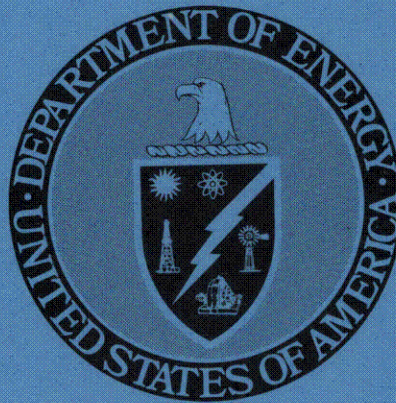


URANIUM DEPOSITS OF THE GRANTS, NEW MEXICO MINERAL BELT (II)

Douglas G. Brookins
University of New Mexico
Department of Geology
Albuquerque, New Mexico 87131

July 1979



PREPARED FOR THE U.S. DEPARTMENT OF ENERGY
Assistant Secretary for Resource Applications
Grand Junction Office, Colorado
Under Contract No. DE-AC-13-76-650-1664
and Bendix Subcontract No. 76-029E

metadc784595

LEGAL NOTICE

This report was prepared as an account of work sponsored by the United States Government as a part of the National Uranium Resource (NURE) Program. Neither the United States nor the Department of Energy and their prime Subcontractor for Uranium Studies, the Bendix Field Engineering Corporation (Grand Junction Branch), nor any of their employees, nor any of their contractors, makes any warranty, express or implied, or assumes any legal liability or responsibility for the accuracy, completeness, or usefulness of any information, apparatus, product or process disclosed, or represents that its use would not infringe privately owned rights.

ERRATA AND NOTES

1. Page 124, Fig. 58: The field for $\text{UO}_2(\text{CO}_3)_2^0$ is not shown as it falls below the pH range for the area designated U-ore (See Langmuir, 1978, for more information).
2. Page 125, Fig. 59: The field for V^{4+} -bearing solid species is not shown. V^{4+} -bearing solid species do occur in the uranium deposits of the Colorado Plateau; the approximate boundaries for a field of V_2O_4 are: Eh + 0.2 to -0.03 volts at pH = 5.9; Eh = - 0.2 volts at pH = 9 (i.e. where the field of V_2O_4 disappears) for an activity of dissolved vanadium = 10^{-7} molal.
3. Page 133, first paragraph: the recommended age of sedimentation is approximately 140 ± 10 m.y. based on published (Lee and Brookins, 1978; data from Jackpile mine area barren montmorillonite) and unpublished data (R.S.Della Valle and D.G.Brookins).
4. Page 144, Fig. 66b: The age for the isochron shown should be 83 ± 11 m.y. with initial $^{87}\text{Sr}/^{86}\text{Sr} = 0.7239 \pm 0.0009$. (note: the correct values are given below Table 12 on p. 143).
5. Pages 271-295, Figs. 264-288: The calibration curves presented here are being revised based on new data representing more standards. The slopes of the curves are not expected to change significantly.
6. Pages 390-394; reactions (i)-(iv) and (a,a',a" and b,b',b") are written for purposes of predicting some of many possible reactions. Thus ΔG_R^0 values calculated from assumed ideal conditions are used instead of ΔG_R because in order to truly use these reactions, one would have to know all reactions, variations in ionic strength, and other parameters. The use of ΔG_R^0 values is, while oversimplified, useful for the purposes of addressing clay mineral-uranium species-iron species. These reactions should not be interpreted as representative of actual reactions which might take place.
7. Page 388: last sentence: The reference is Adams and others (1978); and "Na-feldspar"(not zeolite) should be in the parentheses.

URANIUM DEPOSITS OF THE GRANTS, NEW
MEXICO MINERAL BELT (II)

Douglas G. Brookins
UNIVERSITY OF NEW MEXICO
Department of Geology
Albuquerque, New Mexico 87131

July 1979

PREPARED FOR THE U. S. DEPARTMENT OF ENERGY
ASSISTANT SECRETARY FOR RESOURCE APPLICATIONS
GRAND JUNCTION OFFICE, COLORADO
UNDER CONTRACT NO. DE-AC-13-76-650-1664
AND BENDIX SUBCONTRACT NO. 76-029E

TABLE OF CONTENTS

	Page
PREFACE	xi
Chapter	
1 INTRODUCTION.	1
Geologic Description of the Study Area.	3
Methods of Investigation.	3
Field work.	3
2 SCANNING ELECTRON MICROSCOPY STUDY.	6
Summary	6
Clay Mineralogy	6
Type Samples.	8
Clay Mineral Distribution	9
Discussion.	11
Oxidized and outcrop samples.	11
Ore zone samples.	12
Reduced ground samples.	12
Conclusions	13
3 MOUNT TAYLOR STUDY.	31
Objective of Study.	31
Approaches Used	31
Results	32
Application to Exploration Geochemistry	33
Organic Leaching Experiments.	35
Summary	35
Introduction.	35
Experimental procedures	36
Results	37
Organic Content Study	63
Trace element studies by x-ray fluorescence spectrography	75

TABLE OF CONTENTS (continued)

Chapter	Page
4 Eh-pH DIAGRAMS.	114
Eh-pH Diagrams for V, Mo, Se, As, Sb, REE	117
5 PERIODS OF MINERALIZATION IN THE GRANTS MINERAL BELT.	132
Evidence for Different Periods of Mineralization in the Grants Mineral Belt	133
6 CLAY MINERALOGIC STUDIES.	145
Introduction.	145
7 INSTRUMENTAL NEUTRON ACTIVATION ANALYSIS.	266
Introduction.	266
Sample Preparation.	266
Experimental.	266
Results	269
Delayed Neutron Activation Analysis	327
DNAA Method for U	327
Experimental.	327
DNAA Method for Th.	327
Experimental.	328
Interferences	328
Results	329
8 RARE EARTH ELEMENT (REE) STUDIES.	354
9 THORIUM AND URANIUM ABUNDANCES IN THE ZUNI MOUNTAINS: IMPLICATIONS TO THE GRANTS MINERAL BELT	382
10 DISCUSSION AND CONCLUSIONS.	386
Clay Mineral Relationships and their Bearing on Uranium Mineralization.	386
Chlorite-Pyrite Reactions	392
Reactions Involving Organic Carbon, Chlorite, Sulfur Species, (+) Kaolinite in Redox Zones	393
Clay Minerals from Barren Rocks	394
Clay Minerals from Ore-Bearing and Near-Ore Rocks from Mines	397
Concluding Statements	400

TABLE OF CONTENTS (continued)

	Page
REFERENCES	404
PUBLICATIONS RESULTING FROM AEC-ERDA-DOE/BFEC FUNDING	409

LIST OF FIGURES

Figure	Page
1- 47. S.E.M. Photographs	18- 30
48. Grants Mineral Belt.	34
49- 50. Leach Experiment Conditions.	39- 42
51- 55. Leach Experiment Results	43- 62
56. Organics <u>vs</u> Uranium.	74
57- 65. Eh-pH Diagrams	123-131
66a. Dakota Isochron.	142
66b. Mancos Isochron.	144
67-167. Clay Histograms; Barren Rocks.	155-205
168-263. Clay Histograms; Ore Zones	216-265
264-288. Experimental Correlations.	271-295
289-300. I.N.A.A. Spectra	299-310
301. D.N.A.A. Counter Design.	330
302-303. U and Th Correlations.	332-333
304-309. REE: Kms.	364-381
310-317. REE: Kd	364-368
318-323. REE: Jmj.	369-370
324-329. REE: Jmb.	371-372
330-335. REE: Jmp.c.	373-374
336-341. REE: Jmw.c.	375-376
342-347. REE: Jmr.	377-378
348-350. REE: Jemez.	379-380
351-353. REE: Zuni	381
354. Mg-K-Al-Si-O-H System.	387

LIST OF TABLES

Table		Page
1- 7	Organic Analyses.	64- 73
8-10	XRF Data.	77-113
11	Rb-Sr Data: Dakota	141
12	Rb-Sr Data: Mancos	143
13	Sample Locations.	146-147
14	Rock Descriptions: Barren.	148-154
15-23	Sedimentary Petrography--Summary: Ore Zones.	206-215
24	I.N.A.A. - U.S.G.S. Standards	296-297
25	I.N.A.A. - Nuclides	298
26	I.N.A.A. Results: Kms.	311
27	I.N.A.A. Results: Kd	312
28	I.N.A.A. Results: Jmj.	313
29	I.N.A.A. Results: Jmb.	314
30	I.N.A.A. Results: Jmp.c.	315
31	I.N.A.A. Results: Jmw.c.	316
32	I.N.A.A. Results: Jmr.	317
33	I.N.A.A. Results: Smith Lake	318
34	I.N.A.A. Results: San Mateo.	319-320
35	I.N.A.A. Results: D.O.E. (L.P.).	321
36	I.N.A.A. Results: Jemez.	322
37	I.N.A.A. Results: Zuni	323-326
38	D.N.A.A.: Standards.	331
39	D.N.A.A. Results: Kms.	334
40	D.N.A.A. Results: Kd	335

LIST OF TABLES (continued)

Table		Page
41	D.N.A.A. Results: Jmj.	336
42	D.N.A.A. Results: Jmb.	337
43	D.N.A.A. Results: Jmp.c.	338
44	D.N.A.A. Results: Jmw.c.	339-340
45	D.N.A.A. Results: San Mateo.	341-346
46	D.N.A.A. Results: D.O.E. (L.P.).	347
47	D.N.A.A. Results: Jmr.	348
48	D.N.A.A. Results: Some Sedimentary Rocks	349
49	D.N.A.A. Results: Jemez.	350
50	D.N.A.A. Results: Zuni	351-352
51	D.N.A.A. Results: Hopi Buttes.	353
52	REE Comparisons	358-361
53	Zuni Mts.: Th/U.	384-385

LIST OF PLATES

	Page
Plate 1	Map of Southern San Juan Basin. 4
Plate 2	Tectonic Map of San Juan Basin. 5
Plate 3	Sample Locations of Grants Mineral Belt in pocket

Preface

The report which follows is the second phase of a DOE contract designed to address various aspects of the genesis of the uranium deposits of the Grants mineral belt. Many of the problems outlined in Phase I of this study (Brookins, 1976a) have been answered, others have been raised.

The Data contained herein are many and full data reduction and comprehensive statistical treatment are in progress. It is our intention in Phase III (Pending) of this research to apply the knowledge obtained from Phases I (primarily on ore zones) and II (more data from barren rocks) to continue use of tried techniques plus newer techniques to attempt a realistic genetic model for the Grants mineral belt. It is our contention that we are near this point and should be able to provide the U.S. Department of Energy and Industry with working guides applicable to uranium exploration after completion of Phase III (Proposal Pending).

Student theses and dissertations have been generated during the course of the investigation. Ph.D. Candidates R.S. Della Valle and W.C. Riese have made invaluable contributions to this Report as have M.S. Recipients and Candidates C.S. Sullivan, R.N. Hicks, R. Lowy, J.T. Place. Others supported by DOE/BFEC funds for work on this project include J.S. Bruneau, R.S. Miller, T. Mackeigan, K. Coley, C.I. Mora, D.K. Davidson; all students at UNM. Personnel at the Los Alamos Scientific Laboratory who have rendered invaluable assistance include J.P. Balagna, J.E. Sattizahn, G.A. Cowan, M.P. Bunker.

The availability of some of the facilities at the Los Alamos Scientific Laboratories (LASL) for neutron activation analyses greatly facilitated parts of the research; further, cooperation with personnel of LASL and the

U.S.G.S. (Office of Energy Resources: Branch of Uranium and Thorium)

greatly facilitated the program.

Such research would not be possible without the interest and willingness to cooperate by making sampling of mines and other properties available.

The following companies and their personnel are gratefully acknowledged:

The ARCO-Anaconda Company, The United Nuclear Corporation, Inc., The Kerr-McGee Nuclear Co., The United Nuclear-Homestake Partners Co., Gulf Minerals Resources, Inc., Teton Drilling and Exploration Corporation, The Sohio Minerals Co., CONOCO, Ranchers Mining Exploration and Development Co.

Finally, I wish to thank the many U.S.D.O.E. and Bendix Field Engineering Corporation personnel who have offered constructive advice and been helpful in too many ways to enumerate here.

Chapter 1

INTRODUCTION

Sedimentary uranium deposits in the Grants mineral belt (GMB) occur in a strip nearly one hundred miles long and twenty miles wide that extends from near Gallup on the west to Languna on the east. Of the sedimentary rocks that are exposed in the area, mineable uranium deposits are found only in those of Jurassic and Cretaceous ages. These rocks are, in ascending order, the Entrada Sandstone, Todilto Limestone, Summerville Formation, Bluff Sandstone of the San Rafael Group, and the Morrison Formation, all of Late Jurassic age, and the Dakota Sandstone of Late Cretaceous age.

Deposits in the Morrison Formation, in particular, have been mined extensively and have been the subject of much research since the early 1950's. However, the origin of these deposits is still controversial and many uncertainties exist, even though there are pronounced similarities for many of the deposits.

Most uranium occurrences are closely associated with accumulations of organic matter, and the host sediments either contain granitic or volcanic detritus or are associated with tuffaceous material (Finch, 1967). The most striking feature of the GMB is the similar geochemistry and mineralogy in most of the deposits; iron (as pyrite and, more rarely marcasite), uranium (coffinite; lesser uraninite, U-C complex (?)), vanadium (oxides and silicates), molybdenum (jordisite), selenium (native and ferroselite), and organic carbon (humates and fossil wood) appear in essentially all the uranium deposits (Kendall, 1972) although in differing proportions. In addition, ubiquitous clay mineral assemblages

of montmorillonite, mixed-layer illite-montmorillonite, kaolinite and chlorite exist in most deposits (Keller, 1959; Nash, 1968; Granger, 1962; Kendall, 1972; Brookins 1976a; 1977c). Several hypotheses (or models) have been developed to explain the origin of the ore deposits (ash leach theory, granite leach theory syngenetic, epigenetic, etc.) and agreements are lacking in many aspects of mineralization. Furthermore, although some agreement has been reached on the particular role of organic matter to the uranium mineralization, its role on the dissolution and reprecipitation of the host silicates, its nature and origin have largely been ignored.

Recent investigations (Huang and Keller, 1970, 1971, and 1972a; Ong and others, 1970) show that naturally occurring organic acids, commonly called humic acids, possess significant cation exchange properties (sorption) and are effective agents in the colloidal transport of metallic elements. Since the organic acids are known to dissolve (or reprecipitate) rock-forming silicate minerals (especially clay minerals which also have large cation exchange properties), detailed mineralogical and geochemical studies for both barren and mineralized zones should set further limitations on the origin of the sandstone-type uranium deposits. We therefore, in this study, continued combined sedimentary petrologic, clay mineralogic, geochemical and geochronologic studies with the samples collected from selected localities in the Grants mineral belt.

This investigation was directed toward the mode of ore formation and alterations using geochemical criteria, if possible, use of these criteria as possible ore guides in similar stratigraphic sections in northwestern New Mexico.

GEOLOGIC DESCRIPTION OF THE STUDY AREA

Plate I and II show the study area and major tectonic elements in northwestern New Mexico, respectively. The principal structural-tectonic elements in which the Grants mineral belt occurs have been described by Kelley (1957), Kelley and Clinton (1960), and by Hilpert and Moench (1960).

The area has been subjected to several minor and one major episodes of deformation from Morrison time to the present. The first deformation appears to have accompanied and shortly followed the Morrison sedimentation (Kelley, 1955; Hilpert and Moench, 1960). However, the major deformation of the region probably occurred in Laramide time and gave rise to the Zuni Uplift, the San Juan Basin, and the Acoma Embayment (Kelley, 1963). It is believed that the principal folds and faults in the area were formed and the gently northerly dips were established at this time.

METHODS OF INVESTIGATION

Field Work

Field investigation was concerned with stratigraphic, sedimentologic and structural descriptions in addition to sample collections in both barren and ore zones. Particular attention was paid on the geometrical aspects of the ore bodies, since the pattern of oxidation may have significant correlation to the sedimentary structure (Roach and Thompson, 1959). With access to a significant number of mines, this phase of the research was greatly facilitated. Plate III shows the area of study with sample locations. (Plate III located in pocket)

Plate I. Map of southern San Juan Basin (after Granger, 1968) and the location of study area shown by open circles.

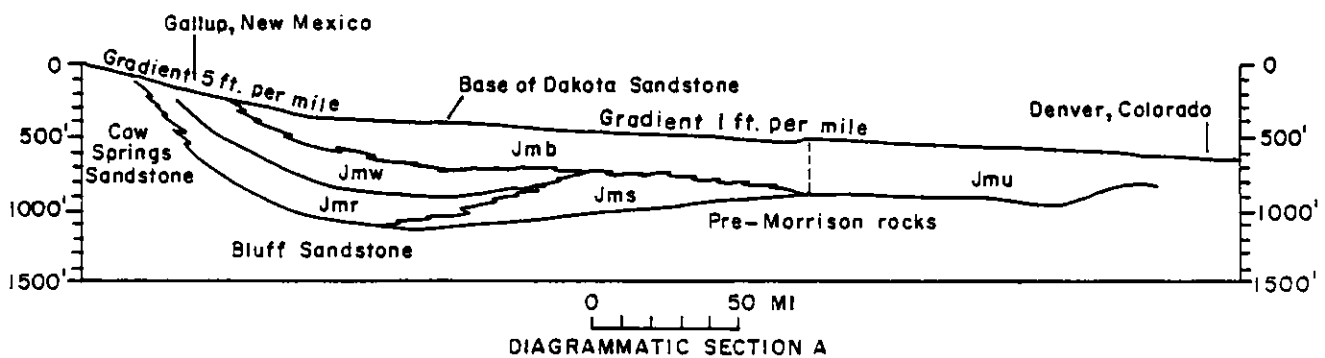
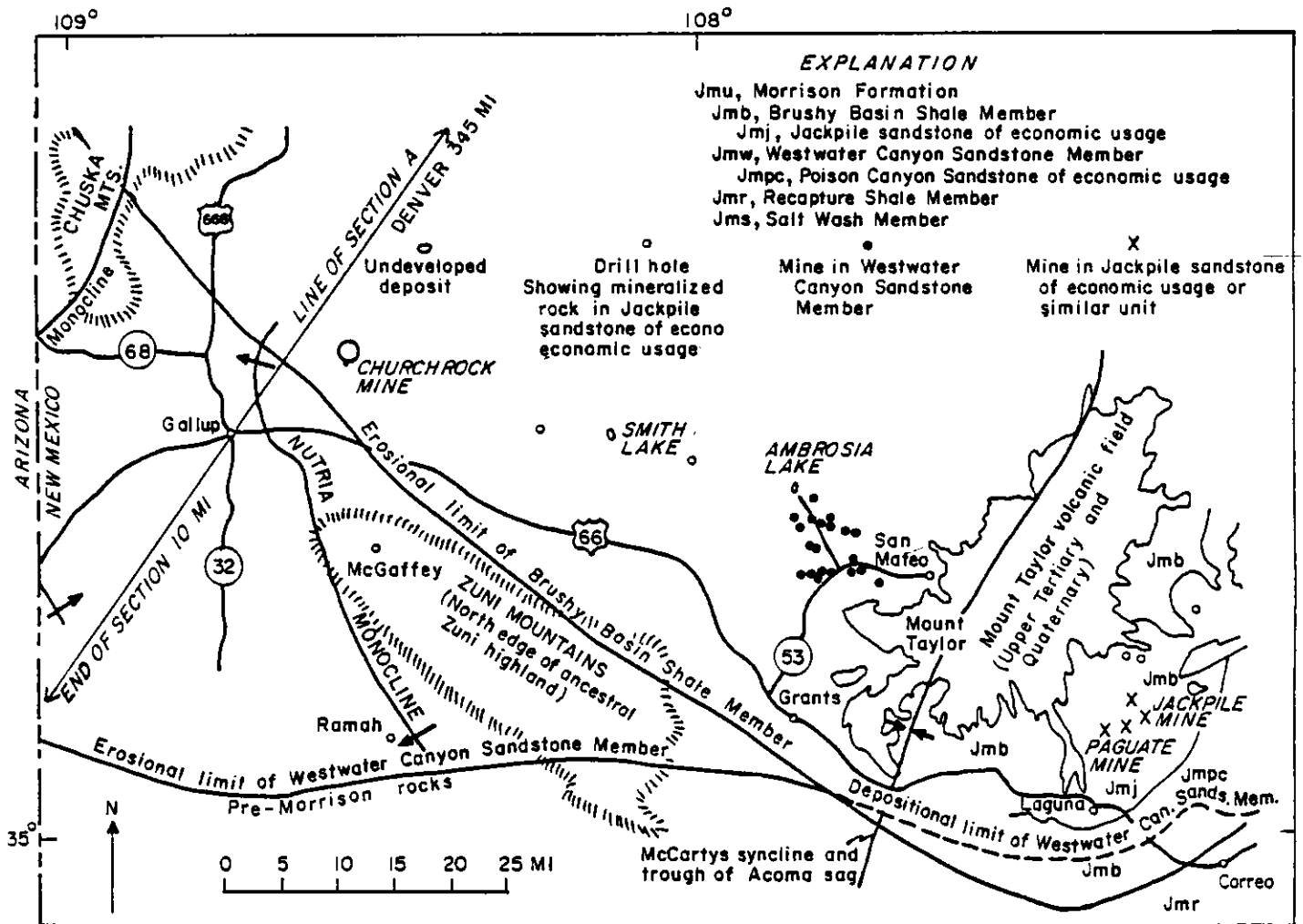
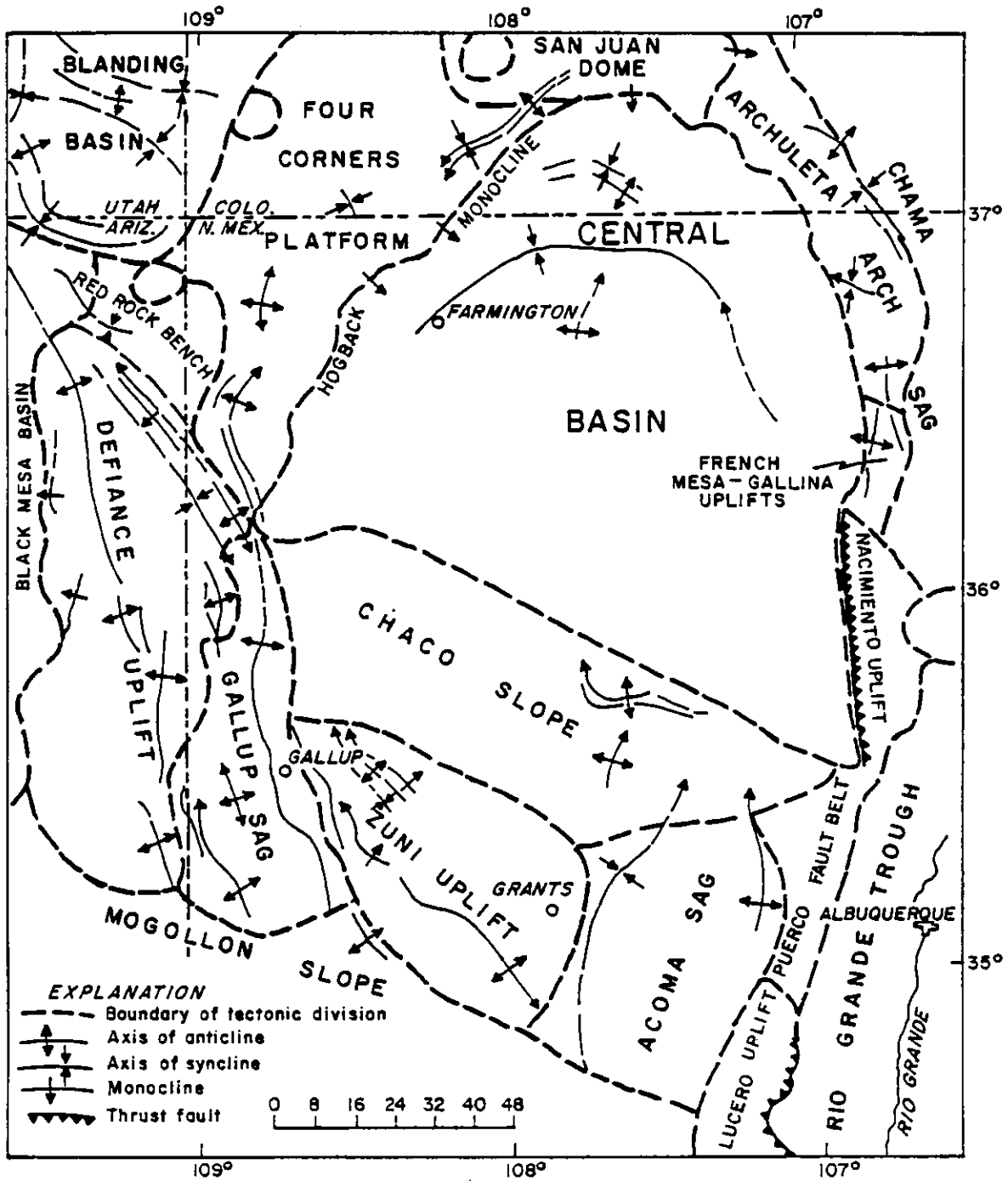


Plate II. Tectonic map of San Juan Basin and adjacent areas (after Kelley, 1963).



Chapter 2

SCANNING ELECTRON MICROSCOPY STUDY

Summary

Scanning electron microscopy study of authigenic minerals in the Westwater Canyon Member of the Morrison Formation (Late Jurassic) reveals compositional variations within and adjacent to sandstone-type uranium deposits. Montmorillonite is the dominant clay mineral in the reduced ground down-dip of the ore body; chlorite is enriched in the ore zones, and kaolinite and altered montmorillonite in the "oxidized" ground up-dip of the ore. Our data also suggest that clay minerals, not pyrite or hematite, may locally be the iron-bearing species of importance.

While it is not possible to positively identify organic materials in SEM photomicrographs, materials deduced to be organic in nature post-date the beginning of authigenic clay formation. This implies that these materials may be carriers of uranium in the ground water system from which the ore deposits precipitated.

Identification of these patterns of clay mineral alteration and the role that organic materials may play as transporting media may significantly alter our exploration techniques. These patterns may be especially useful tools in areas where the ore bodies are known to be removed from the iron species redox interface.

Clay Mineralogy

The clay mineralogy of the Morrison Formation in the Grants mineral belt of New Mexico has been studied extensively by Keller (1962), Granger (1962), Nash (1968), and Kendall (1972) among others. These

studies have for the most part been limited to examination of local aspects of clay mineralogy, and although attempts have been made to establish relationships between clay mineralogy and uranium mineralization in this region, no clear-cut patterns have been recognized. Keller (1962), in particular, has indicated that no specific clay minerals can be used as guides to finding uranium ore, although he did recognize the need for more work, especially with regard to polytypism and trace element studies.

This study has considered a broad, regional assemblage of clay minerals which will be divided into four groups: outcrops, barren "oxidized" samples taken up-dip of the ore, ore zones, and barren "reduced" samples taken down-dip of the ore. Emphasis will be given to samples from the Westwater Canyon Member, particularly subsurface samples which are well removed from the effects of outcrop alteration. The analytical procedures used are outlined in Lee (1976) and will not be elaborated on here. Suffice it to say that in order to calibrate our photos, X-ray diffractograms of oriented samples were obtained for air-dried, glycolated, heated, and acid-treated samples. Random powders were X-rayed mainly for the differentiation of polytypes and identification of non-clay minerals. The criteria used in this phase of the study are also discussed in Lee (1976).

It should be pointed out at this time that we are using the terms "oxidized" and "reduced" for reference purposes and for uniform terminology. Since most of the Wyoming deposits are described in this fashion, and since many of the Grants mineral belt deposits reside at an iron redox interface and show trace element zonation patterns comparable to those

found in the Wyoming deposits, we do not feel that the use of these terms will cause problems. We must emphasize however that the Mount Taylor deposit, from which much of our data has been obtained, does not reside at an iron redox interface although the other transition metals which usually zone across deposits formed by lateral secretion zone here as well. Here, use of the terms "oxidized" and "reduced" is intended to be used for location reference only.

Figure 1 through 16 are photomicrographs of samples taken from the Jackpile sandstone bed of the Brushy Basin Member of the Morrison Formation. These sequences are of significance because they show authigenic mineral development comparable to that found in the Westwater Canyon Member and because they represent the only samples in which primary uranium-bearing minerals have been found.

Figures 17 through 46 represent samples from the Westwater Canyon Member and are arranged into two groups: the first is a sequence of "type" samples and the second, a cross-section through an ore zone. Since most of the production in the Grants mineral belt has been from the Westwater, we will restrict our further discussions to figures 17 through 46.

Type Samples

In order to properly address this topic, it is first necessary to have a feel for what more or less "perfect" samples of each clay look like in SEM photomicrographs. Kaolinite appears as a collection of thick, stacked books (Fig. 17). Kaolinite occasionally assumes a worm-like morphology, and this vermicular form is shown in figure 18. Chlorite can be seen assuming two very distinct morphologies. The

first is an open "edge-to-face" arrangement (Fig. 19) and the second is a collection of small rosettes (Fig. 20). Figure 21 shows montmorillonite in its typical honeycomb morphology. Illite-montmorillonite mixed-layer assemblages, although members of the smectite group, look more like thin, undulating blankets with slightly curling edges (Fig. 22).

Clay Mineral Distributions

While not being "C" shaped, many of the ore bodies in the Grants mineral belt conform to Harshman's 1970 model for roll-fronts in other respects: identifiable iron species are usually reduced down-dip of the ore and oxidized up-dip from it, and various trace elements are distributed in a zoned alteration pattern across the ore (i.e., along dip). Assuming that this chemistry was indicative of the direction that ore-forming fluids had moved, we postulated that if clay minerals formed similar zonation patterns across ore bodies, they would further affirm the lateral secretion hypothesis for genesis of these deposits and might also prove to be useful tools for exploration, especially in areas like the Mount Taylor deposit where much of the iron does not seem to be present in either pyrite or hematite and is therefore less visible. What we have found is that clay minerals are zoned, but in a very subtle fashion: no one clay is exclusively present either in front of, in, or, behind an ore body. This can be illustrated with a sequence of figures that represent a cross-section from the front or down-dip side of an ore body, to the back or up-dip side. Figure 23, the first in this sequence, shows a montmorillonite honeycomb well hidden by what we believe to be amorphous organic material. Also present are rosettes of chlorite, altering from the montmorillonite, and a few authigenic quartz crystals. This sample was taken from core

which was cut approximately one mile down-dip of the nearest known ore. Moving closer to the ore (Fig. 24), we find individual detrital grains covered with chlorite which has formed as an alteration product from montmorillonite. Figure 25 is a closer view of figure 12. We also see a little bit more organic material. This is shown in figure 26. Mixed-layer illite-montmorillonite assemblages are also to be found in close proximity to the ore and are shown in figure 27.

In the ore zones, chlorites such as those shown in figure 28 are the dominant clays. However, as we described earlier, kaolinites and montmorillonites may also be found in the ore zones. Ore zone examples of these are shown in figures 29 and 30, respectively. Other clay minerals which have been identified in the ore zones include illite needles (Fig. 31), chlorite-montmorillonite mixed-layer assemblages (Fig. 32), and chamosite (?) (Fig. 33). Non-clay minerals which have been found in the ore zones include feldspars (Figs. 34 and 35), carbonates (Fig. 36), pyrite (Fig. 37), and titanium oxides (Fig. 38) which form through the alteration of detrital titanomagnetite grains. In at least one deposit (Mount Taylor), we have also found what appears to be plant spores (Figs. 39 and 40). Final identification of these forms has not yet been made because they are smaller than any spore heretofore identified. Primary uranium-bearing species are almost nonexistent in the samples we have studied from the Grants mineral belt; instead, the uranium seems to be complexed by adsorption on clay minerals and by chelation with various humic complexes. Only one sample has shown a primary uranium mineral. This mineral is coffinite and is shown in figure 41.

In oxidized ground, kaolinite becomes the dominant clay as shown in figure 42. Also present in oxidized ground are authigenic feldspars, although in this area they usually look significantly more altered. An example of this alteration is shown in figure 43.

We mentioned earlier that hematite and pyrite are not necessarily the iron-bearing species of importance. This is best illustrated by the Mount Taylor deposit where the only hematite found to date has been a full half mile up-dip of the ore. This sample is shown in figure 44. Note the small size of the nodules. Iron in this ore body has been found in clay minerals such as those shown in figure 45. Elemental X-ray scans, where available, support these findings.

Discussion

Oxidized and Outcrop Samples

The oxidized and outcrop samples appear to have a rather uniform clay mineral distribution, with montmorillonite and kaolinite being the dominant species in the Westwater Canyon Member. In all sections studied, the Westwater Canyon Member contains minor amounts of chlorite. The distribution of minor illitic minerals is very erratic and appears to have no persistent pattern.

Most of the montmorillonite in the Morrison Formation is authigenic and formed by divitrification and hydrolysis of the volcanic ashes. Some may be detrital, but the crystalline, delicate morphology shown in our photomicrographs suggests no multicycle deposition.

Kaolinite in the Westwater Canyon Member occurs as "nests" that fill pore spaces and which often enclose several sand grains. These nests show no oxidation coatings and their size is proportional to grain

size and porosity. The kaolinite in the Jackpile sandstone of the Brushy Basin Member is interstitially distributed throughout the sand and is not restricted to nests. In both units potassium feldspar grains within the nests are fresh and show no signs of kaolinization.

Ore Zone Samples

Chlorite enrichment relative to montmorillonite is the most distinctive alteration feature of these samples. This phenomenon was first reported by Granger (1962) who showed chlorite enrichment to be proportional not only to uranium but to magnesium and organic carbon contents as well. This distribution has been confirmed by Lee (1976) and this study as well.

Chlorite occurs as well developed coatings on detrital grains and is intimately mixed with organic carbonaceous materials. In high grade ores, we have had difficulty detecting chlorite visually due to the abundance of humic materials.

Varying amounts of kaolinite, montmorillonite and illite are also present in the ore zones. Kaolinite is apparently unrelated to the processes of ore formation and is believed to have formed after mineralization. Similarly, the minor illitic constituents which are found in and near the ore zones bear no significant relation to the uranium ore deposits.

Reduced Ground Samples

Two distinctive features mark this suite of samples: the presence of well-crystallized chlorite and of regularly interstratified illite-montmorillonite. The chlorite is ubiquitous whereas the illite-

montmorillonite mixed-layer assemblages are sporadically distributed. Our study suggests that the chlorite was formed by both direct precipitation and solid state alteration of pre-existing montmorillonite (Fig. 46). The mixed-layer clays found in this area are commonly of the 1:1 variety and textural relations suggest that they formed later than montmorillonite but earlier than most chlorite.

Conclusions

We have determined that clay minerals do zone in and near the sandstone-type uranium deposits of the Grants mineral belt, but that they do so in a fairly subtle fashion. No one clay is exclusively present in any given zone. The paragenetic sequence of mineral formation is as follows:

Montmorillonite formed through the devitrification and hydrolysis of volcanic ashfall materials in the Morrison section. The ground water systems of the Colorado Plateau have probably always been high in carbonate content and this partially accounts for the beginning of calcite precipitation early in the ore-forming process. Organic materials (humic acids?) in the ground water system next began to "bleach" the sandstones and acted as a catalyst for the chlorite formation from montmorillonite. Formation of authigenic feldspars began early in the ore-forming process and continued until the second stage of chlorite formation. This second stage is the rosette chlorite and is usually found only near ore zones. Quartz overgrowth formation began before the second influx of organics. It was this second organic phase which probably brought in most of the uranium (Riese, et al., 1978). Finally, kaolinite formation began and at this point some of the ore began to remobilize in what had become an intolerable oxidizing environment. This reprecipitated ore is the stack ore of the

district and further down-dip as well. This sequence is graphically depicted in figure 47.

- Figure 1. SEM photomicrograph showing a bedded mudstone, over which a mantle of illite-montmorillonite mixed-layer assemblage has been deposited. Note the collection of pyrite framboids near the center of the photo.
- Figure 2. SEM photomicrograph depicting a closer view of the pyrite framboids noted in 1. The individual grains of each framboid occasionally show distinct pyritohedral focus, a possible indication that As is substituting in the crystal lattice.
- Figure 3. SEM photomicrograph showing a framework feldspar grain which has been broken, probably during sample preparation. Illite-montmorillonite mixed-layer assemblages may be seen in the first quadrant.
- Figure 4. SEM photomicrograph showing a closer view of the feldspar cleavage and illite-montmorillonite noted in 3.
- Figure 5. SEM photomicrograph showing a framework of detrital grains.
- Figure 6. SEM photomicrograph showing well developed chlorite in typical edge-to-face morphology. Several rosettes appear to be developing in the third and fourth quadrants.
- Figure 7. SEM photomicrograph showing a framework of detrital grains mantled by extremely cryptocrystalline clay materials.
- Figure 8. SEM photomicrograph giving a closer view of 7. Minerals present are still too fine grained to be positively identified, but the morphologies present do allow two possibilities: First, pyrite framboids; this would allow for the high Fe content of this sample. Second, coffinite; this would explain the high Si content of this sample.
- Figure 9. SEM photomicrograph showing a detrital feldspar grain. Note the cleavages in the center of the field of view.
- Figure 10. SEM photomicrograph depicting a closer view of 9.
- Figure 11. SEM photomicrograph showing detrital framework grains.
- Figure 12. SEM photomicrograph showing chlorite in edge-to-face arrangement. Several small rosettes are beginning to develop near the center of the field of view. This is a closer view of 11.
- Figure 13. SEM photomicrograph showing a single detrital grain whose coating of authigenic clays has been broken. Illite-montmorillonite constitutes the outermost coating.
- Figure 14. SEM photomicrograph showing a closer view of 13.

- Figure 15. SEM photomicrograph showing several detrital grains and wispy traces of montmorillonite.
- Figure 16. SEM photomicrograph showing the surface of a detrital grain covered with coffinite. This is a closer view of 15.
- Figure 17. SEM photomicrograph showing a type-sample of kaolinite.
- Figure 18. SEM photomicrograph showing a type-sample of vermicular kaolinite.
- Figure 19. SEM photomicrograph showing a type-sample of chlorite in edge-to-face arrangement.
- Figure 20. SEM photomicrograph showing a type-sample of chlorite rosettes.
- Figure 21. SEM photomicrograph showing a type-sample of montmorillonite in its typical honeycomb morphology.
- Figure 22. SEM photomicrograph showing a type-sample of an illite-montmorillonite mixed-layer assemblage.
- Figure 23. SEM photomicrograph showing a montmorillonite honeycomb well hidden by organic (?) material. Also shown are several rosettes of chlorite and several authigenic quartz grains.
- Figure 24. SEM photomicrograph showing an individual detrital grain completely mantled by authigenic chlorite. Also shown are two dark patches of organic material.
- Figure 25. A closer view of Figure 12, which shows the chlorite to be in edge-to-face arrangement. Several flakes of illite-montmorillonite mixed-layer assemblage are shown near the upper and lower limits of the field of view.
- Figure 26. SEM photomicrograph showing an intergranular accumulation of organic (?) material.
- Figure 27. SEM photomicrograph showing illite-montmorillonite mixed-layer assemblages beginning to mantle a chlorite-coated detrital grain.
- Figure 28. SEM photomicrograph showing chlorite development in an ore zone.
- Figure 29. SEM photomicrograph showing kaolinite development in an ore zone.
- Figure 30. SEM photomicrograph showing montmorillonite development in an ore zone.

- Figure 31. SEM photomicrograph showing illite needles in an ore zone.
- Figure 32. SEM photomicrograph showing a chlorite-montmorillonite (?) mixed-layer assemblage in an ore zone.
- Figure 33. SEM photomicrograph showing chamosite (?) development in an ore zone.
- Figure 34. SEM photomicrograph showing authigenic feldspars in an ore zone.
- Figure 35. SEM photomicrograph showing authigenic feldspars in an ore zone.
- Figure 36. SEM photomicrograph showing carbonate development in an ore zone.
- Figure 37. SEM photomicrograph showing framboidal pyrite development in an ore zone.
- Figure 38. SEM photomicrograph showing titanium oxides (anatase and rutile) developing through the corrosion of detrital titanomagnetite.
- Figure 39. SEM photomicrograph showing plant spores (?).
- Figure 40. A closer view of Figure 39.
- Figure 41. SEM photomicrograph showing coffinite in an ore zone.
- Figure 42. SEM photomicrograph showing kaolinite development in the altered ground up-dip from an ore zone.
- Figure 43. SEM photomicrograph showing authigenic feldspars being altered up-dip from an ore zone.
- Figure 44. SEM photomicrograph showing small hematite nodules on a clay surface up-dip of an ore zone.
- Figure 45. SEM photomicrograph showing high-iron smectites (minnesodaite?).
- Figure 46. SEM photomicrograph showing montmorillonite altering to rosettes of chlorite.
- Figure 47. Paragenetic sequence of mineral formation in the sandstone-type uranium ore deposits of the Grants mineral belt as interpreted from SEM photomicrographs.



Figure 1.

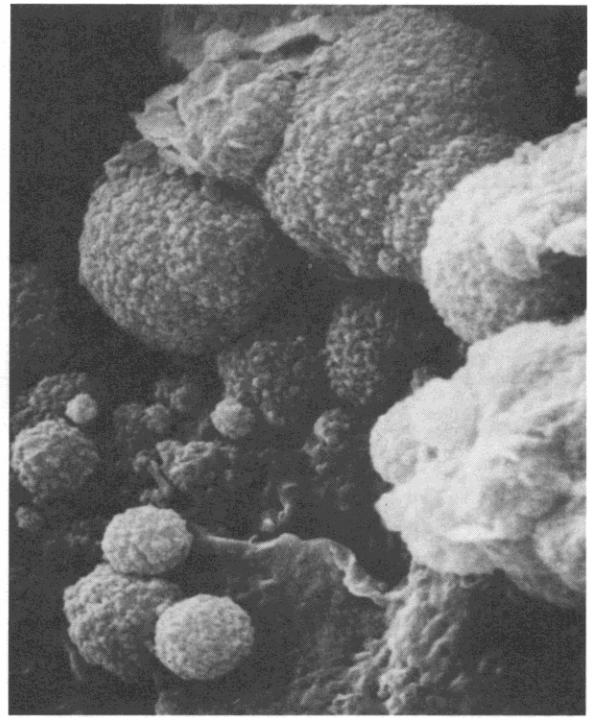


Figure 2.

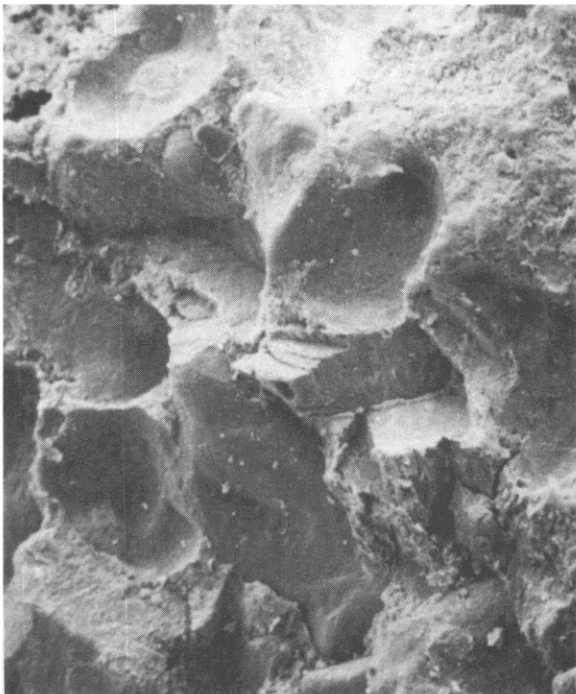


Figure 3.

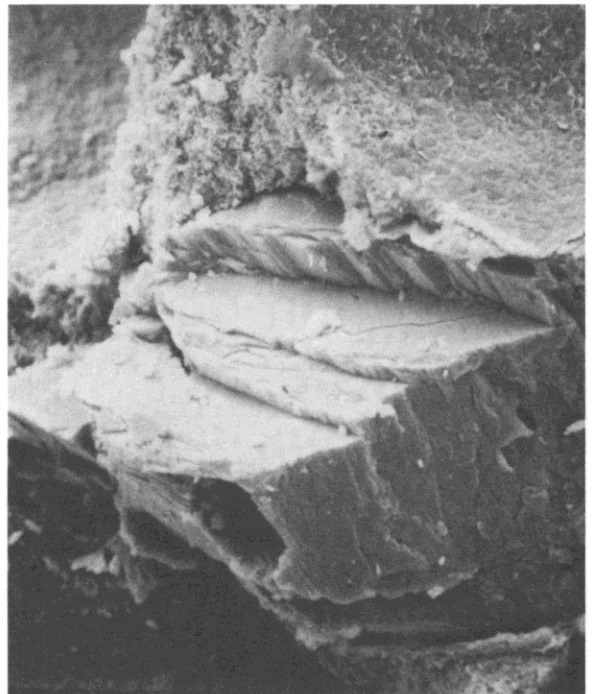


Figure 4.

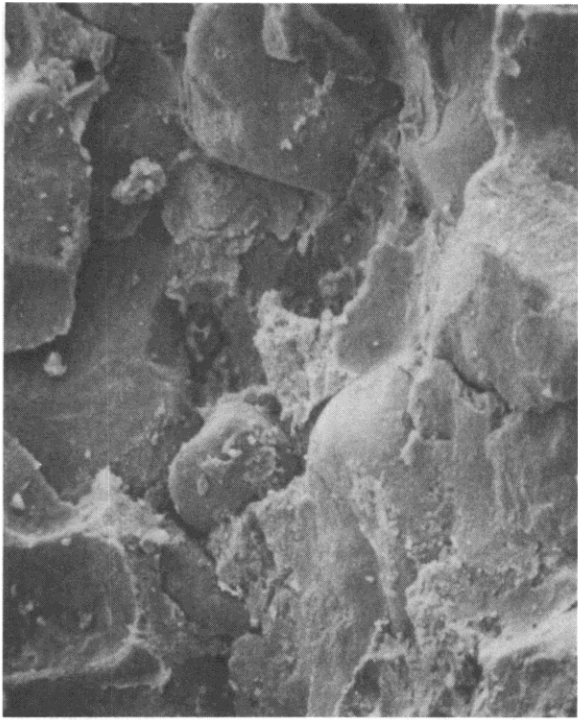


Figure 5.



Figure 6.

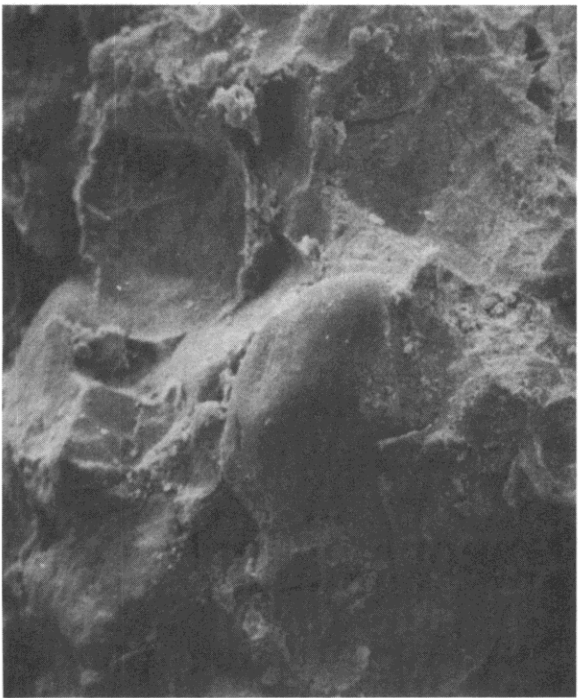


Figure 7.



Figure 8.

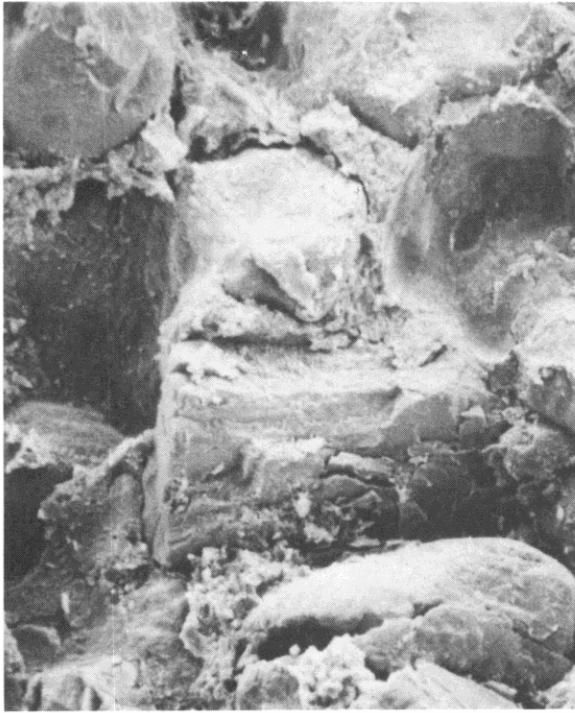


Figure 9.

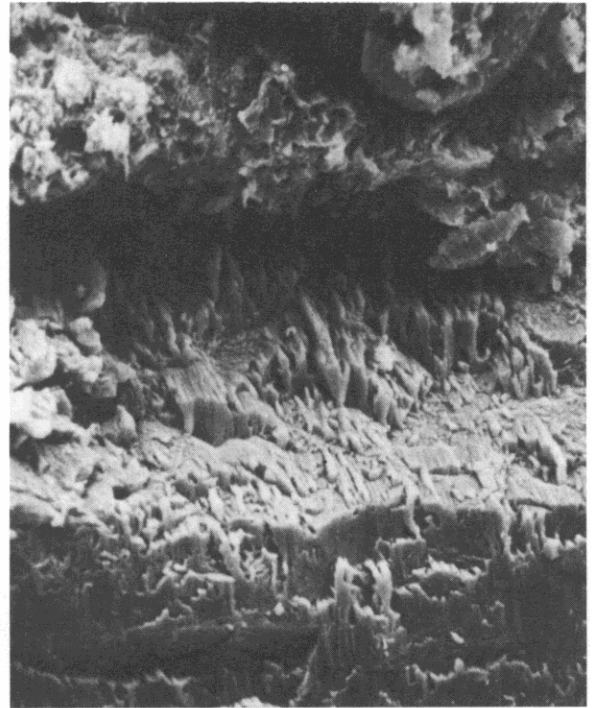


Figure 10.

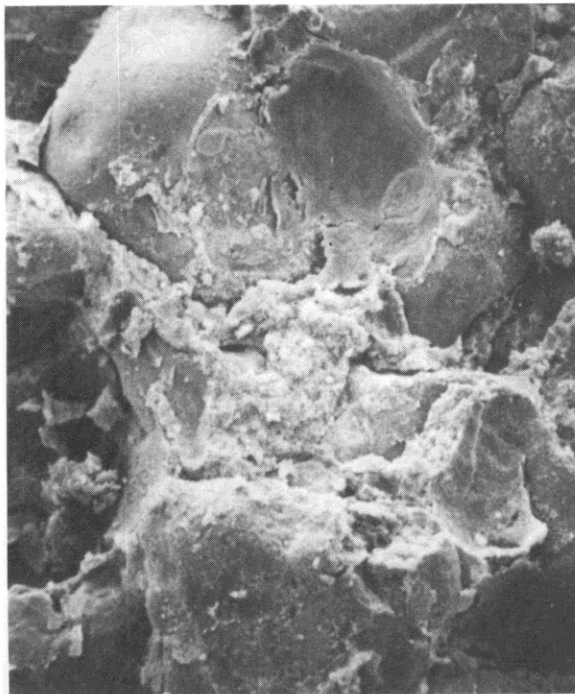


Figure 11.

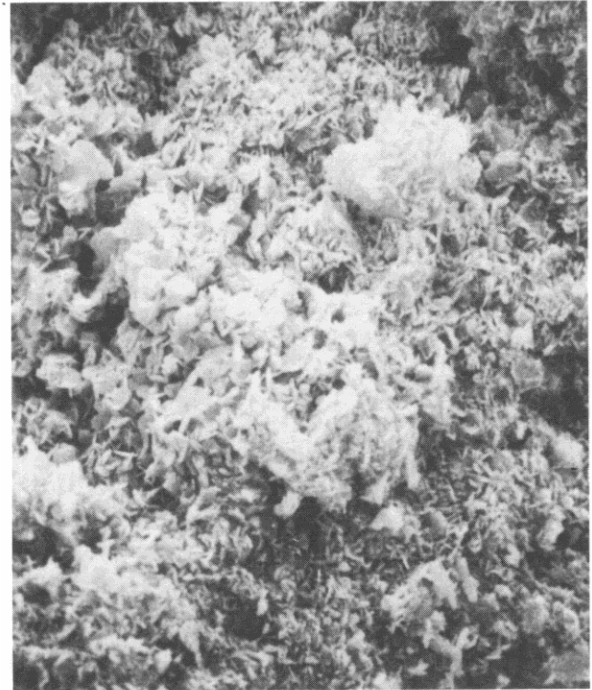


Figure 12.

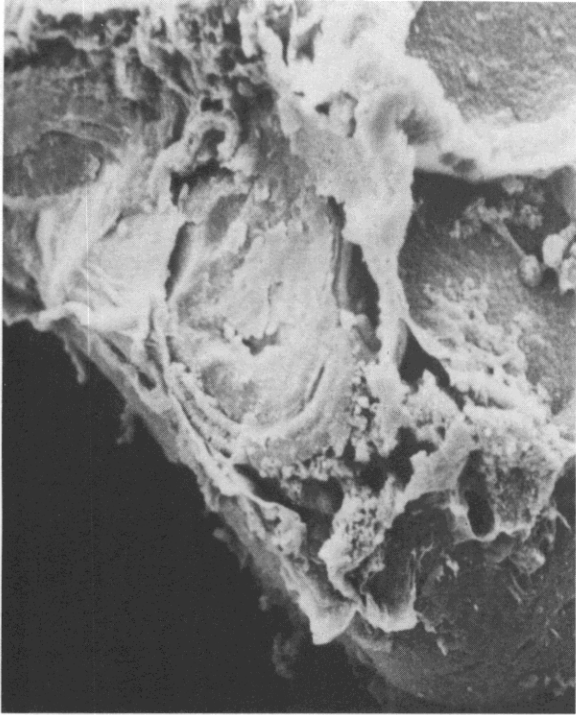


Figure 13.

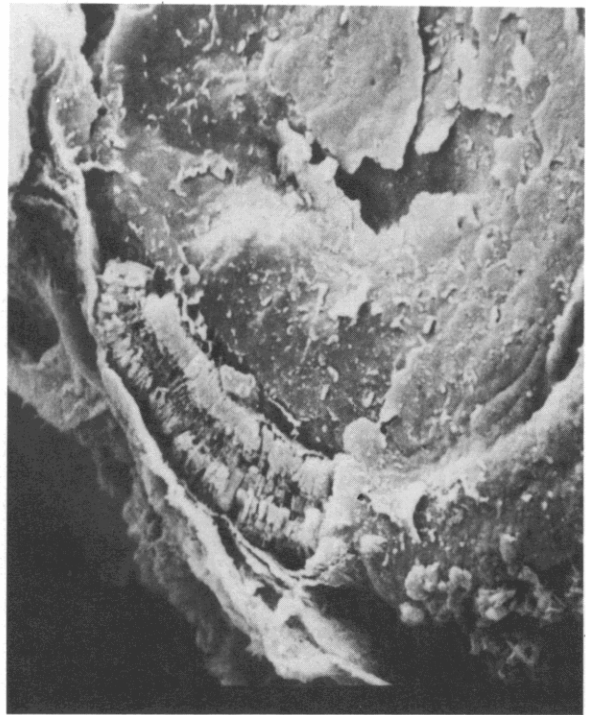


Figure 14.



Figure 15.

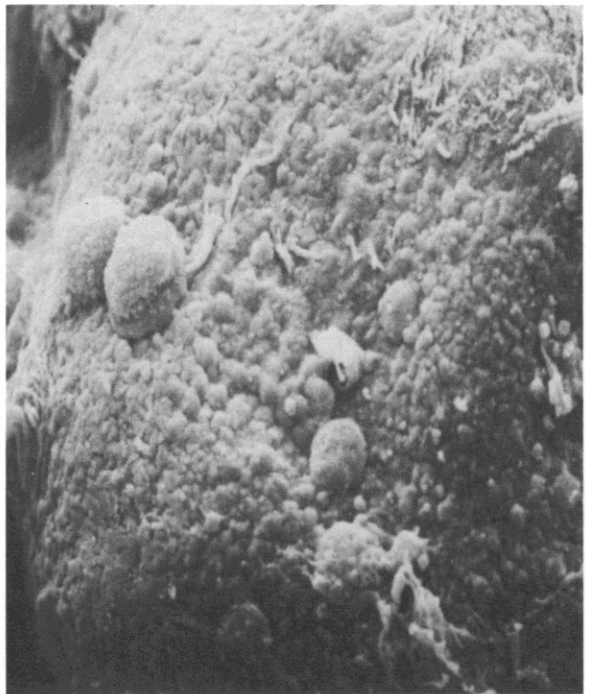


Figure 16.



Figure 17.

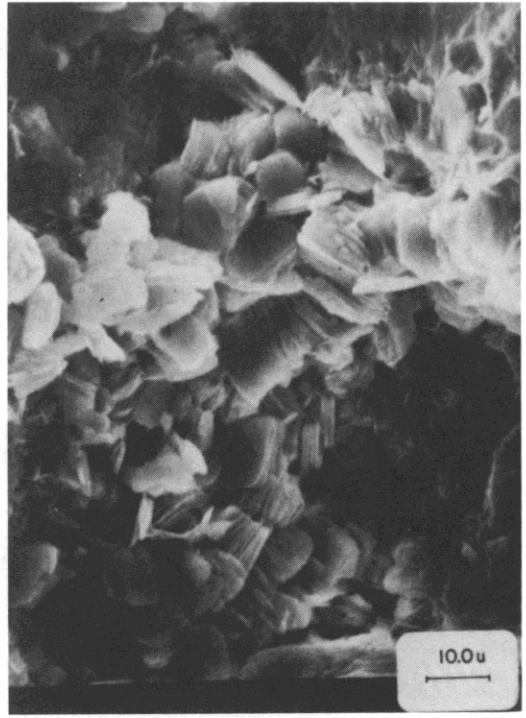


Figure 18.



Figure 19.

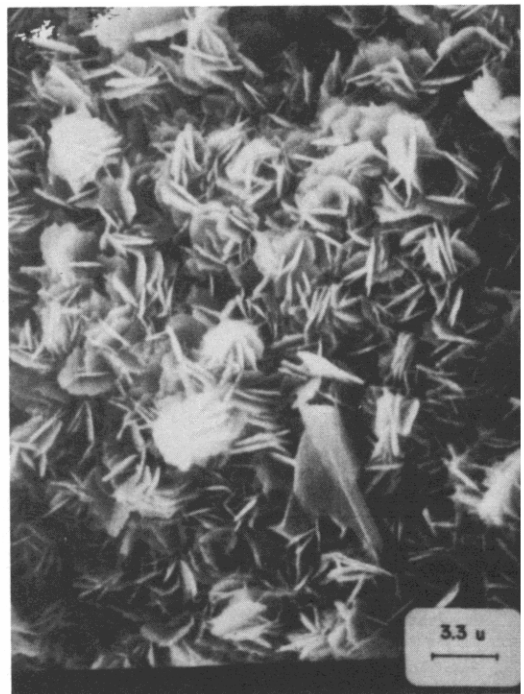


Figure 20.

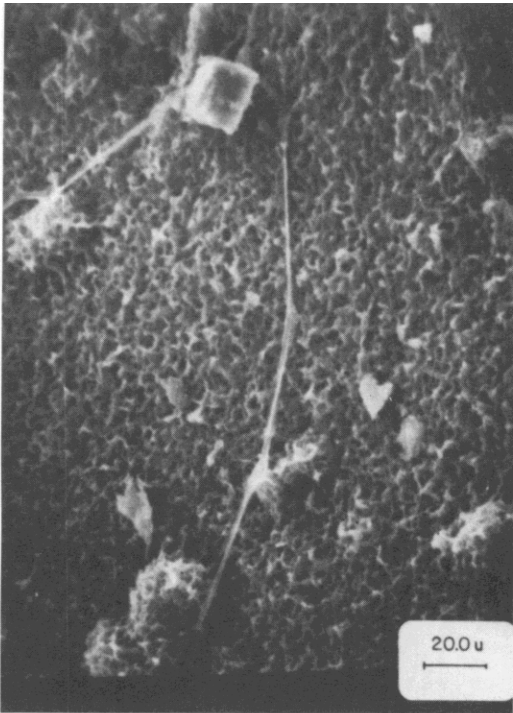


Figure 21.

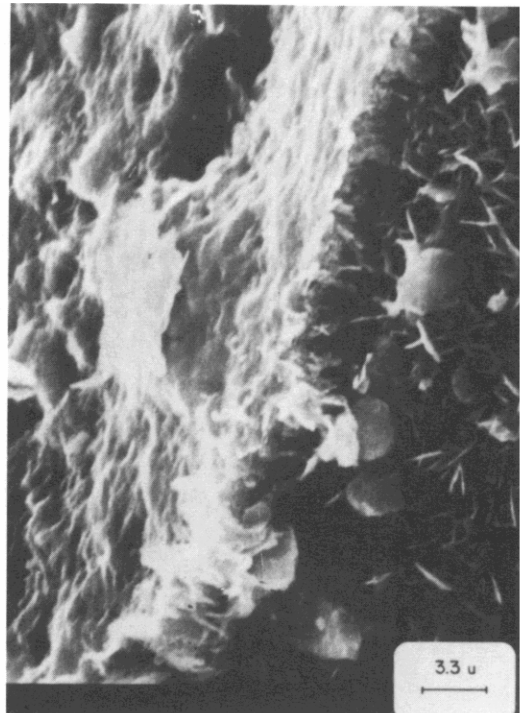


Figure 22.

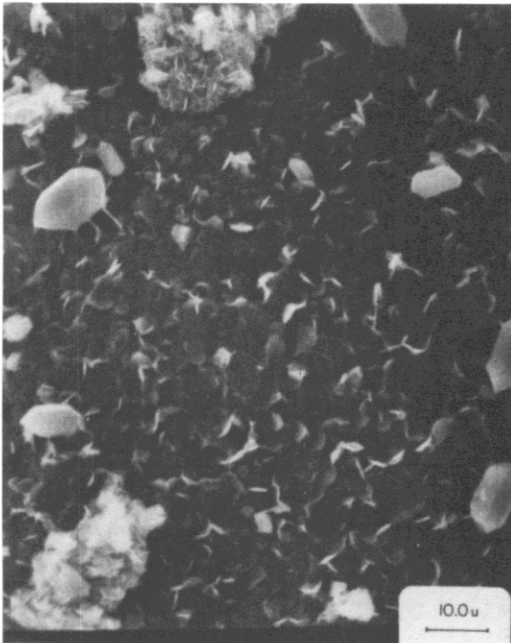


Figure 23.



Figure 24.

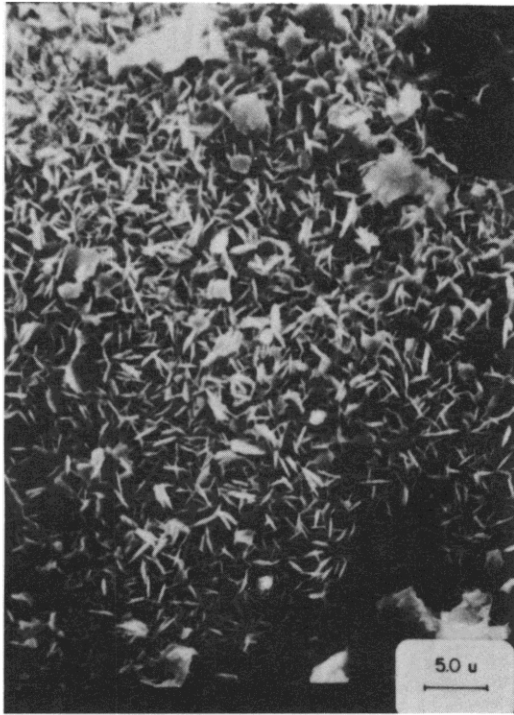


Figure 25.



Figure 26.

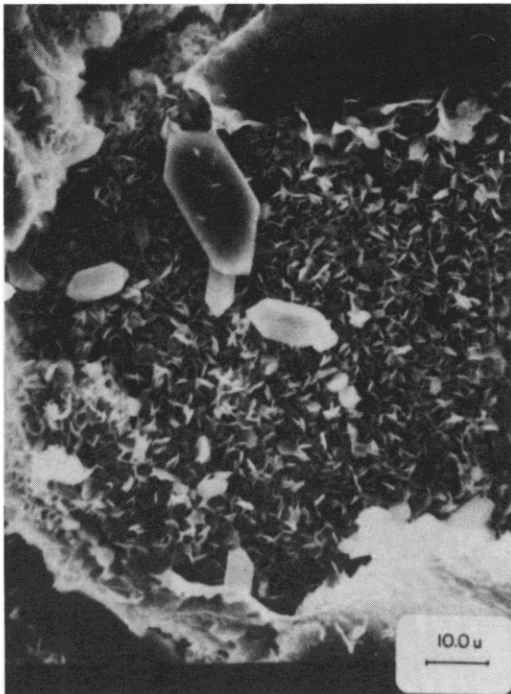


Figure 27.



Figure 28.



Figure 29.

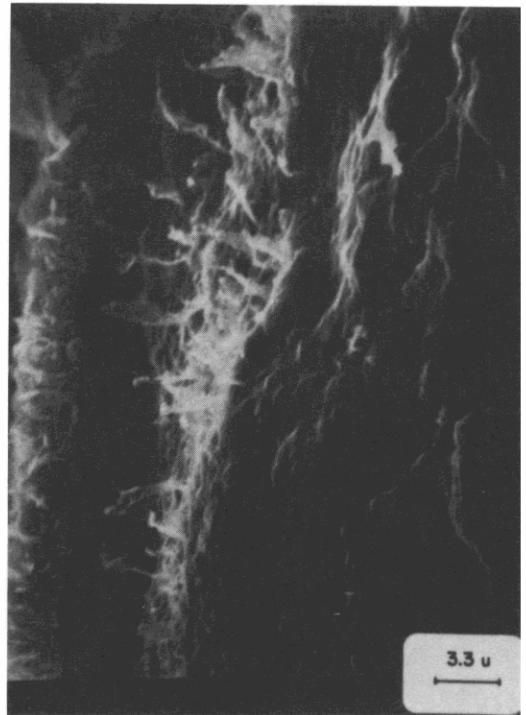


Figure 30.



Figure 31.



Figure 32.



Figure 33.

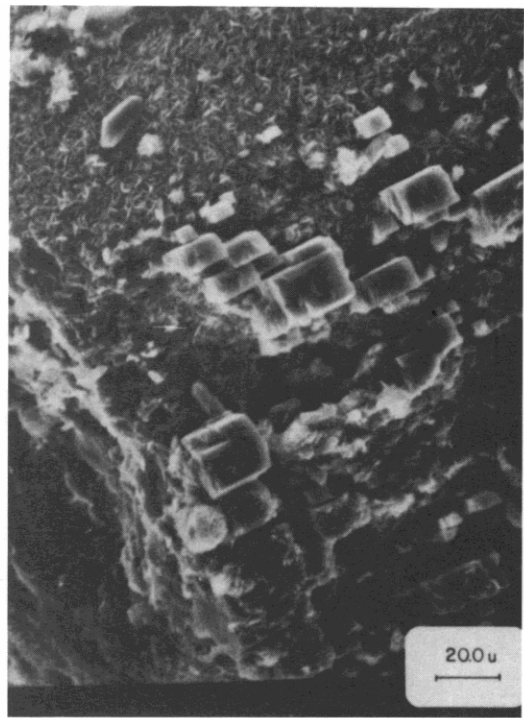


Figure 34.

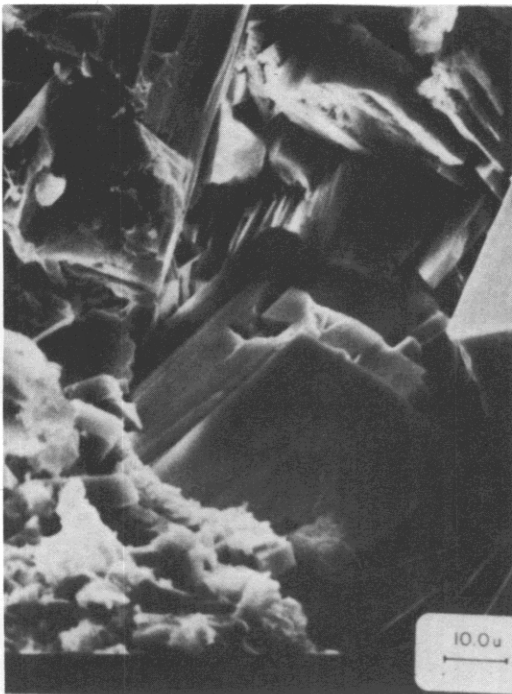


Figure 35.

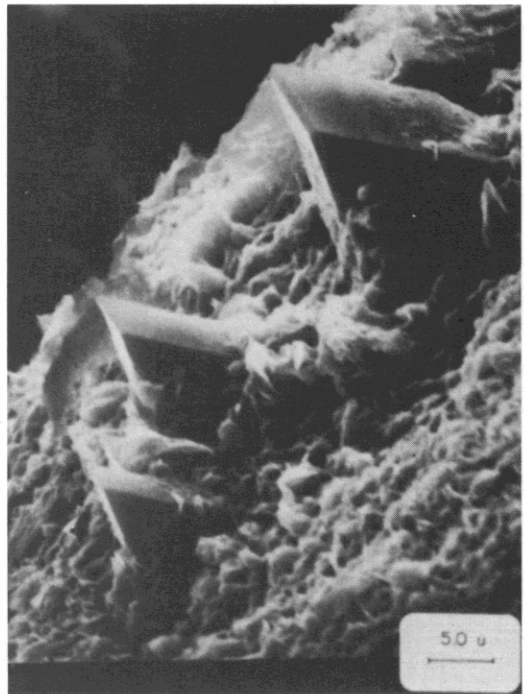


Figure 36.



Figure 37.

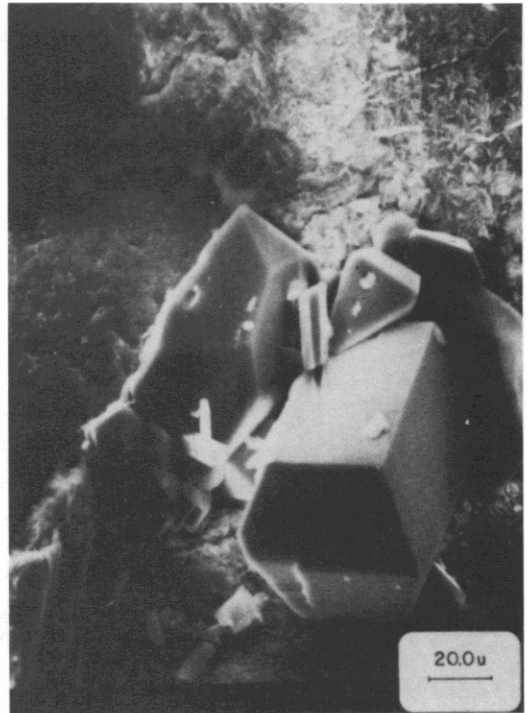


Figure 38.

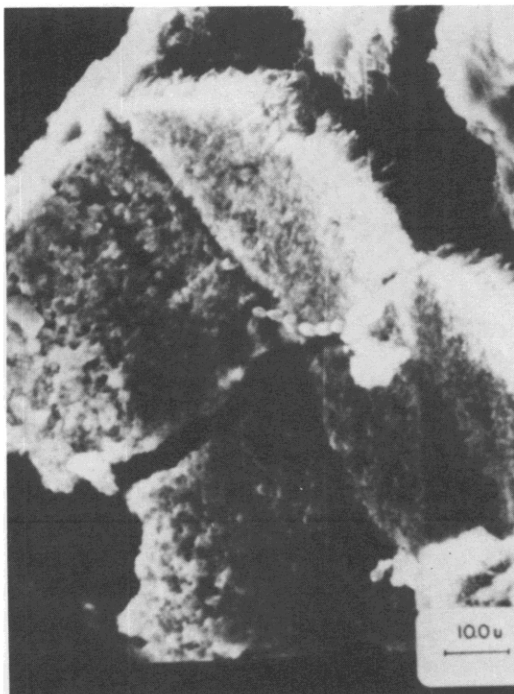


Figure 39.

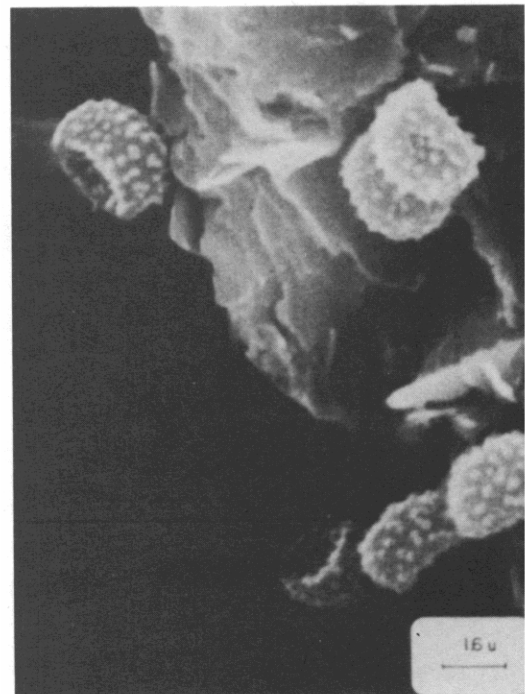


Figure 40.



Figure 41.



Figure 42.

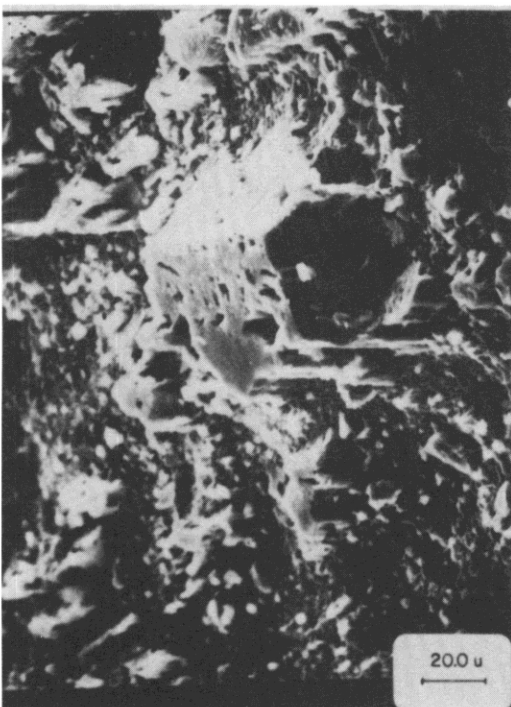


Figure 43.

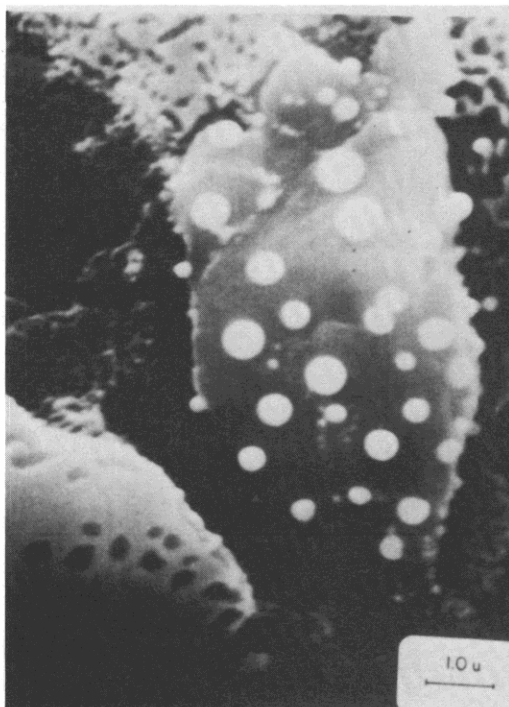


Figure 44.

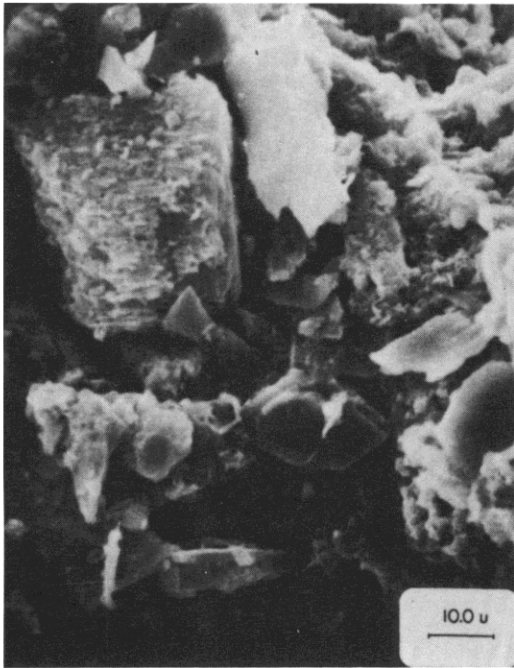


Figure 45.



Figure 46.

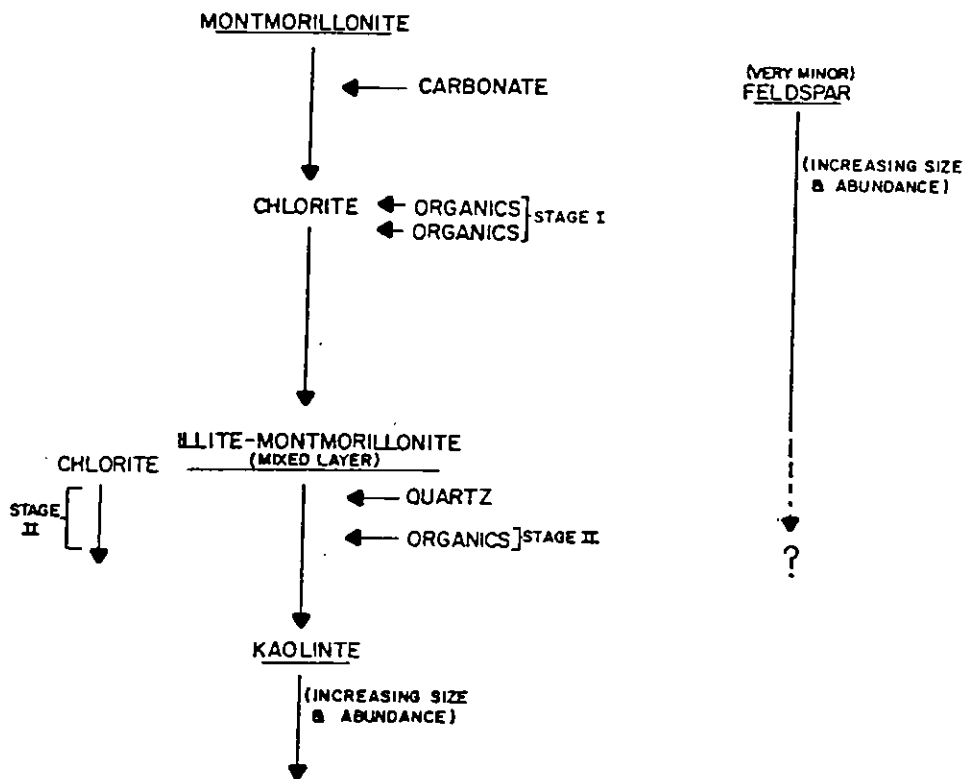


Figure 47

Chapter 3

MOUNT TAYLOR STUDY

Objective of Study

For many years, geologists exploring for sandstone-type uranium deposits have utilized the models of genesis proposed by Harshman (1970) and Rubin (1970). Field investigations rely on location of an iron redox interface and recognition of diagnostic radiometric curves on electric logs. As exploration targets have deepened, the economics of using these models have become prohibitive. Also, deposits are now being discovered which do not reside at the iron redox interface.

With these facts in mind, we have set out to attempt to delineate any other existing elemental (or mineralogical) zonation patterns which would be of use to the explorationist.

Approaches Used

We have looked for patterns of zoning in the distribution of a number of alkaline earths, transition metals, and several lathanide and actinide series elements (Lee, 1976; Riese, 1977; Brookins et al., 1977). Our analytical methods have included x-ray fluorescence (XRF), delayed neutron activation analyses (DNAA), instrumental neutron activation analyses (INAA), loss-on-ignition analyses (LOI), x-ray diffraction (XRD), and scanning electron microscopy (SEM). These techniques were selected with regard to their accuracy, their precision, their speed and facility and their cost. Several were used (INAA and DNAA) more for the purpose of providing data for genetic models than providing viable exploration tools. XRF was used instead of atomic adsorption (AA) or wet chemical techniques because it is relatively fast and inexpensive and because the

expected concentrations of most of the elements analyzed were well within detection limits. XRD was used during the initial phases of study to establish clay zoning patterns (Lee, 1976), and to correlate these patterns with trace element variations. As patterns became more apparent, we turned our attention to SEM both because it is a fast technique for clay mineral identification and because it requires less sample volume. LOI analysis was used to study carbon/organic material distributions.

Results

Our results indicate that a number of trace elements are useful as exploration tools. In addition, clay minerals zoning provides a useful tool for explorationists.

Of particular interest are thorium and multivalent lanthanide series elements. These elements offer much promise in use as pathfinder elements distant from uranium. Molybdenum, titanium and barium may be useful in closer proximity to ore bodies. This data is tabulated in the appendix to this report.

Clay minerals show a variation in composition from montmorillonite in front of the ore, to chlorite in ore zones, and finally to kaolinite behind. The relationship of this para-genetic sequence to trace element geochemistry is still being worked out.

Carbon as present in organic materials shows a direct correlation with uranium in terms of its abundance. This variation shows up in analyses of whole-rock samples and is not enhanced in analyses of the -2μ size fraction.

Application to Exploration Geochemistry

This work has shown that there are exploration alternatives to the models of Harshman (1970) and Rubin (1970). Ratios of Ce/U and Th/U are useful indicators of uranium mobilization as are absolute abundances of titanium, barium, and molybdenum in closer proximity to the ore. The utility of nickel, chromium and cobalt have not yet been fully evaluated. Total carbon as present in organic materials does not show appreciable variation at any distance from ore. Clay mineral changes, while subtle, are also very useful as pathfinders.

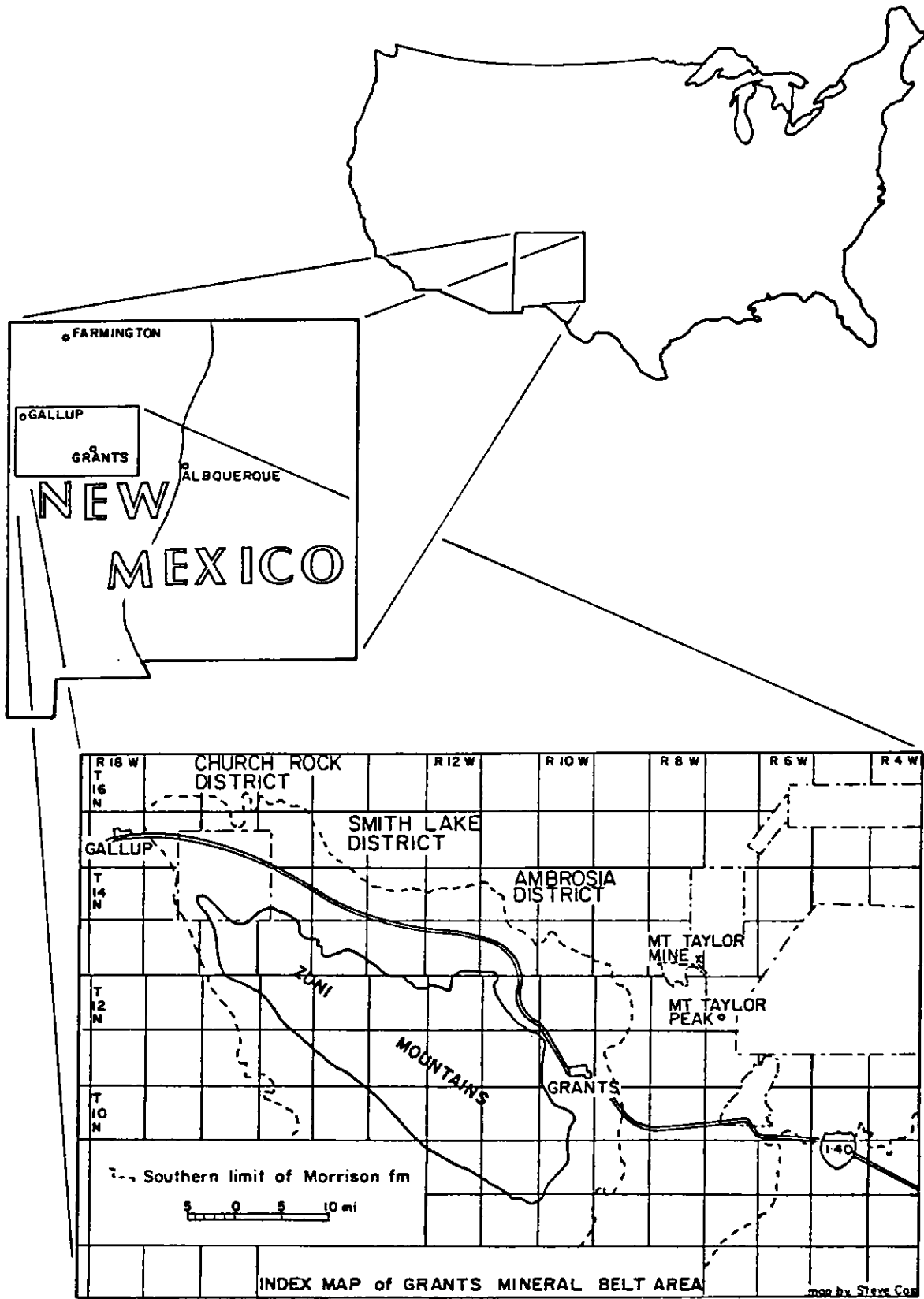


Figure 48

ORGANIC LEACHING EXPERIMENTS

Summary

We have evaluated the effectiveness of acetic, aspartic and tartaric acids in leaching uranium from the Jurassic Morrison Formation of west-central New Mexico. The leach solutions were run under agitation for ten days, at acid concentrations of 0.01M and buffered to 7.0 pH with 0.1N Na_2CO_3 . Aliquots of the leach solutions were taken at regular intervals and analyzed for uranium content by Delayed Neutron Activation (DNAA) at the Los Alamos Scientific Laboratories. Temperature and pH changes were also monitored at regular intervals throughout the duration of the experiment. Our results indicate that organic acids are effective leaching agents of uranium in sediments. Of the three acids studied, tartaric is the most effective. This information, coupled with SEM data, has led us to conclude that organic acids may have provided a significant portion of the uranium present in the ore bodies of the Grants mineral belt.

Introduction

Dissolution of rocks and minerals in aqueous solutions has been studied by a number of individuals over the past two decades, but reports of controlled experiments to evaluate the effectiveness of organic acids as leaching or weathering agents have been conspicuous by their absence. Work done by Drs. Huang and Keller carried out during the late sixties and early seventies at the University of South Florida and the University of Missouri at Columbia represents the vanguard of experimentation in this area of research. These authors have studied the effects of several different organic acids on rock-forming silicate minerals and report

that these acids are very effective leaching agents and may even be solely responsible for the kaolins of central Europe and the bauxites of Israel and Arkansas.

We have attempted in this study to determine the effectiveness of organic acids as leaching agents for uranium in sandstones and mudstones. Specifically, we have used samples from the Jurassic Morrison Formation of west-central New Mexico. We selected this formation because several of its members have anomalously high background concentrations of uranium. A second consideration in selecting samples from this formation was the possibility that leaching of uranium by organic acids from the sediments up-dip and up-gradient from the uranium deposits in the Grants mineral belt might be a significant factor in their genesis. We further hypothesized that the organic acids which functioned as leaching agents might also serve as transporting agents and should be seen in the ore deposits.

Experimental Procedures

The organic acids selected for our experiments were those whose representatives might be present in humic and other soil acids, namely, weakly complexing acetic and aspartic acids, and strongly complexing tartaric acid. These acids also embody representative carboxyl and hydroxyl groups. Deionized water and blank solutions were used for dissolution comparisons.

Our experimental procedures required that three grams of each sample, ground to -200 mesh, be added to 250 ml. of 0.01M organic acid reagent in tightly capped 500 ml. Erlenmeyer flasks and shaken continuously at room temperature of 200 hours. At intervals of one, ten, twenty,

100 and 200 hours, 10 ml. aliquots of solution were withdrawn and replaced with 10 ml. of new reagent. (At this time I should point out that the experiments performed by Huang and Keller have been criticized because they were run under extremely acid conditions of pH 4.0 to 5.0. Since our experiments were expected to simulate the groundwater conditions of the Colorado Plateau, our solutions were all buffered with 0.1N Na_2CO_3 to pH 7.0. During the progress of each experiment, this pH was observed to rise to between 8.0 and 8.5, not unreasonable values for waters of the Colorado Plateau.) Temperature and pH were monitored every eight hours (see Figs. 49 and 50).

The uranium in solution was determined for each aliquot by DNAA. These analyses were carried out at the Los Alamos Scientific Laboratories, using their 8MW Omega West reactor.

Results

Figure 51 shows the results of leaching a sample of the Brushy Basin shale member of the Morrison Formation, -- the often suspected source of the uranium in the Grants mineral belt deposits. The acetic and aspartic acids show no noteworthy enrichments with time, while the tartaric acid shows a marked enrichment. This is a predictable contrast.

Figure 52 shows the results of leaching barren reduced sands from the upper Westwater Canyon member, -- in other words, sands that have not been leached of their uranium by natural processes. No marked contrasts exist. When these results are compared to those for lower Westwater samples (Fig. 53) from an oxidized zone which has been leached, however, it is surprising to find an inexplicable parallel of trends.

Samples from mineralized horizons in the upper Westwater have not all been analyzed. The final data are expected to mitigate the apparent uranium depletion in tartaric acid shown in figure 54.

Finally, samples of lower Westwater ore zones (Fig. 55) show predictable trends, although at concentrations somewhat higher than the other samples we have discussed. (Note the change in scale on the ordinate of these plots; the previous plots had maximum values of 0.5 ppm, while these have maximum values of 1.0 ppm.)

In conclusion, our results indicate that organic acids are effective leaching agents of uranium in sediments. Of the three acids studied, tartaric is the most effective. The information presented so far coupled with SEM data and additional data included after this section has led us to conclude that organic acids may have provided a significant portion of the uranium present in the ore bodies of the Grants mineral belt.

AMBIENT T°C 23 AT ALL TIMES

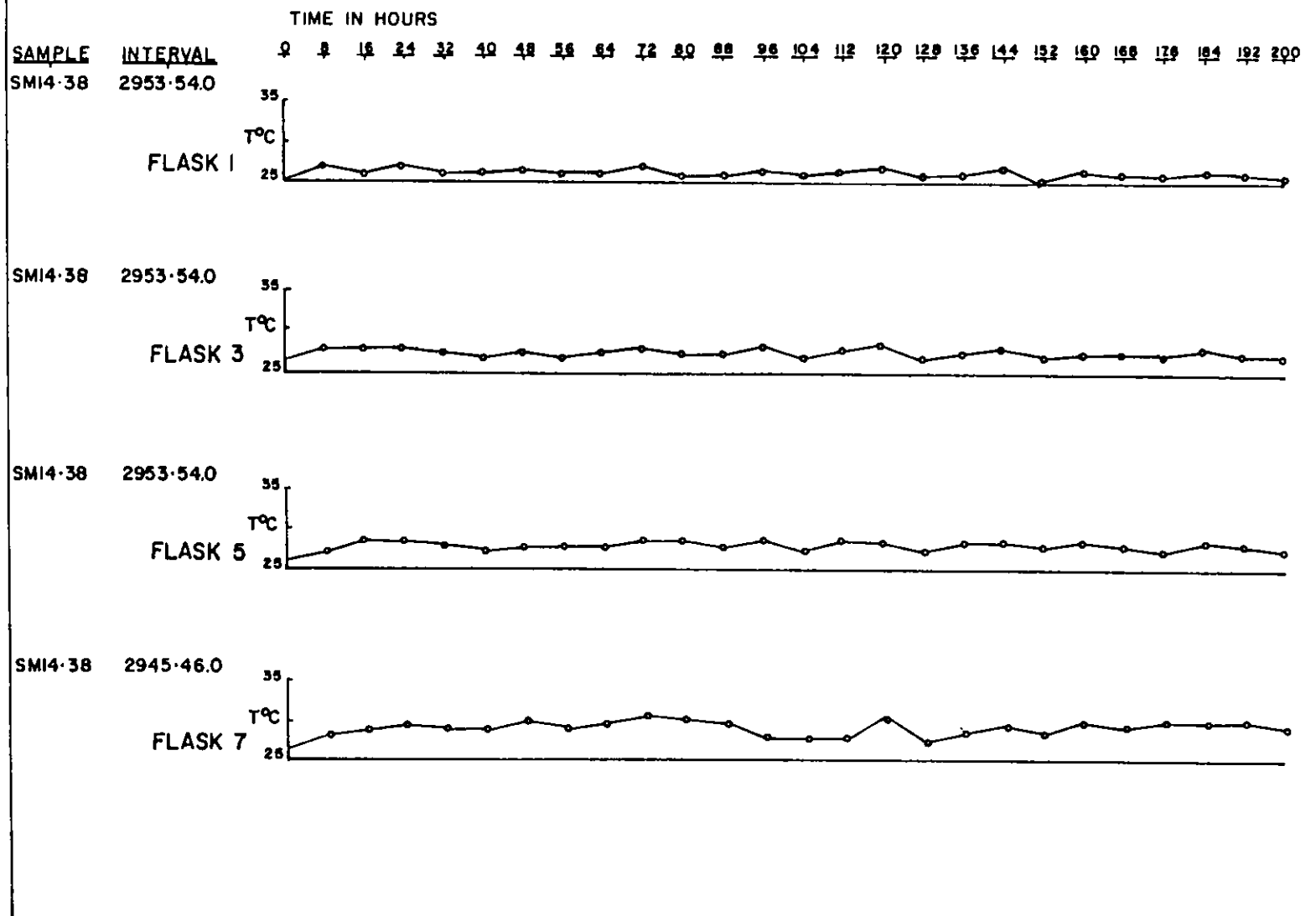
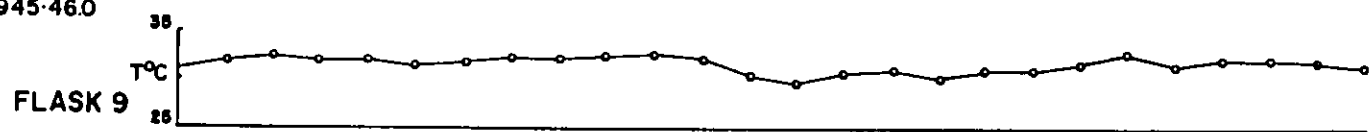


Figure 49a

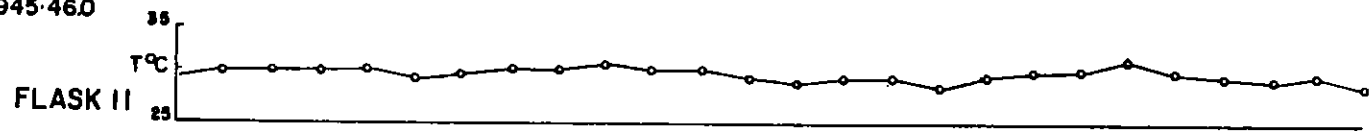
AMBIENT T°C 23 AT ALL TIMES

TIME IN HOURS
0 2 4 6 8 10 12 14 16 18 20 22 24 26 28 30 32 34 36 38 40 42 44 46 48 50 52 54 56 58 60 62 64 66 68 70 72 74 76 78 80 82 84 86 88 90 92 94 96 98 100 102 104 106 108 110 112 114 116 118 120 122 124 126 128 130 132 134 136 138 140 142 144 146 148 150 152 154 156 158 160 162 164 166 168 170 172 174 176 178 180 182 184 186 188 190 192 194 196 198 200

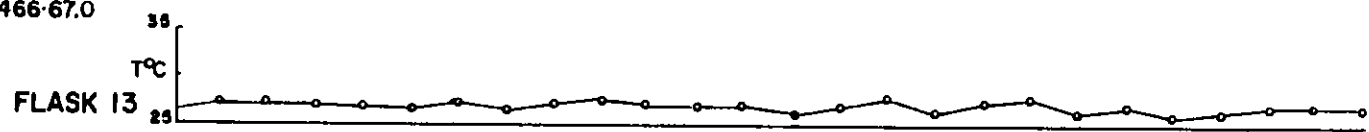
SAMPLE INTERVAL
SM14-38 2945-46.0



SM14-38 2945-46.0



SM13-53 3466-67.0



SM13-53 3466-67.0



-40-
Figure 49b

AMBIENT T°C 23 AT ALL TIMES

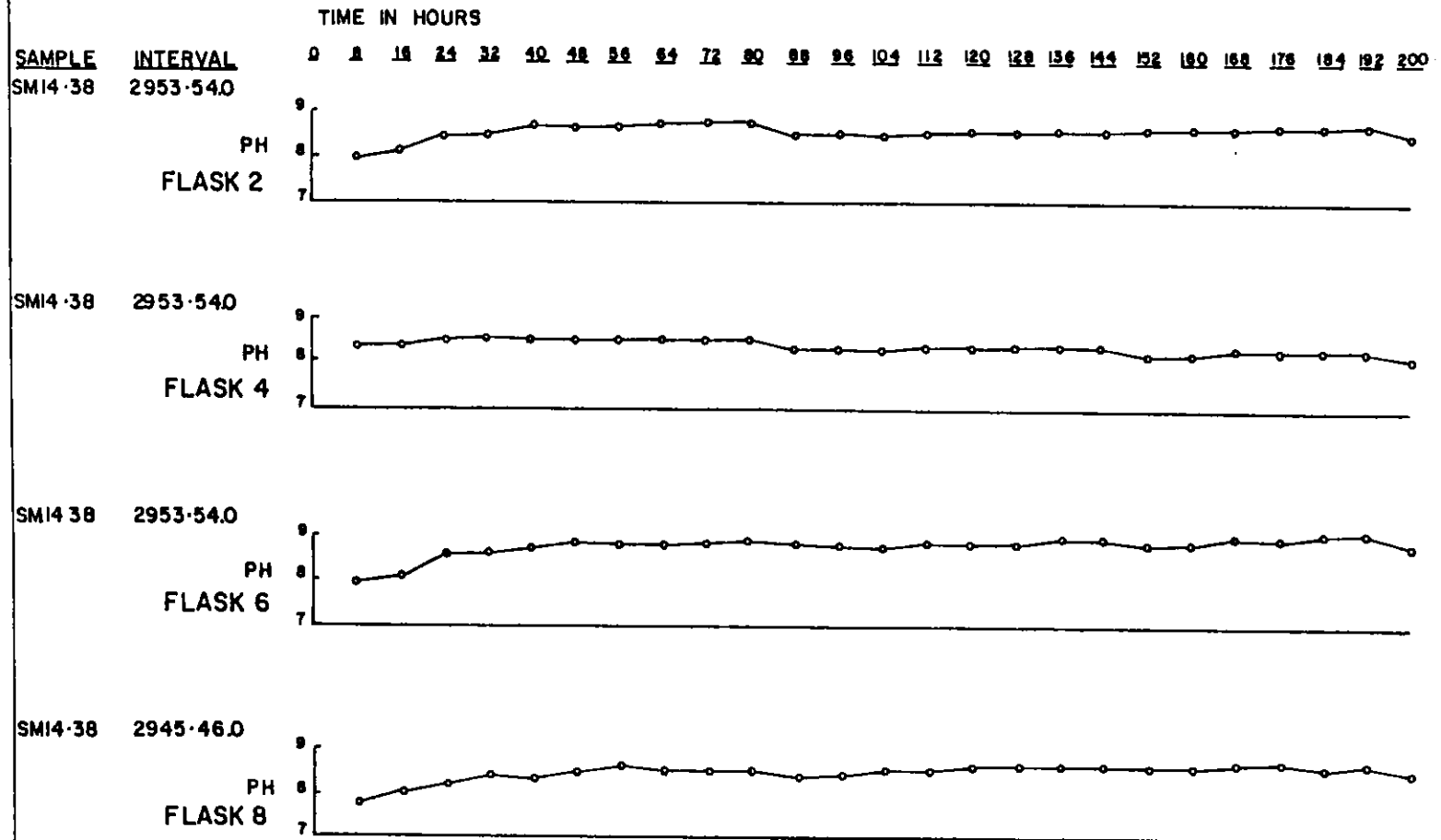


Figure 50a

AMBIENT T°C 23 AT ALL TIMES

TIME IN HOURS
0 2 4 6 8 10 12 14 16 18 20 22 24 26 28 30 32 34 36 38 40 42 44 46 48 50 52 54 56 58 60 62 64 66 68 70 72 74 76 78 80 82 84 86 88 90 92 94 96 98 100 102 104 106 108 110 112 114 116 118 120 122 124 126 128 130 132 134 136 138 140 142 144 146 148 150 152 154 156 158 160 162 164 166 168 170 172 174 176 178 180 182 184 186 188 190 192 194 196 198 200

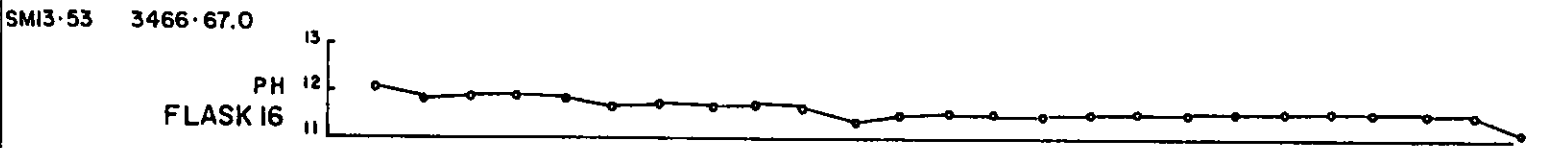
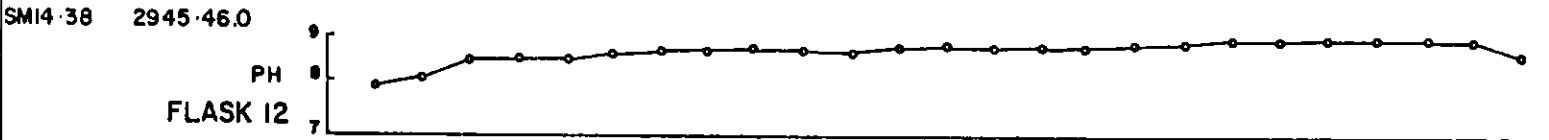
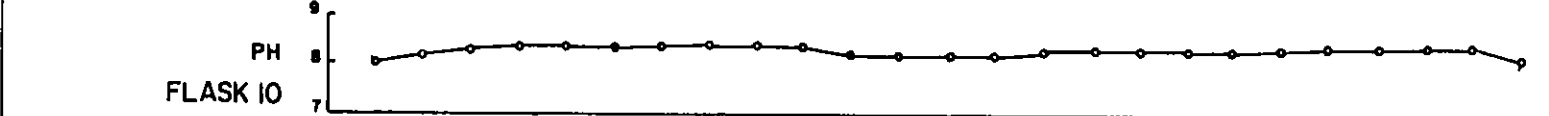


Figure 50b

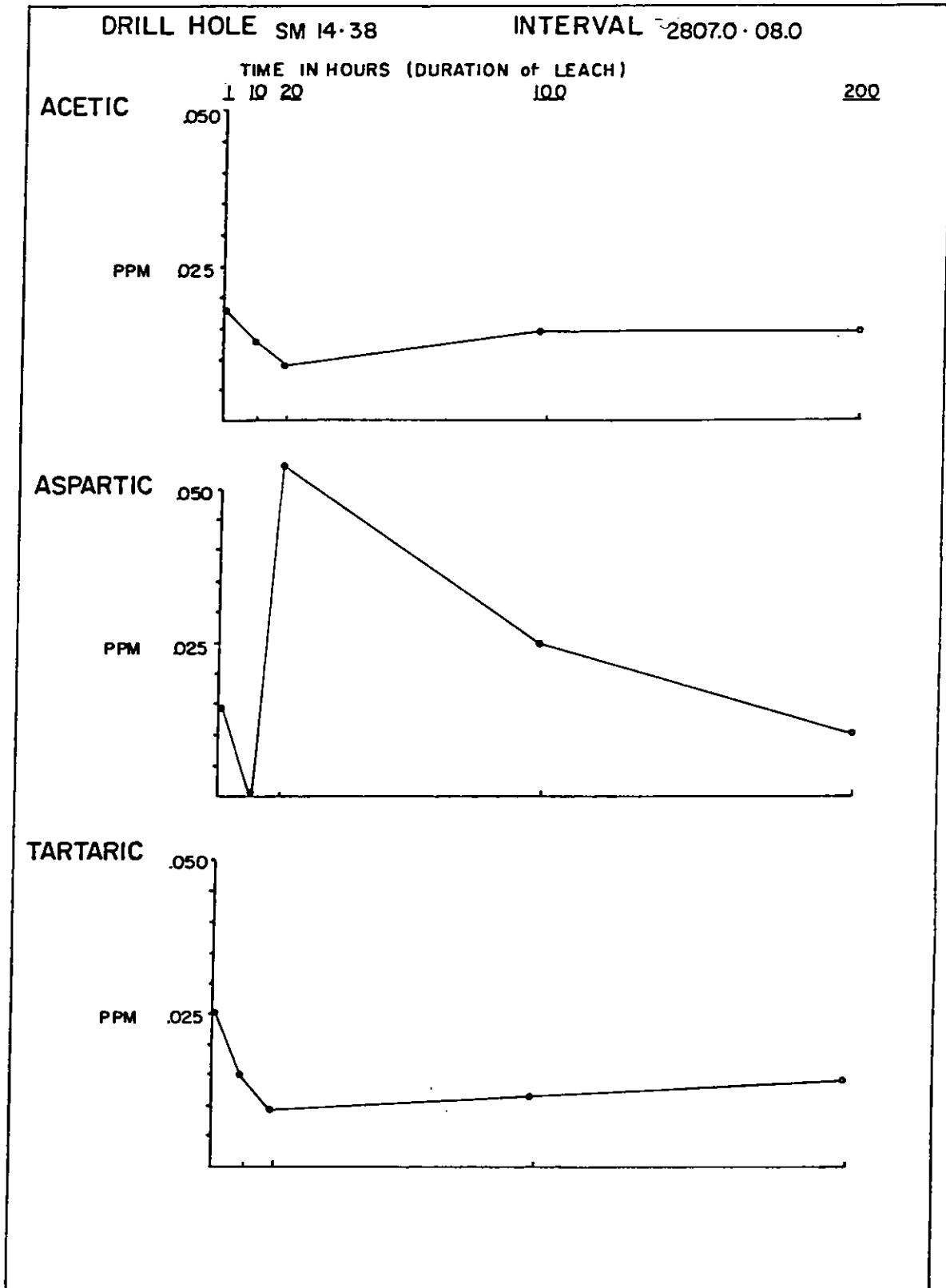


Figure 51b

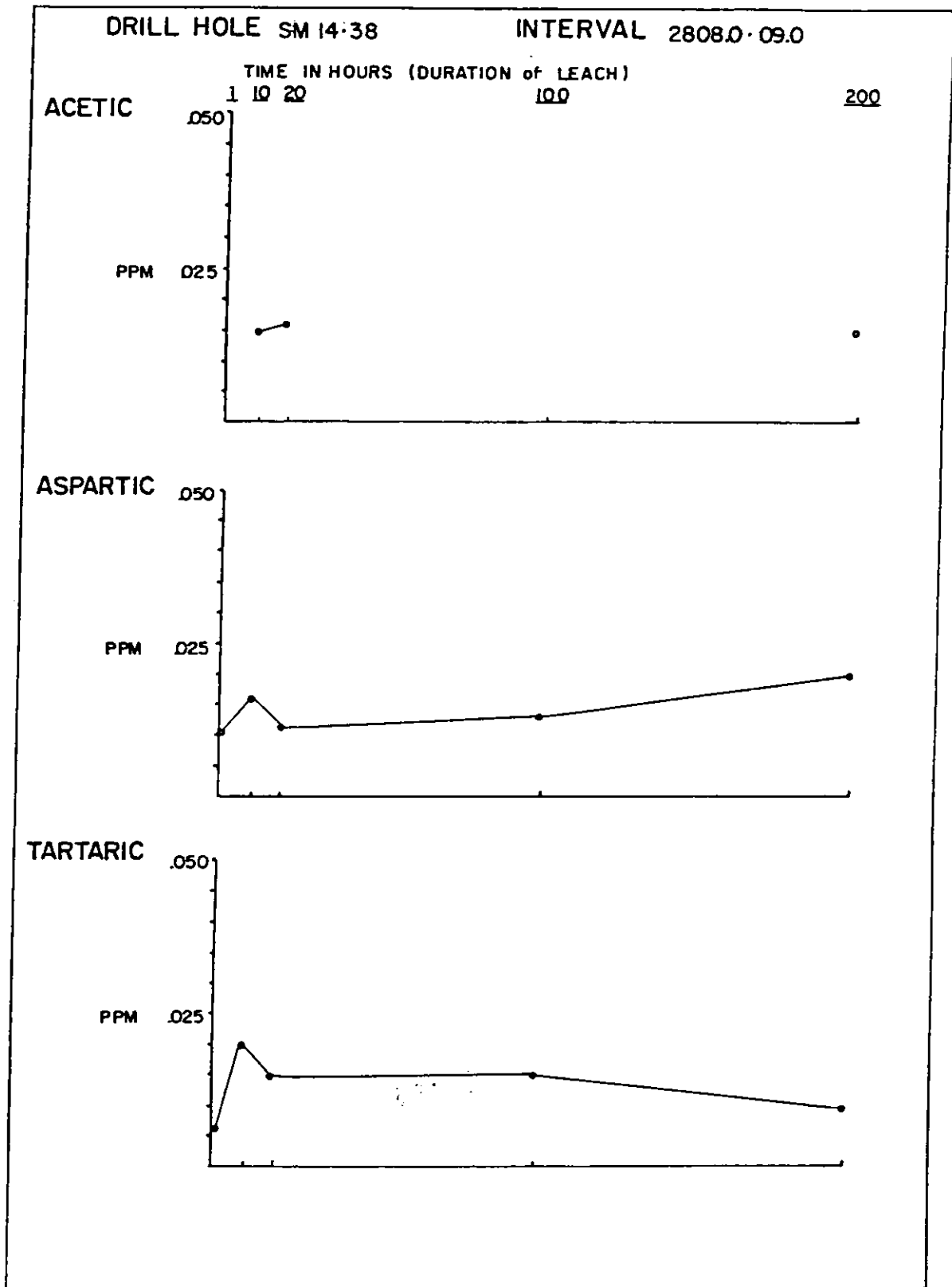


Figure 51c

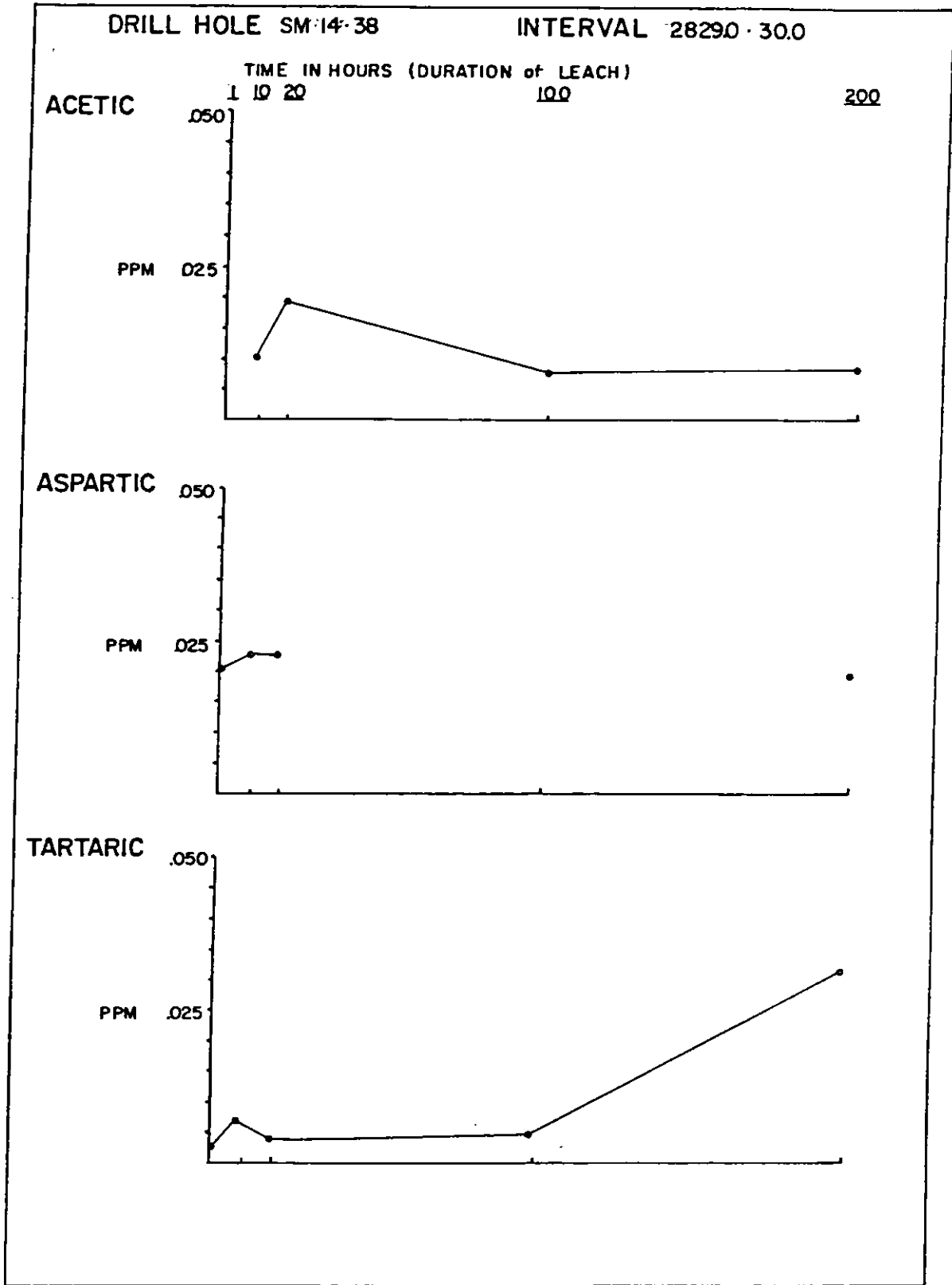


Figure 52a

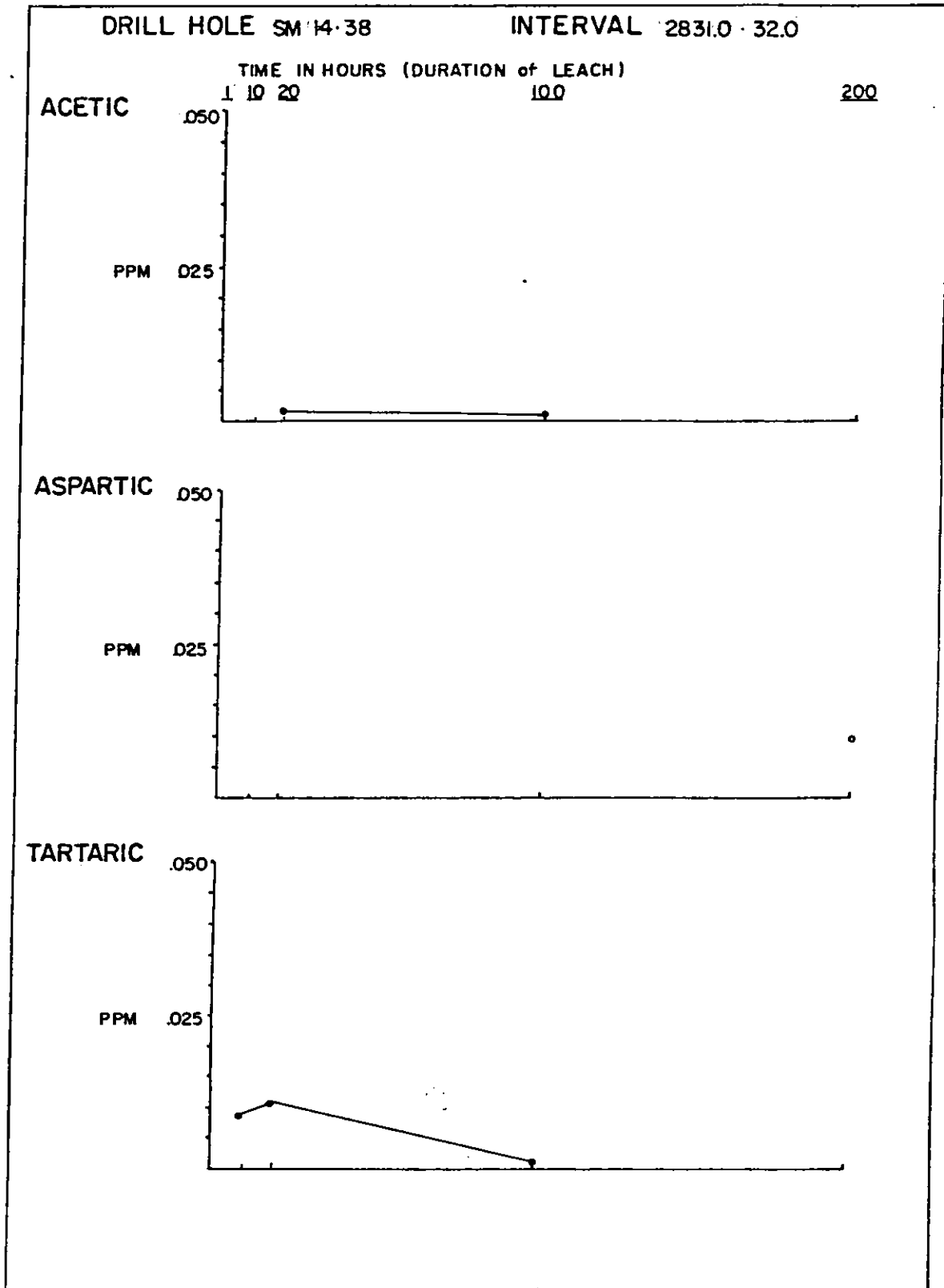


Figure 52b

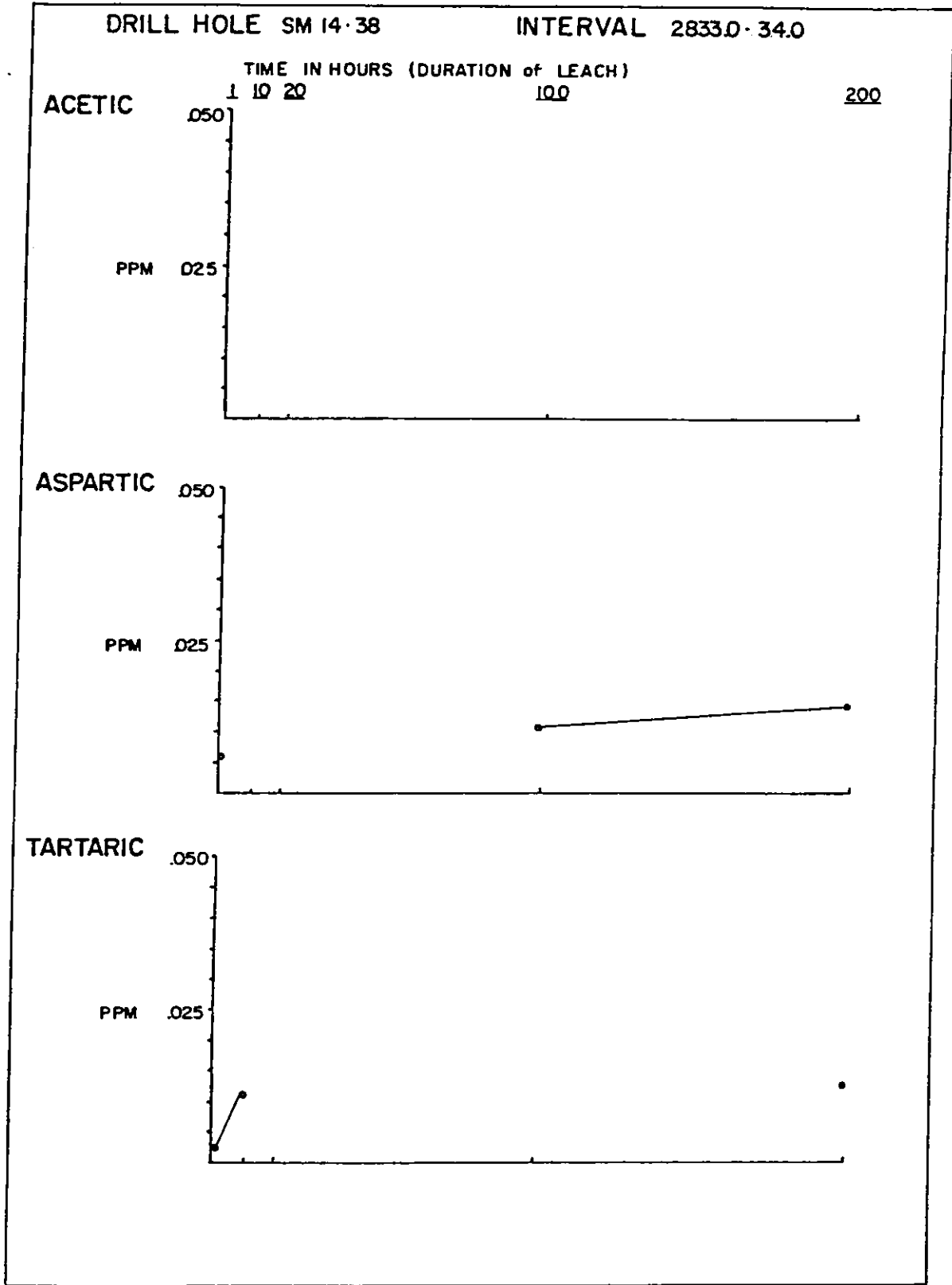


Figure 52c

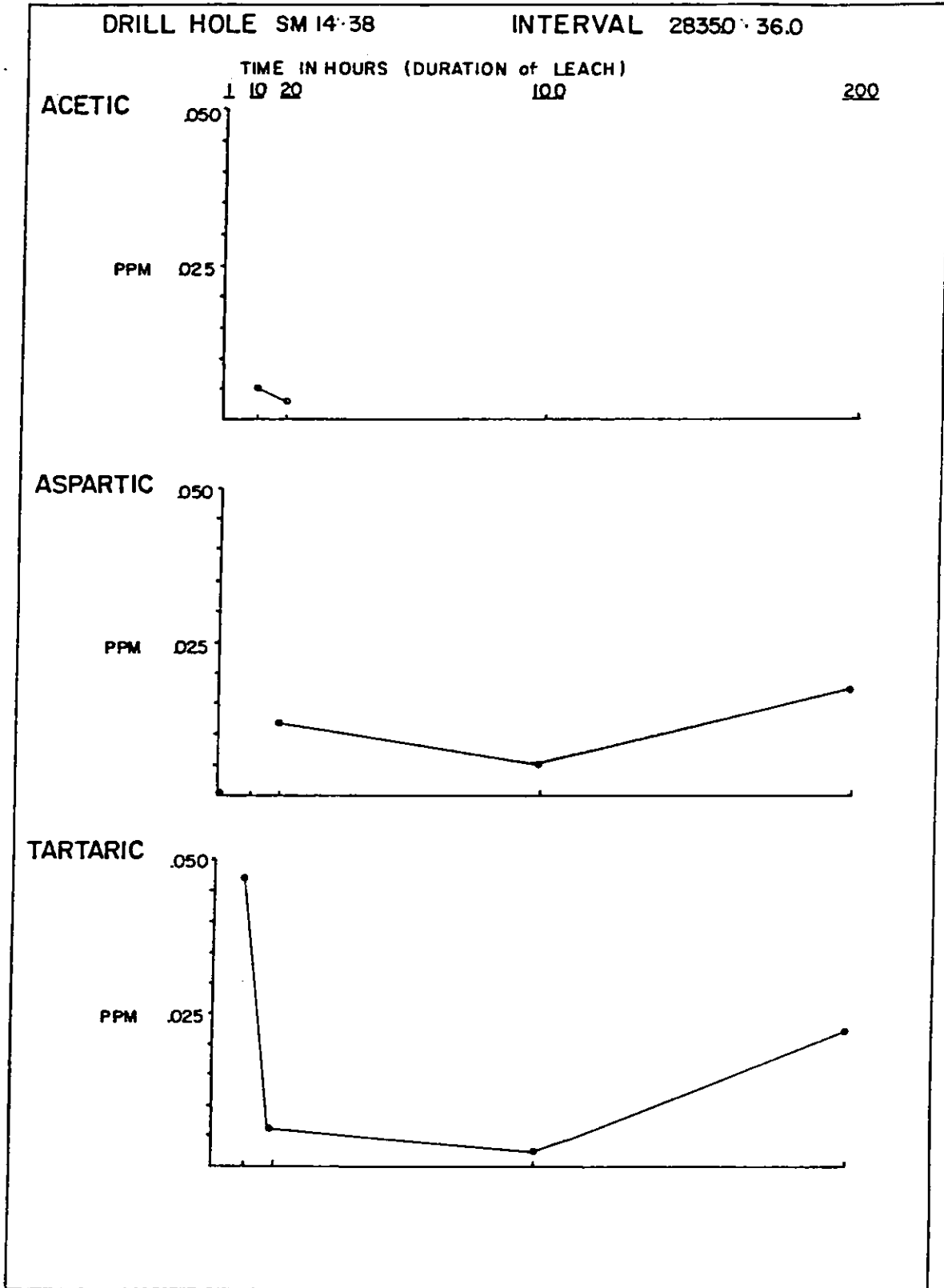


Figure 52d

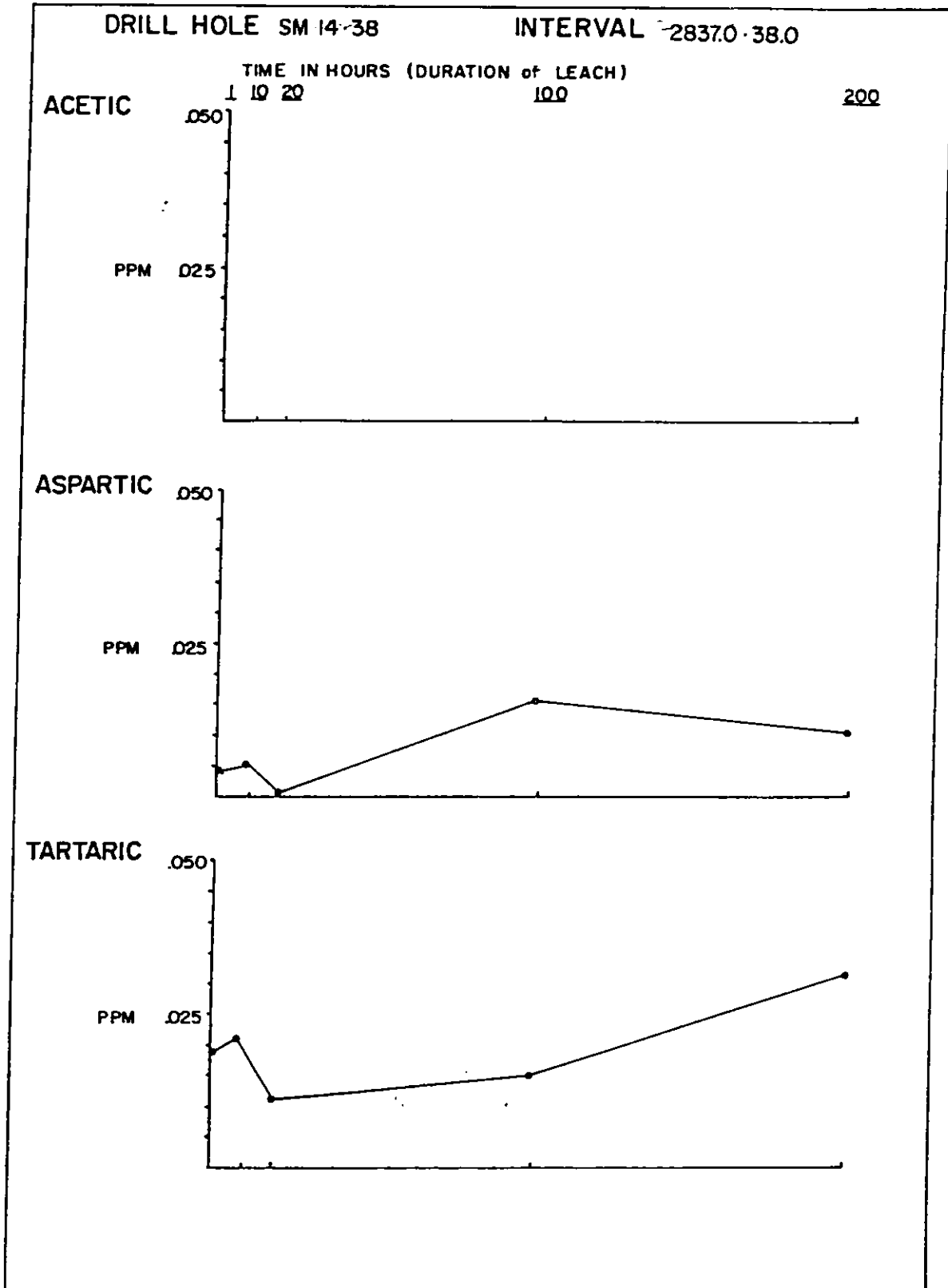


Figure 52e

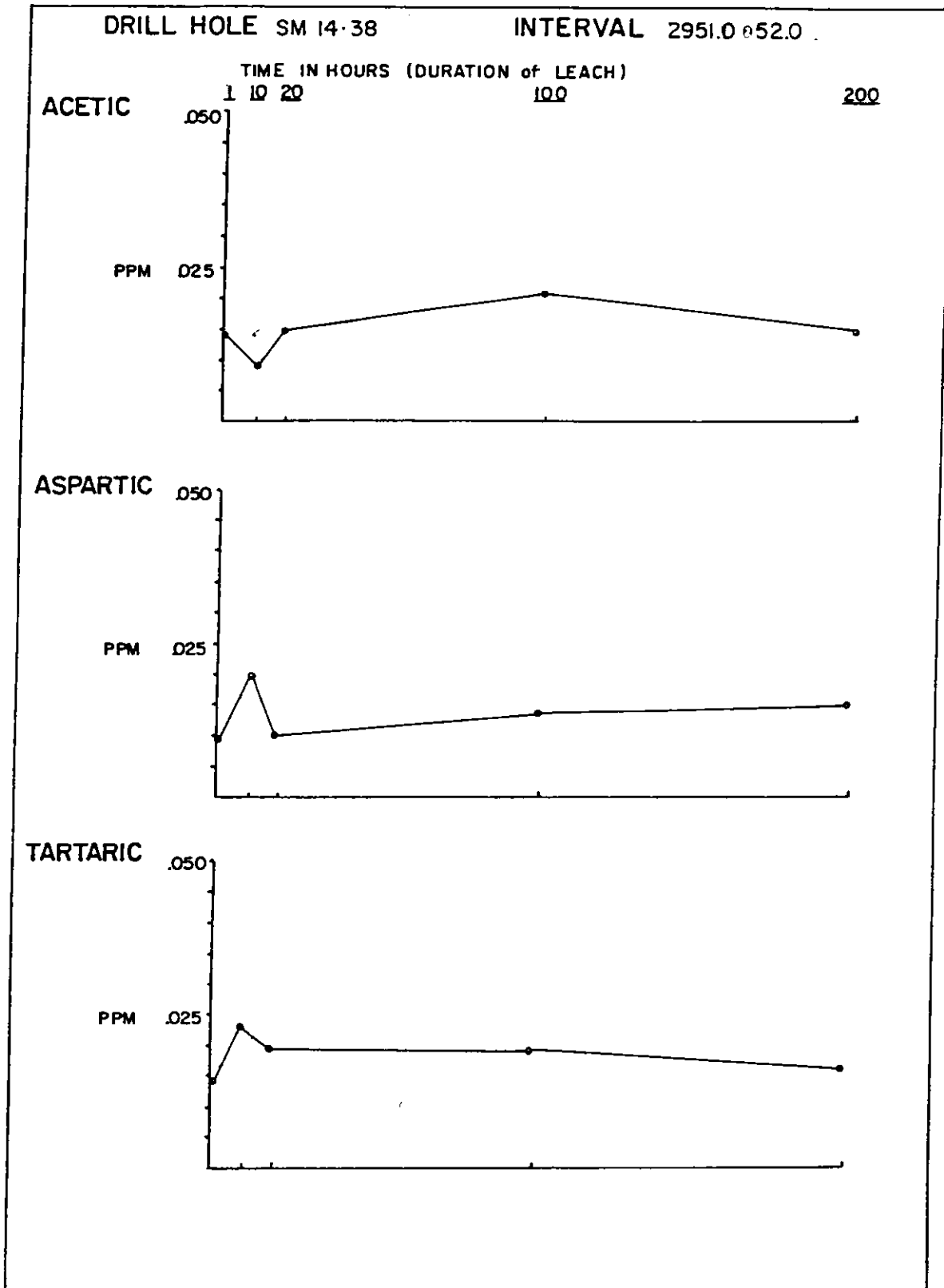


Figure 53b

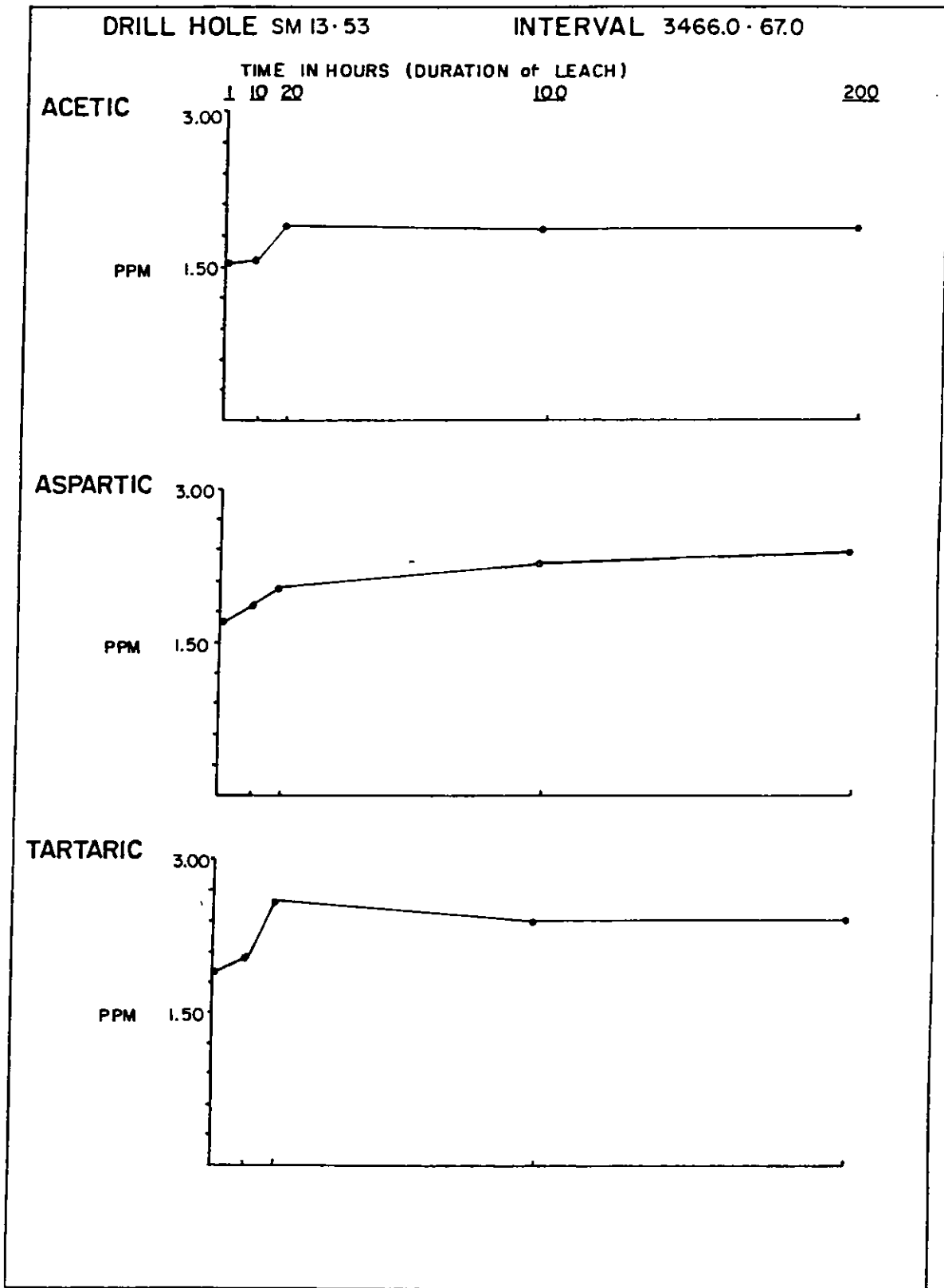


Figure 54c

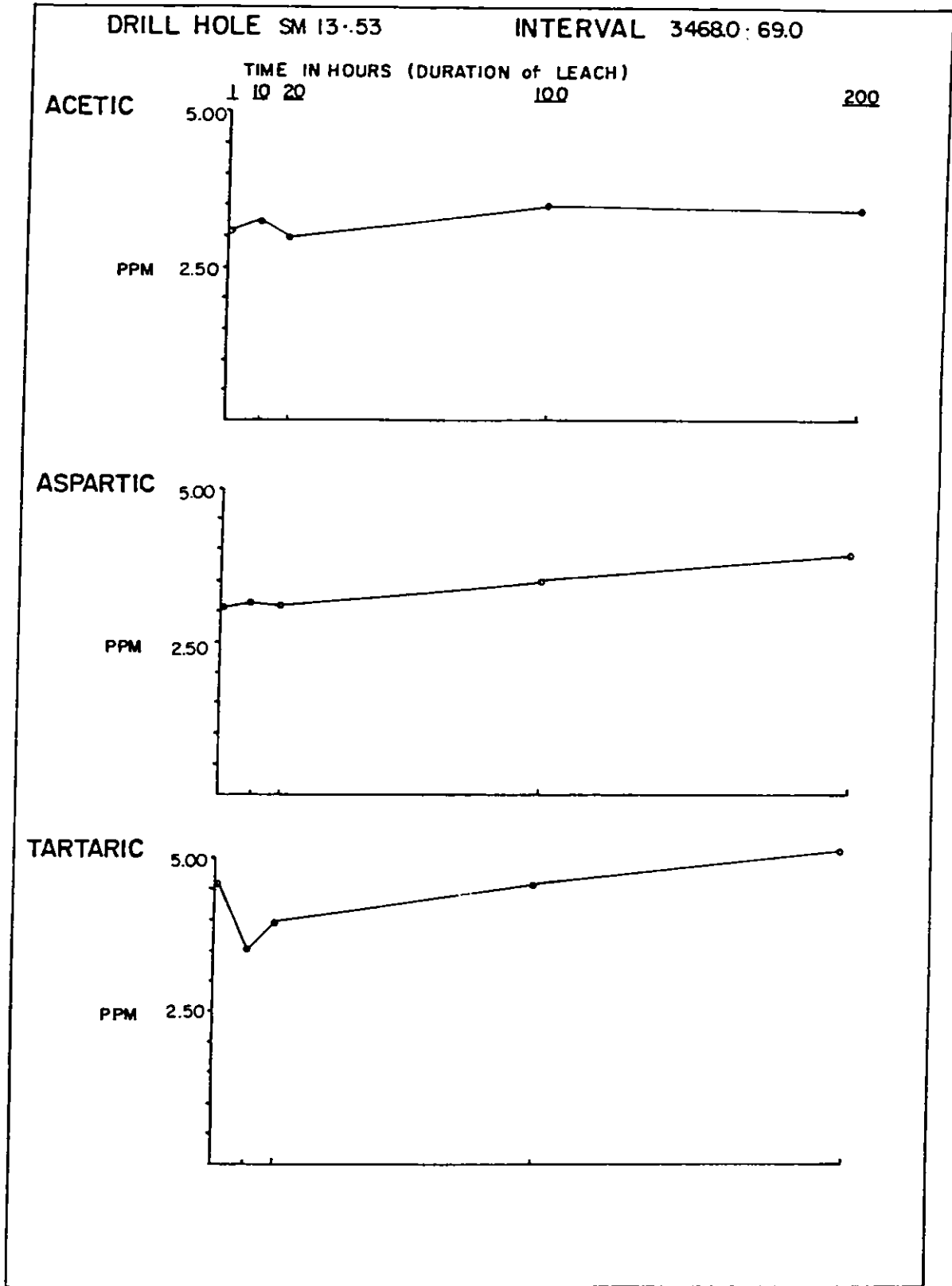


Figure 54d

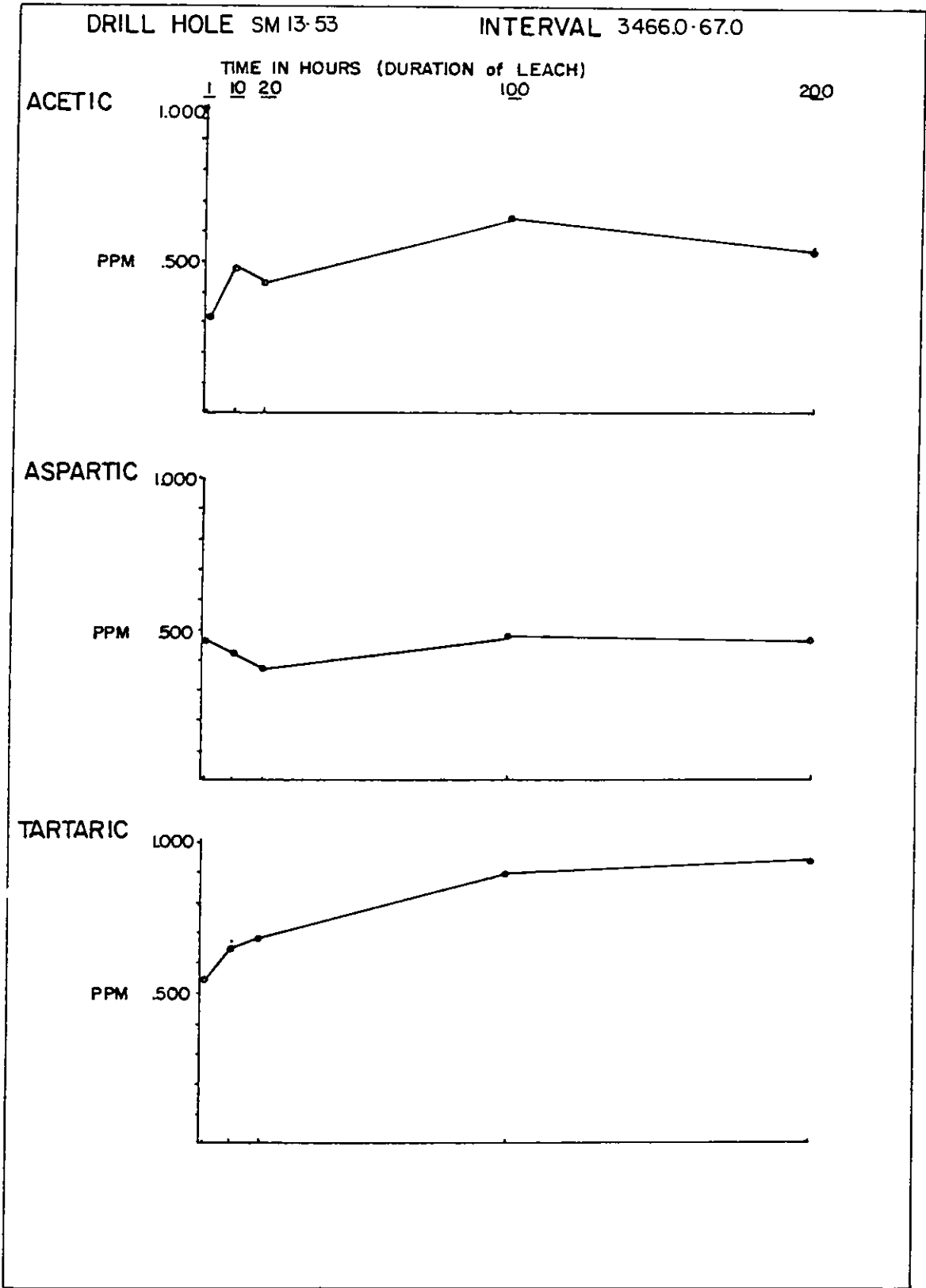


Figure 55a

ORGANIC CONTENT STUDY

Many workers have suggested that ore zones are rich in organic matter because they are dark-colored. While color may be no indication, we have found that uranium content does seem to vary directly with the organic content of the whole rock. This is graphically illustrated in figure 56, which also shows variations in the organic and uranium contents of the -2μ size fraction, in which almost all clay minerals are concentrated. The analyses on which this figure is based are given in tables 1 through 7. The analyses were done by the "loss-on-ignition" technique.

In tables 1 through 7 the $H_2O(-)$ column indicates that amount of adsorbed (or otherwise weakly held) water, the $110^\circ - 500^\circ C$ column indicates volatiles (largely CO_2 and H_2O) from organic matter with the possible inclusion of small amounts of weakly bonded water from clay minerals, and the LOI $110^\circ - 1000^\circ C$ column indicates total volatile release (i.e. CO_2 from organic and inorganic C sources, all H_2O except that lost at $110^\circ C$ (Column $H_2O(-)$), and sulfur oxides, etc.)

TABLE 1.
 SM 13-53 UPPER WESTWATER
 WHOLE-ROCK ORGANIC ANALYSES
 BARREN REDUCED GROUND

<u>Sample</u>	<u>H₂O(-) 1 hour @ 110°C</u>	<u>Organic Content 110°-500°C</u>	<u>LOI 110°-1000°C</u>
13-53 R-17 33-4.0-3305.0 1524 W.R.	3.01	2.04	3.53
13-53 R-1 3311.0-3312.0 1558 W.R.	1.91	2.18	1.87
13-53 R-15 3346.0-3347.0 1553 W.R.	0.12	0.73	0.87
13-53 R-6 3351.0-3352.0 1510 W.R.	0.20	0.94	0.59
13-53 R-1 3356.0-3357.0 W.R.	0.03, 0.09	0.60, 0.70	0.84, 0.74

TABLE 2.
SM 13-53 LOWER WESTWATER
WHOLE-ROCK ORGANIC ANALYSES
ORE ZONE

<u>Sample</u>	<u>H₂O(-) 1 hour @ 110°C</u>	<u>Organic Content 110°-500°C</u>	<u>LOI 110°-1000°C</u>
13-53 3454.0-3455	0.06	0.79	1.73
13-53 3455.0-3456.0	0.16	0.70	1.35
13-53 3456.0-3457.0	0.04	0.65	1.21
13-53 3458.0-3459.0	0.08	0.55	0.82
13-53 3459.0-3460.0	0.06	0.65	0.95
13-53 3461.0-3462.0	1.50	5.18	6.50
13-53 3462.0-3463.0	0.12	0.91	1.35
13-53 3463.0-3464.0	0.20	0.80	1.30
13-53 3464.0-3465.0 "BLK"	0.36	2.05	2.87
13-53 3465.0-3466.0	0.29	1.55	2.60
13-53 3466.0-3467.0	0.36	1.56	2.29
13-53 3467.0-3468.0	0.02	0.89	1.33
13-53 3468.0-3469.0	0.06	1.52	2.33
13-53 3469.0-3470.0 "BLK"	0.10	0.58	0.82
13-53 3470.0-3471.0	0.08	0.56	0.80
13-53 3471.0-3472.0	0.12	0.68	1.14

TABLE 3.
SM 13-53 LOWER WESTWATER
-2u ORGANIC ANALYSES
ORE ZONE

<u>Sample</u>	<u>1 hour @ 110^oC</u>	<u>Organic Content 110^o-500^oC</u>	<u>LOI 110^o-1000^oC</u>
Sm 13-53 R-5 3461.0-3462.0 2 u	1.90	5.05	1.55
Sm 13-53 R-25 3463.0-3464.0 2 u	2.52	5.10	1.99
Sm 13-53 R-4 3464.0-3465.0 2 u	2.44	5.60	1.81
Sm 13-53 R-30 3465.0-3466.0 2 u	2.55	6.24	1.84
Sm 13-53 R-27 3466.0-3467.0 2 u	2.59	6.08	1.69
Sm 13-53 R-21 3467.0-3468.0 2 u	1.88	5.95	1.88
Sm 13-53 R-9 3468.0-3469.0 2 u	1.66	8.23	1.66
Sm 13-53 R-8 3469.0-3470.0 2 u	1.07	4.76	1.65
SM 13-53 R-2 3470.0-3471.0 2 u	0.24	5.86	1.44
Sm 13-53 R-20 3471.0-3472.0 2 u	1.14	5.57	2.19

TABLE 4.
SM 13-53 COMPARISON OF WHOLE-ROCK AND
-2u ORE ZONE ORGANIC ANALYSES

<u>Interval</u>	<u>W.R.</u>	<u>-Zu</u>	<u>Grade</u>
3454-3455	.79		.019
3455-3456	.70		.018
3456-3457	.65		.089
3458-3459	.55		.120
3459-3460	.65		.275
3461-3462	5.18	5.05	.242
3463-3464	.80	5.10	.089
3464-3465	2.05	5.60	.023
3465-3466	1.55	6.24	.007
3466-3467	1.56	6.08	.009
3467-3468	.89	5.95	.006
3468-3469	1.52	8.23	.009
3469-3470	.58	4.76	.009
3470-3471	.56	5.86	.064
3471-3472	.68	5.57	.039

TABLE 5.
 SM 14-38 UPPER WESTWATER
 WHOLE-ROCK ORGANIC ANALYSES
 BARREN OXIDIZED GROUND

<u>Sample</u>	<u>1 hour @ 110°C</u>	<u>Organic Content 110°-500°C</u>	<u>LOI 110°-1000°C</u>
14-38 R-29 2805.0-2806.3 1519 W.R.	0.38	1.04	2.32
14-38 R-24 2806.3-2807.0 1555 W.R.	2.72, 2.50	2.44, 3.33	3.58, 2.97
14-38 R-31 2807.0-2808.0 1561 W.R.	2.05	2.45	3.63
14-38 R-16 2808.0-2809.0 W.R.	1.29	1.51	2.62
14-38 R-19 2809.0-2810.2 1564 W.R.	2.05	2.05	11.56
14-38 R-36 2829.0-2830.0 1506 W.R.	0.17	0.56	0.29
14-38 R-37 2831.0-2832.0 1560 W.R.	0.08, 0.07	0.62, 0.54	0.29, 0.30
14-38 R-35 2833.0-2834.0 1523 W.R.	0.08	0.94	0.27
14-38 R-34 2835.0-2836.0 1556 W.R.	0.21	0.81	0.32
14-38 R-12 2837.0-2838.0 1521 W.R.	0.19	0.82	0.36
14-38 R-38 2839.0-2840.0 1522 W.R.	0.10, 0.11	0.83, 0.78	0.38, 0.43

TABLE 5. (Page 2)

<u>Sample</u>	<u>1 hour @ 110°C</u>	<u>Organic Content 110°-500°C</u>	<u>LOI 110°-1000°C</u>
14-38 R-28 2841.0-2842.0 1509 W.R.	0.47	0.53	0.40
14-38 R-33 2843.0-2844.0 W.R.	0.14	0.86	0.42
14-38 R-32 2845.0-2846.0 1514 W.R.	0.10, 0.13	0.65, 0.60	0.25, 0.26
14-38 R-13 2847.0-2848.0 1547 W.R.	0.10	0.48	0.42

TABLE 6.
 SM 14-38 LOWER WESTWATER
 WHOLE-ROCK ORGANIC ANALYSES
 BARREN OXIDIZED GROUND

<u>Sample</u>	<u>1 hour @ 110°C</u>	<u>Organic Content 110^o-500^oC</u>	<u>LOI 110^o-1000^oC</u>
14-38 R-26 2948.0-2949.0 W.R.	1.99	2.57	1.44
14-38 R-11 2951.0-2952.0 1504 W.R.	0.30	0.99	0.50
14-38 R-23 2952.0-2953.0 1503 W.R.	0.17	1.13	0.63
14-38 R-18 2955.0-2956.0 1508 W.R.	0.23, 0.22	0.86, 0.99	0.51, 0.43
14-38 R-22 2956.0-2957.0 1552 W.R.	0.18, 0.02	0.83, 0.86	1.58, 1.61
14-38 R-14 2957.0-2958.0 W.R.	0.45, 0.32	1.06, 1.13	1.26, 1.43
14-38 R-10 2958.0-2959.0 W.R.	0.14	0.80	0.52
14-38 R-7 2959.0-2960.0 1500 W.R.	0.04	0.80	0.44

Table 7

SUBJECT: H₂O(-), 110°-500°C, L.O.I.

Sample	H ₂ O(-) @ 110°C	110°-500°C	L.O.I. @ 1000°C
HU22-3-1 3640	0.20	0.82	0.48
HU22-3-1 3650	0.33	1.46	0.74
HU22-3-1 3705	0.19	0.18	0.82
HU22-3-1D 3710	0.26	0.53	0.65
HU22-3-1 3715.0-3715.5	0.18	0.58	0.60
HU22-3-1 3719.5-3720.0	0.31	1.23	0.56
HU22-3-1D 3720	0.22	0.87	0.42
HU22-3-1 3724.5-3725.0	0.27, 0.30 0.28*	2.36, 2.34 2.35*	0.61, 0.60 0.60*
HU22-3-1D 3730.0-3730.5	0.22	0.94	0.38
HU22-3-1D 3735.0-3735.5	0.16	0.84	0.26
HU22-3-1D 3739.5-3740.0	0.17	0.66	0.36
HU22-3-2D 3759.5-3760.0	0.18, 0.24 0.21*	0.98, 1.12 1.05*	0.58, 0.41 0.50*
HU22-3-3D 3799.5-3800.0	0.18	0.75	0.53

*Average value on samples ran in duplicate.

Table 7 (cont'd)

SUBJECT: H₂O(-), 110°-500°C, L.O.I.

Sample	H ₂ O(-) @ 110°C	110°-500°C	L.O.I. @ 1000°C
HU22-3-3D 3805.0-3805.5	0.45	1.18	0.43
HU22-3-3D 3809.5-3810.0	0.20, 0.22 0.21*	1.39, 1.32 1.36*	0.32, 0.36 0.34*
HU22-3-3D 3819.5-3820.0	0.23	0.86	0.40
HU22-3-3D 3829.5-3830.0	0.18	0.87	1.60
HU22-3-3D 3834.5-3835.0	0.12, 0.14 0.13*	0.58, 0.58 0.58*	0.81, 0.77 0.79*
HU22-3-4D 3785	1.77	2.28	1.28
HU22-3-4D 3809.5-3810.0	0.47	0.92	1.00
HU22-3-4D 3830	0.16	0.51	0.92
HU22-3-4D 3840.0-2840.5	0.34	2.25	0.58
HU22-3-4D 3870	0.30	0.85	0.77
HU22-3-4D 3880	1.85	1.71	1.56
HU22-3-4D 3890	0.37	0.77	0.79
HU22-3-4D 3905	0.16	0.58	0.20

*Average value on samples run in duplicate.

Table 7 (cont'd)

SUBJECT: H₂O(-), 110°-500°C, L.O.I.

Sample	H ₂ O(-) @ 110°C	110°-500°C	L.O.I. @ 1000°C
HU22-3-4D 3935	0.12	0.81	0.36
Sm 13-53 3357.0-3358.0	0.24	0.90	2.31
Sm 13-53 3358.0-3359.0	0.28	0.82	4.40
Sm 13-53 3359.0-3360.0	0.39	1.08	7.73
Sm 13-53 3457.0-3458.0	0.16	0.74	0.20
Sm 13-53 3460.0-3461.0	0.20	0.77	0.37

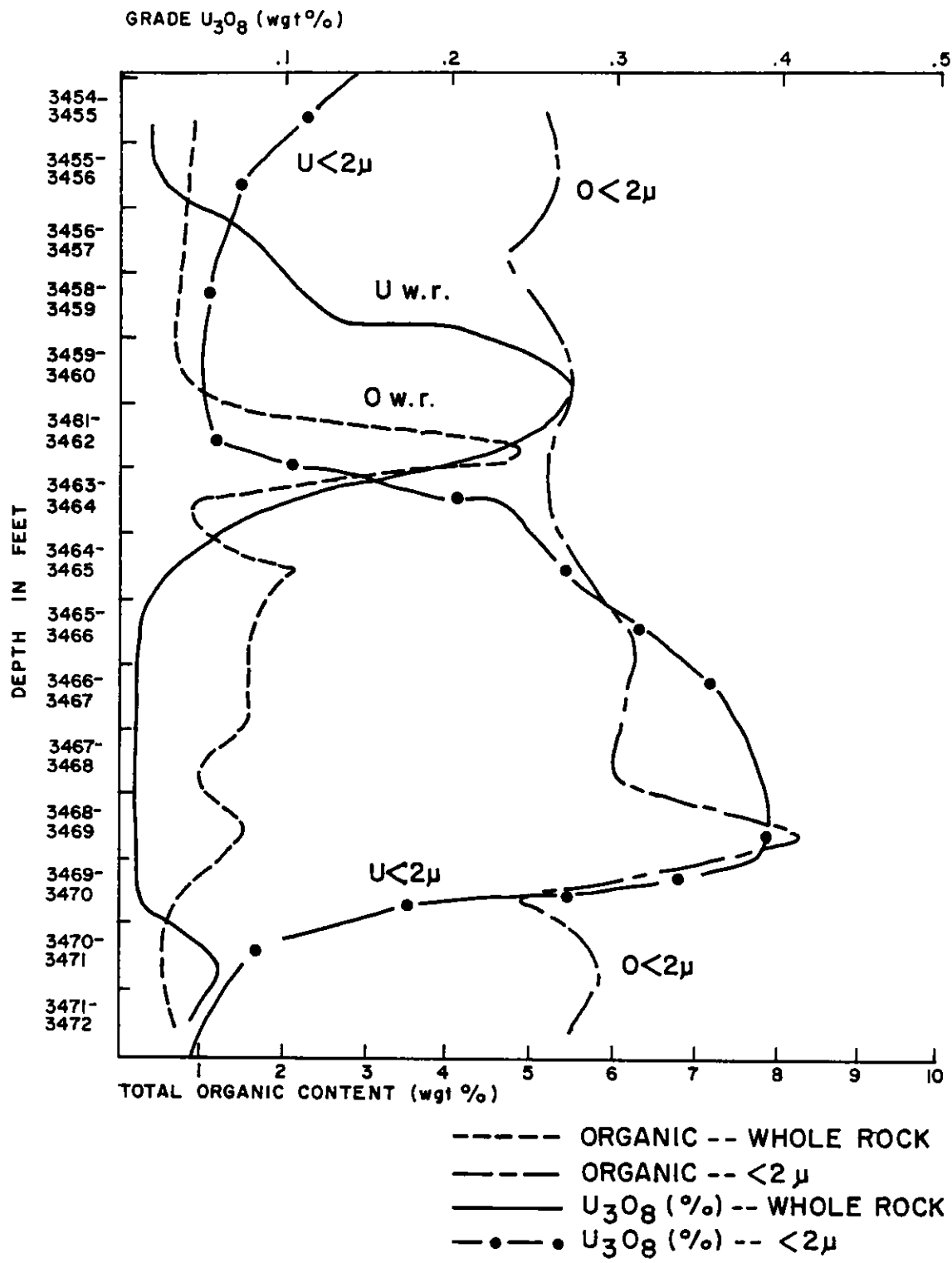


Figure 56

Trace Element Studies by X-Ray Fluorescence Spectrography

Approximately 190 whole rock samples from the vicinity of the Mount Taylor deposit near San Mateo, New Mexico, were analyzed by X-ray fluorescence spectrography to determine if certain correlations could be made without separating the minus-two micron, clay size fraction. The lithologies are only briefly described (Table 10), hence correlation of elemental variation with lithology is speculative at best. In the tabulation of data the reader will note that in table 8 all data are reported as ppm except Ca, Fe and K and in table 9 all data are reported in percentages. These last data were the first samples to be run and precision was poorer than in subsequent work, hence data are reported in percentages.

In an earlier study we attempted to demonstrate that it is necessary to separate the clay size fraction; the lack of many apparent trends in elemental ratios for trace elements based on study of the San Mateo whole rocks supports our earlier view (Brookins, 1976a).

Throughout this report attention is called to the suite Mo-V-Se-As which, under many conditions in nature, are carried with U as oxyanions in solution and the entire group precipitated together under reducing conditions. While we adhere to this belief in principle, the data of table 8 do not convincingly support this hypothesis. For example, in the depth interval 3463 feet to 3469 feet (SM 13-53) high U values correlate with high V values and with As for several samples. Both Se and Mo do not show any positive correlation with U, however, and Se is commonly high in many samples regardless of U concentration. These data are thus difficult to use because of the erratic background of Se in general

and the Mo levels in whole rocks are typically low. In samples from southeast of the Mount Taylor deposit (HU 22-3-4d), high U concentrations correlate with V at the approximate footages of 3720, 3724, 3750, 3760, 3805, 3845 and 3850 feet. Here, too, positive correlation of high U with Mo and Se are noted, yet As does not correlate with U. Further, while Se is abundant in U-rich samples, high values are also noted at depth intervals where U is present in amounts less than 100 ppm. These samples are presumably all from reduced (pyrite stable) parts of the Westwater Canyon Member and enrichment of Mo, Se, V with U are predictable; yet so too is As with U. The V/Mo ratio is of interest for the last group of samples, ranging from 3/1 to 10/1 ($\bar{X} = 6/1$) although the controlling mineralogy is not known.

Until such time as clay minerals are separated (with the other minus two micron phases) we propose no universal elemental ratios from whole rocks. The correlations of U with V or Mo or Se or As are too spotty to warrant use for pathfinder applications in the absence of other data.

A more thorough discussion of possible pathfinder elements for U will be included with the discussion on trace element studies of clay sized materials based on neutron activation analyses.

Table 8
XRF Data (ppm except where noted)

Sample:	SM 13-53	SM 13-53	SM 13-53	SM 13-53	SM 13-53	SM 13-53	SM 13-53
Depth	3304.0-	3305.0-	3306.0-	3307.0-	3308.0-	3311.0-	3344.0-
Interval:	3305.0	3306.0	3307.0	3308.0	3309.0	3312.0	3345.0
<u>Element</u>							
Ca	2.10%	2.00%	8.05%	0.67%	0.65%	1.03%	1.07%
Fe	3.25%	5.22%	2.32%	4.58%	3.94%	3.28%	1.08%
K	3.47%	5.46%	2.76%	3.24%	3.35%	3.85%	3.10%
As	11	29	9	16	14	11	A
Ba	454	459	333	742	847	807	3059
Ce	153	131	135	250	247	203	435
Cr	109	159	89	140	119	98	A
Cu	340	299	201	265	209	251	A
La	25	4	1	46	44	26	6
Mn	258	436	1066	216	199	204	137
Mo	6	3	1	2	4	8	2
Nb	-	-	-	-	-	-	-
Nd	-	-	-	-	-	-	-
Ni	9	13	20	20	17	16	10
Pb	24	9	38	5	10	22	38
Rb	73	154	55	90	83	82	88
Se	27	37	29	23	17	25	10
Sr	282	237	135	193	196	230	109
Ta	16	17	10	A	9	19	17
Th	27	18	30	19	20	15	17
Ti	1922	2684	1211	2091	2042	2121	323
U	111	115	85	79	59	98	25
V	37	141	20	18	13	47	13
Y	42	50	42	35	29	38	19
Yb	38	77	21	8	19	24	34
Zn	14	20	14	15	13	14	A
Zr	263	267	96	172	199	247	65

Table 8 (cont'd)
XRF Data (ppm except where noted)

Sample:	SM 13-53	SM 13-53	SM 13-53	SM 13-53	SM 13-53	SM 13-53	SM 13-53
Depth	3345.0-	3346.0-	3347.0-	3348.0-	3349.0-	3350.0-	3351.0-
Interval:	3346.0	3347.0	3348.0	3349.0	3350.0	3351.0	3352.0
<u>Element</u>							
Ca	1.37%	1.12%	1.57%	5.50%	0.70%	0.48%	0.53%
Fe	0.98%	0.88%	0.80%	1.28%	1.50%	1.19%	1.93%
K	2.87%	2.98%	2.99%	2.46%	2.28%	2.10%	2.40%
As	A	A	A	A	A	A	0
Ba	3383	2072	2072	875	940	1064	1072
Ce	482	423	323	182	202	238	217
Cr	A	A	A	18	16	A	24
Cu	A	A	A	A	A	A	A
La	12	12	12	12	15	22	23
Mn	174	147	149	458	108	67	127
Mo	10	10	5	12	9	19	14
Nb	-	-	-	-	-	-	-
Nd	-	-	-	-	-	-	-
Ni	5	9	2	3	5	4	9
Pb	35	44	23	45	37	36	22
Rb	74	83	85	60	56	43	52
Se	13	21	13	18	14	17	21
Sr	111	118	116	114	102	101	103
Ta	20	31	23	18	14	15	11
Th	15	13	17	22	8	9	12
Ti	483	533	450	817	1132	2630	1227
U	22	40	13	20	31	73	31
V	3	95	30	76	116	122	90
Y	22	20	17	28	18	21	19
Yb	64	61	62	69	66	56	56
Zn	A	0	A	0	A	4	0
Zr	88	87	74	112	141	290	135

Table 8 (cont'd)
XRF Data (ppm except where noted)

Sample:	SM 13-53	SM 13-53	SM 13-53	SM 13-53	SM 13-53	SM 13-53	SM 13-53
Depth	3352.0-	3353.0-	3354.0-	3355.0-	3356.0-	3357.0-	3358.0-
Interval:	3353.0	3354.0	3355.0	3356.0	3357.0	3358.0	3359.0
<u>Element</u>							
Ca	0.93%	0.58%	0.46%	0.62%	0.99%	3.25%	6.98%
Fe	1.60%	2.39%	1.70%	1.29%	1.15%	1.54%	2.06%
K	2.17%	2.02%	2.05%	2.05%	2.03%	2.37%	2.21%
As	A	2	A	A	A	A	1
Ba	1497	1645	1265	1383	1416	1046	3343
Ce	289	333	255	256	250	203	530
Cr	0	11	A	A	A	27	35
Cu	A	4	A	A	A	A	6
La	23	52	37	7	A	5	9
Mn	140	166	105	117	156	365	472
Mo	17	17	17	7	9	5	9
Nb	-	-	-	-	-	-	-
Nd	-	-	-	-	-	-	-
Ni	1	6	4	A	8	6	8
Pb	16	20	19	24	20	25	29
Rb	43	34	43	49	51	57	47
Se	16	12	10	13	10	14	25
Sr	91	80	84	90	86	106	117
Ta	11	A	A	19	11	11	2
Th	9	A	2	2	11	A	11
Ti	1442	2796	1750	1179	1240	723	814
U	41	80	33	27	A	18	42
V	69	52	87	126	93	81	A
Y	17	23	20	20	17	20	25
Yb	64	45	62	74	49	48	45
Zn	A	4	A	A	A	0	5
Zr	149	288	196	129	122	79	89

Table 8 (cont'd)
XRF Data (ppm except where noted)

Sample:	SM 13-53	SM 13-53	SM 13-53	SM 13-53	SM 13-53	SM 13-53	SM 13-53
Depth	3359.0-	3361.0-	3454.0-	3455.0-	3456.0-	3457.0-	3458.0-
Interval:	3360.0	3362.0	3455.0	3456.0	3457.0	3458.0	3459.0
<u>Element</u>							
Ca	30.41%	0.30%	1.07%	0.53%	0.40%	0.21%	0.21%
Fe	1.93%	1.28%	0.81%	1.21%	0.90%	1.22%	0.86%
K	2.02%	2.24%	1.65%	1.77%	1.82%	1.66%	1.58%
As	10	A	A	A	A	A	A
Ba	687	786	1453	1203	1203	802	986
Ce	162	143	243	209	218	140	165
Cr	51	A	A	A	A	A	A
Cu	5	A	A	A	A	14	2
La	10	A	A	A	A	A	A
Mn	997	44	82	68	44	25	13
Mo	19	0	18	21	25	12	24
Nb	-	-	-	-	-	-	-
Nd	-	-	-	-	-	-	-
Ni	A	6	A	4	A	A	A
Pb	29	55	139	130	130	33	47
Rb	36	50	42	42	40	35	38
Se	20	225	742	703	696	174	217
Sr	137	79	62	63	64	55	54
Ta	A	6	11	26	24	A	41
Th	15	6	3	A	2	0	5
Ti	2109	531	889	1111	984	601	662
U	68	50	A	A	29	5	A
V	53	170	186	178	184	169	161
Y	31	15	11	11	15	9	7
Yb	95	56	83	60	89	156	97
Zn	5	A	A	A	A	A	A
Zr	205	80	109	117	132	62	80

Table 8 (cont'd)
XRF Data (ppm except where noted)

Sample:	SM 13-53	SM 13-53	SM 13-53	SM 13-53	SM 13-53	SM 13-53	SM 13-53
Depth	3459.0-	3460.0-	3463.0-	3463.0-	3464.0-	3465.0-	3466.0-
Interval:	3460.0	3461.0	3464.0	3464.0	3465.0	3466.0	3467.0
<u>Element</u>							
Ca	0.24%	0.33%	0.23%	0.25%	0.37%	0.76%	0.45%
Fe	0.93%	1.40%	1.22%	1.44%	3.19%	2.97%	2.37%
K	1.69%	1.98%	2.08%	2.11%	2.33%	2.08%	2.21%
As	A	A	A	A	41	21	20
Ba	1420	1039	758	781	829	775	829
Ce	222	174	141	154	220	218	185
Cr	A	A	2	25	113	93	74
Cu	A	14	A	A	107	76	29
La	A	A	2	11	31	38	19
Mn	35	46	43	70	191	220	171
Mo	13	7	8	A	0	A	11
Nb	-	-	-	-	-	-	-
Nd	-	-	-	-	-	-	-
Ni	3	A	2	6	12	15	18
Pb	107	83	37	50	33	49	52
Rb	42	52	47	86	22	5	24
Se	386	312	27	40	68	83	75
Sr	69	80	77	81	115	106	111
Ta	14	A	12	30	50	47	67
Th	5	A	6	38	55	69	70
Ti	609	553	512	840	1697	1306	1473
U	0	6	75	583	1384	1910	1437
V	212	124	261	551	681	479	661
Y	4	9	17	28	42	45	56
Yb	7	154	62	61	60	53	50
Zn	A	A	A	4	18	21	18
Zr	81	71	79	109	218	165	188

Table 8 (cont'd)
XRF Data (ppm except where noted)

Sample:	SM 13-53	SM 13-53	SM 13-53	SM 13-53	SM 13-53	SM 14-38	SM 14-38
Depth	3367.0-	3468.0-	3469.0-	3470.0-	3471.0-	2805.0-	2806.0-
Interval:	3468.0	3469.0	3470.0	3471.0	3472.0	2806.2	2807.0
<u>Element</u>							
Ca	0.41%	0.67%	0.20%	0.19%	0.22%	3.10%	1.79%
Fe	0.99%	1.88%	0.65%	0.75%	0.99%	1.31%	4.32%
K	2.06%	2.08%	1.69%	1.64%	1.80%	2.05%	3.65%
As	A	16	A	A	A	A	29
Ba	1913	3532	1440	1322	1713	8024	503
Ce	301	547	205	227	284	945	98
Cr	A	52	A	A	A	11	164
Cu	A	46	A	A	A	23	491
La	0	23	A	8	9	A	31
Mn	56	155	17	30	45	456	281
Mo	A	A	9	10	A	10	15
Nb	-	-	-	-	-	-	-
Nd	-	-	-	-	-	-	-
Ni	3	12	A	A	A	5	17
Pb	57	68	53	30	48	38	4
Rb	49	47	37	39	39	51	87
Se	38	87	28	24	36	28	38
Sr	91	98	75	69	74	181	233
Ta	54	72	42	42	52	36	26
Th	66	94	47	34	44	30	35
Ti	430	336	326	980	930	936	2416
U	765	2276	336	156	759	85	151
V	504	324	324	295	239	68	A
Y	30	43	18	15	34	23	47
Yb	89	59	120	94	101	71	23
Zn	0	11	A	A	5	4	18
Zr	79	85	57	127	125	93	208

Table 8 (cont'd)
XRF Data (ppm except where noted)

Sample:	SM 14-38	SM 14-38	SM 14-38	SM 14-38	SM 14-38	SM 14-38	SM 14-38
Depth	2807.0-	2808.0-	2809.0-	2829.0-	2830.0-	2831.0-	2832.0-
Interval:	2808.0	2809.0	2810.2	2830.0	2831.0	2832.0	2833.0
<u>Element</u>							
Ca	3.12%	2.50%	23.15%	0.32%	0.32%	0.31%	0.31%
Fe	2.70%	2.32%	2.11%	0.67%	0.64%	0.61%	0.87%
K	3.33%	2.86%	3.49%	2.32%	2.42%	2.51%	2.37%
As	21	11	14	A	A	A	A
Ba	745	721	445	762	743	870	781
Ce	137	132	120	88	76	98	87
Cr	102	78	87	A	A	A	4
Cu	277	87	472	A	A	A	A
La	18	8	22	A	A	A	A
Mn	314	659	654	20	18	15	24
Mo	15	22	14	43	19	12	18
Nb	-	-	-	-	-	-	-
Nd	-	-	-	-	-	-	-
Ni	15	5	13	A	A	2	A
Pb	23	28	55	40	46	41	23
Rb	62	56	69	63	72	75	67
Se	33	28	43	28	19	14	20
Sr	248	215	227	102	97	91	97
Ta	29	36	39	47	55	18	32
Th	40	42	48	35	31	13	4
Ti	2385	1654	1521	659	450	432	460
U	163	145	156	112	92	27	A
V	14	75	A	165	187	117	139
Y	45	37	49	20	19	17	16
Yb	31	59	38	113	86	77	95
Zn	28	19	18	A	A	A	A
Zr	254	203	159	74	66	56	72

Table 8 (cont'd)
XRF Data (ppm except where noted)

Sample:	SM 14-38	SM 14-38	SM 14-38	SM 14-38	SM 14-38	SM 14-38	SM 14-38
Depth	2833.0-	2834.0-	2835.0-	2836.0-	2837.0-	2838.0-	2839.0-
Interval:	2834.0	2835.0	2836.0	2837.0	2838.0	2839.0	2840.0
<u>Element</u>							
Ca	0.32%	0.28%	0.36%	0.35%	0.33%	0.32%	0.33%
Fe	0.87%	0.94%	1.16%	1.21%	1.16%	1.72%	1.06%
K	2.49%	2.08%	2.53%	2.67%	2.63%	2.42%	2.54%
As	A	A	A	A	A	A	A
Ba	835	1594	883	1229	1821	891	848
Ce	110	197	123	152	227	117	115
Cr	2	A	5	1	A	25	9
Cu	A	A	A	A	A	A	A
La	A	3	A	6	A	6	1
Mn	43	48	63	68	76	95	57
Mo	9	16	10	12	11	14	9
Nb	-	-	-	-	-	- -	-
Nd	-	-	-	-	-	-	-
Ni	A	8	10	7	6	5	2
Pb	30	31	39	33	33	31	43
Rb	69	49	66	72	71	60	72
Se	20	14	21	17	23	23	25
Sr	97	82	95	102	102	94	100
Ta	30	23	39	23	31	13	38
Th	12	A	20	14	17	7	14
Ti	468	1827	1263	1041	947	924	798
U	A	28	69	A	34	40	18
V	115	175	155	128	159	132	144
Y	16	16	22	22	19	17	20
Yb	86	48	54	56	67	66	75
Zn	A	A	A	A	A	1	A
Zr	61	155	128	102	116	115	99

Table 8 (cont'd)
XRF Data (ppm except where noted)

Sample:	SM 14-38	SM 14-38	SM 14-38	SM 14-38	SM 14-38	SM 14-38	SM 14-38
Depth	2840.0-	2841.0-	2842.0-	2843.0-	2844.0-	2845.0-	2846.0-
Interval:	2841.0	2842.0	2843.0	2844.0	2845.0	2846.0	2847.0
<u>Element</u>							
Ca	0.32%	0.32%	0.32%	0.31%	0.35%	0.29%	0.29%
Fe	1.81%	1.24%	1.07%	0.96%	1.11%	0.62%	1.23%
K	2.28%	2.59%	2.56%	2.39%	2.69%	2.61%	2.34%
As	2	A	A	A	A	A	A
Ba	843	897	1056	1237	900	843	956
Ce	135	132	170	200	141	123	147
Cr	40	37	A	A	19	A	7
Cu	A	A	A	A	A	A	A
La	6	1	0	12	6	0	12
Mn	91	59	59	57	58	24	64
Mo	9	4	13	22	41	8	51
Nb	-	-	-	-	-	-	-
Nd	-	-	-	-	-	-	-
Ni	10	7	8	A	A	2	7
Pb	24	24	29	40	25	33	32
Rb	60	71	68	63	61	78	61
Se	17	18	19	24	23	8	21
Sr	87	96	95	97	105	84	89
Ta	23	37	33	35	22	28	35
Th	9	8	8	20	14	11	19
Ti	796	827	1519	1832	1379	431	1030
U	60	11	84	76	65	37	58
V	121	152	138	147	152	160	144
Y	17	19	22	24	21	22	25
Yb	44	55	57	87	76	60	62
Zn	1	A	A	A	A	A	A
Zr	85	101	164	195	158	64	125

Table 8 (cont'd)
XRF Data (ppm except where noted)

Sample:	SM 14-38	SM 14-38	SM 14-38	SM 14-38	SM 14-38	SM 14-38	SM 14-38
Depth	2847.0-	2848.0-	2945.0-	2946.0-	2947.0-	2948.0-	2949.0-
Interval:	2848.0	2849.0	2946.0	2947.0	2948.0	2949.0	2950.0
<u>Element</u>							
Ca	0.25%	0.28%	0.37%	1.29%	0.88%	0.71%	0.69%
Fe	0.99%	0.95%	2.56%	2.82%	3.68%	3.66%	3.55%
K	2.21%	2.45%	1.61%	1.94%	4.24%	3.71%	3.84%
As	A	A	1	2	38	6	14
Ba	735	781	629	564	625	556	500
Ce	164	141	105	88	194	176	141
Cr	A	6	55	72	142	118	114
Cu	A	A	A	A	597	293	305
La	43	A	A	A	25	31	12
Mn	36	38	126	187	178	164	170
Mo	53	45	9	8	9	10	12
Nb	-	-	-	-	-	-	-
Nd	-	-	-	-	-	-	-
Ni	7	8	0	4	20	15	9
Pb	28	35	12	16	51	25	32
Rb	58	66	30	37	114	90	100
Se	19	23	18	23	66	30	43
Sr	79	82	57	67	225	166	151
Ta	35	32	8	A	41	18	16
Th	15	19	11	6	43	27	37
Ti	647	623	1470	512	2854	2052	2093
U	47	43	52	51	210	124	158
V	135	148	139	127	202	62	64
Y	19	18	17	18	58	45	50
Yb	59	55	72	70	26	29	58
Zn	A	A	6	8	23	15	30
Zr	70	76	120	61	174	180	171

Table 8 (cont'd)
XRF Data (ppm except where noted)

Sample:	SM 14-38	SM 14-38	SM 14-38	SM 14-38	SM 14-38	SM 14-38	SM 14-38
Depth	2950.3-	2951.0-	2952.0-	2953.0-	2954.0	2955.0	2956.0-
Interval:	2951.0	2952.0	2953.0	2954.0	2955.0	2956.0	2957.0
<u>Element</u>							
Ca	4.40%	0.40%	0.99%	0.45%	0.27%	0.41%	2.41%
Fe	4.35%	2.88%	5.40%	3.61%	3.29%	2.95%	1.75%
K	1.36%	1.94%	3.25%	1.37%	1.33%	1.69%	1.66%
As	1	7	19	27	17	13	5
Ba	581	489	745	578	497	562	478
Ce	94	70	147	105	70	102	76
Cr	115	64	107	81	69	43	16
Cu	11	A	A	18	A	A	1
La	A	A	A	0	A	A	A
Mn	390	140	274	212	184	175	228
Mo	3	5	10	12	10	5	18
Nb	-	-	-	-	-	-	-
Nd	-	-	-	-	-	-	-
Ni	5	19	39	23	25	20	34
Pb	19	29	16	12	16	16	57
Rb	17	34	42	7	15	15	18
Se	31	34	26	31	27	21	24
Sr	54	79	112	54	57	61	69
Ta	A	36	14	21	19	30	50
Th	2	37	45	59	45	38	64
Ti	453	851	1833	1832	1141	1564	799
U	109	113	176	165	123	135	180
V	61	244	354	247	276	238	240
Y	22	27	34	29	26	25	32
Yb	56	49	27	46	46	10	20
Zn	11	7	14	16	15	11	17
Zr	60	86	109	59	83	68	44

Table 8 (cont'd)
XRF Data (ppm except where noted)

Sample:	SM 14-38	SM 14-38	SM 14-38	SM 14-38
Depth	2957.0-	2958.0-	2959.0	2960.0-
Interval	2958.0	2959.0	2960.0	2961.0
<u>Element</u>				
Ca	1.30%	0.71%	0.49%	0.45%
Fe	2.03%	1.68%	1.66%	1.58%
K	1.99%	1.81%	1.84%	1.74%
As	11	3	9	1
Ba	567	713	581	581
Ce	152	188	152	154
Cr	46	A	A	A
Cu	41	A	A	A
La	0	0	A	A
Mn	200	134	119	105
Mo	14	10	13	7
Nb	-	-	-	-
Nd	-	-	-	-
Ni	27	16	31	14
Pb	61	40	42	34
Rb	21	17	18	19
Se	55	17	20	16
Sr	82	64	65	59
Ta	61	42	50	36
Th	61	44	48	30
Ti	1226	1483	845	1391
U	217	169	199	153
V	245	226	262	272
Y	35	27	28	25
Yb	48	47	21	83
Zn	16	8	10	8
Zr	79	58	46	62

Table 8 (cont'd)
XRF Data (ppm except where noted)

Sample:	HU 22- 3-1	HU 22- 3-1	HU 22- 3-1	HU 22- 3-1	HU 22- 3-1	HU 22- 3-1	HU 22- 3-1
Depth	3640.0-	3650.0-	3670.0-	3680.0-	3690.0-	3695.0-	3700.0-
Interval:	3640.5	3650.5	3670.5	3680.5	3690.5	3695.5	3700.5
<u>Element</u>							
Ca	0.22%	0.58%	0.66%	0.69%	0.60%	0.26%	0.64%
Fe	0.40%	0.85%	2.68%	4.27%	2.59%	1.28%	3.10%
K	1.49%	1.64%	3.10%	3.22%	2.42%	1.46%	2.65%
As	A	2	16	33	39	A	81
Ba	1522	1041	519	476	496	622	490
Ce	610	466	348	455	330	324	408
Cr	29	25	14	30	21	35	16
Cu	2	2	17	10	16	3	13
La	2	7	9	25	10	10	20
Mn	68	141	233	377	266	159	315
Mo	2	2	2	3	A	12	A
Nb	-	-	-	-	-	-	-
Nd	-	-	-	-	-	-	-
Ni	52	44	29	25	69	68	23
Pb	11	A	6	A	0	34	A
Rb	65	81	180	173	128	63	147
Se	9	A	30	0	19	23	31
Sr	128	152	502	483	507	119	485
Ta	45	A	148	A	92	167	65
Th	10	A	38	A	34	21	43
Ti	1213	614	8489	4193	5083	5982	5375
U	50	16	129	61	103	210	87
V	64	36	A	A	A	42	A
Y	11	15	35	48	45	13	45
Yb	41	A	135	A	83	151	59
Zn	0	0	16	11	31	A	20
Zr	86	73	270	278	274	254	269

Table 8 (cont'd)
XRF Data (ppm except where noted)

Sample:	HU 22- 3-1	HU 22- 3-1	HU 22- 3-1	HU 22- 3-1	HU 22- 3-1	HU 22- 3-1	HU 22- 3-1D
Depth	3705.0-	3710.0-	3715.0-	3719.5-	3724.5-	3710.0-	3716.0-
Interval:	3705.5	3710.5	3715.5	3720.0	3725.0	3710.5	3716.5
<u>Element</u>							
Ca	0.22%	0.17%	0.19%	0.28%	0.58%	0.21%	0.27%
Fe	1.11%	0.49%	0.56%	0.66%	0.92%	0.87%	0.88%
K	1.30%	1.03%	1.24%	2.01%	1.93%	1.34%	1.97%
As	21	A	28	A	A	A	1
Ba	567	419	577	604	1158	874	712
Ce	315	208	318	444	364	444	382
Cr	78	32	22	9	28	14	32
Cu	1	3	4	9	8	2	6
La	3	A	7	14	11	14	A
Mn	249	72	78	205	198	64	130
Mo	32	44	409	441	121	17	14
Nb	-	-	-	-	-	-	-
Nd	-	-	-	-	-	-	-
Ni	201	37	78	116	126	A	16
Pb	32	21	53	112	135	15	A
Rb	48	49	62	192	181	87	88
Se	49	12	160	334	119	13	179
Sr	97	89	106	136	154	130	107
Ta	137	A	A	73	169	A	1
Th	39	7	4	11	58	A	A
Ti	4918	441	1526	A	A	3612	555
U	85	48	117	4670	7678	40	508
V	68	22	34	4067	657	44	89
Y	17	2	3	A	12	4	3
Yb	124	A	A	66	153	A	1
Zn	A	2	A	8	5	A	18
Zr	378	59	123	120	145	118	76

Table 8 (cont'd)
XRF Data (ppm except where noted)

Sample:	HU 22- 3-1D	HU 22- 3-1D	HU 22- 3-1D	HU 22- 3-1D	HU 22- 3-1D	HU 22- 3-2D	HU 22- 3-2D
Depth	3720.0-	3730.0-	3735.0-	3739.5-	3745.5-	3705.0-	3710.0-
Interval:	3720.5	3730.5	3735.5	3740.0	3746.0	3705.5	3710.5
<u>Element</u>							
Ca	0.56%	0.21%	0.18%	0.69%	0.28%	0.57%	3.58%
Fe	1.82%	0.91%	0.87%	4.27%	0.74%	2.26%	2.30%
K	1.94%	1.48%	1.32%	3.22%	2.30%	2.67%	2.42%
As	1	21	8	33	A	A	10
Ba	567	462	614	679	3155	528	561
Ce	338	343	371	390	1078	338	428
Cr	2	13	30	30	21	16	5
Cu	10	2	1	10	5	16	12
La	10	21	11	21	3	6	54
Mn	1809	91	114	377	143	231	320
Mo	5	27	30	3	18	A	4
Nb	-	-	-	-	-	-	-
Nd	-	-	-	-	-	-	-
Ni	10	20	68	25	111	14	4
Pb	A	24	22	A	84	68	11
Rb	75	78	65	173	126	131	117
Se	A	19	33	A	273	15	29
Sr	350	128	103	483	135	421	566
Ta	A	11	A	A	37	90	41
Th	A	3	9	A	39	47	24
Ti	3188	903	1604	4055	492	4920	4449
U	122	63	26	61	440	181	58
V	A	24	32	A	327	14	A
Y	55	11	7	48	13	34	32
Yb	A	10	A	A	34	81	37
Zn	35	A	A	11	3	23	22
Zr	319	103	99	278	84	347	335

Table 8 (cont'd)
XRF Data (ppm except where noted)

Sample:	HU 22- 3-2D	HU 22- 3-2D	HU 22- 3-2D	HU 22- 3-2D	HU 22- 3-2D	HU 22- 3-2D	HU 22- 3-2D
Depth	3715.0-	3719.0-	3725.0-	3730.0-	3739.5-	3744.5-	3749.9-
Interval	3715.5	3719.5	3725.5	3730.5	3740.0	3745.0	3750.0
<u>Element</u>							
Ca	0.65%	0.67%	0.29%	0.30%	0.68%	0.30%	0.24%
Fe	3.45%	3.38%	0.52%	0.92%	2.73%	1.57%	1.51%
K	2.53%	2.83%	1.60%	1.46%	2.85%	1.74%	1.38%
As	A	52	A	A	169	10	A
Ba	542	572	632	716	624	692	625
Ce	495	376	271	404	372	325	354
Cr	28	9	24	20	14	23	30
Cu	15	* 16	5	5	14	5	13
La	30	A	A	A	5	A	A
Mn	358	320	108	129	272	188	224
Mo	5	A	9	4	2	9	43
Nb	-	-	-	-	-	-	-
Nd	-	-	-	-	-	-	-
Ni	59	14	46	81	23	23	53
Pb	61	A	24	14	A	A	58
Rb	132	154	83	55	165	82	87
Se	10	A	A	A	9	A	63
Sr	400	580	124	99	454	121	120
Ta	75	11	22	14	A	A	30
Th	58	15	18	7	24	A	19
Ti	4652	6819	595	6547	4866	543	844
U	108	10	24	60	99	569	2788
V	A	A	15	52	A	116	243
Y	45	35	4	8	33	A	17
Yb	68	10	20	12	A	A	28
Zn	41	41	A	4	28	8	38
Zr	231	286	76	203	220	83	143

Table 8 (cont'd)
XRF Data (ppm except where noted)

Sample:	HU 22- 3-2D	HU 22- 3-2D	HU 22- 3-3D	HU 22- 3-3D	HU 22- 3-3D	HU 22- 3-3D	HU 22- 3-3D
Depth	3754.5-	3759.5-	3790.0-	3795.0-	3799.5-	3805.0-	3809.5-
Interval:	3755.0	3760.0	3790.5	3795.5	3800.0	3805.5	3810.0
<u>Element</u>							
Ca	0.20%	0.34%	0.64%	0.29%	0.31%	0.30%	0.22%
Fe	0.50%	0.78%	3.20%	1.23%	0.58%	1.36%	2.01%
K	0.85%	1.95%	2.31%	1.67%	1.40%	1.45%	1.18%
As	A	A	6	A	A	A	13
Ba	494	775	491	665	735	500	524
Ce	287	410	319	341	366	278	343
Cr	9	23	21	21	11	20	17
Cu	3	12	13	5	2	4	9
La	A	5	9	A	7	4	1
Mn	17	147	319	147	54	163	257
Mo	10	84	4	9	5	49	21
Nb	-	-	-	-	-	-	-
Nd	-	-	-	-	-	-	-
Ni	7	102	14	64	14	62	33
Pb	79	209	A	40	191	29	34
Rb	43	118	139	64	67	74	71
Se	341	843	9	11	9	22	50
Sr	72	121	453	126	110	170	100
Ta	43	93	10	30	7	1	17
Th	16	6	48	8	2	14	15
Ti	5302	119	3963	1399	1576	1164	2179
U	241	2107	98	34	30	A	1823
V	119	584	A	28	39	9	91
Y	7	8	37	17	13	5	20
Yb	39	85	9	27	7	1	15
Zn	A	16	22	2	A	3	21
Zr	128	128	233	149	100	103	222

Table 8, (cont'd)
XRF Data (ppm except where noted)

Sample:	HU 22- 3-3D	HU 22- 3-3D	HU 22- 3-3D	HU 22- 3-3D	HU 22- 3-3D	HU 22- 3-4D	HU 22- 3-4D
Depth	3814.5-	3819.5-	3825.0-	3829.5-	3834.5-	3805.0-	3809.5-
Interval:	3815.0	3820.0	3825.5	3830.0	3835.0	3805.5	3810.0
<u>Element</u>							
Ca	0.29%	0.27%	0.45%	1.36%	0.98%	0.35%	0.30%
Fe	1.61%	0.90%	0.67%	0.40%	0.55%	1.15%	0.54%
K	1.76%	1.89%	1.49%	1.58%	2.13%	2.35%	1.85%
As	11	A	A	8	4	7	9
Ba	687	678	2854	570	771	686	757
Ce	383	259	737	317	391	493	339
Cr	48	25	27	33	34	32	26
Cu	8	6	2	2	3	6	10
La	6	7	8	3	4	41	15
Mn	239	156	134	175	166	223	132
Mo	31	152	24	10	6	106	63
Nb	-	-	-	-	-	-	-
Nd	-	-	-	-	-	-	-
Ni	121	72	52	99	92	101	98
Pb	36	39	33	51	85	99	44
Rb	73	92	78	84	126	168	98
Se	42	97	A	18	37	72	57
Sr	145	124	117	122	127	145	155
Ta	A	102	A	12	54	143	157
Th	7	23	16	3	5	28	7
Ti	968	497	690	648	423	686	1593
U	100	26	53	48	29	6948	55
V	42	43	262	98	77	290	62
Y	6	6	3	1	9	15	15
Yb	A	93	A	11	49	130	142
Zn	57	10	3	1	3	A	21
Zr	95	65	69	64	71	162	124

Table 8 (cont'd)
XRF Data (ppm except where noted)

Sample:	HU 22- 3-4D	HU 22- 3-4D	HU 22- 3-4D	HU 22- 3-4D	HU 22- 3-4D	HU 22- 3-4D	HU 22- 3-4D
Depth	3814.5-	3819.5-	3825.0-	3834.5-	3840.0-	3845.0-	3850.0-
Interval:	3815.0	3820.0	3825.5	3835.0	3840.5	3845.5	3850.5
<u>Element</u>							
Ca	0.30%	0.26%	0.27%	0.24%	0.64%	0.39%	0.27%
Fe	1.17%	1.93%	0.69%	1.00%	3.10%	1.08%	0.99%
K	1.59%	1.51%	1.80%	1.52%	2.64%	2.69%	1.67%
As	12	A	A	8	81	39	A
Ba	526	521	713	714	2236	661	509
Ce	341	435	438	353	800	313	289
Cr	15	16	18	18	13	77	44
Cu	4	6	5	4	13	A	15
La	12	25	22	13	9	11	29
Mn	114	194	77	96	316	381	270
Mo	47	21	A	19	A	198	126
Nb	-	-	-	-	-	-	-
Nd	-	-	-	-	-	-	-
Ni	64	52	71	32	23	258	157
Pb	16	11	14	A	A	241	149
Rb	94	59	85	55	147	200	176
Se	31	13	A	15	31	156	104
Sr	152	108	113	99	485	172	137
Ta	A	A	26	A	65	251	203
Th	4	10	19	A	43	44	49
Ti	2537	2192	1989	663	4772	A	A
U	81	76	11	A	87	11484	8114
V	18	23	41	21	81	2271	946
Y	16	11	5	A	45	16	11
Yb	A	A	23	A	59	228	185
Zn	5	8	10	9	20	A	A
Zr	164	147	107	48	269	218	146

Table 8 (cont'd)
XRF Data (ppm except where noted)

Sample:	HU 22- 3-4D	HU 22- 3-4D	HU 22- 3-4D	HU 22- 3-4D	HU 22- 3-4D	HU 22- 3-4D	HU 22- 3-4D
Depth	3855.0-	3865.0-	3868.0-	3870.0-	3875.0-	3880.0-	3885.0-
Interval:	3855.5	3865.5	3868.5	3870.5	3875.5	3880.5	3885.5
<u>Element</u>							
Ca	0.20%	0.94%	0.64%	0.29%	0.40%	0.56%	0.56%
Fe	0.57%	2.18%	2.81%	1.61%	1.45%	2.45%	3.33%
K	1.44%	1.60%	2.42%	1.76%	1.25%	2.30%	2.51%
As	A	17	21	11	A	31	8
Ba	476	1220	696	504	693	485	446
Ce	355	502	433	350	421	349	376
Cr	A	4	16	48	19	24	21
Cu	8	4	13	8	5	17	12
La	14	1	25	12	9	12	7
Mn	43	236	265	239	198	231	310
Mo	29	A	A	31	10	16	A
Nb	-	-	-	-	-	-	-
Nd	-	-	-	-	-	-	-
Ni	21	8	33	121	15	45	38
Pb	10	A	A	36	33	A	A
Rb	74	60	145	73	50	105	127
Se	A	A	6	42	3	35	15
Sr	106	104	375	145	87	243	374
Ta	A	A	37	A	32	96	13
Th	A	14	20	7	14	19	23
Ti	511	3349	4805	986	4864	3538	4613
U	18	12	83	100	118	96	205
V	29	76	8	37	33	72	A
Y	6	5	27	6	10	34	31
Yb	A	A	34	A	29	87	11
Zn	7	2	14	57	4	29	43
Zr	68	307	223	95	236	302	243

Table 8 (cont'd)
XRF Data (ppm except where noted)

Sample:	HU 22- 3-4D	HU 22- 3-4D	HU 22- 3-4D	HU 22- 3-4D	HU 22- 3-4D	HU 22- 3-4D	HU 22- 3-4D
Depth	3890.0-	3895.0-	3900.0-	3915.0-	3925.0-	3935.0-	3945.0-
Interval:	3890.5	3895.5	3900.5	3915.5	3925.5	3935.5	3945.5
<u>Element</u>							
Ca	0.51%	0.15%	0.27%	0.31%	0.21%	0.30%	0.21%
Fe	1.29%	0.50%	4.40%	0.97%	1.28%	0.68%	0.73%
K	.139%	0.95%	1.29%	1.22%	1.47%	1.17%	1.17%
As	1	335	9	A	A	A	2
Ba	1227	570	598	541	559	454	404
Ce	636	367	354	293	349	290	195
Cr	5	27	25	12	31	31	3
Cu	4	5	16	4	5	2	7
La	55	4	A	A	5	2	20
Mn	122	201	486	115	152	67	71
Mo	A	295	21	12	15	3	8
Nb	-	-	-	-	-	-	-
Nd	-	-	-	-	-	-	-
Ni	7	177	43	44	83	66	A
Pb	2	69	2	17	25	4	6
Rb	55	146	57	39	52	43	48
Se	A	408	21	11	17	A	32
Sr	130	181	99	72	92	71	77
Ta	80	117	116	A	A	A	39
Th	A	80	68	A	16	A	13
Ti	4862	678	18463	2034	2352	1117	1060
U	91	419	153	76	68	A	13
V	167	76	A	25	33	24	17
Y	13	109	24	14	15	5	4
Yb	73	106	105	A	A	A	35
Zn	A	1	44	A	18	A	10
Zr	326	156	629	152	281	82	133

Table 9

SRF Data (ppm except where noted)

Sample:	SM 15-24	SM 15-24	SM 15-24
Depth	2594.0	2608.5-	2611.0-
Interval	2595.0	2609.0	2612.0
<u>Element</u>			
Ca	-	-	-
Fe	-	-	-
K	-	-	-
As	0.001	0.001	0.001
Ba	0.131	0.083	0.064
Ce	0.093	0.001	0.001
Cr	-	-	-
Cu	0.021	0.017	0.009
La	-	-	-
Mn	0.001	0.001	0.001
Mo	0.005	0.023	0.006
Nb	-	-	-
Nd	-	-	-
Ni	-	-	-
Pb	-	-	-
Rb	0.014	0.009	0.016
Se	0.001	0.001	0.001
Sr	0.056	0.029	0.043
Ta	0.002	0.002	0.001
Th	0.009	0.007	0.005
Ti	0.347	0.258	0.117
U	0.005	0.005	0.005
V	0.014	0.083	0.018
Y	0.003	0.002	0.002
Yb	0.091	0.080	0.140
Zn	-	-	-
Zr	0.051	0.031	0.032

Table 9 (cont'd)
SRF Data (ppm except where noted)

Sample:	SM 15-25	SM 15-25	SM 15-25	SM 15-25	SM 15-25	SM 15-25	SM 15-28
Depth	2596.0-	2604.5-	2609.0-	2610.5-	2627.0-	2632.5-	2650.0-
Interval	2597.0	2605.0	2610.0	2611.0	2628.0	2632.8	2651.0
<u>Element</u>							
Ca	-	-	-	-	-	-	-
Fe	-	-	-	-	-	-	-
K	-	-	-	-	-	-	-
As	0.001	0.001	0.001	0.001	0.010	0.001	0.001
Ba	0.117	0.073	0.143	0.120	0.073	0.048	0.072
Ce	0.010	0.005	0.001	0.011	0.001	0.001	0.001
Cr	-	-	-	-	-	-	-
Cu	0.012	0.009	0.007	0.005	0.010	0.010	0.007
La	-	-	-	-	-	-	-
Mn	0.001	0.001	0.001	0.001	0.001	0.443	0.001
Mo	0.005	0.005	0.005	0.005	0.006	0.005	0.006
Nb	-	-	-	-	-	-	-
Nd	-	-	-	-	-	-	-
Ni	-	-	-	-	-	-	-
Pb	-	-	-	-	-	-	-
Rb	0.014	0.010	0.011	0.011	0.017	0.005	0.018
Se	0.001	0.001	0.001	0.001	0.001	0.001	0.001
Sr	0.040	0.039	0.041	0.061	0.038	0.040	0.040
Ta	0.001	0.001	0.001	0.001	0.001	0.001	0.001
Th	0.004	0.004	0.003	0.001	0.005	0.001	0.004
Ti	0.291	0.138	0.273	0.333	0.122	0.091	0.115
U	0.005	0.013	0.010	0.005	0.005	0.005	0.005
V	0.011	0.012	0.015	0.010	0.017	0.009	0.012
Y	0.002	0.003	0.003	0.002	0.002	0.002	0.002
Yb	0.019	0.060	0.037	0.005	0.076	0.014	0.140
Zn	-	-	-	-	-	-	-
Zr	0.054	0.032	0.061	0.045	0.029	0.017	0.030

Table 9 (cont'd)
XRF Data (ppm except where noted)

Sample:	SM 15-28	SM 15-28	SM 15-31	SM 15-31	SM 15-31	SM 15-31	SM 15-31
Depth	2674.0-	2684.0-	2763.0-	2810.0-	2840.0-	2868.0-	2869.5
Interval:	2675.0	2685.0	2764.0	2811.0	2841.0	2869.0	2870.0
<u>Element</u>							
Ca	-	-	-	-	-	-	-
Fe	-	-	-	-	-	-	-
K	-	-	-	-	-	-	-
As	0.001	0.001	0.001	0.001	0.001	0.001	0.001
Ba	0.124	0.078	0.082	0.104	0.087	0.044	0.068
Ce	0.026	0.017	0.001	0.001	0.001	0.029	0.001
Cr	-	-	-	-	-	-	-
Cu	0.008	0.008	0.012	0.009	0.008	0.013	0.012
La	-	-	-	-	-	-	-
Mn	0.001	0.001	0.001	0.013	0.028	0.001	0.132
Mo	0.005	0.005	0.006	0.005	0.005	0.005	0.005
Nb	-	-	-	-	-	-	-
Nd	-	-	-	-	-	-	-
Ni	-	-	-	-	-	-	-
Pb	-	-	-	-	-	-	-
Rb	0.011	0.005	0.012	0.012	0.008	0.006	0.006
Se	0.001	0.030	0.001	0.001	0.001	0.001	0.001
Sr	0.037	0.039	0.012	0.033	0.038	0.048	0.026
Ta	0.001	0.001	0.001	0.001	0.001	0.001	0.001
Th	0.006	0.001	0.004	0.001	0.001	0.001	0.001
Ti	0.216	0.228	0.147	0.251	0.157	0.258	0.105
U	0.005	0.057	0.005	0.005	0.005	0.005	0.005
V	0.013	0.064	0.015	0.009	0.009	0.015	0.006
Y	0.002	0.022	0.002	0.002	0.002	0.002	0.002
Yb	0.088	0.031	0.051	0.005	0.044	0.005	0.047
Zn	-	-	-	-	-	-	-
Zr	0.049	0.055	0.006	0.022	0.028	0.040	0.004

Table 9 (cont'd)
XRF Data (ppm except where noted)

Sample:	SM 15-36	SM 15-36	SM 15-36	SM 15-36	SM 15-36	SM 15-43	SM 15-43
Depth	2576.0-	2585.0-	2588.5-	2590.0-	2597.0-	2564.0-	2582.0-
Interval:	2577.0	2586.0	2589.0	2591.0	2597.5	2565.0	2583.0
<u>Element</u>							
Ca	-	-	-	-	-	-	-
Fe	-	-	-	-	-	-	-
K	-	-	-	-	-	-	-
As	0.001	0.001	0.001	0.001	0.001	0.001	0.001
Ba	0.103	0.131	0.068	0.090	0.104	0.139	0.079
Ce	0.002	0.001	0.001	0.001	0.001	0.013	0.001
Cr	-	-	-	-	-	-	-
Cu	0.011	0.014	0.005	0.005	0.012	0.012	0.012
La	-	-	-	-	-	-	-
Mn	0.001	0.001	0.261	0.197	0.292	0.001	0.001
Mo	0.005	0.005	0.005	0.005	0.005	0.005	0.006
Nb	-	-	-	-	-	-	-
Nd	-	-	-	-	-	-	-
Ni	-	-	-	-	-	-	-
Pb	-	-	-	-	-	-	-
Rb	0.015	0.015	0.007	0.005	0.011	0.015	0.017
Se	0.001	0.001	0.001	0.001	0.001	0.001	0.001
Sr	0.040	0.026	0.051	0.099	0.061	0.063	0.040
Ta	0.001	0.001	0.001	0.001	0.001	0.001	0.001
Th	0.003	0.004	0.001	0.001	0.001	0.001	0.004
Ti	0.190	0.237	0.237	0.137	0.203	0.338	0.141
U	0.005	0.005	0.026	0.005	0.005	0.005	0.005
V	0.012	0.017	0.055	0.033	0.069	0.-07	0.018
Y	0.002	0.003	0.005	0.005	0.002	0.002	0.002
Yb	0.072	0.063	0.018	0.008	0.012	0.007	0.057
Zn	-	-	-	-	-	-	-
Zr	0.034	0.027	0.027	0.041	0.044	0.044	0.031

Table 9 (cont'd)
XRF Data (ppm except where noted)

Sample:	SM 15-43	SM 15-43	SM 15-43	SM 15-43	SM 15-43	SM 15-43	SM 15-48
Depth	2592.9-	2593.5-	2605.0-	2611.5-	2635.0-	2641.0-	2582.0-
Interval:	2593.4	2594.0	2606.0	2612.0	2636.0	2641.4	2583.0
<u>Element</u>							
Ca	-	-	-	-	-	-	A
Fe	-	-	-	-	-	-	-
K	-	-	-	-	-	-	-
As	0.001	0.001	0.001	0.001	0.001	0.001	0.001
Ba	0.100	0.120	0.183	0.150	0.090	0.113	A
Ce	0.071	0.013	0.001	0.004	0.002	0.001	A
Cr	-	-	-	-	-	-	-
Cu	0.010	0.001	0.009	0.008	0.014	0.009	-
La	-	-	-	-	-	-	-
Mn	0.001	0.001	0.001	0.001	0.001	0.067	A
Mo	0.001	0.005	0.005	0.005	0.005	0.005	0.005
Nb	-	-	-	-	-	-	-
Nd	-	-	-	-	-	-	-
Ni	-	-	-	-	-	-	-
Pb	-	-	-	-	-	-	-
Rb	A	0.006	0.016	0.012	0.015	0.010	0.005
Se	0.040	0.001	0.001	0.001	0.001	0.001	0.001
Sr	0.029	0.047	0.002	0.031	0.026	0.037	0.090
Ta	0.002	0.001	0.001	0.001	0.001	0.001	0.001
Th	0.008	0.-03	0.003	0.003	0.002	0.001	0.001
Ti	0.233	0.257	0.404	0.298	0.221	0.197	A
U	A	0.121	0.005	0.005	0.005	0.005	0.005
V	A	0.014	0.015	0.017	0.010	0.006	A
Y	A	0.011	0.003	0.002	0.002	0.002	0.001
Yb	0.032	0.042	0.032	0.071	0.014	0.023	0.010
Zn	-	-	-	-	-	-	-
Zr	0.041	0.054	0.080	0.046	0.012	0.040	0.012

Table 9 (cont'd)
XRF Data (ppm except where noted)

Sample:	SM 15-48	SM 15-48	SM 15-48	SM 15-48	SM 15-48	SM 15-48	SM 15-48
Depth	2591.0-	2618.5-	2626.0-	2637.0-	2654.0-	2666.3-	2670.0-
Interval:	2592.1	2619.0	2627.0	2638.0	2655.0	2666.5	2670.5
<u>Element</u>							
Ca	-	-	-	-	-	-	-
Fe	-	-	-	-	-	-	-
K	-	-	-	-	-	-	-
As	0.001	0.001	0.001	0.001	0.001	0.001	0.001
Ba	0.084	0.081	0.135	0.080	0.071	0.096	0.057
Ce	0.005	0.001	0.006	0.001	0.001	0.017	0.002
Cr	-	-	-	-	-	-	-
Cu	0.010	0.012	0.004	-	0.001	-	0.007
La	-	-	-	-	-	-	-
Mn	0.001	0.001	0.001	0.001	0.011	0.001	0.001
Mo	0.005	0.005	0.008	0.006	0.005	0.006	0.007
Nb	-	-	-	-	-	-	-
Nd	-	-	-	-	-	-	-
Ni	-	-	-	-	-	-	-
Pb	-	-	-	-	-	-	-
Rb	0.013	0.016	0.015	0.016	0.010	0.018	0.014
Se	0.001	0.001	0.001	0.001	0.001	0.001	0.001
Sr	0.045	0.043	0.038	0.037	0.039	0.038	0.034
Ta	0.001	0.001	0.001	0.001	0.001	0.001	0.001
Th	0.004	0.005	0.002	0.003	0.001	0.006	0.006
Ti	0.148	0.009	0.012	0.009	0.008	0.012	0.008
U	0.005	0.005	0.007	0.006	0.005	0.005	0.005
V	0.012	0.018	0.020	0.016	0.010	0.038	0.010
Y	0.002	0.002	0.002	0.002	0.002	0.002	0.002
Yb	0.061	0.084	0.095	0.073	0.019	0.096	0.140
Zn	-	-	-	-	-	-	-
Zr	0.034	0.030	0.035	0.031	0.032	0.028	0.030

Table 9 (cont'd)
XRF Data (ppm except where noted)

Sample:	SM 22-14	SM 22-14	SM 22-14	SM 22-14	SM 22-14	SM 22-14	SM 22-14
Depth	2627.0-	2645.0-	2651.0-	2655.0-	2660.0-	2672.5-	2673.0-
Interval:	2628.0	2646.0	2652.0	2656.0	2661.0	2673.0	2673.5
<u>Element</u>							
Ca	-	-	-	-	-	-	-
Fe	-	-	-	-	-	-	-
K	-	-	-	-	-	-	-
As	0.001	0.001	0.001	0.004	0.001	0.001	0.001
Ba	0.104	0.128	0.121	3.500	0.110	0.270	2.200
Ce	0.105	0.011	0.011	0.019	0.016	0.001	0.018
Cr	-	-	-	-	-	-	-
Cu	0.009	0.005	0.008	0.001	0.001	0.001	0.001
La	-	-	-	-	-	-	-
Mn	0.001	0.001	0.001	0.045	0.084	0.044	0.040
Mo	0.005	0.005	0.005	0.017	0.002	0.002	0.004
Nb	-	-	-	0.004	0.003	0.002	0.001
Nd	-	-	-	-	-	-	-
Ni	-	-	-	-	0.001	0.001	0.001
Pb	-	-	-	-	-	-	-
Rb	0.015	0.016	0.015	0.011	0.011	0.005	0.008
Se	0.001	0.001	0.001	0.021	0.001	0.006	0.001
Sr	0.142	0.038	0.067	0.017	0.019	0.040	0.066
Ta	0.001	0.001	0.001	0.009	0.001	0.001	0.001
Th	0.004	0.002	0.003	0.003	0.001	0.001	0.001
Ti	0.010	0.012	0.012	0.400	0.096	0.039	0.310
U	0.005	0.005	0.005	0.056	0.010	0.015	0.001
V	0.012	0.017	0.014	0.001	0.001	0.001	0.001
Y	0.003	0.002	0.003	0.001	0.001	0.003	0.002
Yb	0.010	0.029	0.010	0.060	0.010	0.001	0.001
Zn	-	-	-	-	-	-	-
Zr	0.088	0.046	0.070	0.012	0.014	0.027	0.084

Table 9 (cont'd)
XRF Data (ppm except where noted)

Sample:	SM 22-15	SM 22-15	SM 22-15	SM 23-15	SM 23-15	SM 23-15
Depth	2635.0-	2658.0-	2679.0-	2804.0-	2809.0-	2815.0-
Interval:	2636.0	2659.0	2680.0	2805.0	2810.0	2816.0
<u>Element</u>						
Ca	-	-	-	-	-	-
Fe	-	-	-	-	-	-
K	-	-	-	-	-	-
As	0.001	0.005	0.001	0.001	0.001	0.001
Ba	0.042	0.089	0.100	0.065	0.120	0.090
Ce	0.016	0.001	0.014	0.015	0.001	0.017
Cr	-	-	-	-	-	-
Cu	0.001	0.001	0.001	0.001	0.001	0.001
La	-	-	-	-	-	-
Mn	0.001	0.037	0.020	0.030	0.014	0.028
Mo	0.012	0.110	0.003	0.004	0.003	0.004
Nb	0.005	0.010	0.001	0.010	0.003	0.005
Nd	-	-	-	-	-	-
Ni	0.001	0.001	0.001	0.001	0.002	0.001
Pb	-	-	-	-	-	-
Rb	0.006	0.009	0.010	0.007	0.010	0.014
Se	0.007	0.004	0.001	0.005	0.014	0.010
Sr	0.014	0.020	0.015	0.017	0.056	0.016
Ta	0.001	0.001	0.001	0.009	0.003	0.008
Th	0.001	0.005	0.001	0.001	0.001	0.001
Ti	0.290	0.180	0.100	0.410	0.130	0.210
U	0.018	0.011	0.010	0.010	0.600	0.010
V	0.010	0.001	0.069	0.020	0.001	0.011
Y	0.001	0.003	0.002	0.002	0.002	0.002
Yb	0.200	0.010	0.200	1.000	1.000	0.080
Zn	-	-	-	-	-	-
Zr	0.018	0.029	0.015	0.022	0.038	0.018

Table 10

Lithology of Samples Analyzed by XRF

<u>Drill Hole</u>	<u>Interval</u>	<u>Description</u>
SM 13-53	3304.0-3305.0	Shale, light green, laminated
SM 13-53	3305.0-3306.0	Silty shale, light green with red mottling
SM 13-53	3306.0-3307.0	Shale, reddish brown and silty shale, light green, trace calcite and limonite
SM 13-53	3307.0-3308.0	Sandy shale, reddish brown, trace light green shale galls
SM 13-53	3308.0-3309.0	Sandy shale, light green, trace gray clay galls
SM 13-53	3311.0-3312.0	Sandy shale, light green, trace gray clay galls
SM 13-53	3344.0-3345.0	Sandstone, medium to coarse grained, gray, trace light green clay, kaolinite, green clay galls
SM 13-53	3345.0-3346.0	Sandstone, medium to coarse grained, gray, trace light green clay, kaolinite, green clay galls
SM 13-53	3346.0-3347.0	Sandstone, medium to coarse grained, gray, trace light green clay, kaolinite, light green clay galls
SM 13-53	3347.0-3348.0	Sandstone, medium to coarse grained, gray, trace light green clay, kaolinite, green clay galls
SM 13-53	3348.0-3349.0	Sandstone, medium to fine grained, gray, trace feldspar, kaolinite, magnetite(?)
SM 13-53	3349.0-3350.0	Sandstone, medium to coarse grained, trace feldspar, green clay, kaolinite
SM 13-53	3350.0-3351.0	Sandstone, medium to fine grained, gray, trace feldspar, abundant kaolinite
SM 13-53	3351.0-3352.0	Sandstone, medium to fine grained, gray, trace feldspar, abundant kaolinite
SM 13-53	3352.0-3353.0	Sandstone, medium to fine grained, gray, trace feldspar, abundant kaolinite
SM 13-53	3353.0-3354.0	Sandstone, medium to fine grained, gray, trace feldspar, abundant kaolinite
SM 13-53	3354.0-3355.0	Sandstone, medium to fine grained, gray, trace feldspar, abundant kaolinite
SM 13-53	3355.0-3356.0	Sandstone, medium to coarse grained, trace feldspar, kaolinite, green clay galls
SM 13-53	3356.0-3357.0	Sandstone, medium grained, gray, trace feldspar and kaolinite
SM 13-53	3357.0-3358.0	Sandstone, medium to coarse grained, gray with green shale galls, trace feldspar and kaolinite
SM 13-53	3358.0-3359.0	Sandstone, medium to coarse grained, gray, trace feldspar and kaolinite, abundant green shale galls
SM 13-53	3359.0-3360.0	Sandstone, fine to very fine grained, light gray, trace feldspar and kaolinite
SM 13-53	3361.0-3362.0	Sandstone, medium to fine grained, gray, trace feldspar, pyrite, carbon frags
SM 13-53	3554.0-3455.0	Sandstone, medium to fine grained, gray, trace carbon, limonite, kaolinite, abundant green shale galls

<u>Drill Hole</u>	<u>Interval</u>	<u>Description</u>
SM 13-53	3455.0-3456.0	Sandstone, medium to fine grained, gray, trace carbon, limonite, kaolinite, abundant green shale galls
SM 13-53	3456.0-3457.0	Sandstone, medium to fine grained, gray, trace carbon and feldspar, abundant kaolinite
SM 13-53	3457.0-3458.0	Sandstone, medium to fine grained, gray, trace carbon and feldspar, abundant kaolinite
SM 13-53	3458.0-3459.0	Sandstone, medium to fine grained, gray, trace carbon, feldspar, pyrite, kaolinite, uranium(?)
SM 13-53	3459.0-3460.0	Sandstone, medium to fine grained, gray, trace carbon, feldspar, pyrite, kaolinite, uranium(?)
SM 13-53	3460.0-3461.0	Sandstone, medium to fine grained, gray, trace carbon, feldspar, pyrite, kaolinite
SM 13-53	3461.0-3463.0	Sandstone, medium to fine grained, gray, trace carbon, feldspar, pyrite, kaolinite
SM 13-53	3463.0-3464.0	Sandstone, medium to fine grained, gray, trace carbon, feldspar, pyrite, kaolinite
SM 13-53	3464.0-3465.0	Sandstone, medium to coarse, gray, trace feldspar, pyrite, kaolinite, and green shale partings
SM 13-53	3465.0-3466.0	Sandstone, medium to fine grained, black, abundant carbon films, pyrite, and light green shale partings and galls
SM 13-53	3466.0-3467.0	Sandstone, fine to silty, gray, trace feldspar, kaolinite, pyrite, and light green shale partings
SM 13-53	3467.0-3468.0	Sandstone, fine to silty gray, trace feldspar kaolinite, pyrite, and light green shale partings
SM 13-53	3468.0-3469.0	Sandstone, medium to coarse grained, gray, abundant kaolinite, light green shale partings, and bands of carbonaceous material
SM 13-53	3469.0-3470.0	Sandstone, medium to fine grained, gray, trace feldspar, kaolinite, carbon, uranium
SM 13-53	3470.0-3471.0	Sandstone, medium to fine grained, gray, trace feldspar, kaolinite, carbon, uranium
SM 13-53	3471.0-3472.0	Sandstone, medium to fine grained, gray, trace feldspar, kaolinite, carbon, uranium
SM 14-38	2805.0-2806.0	Sandstone, medium to fine, gray, trace feldspar, mafics, green clay galls
SM 14-38	2806.0-2807.0	Shale, light green, finely laminated
SM 14-38	2807.0-2808.0	Sandy shale, greenish gray
SM 14-38	2808.0-2809.0	Sandy shale, greenish gray
SM 14-38	2809.0-2810.0	Silty shale, light green
SM 14-38	2829.0-2830.0	Sandstone, medium to fine to coarse grained, trace feldspar, kaolinite, light green clay lenses
SM 14-38	2830.0-2831.0	Sandstone, medium to fine to coarse grained, trace feldspar, kaolinite, light green clay lenses

<u>Drill Hole</u>	<u>Interval</u>	<u>Description</u>
SM 14-38	2831.0-2832.0	Sandstone, medium to fine to coarse grained, trace feldspar, kaolinite, light green clay lenses
SM 14-38	2832.0-2833.0	Sandstone, medium to fine to coarse grained, trace feldspar, kaolinite, light green clay lenses
SM 14-38	2833.0-2834.0	Sandstone, medium to fine to coarse grained, trace feldspar, kaolinite, light green clay lenses
SM 14-38	2834.0-2835.0	Sandstone, medium to fine grained, dark gray, trace kaolinite, feldspar, carbonaceous streaks
SM 14-38	2835.0-2836.0	Sandstone, medium to fine grained, dark gray, trace feldspar, kaolinite, carbon, abundant light green shale lenses
SM 14-38	2836.0-2837.0	Sandstone, medium to fine to coarse grained, dark gray, trace feldspar, kaolinite, carbon, abundant light green shale lenses
SM 14-38	2837.0-2838.0	Sandstone, medium to fine grained, gray, trace feldspar, kaolinite, carbon
SM 14-38	2838.0-2839.0	Sandstone, medium to fine grained, gray, trace feldspar, kaolinite, carbon
SM 14-38	2839.0-2840.0	Sandstone, fine to medium grained, gray, trace feldspar and light green shale lenses
SM 14-38	2840.0-2841.0	Sandstone, medium to fine grained, gray, bedded with coarse sands and light green shales, trace feldspar and kaolinite
SM 14-38	2841.0-2842.0	Sandstone, medium to fine grained, gray, bedded with coarse sands and light green shales, trace feldspar and kaolinite
SM 14-38	2842.0-2843.0	Sandstone, medium to fine grained, gray, bedded with coarse sands and light green shales, trace feldspar and kaolinite
SM 14-38	2843.0-2844.0	Sandstone, medium to fine grained, dark gray, trace kaolinite and carbon
SM 14-38	2844.0-2845.0	Sandstone, medium to fine grained, dark gray, trace kaolinite and carbon
SM 14-38	2845.0-2846.0	Sandstone, medium to fine grained, dark gray, trace kaolinite and carbon
SM 14-38	2846.0-2847.0	Sandstone, medium to fine grained, gray, trace feldspar, kaolinite, mafics
SM 14-38	2847.0-2848.0	Sandstone, medium to fine grained, gray, trace feldspar, kaolinite, mafics
SM 14-38	2848.0-2849.0	Sandstone, medium to fine grained, gray, trace feldspar, kaolinite, mafics
SM 14-38	2945.0-2946.0	Sandstone, medium grained, grayish green, trace feldspar, kaolinite, montmorillinite
SM 14-38	2946.0-2947.0	Sandstone, medium grain, grayish green, trace feldspar, kaolinite, montmorillinite

<u>Drill Hole</u>	<u>Interval</u>	<u>Description</u>
SM 14-38	2947.0-2948.0	Shale, light green, laminated
SM 14-38	2948.0-2949.0	Shale, light green, laminated
SM 14-38	2949.0-2950.0	Shale, light green, laminated
SM 14-38	2950.0-2951.0	Sandstone, medium to fine grained, grayish green, trace feldspar, kaolinite, montmorillinite
SM 14-38	2951.0-2952.0	Sandstone, medium to fine grained, grayish green, trace feldspar, kaolinite, montmorillinite
SM 14-38	2952.0-2953.0	Sandstone, medium to fine grained, grayish green, trace feldspar, kaolinite, montmorillinite
SM 14-38	2953.0-2954.0	Sandstone, medium to fine grained, grayish green, trace feldspar, kaolinite, montmorillinite
SM 14-38	2954.0-2955.0	Sandstone, medium to fine grained, grayish green, trace feldspar, kaolinite, montmorillinite
SM 14-38	2955.0-2956.0	Sandstone, medium to fine grained, grayish green, trace feldspar, kaolinite, montmorillinite
SM 14-38	2956.0-2957.0	Sandstone, medium to fine grained, grayish green, trace feldspar, kaolinite, montmorillinite
SM 14-38	2957.0-2958.0	Sandstone, medium to fine grained, grayish green, trace feldspar, kaolinite, montmorillinite
SM 14-38	2958.0-2959.0	Sandstone, medium to fine grained, grayish green, trace feldspar, kaolinite, montmorillinite
SM 14-38	2959.0-2960.0	Sandstone, medium to fine grained, grayish green, trace feldspar, kaolinite, montmorillinite
SM 14-38	2960.0-2961.0	Sandstone, medium to fine grained, grayish green, trace feldspar, kaolinite, montmorillinite
SM 15-24	2594.0-2595.0	Sandstone, fine grained, light gray, trace feldspar, carbon, pyrite and kaolinite
SM 15-24	2608.5-2609.0	Sandstone, fine grained, yellowish gray to dark greenish gray, trace feldspar, carbon, kaolinite and pyrite
SM 15-24	2611.0-2612.0	Sandstone, medium grained, pinkish gray, trace feldspar, carbon and kaolinite
SM 15-25	2596.0-2597.0	Siltstone, grayish yellow green
SM 15-25	2604.5-2605.0	Sandstone, coarse, greenish black, trace feldspar, kaolinite and carbon
SM 15-25	2609.0-2610.0	Sandstone, fine grained, light brownish gray to yellowish gray, trace feldspar and carbon

<u>Drill Hole</u>	<u>Interval</u>	<u>Description</u>
SM 15-25	2610.5-2611.0	Thucolite (?), grayish black
SM 15-25	2627.0-2628.0	Sandstone, coarse grained, yellowish gray, trace feldspar, kaolinite and carbon
SM 15-25	2632.5-2632.8	Sandstone, medium to coarse grained, light gray, trace kaolinite, carbon and feldspar
SM 15-28	2650.0-2651.0	Sandstone, very coarse, poorly sorted, light gray, trace feldspar, kaolinite, carbon, mica
SM 15-28	2674.0-2675.0	Sandstone, fine grained, light gray, trace feldspar, kaolinite and hematite
SM 15-28	2684.0-2685.0	Siltstone, yellowish gray, trace feldspar, kaolinite and carbon
SM 15-31	2763-2764.0	Sandstone, medium grained, light gray, trace feldspar and carbon
SM 15-31	2810.0-2811.0	Siltstone, brownish gray, trace kaolinite and hematite
SM 15-31	2840.0-2841.0	Siltstone, dusky yellow, abundant hematite
SM 15-31	2868.0-2869.0	Siltstone, greenish gray, questionable U mineralization
SM 15-31	2869.0-2870.0	Sandstone, fine grained, very light gray, trace feldspar, kaolinite and carbon
SM 15-36	2576.0-2577.0	Sandstone, very coarse, light olive gray, trace feldspar, hematite and carbon
SM 15-36	2585.0-2586.0	Sandstone, medium grained, pinkish gray, trace feldspar and carbon
SM 15-36	2588.5-2589.0	Sandstone, coarse to very coarse, medium dark gray to dark gray, trace feldspar and carbon
SM 15-36	2590.0-2591.0	Mudstone, greenish gray
SM 15-36	2597.0-2597.5	Siltstone, greenish gray with brownish gray
SM 15-43	2564.0-2565.0	Mudstone, brownish gray
SM 15-43	2582.0-2583.0	Sandstone, medium grained, greenish gray, trace feldspar and carbon
SM 15-43	2592.9-2593.4	Interbedded mudstones and coarse sandstones, dark gray and dark greenish gray, trace feldspar and carbon
SM 15-43	2593.5-2594.0	Sandstone, fine grained, medium light gray, trace feldspar and carbon
SM 15-43	2605.0-2606.0	Sandstone, fine grained, light gray, trace feldspar and carbon
SM 15-43	2611.5-2612.0	Siltstone to fine grained sandstone, graded, light gray, trace feldspar, hematite, carbon and questionable U mineralization
SM 15-43	2635.0-2636.0	Siltstone, dark greenish gray with brownish gray, coloring is irregular in distribution
SM 15-43	2641.0-2641.4	Sandstone, very fine grained, greenish gray, trace feldspar and carbon
SM 15-48	2582.0-2583.0	Siltstone, pale yellowish green, trace pyrite
SM 15-48	2591.0-2592.1	Sandstone, medium grained, greenish gray, trace carbon
SM 15-48	2618.5-2619.0	Sandstone, medium grained, light olive gray, trace carbon, feldspar, hematite

<u>Drill Hole</u>	<u>Interval</u>	<u>Description</u>
SM 15-48	2626.0-2627.0	Sandstone, medium to coarse grained, greenish gray, trace carbon and feldspar
SM 15-48	2637.0-2638.0	Sandstone, medium grained, greenish gray, trace carbon and feldspar
SM 15-48	2654.0-2655.0	Sandstone, fine grained, mottled-greenish gray and light brownish gray, trace feldspar, carbon, hematite
SM 15-48	2666.3-2666.5	Pebbly sand, light olive gray, trace feldspar, hematite, bornite, chalcopyrite
SM 15-48	2670.0-2670.5	Sandstone, very coarse, light olive gray, trace feldspar, carbon, abundant hematite
SM 22-14	2627.0-2628.0	Mudstone, greenish gray, abundant montmorillonite
SM 22-14	2645.0-2646.0	Siltstone, very light gray, trace feldspar, carbon and hematite
SM 22-14	2651.0-2652.0	Siltstone, very light gray to light brownish gray, trace feldspar and carbon
SM 22-14	2655.0-2656.0	Sandstone, light gray, medium grained, well sorted, traces of kaolinite and carbon
SM 22-14	2660.0-2661.0	Sandstone, coarse and conglomeratic, light gray, traces of kaolinite and carbon
SM 22-14	2672.5-2673.0	Sandstone, light gray, medium to fine grained, fair sorting, trace kaolinite, carbon, hematite
SM 22-14	2673.0-2673.5	Siltstone, light gray to pale reddish purple, trace feldspar and hematite
SM 22-15	2635.0-2636.0	Mudstone, brownish gray and very light gray, abundant montmorillonite
SM 22-15	2658.0-2659.0	Sandstone, medium to fine grained, yellowish gray, trace kaolinite and feldspar
SM 22-15	2679.0-2680.0	Sandstone, medium to coarse grained, grayish black, trace feldspar, carbon, pyrite and kaolinite
SM 23-15	2804.0-2805.0	Silty mudstone, greenish gray, trace pyrite
SM 23-15	2809.0-2810.0	Sandstone, coarse, light olive gray, trace pyrite and feldspar
SM 23-15	2815.0-2816.0	Sandstone, medium grained, light gray, trace feldspar and carbon
HU 22-3-1	3640.0-3640.5	Sandstone, medium to coarse grained, light gray, trace feldspar
HU 22-3-1	3650.0-3650.5	Silty sandstone, medium brown, trace feldspar
HU 22-3-1	3670.0-3670.5	Shale, light green
HU 22-3-1	3680.0-3680.5	Shale, medium brown
HU 22-3-1	3690.0-3690.5	Shale, light green
HU 22-3-1	3695.0-3695.5	Sandstone, fine grained, light gray
HU 22-3-1	3700.0-3700.5	Shale, light green
HU 22-3-1	3705.0-3705.5	Sandstone, medium green, gray, trace feldspar
HU 22-3-1	3710.0-3710.5	Sandstone, silty to fine grained, light gray, trace feldspar and pyrite
HU 22-3-1	3715.0-3715.5	Sandstone, silty to fine grained, light gray, trace feldspar and pyrite

<u>Drill Hole</u>	<u>Interval</u>	<u>Description</u>
HU 22-3-1	3719.5-3720.0	Sandstone, silty to fine grained, light gray, trace feldspar and pyrite
HU 22-3-1	3724.5-3725.0	Sandstone, silty to fine grained, light gray, trace feldspar and pyrite
HU 22-3-1D	3710.0-3710.5	Sandstone, silty to fine grained, light gray, trace feldspar and pyrite
HU 22-3-1D	3716.0-3716.5	Sandstone, silty to fine grained, light gray, trace feldspar and pyrite
HU 22-3-1D	3720.0-3720.5	Sandstone, silty to fine grained, light gray, trace feldspar and pyrite
HU 22-3-1D	3730.0-3730.5	Sandstone, coarse to very coarse grained, light gray, trace feldspar and pyrite
HU 22-3-1D	3735.0-3735.5	Sandstone, fine grained, gray, trace feldspar and pyrite
HU 22-3-1D	3739.5-3740.0	Sandstone, coarse to very coarse grained, light gray, trace feldspar and pyrite
HU 22-3-1D	3745.5-3746.0	Sandstone, coarse to very coarse grained, light grayish brown, trace feldspar and pyrite
HU 22-3-2D	3705.0-3705.5	Shale, light green
HU 22-3-2D	3710.0-3710.5	Shale, light green
HU 22-3-2D	3715.0-3715.5	Shale, light green
HU 22-3-2D	2719.0-2719.5	Shale, light green
HU 22-3-2D	3725.0-3725.5	Sandstone, medium grained, light brown, trace feldspar and pyrite
HU 22-3-2D	3730.0-3730.5	Sandstone, medium to coarse grained, light grayish brown, trace feldspar and pyrite
HU 22-3-2D	3739.5-3740.0	Shale, light green
HU 22-3-2D	3744.5-3745.0	Sandstone, medium to coarse grained, black, trace feldspar, pyrite, and organics
HU 22-3-2D	3749.5-3750.0	Sandstone, fine to medium grained, dark gray, trace feldspar, pyrite, and organics
HU 22-3-2D	3754.5-3755.0	Sandstone, coarse to very coarse grained, medium brown, trace feldspar, pyrite, organics
HU 22-3-2D	3759.5-3760.0	Sandstone, medium to coarse grained, dark gray, trace feldspar, pyrite, organics
HU 22-3-3D	3790.0-3790.5	Shale, light green
HU 22-3-3D	3795.0-3795.5	Sandstone, fine grained, light brown
HU 22-3-3D	3799.5-3800.0	Sandstone, medium to coarse grained, medium brown, trace feldspar, pyrite, organics
HU 22-3-3D	3805.0-3805.5	Sandstone, fine to medium grained, light brown, trace feldspar, pyrite, organics
HU 22-3-3D	3809.5-3810.0	Sandstone, fine grained, gray, trace feldspar, pyrite, organics
HU 22-3-3D	3814.5-3815.0	Sandstone, medium to coarse grained, dark gray, trace feldspar, pyrite, organics

<u>Drill Hole</u>	<u>Interval</u>	<u>Description</u>
HU 22-3-3D	3819.5-3820.0	Sandstone, fine to medium grained, dark gray, trace feldspar, pyrite, organics
HU 22-3-3D	3825.0-3825.5	Sandstone, medium to coarse grained, gray, trace feldspar and organics
HU 22-3-3D	3829.5-3830.0	Sandstone, medium to coarse grained, brown, trace feldspar
HU 22-3-3D	3834.5-3835.0	Sandstone, medium to coarse grained, brown, trace feldspar
HU 22-3-4D	2805.0-3805.5	Sandstone, fine to medium grained, gray, trace feldspar
HU 22-3-4D	3809.5-3810.0	Sandstone, coarse to very coarse, grayish brown, trace feldspar
HU 22-3-4D	3814.5-3815.0	Sandstone, coarse, brown, trace feldspar
HU 22-3-4D	3819.5-3820.0	Sandstone, medium to coarse grained, light gray, trace feldspar
HU 22-3-4D	3825.0-3825.5	Sandstone, fine to medium grained, light brown, trace feldspar
HU 22-3-4D	3834.5-3835.0	Sandstone, medium to coarse grained, light brown, trace feldspar
HU 22-3-4D	3840.0-3840.5	Sandstone, medium to coarse grained, black, trace feldspar
HU 22-3-4D	3845.0-3845.5	Sandstone, medium to coarse grained, black, trace feldspar and organics
HU 22-3-4D	3850.0-3850.5	Sandstone, medium to coarse grained, black, trace feldspar and organics
HU 22-3-4D	3855.0-3855.5	Shale, light grayish green
HU 22-3-4D	3865.0-3865.5	Sandstone, silty, light gray
HU 22-3-4D	3868.0-3868.5	Sandstone, medium to coarse grained, light grayish brown
HU 22-3-4D	3870.0-3870.5	Sandstone, medium to coarse grained, light grayish brown, trace feldspar
HU 22-3-4D	3875.0-3875.5	Sandstone, medium to coarse grained, light grayish brown, trace feldspar
HU 22-3-4D	3880.0-3880.5	Sandy shale, light grayish green
HU 22-3-4D	3885.0-3885.5	Sandy shale, light grayish green
HU 22-3-4D	3890.0-3890.5	Sandy shale, light greenish gray
HU 22-3-4D	3895.0-3895.5	Shale, light green
HU 22-3-4D	3900.0-3900.5	Sandy shale, light gray
HU 22-3-4D	3915.0-3915.5	Sandstone, medium to coarse grained, light gray, trace feldspar
HU 22-3-4D	3925.0-3925.5	Sandstone, fine to medium grained, light gray, trace feldspar
HU 22-3-4D	3935.0-3935.5	Sandstone, medium grained, light gray
HU 22-3-4D	3945.0-3945.5	Sandstone, medium grained, light gray, trace feldspar

Chapter 4

Eh - pH Diagrams

Much attention has been given to Eh - pH diagrams in attempting to interpret the paragenesis of uranium deposits in recent years. The first rigorous attempt at explaining uranium minerals in sedimentary deposits was that by Hostetler and Garrels (1962) although coffinite was not included in their study due to lack of thermodynamic data. They did propose, however, that the uraninite-dissolved species and coffinite-dissolved species must be close to each other in Eh - pH space because of the common occurrence of both solid species. More recently Brookins (1976a) and Langmuir (1978) have presented revised Eh - pH diagrams (the former is shown as Figure 58). The value for ΔG_f° for coffinite, taken to be stoichiometric $USiO_4$, has always been problematic since measured values have been impossible to obtain to date. Brookins (1976b) estimated this value at -456 ± 5 kcal/mole using ΔG differences for $ThO_2-TH(OH)_4-ThSiO_4$ and $ZrO_2-Zr(OH)_4-ZrSiO_4$ to estimate the coffinite value since data are available for $UO_2-U(OH)_4$. The calculated value of -456 kcal/mole can be used in turn to estimate the ΔG_f° values for either zircon or thorite with a small uncertainty. It should be pointed out that Brookins' (1976b) estimate of the ΔG_f° for coffinite was not calculated assuming equilibrium conditions between UO_2 and $USiO_4$ in the presence of H_2O and dissolved silica which Langmuir (1978, p. 559) has indicated. Langmuir's (1978) estimate of ΔG_f° for coffinite based on UO_2-USiO_4 equilibrium in the presence of water and dissolved silica is -452 kcal/mole, a value within the stated limits of error (± 5 kcal) by Brookins (1976b). The point is well taken that this method of estimating the ΔG_f° for coffinite must be made in order to assess the coffinite-uraninite

problem. Further, in Langmuir's (1978) comprehensive treatment of uranium species, he presents diagrams (Figs. 12,13) based partly on the work of Nord (1977) who studied coffinite-uraninite in natural samples using the transmission electron microscope, electron microprobe and electron diffraction. Nord's (1977) study showed uraninite (determined to be $UO_{2.08}$) forming from coffinite in the absence of quartz.

For purposes of this report some reference framework assumptions concerning the important species Fe, CO_2 , S, and Si in the presence of water are necessary. In figure 57 is shown the Eh - pH diagram for some Fe species in the presence of sulfur. Total dissolved S is assumed to be 10^{-3} molal since higher amounts would extend the native sulfur field into the area designated U-ore, and native sulfur is not considered to be a primary phase in the Grants mineral belt deposits. The Fe-S-H-O diagram is greatly simplified. Dissolved Fe = 10^{-6} m. is assumed based on data from Phoenix (1959), CO_2 (which is taken to be approximately 10^{-2} from Phoenix's (1959) data) is not considered, and the field of magnetite (Fe_3O_4) is not shown. Omission of the magnetite field is not serious as the work of Lee (1976) has shown most (if not all?) magnetite to be detrital in the Grants mineral belt. Further, the magnetite field occurs at pH values greater than the upper limit for the area marked U-ore (see Garrels and Christ, 1965). The fact that this area slightly overlaps the pyrite-hematite boundary is based on the mineralogy of the deposits; the assemblage coffinite (less frequently uraninite)-pyrite is very common while coffinite-hematite is very much less common but nevertheless still noted.

In figure 58 is shown a composite diagram for U-Si-C-H-O-S; the boundary for $H_2S-SO_4^{2-}-HS^- -SO_4^{2-}$ is used for pyrite-hematite. The boundary between

reduced carbon (C) and oxidized carbon (H_2CO_3 , HCO_3^- , CO_3^{2-}) assumes total dissolved C = 10^{-2} . The importance of this boundary is severalfold. First, the boundary must be close to that for organic carbonaceous matter-calcite as both are observed in several deposits. Second, primary coffinite is intimately mixed with organic carbonaceous matter and calcite present may be the product of reactions controlled by U-C-organic acids (see discussion later in this report). Third, framboidal pyrite is often found in association with U-ore and organic carbonaceous matter. The U species of interest considered here are not as complete as those shown by Langmuir (1978). In figure 58, for example, no fields for $(\text{UO}_2(\text{CO}_3)_2)^0$ nor U_4O_9 are shown. Important dissolved species are considered to be: UO_2^{2+} , $\text{UO}_2(\text{CO}_3)_2 \cdot 2\text{H}_2\text{O}^{2-}$ (i.e., UDC), and $\text{UO}_2(\text{CO}_3)_3^{4-}$ (i.e., UTC) as well as a small field of U^{4+} . Fields for complexes U with P, S, Cl, etc., are not included and the reader is again referred to Langmuir (1978) for more detail. The main aqueous species of importance are taken as UDC and UTC as the pH range of interest is thought to be from about 6.5 to approximately 8.3. The positions of the boundaries between USiO_4 (for coffinite) or UO_2 (for uraninite) and aqueous species are different because of assumed activities of $\text{U} = 10^{-6}$ and $\text{H}_4\text{SiO}_4 = 10^{-6.9}$ (an hypothetical equilibrium value). Since most of the rocks are quartz saturated and some amorphous silica saturated, then $a_{\text{H}_4\text{SiO}_4} = 10^{-3.5}$ to $10^{-2.7}$ which will have the effect of bringing the coffinite-dissolved species and uraninite-dissolved species closer together. This certainly must be the case as, although coffinite is more common than uraninite in the Grants mineral belt, uraninite is noted from several deposits. Further, for reactions involving dissolved species in the absence of any dissolved silica (i.e., such as might be the case where organic matter, sulfur, iron

species only are involved) then U(IV) must precipitate as uraninite. Further, if one assumes the formula for pitchblende (i.e., not igneous uraninite) to be $UO_{2.6}$, then the coffinite-dissolved U species and pitchblende-dissolved U species are very nearly coincident. Finally, with reference to figure 58, one can state with any degree of confidence only that coffinite should be stable relative to stoichiometric UO_2 under quartz-saturated conditions but that since the organic matter-choked, grain rimming material is often cryptocrystalline to amorphous silica-deficient conditions might be quite easy to achieve in which case pitchblende will precipitate. The presence of both coffinite and pitchblende indicates this to be the case.

Eh - pH Diagrams for V, Mo, Se, As, Sb, REE

A characteristic of many sedimentary uranium deposits is the suite of metals present in trace quantities in most rocks which are concentrated along with uranium to an appreciable degree. Suggested transport of many of these metals as oxyanions allows them to be segregated from metals such as Th, Al, etc., which form insoluble hydroxides instead of soluble oxyanions. When conditions favorable for reduction of U(VI) to U(IV) occur, metals such as V, Mo, Se are also reduced and concentrated in the uranium deposits. While V, Mo and Se are the three most common trace metals commonly associated with sedimentary uranium deposits, our work (Brookins, 1976a; and this report) indicate significant concentrations of As, Sb and the rare earth elements (REE). It is likely that As and Sb are also transported as oxyanions and concentrated in sulfides when U reduction occurs. The REE, on the other hand, pose a different problem in that while enrichment of europium can readily be explained by reduction of Eu^{3+} to Eu^{2+} , the mechanism of transport of all the trivalent REE is not known. Based on our data (discussed

later) it is possible that the REE are derived from more local sources (i.e., Brushy Basin shale, etc.) than the U, V, Mo, Se, As, Sb suite which has probably been derived in large part from a more far-removed source. This will be discussed later.

The Eh - pH diagram for V species is shown as figure 59. In this diagram several assumptions need clarification. First, the work of many investigators (see Brookins, 1976b; Lee, 1976; Hostetler and Garrels, 1962) clearly shows the enrichment of V with U. When V/U is very high, V-minerals such as roscoelite may form; at lower V/U ratios the V may be incorporated into chlorite or other clay minerals formed as coffinite (or pitchblende) are forming. Lee's (1976) data clearly show this. For purposes of Eh - pH treatment, the more recent thermodynamic data summarized by Naumov and others (1974) have been used by Hem (1977) for aqueous species and LaPointe and Markos (1977) have constructed a diagram for roscoelite stability. For purposes more applicable to the Grants mineral belt, use of data for V_2O_3 for V(III) is justified since, analogous to $FeO(OH)-Fe_2O_3$, $VO(OH)$ must age to V_2O_3 quickly in terms of geologic time. Since V(III) is readily incorporated into the octahedral sites of clay minerals such as chlorite which otherwise do not usually contain appreciable amounts of M^{3+} ions (note: under reducing conditions most Fe is present as Fe^{2+} and chlorites assumed penecontemporaneous with coffinite are typically Mg-rich rather than Fe-rich), hence the field of V_2O_3 can be used to approximate not only $VO(OH)$, but, following the method of Tardy and Garrels (1974) for estimation of free energies of formation for layered silicates, this field will represent the approximate stability field for a vanadiferous chlorite in Eh - pH space. That the field of V_2O_3 encompasses the Eh - pH field marked U-ore (Figs. 57, 58) is consistent with observation which allows one to

predict that slightly vanadiferous clay minerals will be noted before the iron-controlled redox front is encountered. Of more importance is the fact that although many V(IV,V) species are shown in figure 59, all the ionic radii for V species are sufficiently small for retention in the octahedral sites of clay minerals. Thus when local oxidation occurs and U is remobilized, V will be remobilized only if the clay minerals hosting it are broken down as well. This allows potential for V as a pathfinder element which will be discussed later.

In figure 60 is shown the Eh - pH diagram for Se species. Howard (1977) has presented a much more comprehensive treatment of the problem of Se species and only a brief summary will be attempted here. When Se-oxyanions first start to encounter reducing conditions the stable phase under Fe-poor, S-poor conditions may well be native Se. Under more reducing conditions, and again dependent on the Fe-S budget, Se will be present as selenide ion either as ferroselite, FeSe_2 , or seleniferous pyrite, $\text{Fe}(\text{S},\text{Se})_2$. Based on figure 60 one can argue that a zonation of native Se - seleniferous pyrite - ferroselite may occur across U ore zones and indeed this is apparent in some Wyoming deposits, especially the enrichment of Se on the up-gradient side of U ore. Local oxidation of any seleniferous pyrite may result in a younger generation of native Se such as observed by Kendall (1971) for the Section 27 Mine, Grants mineral belt.

In figure 61 is shown the Eh - pH diagram for molybdenum. There exist many uncertainties in the thermodynamic data for Mo species; in fact the ΔG_f° for ilsemanite, Mo_3O_8 , is only available by calculation (Titley and Anthony, 1962). Recent calculations by the author (Brookins, unpub.) indicates that the Mo_3O_8 field disappears by 200°C which can, if primary

ilsemannite is advocated, be used as an upper limit on temperature of formation of the uranium deposits where this mineral occurs. Molybdenum-oxyanions such as HMO_4^- or MoO_4^{2-} will, from inspection of figures 57 and 58 persist to lower Eh values than the pyrite-hematite boundary. This allows prediction that Mo as MoS_2 (note: this compound in uranium deposits is often referred to as amorphous material known as jordisite; the work of Kendall, 1971, suggests that it may be cryptocrystalline molybdenite) will be concentrated on the down-gradient side of U-ore deposition sites such as noted in Wyoming (Harshman, 1970) and in some Russian deposits (Lisitsin, 1968). While a zoning of Se-U-Mo is noted on occasions in the Grants mineral belt (Kendall, 1971), the direction of such zonation is problematic and the topic for more discussion under paragenesis. At this point it is sufficient to again point out that although U, V, Se, Mo may be carried as oxyanions as a group, each will commonly be incorporated into different phases under reducing conditions. If, for example, very slight oxidation occurs, then V(III)-V(IV,V) and U(IV)-U(VI) and possibly Se(-II)-Se(0) may occur while Mo(IV) remains unoxidized. The result would be vanadiferous oxychlorite, native selenium, MoS_2 left in situ with U remobilized. This assemblage can easily be misinterpreted to mean lack of uranium in a larger system when in actuality it may merely be indicative of U remobilization to another favorable site.

Eh - pH diagrams for As, Sb and Eu and Sm are shown as figures 62 through 65. Not enough detail is known yet about detail of zonation of these elements across U ore. In the case of As (Fig. 62) it is probable that, under reducing conditions, As^{3+} can be easily incorporated into pyrite. AsS or As_2S_3 will form only in Fe-poor systems. Of interest is the small field of As_2O_3 which suggests, somewhat analogous to Se, that slight oxidation

might leave fingerprints of As in hematitic rocks when U(IV)-U(VI) oxidation occurs. Certainly this possibility should not be overlooked.

The behavior of antimony is somewhat easier to predict. Transport of Sb(III) as either SbO^+ or SbO_2^- on either side of the field for Sb_2O_3 depends on breakdown of Sb(V) (shown as Sb_2O_5). That such transport has occurred in the Grants mineral belt is suggested by the concentration of Sb with U when evidence for Sb camouflage in resistate minerals is lacking. Under pyrite-stable conditions Sb will easily substitute for Fe^{2+} in pyrite and, under more oxidizing conditions, Sb^{3+} for Fe^{3+} in hematite. Only under iron-poor conditions are stibnite or Sb_2O_3 likely. Antimony thus, like As and Se, may be useful as a pathfinder element for U.

The REE Eh - pH diagrams in general are simple in that all but Ce and Eu are commonly present as M^{3+} ions. Yet our data show enrichment of total REE and pronounced positive Eu anomalies. When a $\text{M}_2(\text{CO}_3)_3$ phase is considered (i.e., Fig. 65 for Sm) then the pH range is essentially identical to that for U-ore (Fig. 58). Data for $\text{Eu}_2(\text{CO}_3)_3$ are similar. Eu^{2+} must be enriched by oxidation to Eu^{3+} as oxidized samples of rocks above the Jurassic Westwater Canyon Member of the Morrison Formation (i.e., Cretaceous Dakota and Mancos Formations; Jurassic Brush Basin Member of the Morrison Formation) all show rather normal REE distribution patterns with negative Eu anomalies. This in turn implies that the REE, unlike the metals thought to be transported in as oxyanions (U, V, Se, Mo, As), may be more locally derived. However, as argued above, upon oxidation the total REE and positive Eu anomaly will be preserved in the oxidized rocks, probably in oxides or hydroxides (and possibly in carbonates).

FIGURES 57 - 65

Eh-pH Diagrams

Note: All diagrams constructed using 25°C, 1 atm. P data.

Figure 57
IRON - SULFUR

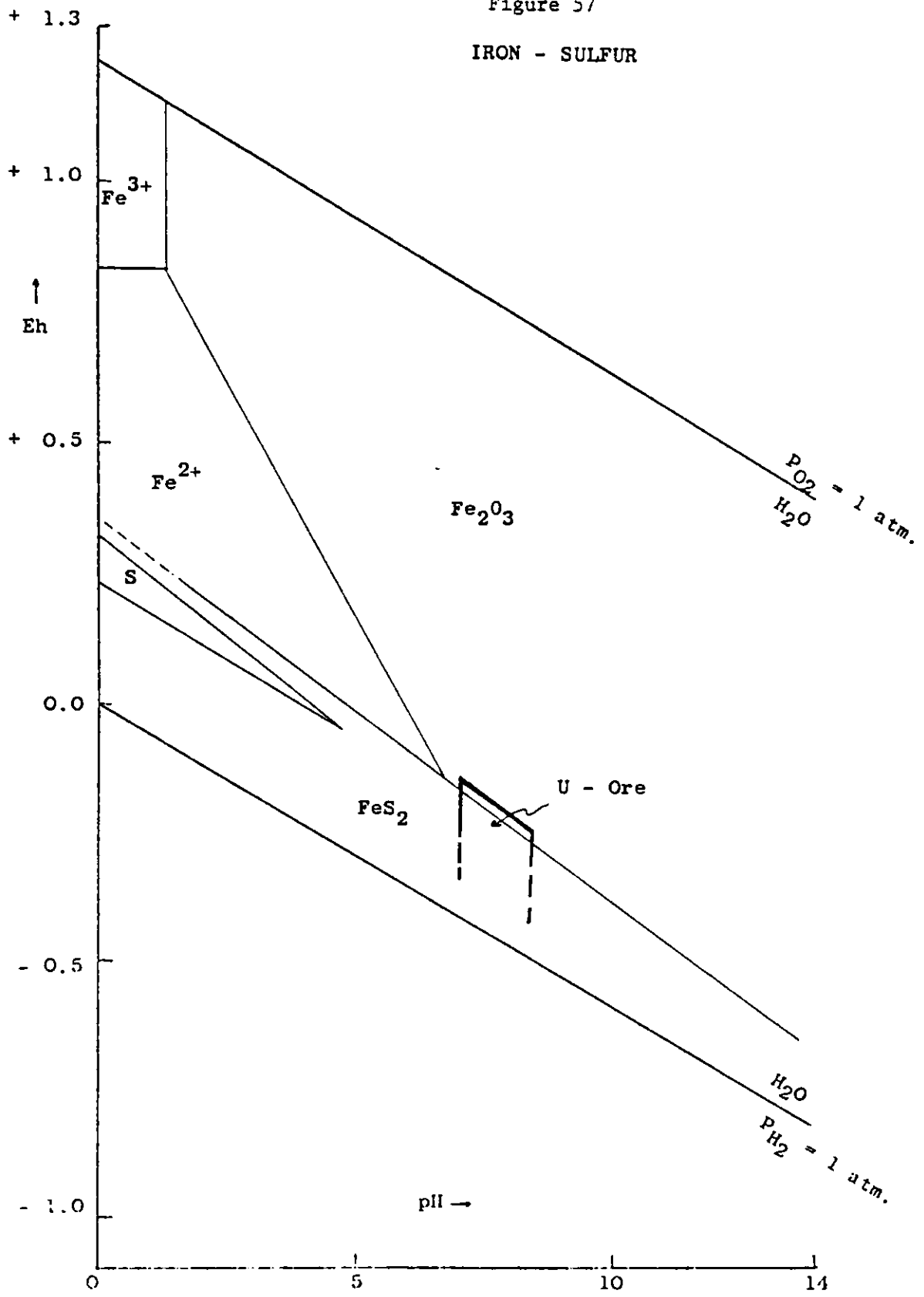


Figure 58

URANIUM - CARBON - SULFUR

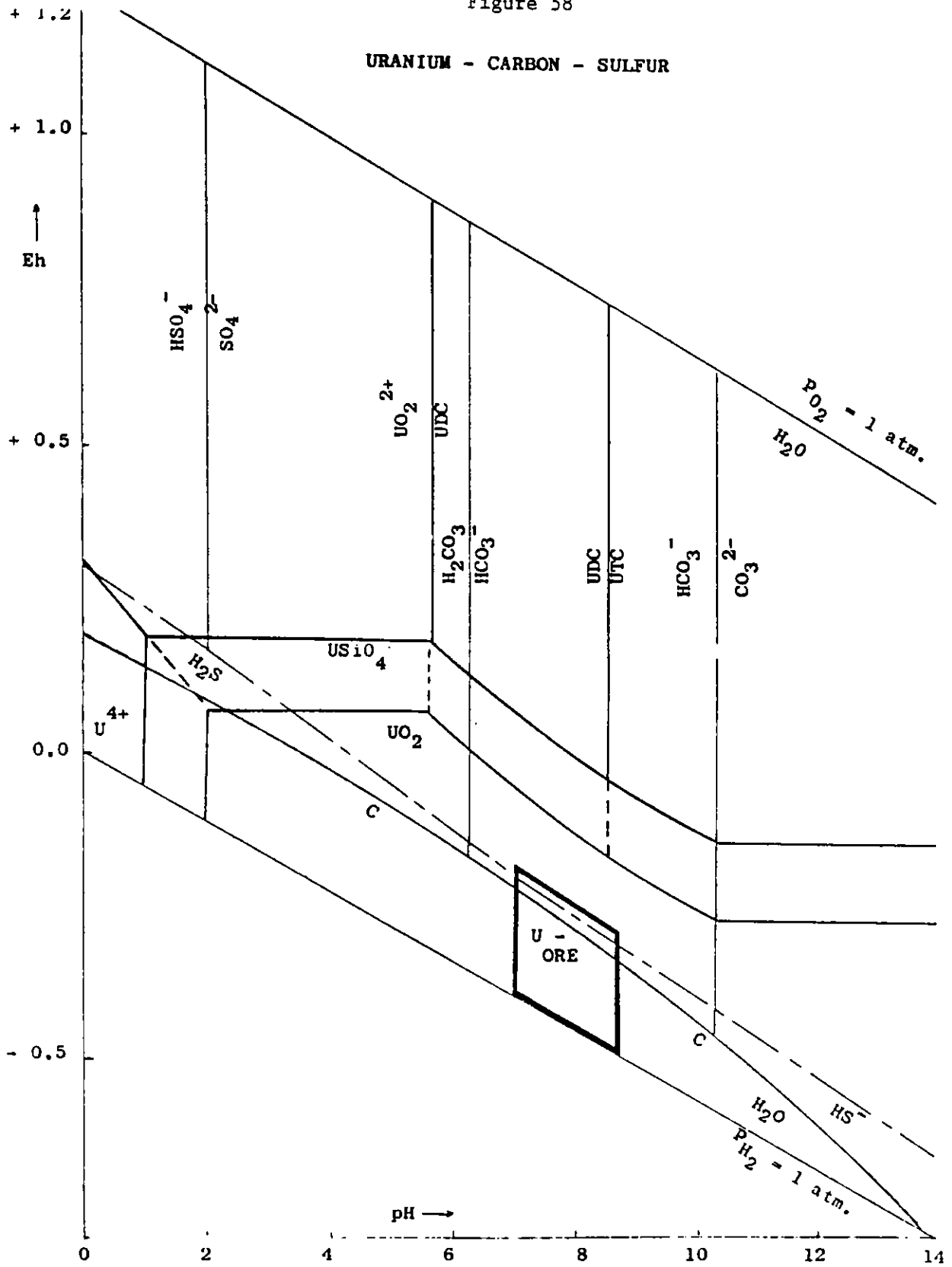


Figure 59

VANADIUM

Total V = 10^{-7} and 10^{-3}

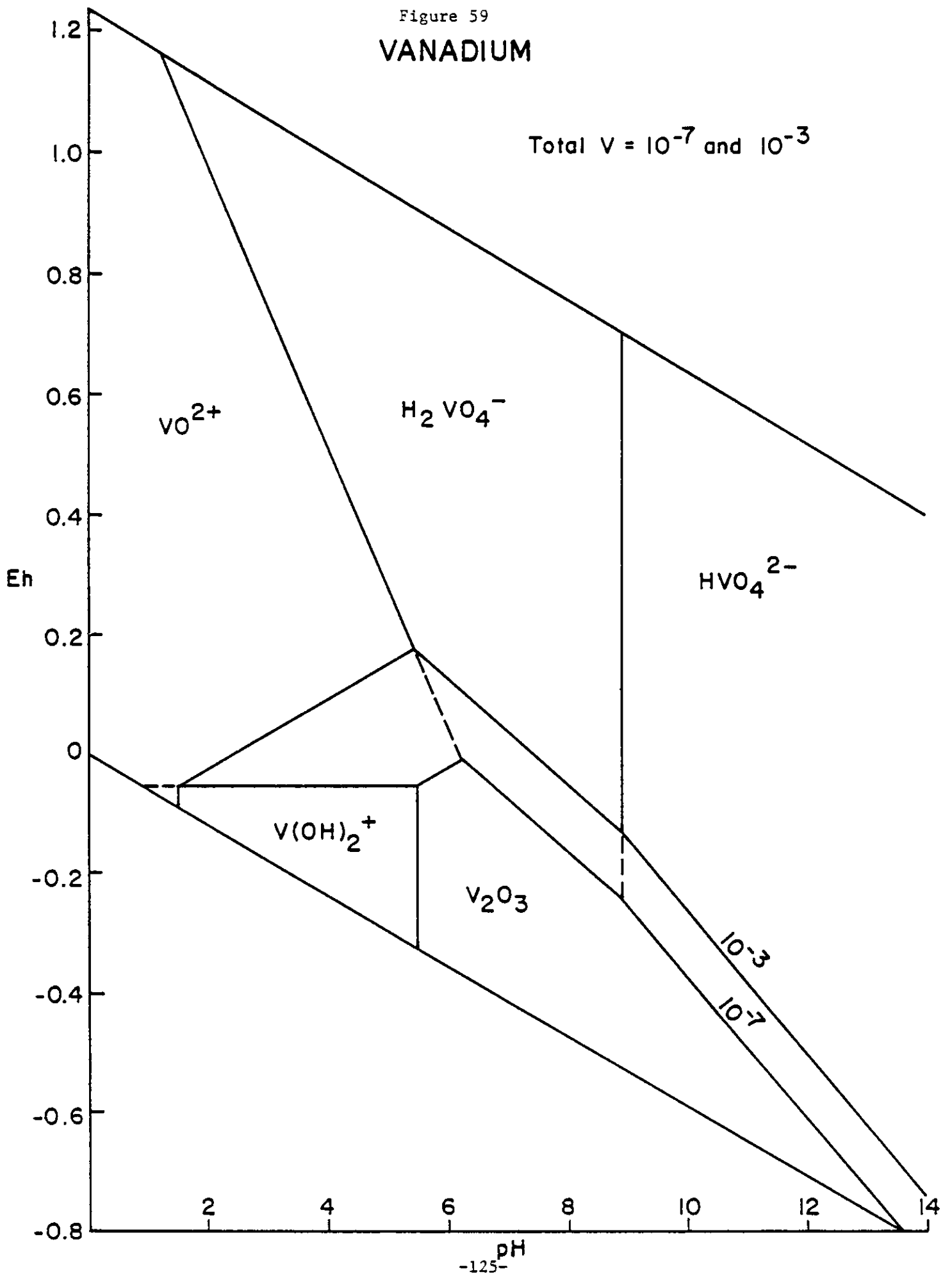


Figure 60

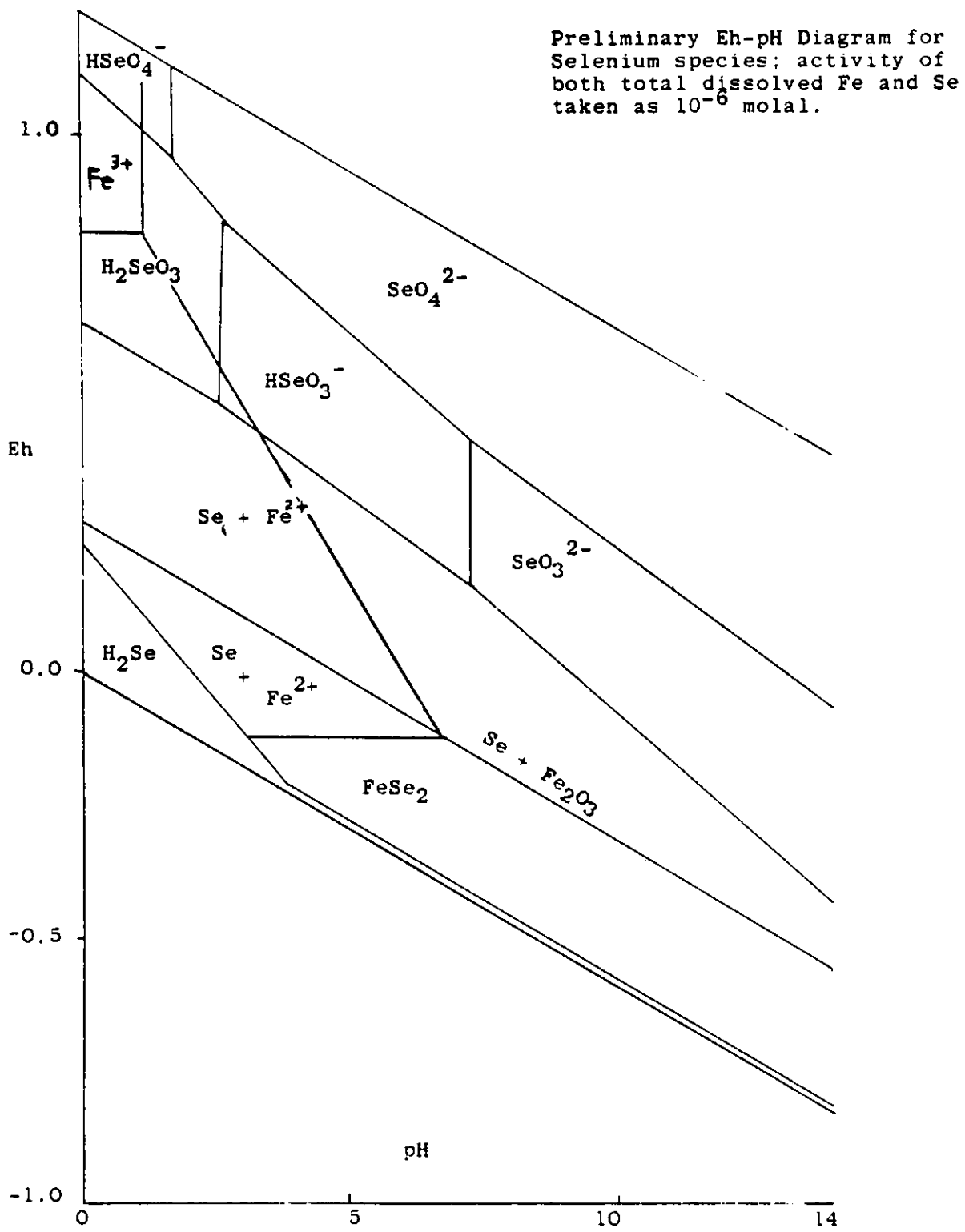


Figure 61

MOLYBDENUM - 25° C -

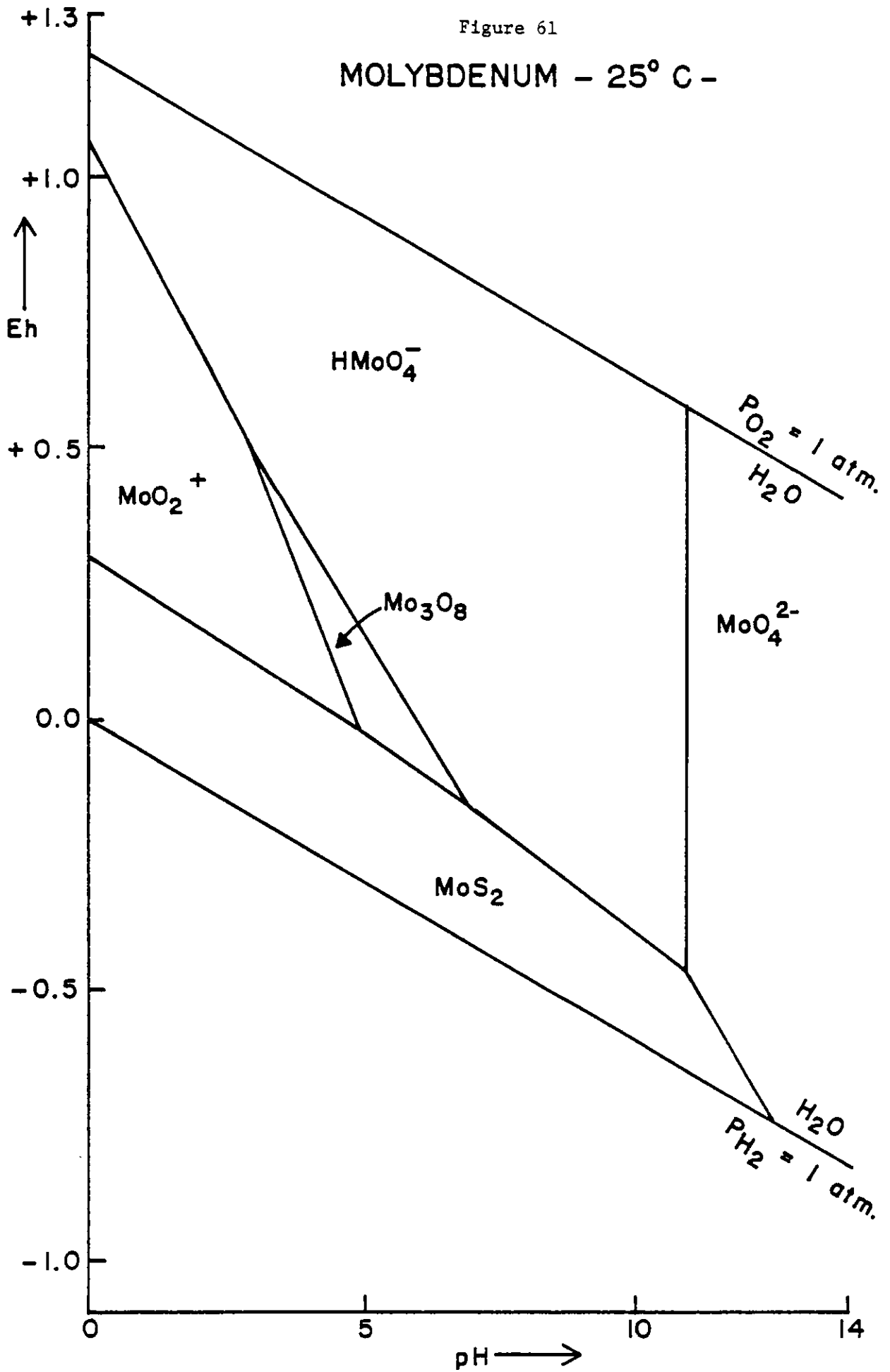


Figure 62

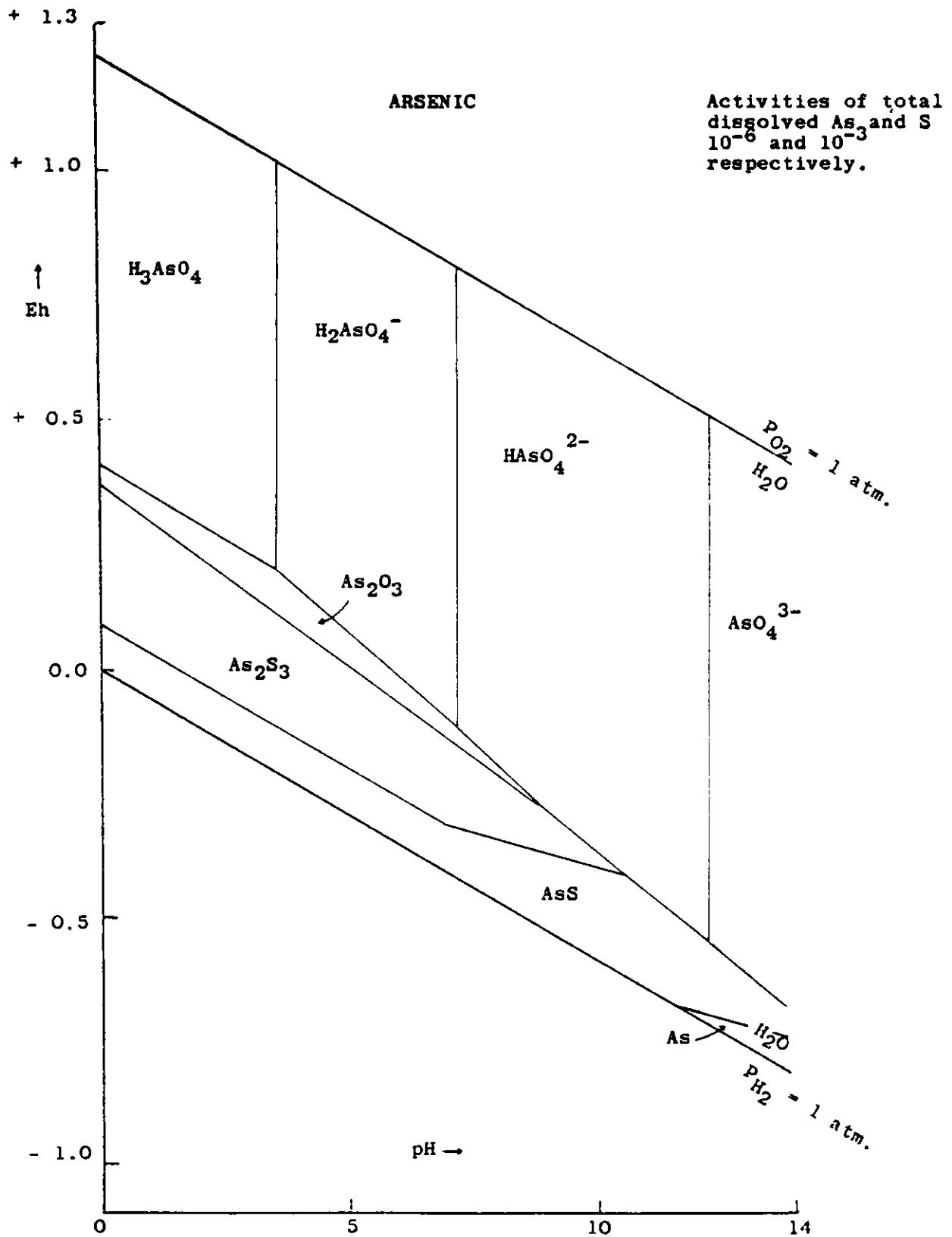


Figure 63

ANTIMONY - 25° C -

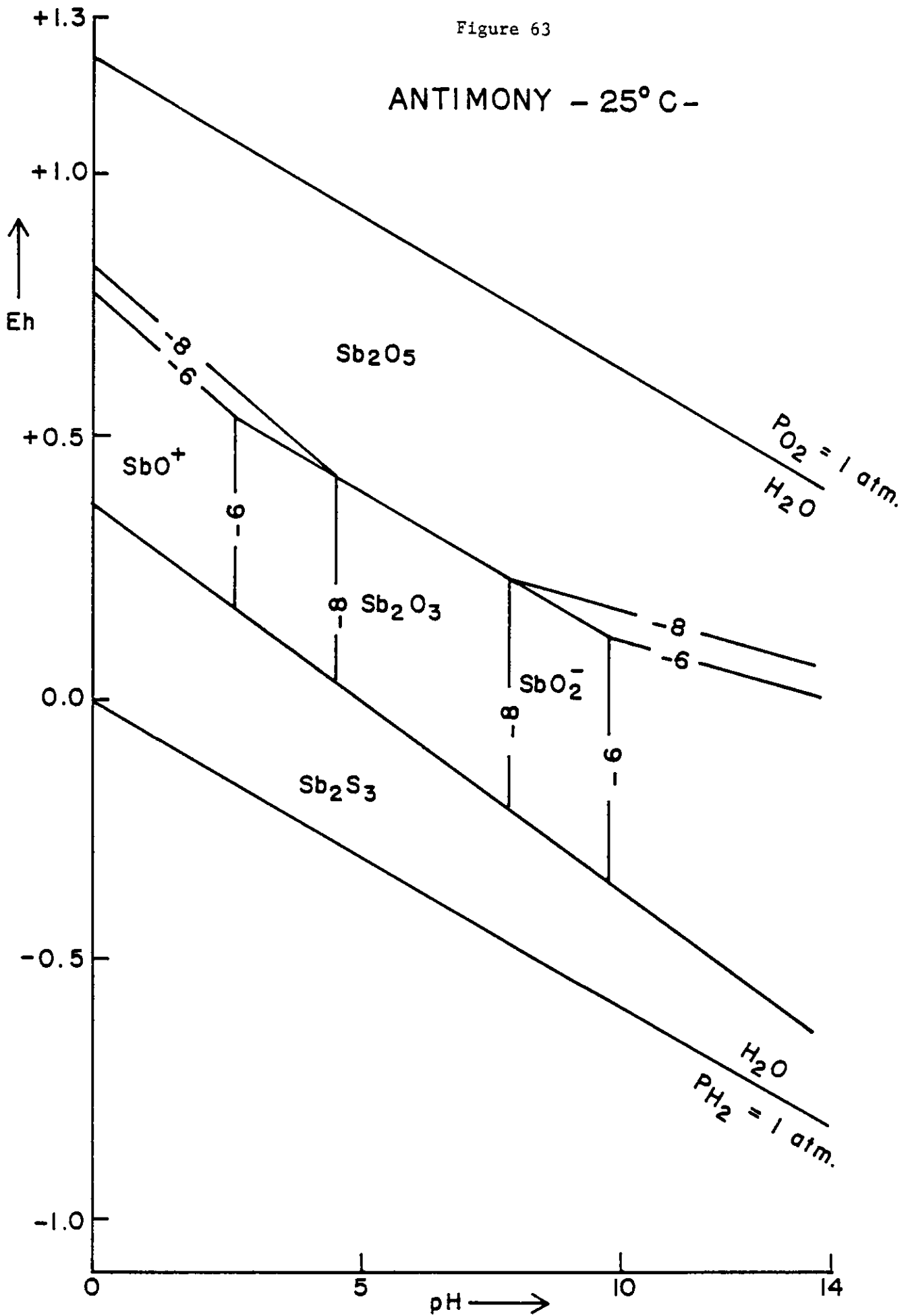


Figure 64

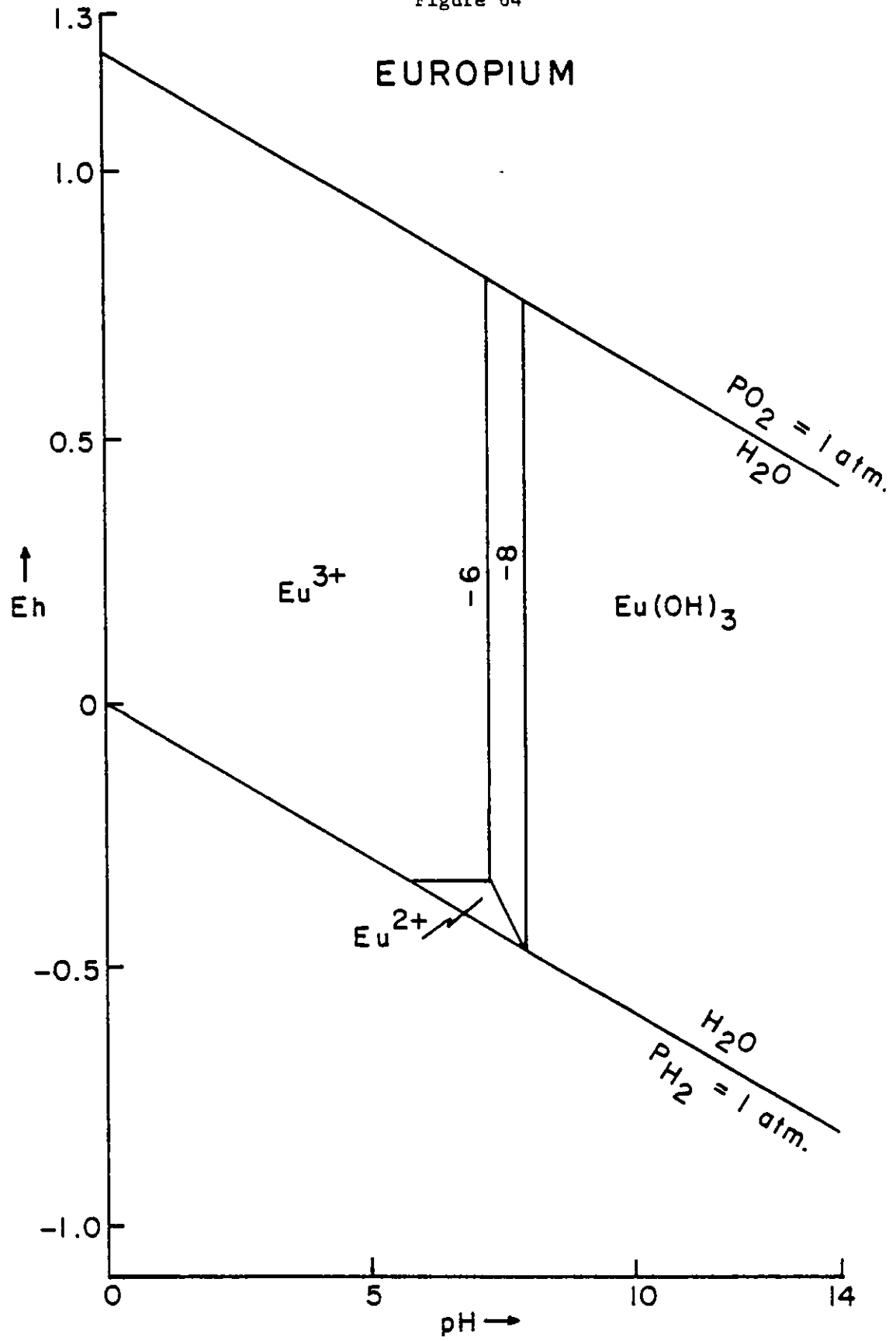
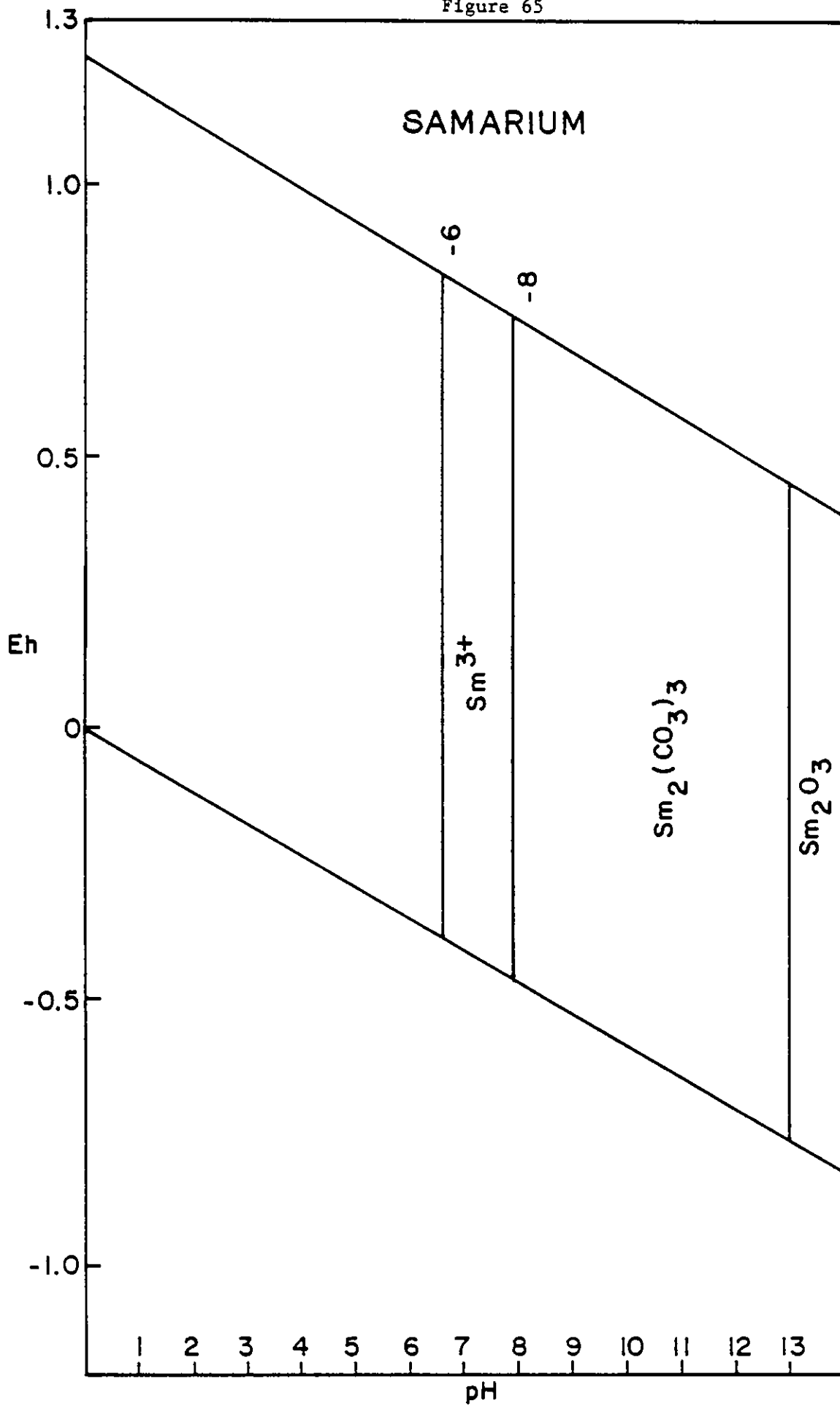


Figure 65



Chapter 5

Periods of Mineralization in the Grants Mineral Belt

Radiometric age determinations for the uranium ores and their host rocks in the Grants mineral belt are extremely valuable in defining areas where exploration should be concentrated as well as providing insight into processes responsible for the ore formation.

Age determinations to date have been attempted by the conventional U-Pb, K-Ar and Rb-Sr methods. The U-Pb method may be directly applied to uranium ore minerals but with usually only limited success due to possible loss of intermediate radioactive species from the ^{238}U decay chain, anomalous Pb in sulfides admixed with the uranium minerals, and other factors. Brookins (1976a) has discussed the limitations of the U-Pb method for previous studies in the Grants mineral belt.

The K-Ar and Rb-Sr dates are usually attempted on clay and other minerals assumed from SEM or other data to be penecontemporaneous with ore formation. The K-Ar dates reported by Brookins (1976a) and Brookins and others (1977) vary widely. This is due to radiogenic ^{40}Ar loss and to presence of authigenic K-feldspar which, from SEM evidence, is post-mineralization (but how much younger is unknown). Combined, these two factors usually result in ages which are too young, and the method is not yet useful. Rb-Sr dates on authigenic clay minerals have (Brookins, 1976a) proven to be most useful for determining ages of sedimentation, primary and some secondary mineralization, etc.; these dates are discussed below.

Evidence for Different Periods of Mineralization in the Grants Mineral Belt

1. Syngenetic ores in Morrison Formation sedimentary rocks. These deposits, if truly syngenetic, must be approximately 145 ± 10 m.y. old as the Morrison Formation is Late Jurassic. Further, Rb-Sr dates on authigenic montmorillonites in reduced rocks removed from ore zones yield ages of sedimentation of 145 ± 8 m.y. (Brookins, 1976a; Lee and Brookins, in press.)
2. Early epigenetic ores in the Morrison Formation contain chlorite which is penecontemporaneous with uranium mineralization. This material has been dated at 139 ± 9 m.y. by Lee (1976; see also Brookins, 1976a; Lee and Brookins, in press). While the ages of primary sedimentation (145 ± 10 m.y.) and the age of chlorite formation (139 ± 10 m.y.) are within the limits of error, cross cutting of sedimentary features by uranium mineralization indicates the epigenetic nature of the mineralization.
3. Early to Mid-Cretaceous (Pre-Dakota) mineralization in Morrison Formation sedimentary rocks. The Rb-Sr dates on both minus-two and minus-0.5 micron clay minerals from ore zones from the Jackpile Sandstone range from 110 to 115 m.y.; these dates are not very different from the minimum U-Pb date of 95 ± 8 m.y. for uranium ore reported by Nash (1968). However, the Rb-Sr dates are considered more reliable as some ore at the Jackpile Mine is truncated by the unconformity between the Jurassic Jackpile Sandstone and the Mid- to Late-Cretaceous Dakota Formation (Melvin, 1976). Thus the 110-115 m.y. date represents a period of mineralization due to remobilization of pre-existing, presumably early Late Jurassic, mineralization (possibly as old as the

Ambrosia Lake ore?). Since uplift of the southern San Juan Basin is indicated during the Mid-Cretaceous, this may account for the present day position of the Jackpile ores. If substantiated, this will be of great assistance in defining zones for mineralization.

4. Primary Dakota Formation (Mid- to Late-Cretaceous) Mineralization.

Granger (1968) proposed a model in which uranium was leached from basal Dakota Formation rocks into the underlying Late Jurassic Morrison Formation. While the radiometric and geologic criteria have refuted this model, ore occurrences are known from some parts of the Dakota Formation. Recent Rb-Sr dating (Brookins, 1977) indicates the Dakota Formation age of sedimentation to be 94 ± 8 m.y.; this date is consistent with the K-Ar dating by the U.S. Geological Survey which places the age of the Dakota Formation at approximately 92 m.y.

We have noted uranium mineralization in several parts of the Dakota Formation as have others; the problem is whether or not the mineralization occurred at or close to the time of sedimentation or in much later times. Ludwig and others (1977) suggest a Pleistocene age of mineralization for some uranium ore from the Hogback No. 4 Mine in the Dakota Formation; no other radiometric dates are available.

In close proximity to the St. Anthony Mine in the Laguna District uranium mineralization is noted along bedding plane fractures in the Dakota Formation close to, but slightly above, the basal swamp deposits in contact with the Jackpile Sandstone. This material is clay mineral rich and we intend to use the Rb-Sr method to study this, and the Silver Spur Deposit near Ambrosia Lake, to test for the age of mineralization.

First results on the Mancos Shale (Cretaceous) which overlies the Dakota Formation yield an isochron Rb-Sr date of 83 ± 15 m.y.; this date agrees with its stratigraphic position, the date on the Dakota Formation (94 ± 8 m.y.), the range in dates by the U.S. Geological Survey (78-85 m.y.). The Rb-Sr isochron for the Mancos Shale is shown as figure 66. Of interest is that the minus two micron clay size material yields a high $^{87}\text{Sr}/^{86}\text{Sr}$ ratio of about 0.72 which is consistent with results obtained on other argillaceous rocks.

5. Laramide Mineralization. Many (see summary in Roebber, 1970) investigators have pointed out that the stack (redistributed) ore of the Grants mineral belt is due to tectonism accompanied by dissolution and reprecipitation of early formed ore into joint or fault parts of the sedimentary rocks. Presumably this period of ore formation is Laramide; i.e., roughly 60 m.y. in age. Yet, since uplift occurred in post-Laramide time, it can also be argued that perhaps the favorable structural traps were formed during the Laramide but that ore filling occurred in much younger times (?). What is clear is that these stack deposits contain a series of authigenic clay minerals which, on first inspection, are different from those associated with the early epigenetic ores of Ambrosia Lake or the Mid-Cretaceous ores of the Jackpile Sandstone. Different illite/chlorite ratios and an abundance of kaolinite are common in these deposits. Similarly, trace element abundance and distribution is apparently different between stack and primary ores.

We are studying the clay minerals of the stack ores by the Rb-Sr method to see if one or more periods of mineralization were involved. If more than one (including a more or less continuous sequence of

dissolution followed by reprecipitation from the Laramide to the Present?), then this would be of significance to the explorationist.

6. Tertiary Mineralization (?). In some barren, oxidized parts of the Morrison Formation at Ambrosia Lake, ore pods occur which may be interpreted as either remnant (i.e., Late Jurassic) pods or new (i.e., Tertiary) zones of mineralization. Some of these ore accumulations are clearly remnant when it is noted that they contain pyrite, organic carbon, etc., typical of primary ore in the area; the explanation for their existence is one of armoring of the ore by clay and other minerals or some factors affecting fluid flow such that these parts of the ore were not destroyed. If, on the other hand, the ore contains coffinite (or uraninite) plus hematite, then a possible Tertiary age of mineralization can be inferred. In the latter case the Eh conditions were such that uranium mineralization occurred in the hematite stability field (see Brookins, 1976b). We attempted to date these remnant ore pods by the Rb-Sr method. If they turned out to be Tertiary, then this, in effect, would indicate that other such ore occurrences in barren oxidized rocks might be present (note: the reader is reminded that some production has come from such deposits; Kelley, 1963).

Preliminary data for Rb-Sr study of a possible post-Laramide uranium deposit* (*Site not yet disclosed pending more work and for proprietary reasons) yield a date of 48 m.y., but with an uncertainty of ± 45 m.y. The larger error is due to a restrictive range in $^{87}\text{Rb}/^{86}\text{Sr}$ (1.8 to 3.4), scatter in $^{87}\text{Sr}/^{86}\text{Sr}$ (0.717-0.724), and uncertainty in the initial $^{87}\text{Sr}/^{86}\text{Sr}$ ratio. The data do not, however, fall on any of the other isochrons for clay minerals from the Grants

mineral belt, but rather they appear to be confined to a restrictive envelope of younger age. These particular samples are all kaolinite rich, but the kaolinite appears to be penecontemporaneous with U mineralization. If the redox front is (a) Laramide and (b) has remained essentially stationary since approximately 60-70 m.y. ago, then it is possible that the U deposited at this site is indeed representative of Tertiary mineralization where ore previously described from other similar sites as redistributed may actually be analogous to Wyoming or Texas roll ore, except that the redox front is largely stationary and tectonically controlled. A series of complex reactions essentially controlled by sulfide-sulfate equilibrium is postulated where U(VI) reduction to U(IV) is accompanied by K-feldspar destruction and kaolinite formation. The postulated amount of aqueous Mg^{2+} is lower than for ore deeper in the San Juan Basin as only sparse montmorillonite (or mixed layer illite-montmorillonite) and chlorite are noted. The processes responsible for the U reduction may not be very different from those proposed by Siever and Kastner (1972), i.e., chlorite, + organic C + SO_4^{2-} + H^+ = chlorite₂ + pyrite + kaolinite + H_4SiO_4 + siderite + HCO_3^- + water, where chlorite₁ is more Fe-rich than chlorite₂. If excess sulfur is present than siderite in the above reaction will be replaced by more pyrite. The importance of the above reaction is that SO_4^{2-} present in the redox zone may be reduced to form pyrite in the presence of organic carbon and either chlorite or montmorillonite resulting in an assemblage of kaolinite-pyrite-(+ Mg-chlorite). Further, the released silica (H_4SiO_4) will facilitate coffinite formation.

7. Age of the Redox Interface present in the Grants mineral belt. The redox front between pyritiferous, reduced rocks and hematitic, oxidized rocks is actively explored for uranium occurrences. It is recognized that trend ore is commonly located at or near this interface and that much stack ore occurs directly in the interface. Wyoming- or Texas-type rolls at the interface are difficult to demonstrate, possibly because the ancient age of the Jurassic deposits has destroyed the more readily observable roll-like features or a different or combination of other factor or factors were involved with ore deposition. From the comments made above (see items 4, 5, 6) mechanisms for destruction of very early formed ore, presumably oxidation, are indicated. If this indicates a slow moving redox front due to gradual, or at times episodic, uplift, which a pronounced control over the ore, then demonstrating whether or not the present front is relatively young (i.e., formed in relatively recent times) or has formed progressively, is of utmost importance.

We are attempting to date authigenic minerals from the redox front from ore zones and from barren rocks to test this point. If, for example, it showed that much of the front is a very young feature and not responsible for much of the ore control, then less exploration would be dictated by the presence of the front. Alternately, if the opposite is true, e.g., the front had progressed slowly throughout the last 100 m.y. or so to its present position, with a strong control over ore formation, then even more exploration would be focused on the front's position.

It should be emphasized that, thanks to the internal funding from University of New Mexico sources for mass spectrometric modification, that we now have the analytical capability to investigate this problem in the detail it warrants.

8. We systematically gathered all the existing radiometric and geological data relevant to ages of sedimentation, mineralization, tectonism in the GMB and summarized it for the public. It has been very apparent to us for several years that age relationships in the GMB are hazily understood, in large part due to the quality of the data, the quality of samples studied, etc., and we felt that we were in a position to properly tabulate all data and attempt an interpretation.
9. Other age studies. We further examined in more detail the volcanogenic and plutonic detrital material noted in the Morrison Formation. Our first results (see Brookins, 1976a) demonstrated that plutonic 2- to 62-micron (slit size) detritus was Precambrian as were microcline-quartz pebbles from Morrison Formation outcrops; yet we could not determine the relationship of either to the presently exposed core rocks of the Zuni Mountains which have been dated at 1.4 b.y. (Brookins and others, in press).

As part of NURE Program, others (see Ragland, 1977) have attempted to correlate uranium abundances with initial $^{87}\text{Sr}/^{86}\text{Sr}$ ratios for granitic rocks. While this relationship has not, to our satisfaction, been demonstrated, we are in a position to address the problem in some detail both for the GMB and Precambrian rocks elsewhere in New Mexico as we have been systematically gathering the Sr data for several years and uranium data for the last three or four.

The first Rb-Sr date on volcanogenic material indicated a Permian-Triassic source (Lee, 1975; Brookins, 1976a). We followed up on this study and examined the proposed source rocks of this age from southeastern Arizona; trace and other elemental studies supplemented this work.

Table 11

Dakota Sandstones and Bentonites

Minus Two Micron Size Fraction

Sample No.		Rbppm	Srppm	Rb/Sr	$^{87}\text{Rb}/^{86}\text{Sr}$	$^{87}\text{Sr}/^{86}\text{Sr}$
Kd - 9J	2u	19.3	185.4	0.1041	0.3014	0.7098
Kd - 8J	2u	13.8	42.7	0.3232	0.9359	0.7105
Kd - 7J	2u	17.8	209.4	0.0850	0.2461	0.7102
Kd - 2J	2u	12.4	81.8	0.1516	0.4389	0.7105
Kds - 1J	2u	19.1	40.0	0.4775	1.3829	0.7114
KdBs - 1J	2u	178.1	192.5	0.9252	2.6798	0.7130
Kds - 1 P.C.	2u	46.2	63.9	0.7230	2.0943	0.7130
Kd 4 - J	2u	9.0	90.1	0.0999	0.2893	0.7101
Kd 3 - J	2u	20.3	121.3	0.1674	0.4848	0.7103
Kds 12 - J	2u	18.3	68.8	0.2660	0.1889	0.7101

Isochron Age = $93 \text{ m.y.} \pm 8 \text{ m.y.}$

$^{87}\text{Sr}/^{86}\text{Sr}$ Init. = $0.7097 \pm .0001$

DAKOTA SANDSTONE
-2 μ Clay Fraction

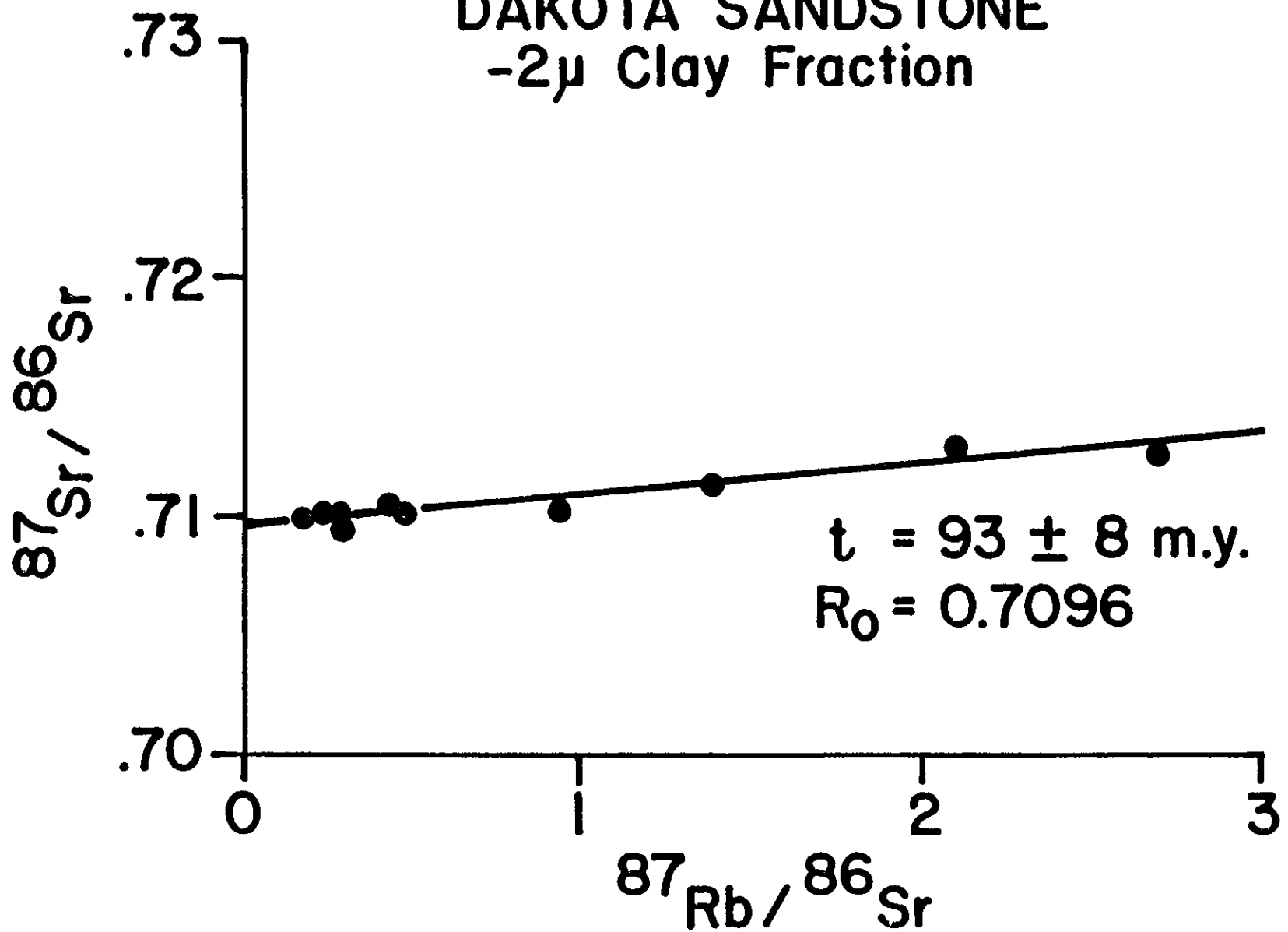


Figure 66a

Table 12

Mancos Shale Minus Two Micron Size Fraction

Sample No.		Rbppm	Srppm	Rb/Sr	$^{87}\text{Rb}/^{86}\text{Sr}$	$^{87}\text{Sr}/^{86}\text{Sr}$
Kms - 3	2u	137.53	225.90	0.61	1.77	0.7256
Kms - 9	2u	131.61	117.10	1.12	3.26	0.7279
Kms - 1	2u	139.10	64.40	2.16	6.27	0.7322
Kms - 4	2u	154.49	49.83	3.10	9.00	0.7339

Isochron Age = 83 m.y. 11 m.y.

$^{87}\text{Sr}/^{86}\text{Sr}$ Init. = 0.7239 0.0009

MANCOS SHALE
-2 μ Fraction

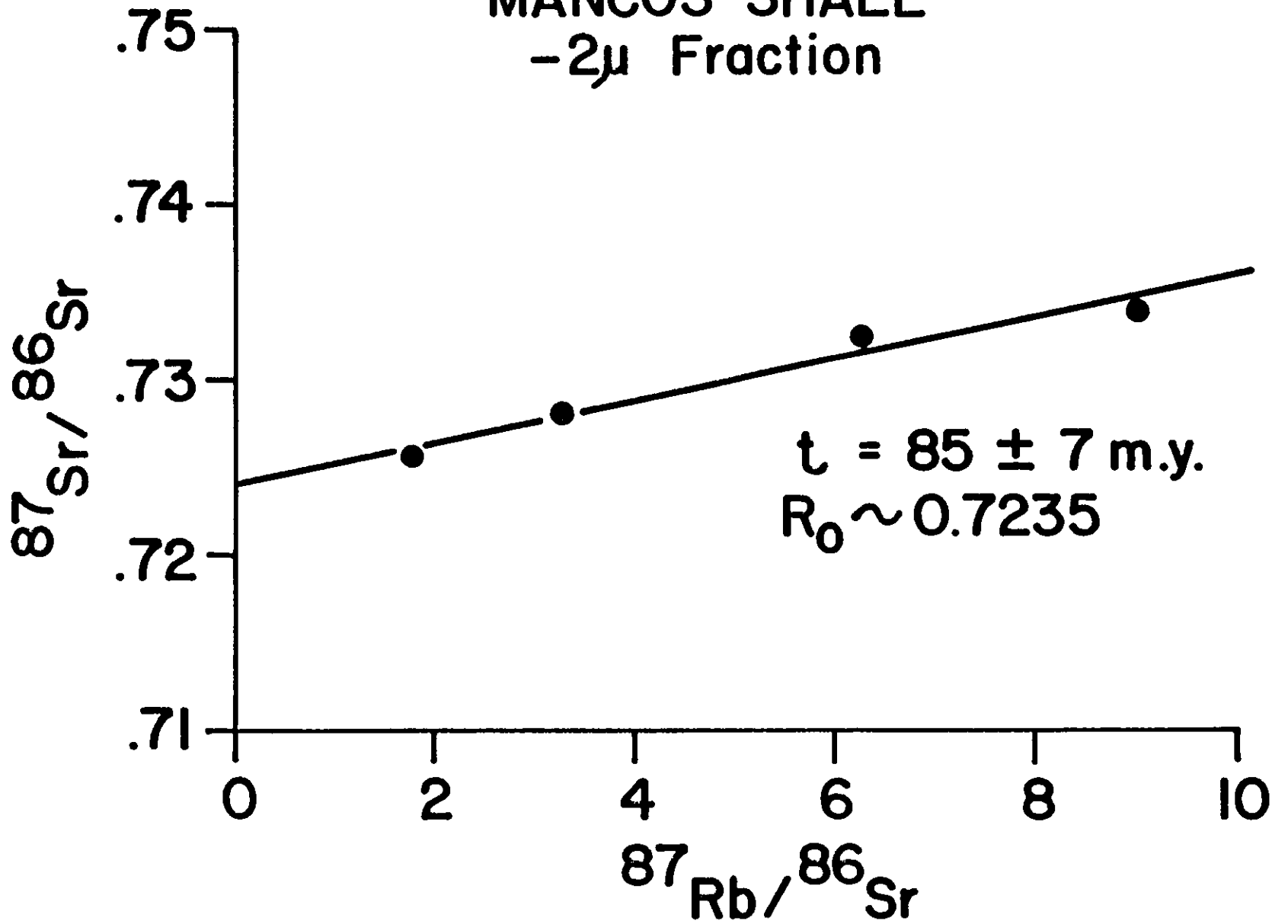


Figure 66b

Chapter 6

CLAY MINERALOGIC STUDIES

Introduction

Clay mineralogical analyses are important for understanding the paragenesis of much of the ore of the Grants mineral belt. Brookins (1976a,b) has pointed out the importance of the clay mineralogical associations with the ore deposits. In brief, high chlorite/montmorillonite or illite/montmorillonite or chlorite + illite/montmorillonite are typical of many ore zones whereas montmorillonitic clays are more typical of barren, reduced rocks. Kaolinite may be important in possible Tertiary or Laramide (i.e., stack) ore deposits; in the deeper, reduced rocks it is usually secondary.

Elemental distribution in the clay minerals (-2μ fraction) is discussed elsewhere. This section is included to provide a tabulation of the clay mineralogic data for various ore deposits and barren reduced, barren oxidized Morrison Formation samples and some Cretaceous samples as well.

The integration of chemical data with the clay mineralogic data is on-going and will be reported in Phase III.

Table 13

Sample Locations

<u>Sample</u>	<u>Latitude</u>			<u>Longitude</u>			<u>Description</u>
	Deg.	Min.	Sec.	Deg.	Min.	Sec.	
HGQ	35	41	12	106	54	21	Holyghost Quadrangle
JJ	35	9	56	107	20	4	JJ Mine
SA	35	9	22	107	19	25	Saint Anthony Mine
P	35	7	50	107	23	5	Paguata Mine
MQ	35	5	19	107	23	13	Mesita Quadrangle
LQ	35	4	37	107	24	27	Laguna Quadrangle
SM	35	19	39	107	38	37	Gulf Mine
JOM	35	22	0	107	43	19	Johnny M. Mine
D	35	20	5	107	48	51	Doris Mine
DLQ	35	19	53	107	49	54	Dos Lomas Quadrangle
SS	35	23	26	107	57	8	Silver Spur Mine
Sec. 36	35	24	5	107	51	20	Kerr McGee Sec. 36 Mine
Sec. 30	35	24	45	107	50	19	" " " 30 "
Sec. 23	35	25	39	107	52	54	U.N.H.P Sec. 23 Mine
DOE	35	21	48	107	39	44	Reduced Ground Cover
" SM-2	35	23	49	107	43	10	" " "
" G-1	35	23	51	107	42	7	" " "
" G-9	35	24	40	107	4	5	" " "
" R-3	35	29	30	107	35	24	" " "
" R-5	35	29	50	107	41	51	" " "
" R-8	35	29	58	107	44	31	" " "
" R-7	35	33	19	107	43	54	" " "
" R-6	35	35	3	107	48	27	" " "

Table 13 (cont'd.)

Sample Locations (cont'd)

DOE R-9	35	36	3	107	36	37	Reduced Ground Cover
PC	35	19	35	107	49	9	Poison Canyon Location
K	35	21	43	107	46	58	Mancos Samples Location
TG	35	28	23	108	9	4	Thoreau Quadrangle
SL	35	39	53	108	9	72	Smith Lake Location
Z (###)	35	10	53	108	10	25	Zuni 100 Series Loc.
Z (###)	35	9	49	108	10	59	" " " "

Table 14

Mancos Shale

Sample	K	CH	M	CH-M	I	I-M	Description
Kms-1	40	-	tr	-	39	20	Gray-Black shale
Kms-2	54	-	tr	-	26	19	do.
Kms-3	46	-	tr	-	18	35	do.
Kms-4	43	-	-	-	28	30	do.
Kms-5	61	-	-	-	38	tr	do.
Kms-6	25	-	41	-	11	23	do.
Kms-7	29	31	-	-	11	29	do.
Kms-8	40	tr	11	-	25	33	do.
Kms-9	4	tr	-	-	tr	94	do.
Kms-10	28	39	-	-	5	28	do.
Kms-11	45	tr	19	-	34	tr	do.
Kms-12	39	-	-	-	26	35	do.

Kms location is at Ambroisa Lake area one mile north of Doris Mine

--concentrations in percent--

Table 14 (cont'd.)

Dakota Formation

Sample	K	CH	M	CH-M	I	I-M	Description
Kd 1-J	20	-	56	-	23	-	Carbonaceous shale
Kd 2J	tr	-	95	-	-	tr	Bentonite
Kd 3J	tr	-	95	-	-	tr	Bentonite
Kd 4J	2	-	97	-	-	tr	Bentonite
Kd 5J	41	-	58	-	-	tr	Bentonite
Kd 7J	2	-	95	-	-	tr	Carbonaceous shale
Kd 8J	5	-	95	-	-	-	Bentonite
Kd 9J	7	-	93	-	tr	-	Bentonite
Kds 11J	4	-	95	-	tr	-	Bentonitic shale
Kds 12J	-	tr	97	-	-	-	Limonitic ss. with carb. shale layers
Kds-1 PC	72	-	-	-	-	28	Carbonaceous shale
Kds-2 PC	tr	-	-	-	-	96	Carbonaceous shale
Kds-3 PC	95	-	-	-	-	-	Fine grained sandstone
Kds-4 PC	78	-	5	-	17	-	Limonite-stained sandstone
Kds-5 PC	96	-	-	-	-	-	Limonitic sandstone
Kds-6 PC	97	-	-	-	-	-	Limonitic sandstone
Kds-7 PC	69	-	-	-	tr	30	Carbonaceous shale
Avg. Sh.	47	-	-	-	-	53	---
Avg. Ss.	95	-	tr	-	-	-	---

KdJ samples collected five miles south of San Ysidro, NM; Kd PC samples collected one mile south of the Doris Mine near Ambrosia Lake.

Table 14 (cont'd.)

Jackpile Sandstone

sample	K	CH	M	CH-M	I	I-M	Description
MQ Kd-Jmj	91	-	7	-	tr	tr	Carbonaceous sh., Dakota ss.
MQ Jmj-1	89	2	7	-	-	tr	Dark gray sandstone
MQ Jmj-2	5	-	5	-	26	64	Limonitic sandstone
MQ Jmj-3	32	-	13	53	tr	tr	Gray sandstone
MQ Jmj-4	24	5	-	tr	20	50	Gray sandstone
MQ Jmj-5	65	tr	-	-	23	tr	White, coarse sandstone

MQ = Mesita Quadrangle location

Table 14 (cont'd.)

sample	Brushy Basin Member						Description
	K	CH	M	CH-M	I	I-M	
LQ Jmb-1	5	-	-	-	-	95	Green silty mudstone
LQ Jmb-3	3	13	79	-	5	-	Green silty mudstone
LQ Jmb-5	-	-	-	-	-	100	Greenish mudstone
TQ Jmb-1	42	-	58	-	-	-	Carbonaceous shale; some ss.
TQ Jmb-2	5	-	85	-	5	5	Green mudstone
TQ Jmb-3	6	-	50	-	tr	43	Limonitic sandstone
TQ Jmb-4	tr	-	-	-	-	99	Hematitic mudstone
DLQ Jmb-1	93	-	6	-	-	tr	Carbonaceous sh; Dakota ss.
DLQ Jmb-2	5	-	93	-	tr	tr	Green silty mudstone
DLQ Jmb-3	18	-	81	-	-	tr	Limonitic sandstone
DLQ Jmb-4	-	-	95	-	-	tr	Limonitic ss-sh.

TQ = Thoreau Quadrangle

MQ = Mesita Quadrangle

DLQ = Dos Lomas Quadrangle

Table 14 (cont'd)

Sample	Poison Canyon Member						Description
	K	Ch	M	CH-M	I	I-M	
PCU-1	69	-	7	-	14	10	Limonitic sandstone
PCU-2	59	-	-	-	15	27	Oxidized sandstone
PCU-3	64	-	-	-	10	27	Limonitic sandstone
PCU-4	83	-	15	-	tr	tr	Limonitic sandstone
PCU-5	52	-	-	-	-	48	Oxidized sandstone
PCU-6	41	-	-	-	25	35	Oxidized sandstone
PCU-7	32	-	-	-	-	68	Oxidized sandstone
PCU-8	27	-	tr	-	9	63	Oxidized sandstone
PCU-9	34	-	tr	-	12	53	Oxidized sandstone
PCU-10	4	-	-	-	18	78	Oxidized sandstone
PCU-11	95	-	-	-	-	-	Oxidized sandstone
PCU-12	58	-	tr	-	10	31	Oxidized sandstone
PCL-1	89	-	-	-	-	11	Hematitic sandstone
PCL-4	86	-	-	-	4	10	Hematitic sandstone
PCL-6	-	-	-	-	45	55	Green, bentonitic mudstone
PCL-7	78	-	5	-	7	9	Oxidized arkose
PCL 7&10	95	-	-	-	tr	4	(see PCL-7, PCL-10)
PCL-8	100	-	-	-	-	-	Limonitic sandstone
PCL-10	81	-	tr	-	11	7	Limonitic sandstone
DLQ Jmpc-2	62	-	32	-	-	6	Hematitic sandstone
DLQ Jmpc-3	-	-	65	-	-	35	Gray sandstone
avg. PC	60	-	-	-	12	28	---

PC = Ambrosia Lake, near Doris Mine (L=lower unit; U=upper unit)

DLQ = Dos Lomas Quadrangle

Table 14 (cont'd)

Westwater Canyon Member

sample	K	CH	M	CH-M	I	I-M	Description
HG Jmwc-1-2c	-	-	-	-	-	100	Limonitic sandstone
HG Jmwc-1-2D	-	-	-	13	-	87	Limon. ss; below channel
HG Jmwc-1-2Di	3	-	-	-	-	97	Limonitic sandstone
HG Jmwc-1-3a	-	47	-	-	-	53	Hematitic sandstone
HG Jmwc-1-6a	-	-	-	-	-	100	Bleached sandstone
HG Jmwc-1-7a	-	-	85	-	7	8	Oxid., limon. sandstone
HG Jmwc-1-8a	-	tr	-	-	-	99	Hematitic sandstone
clay armour	tr	4	-	-	3	92	Limon. armour, green clay
TQ Jmw-3	61	-	12	27	-	-	Hematitic sandstone
TQ Jmw-4	4	-	23	-	tr	72	Green mudstone (Na mont.)
TQ Jmw-6	44	27	tr	tr	7	20	Hem. ss, green mudstone
TQ Jmw-7	55	35	9	-	-	tr	Hematitic sandstone
TQ Jmw-9	49	36	tr	-	-	14	Hematitic silty mudstone
TQ Jmw-12	tr	13	86	-	-	-	Unoxid. calcitic sandstone
DLQ Jmw-2	5	5	50	-	-	40	Limon. ss. with mudstone pel's.
DLQ Jmw-4	69	-	10	-	-	21	Hematitic sandstone
DLQ Jmw-5	-	7	26	-	5	62	Green mudstone
DLQ Jmw-6	8	10	23	-	5	54	Limon. ss, mudst. pellets
LQ Jmw-2	-	-	95	-	tr	-	Limon. sandy mudstone
LQ Jmw-4	67	-	24	9	tr	-	Limon. sandy mudstone
LQ Jmw-5	50	-	40	10	-	-	Hematitic sandstone
LQ Jmw-6	5	-	72	23	-	-	Limonitic sandstone
LQ Jmw-7	17	25	57	tr	-	-	Limonitic sandstone
LQ Jmw-9	5	12	82	-	tr	-	Green mudstone

HG= Holyghost Quadrangle. TQ=Thoreau Quadrangle. DLQ=Dos Lomas Quadrangle. LQ=Lomas Quadrangle.

Table 14 (cont'd)

sample	Recapture Member						Description
	K	CH	M	CH-M	I	I-M	
HG Jmr-2	9	-	90	-	-	-	Red-green mudstone
BLQ Jmr-1	-	-	-	-	-	100	Brown silty mudstone
DLQ Jmr-2	15	-	tr	-	22	62	Green silty mudstone
DLQ Jmr-6	-	-	-	-	-	100	Red siltstone
TQ Jmr-1	19	-	61	-	tr	19	Gray silty mudstone
TQ Jmr-3	14	tr	-	-	32	53	Brown mudstone
TQ Jmr-2	24	19	43	-	5	9	Green mudstone

HG = Holyghost Quadrangle

DLQ = Dos Lomas Quadrangle

TQ = Thoreau Quadrangle

Figure 67

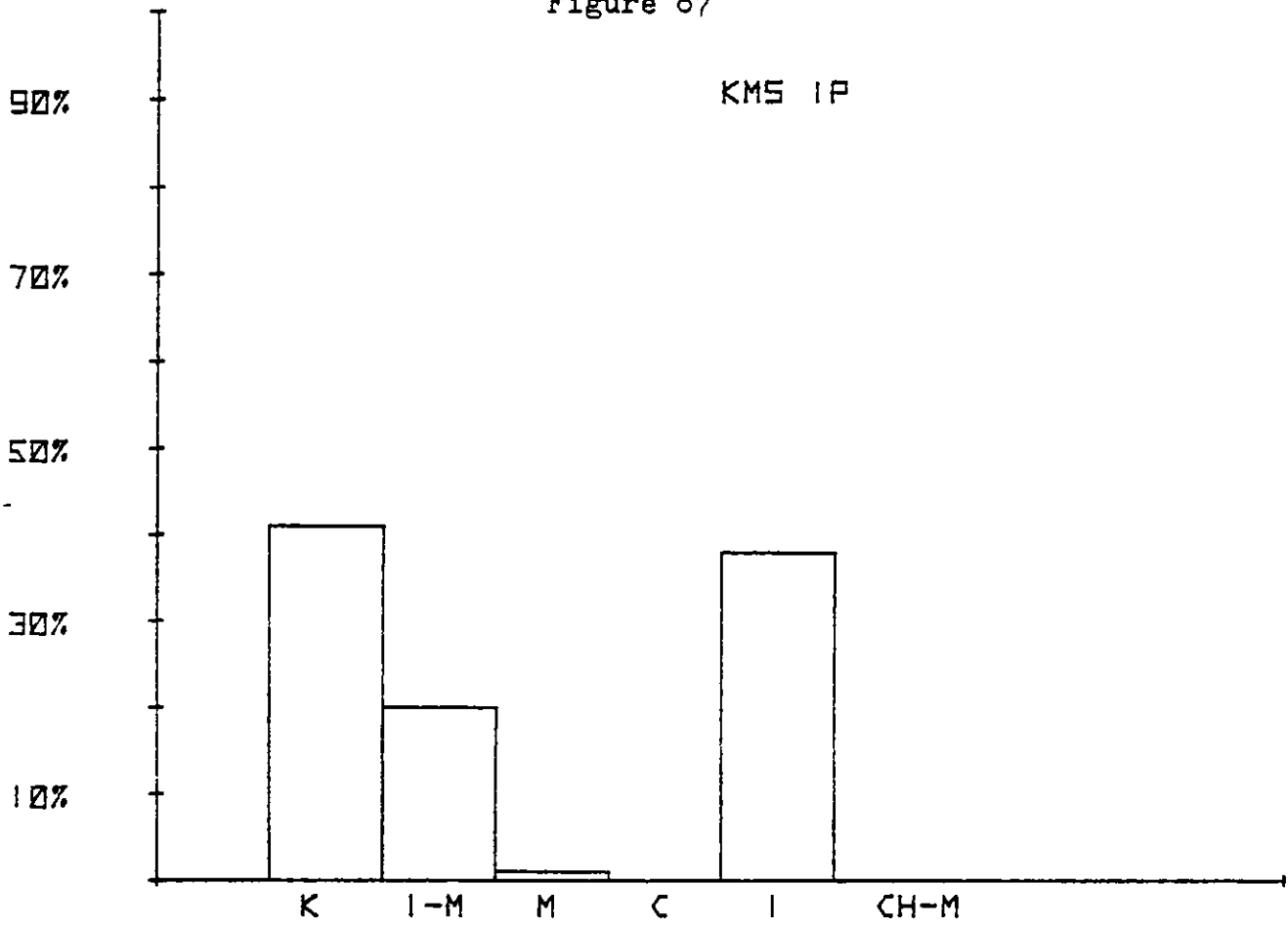


Figure 68

KMS 2P

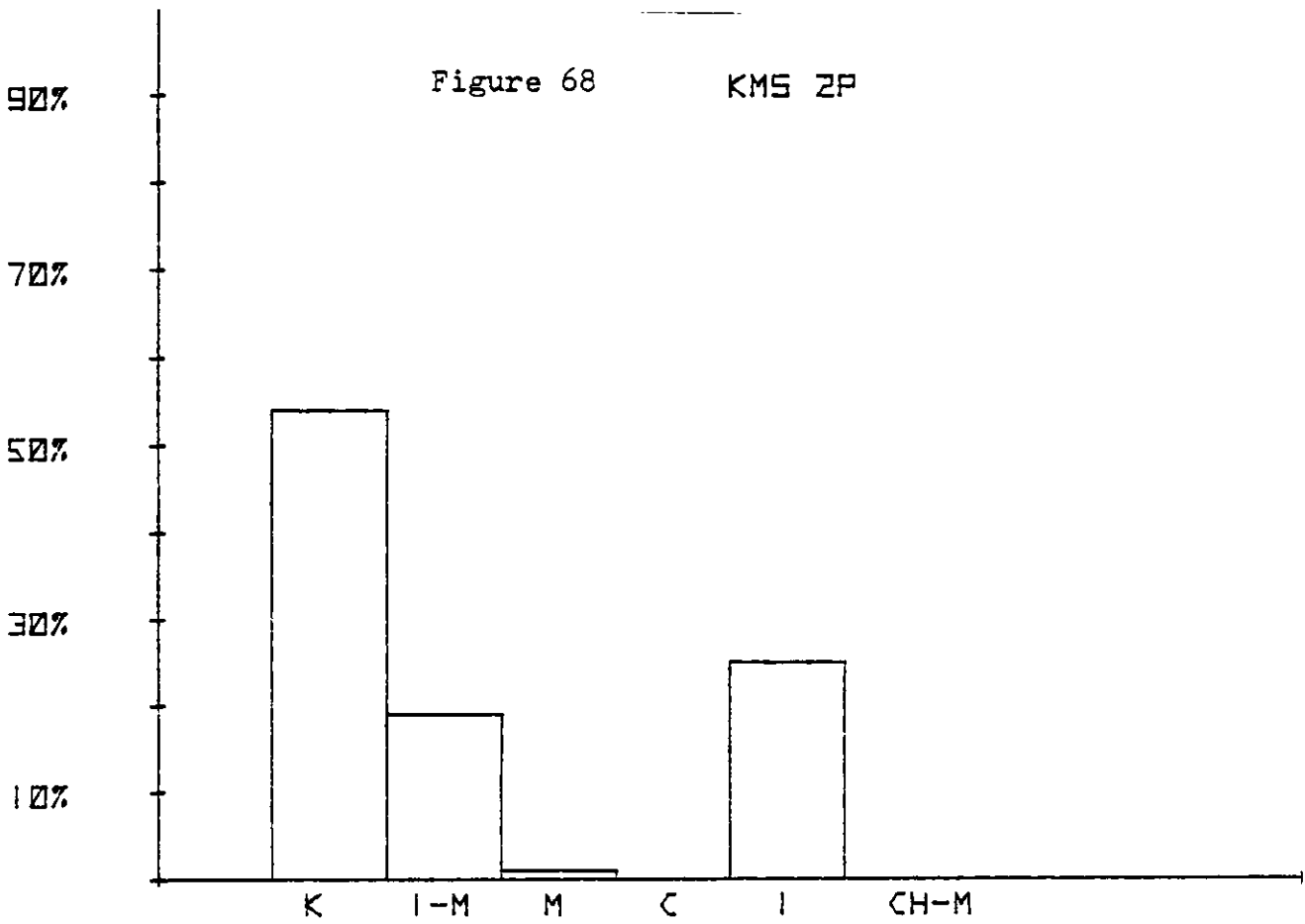


Figure 69

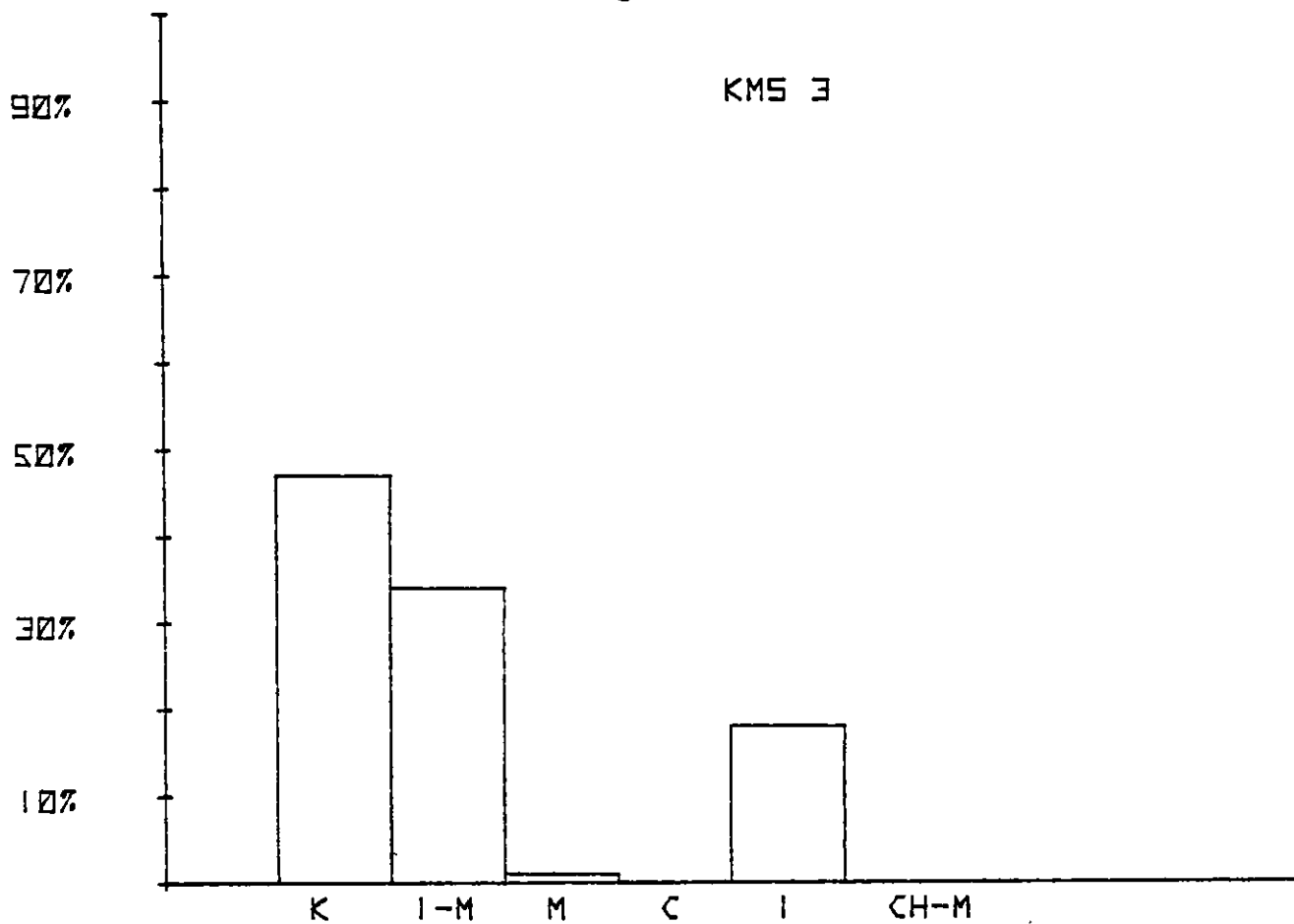


Figure 70

KMS 4P

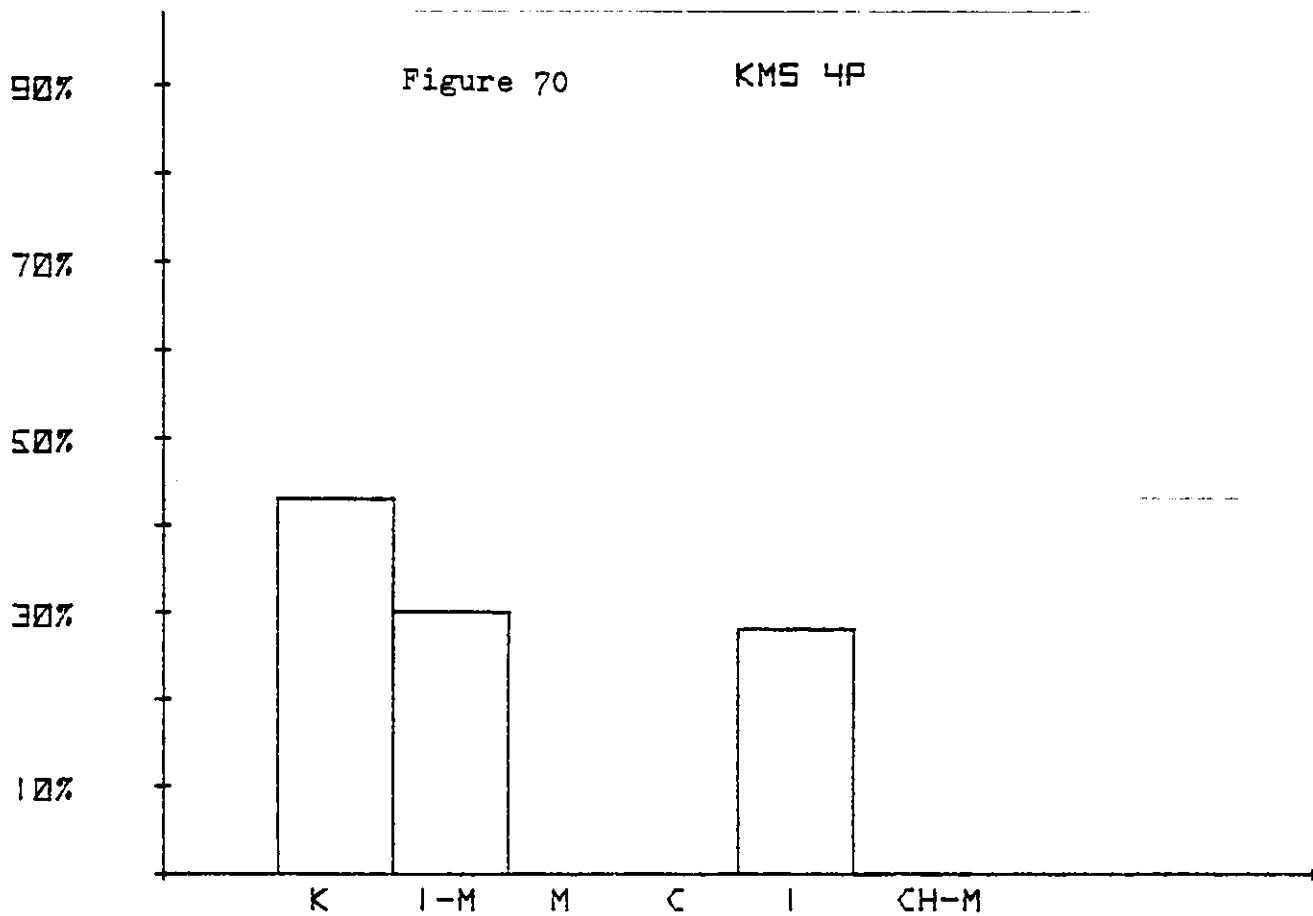


Figure 71

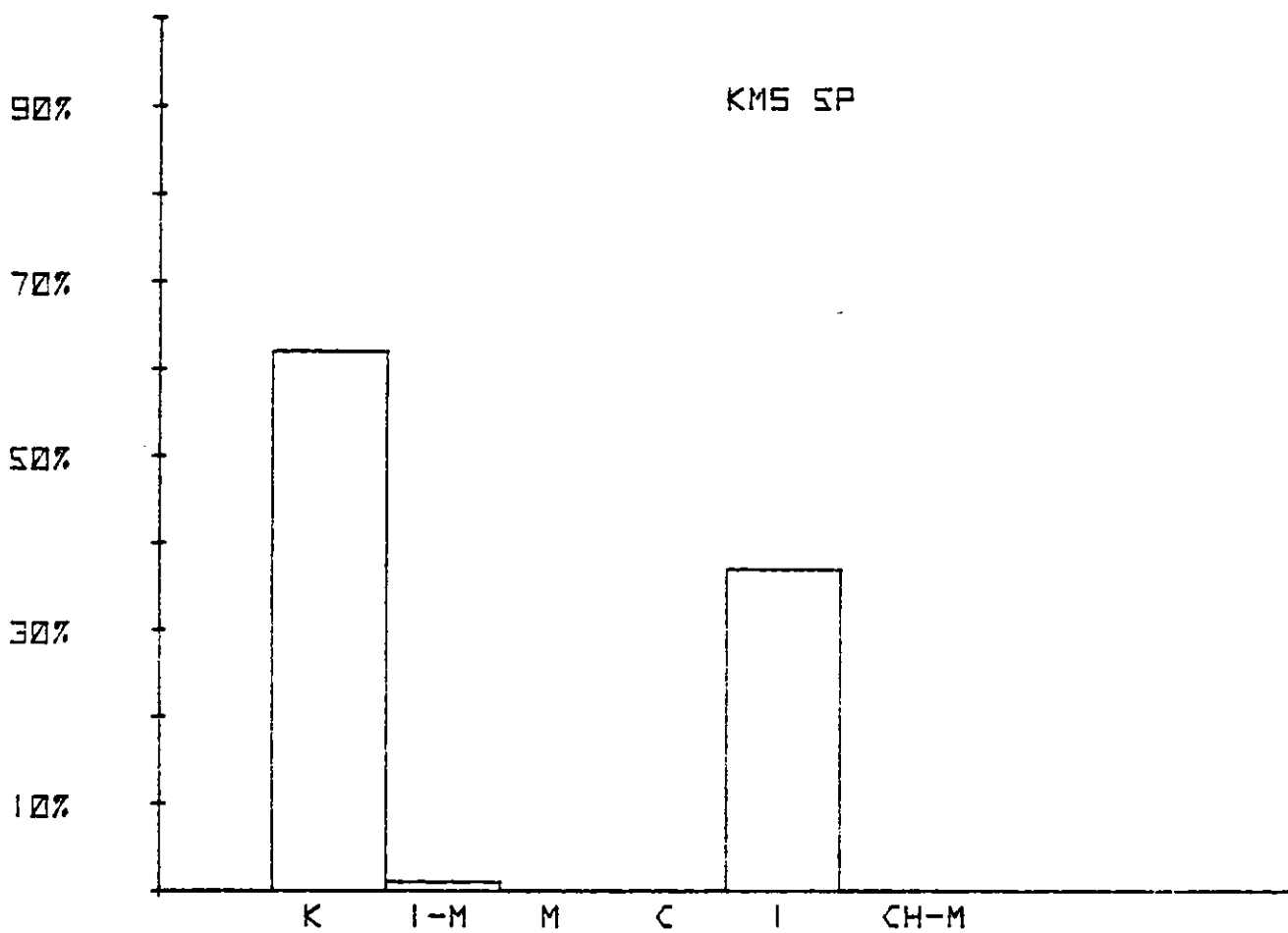


Figure 72

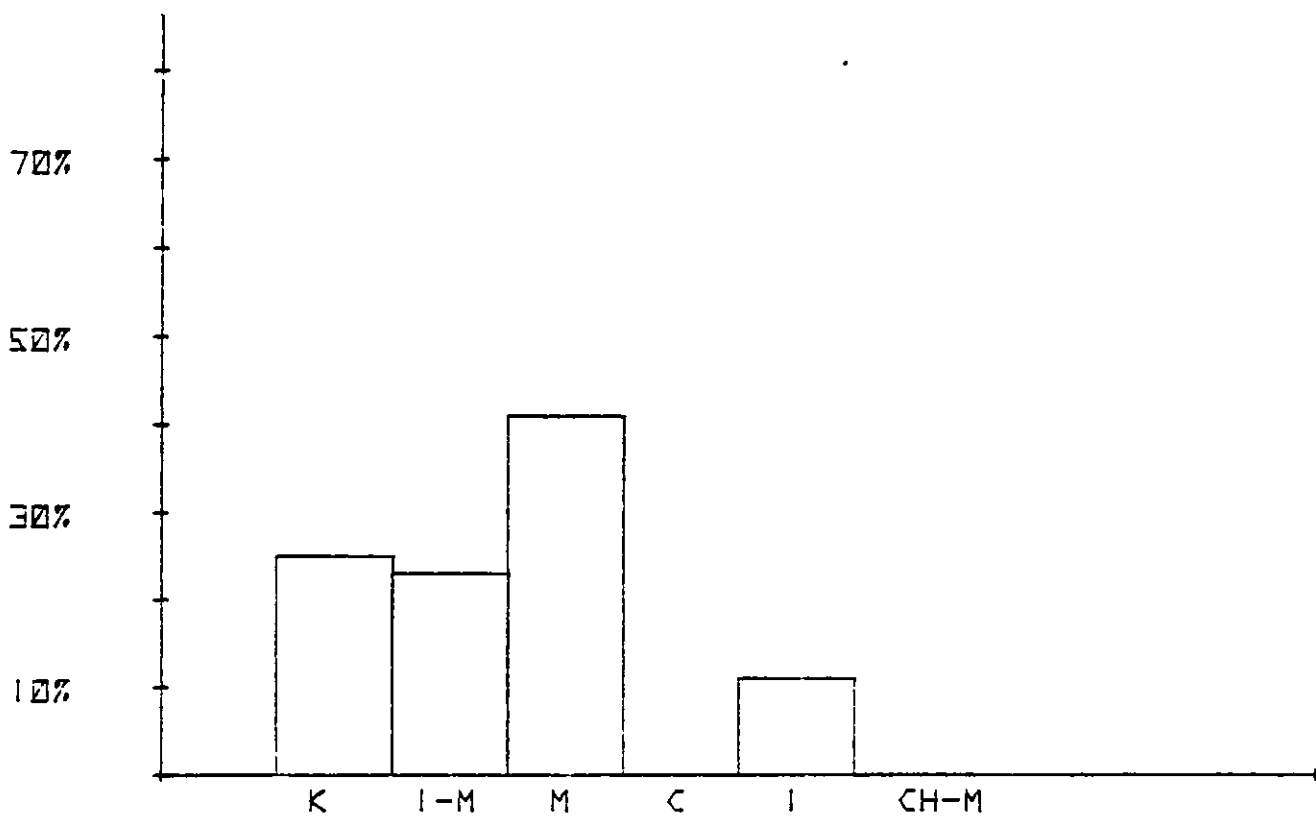


Figure 73

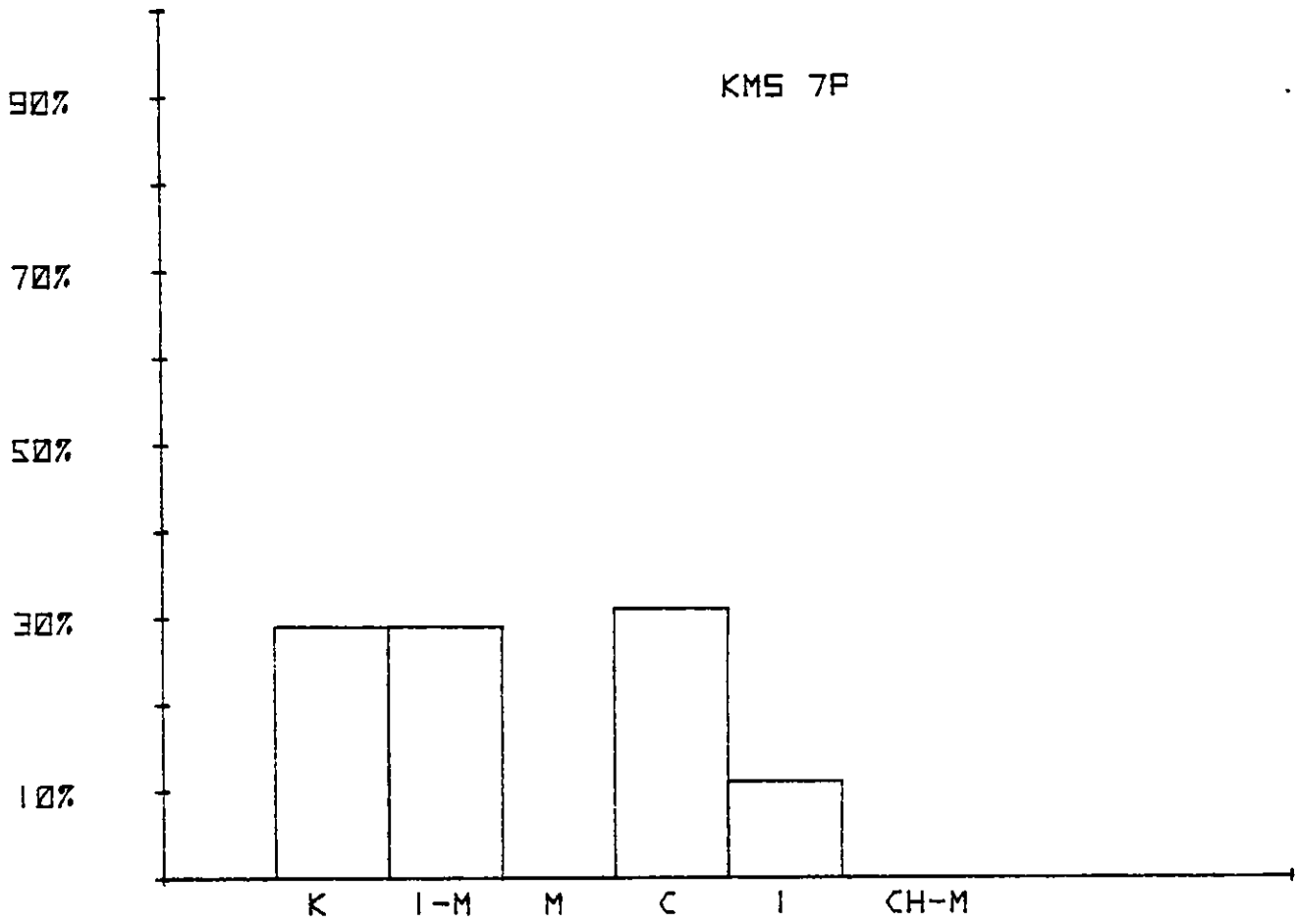


Figure 74

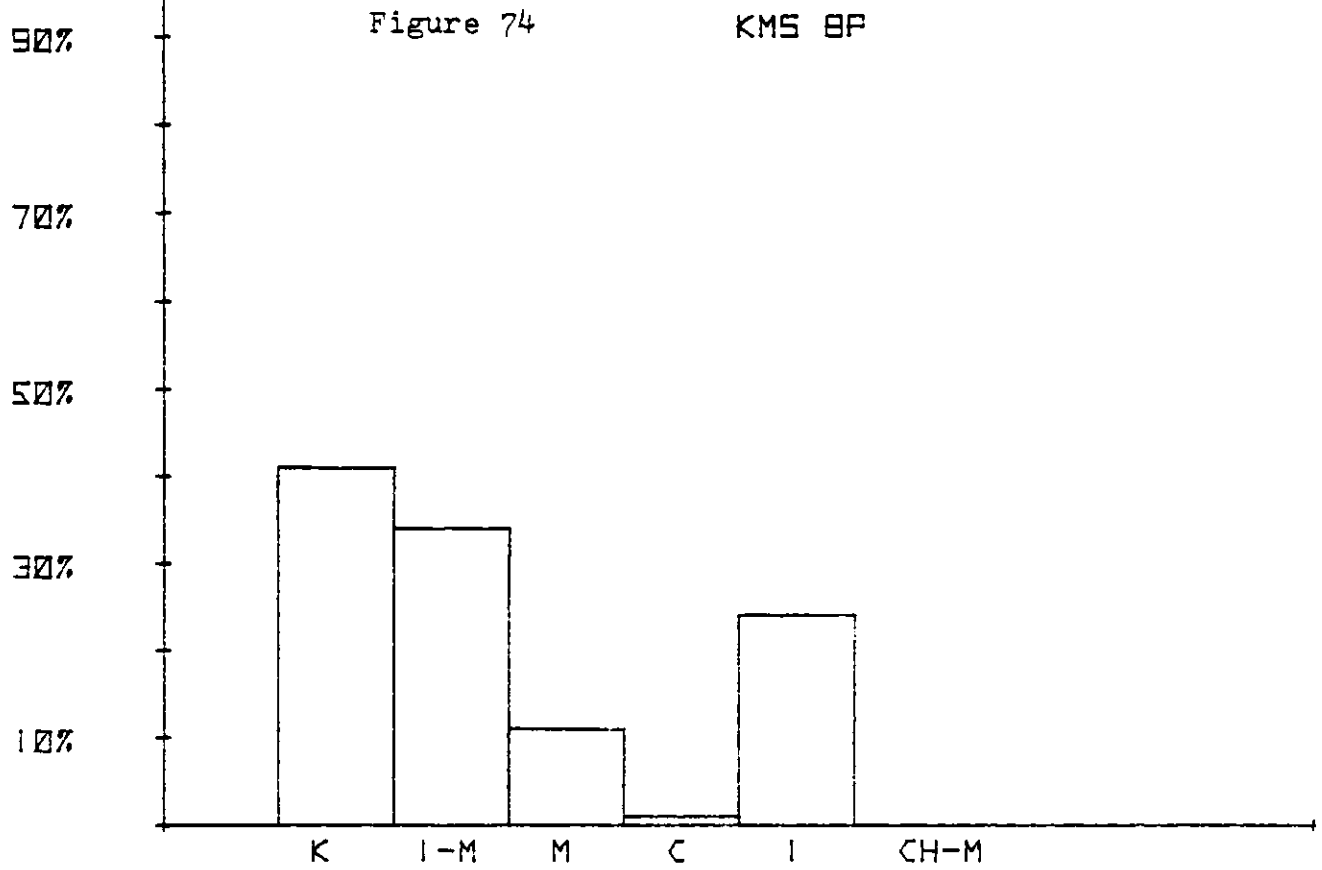


Figure 75

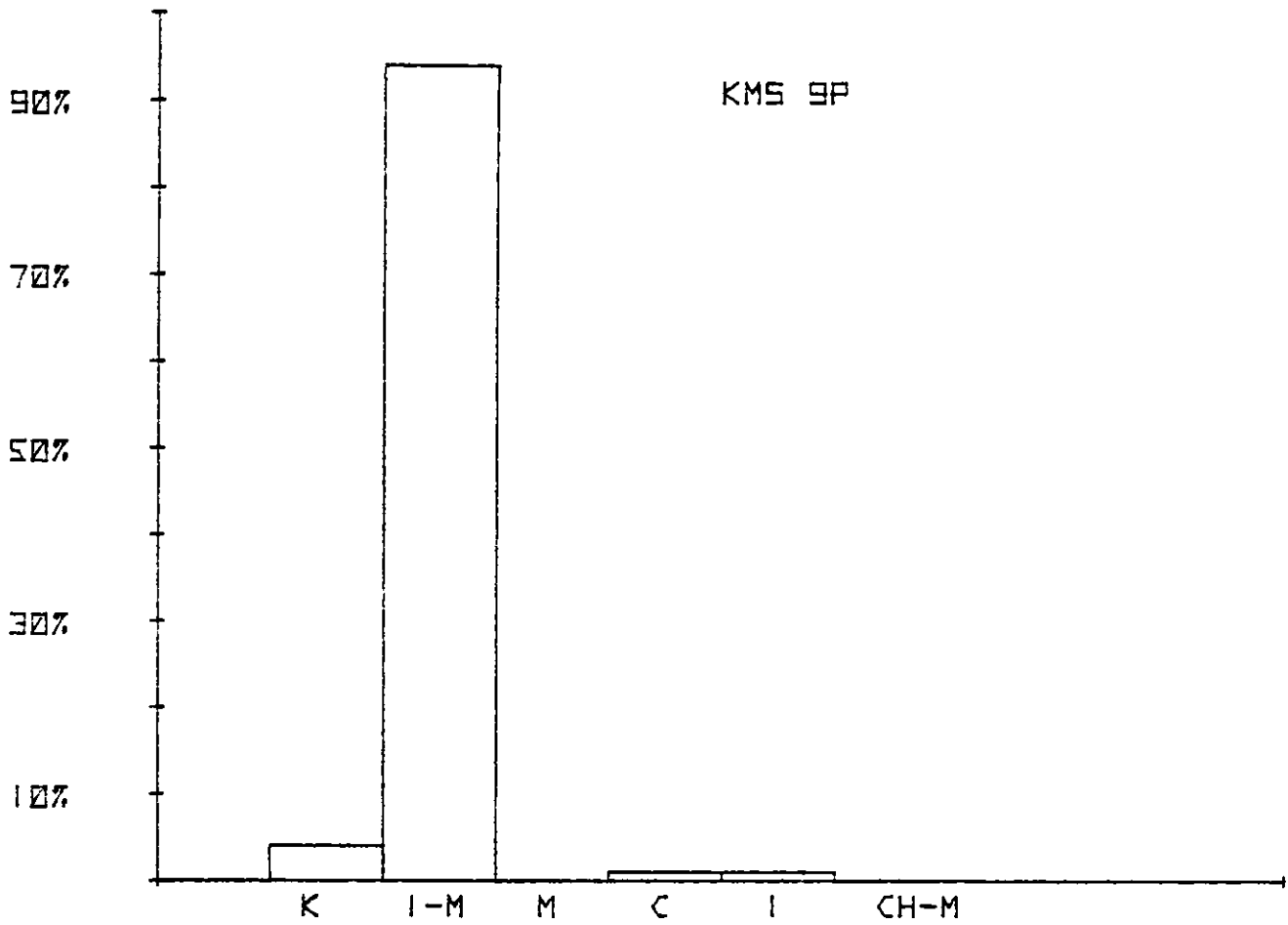


Figure 76

KMS 10P

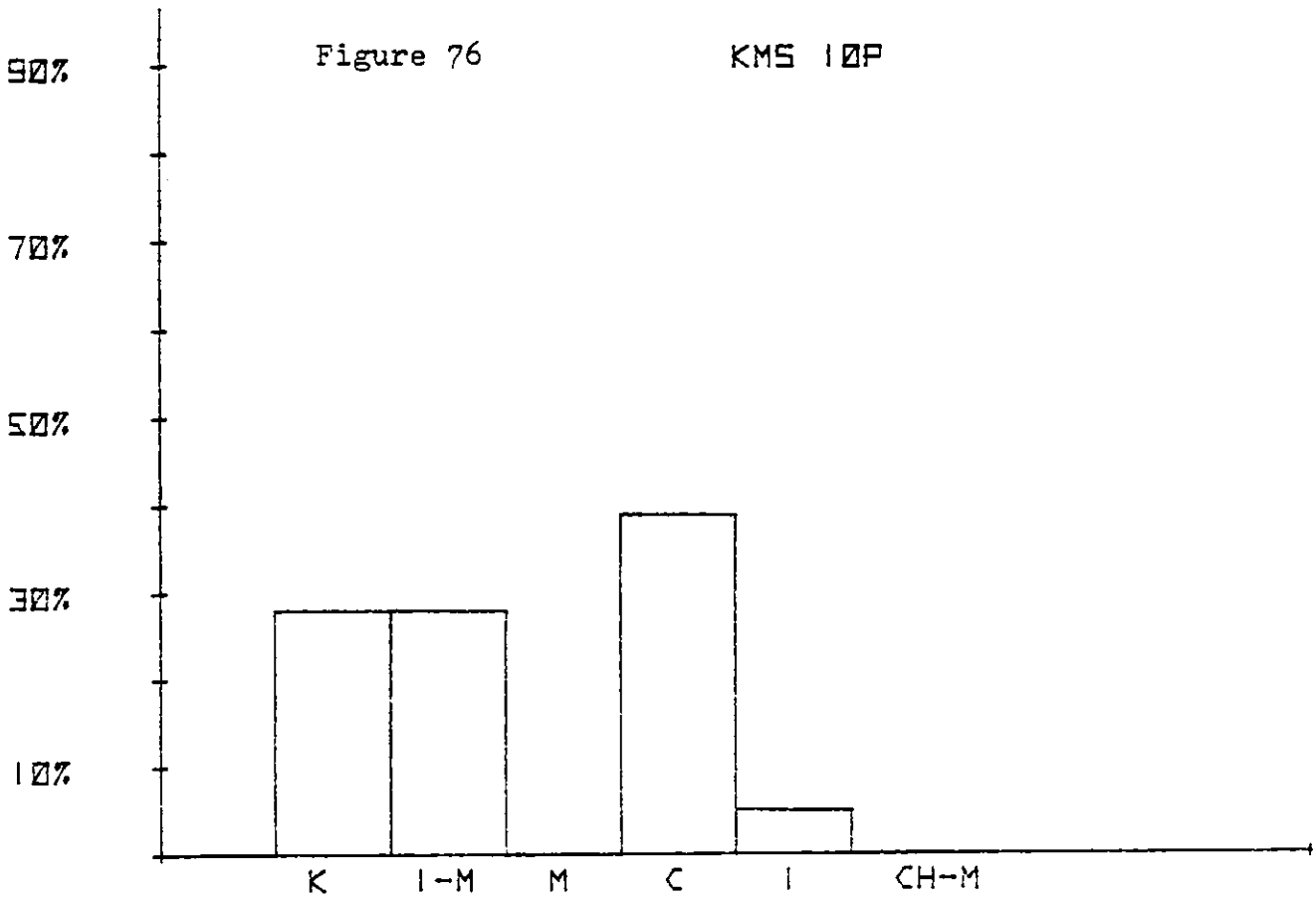


Figure 77

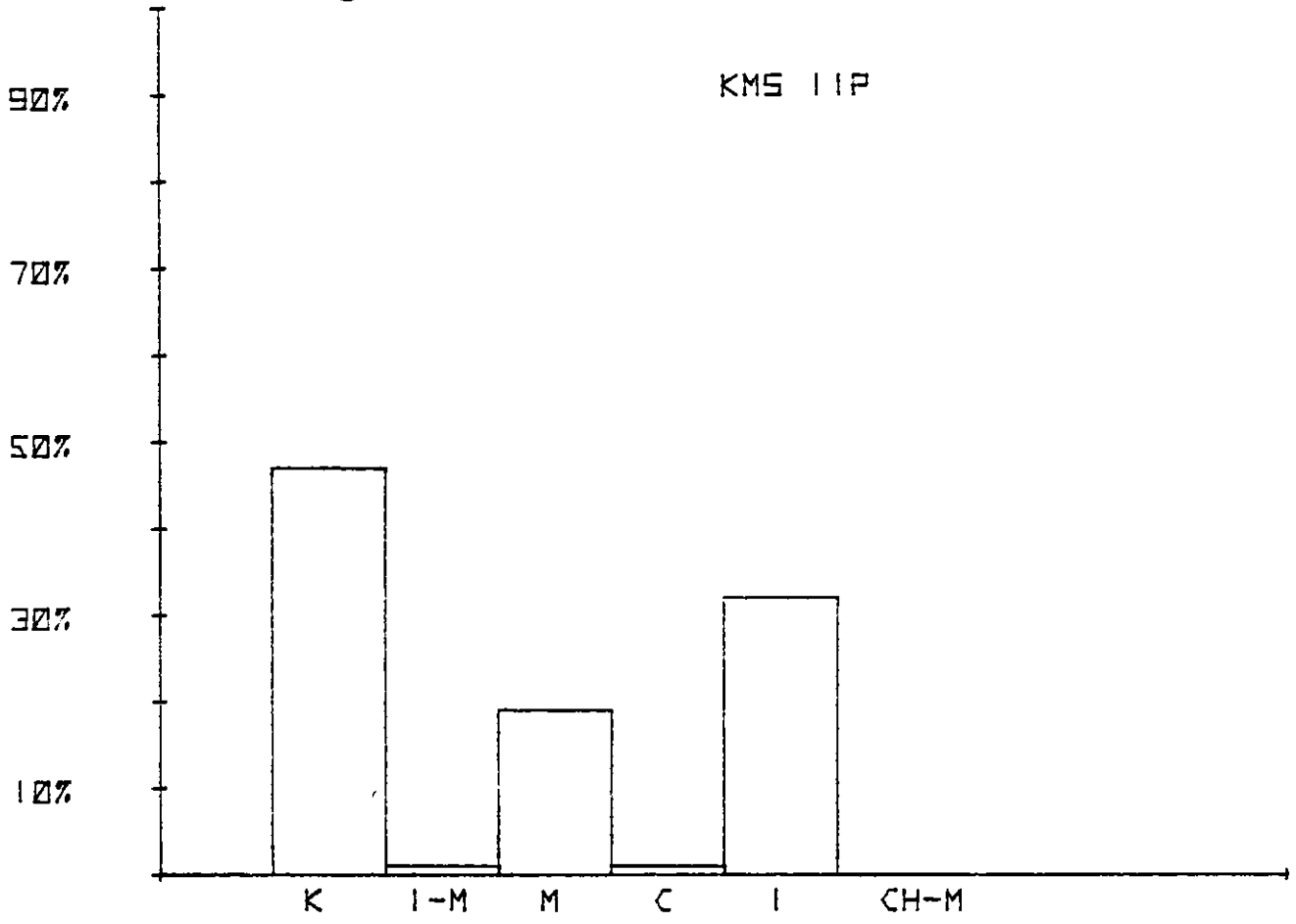


Figure 78

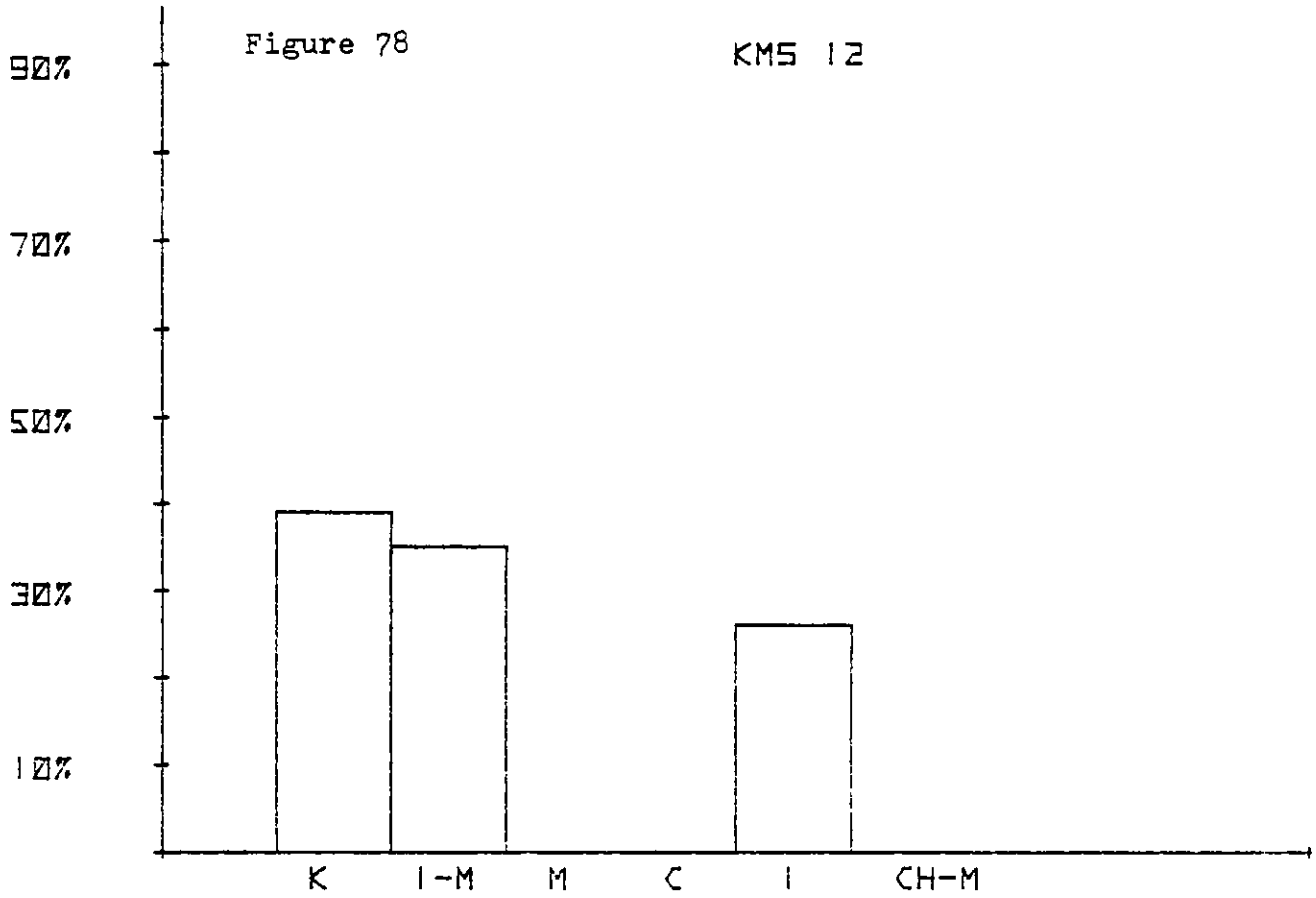


Figure 79

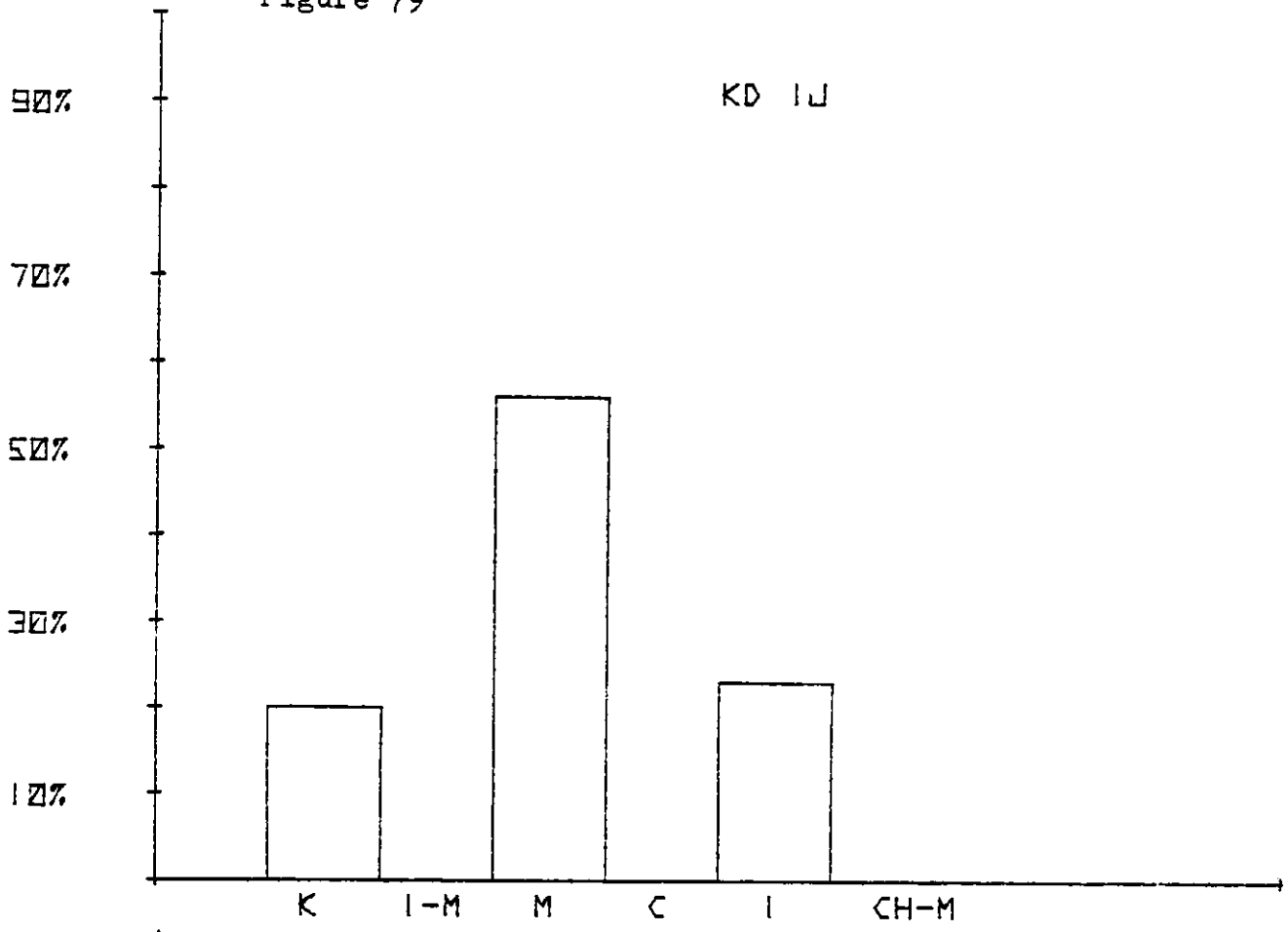


Figure 80

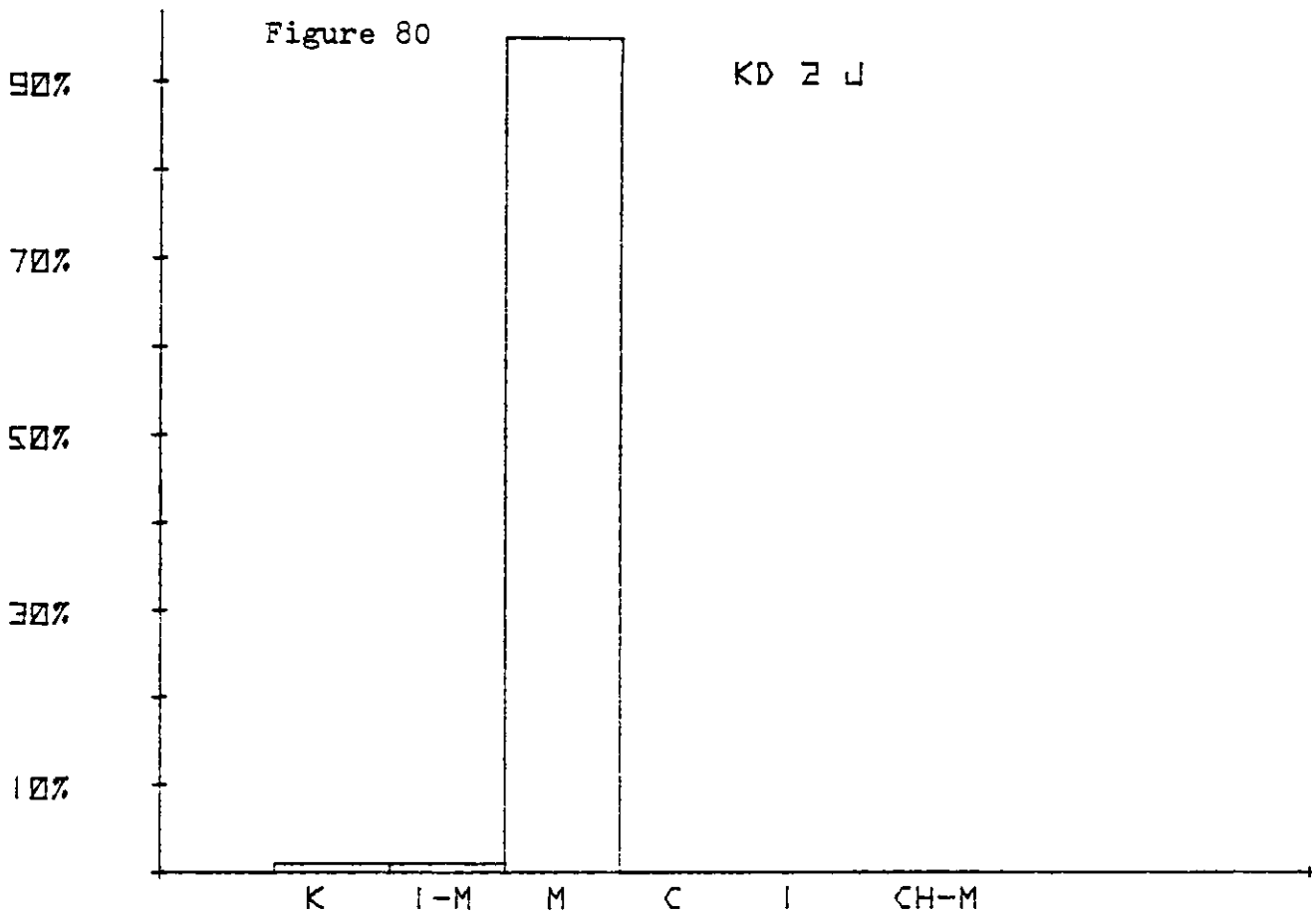
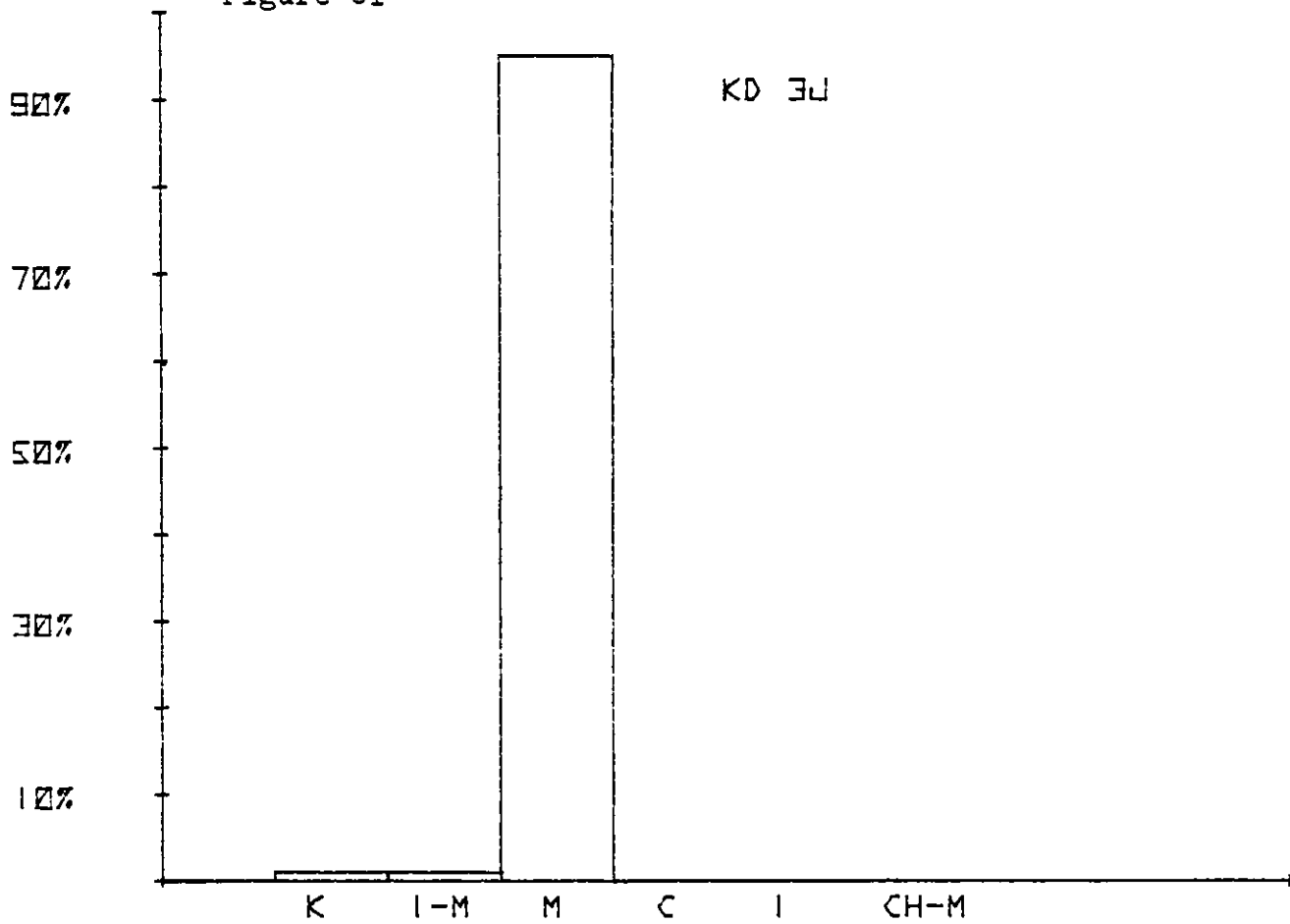
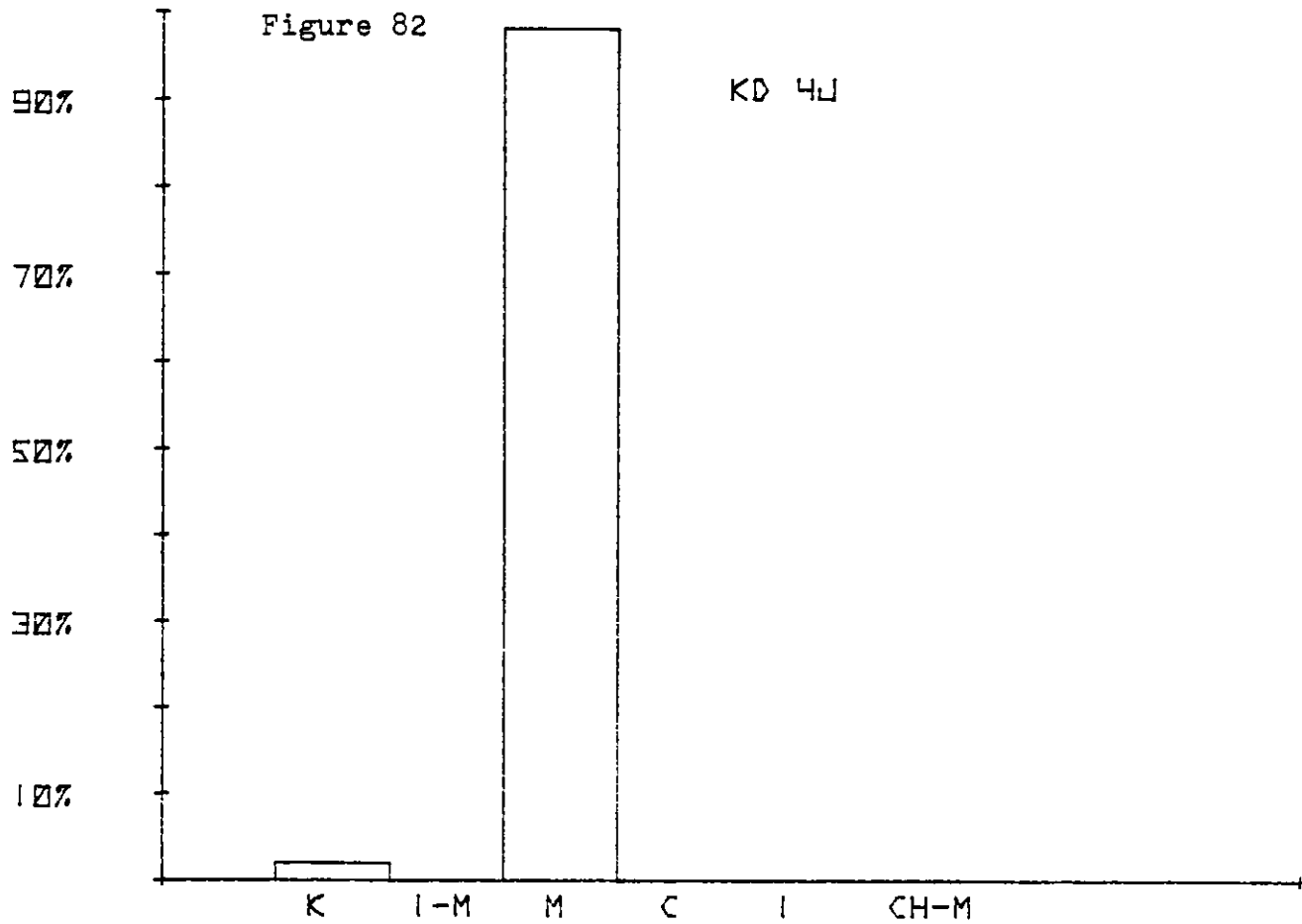


Figure 81



KD 3J

Figure 82



KD 4J

Figure 83

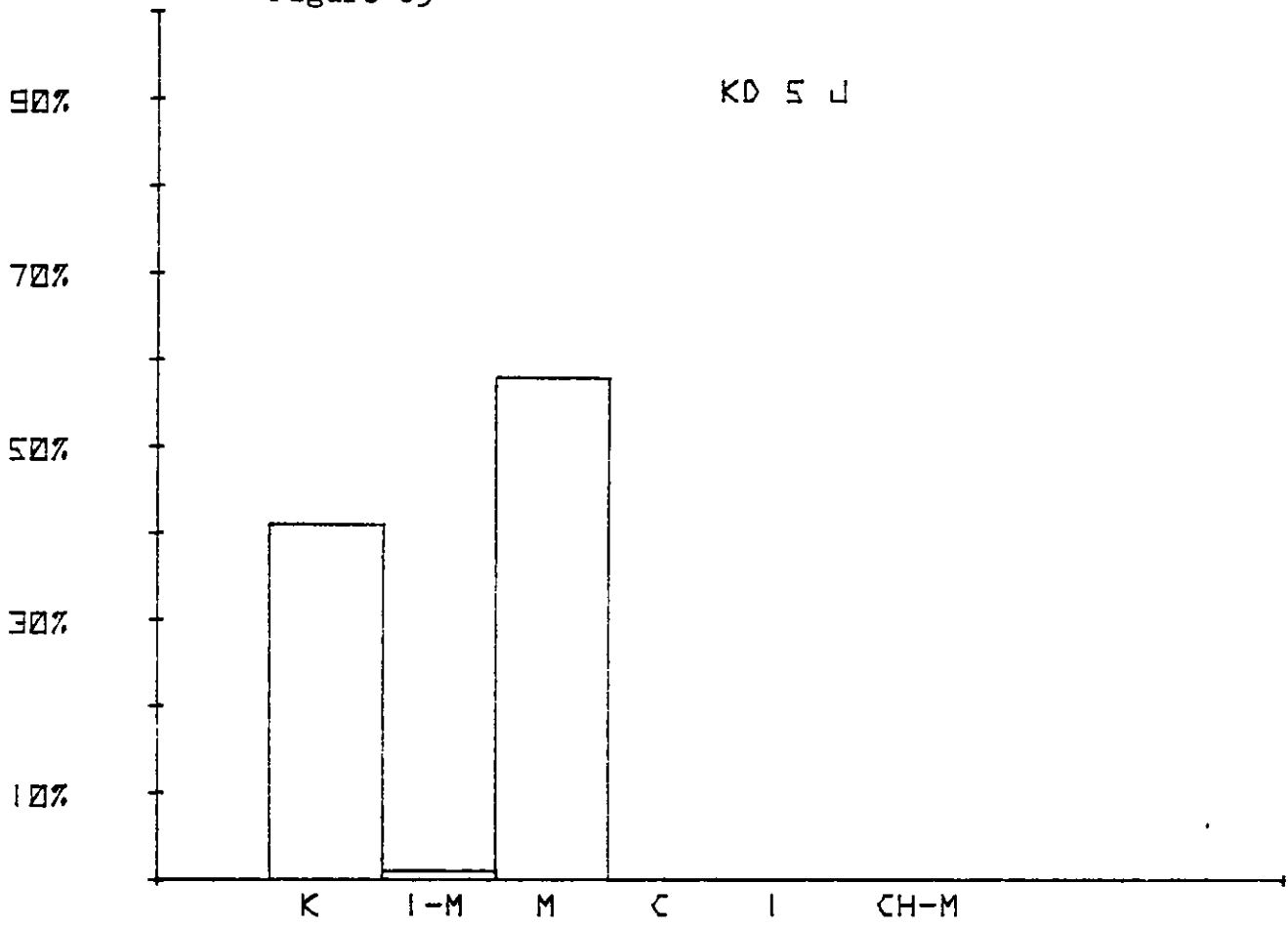


Figure 84

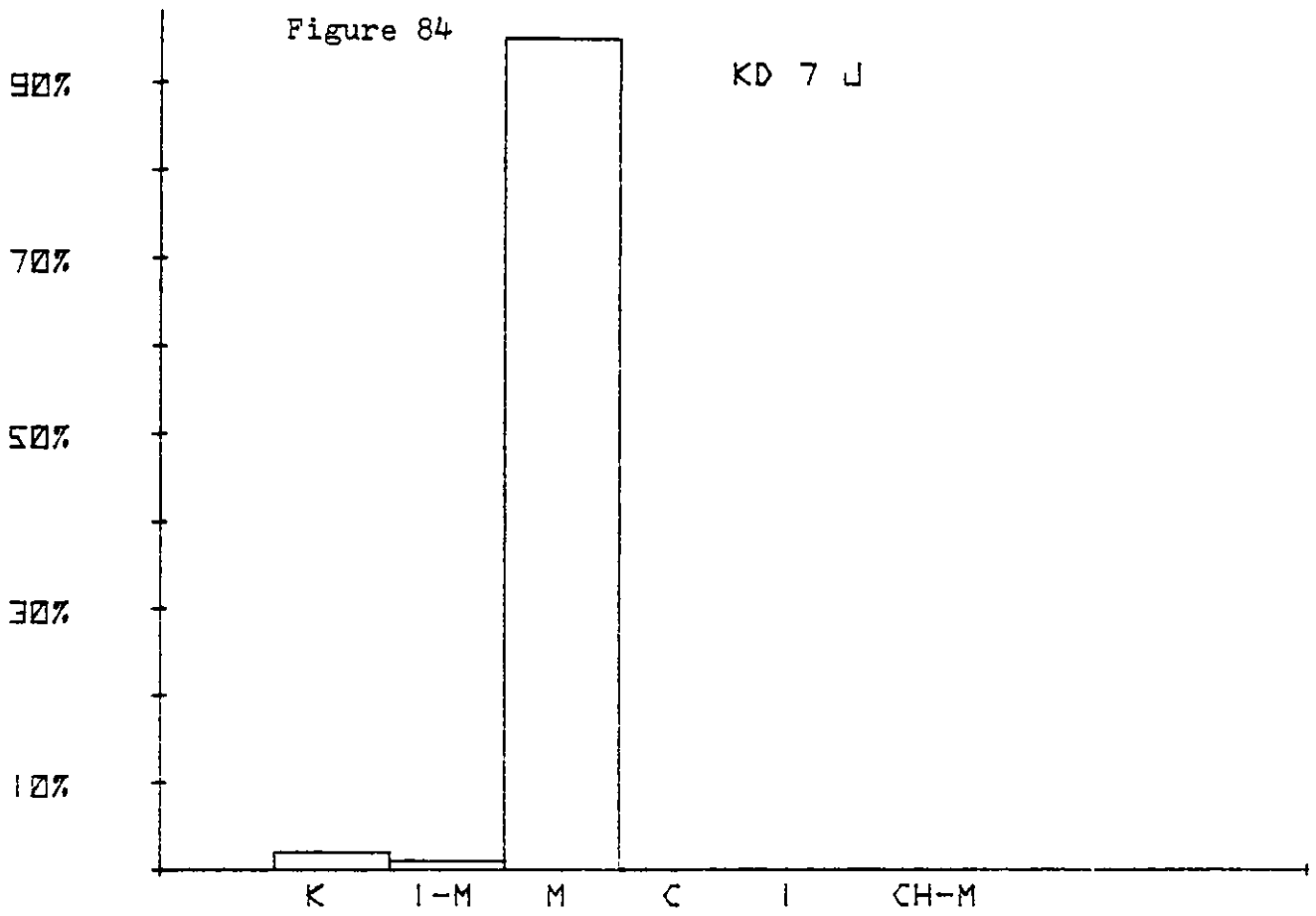


Figure 85

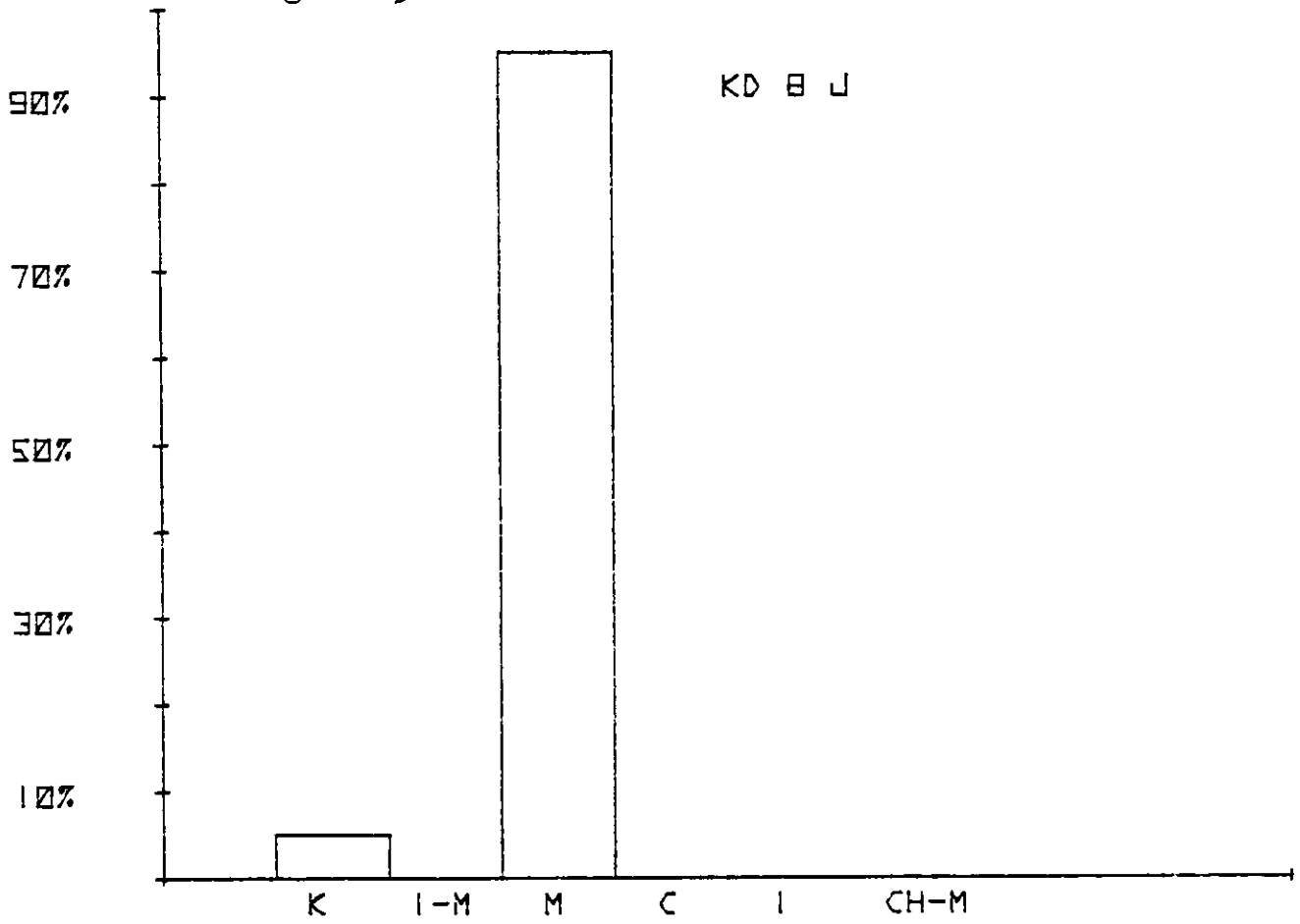


Figure 86

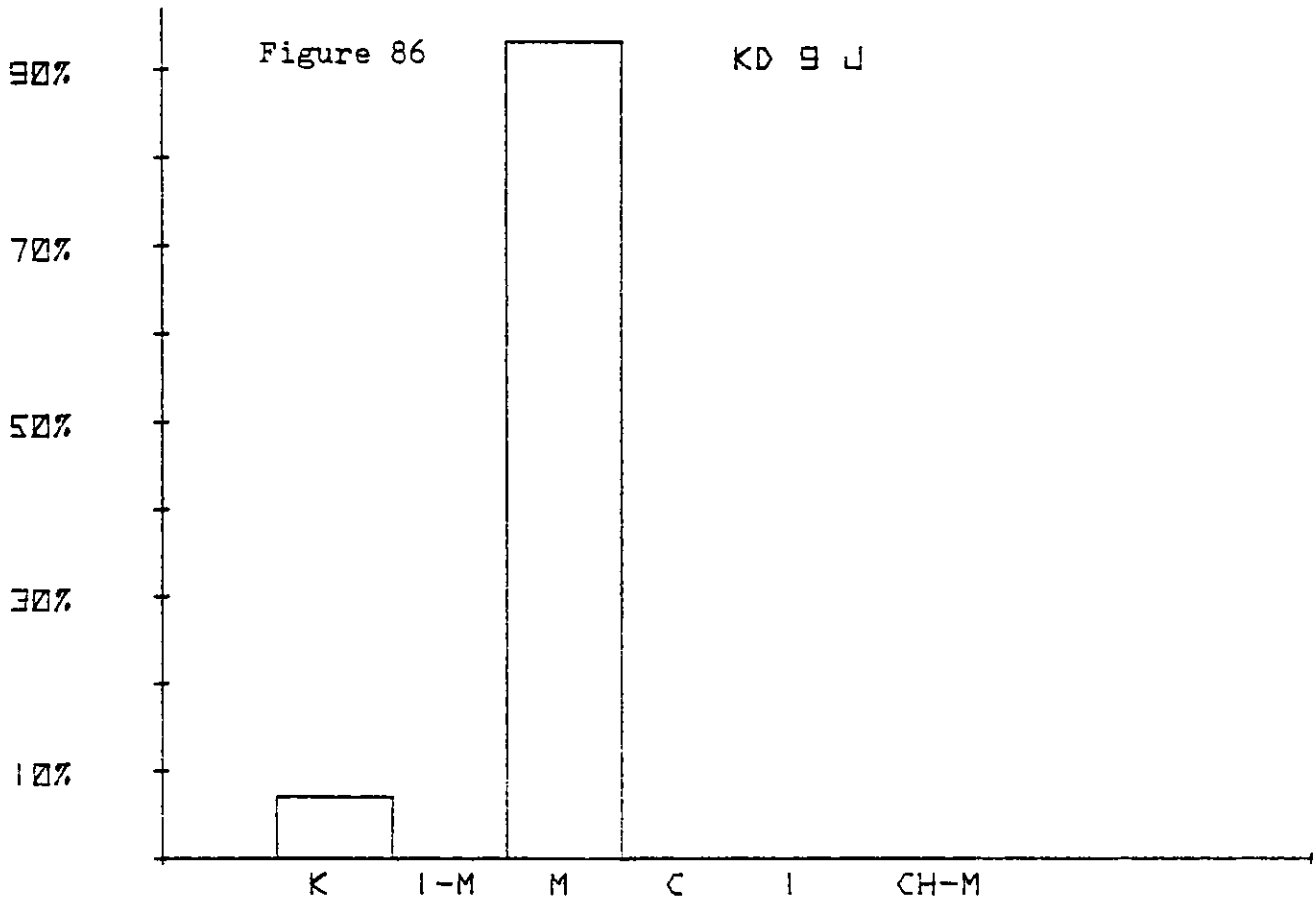


Figure 87

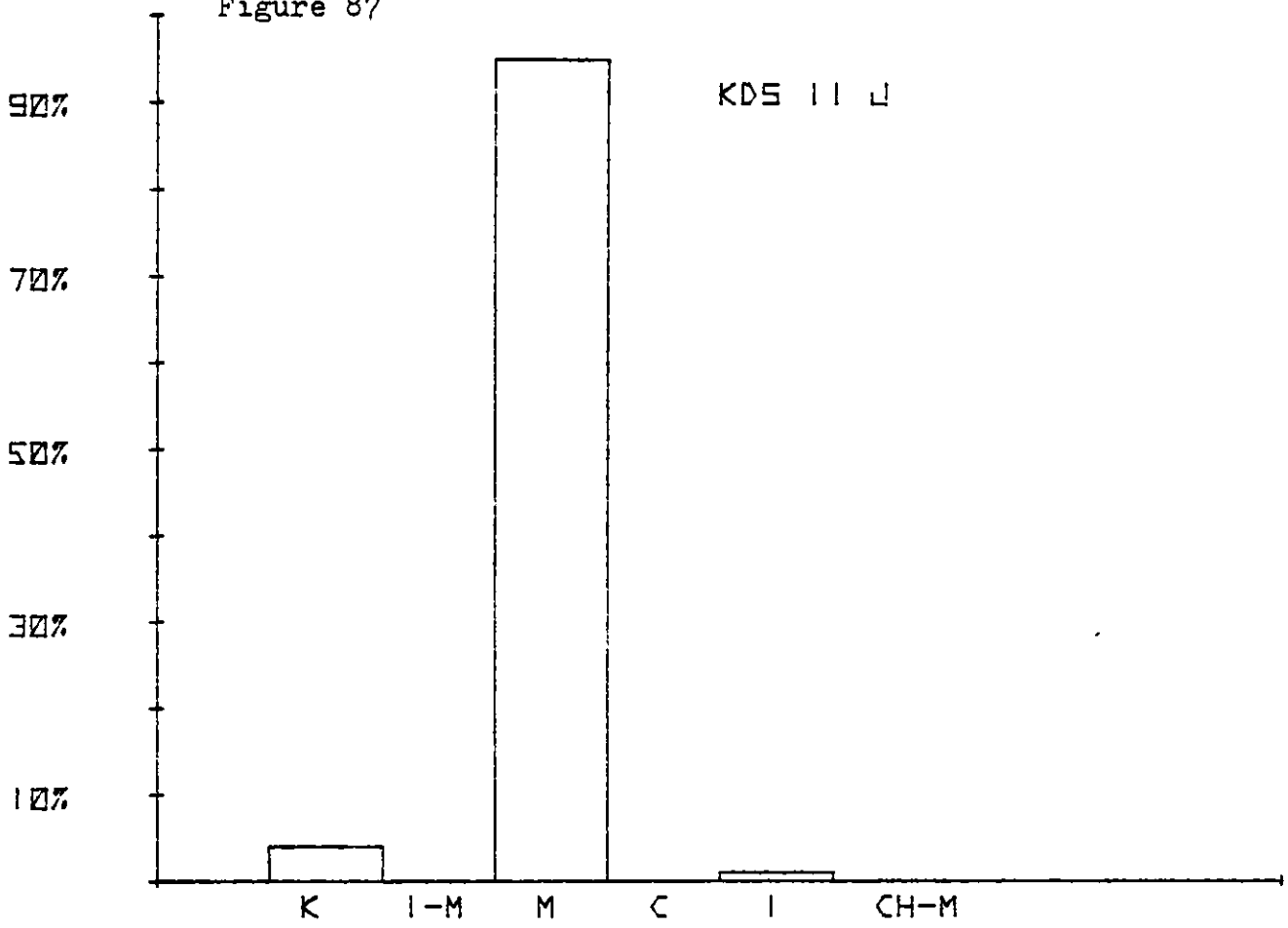


Figure 88

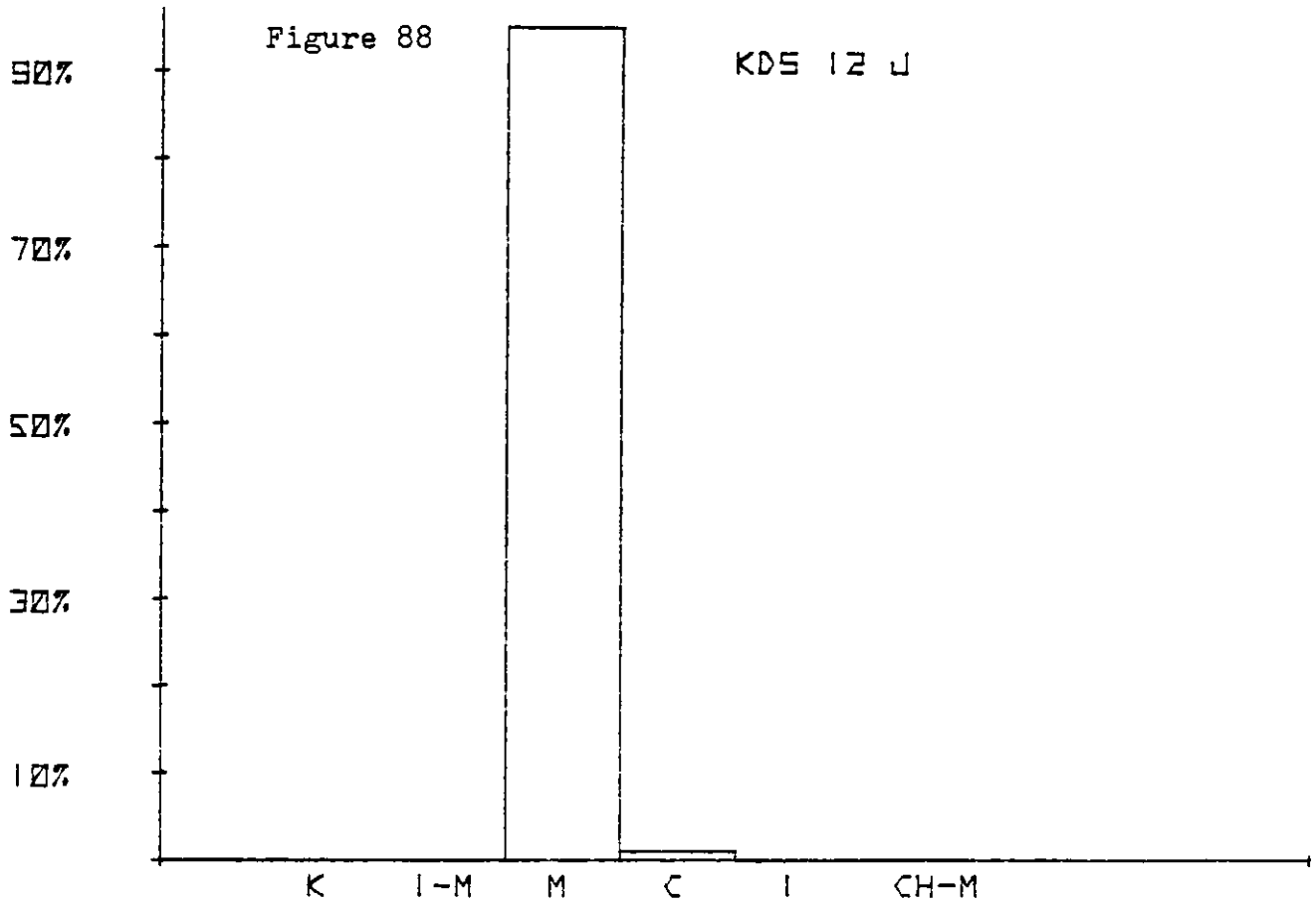


Figure 89

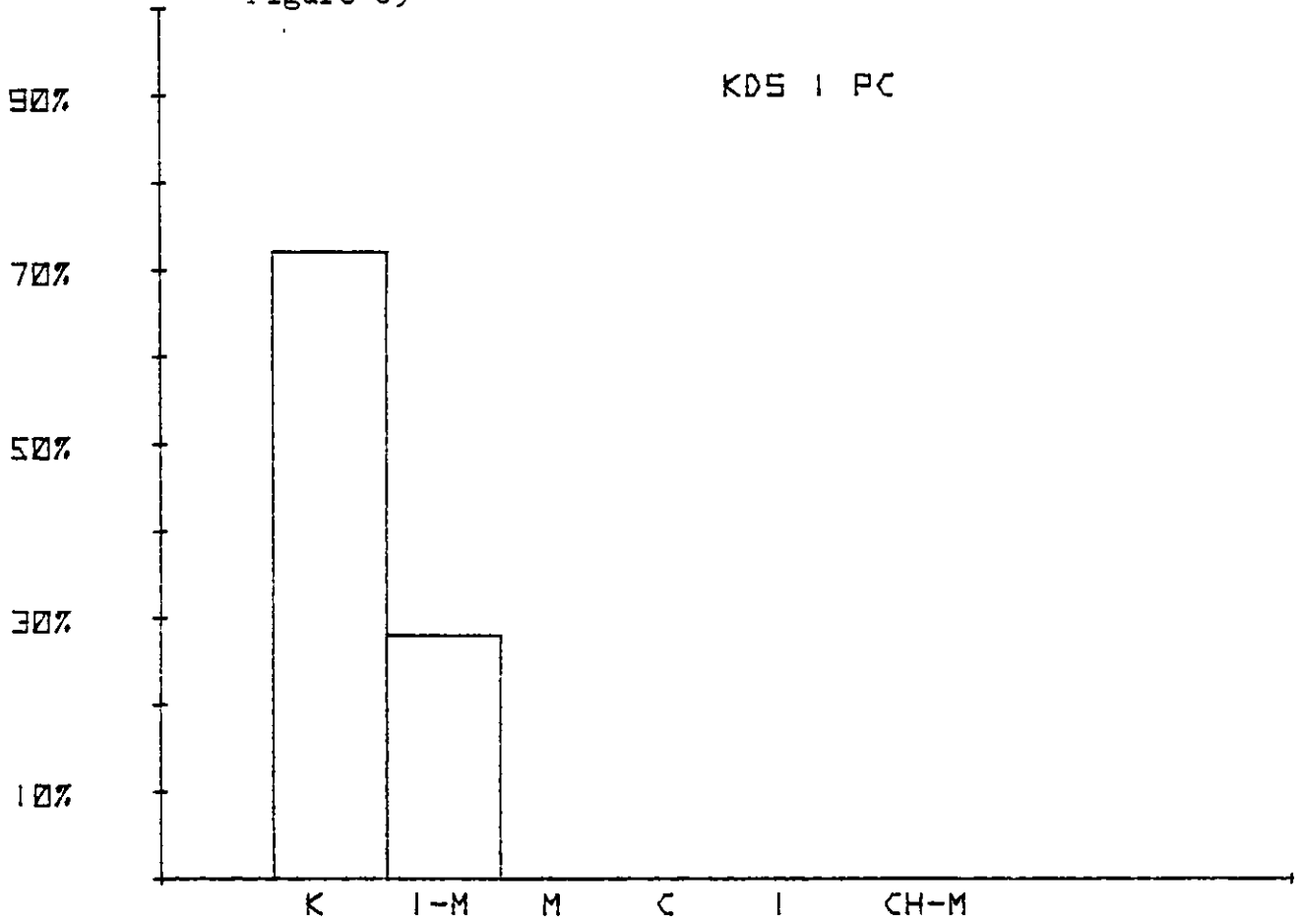


Figure 90

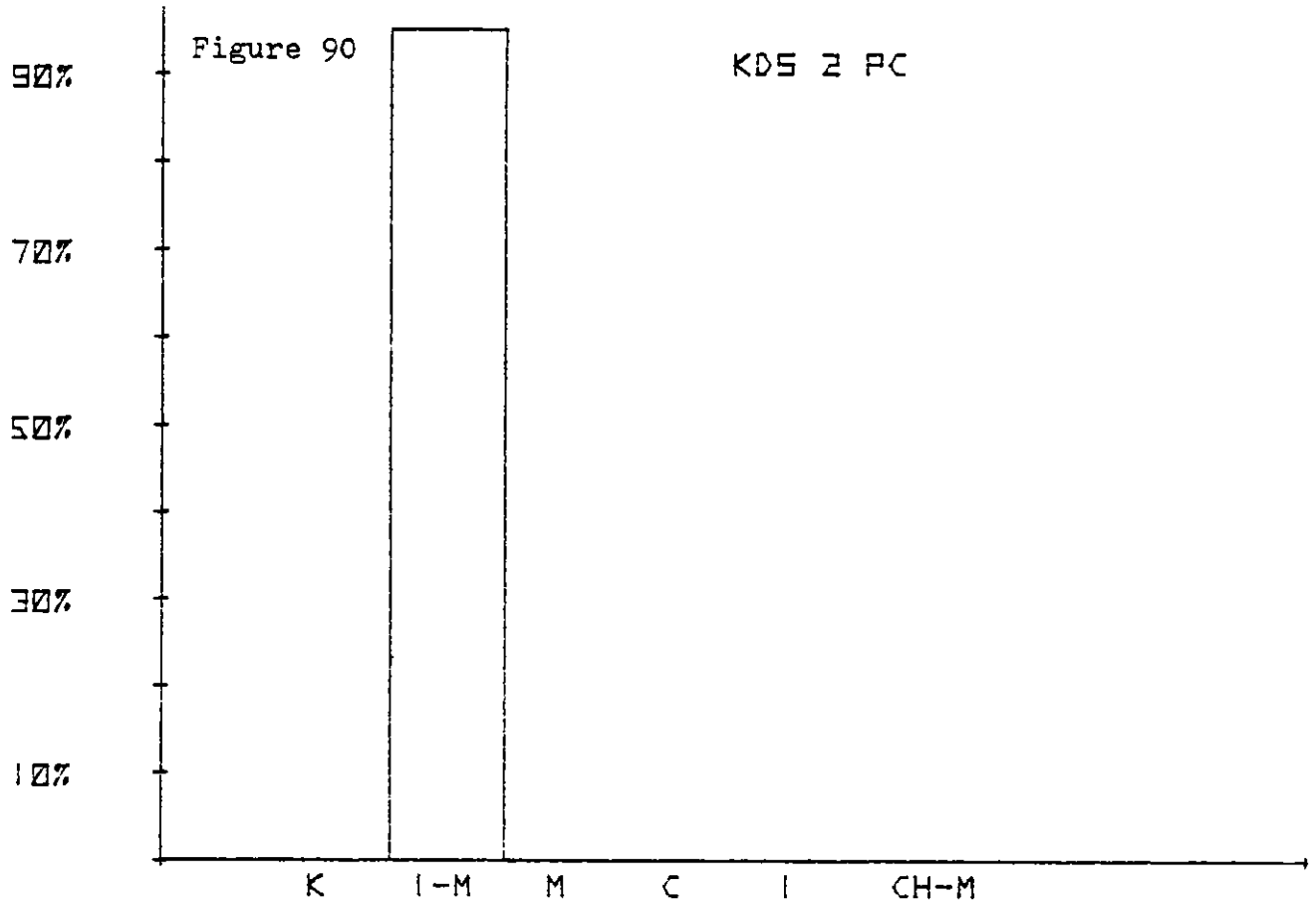


Figure 91

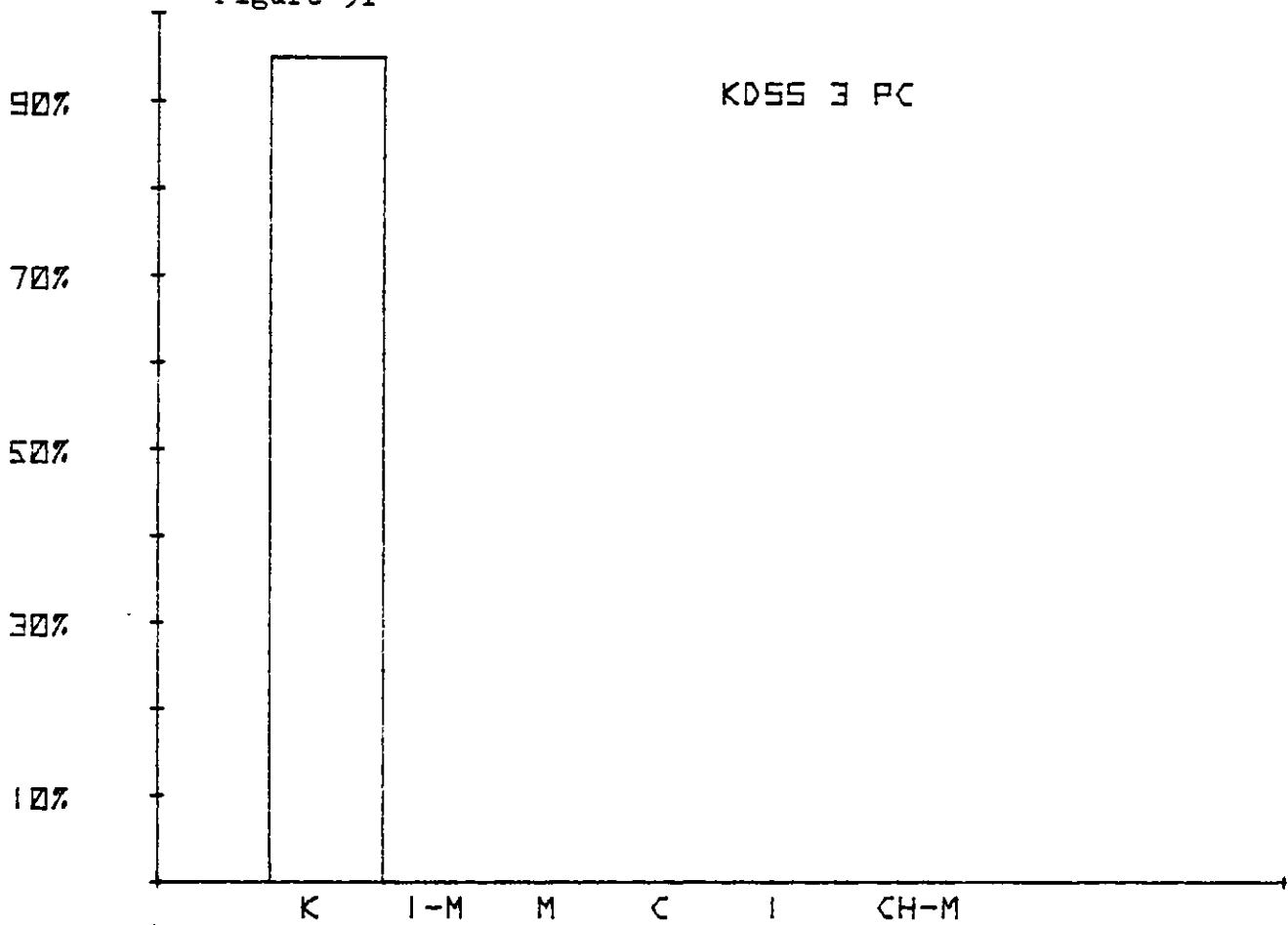


Figure 92

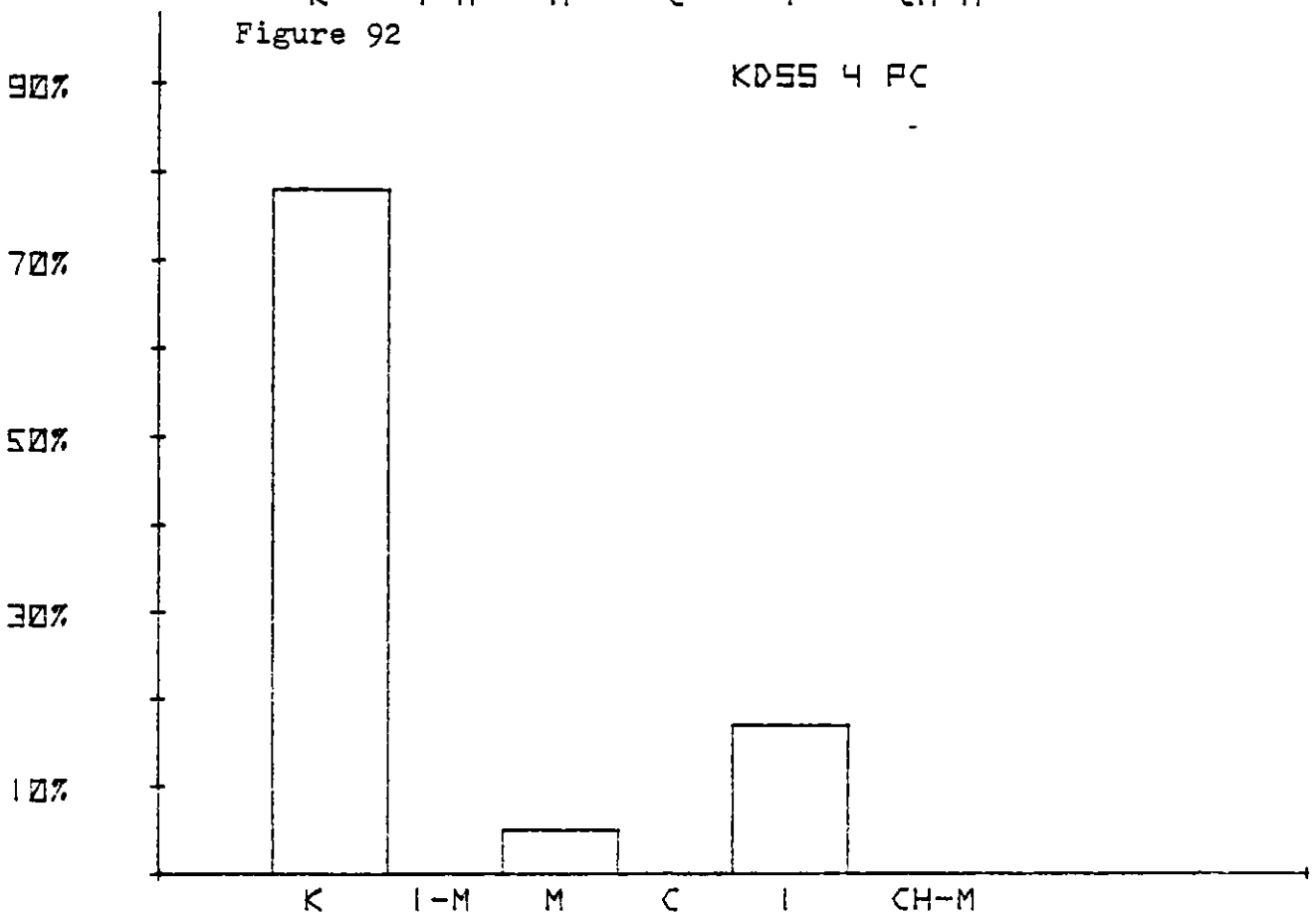


Figure 93

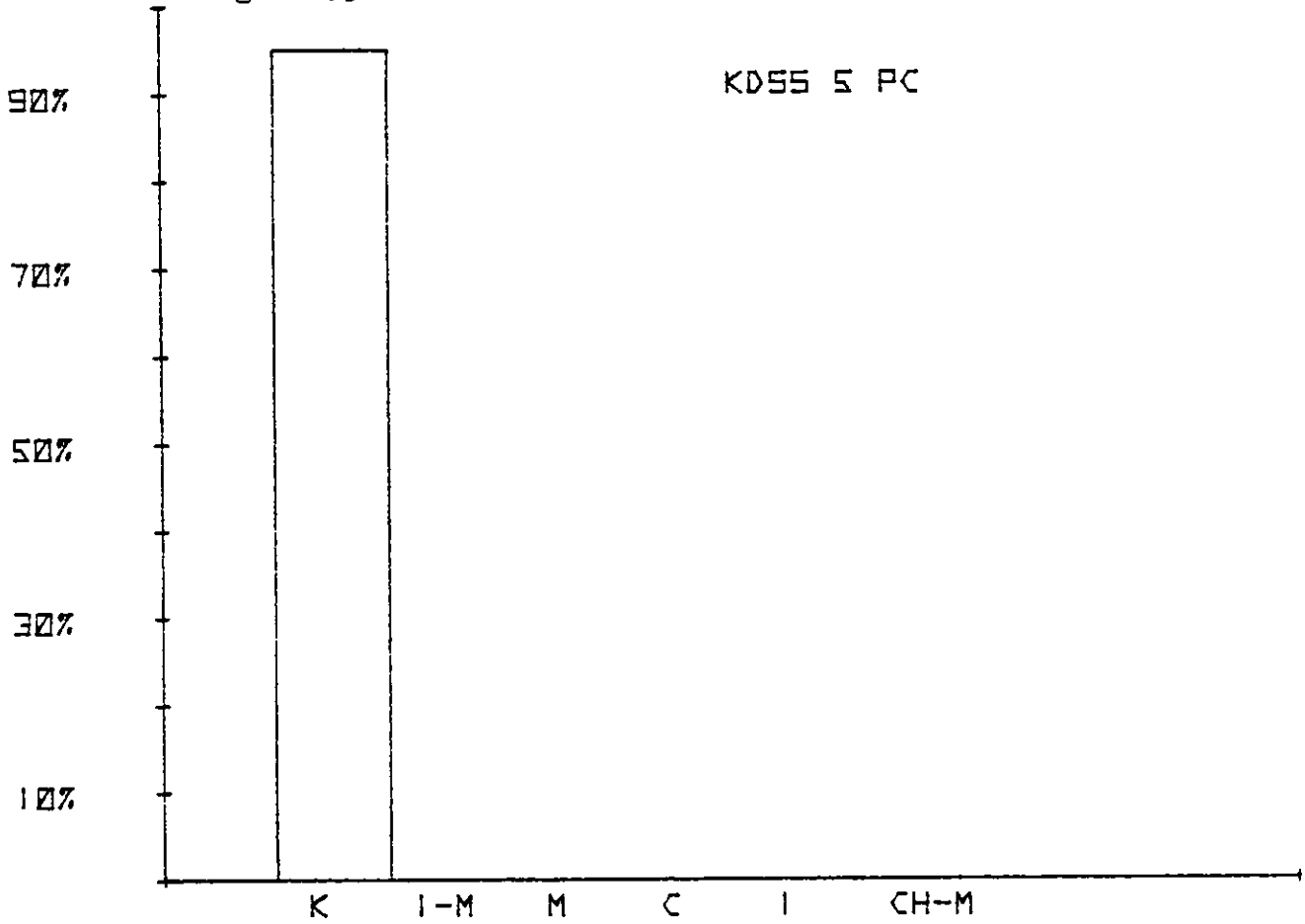


Figure 94

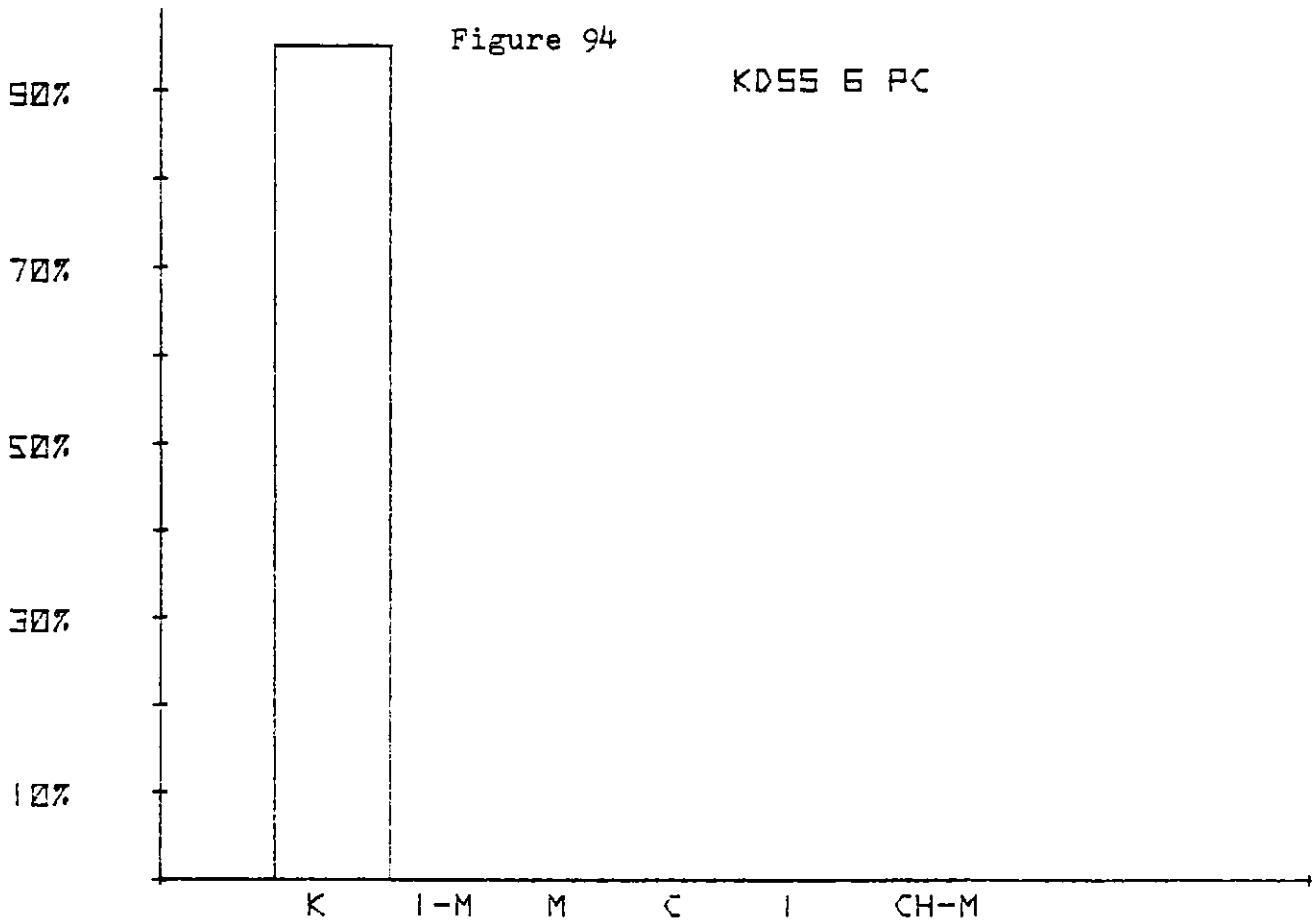


Figure 95

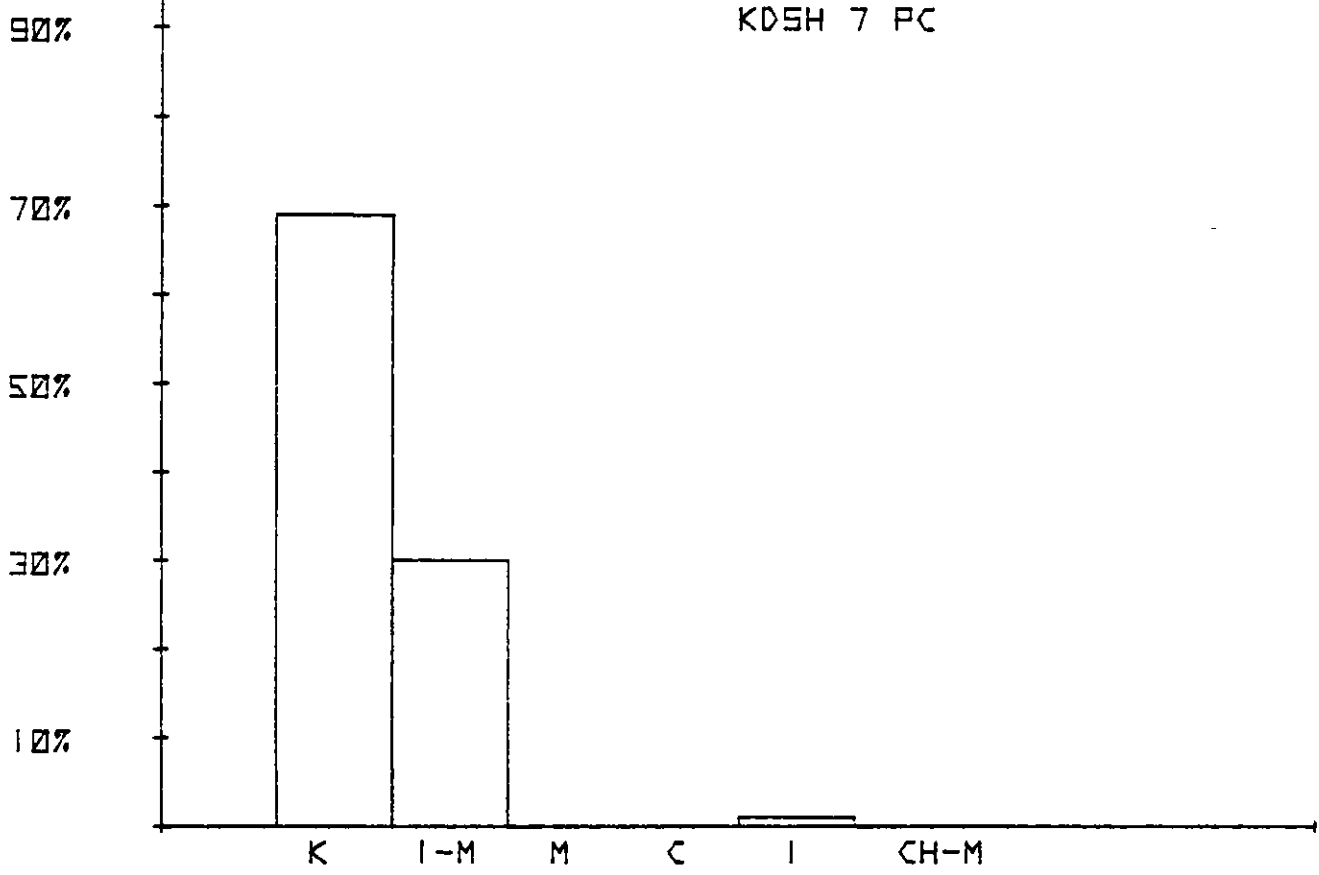


Figure 96

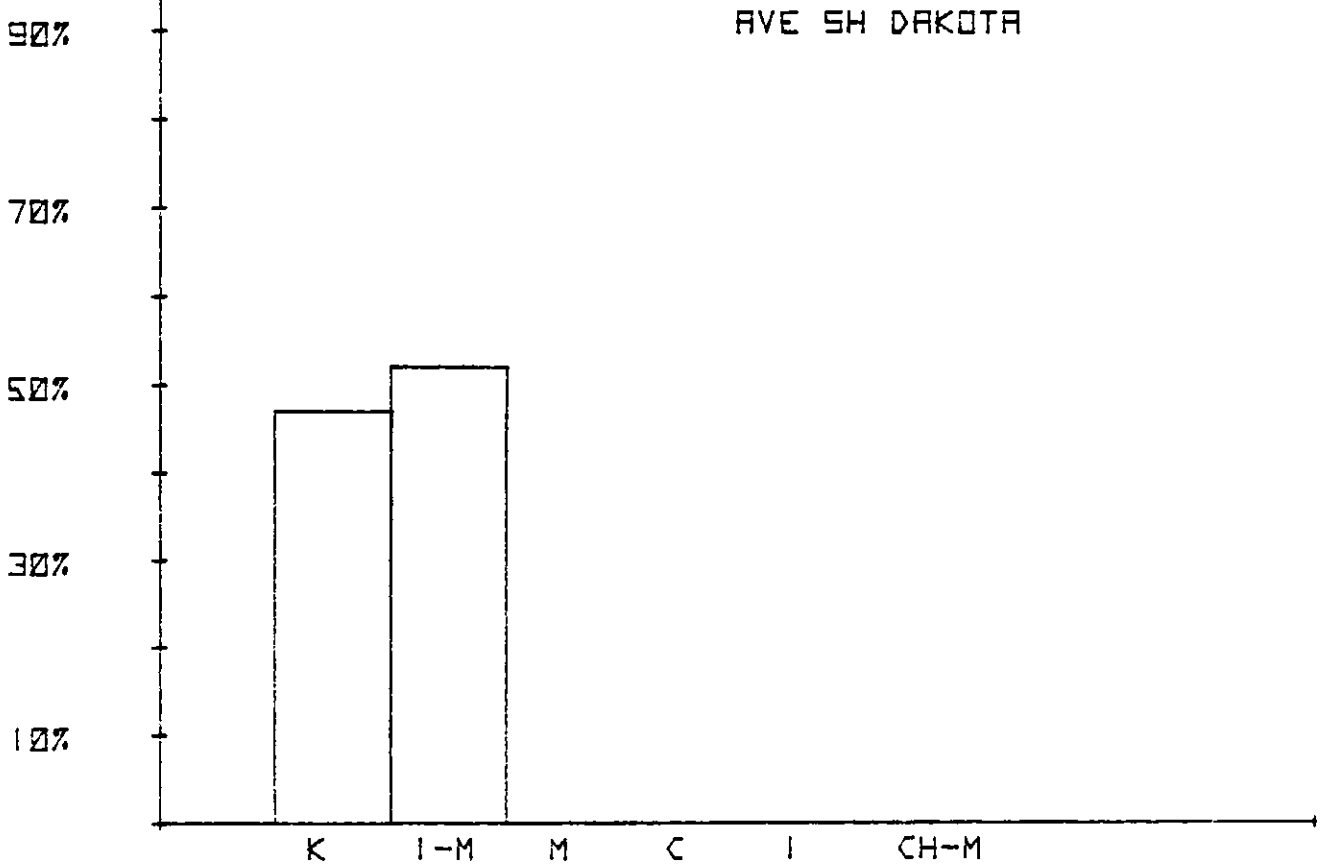


Figure 97

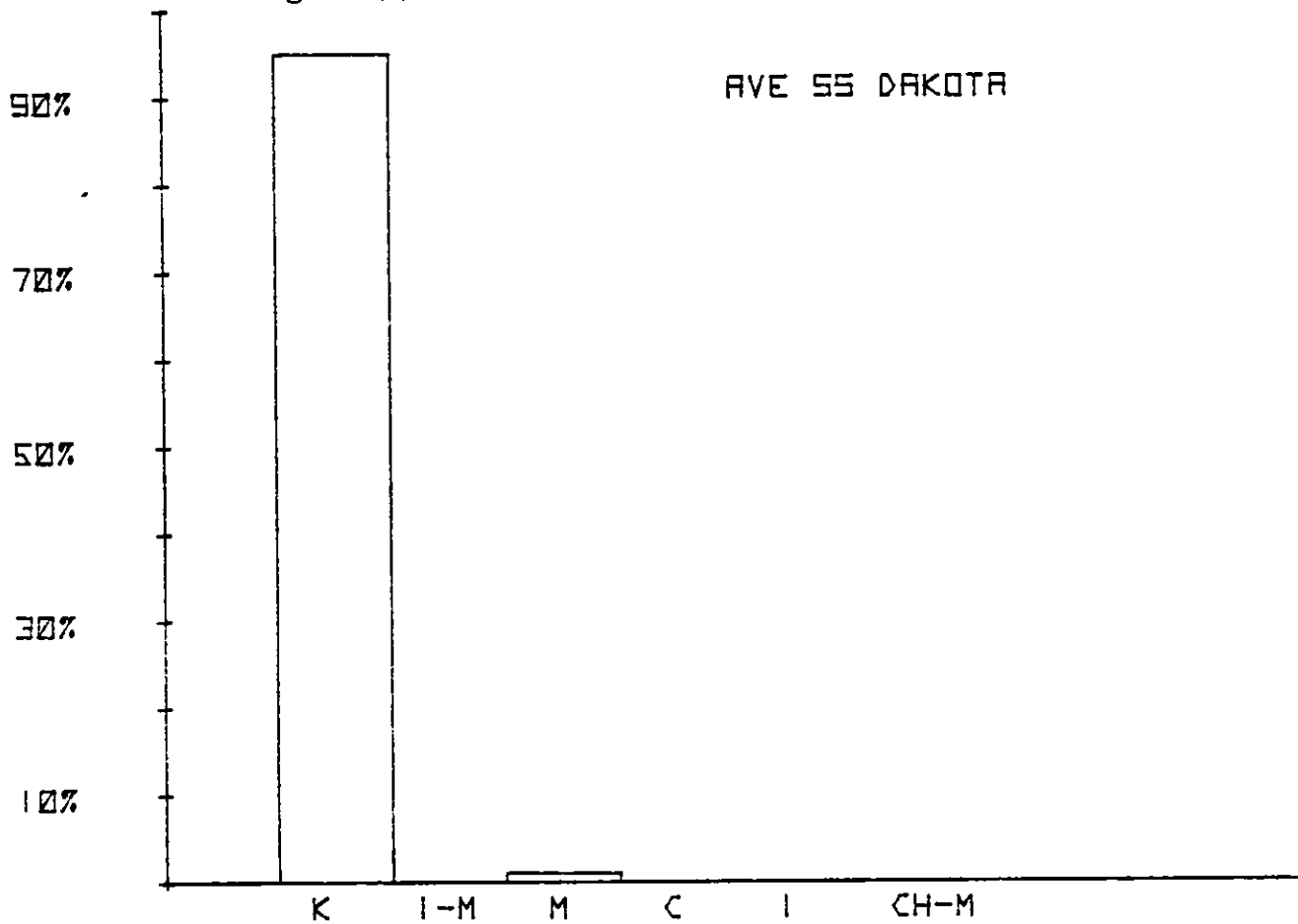


Figure 98

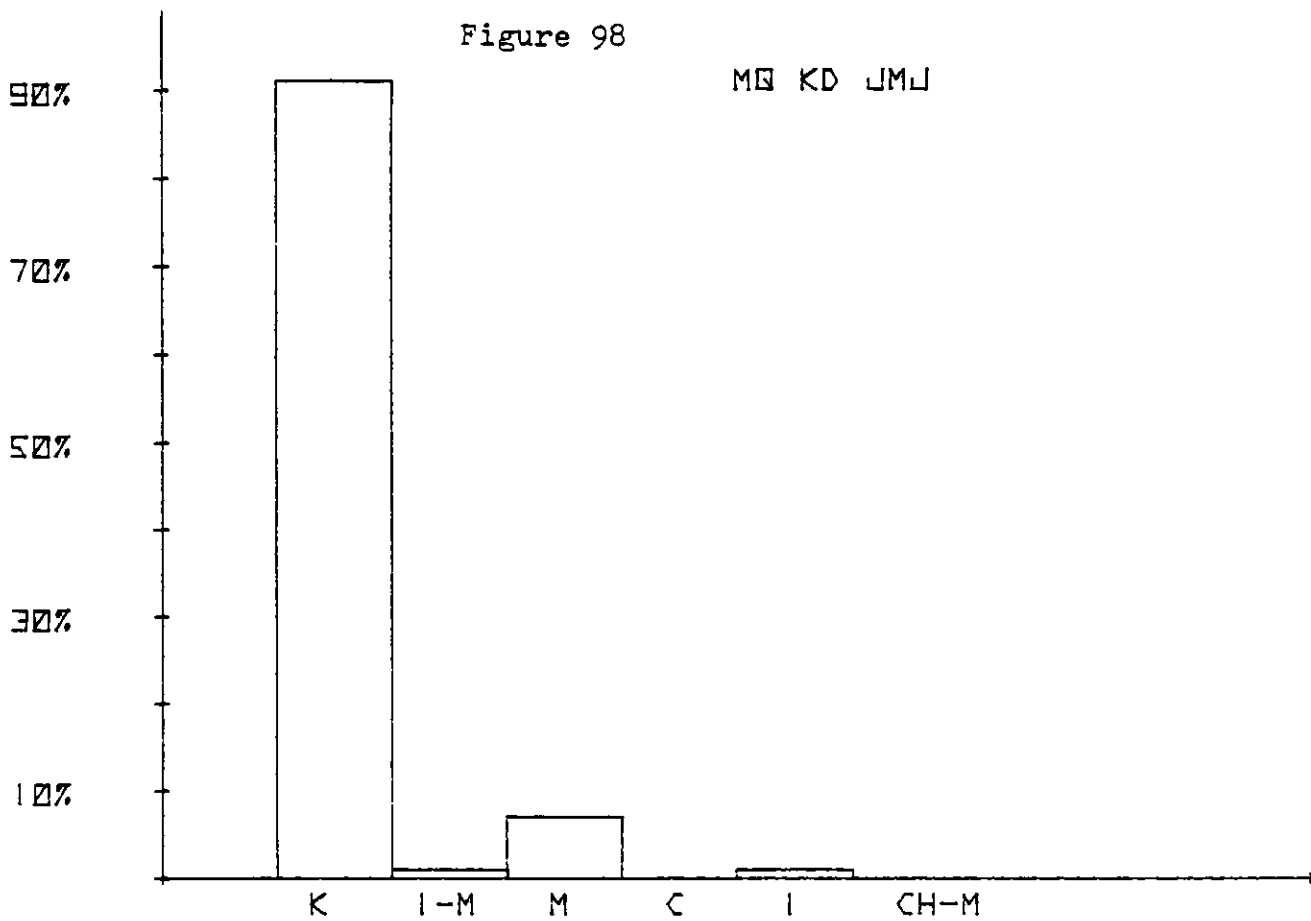
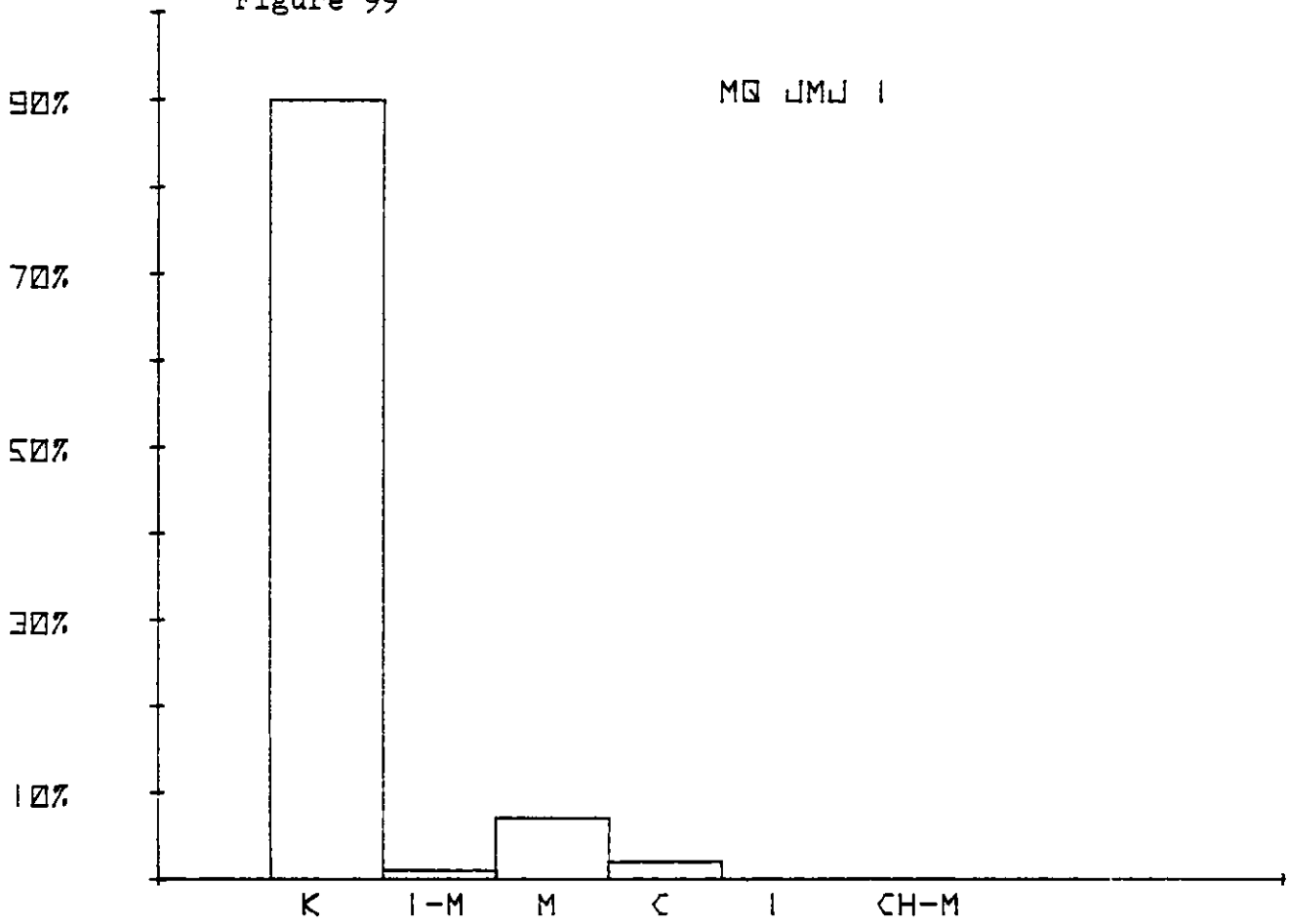
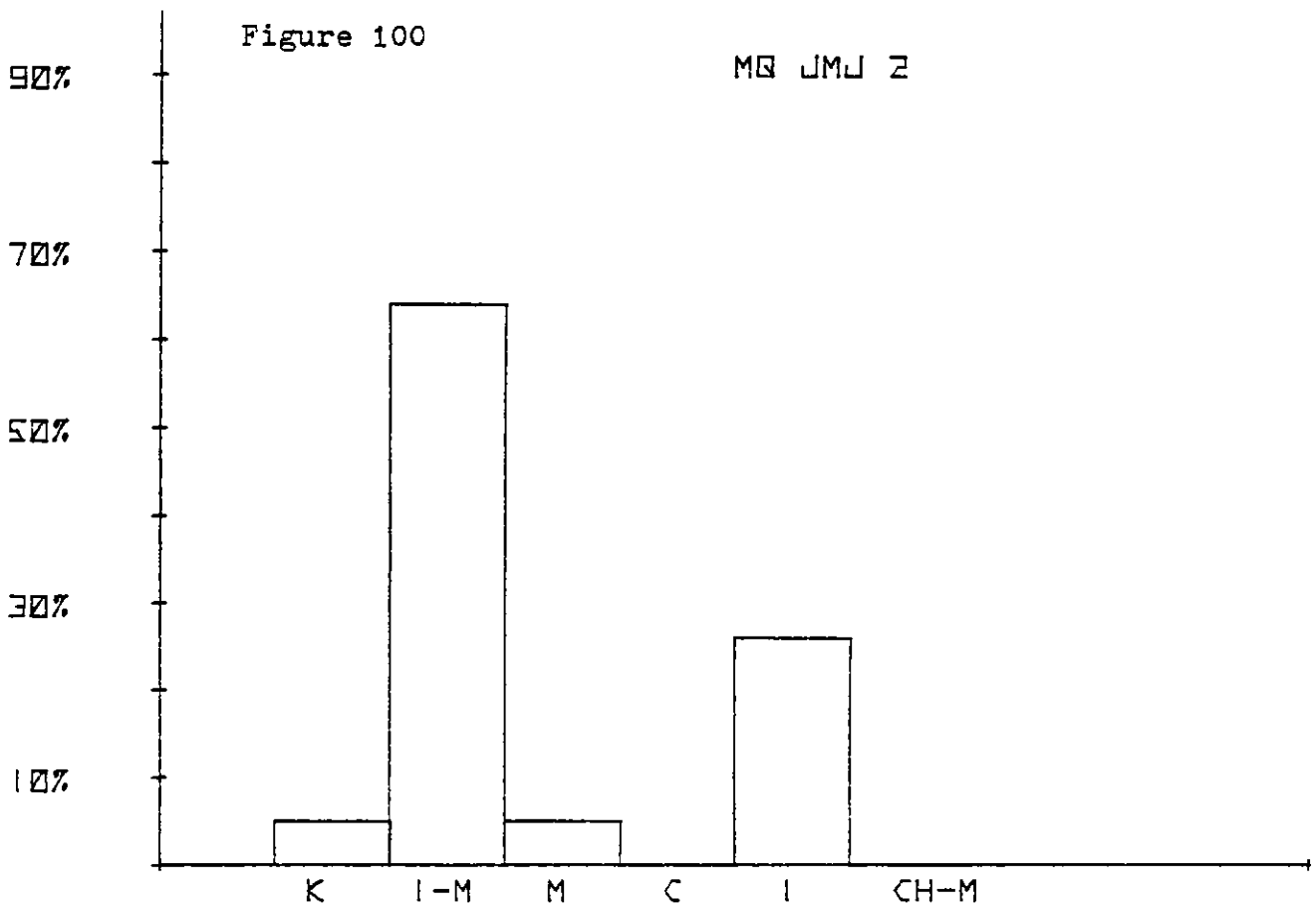


Figure 99



MQ JMJ 1

Figure 100



MQ JMJ 2

Figure 101

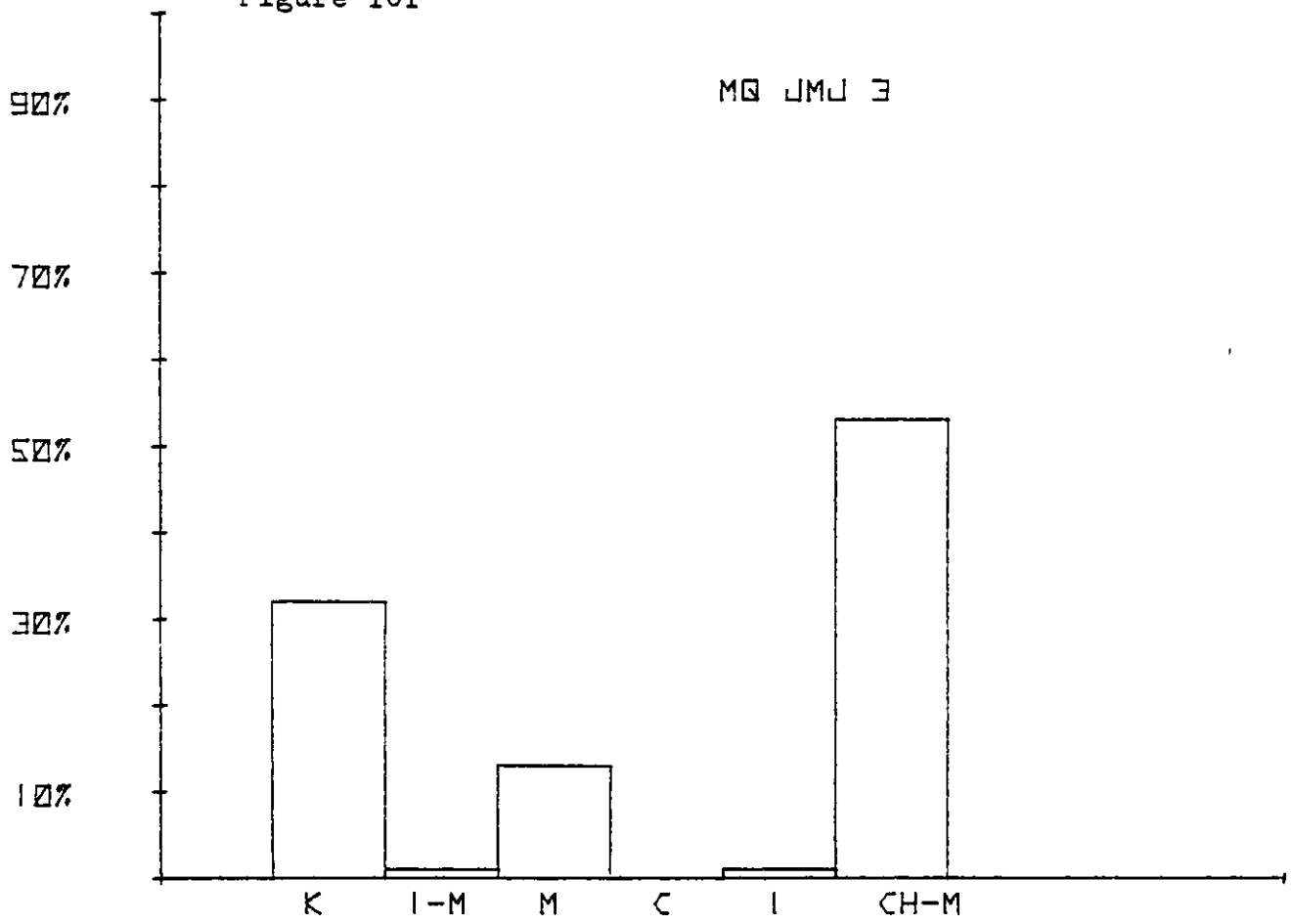


Figure 102

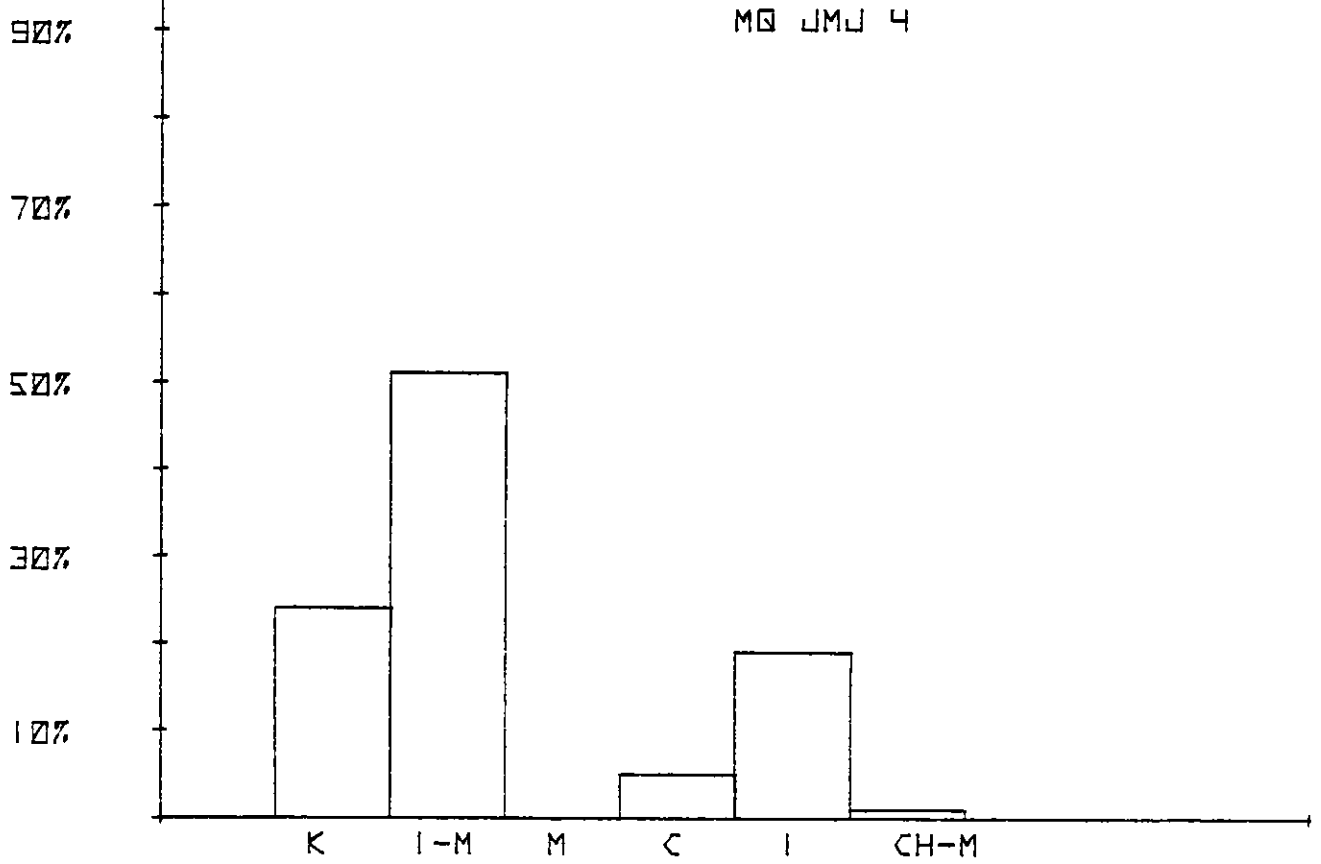


Figure 103

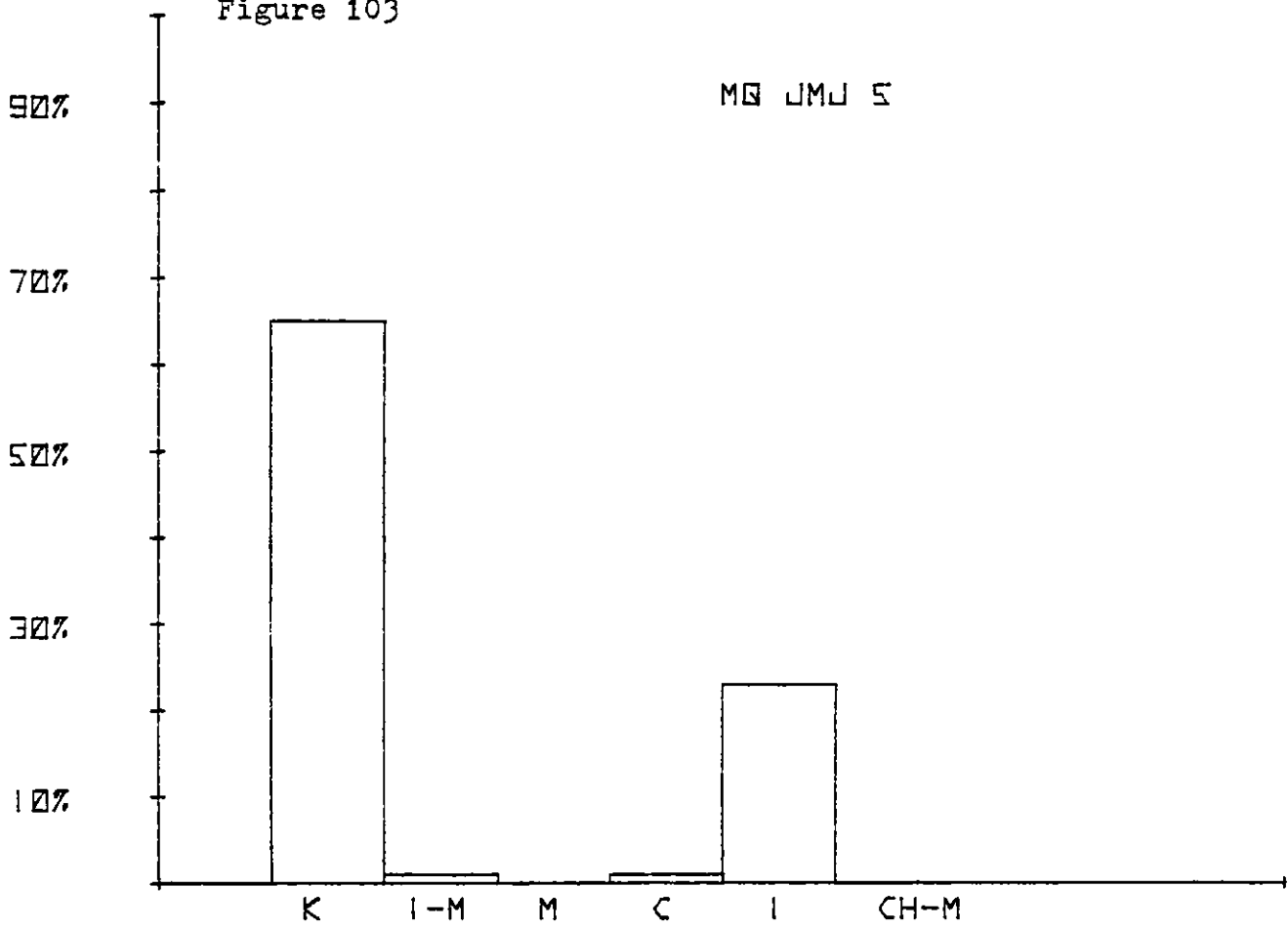


Figure 104

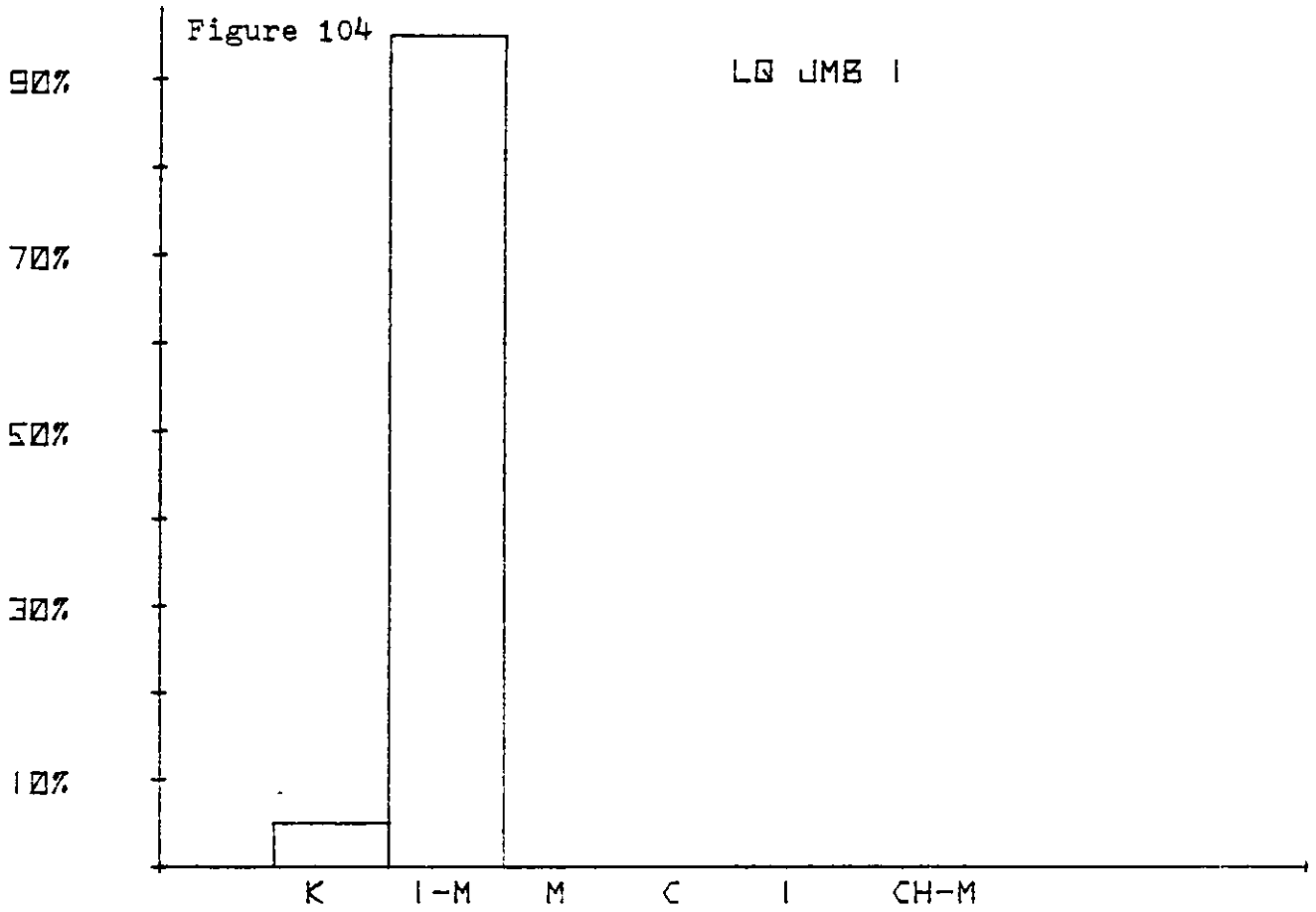


Figure 105

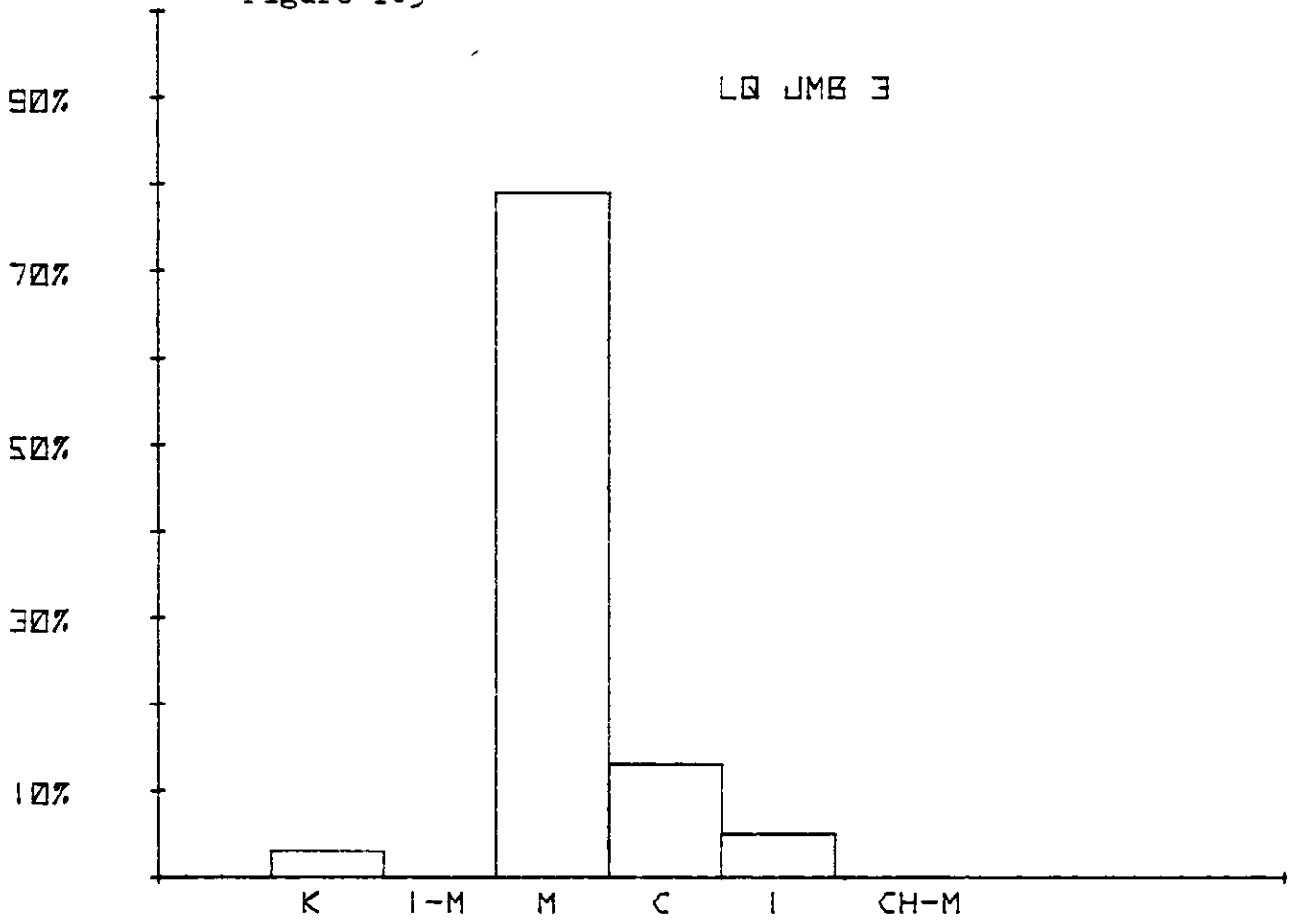


Figure 106

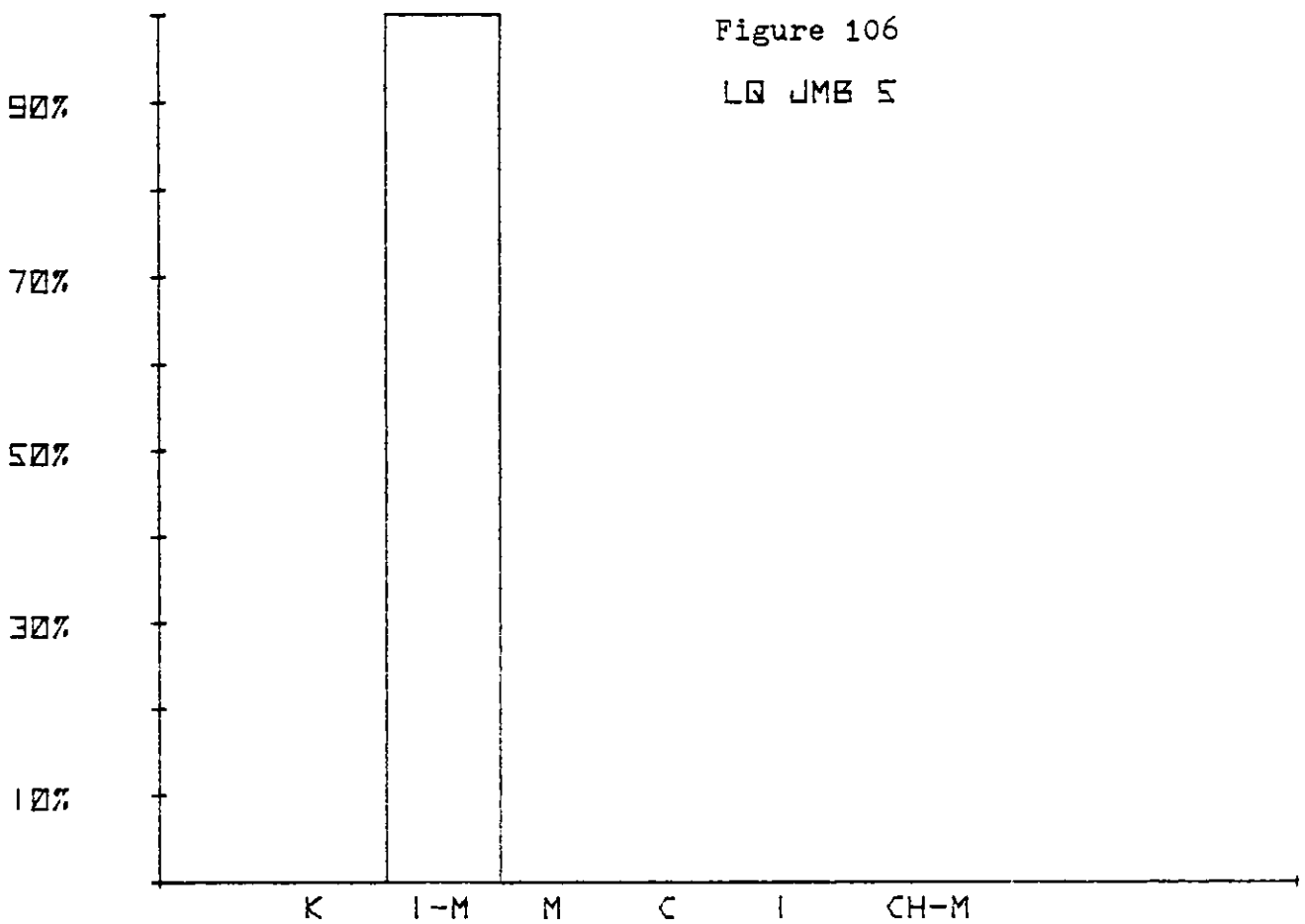


Figure 107

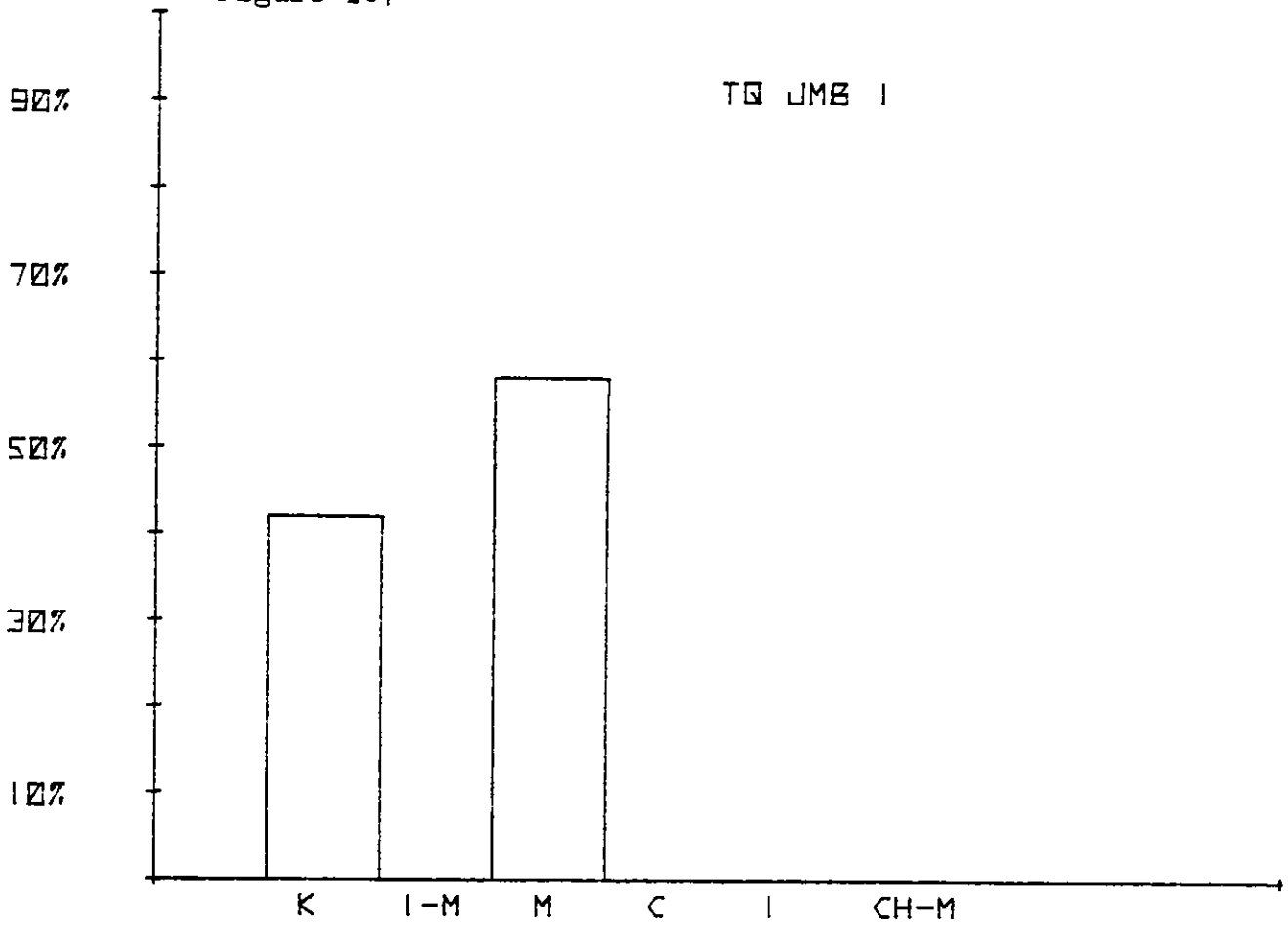


Figure 108

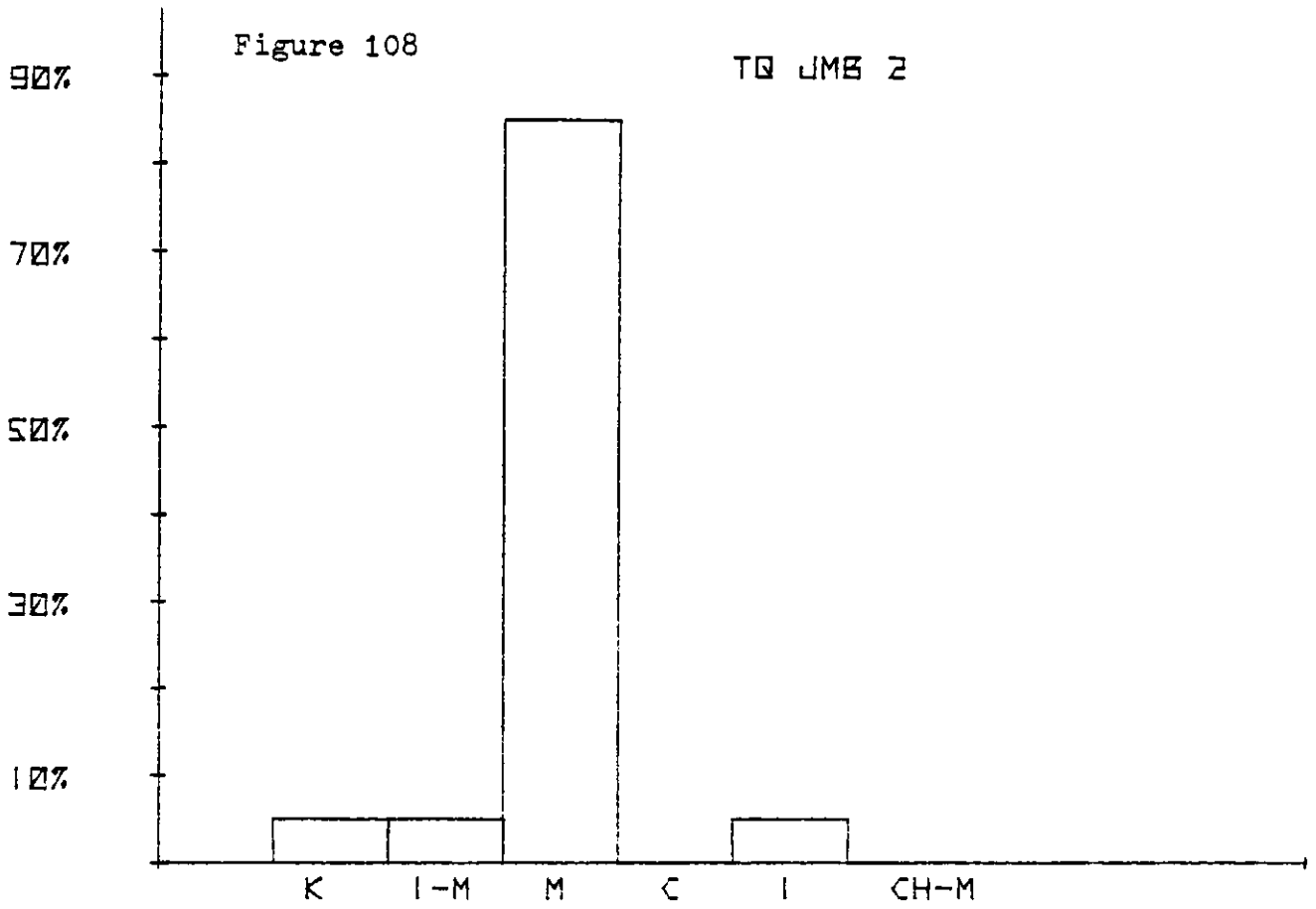


Figure 109

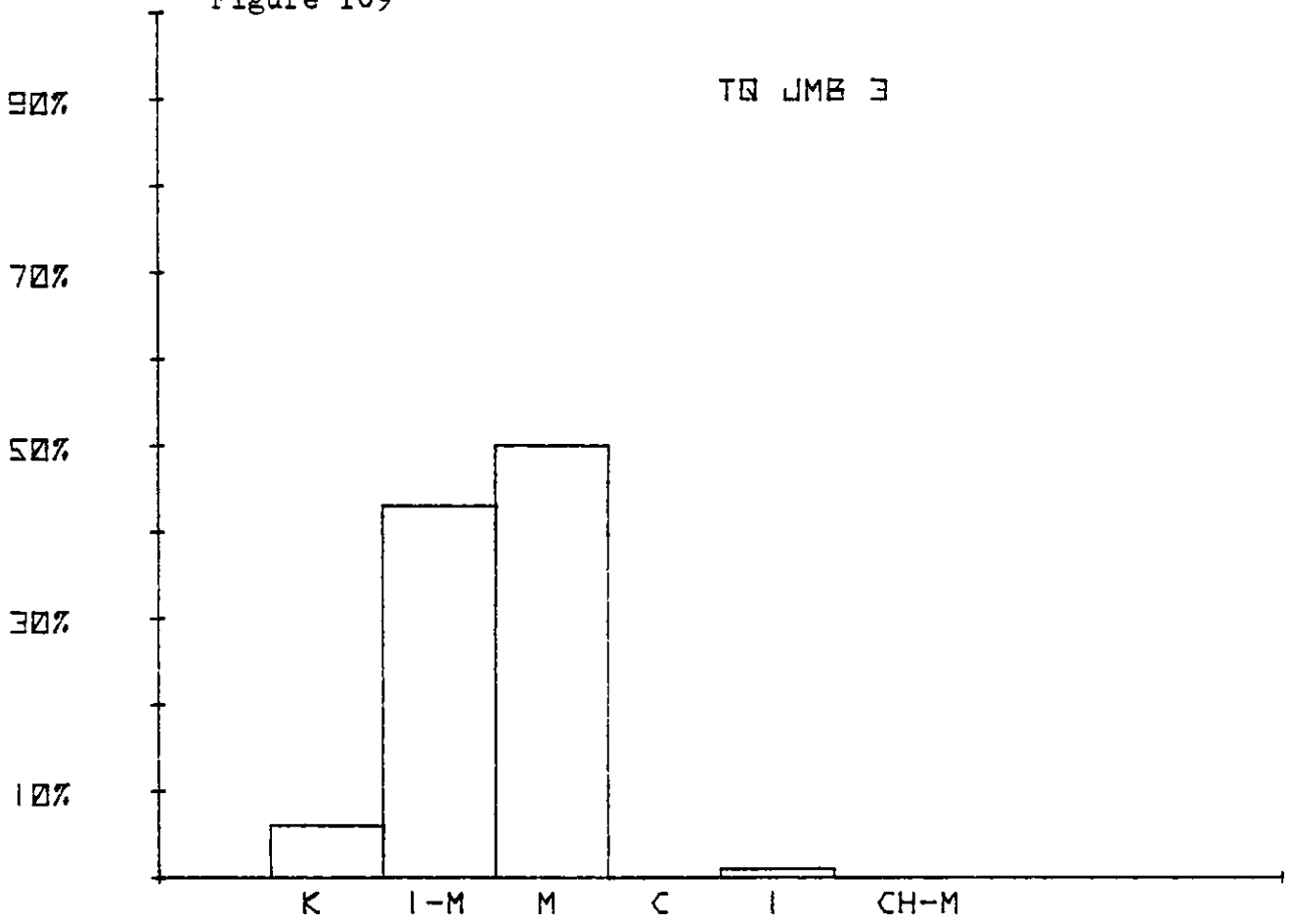


Figure 110

TQ JMB 4

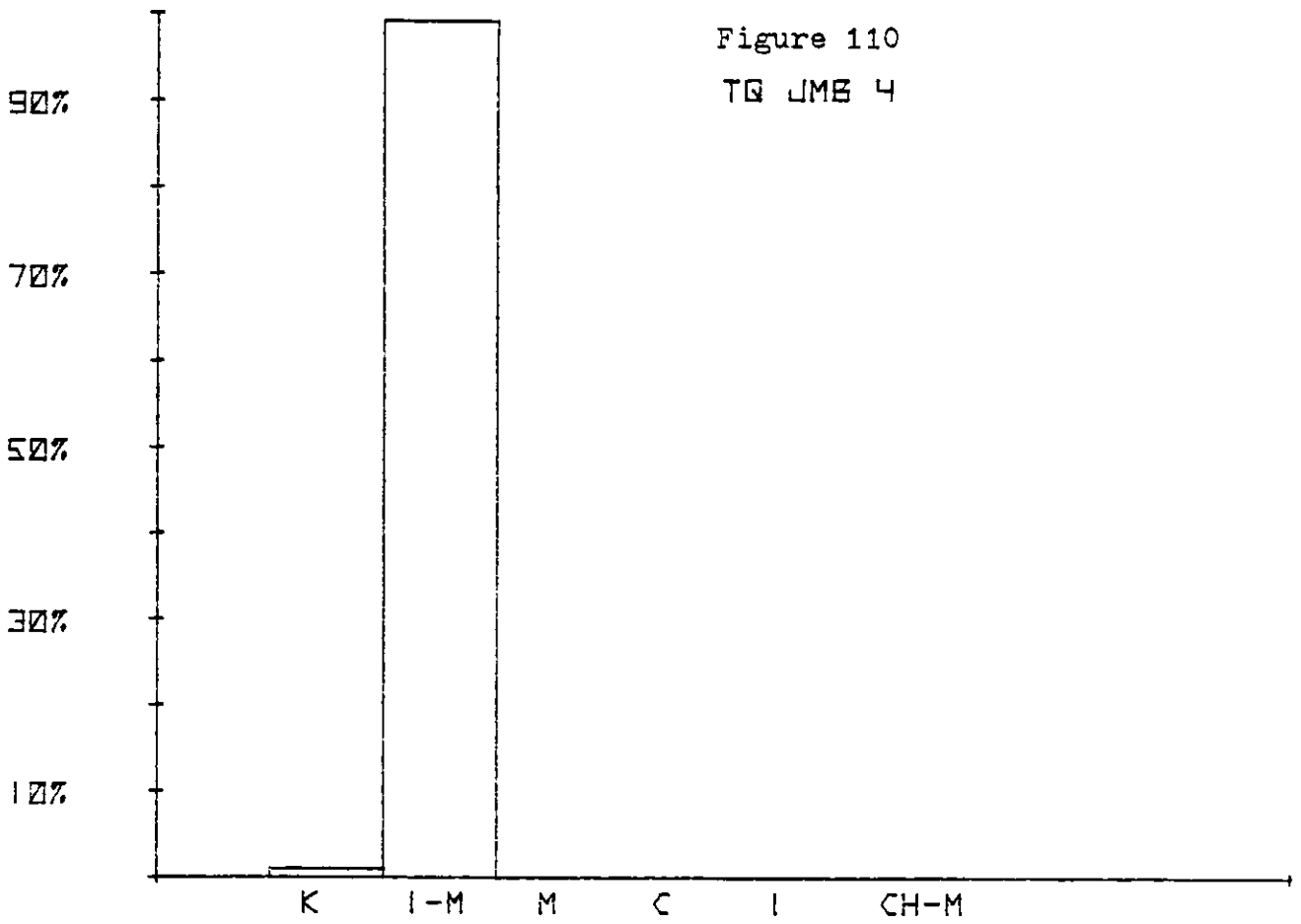


Figure 111

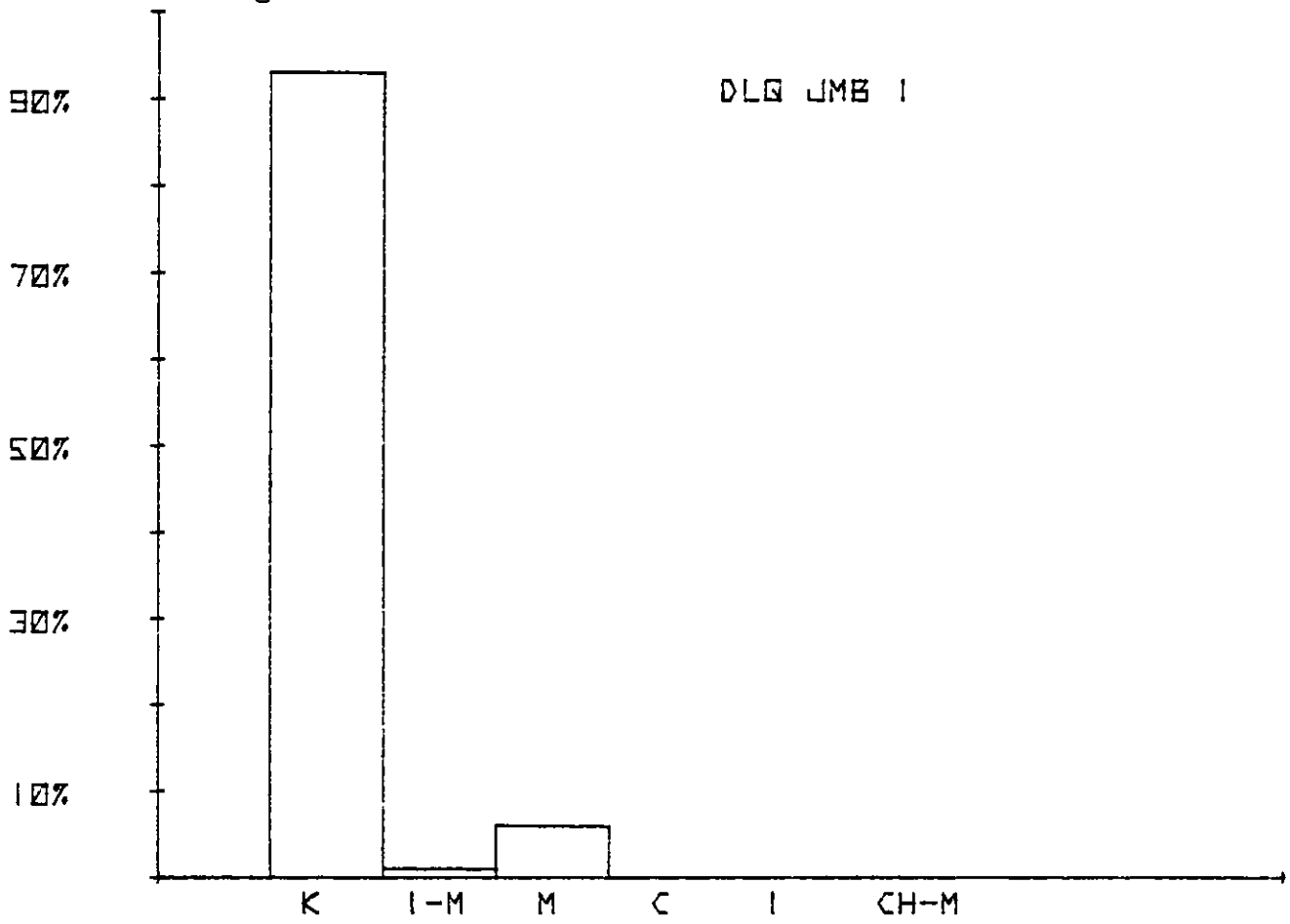


Figure 112

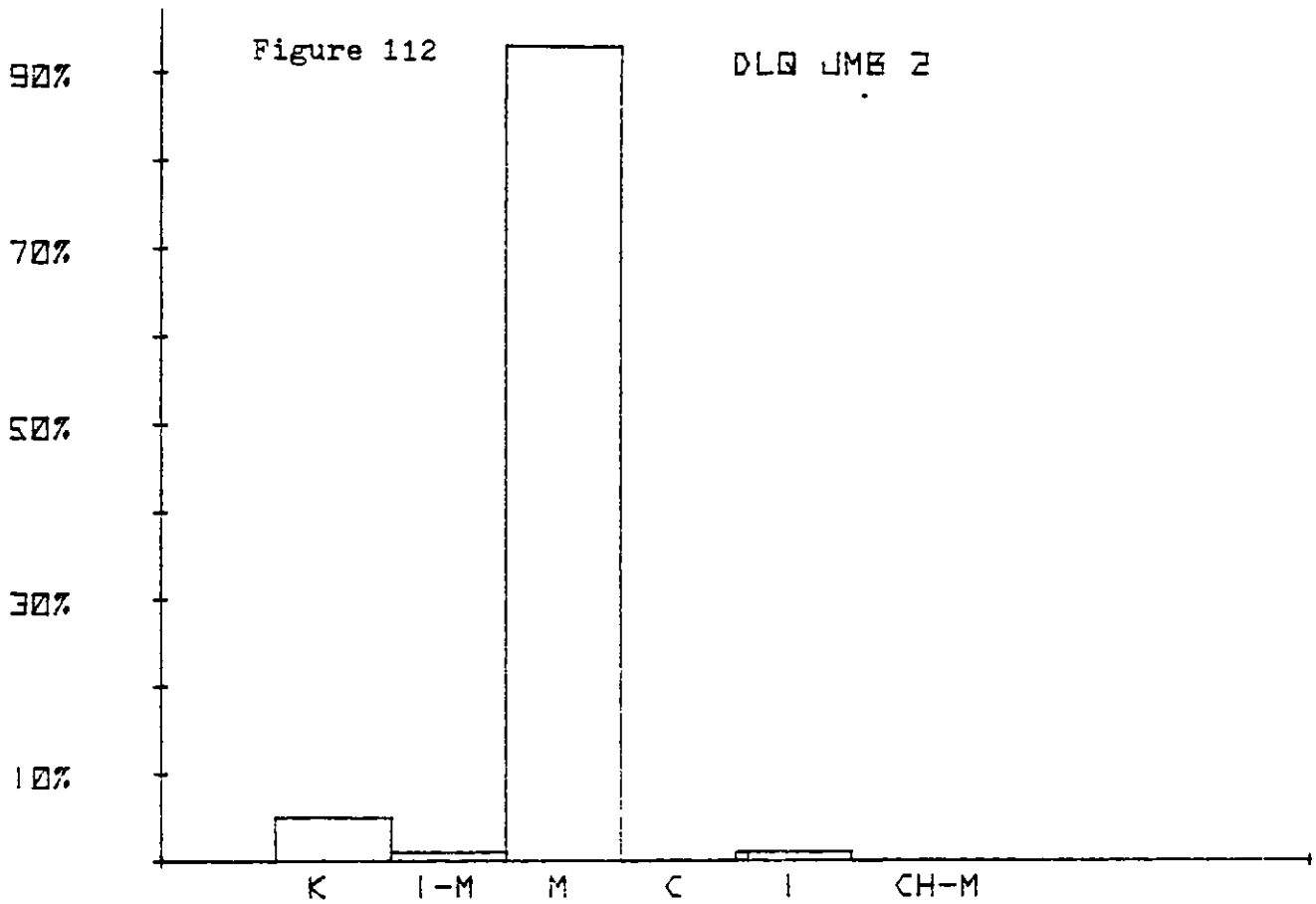


Figure 113

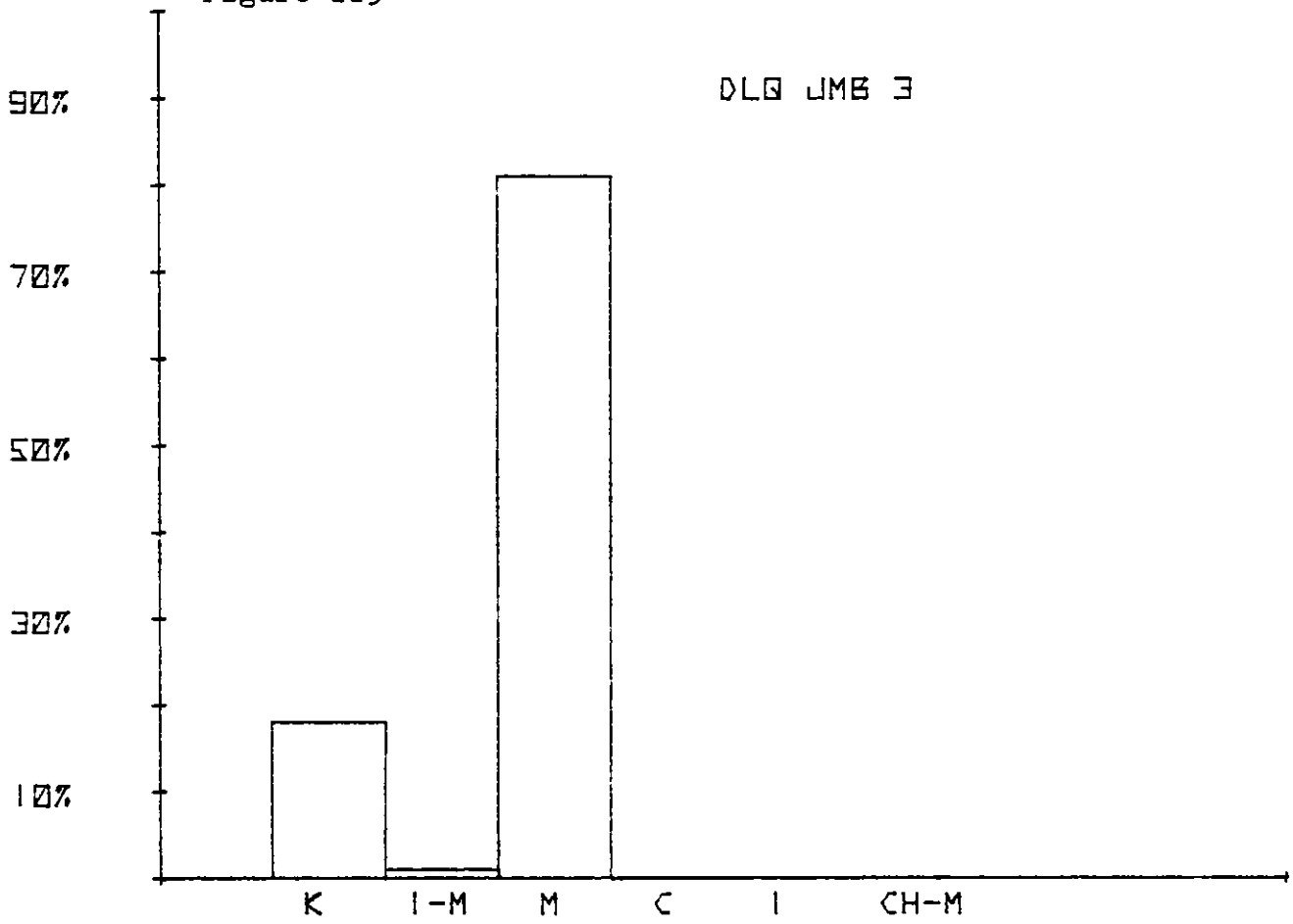


Figure 114

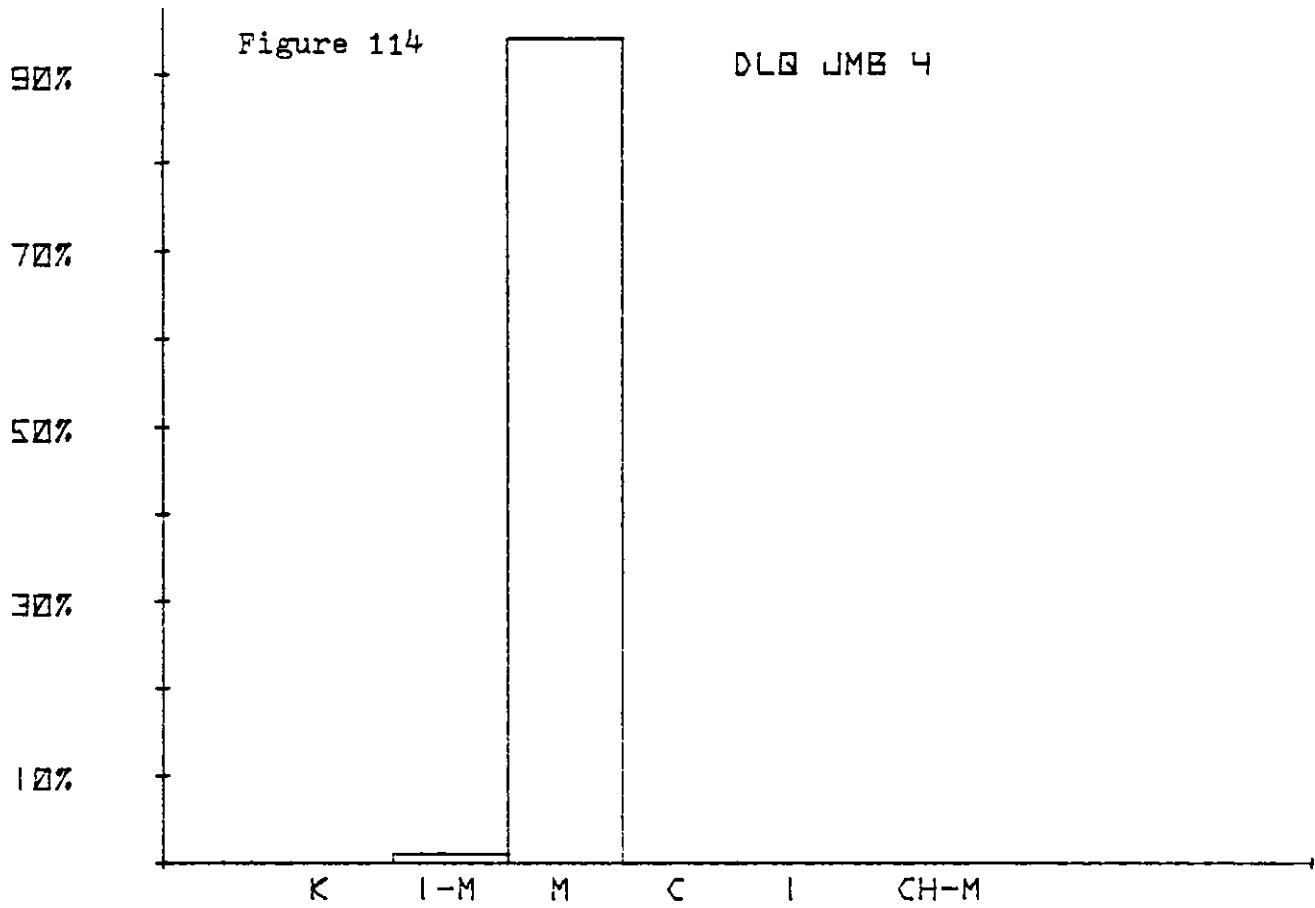


Figure 115

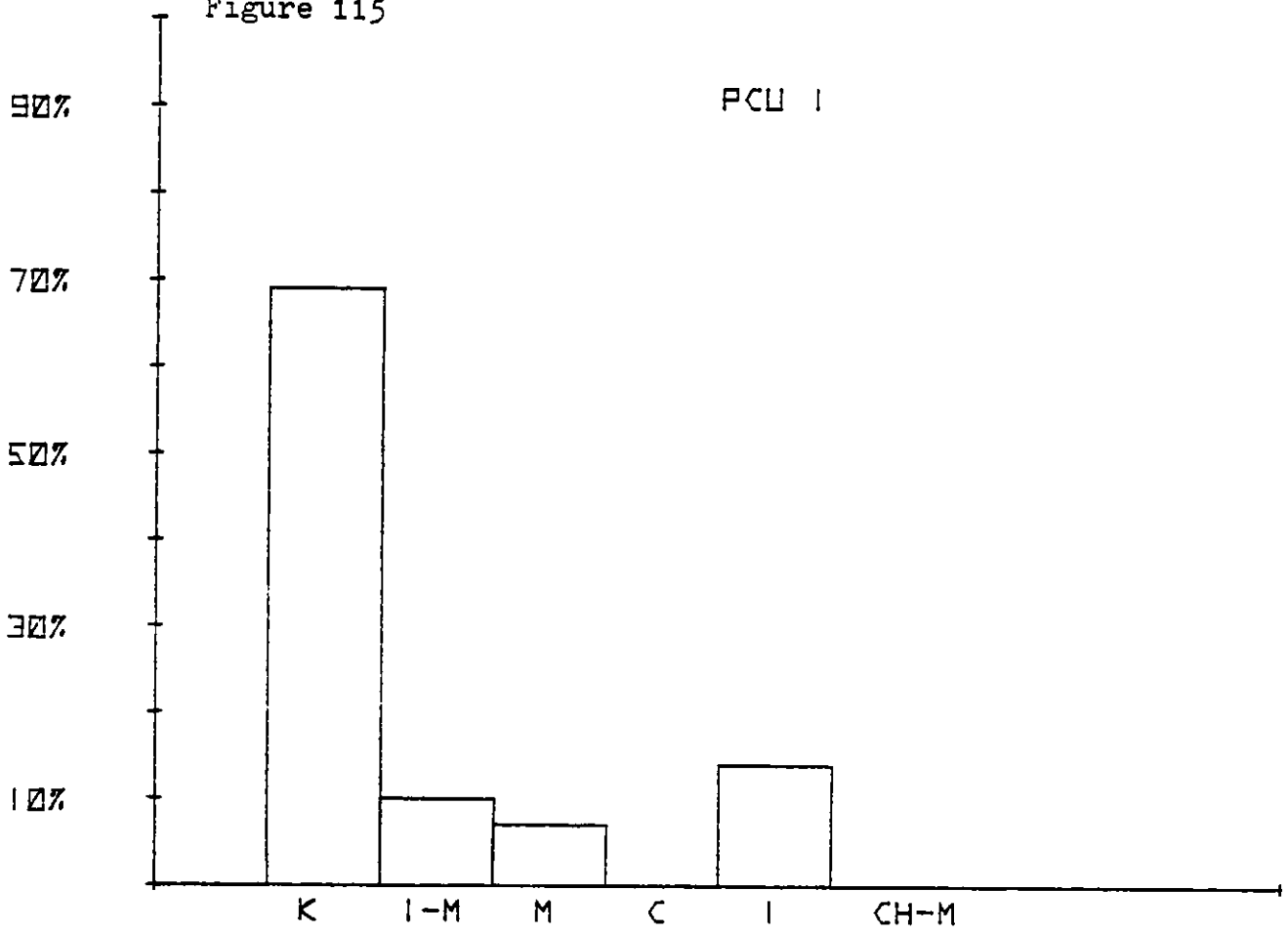


Figure 116

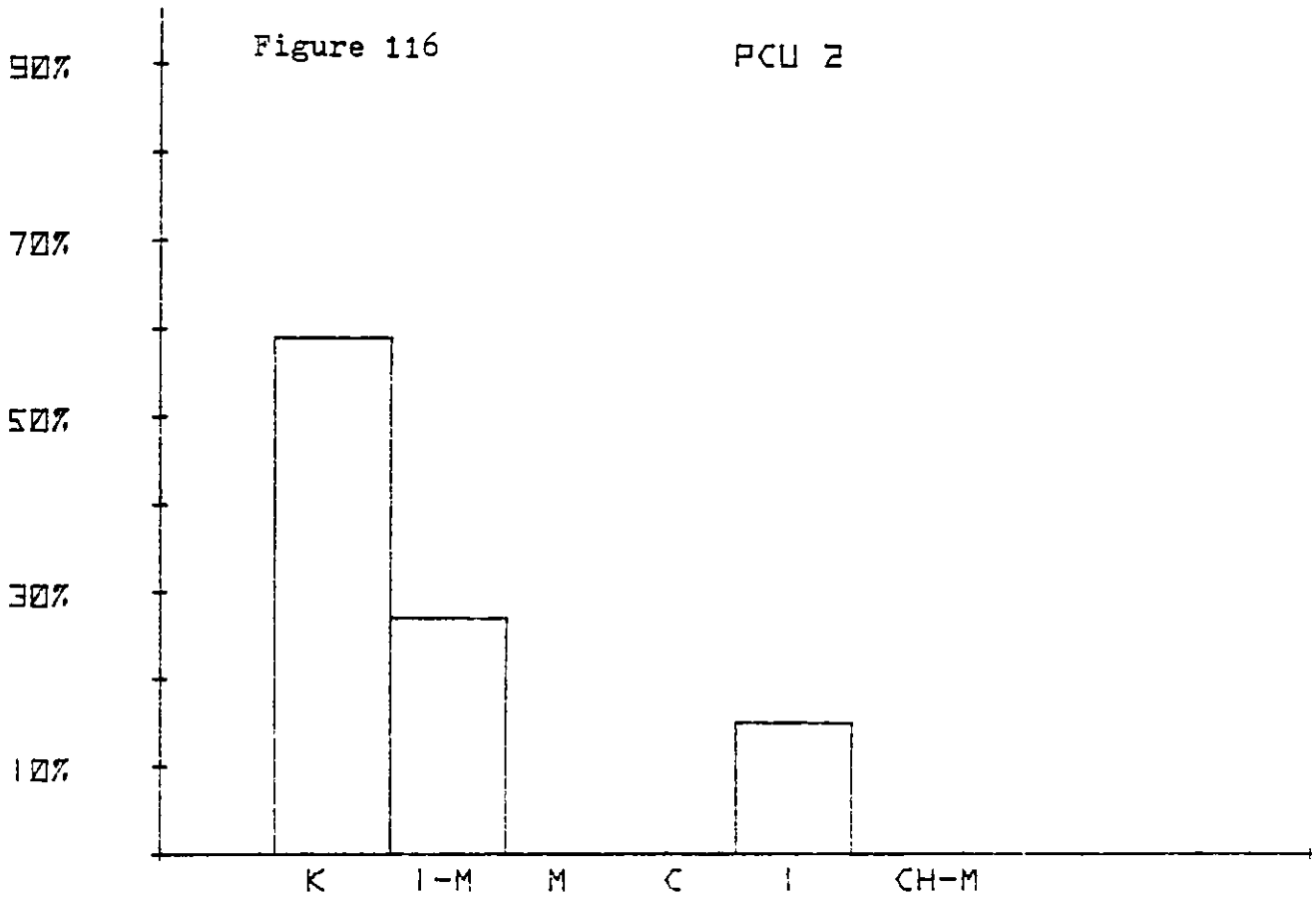


Figure 117

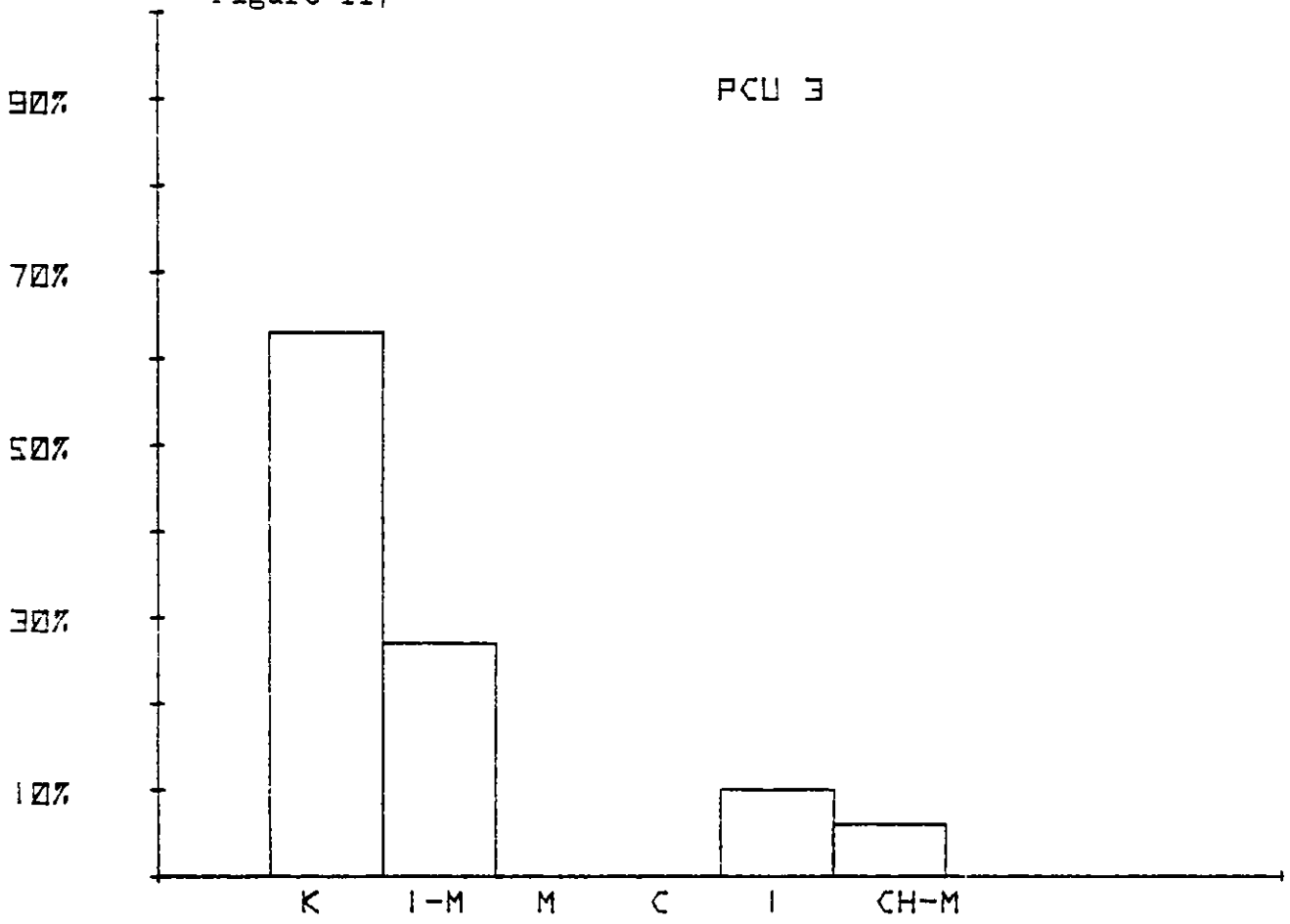


Figure 118

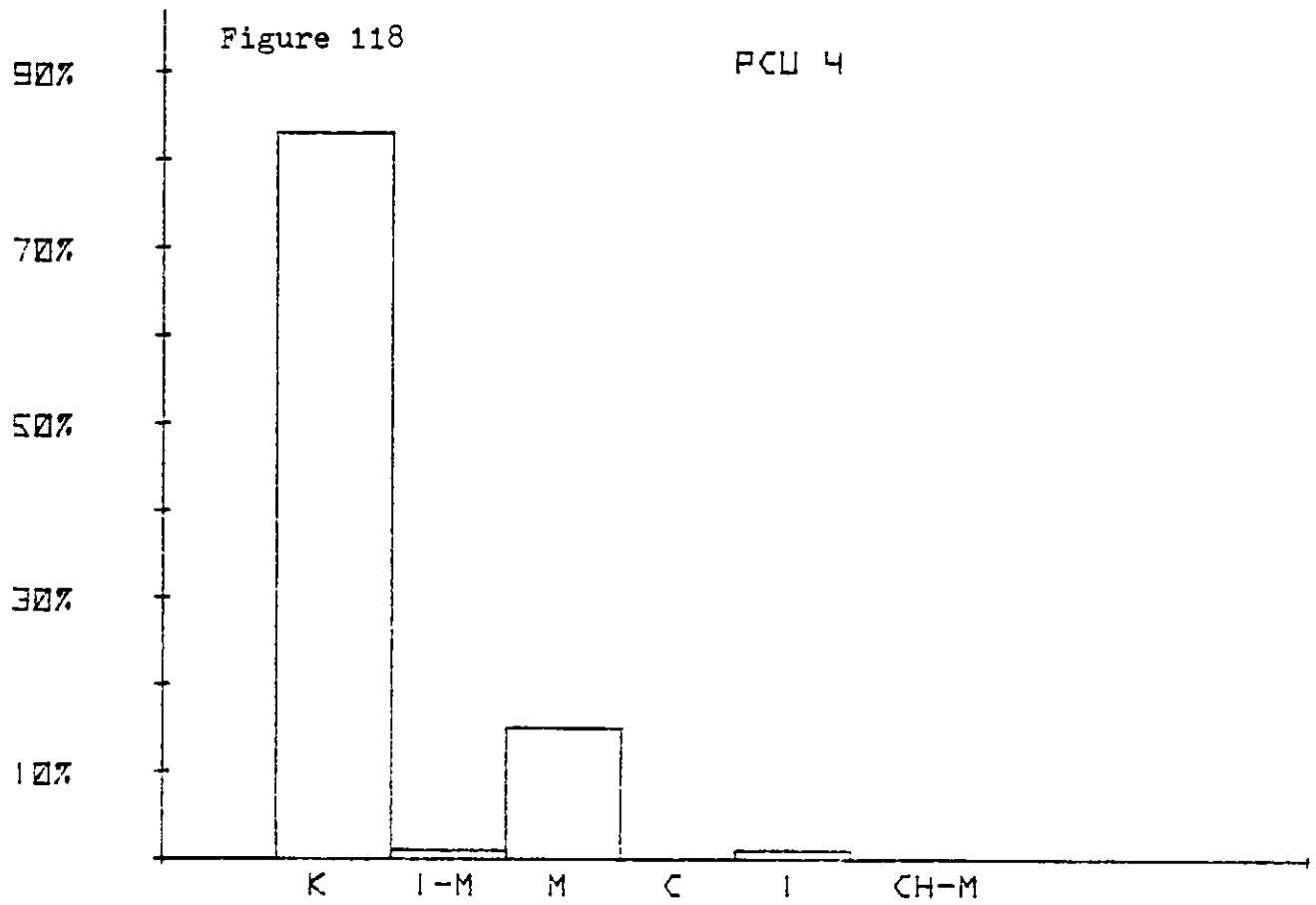


Figure 119

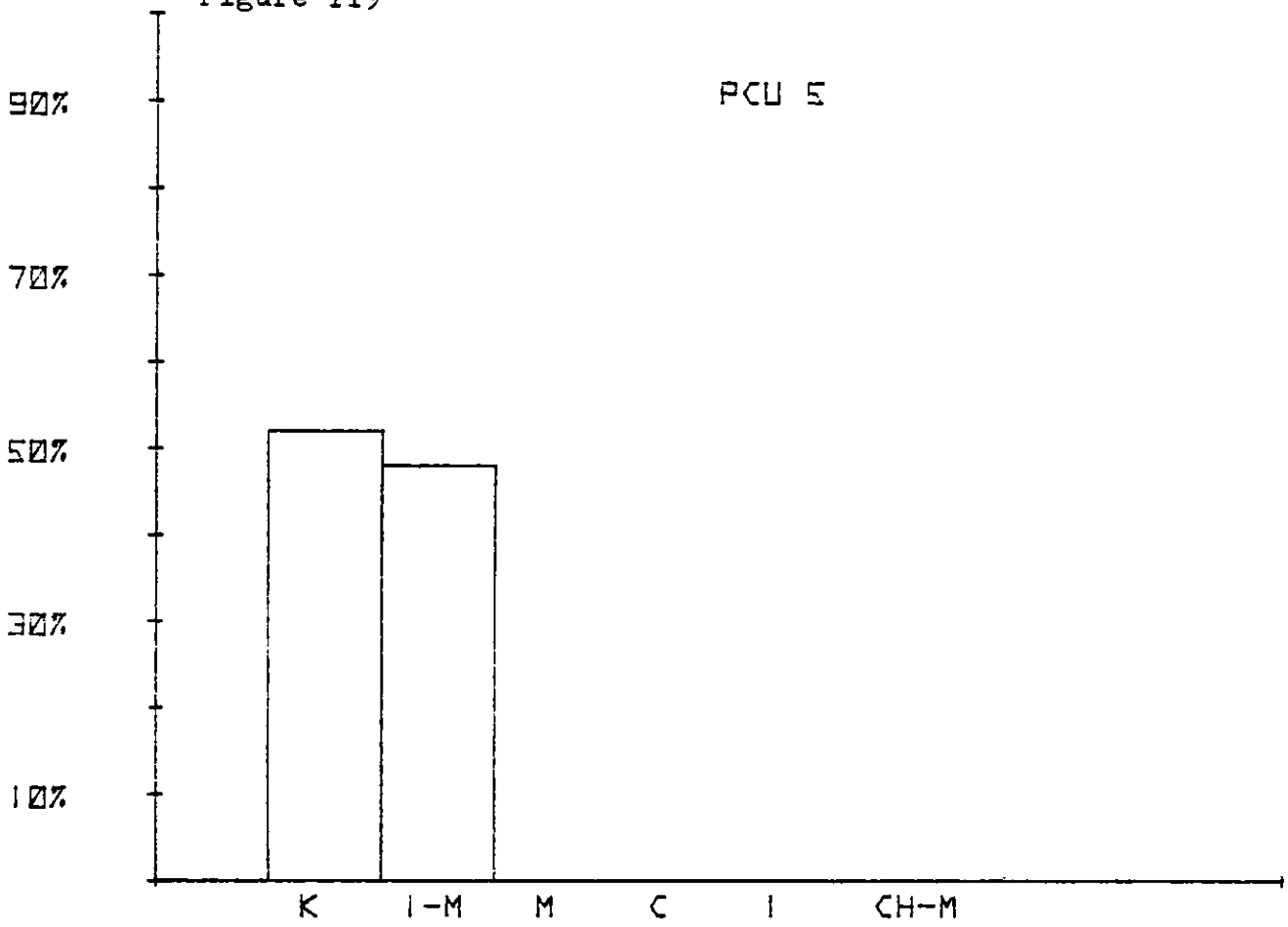


Figure 120

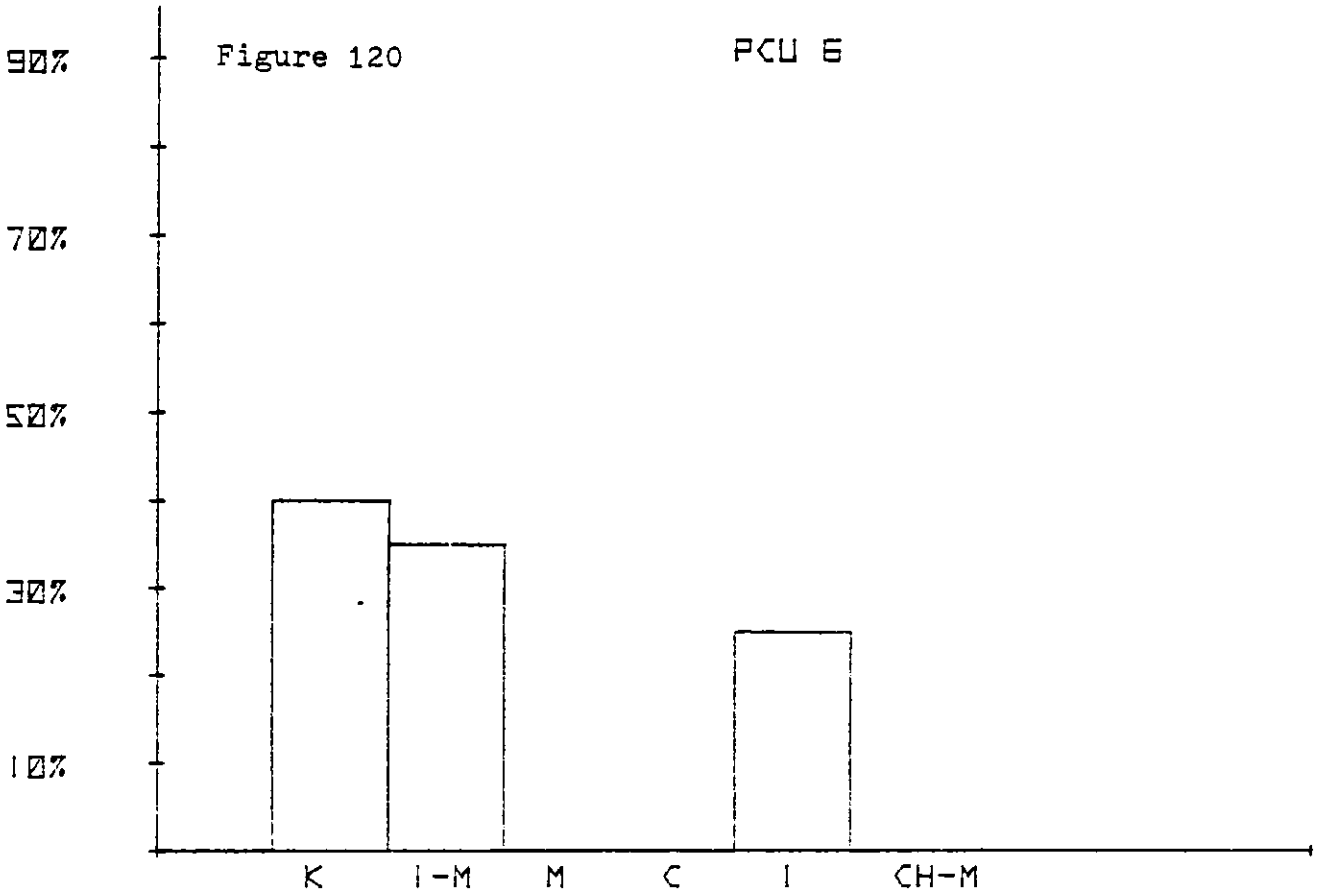


Figure 121

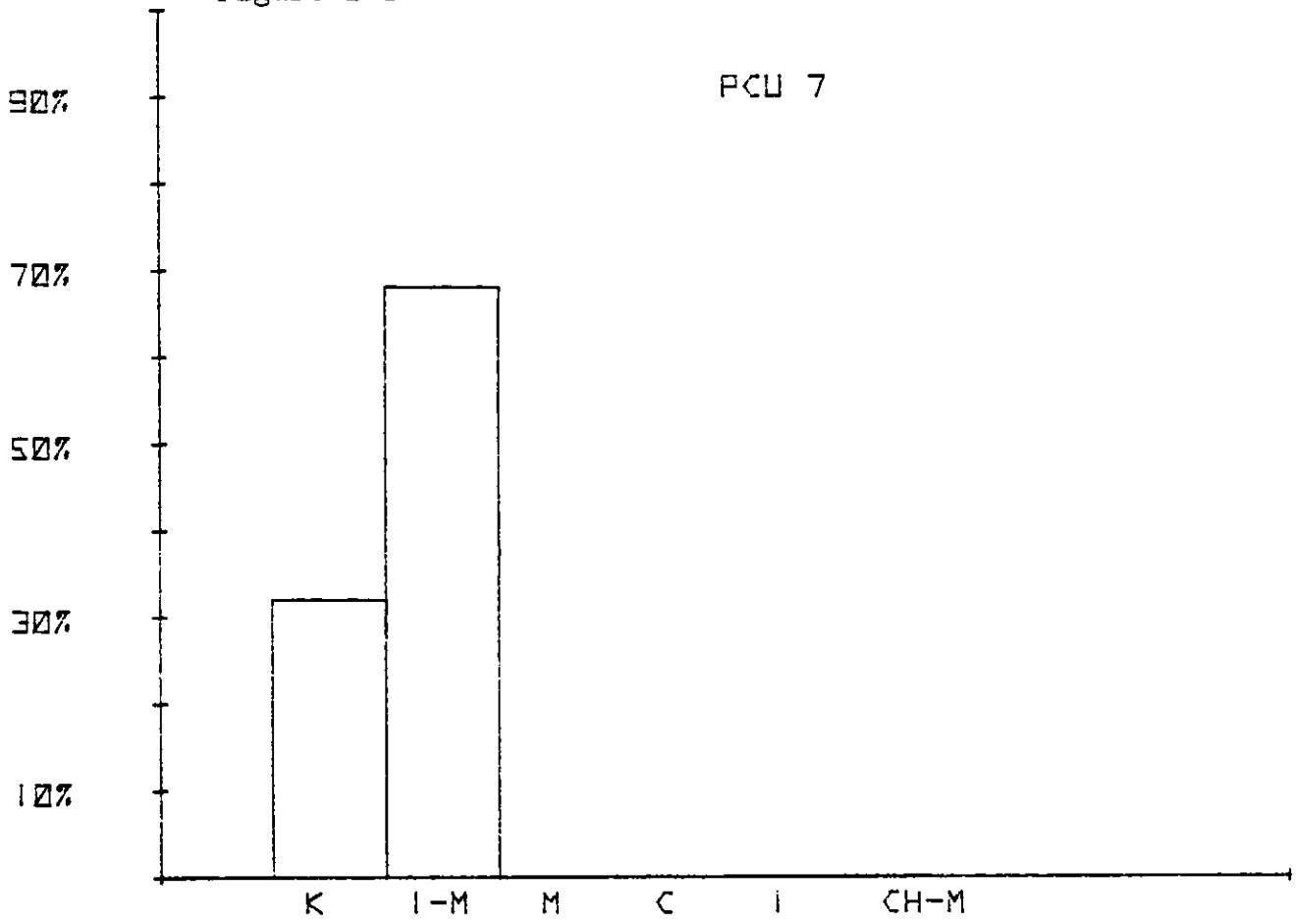


Figure 122

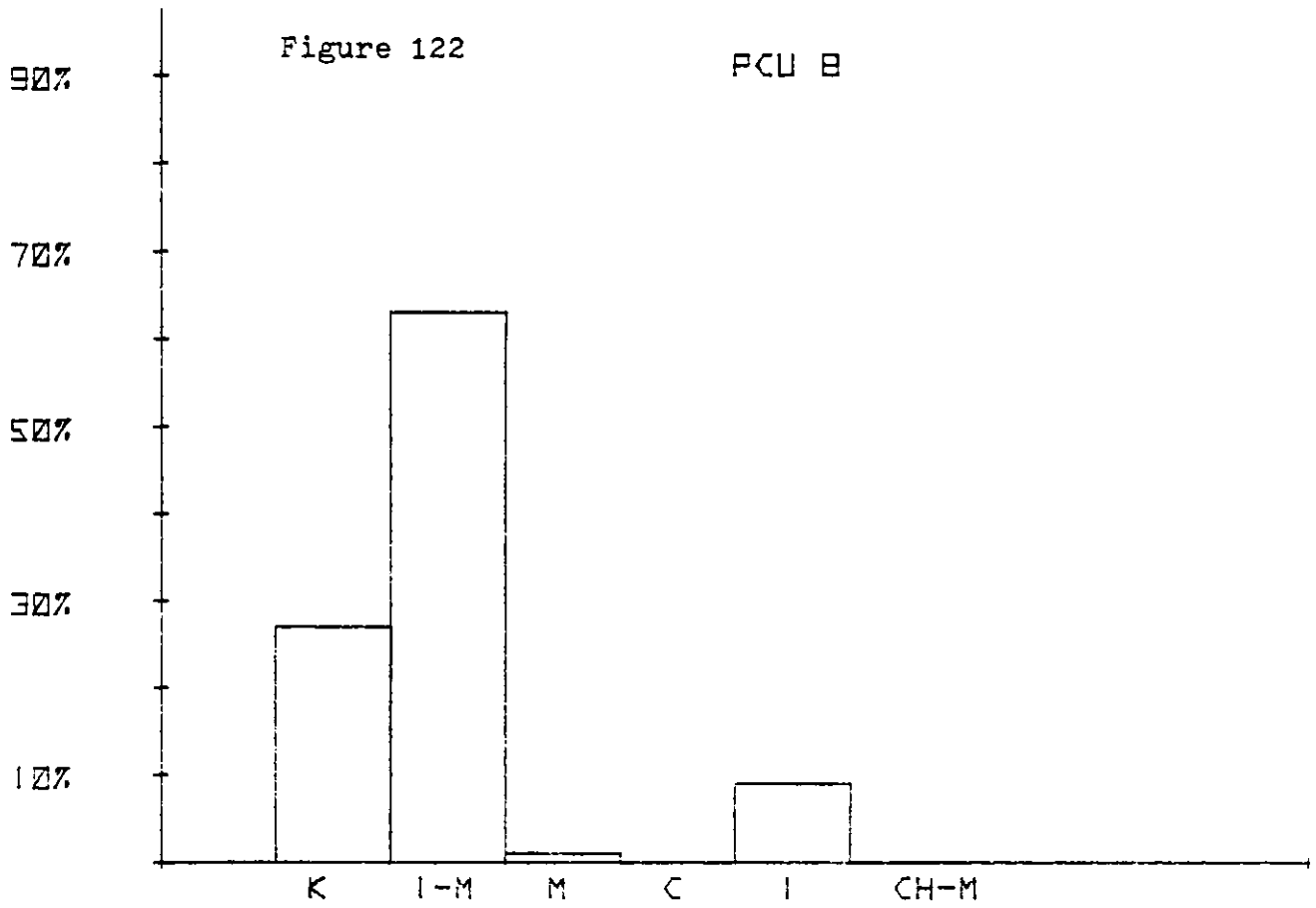


Figure 123

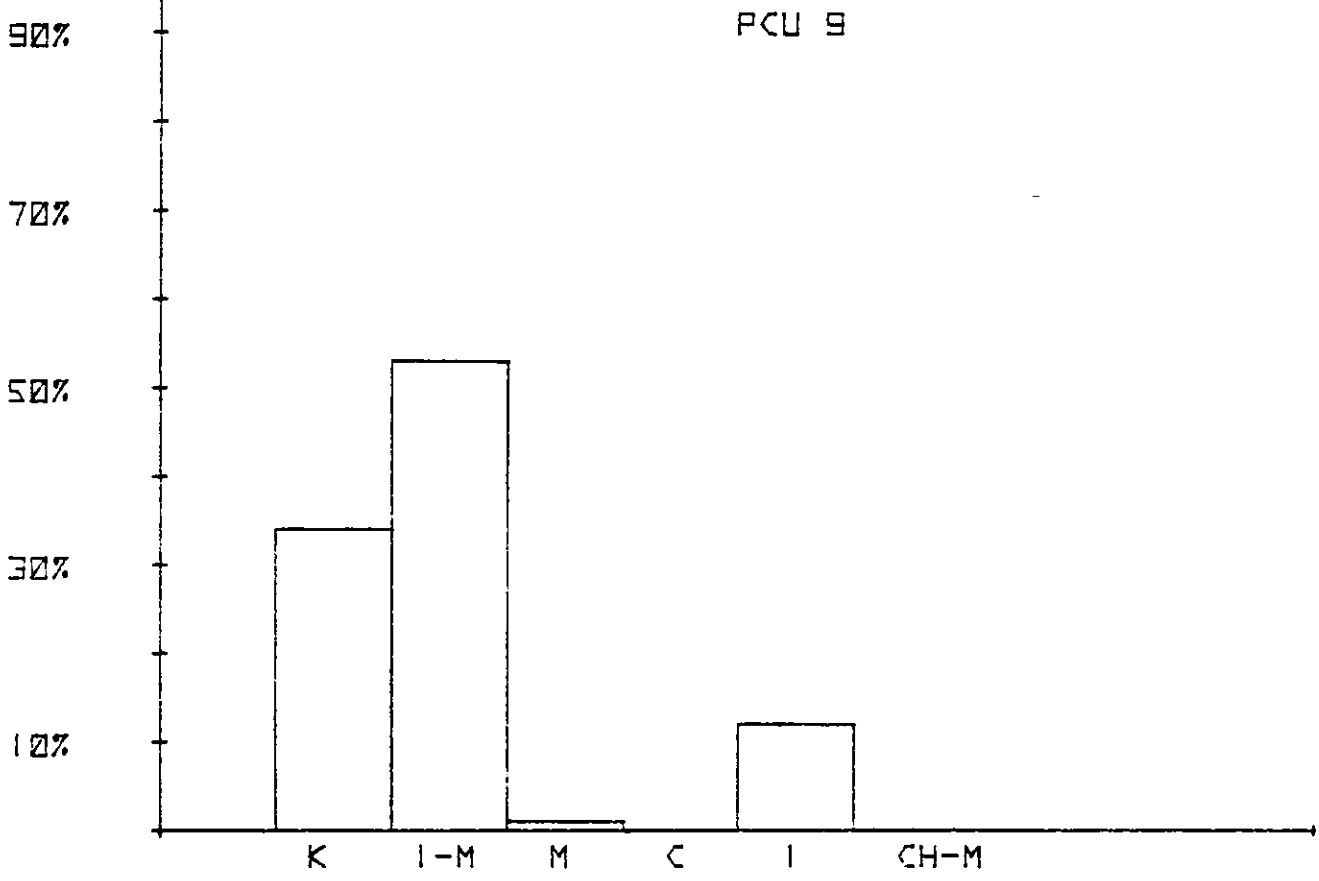


Figure 124

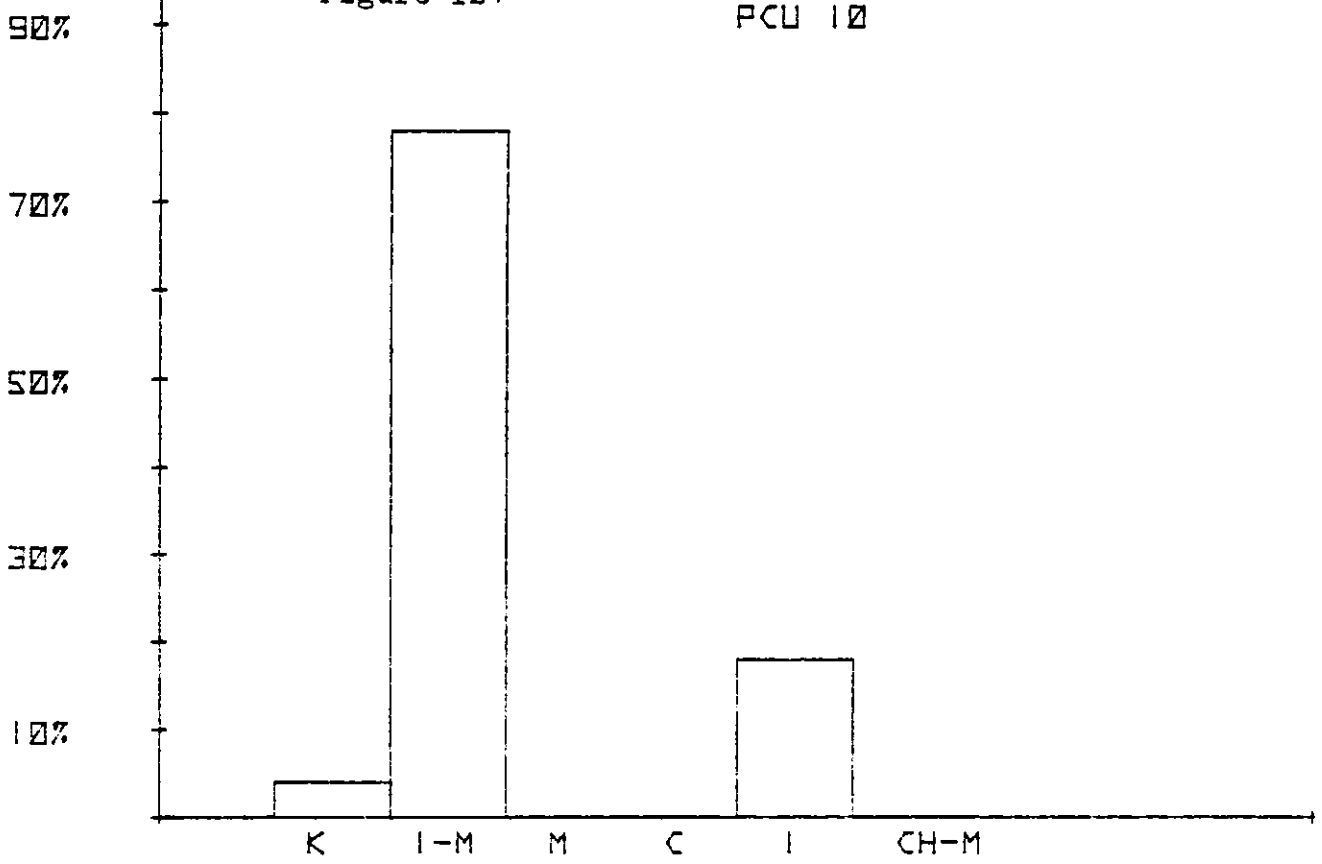


Figure 125

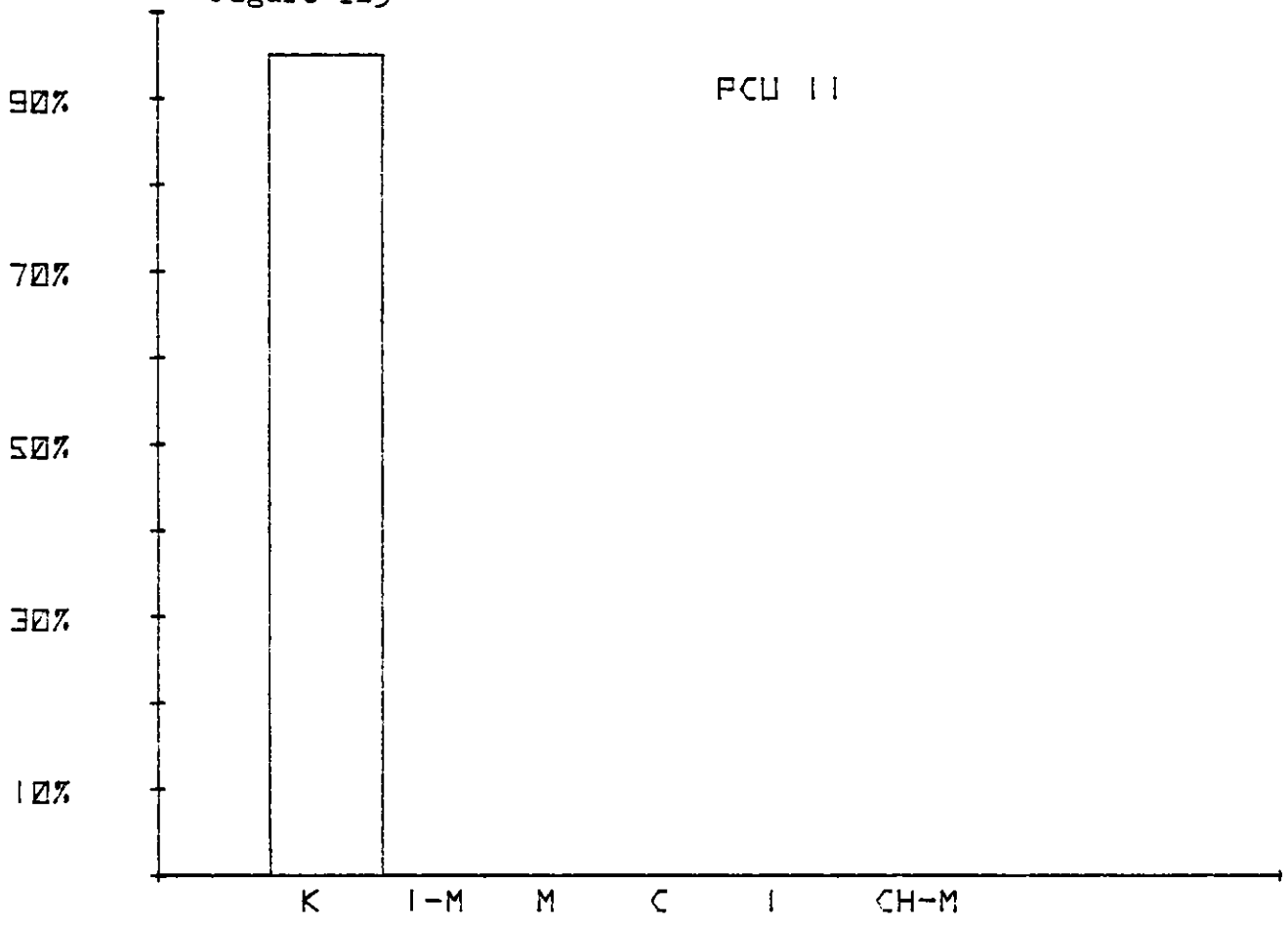


Figure 126

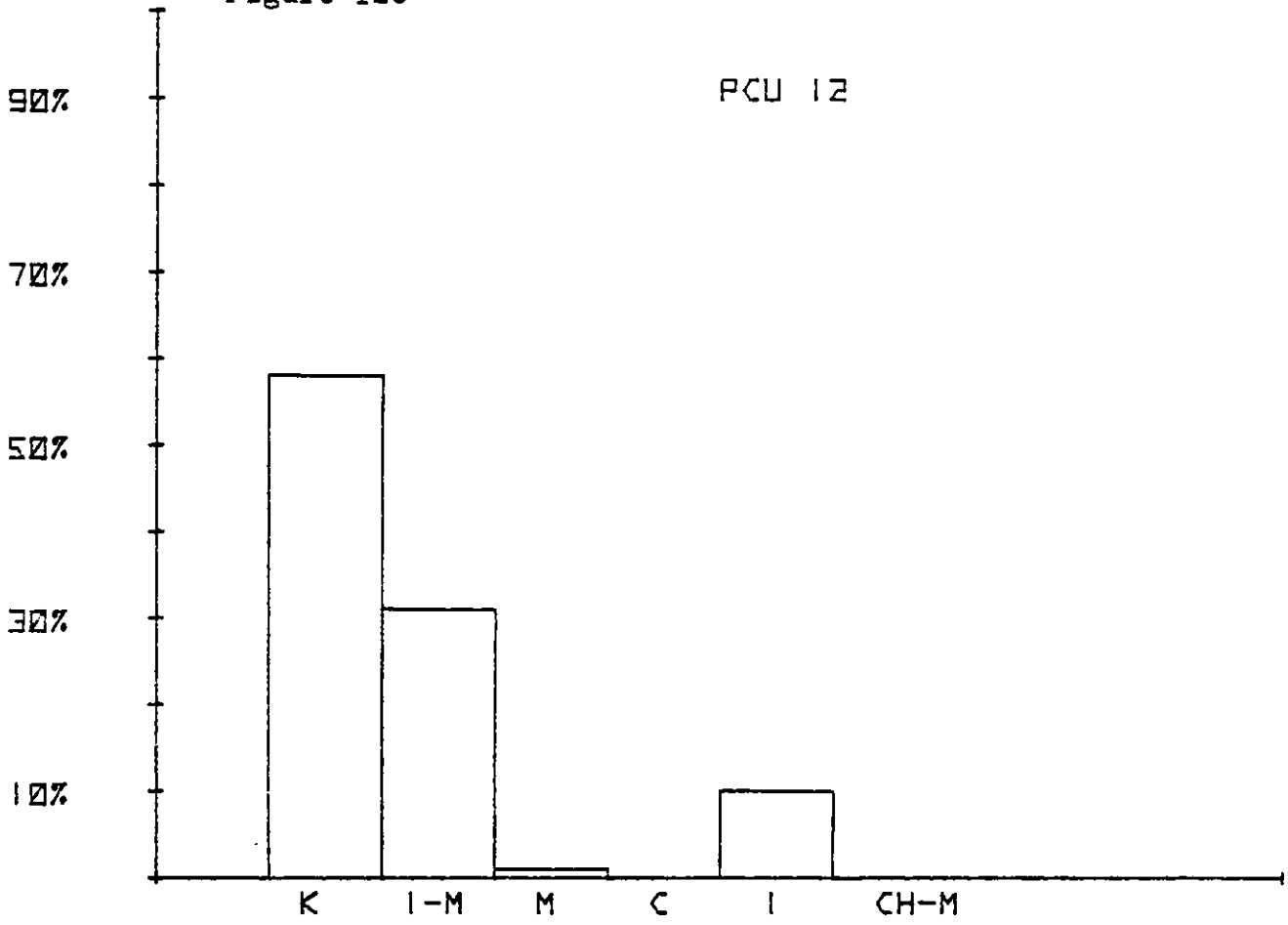


Figure 127

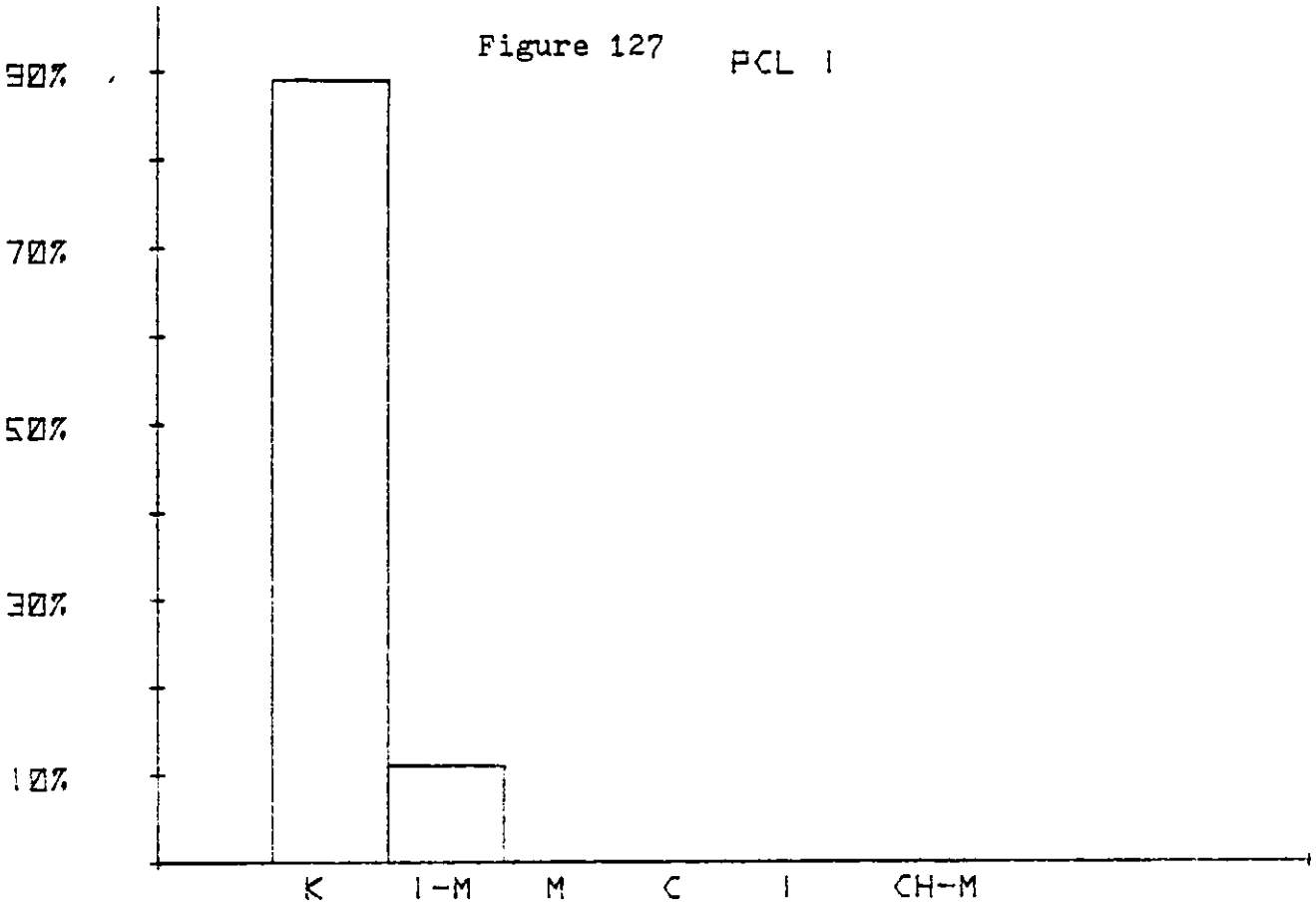


Figure 128

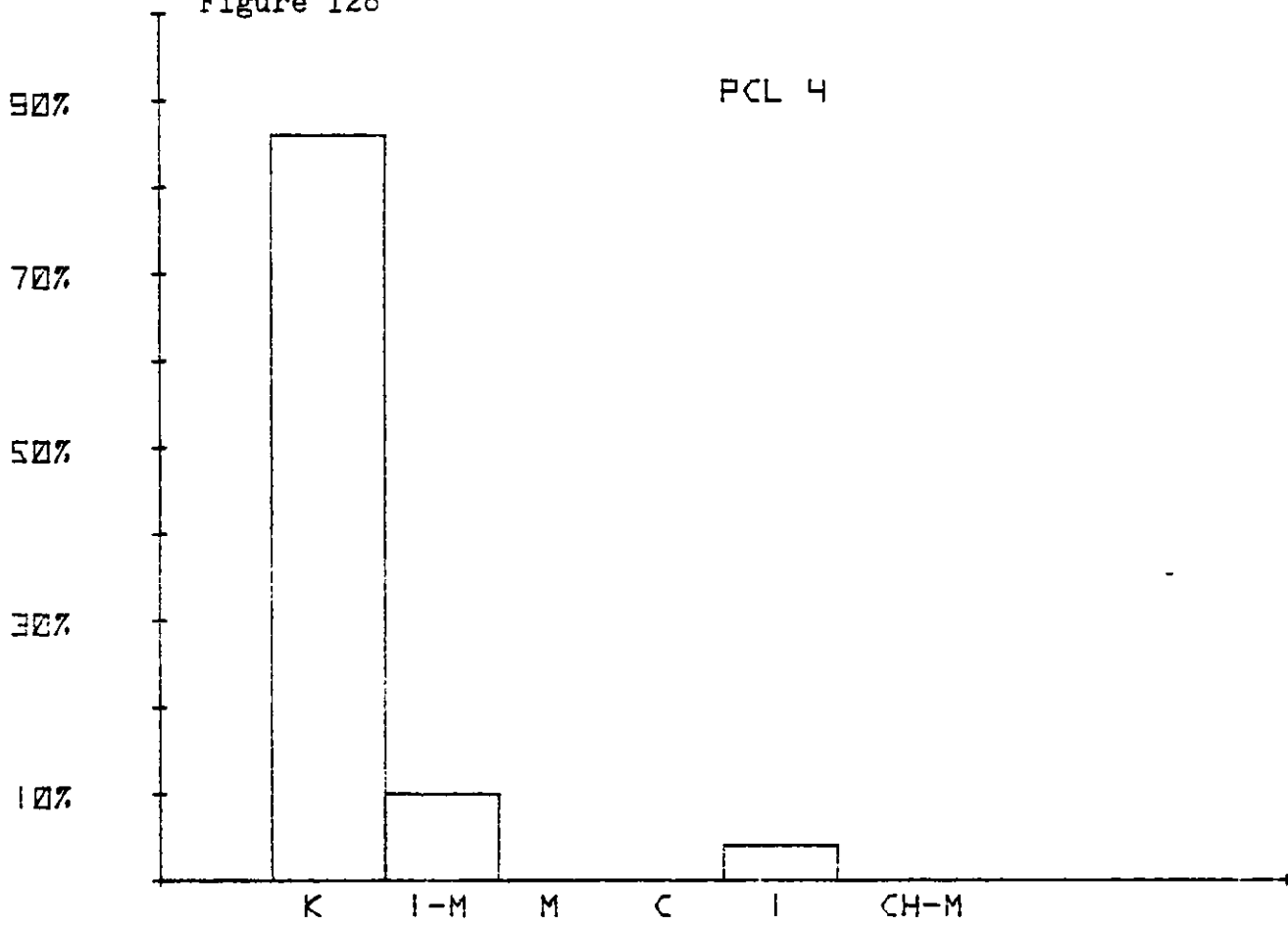


Figure 129

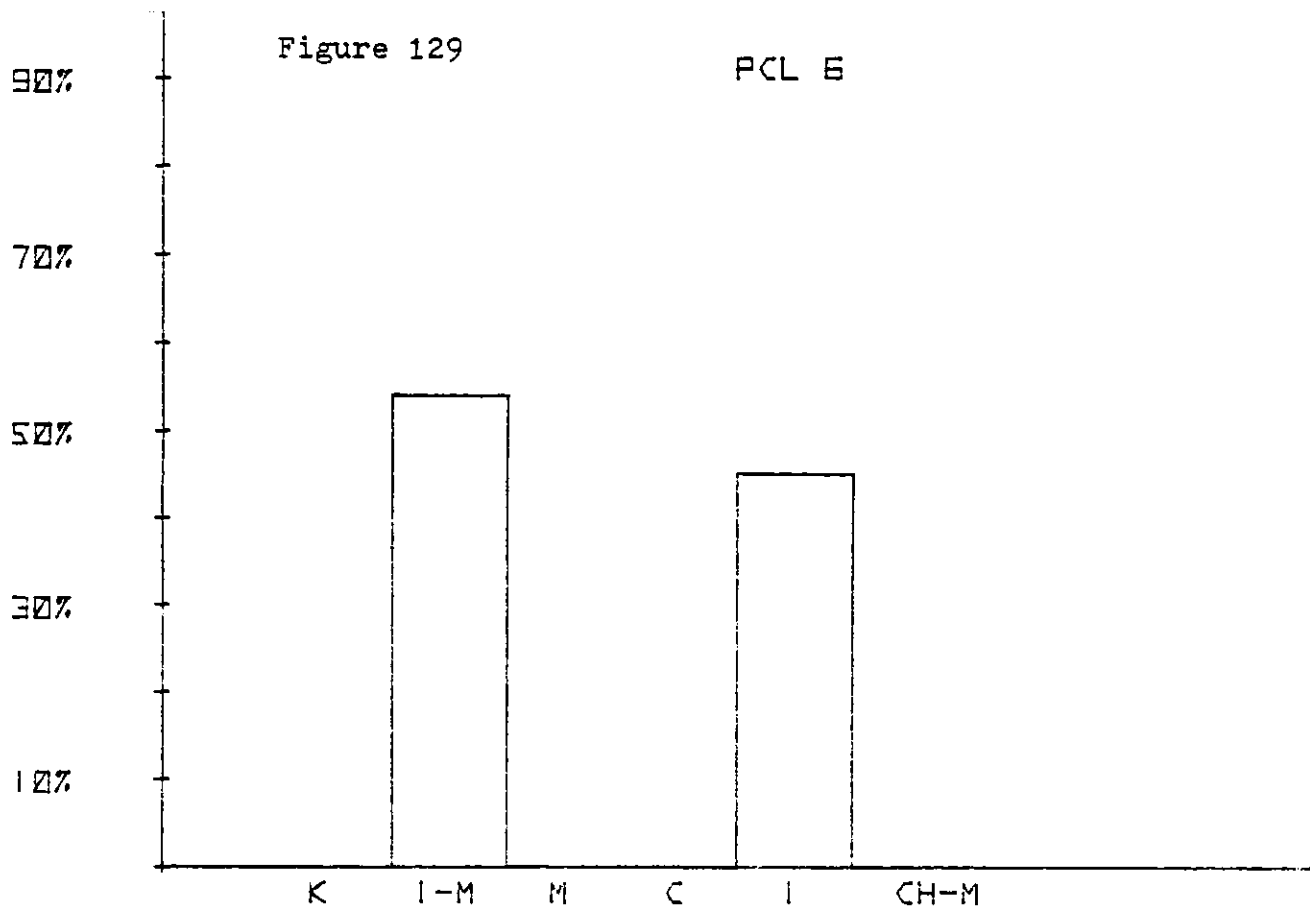


Figure 130

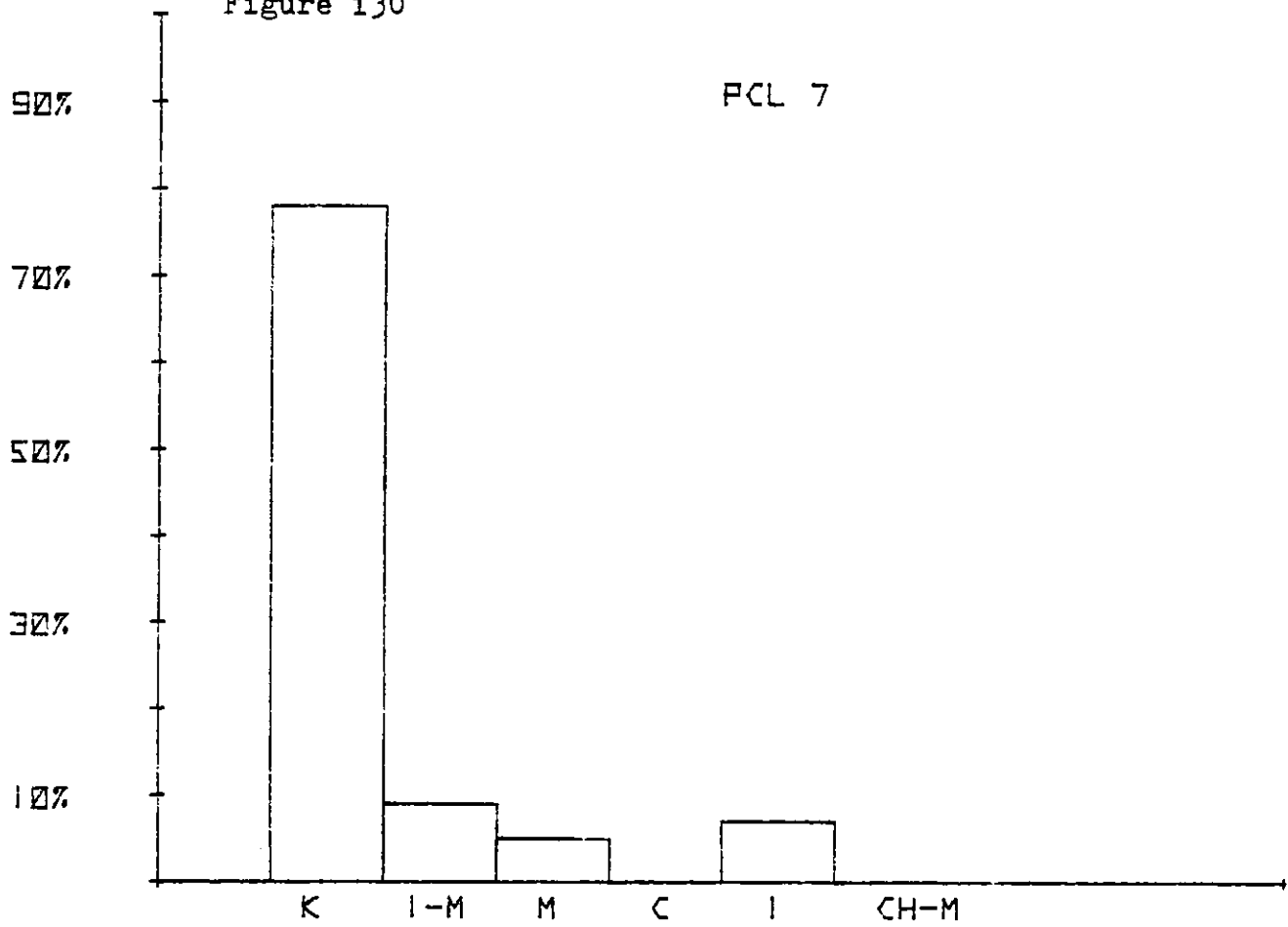


Figure 131

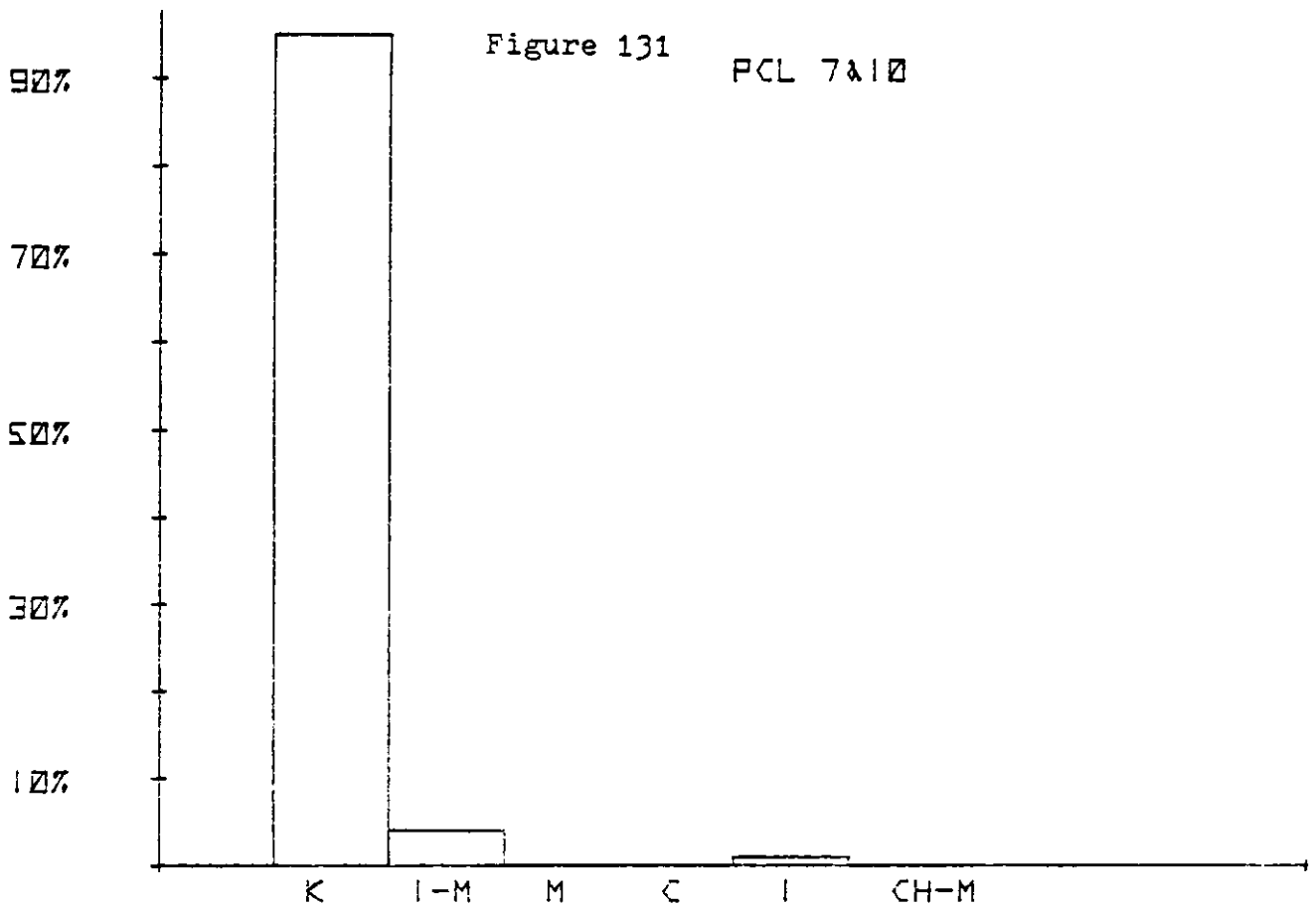


Figure 132

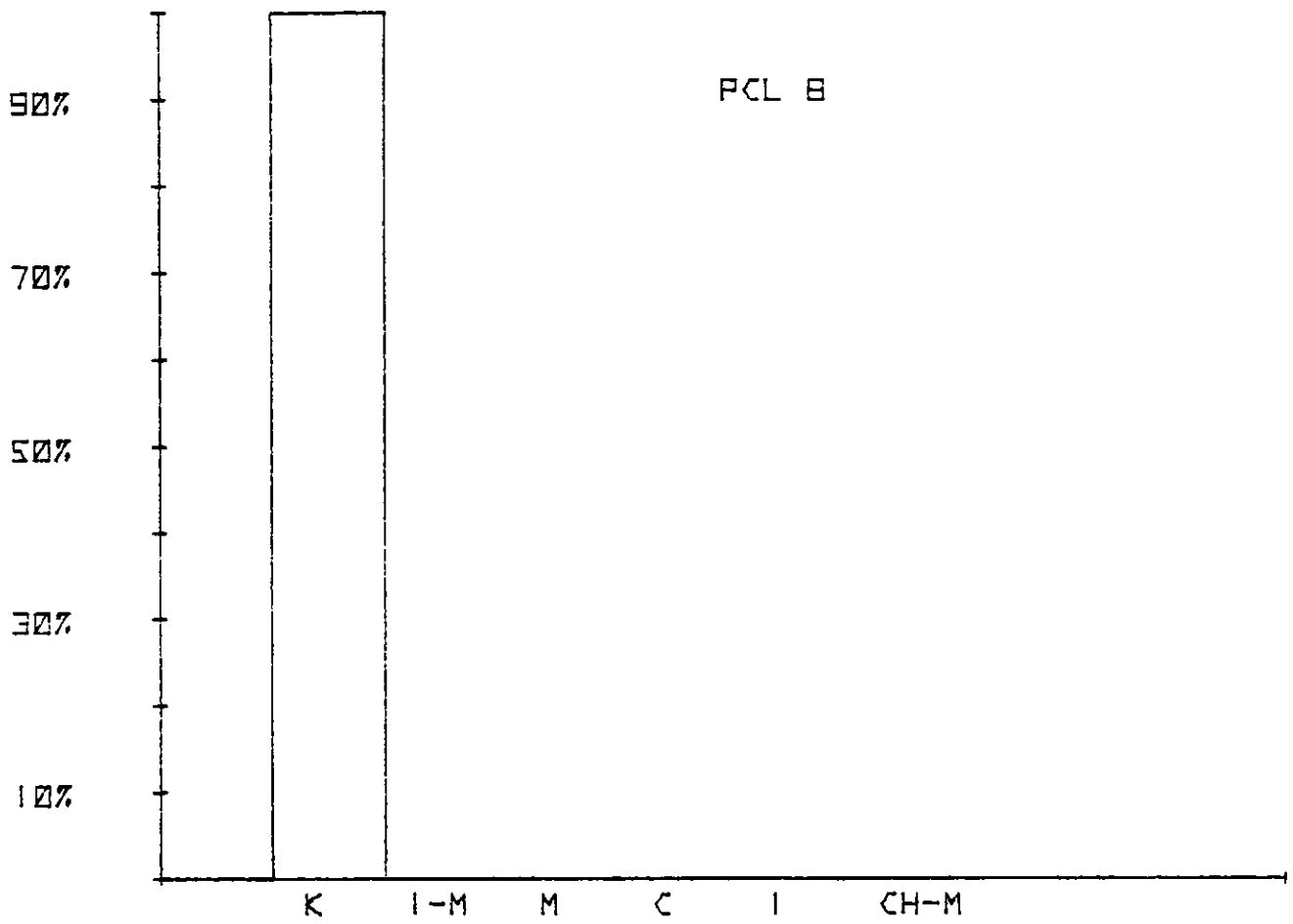


Figure 133

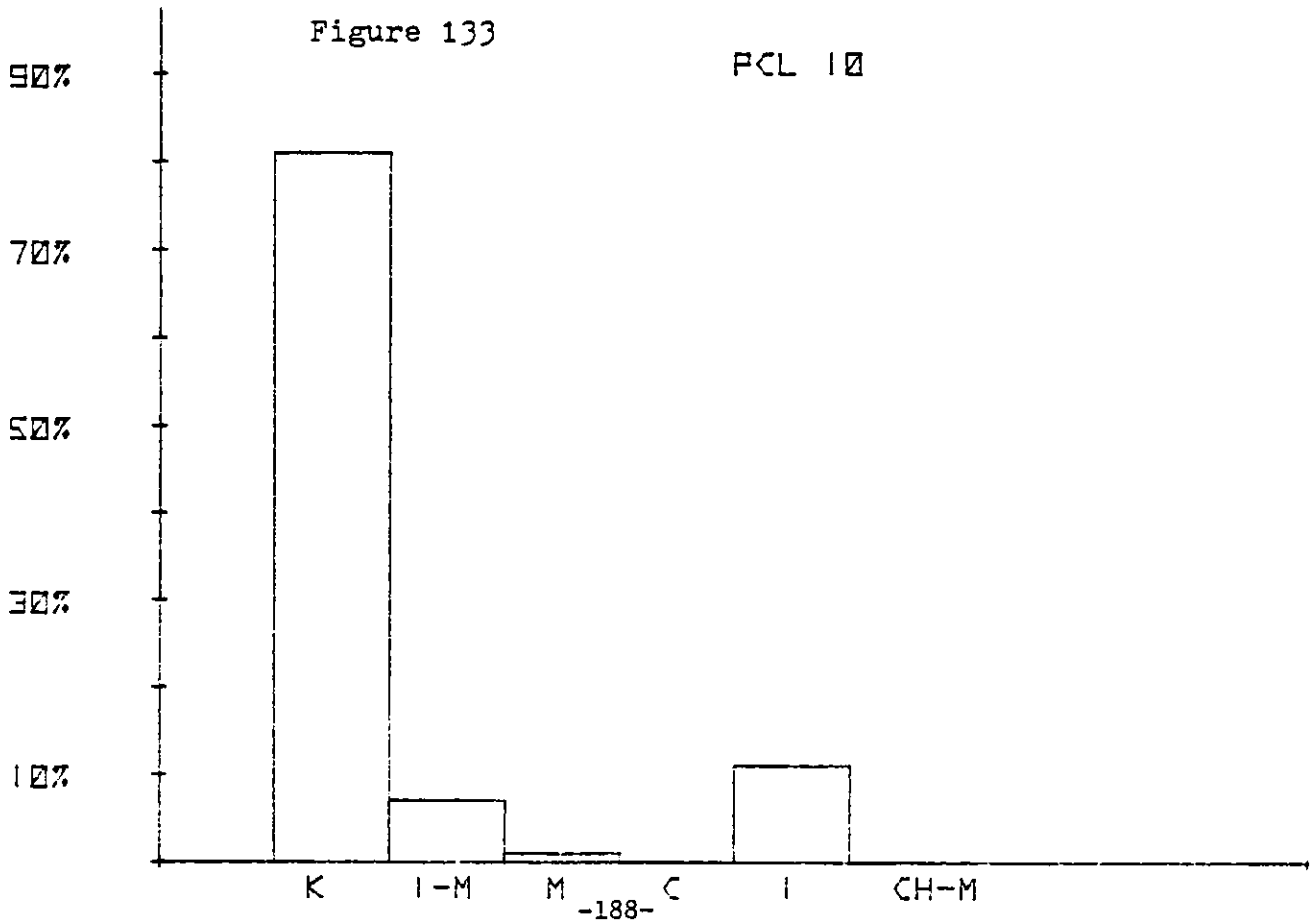


Figure 134

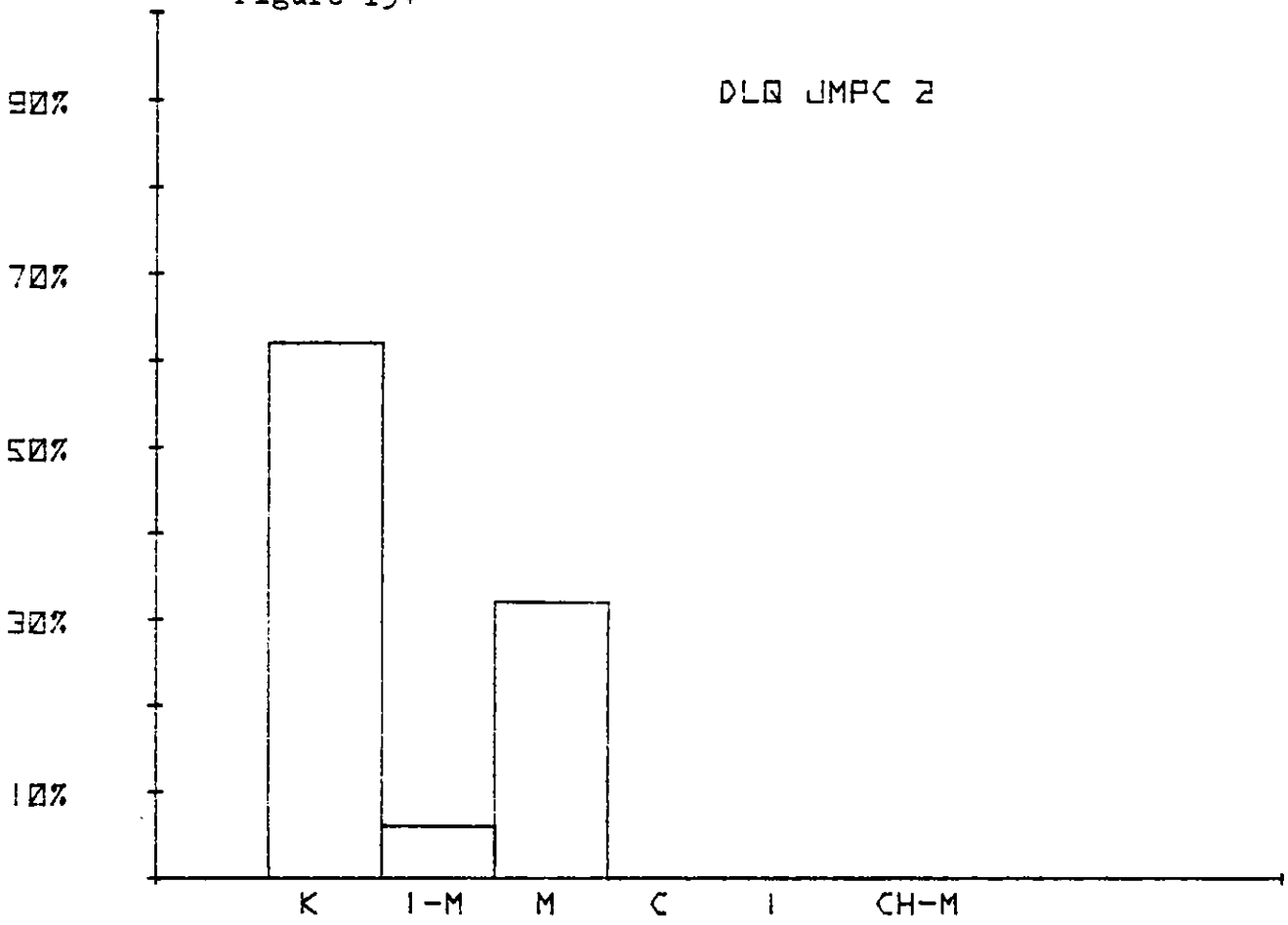


Figure 135

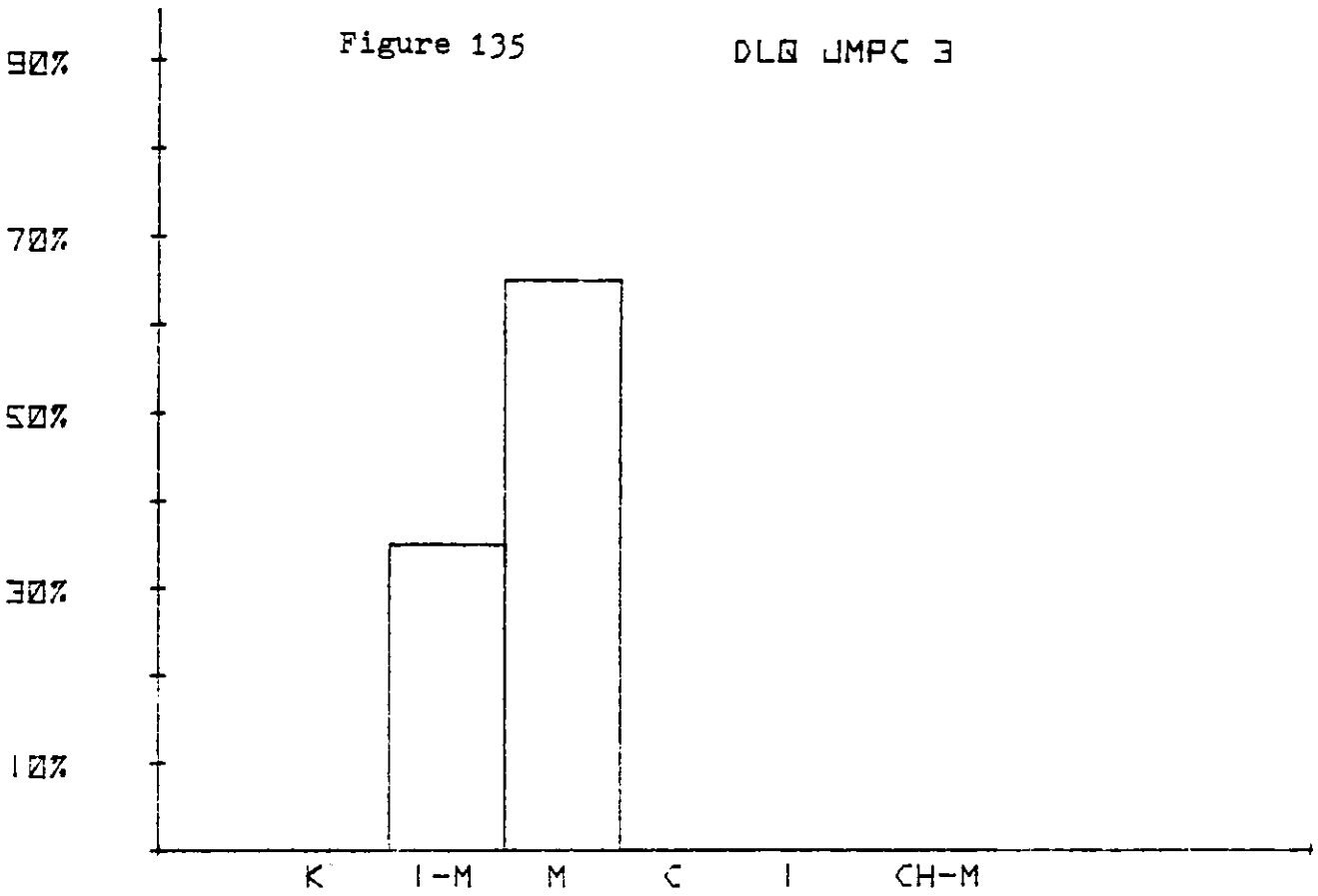


Figure 136

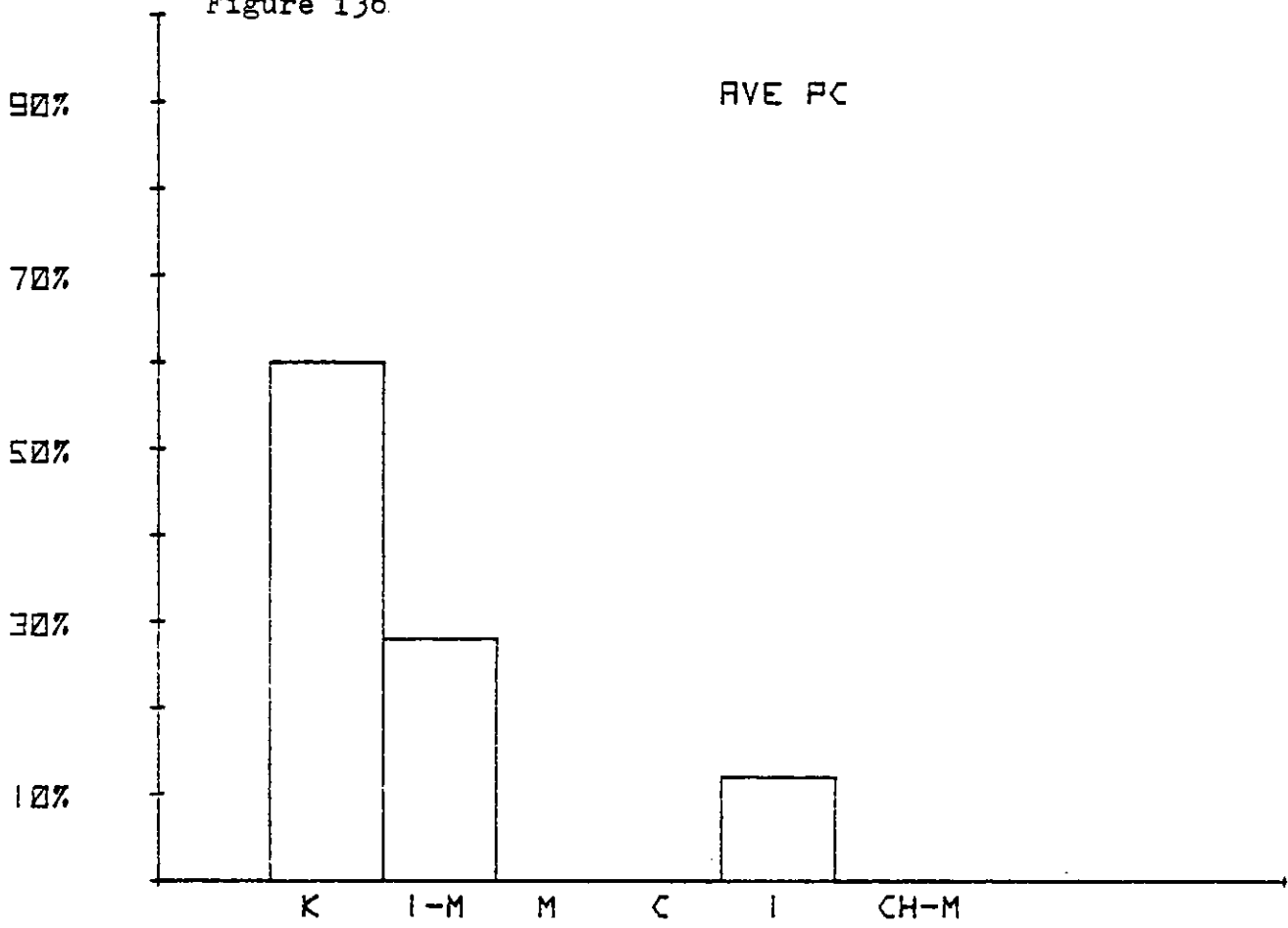


Figure 137
HG JMWC 1-2C

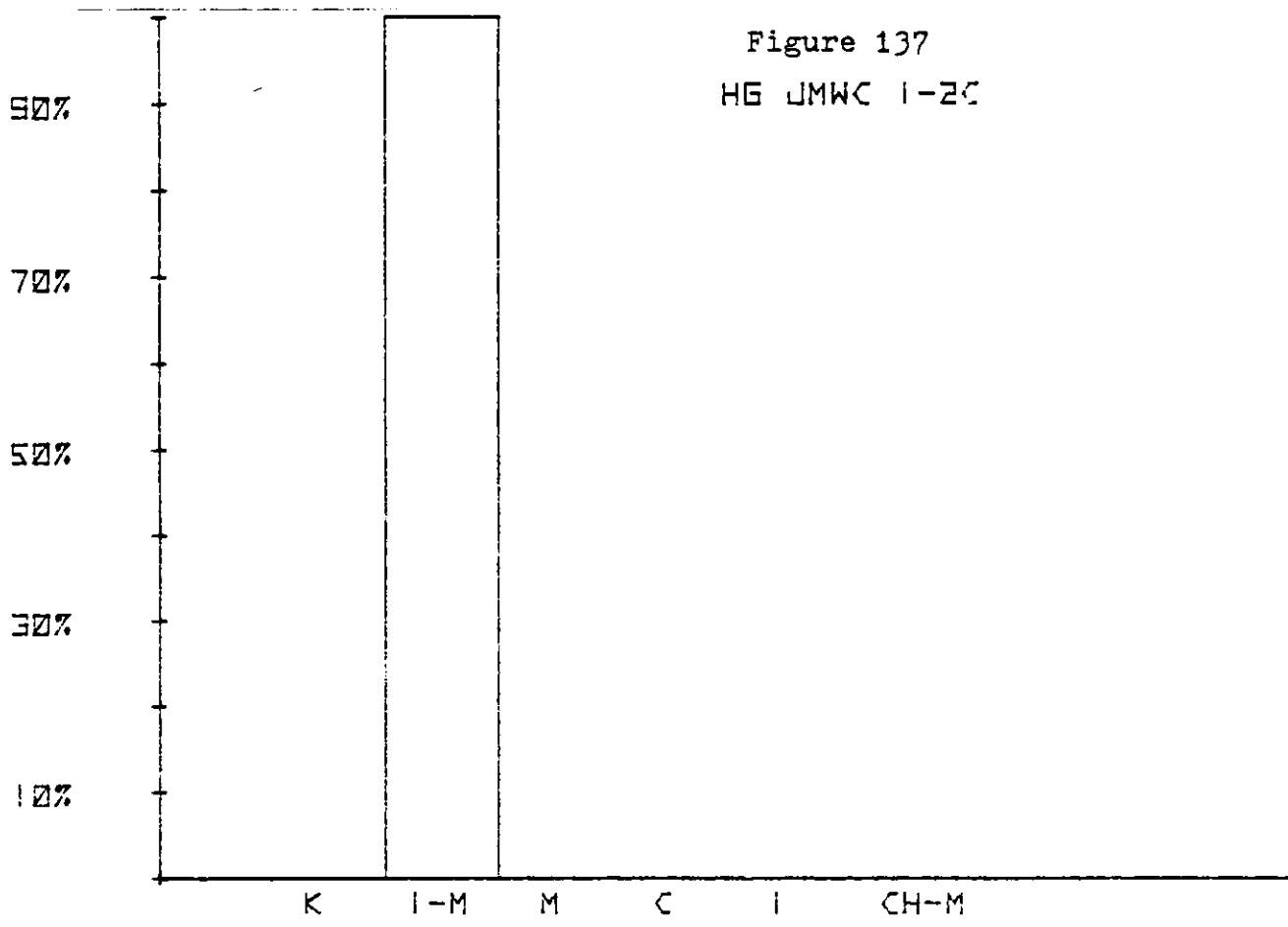


Figure 138

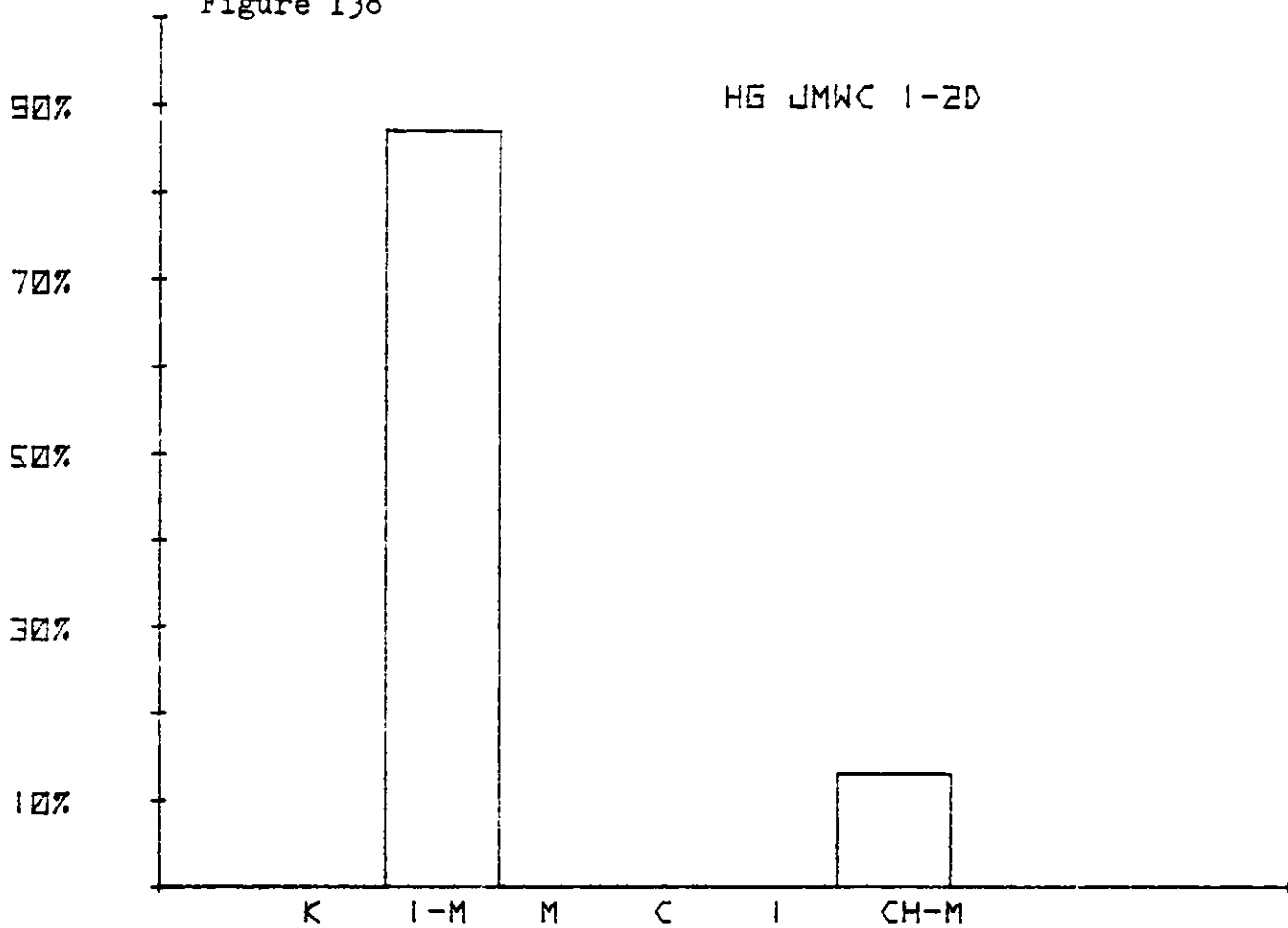


Figure 139

HG JMWC 1-201

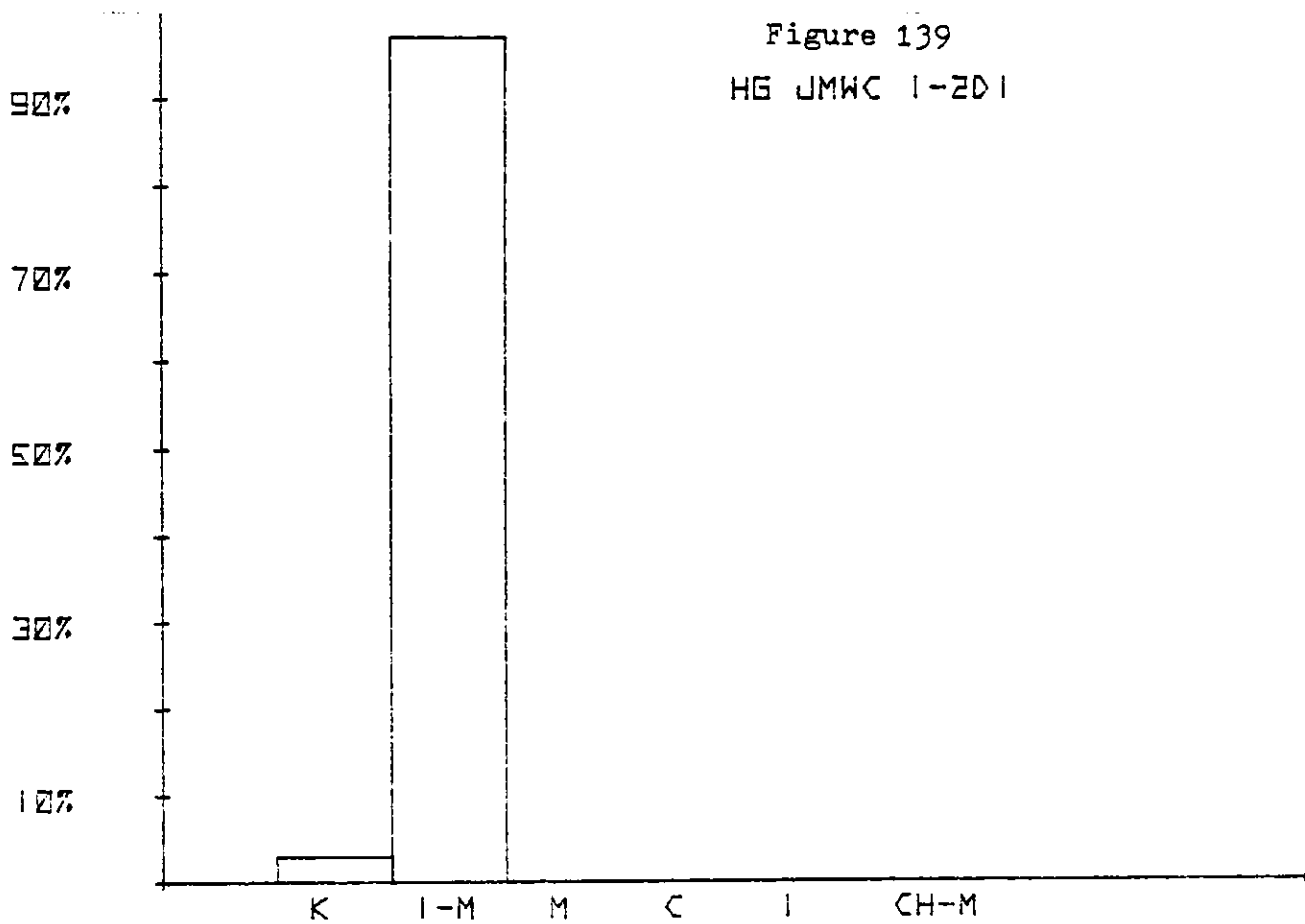


Figure 140

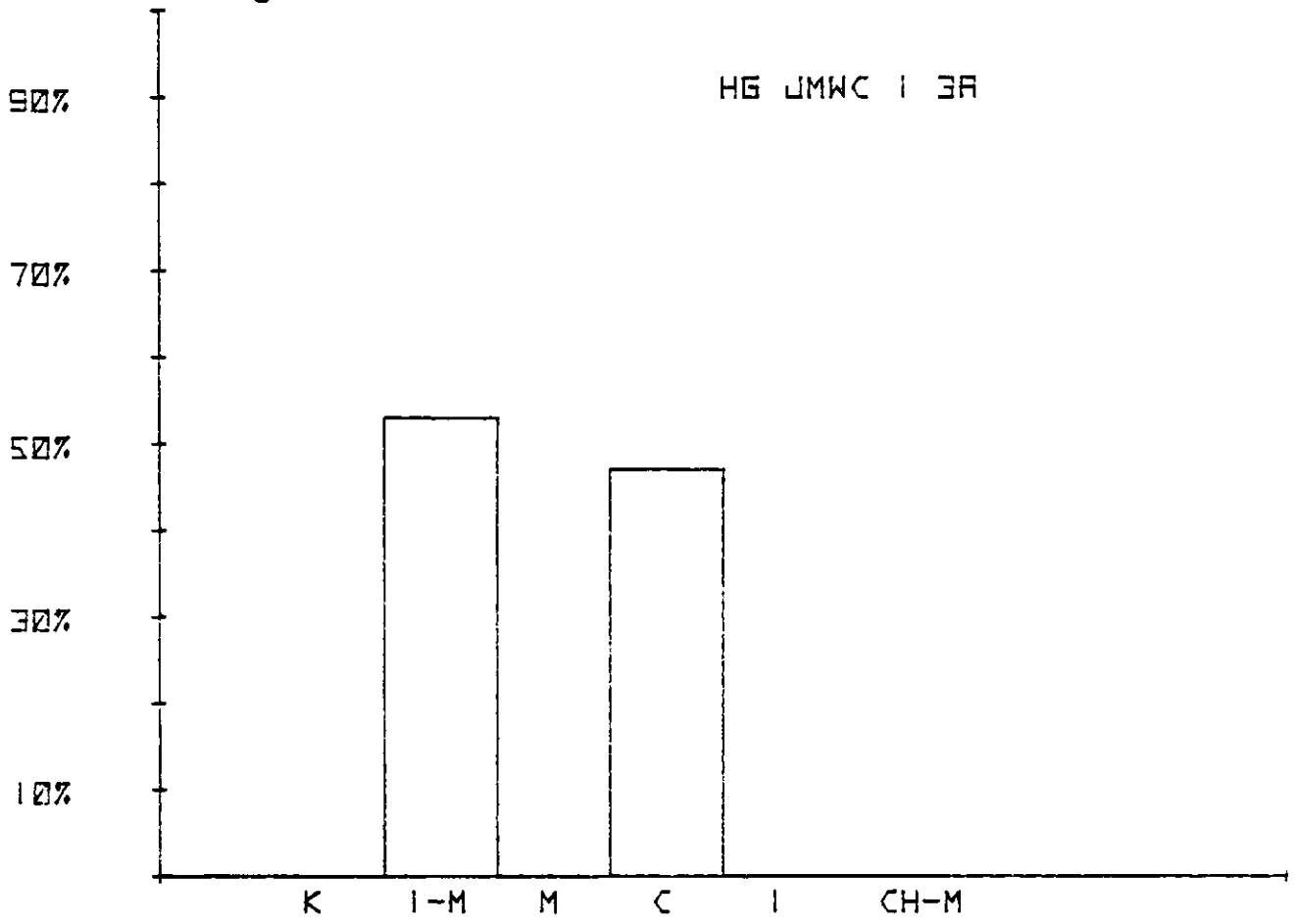


Figure 141

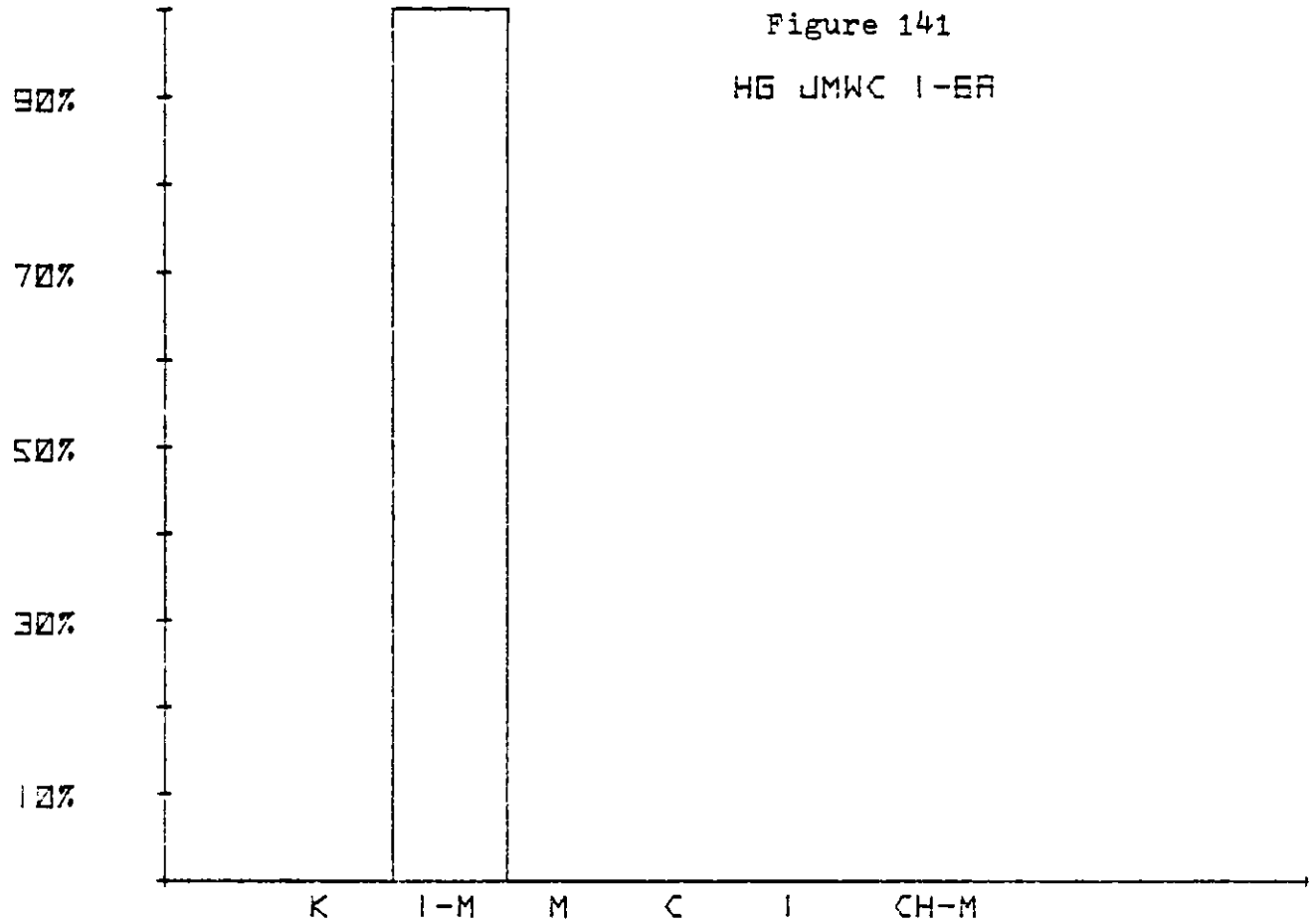


Figure 142

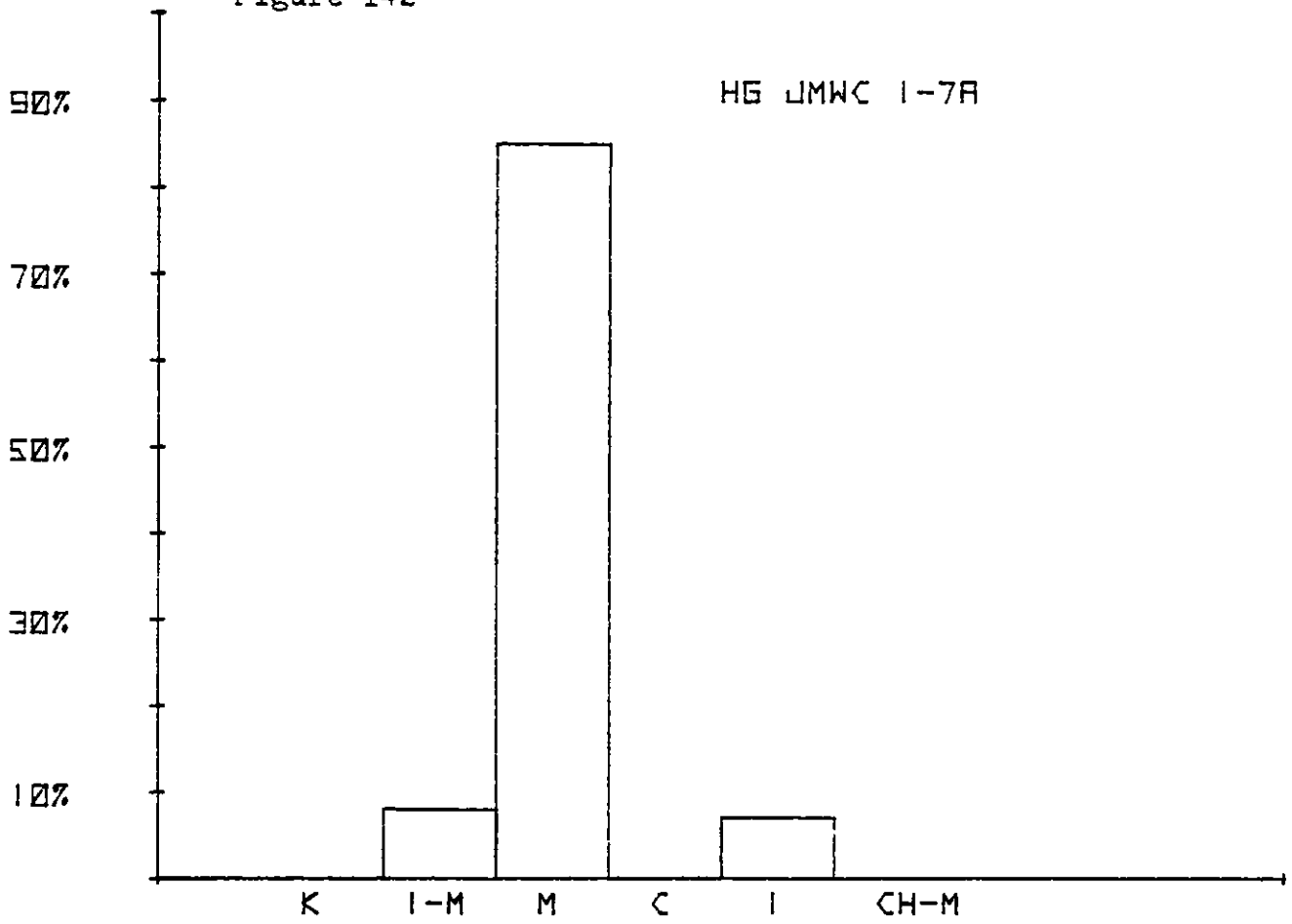


Figure 143

HG LMWC 1-8A

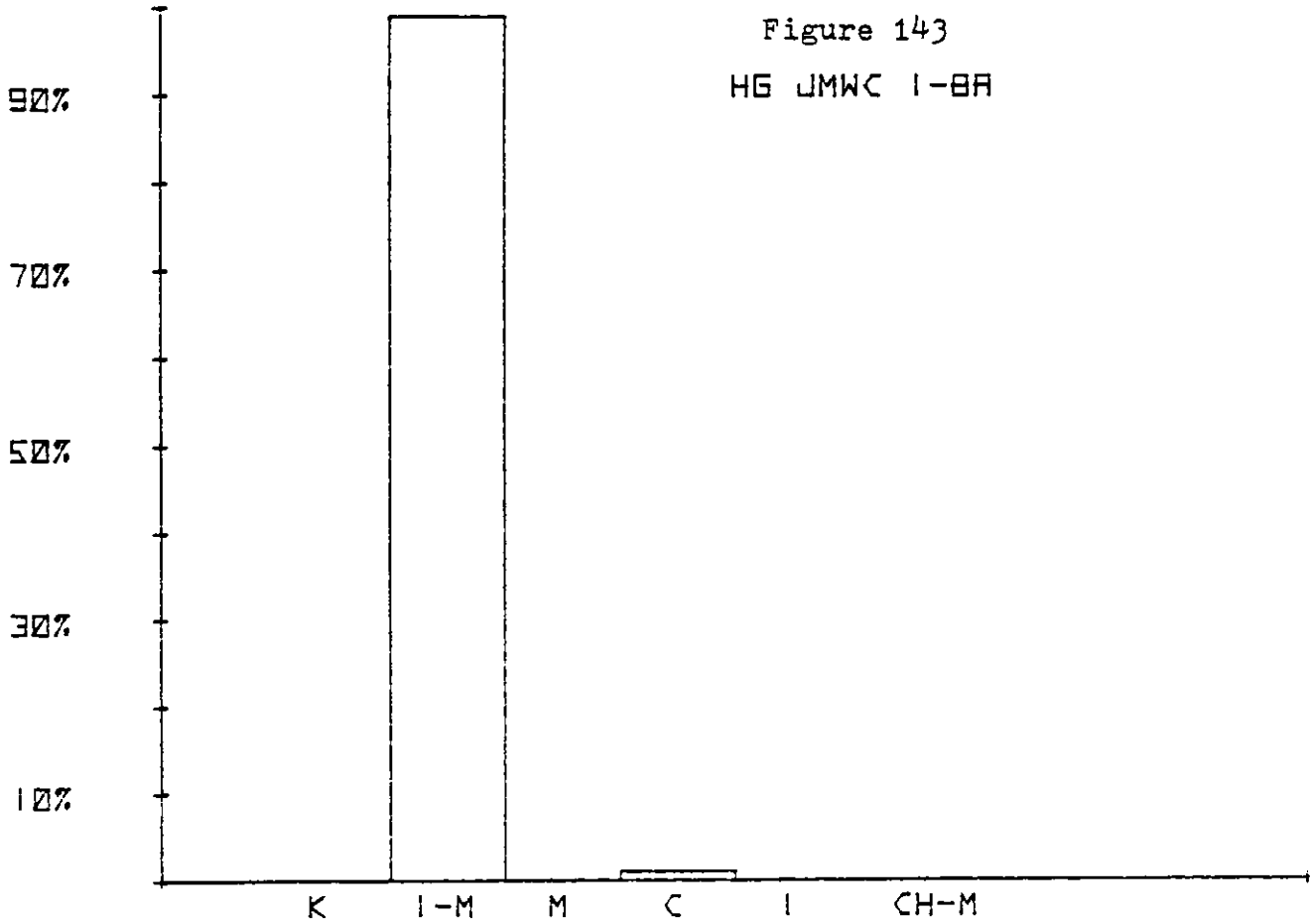


Figure 144

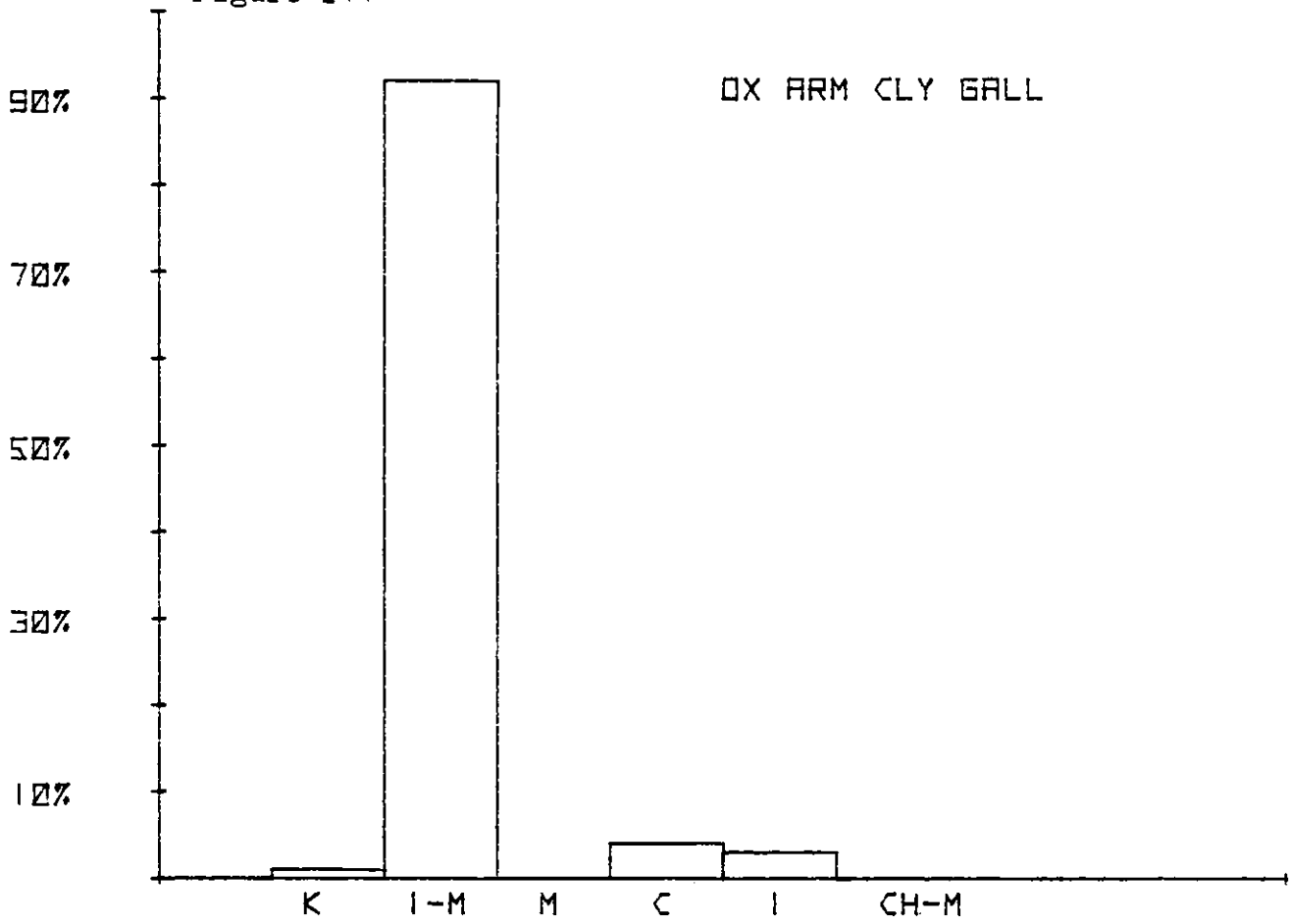


Figure 145

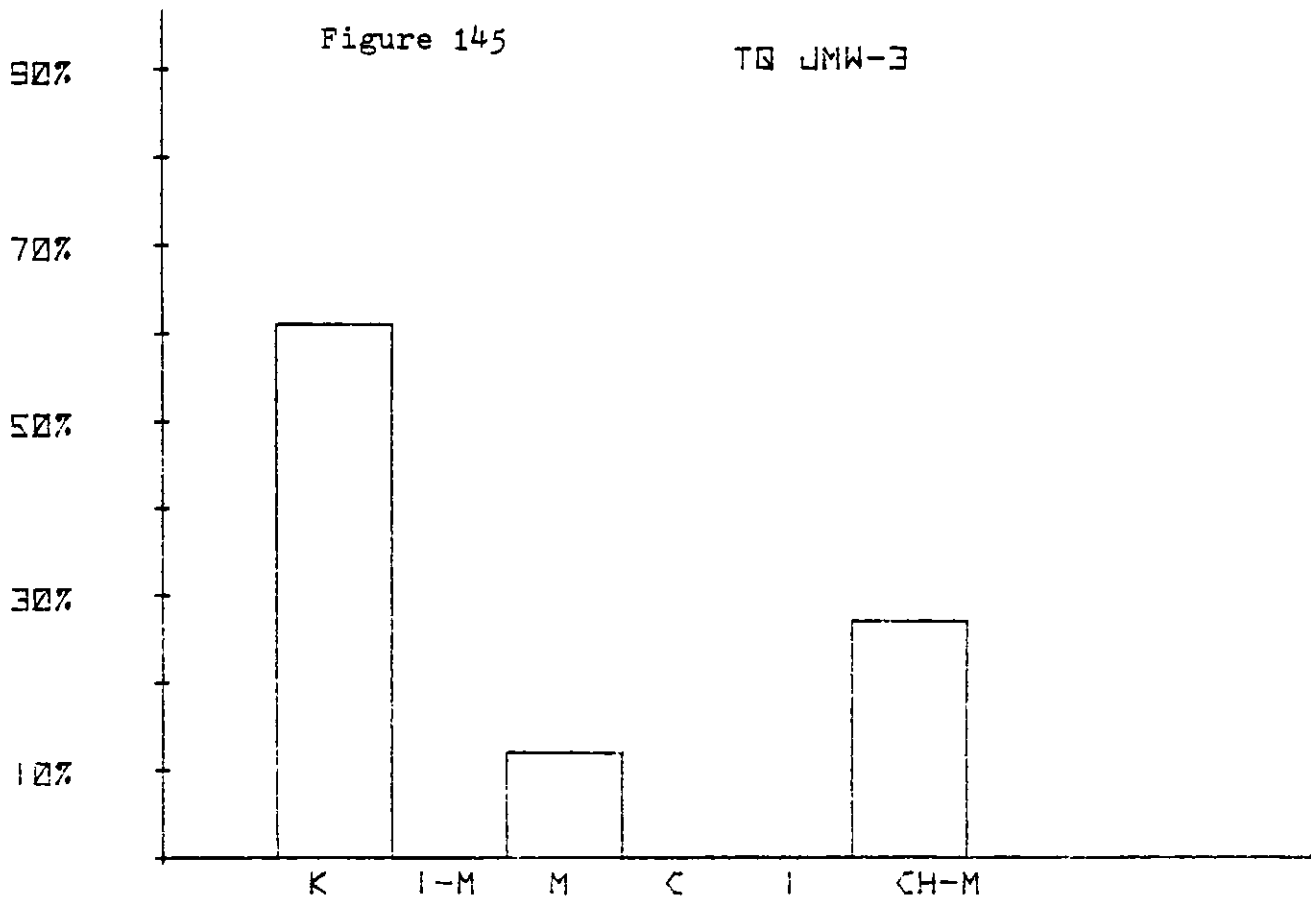


Figure 146

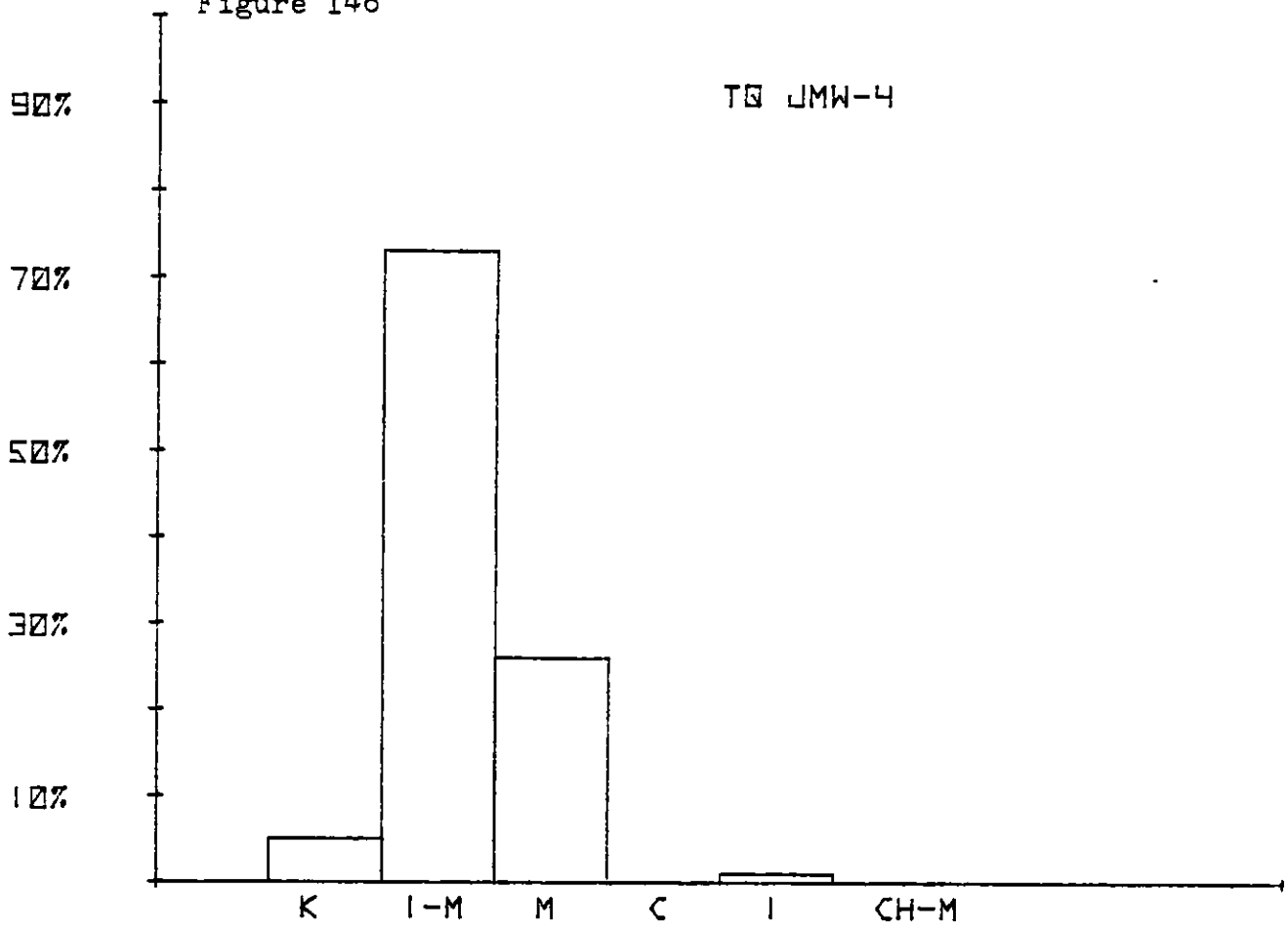


Figure 147

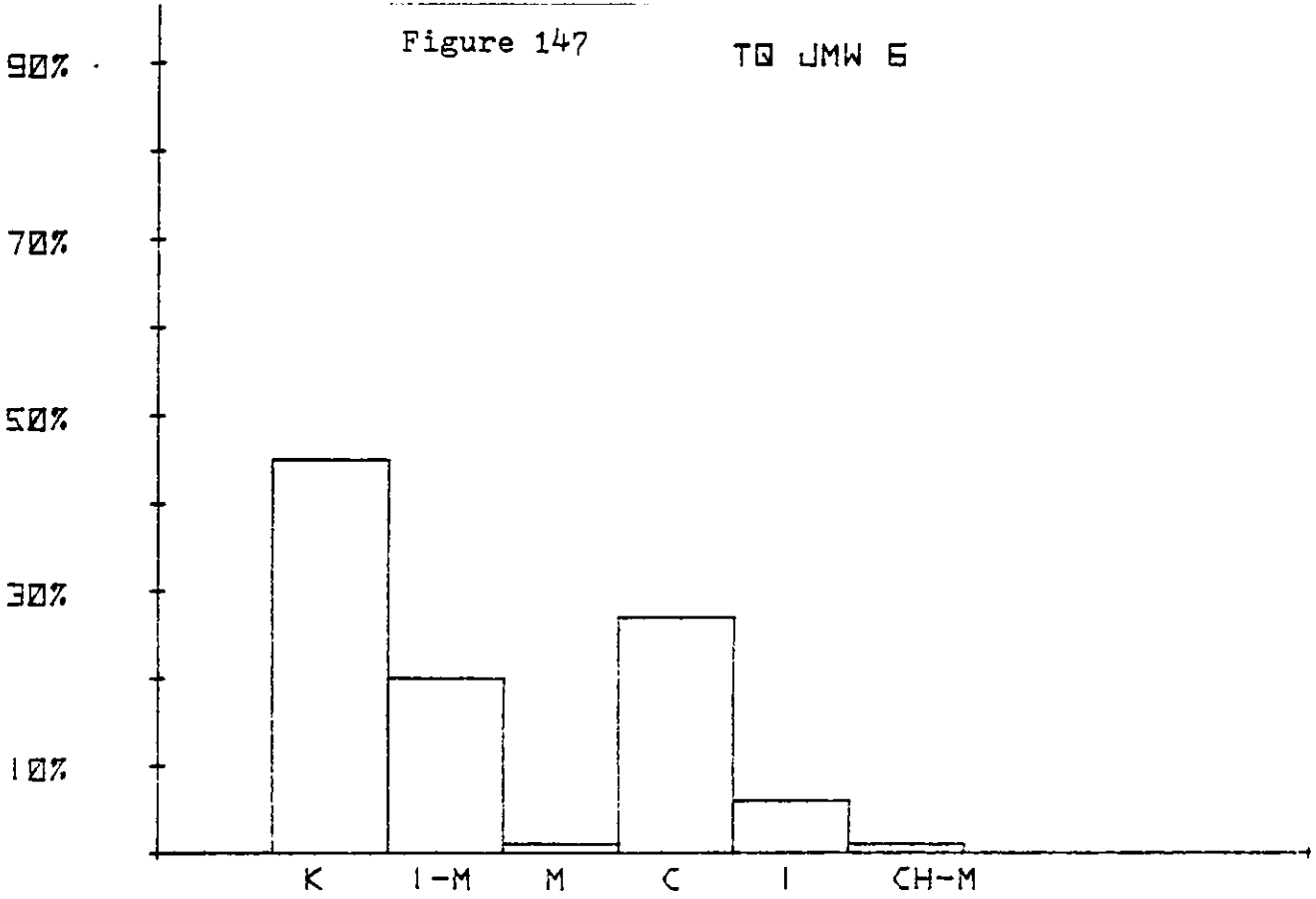


Figure 148

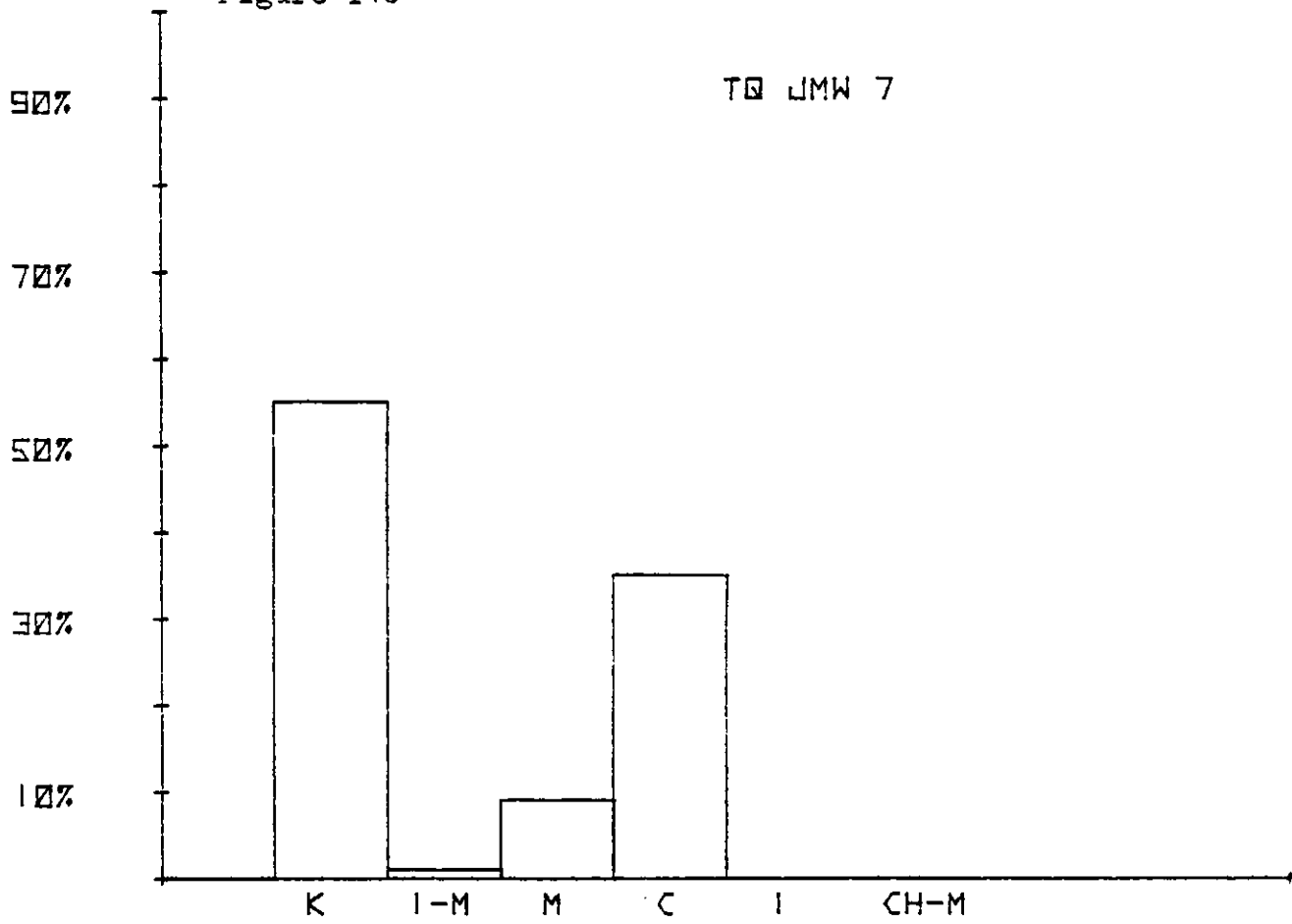


Figure 149

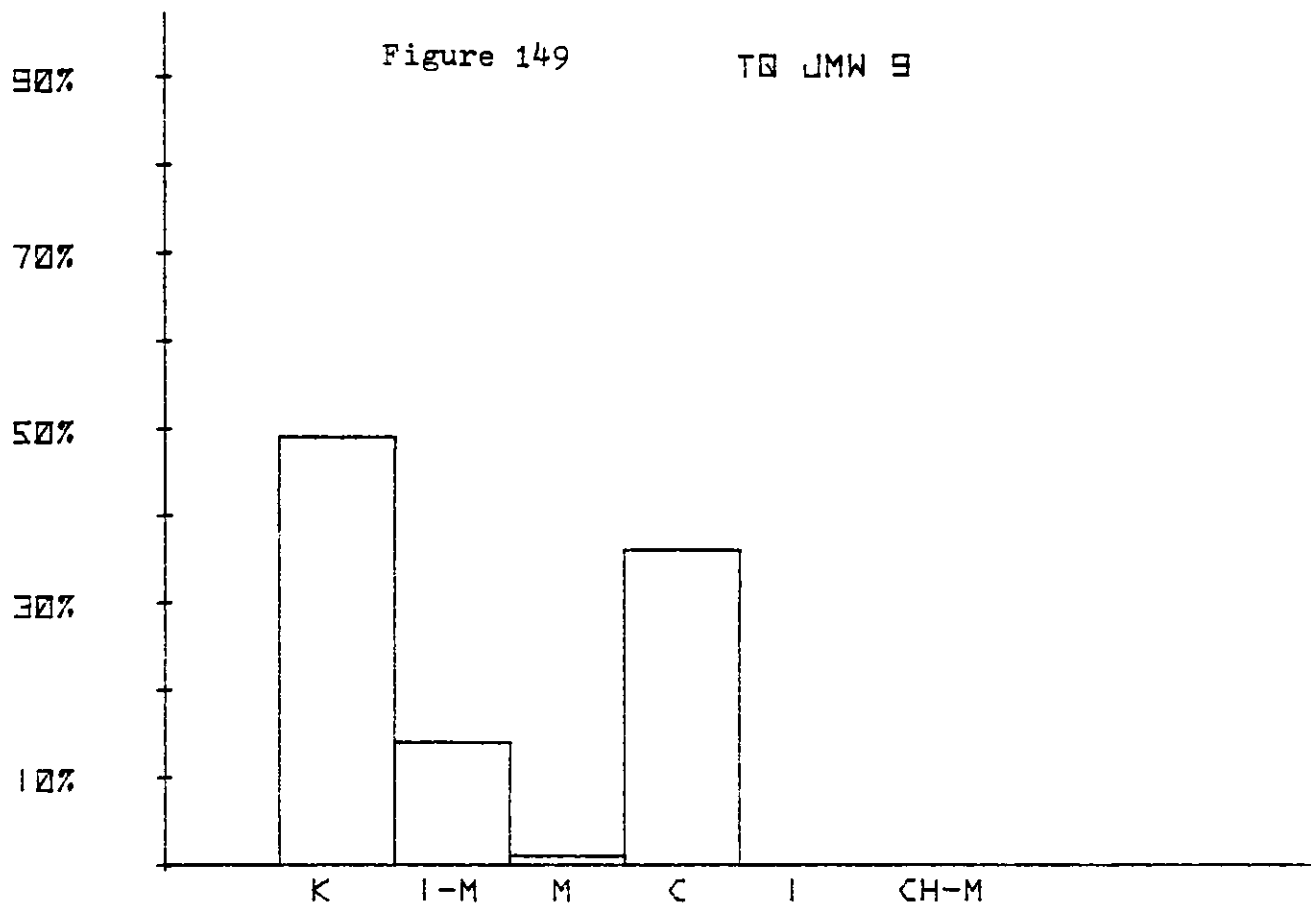
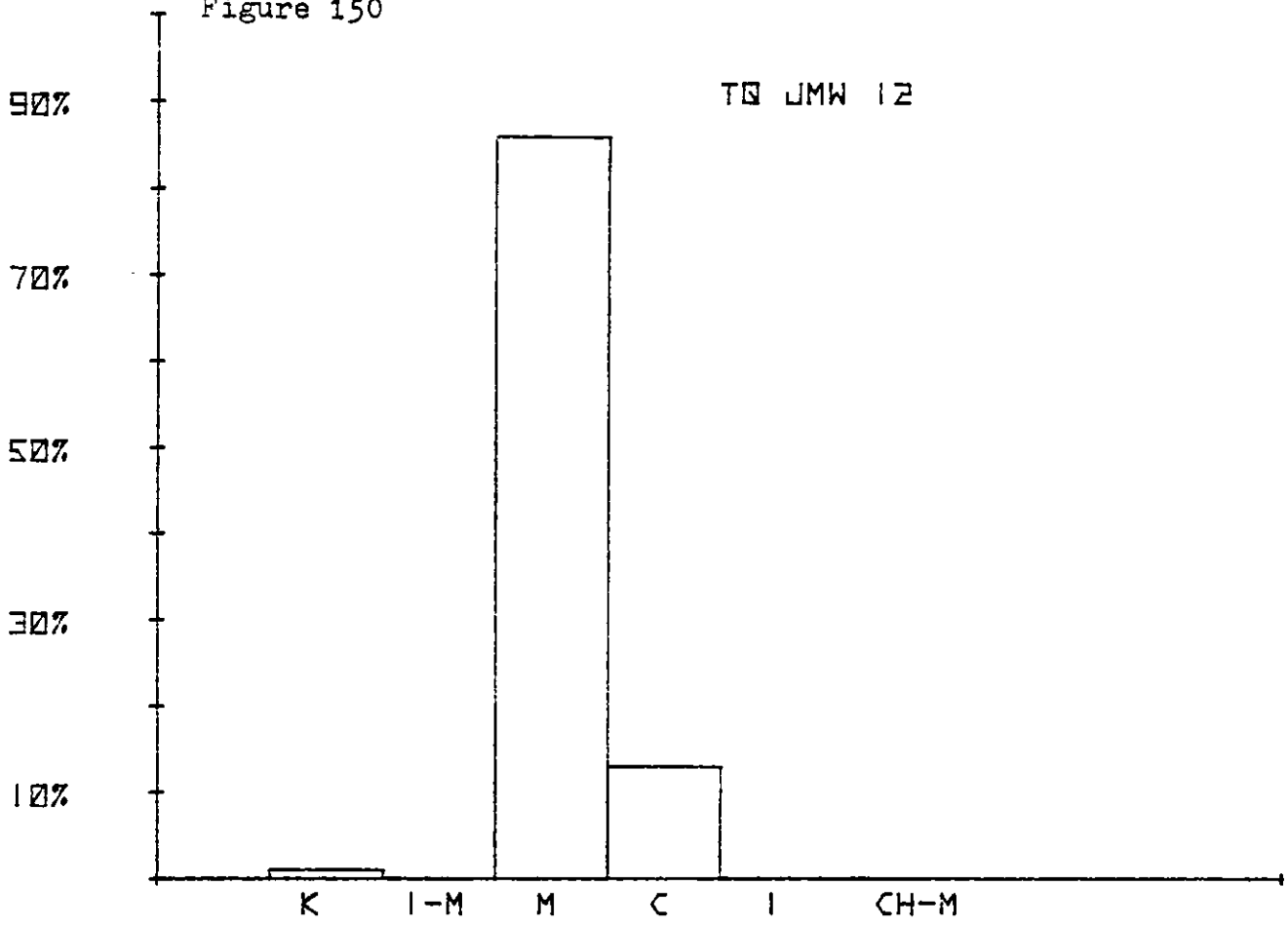
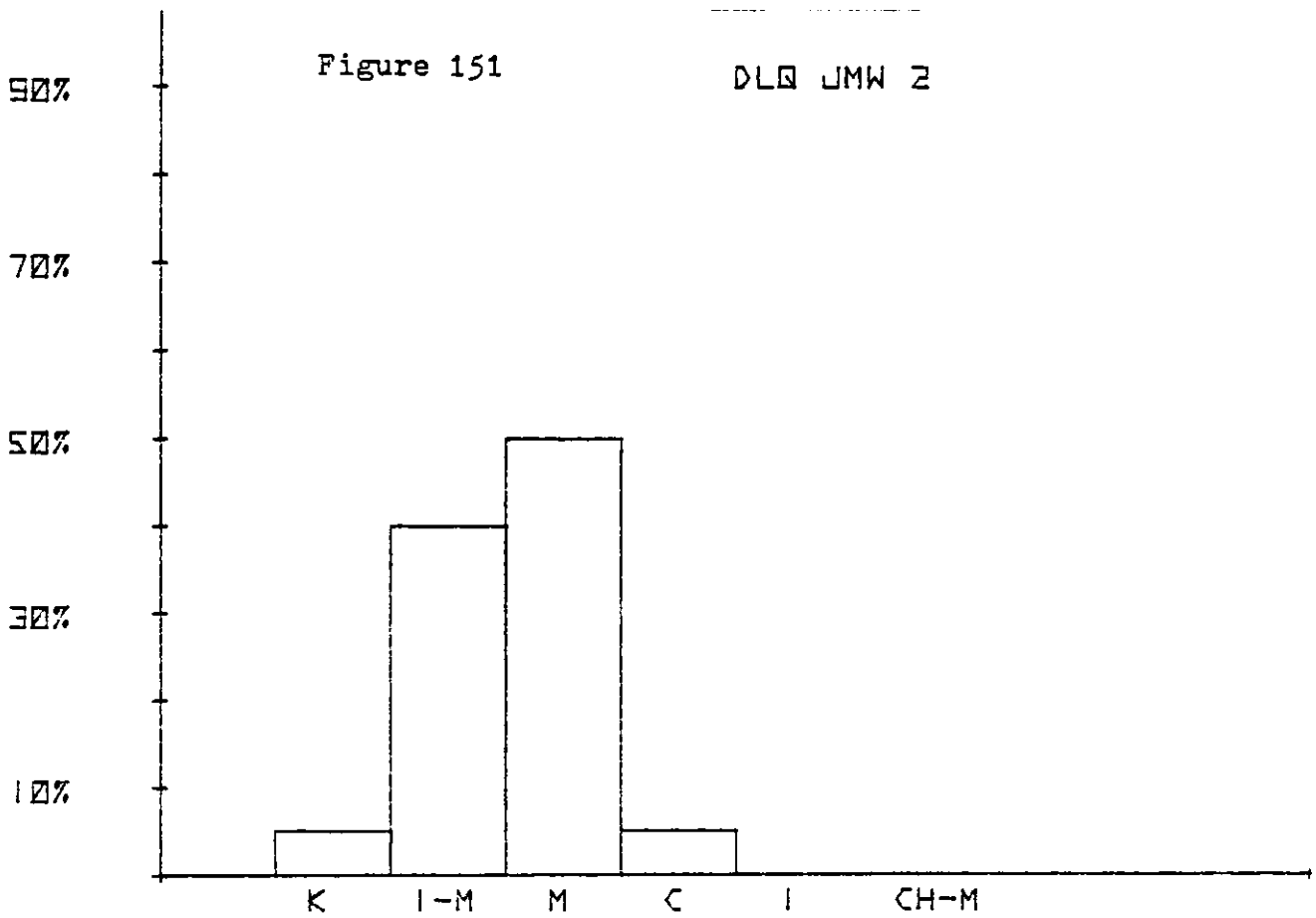


Figure 150



TQ JMW 12

Figure 151



DLQ JMW 2

Figure 152

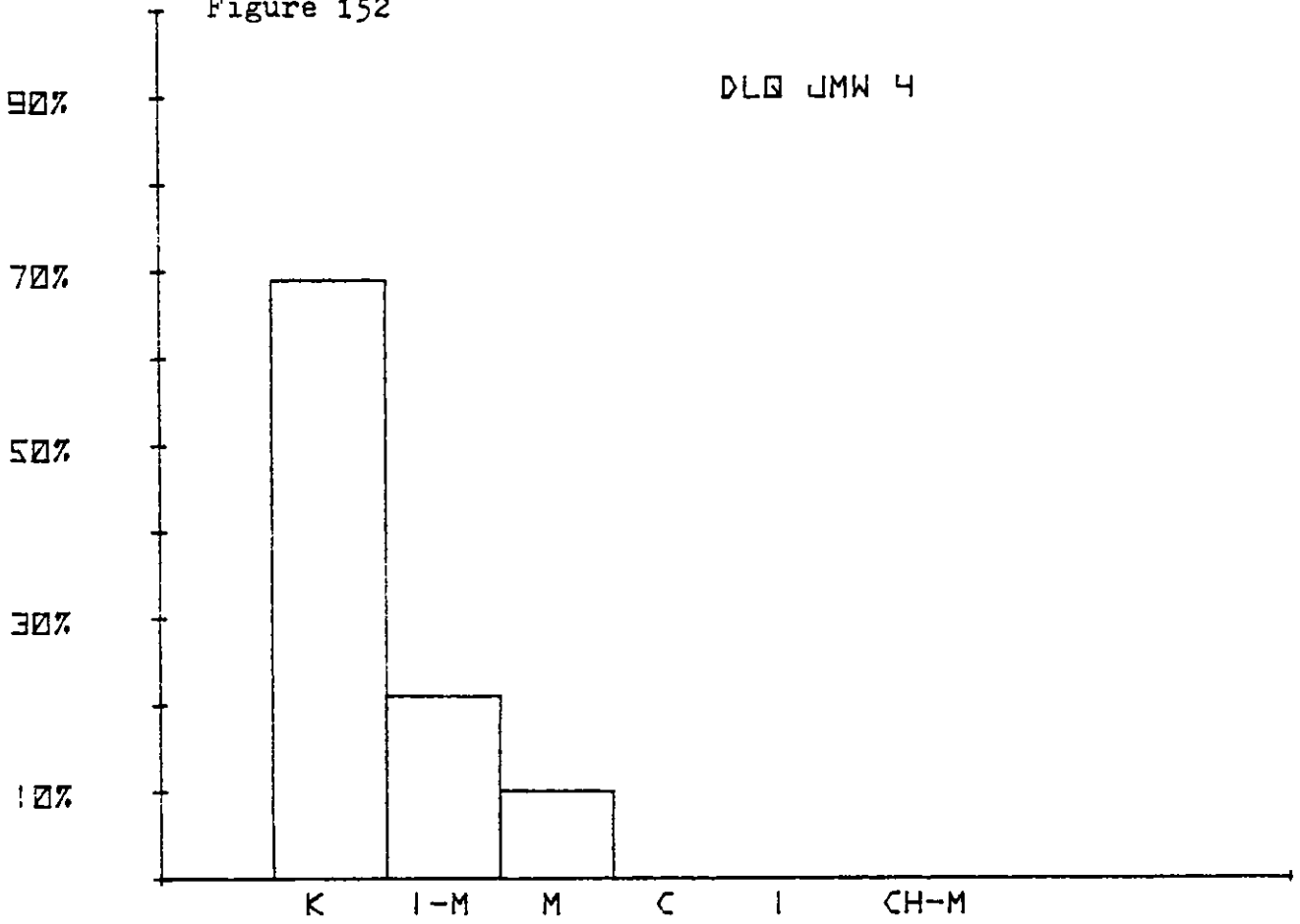


Figure 153

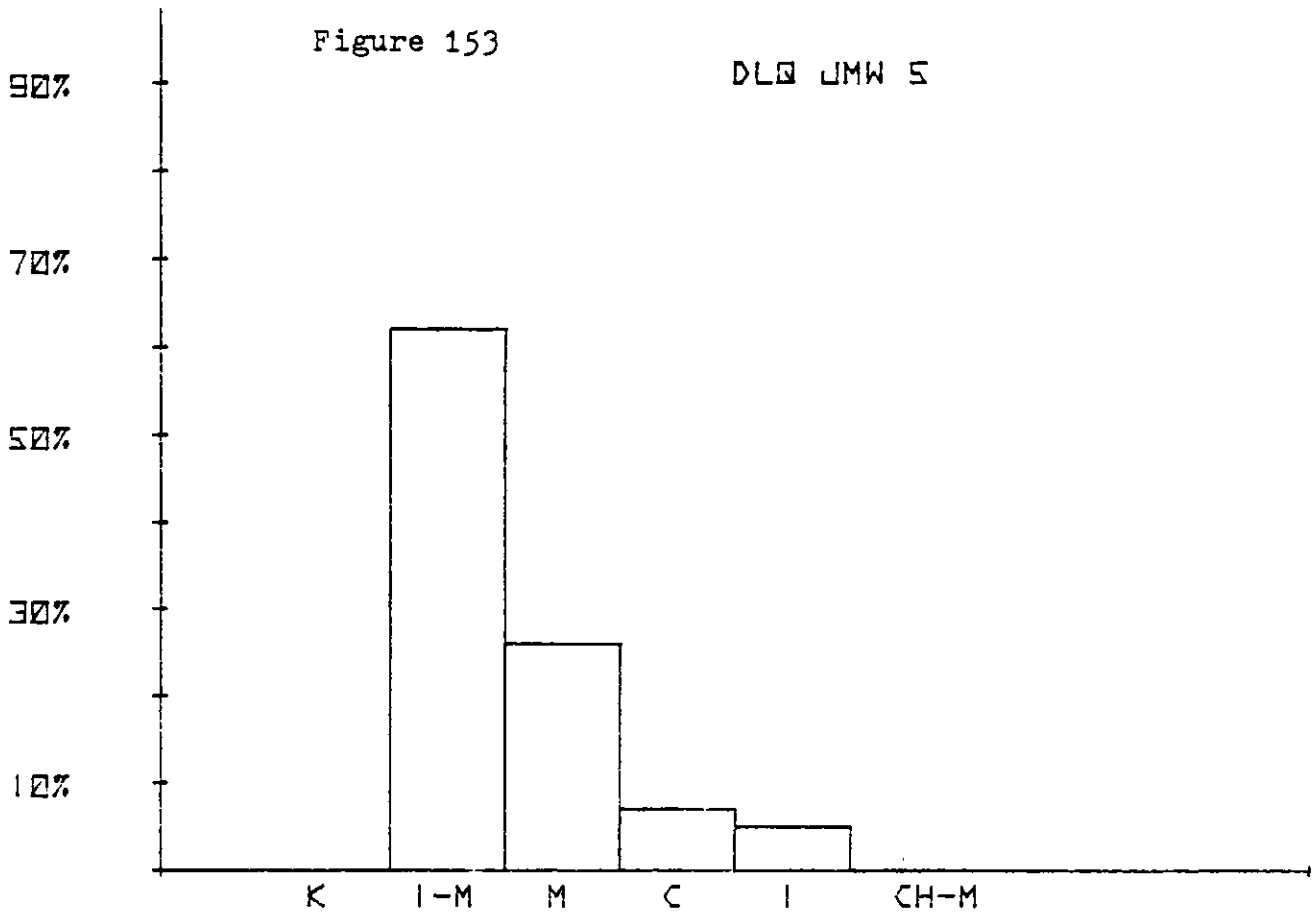


Figure 154

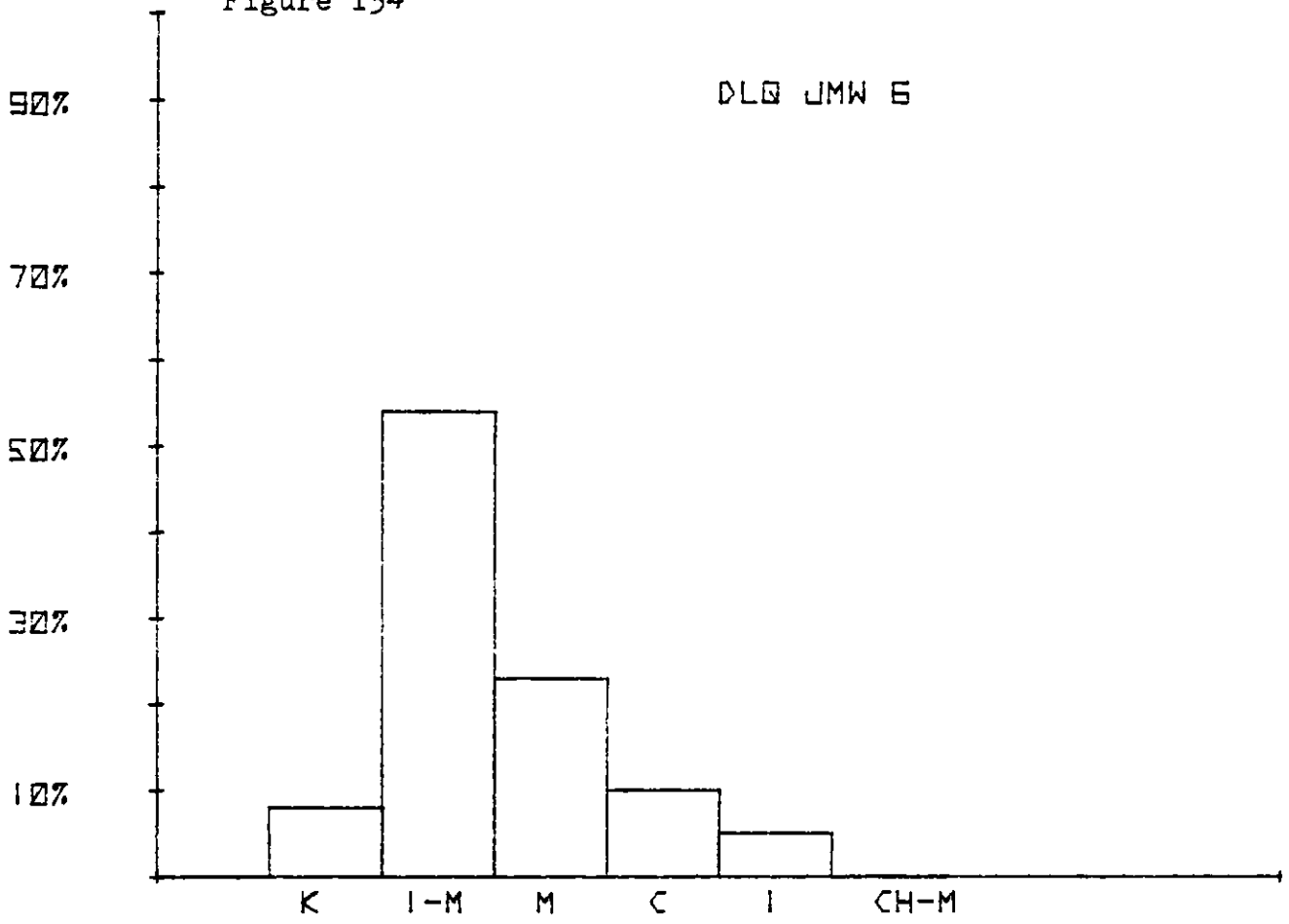


Figure 155

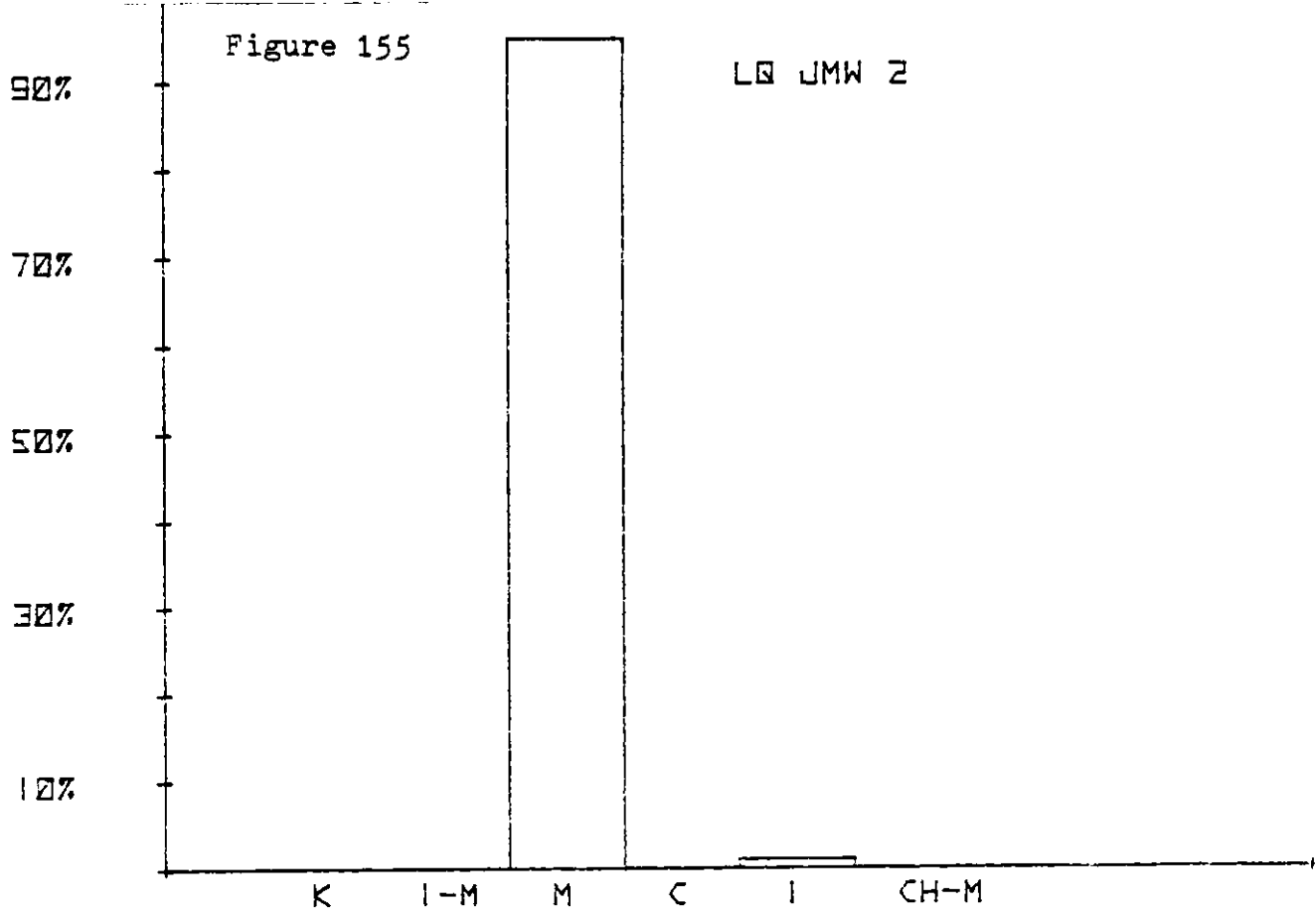


Figure 156

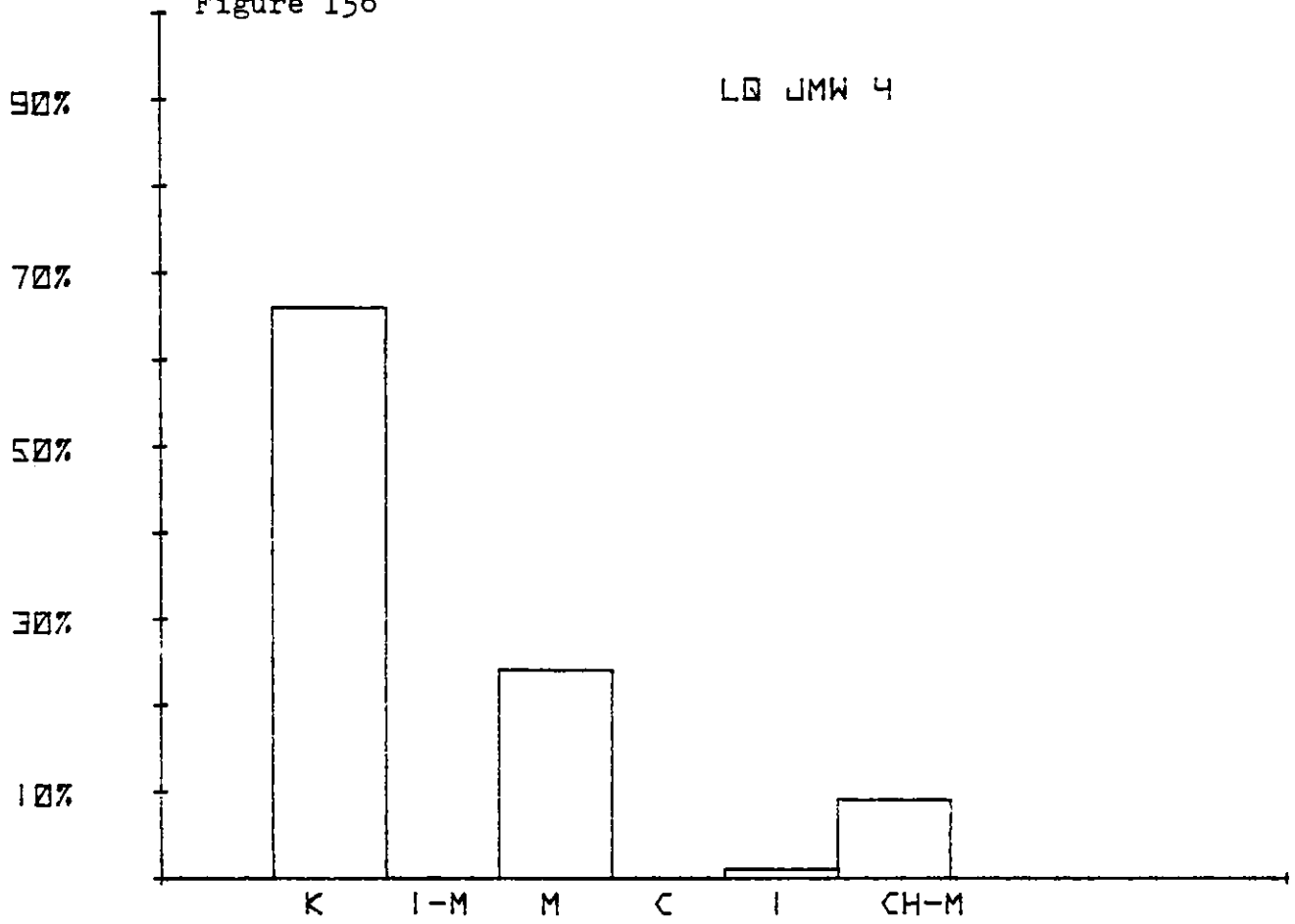


Figure 157

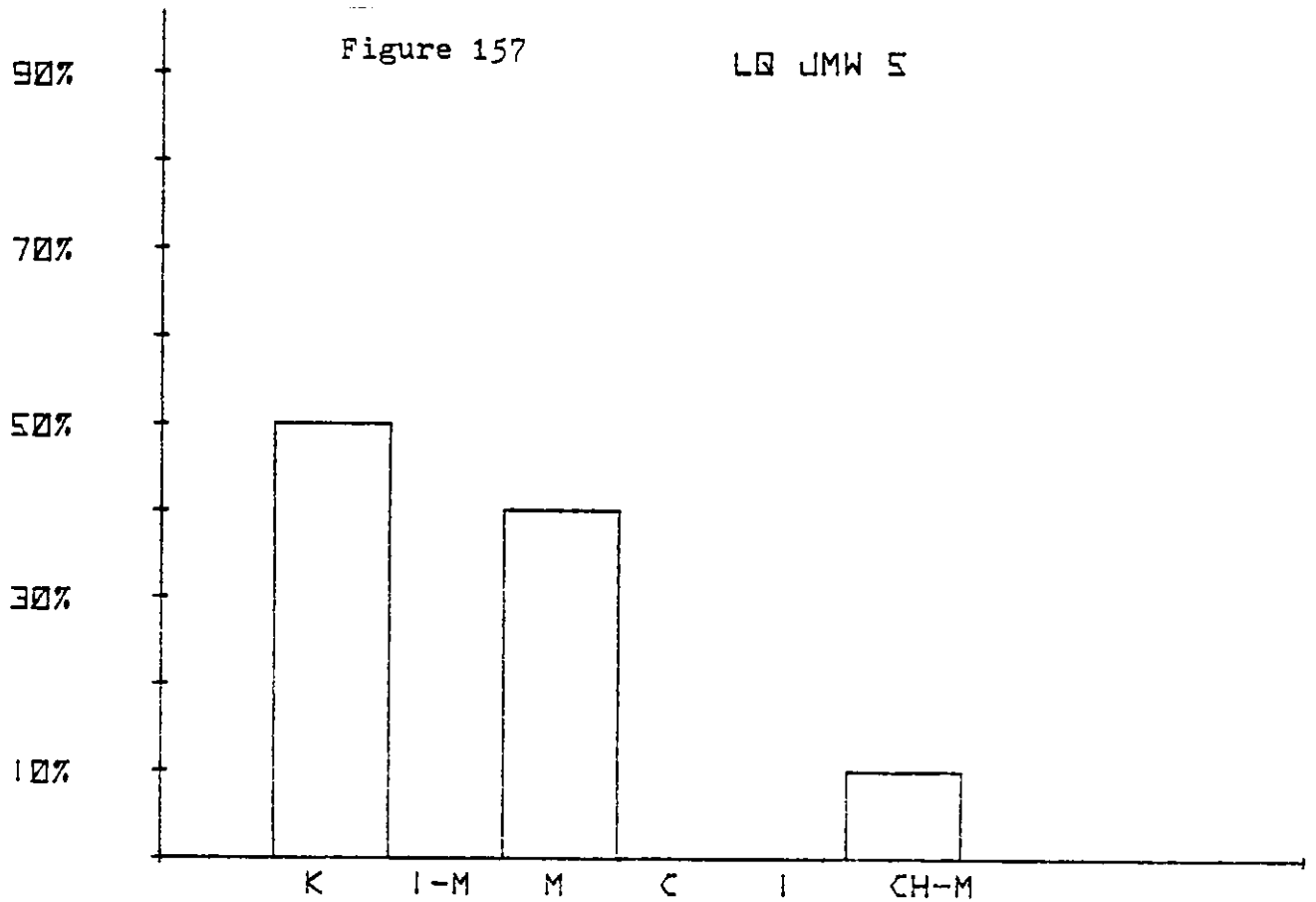


Figure 158

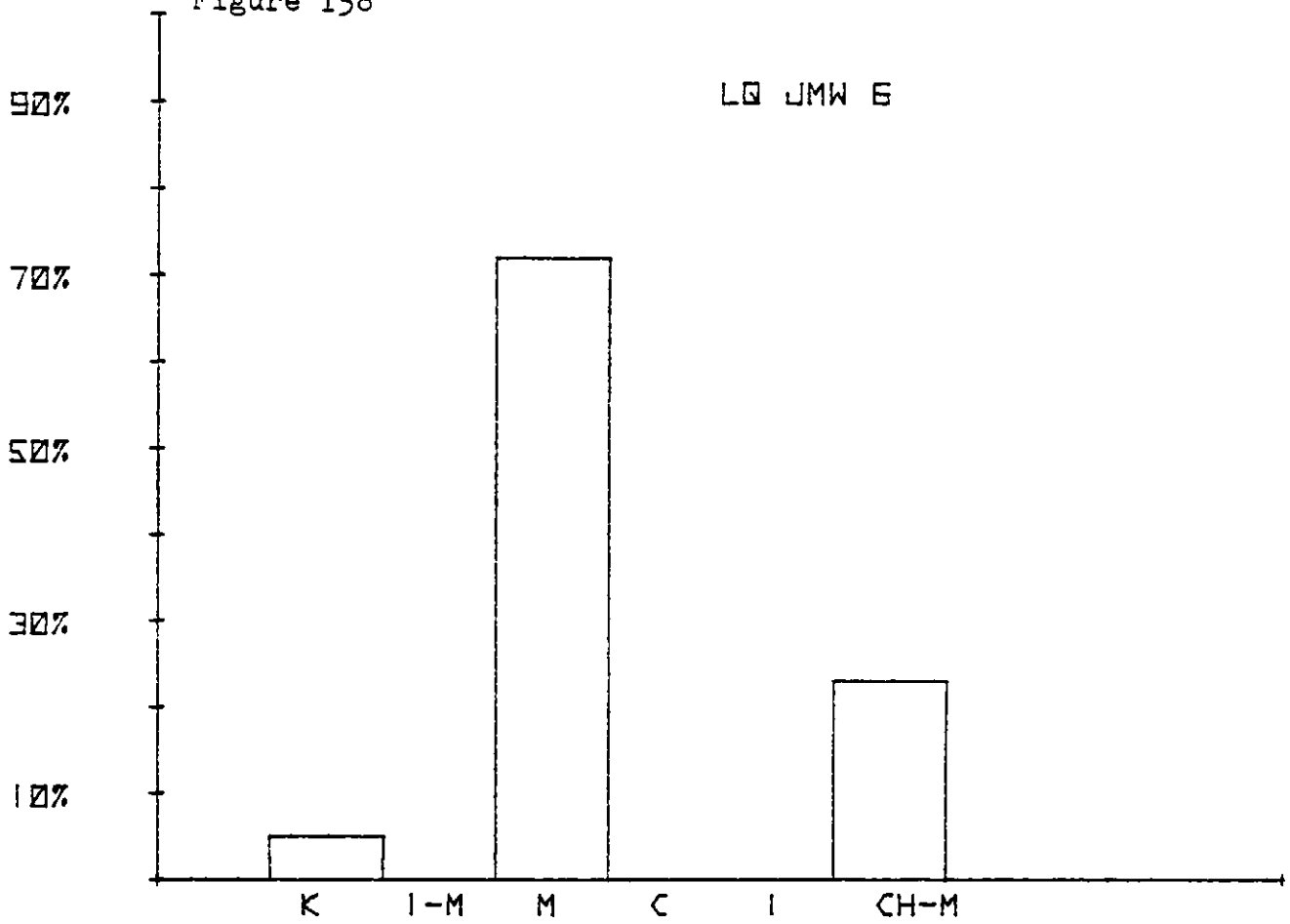


Figure 159

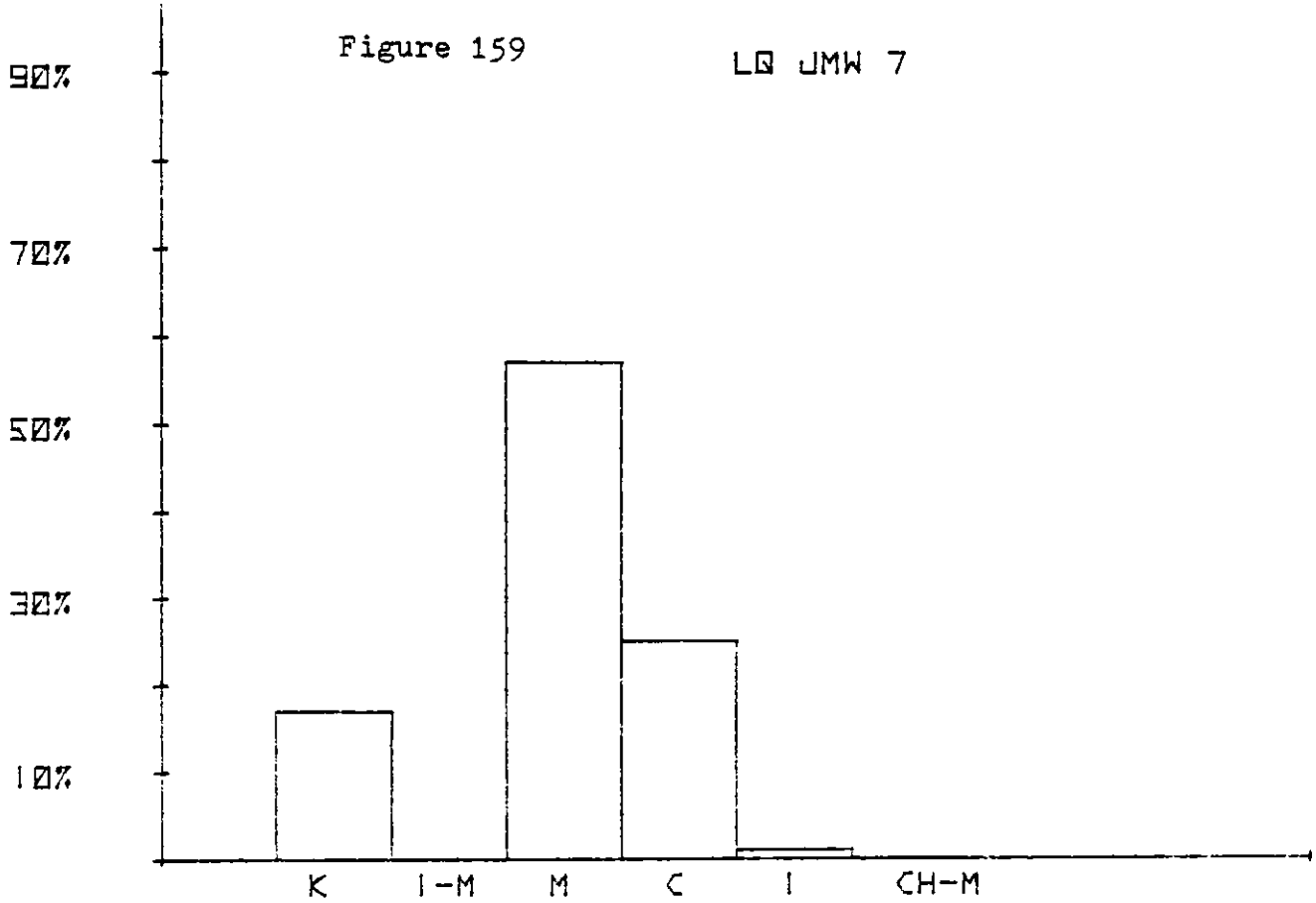


Figure 160

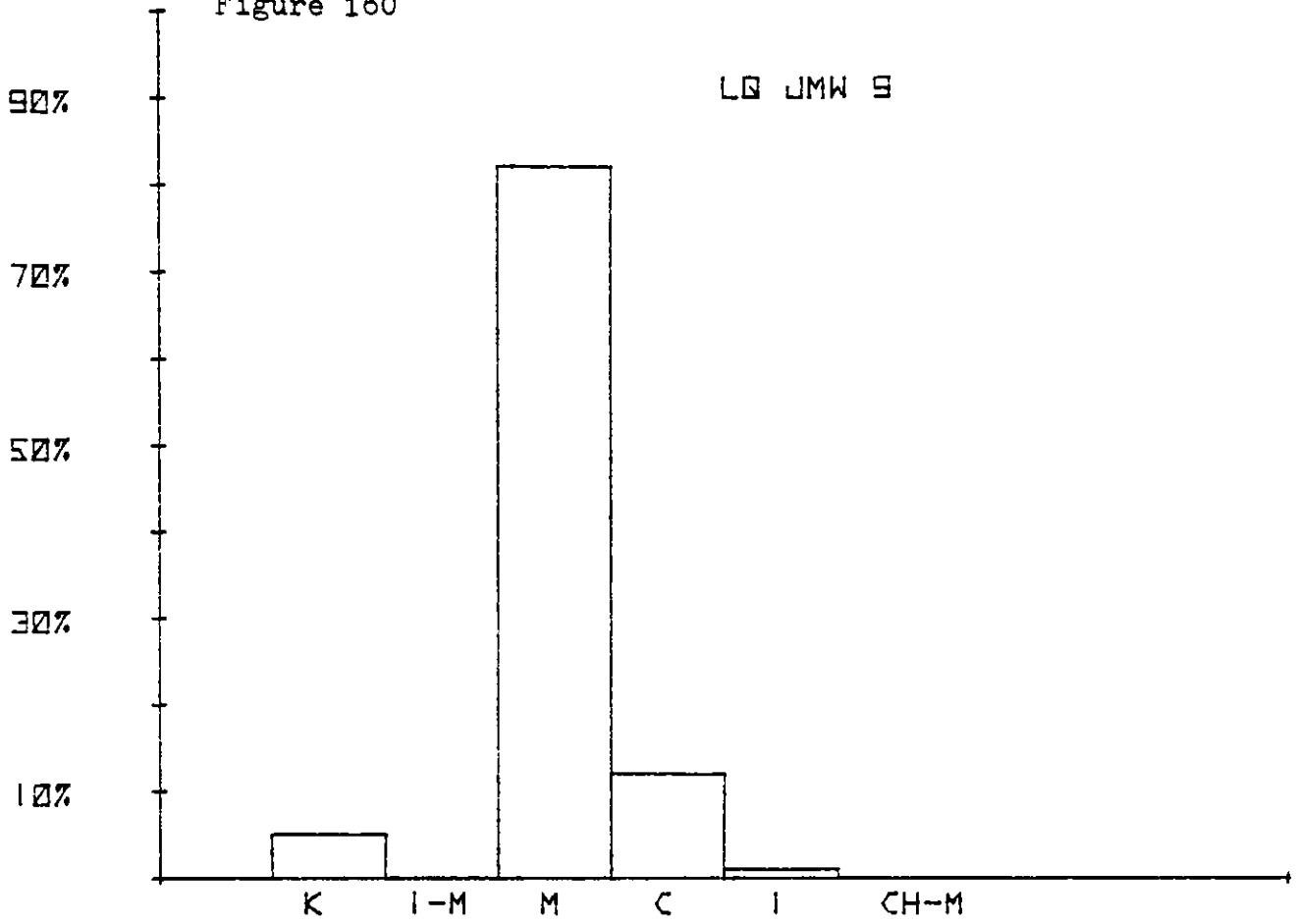


Figure 161

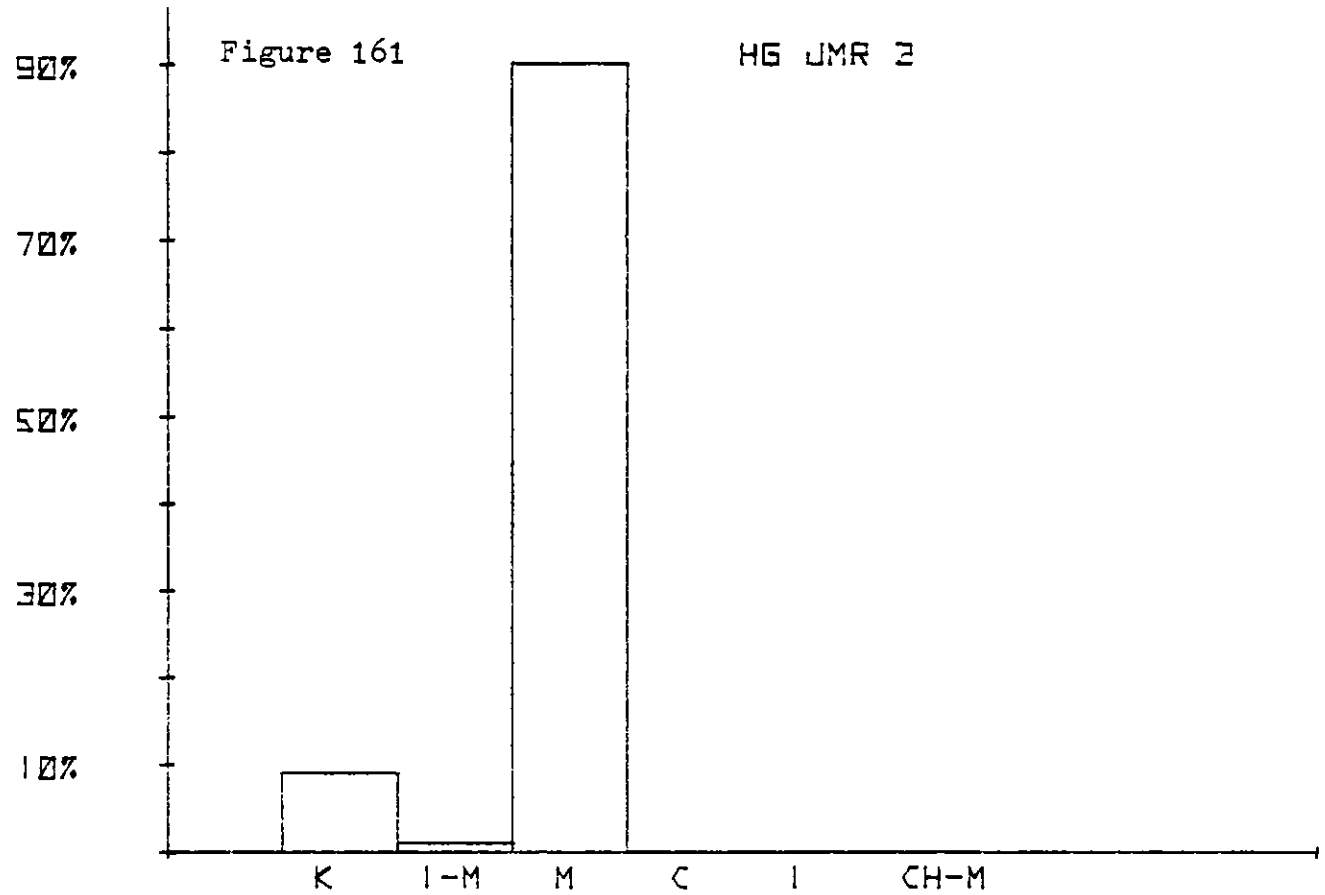


Figure 162

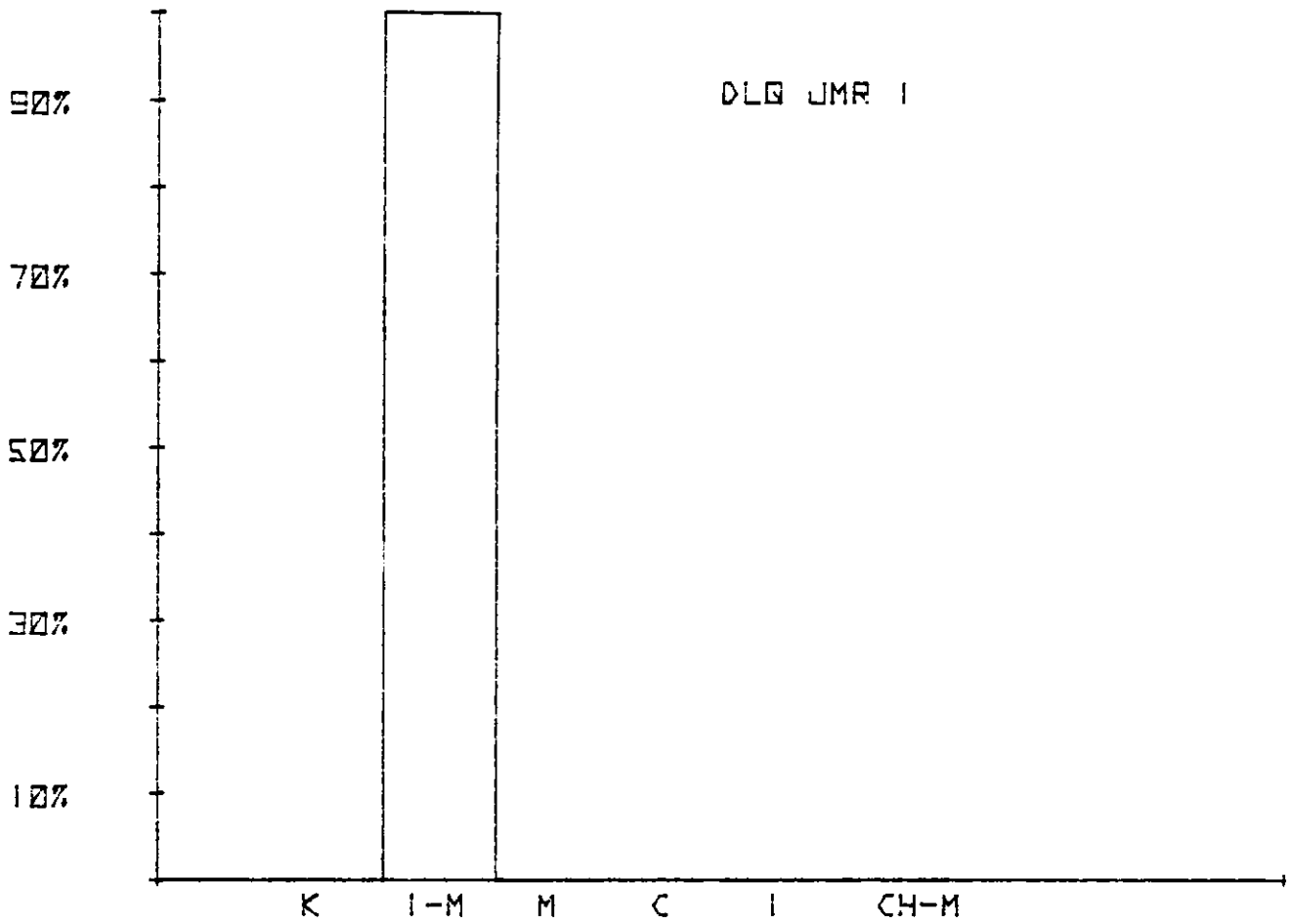


Figure 163

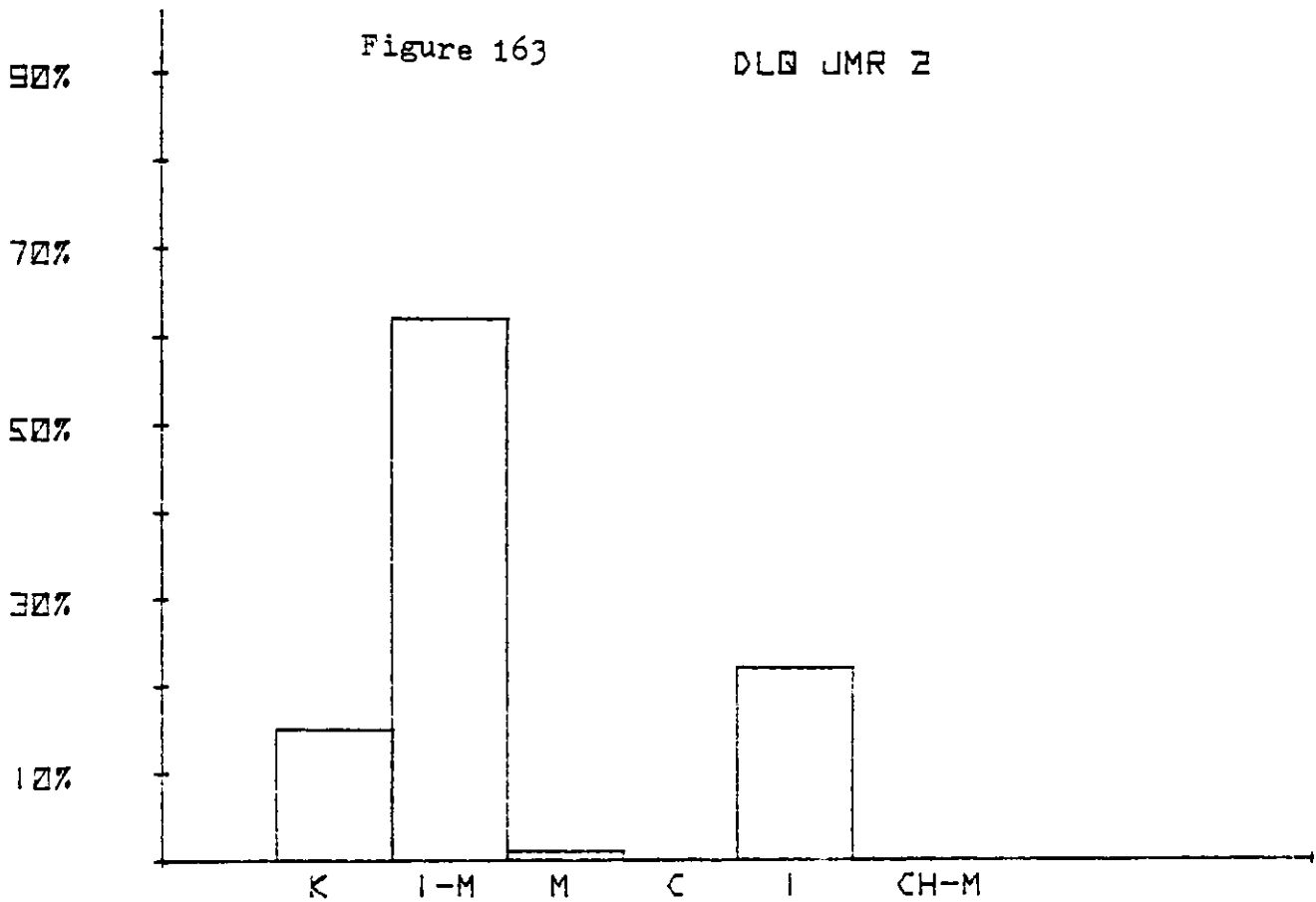


Figure 164

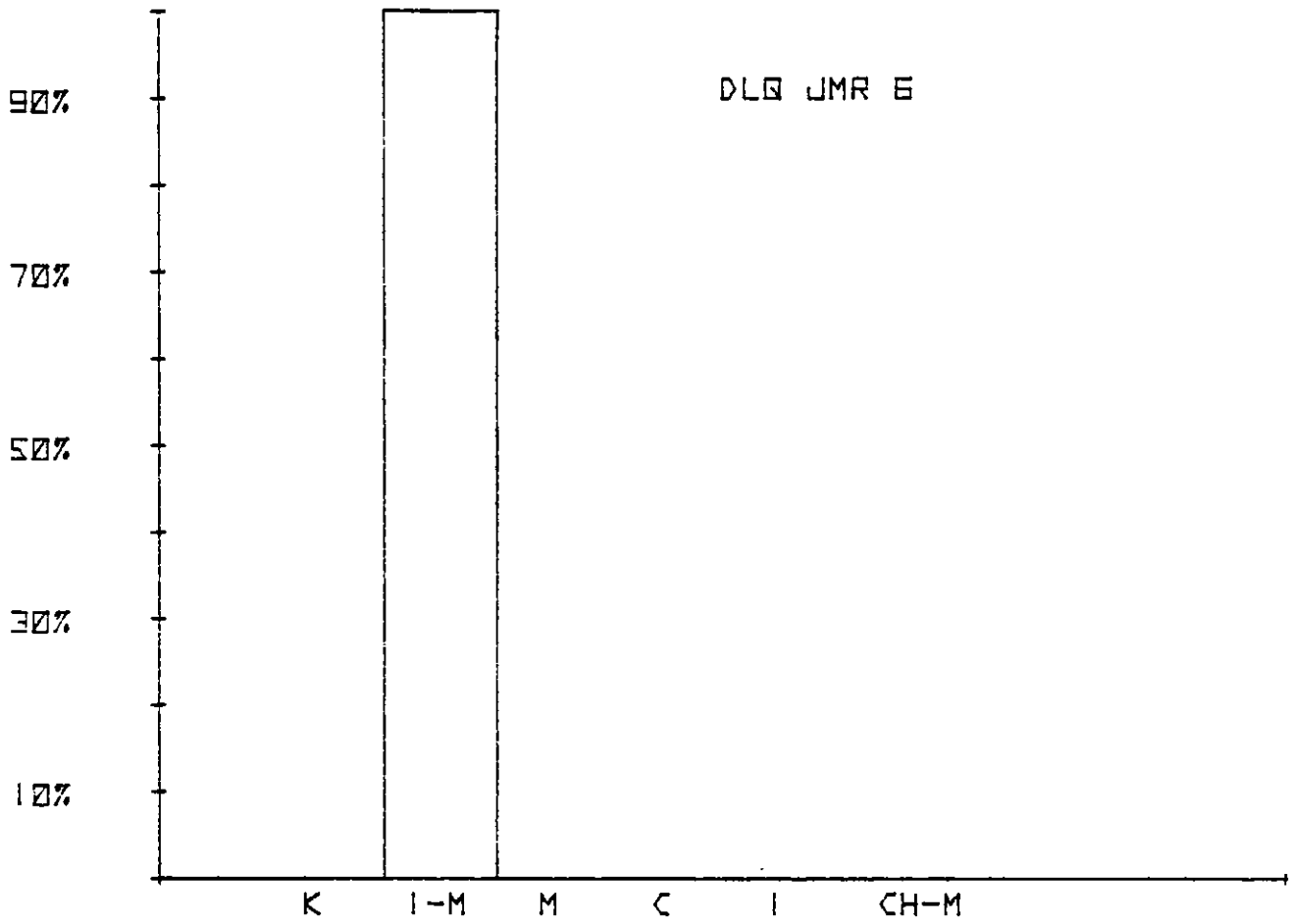


Figure 165

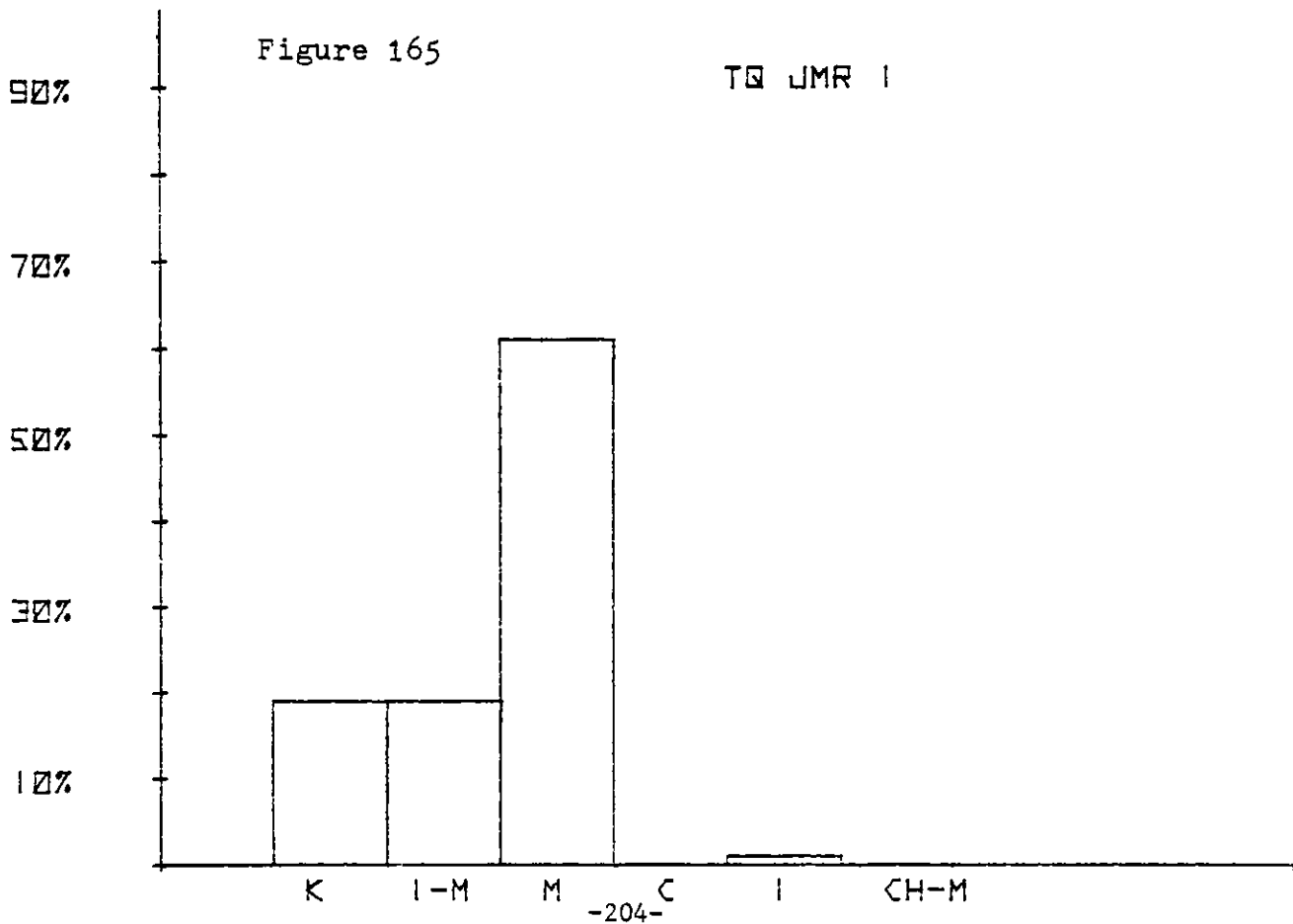


Figure 166

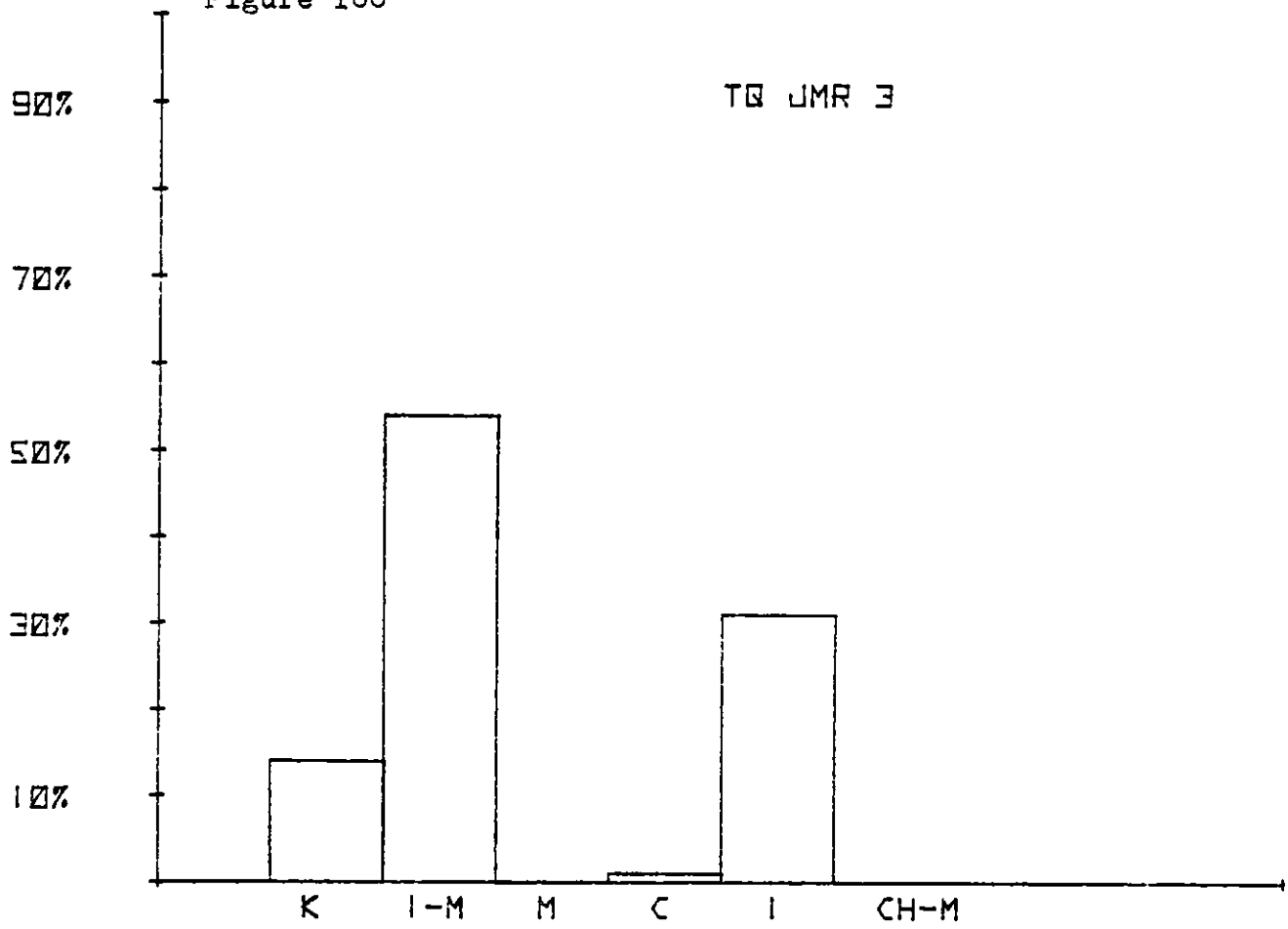
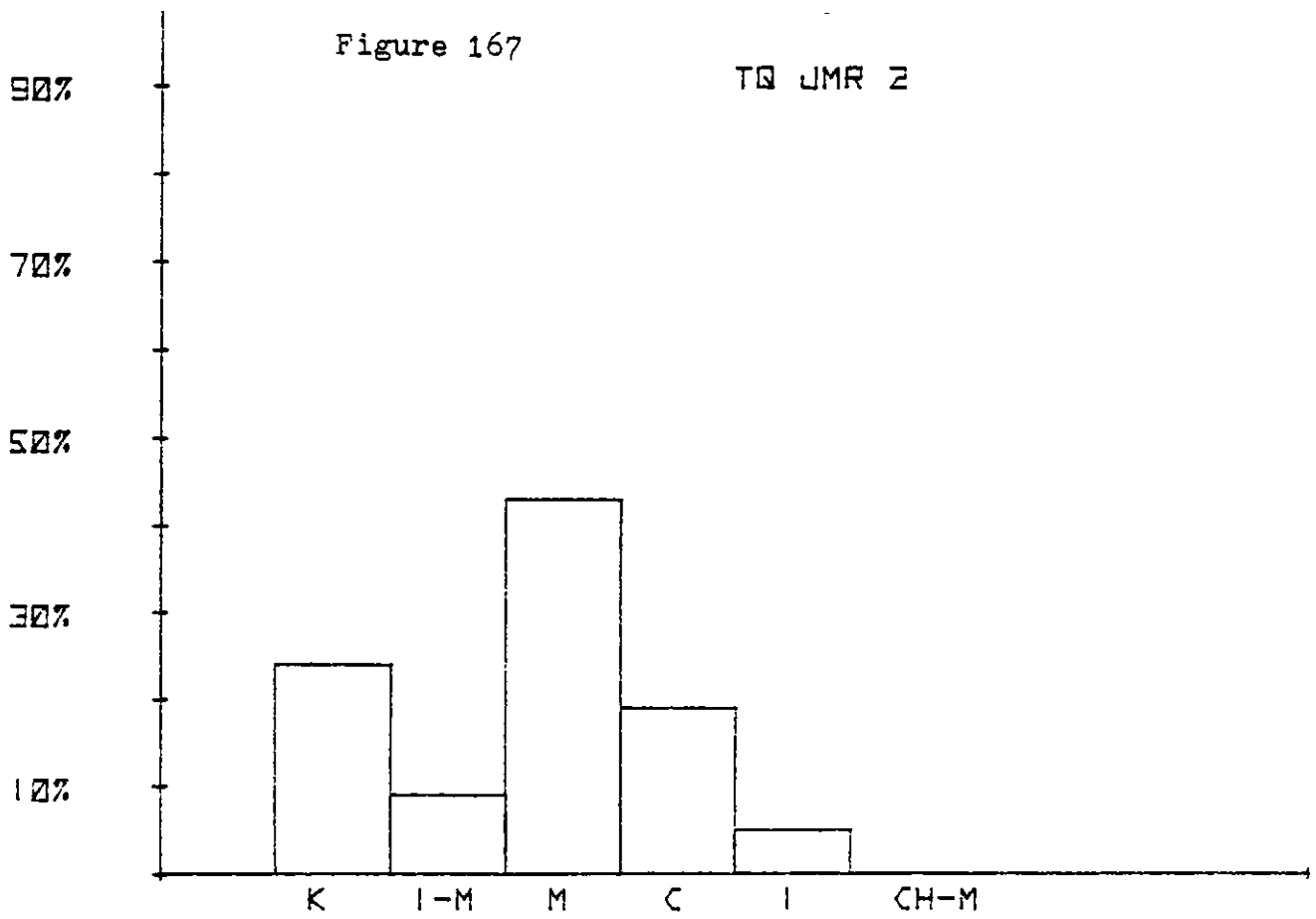


Figure 167



SEDIMENTARY PETROGRAPHY

SAMPLE	ALTERATION											CLAY HABIT										
	COLOR	GRAIN SIZE	SORTING	POROSITY	MATRIX	CALCITE	FELDSPAR	QUARTZ	HEAVY MIN.	PYRITE	REDISTRIBUTED OCM	PARTICULATE OCM	OTHER	PORE FILLING	GRAIN COATING	DETRITAL	KAOLINITE %	CHLORITE %	MONTMORILLONITE %	ILLITE %	I-M %	
SA-1	Gn	F	Fr	P	Cly								X	X	X	50			10	40		
SA-2A	B			P						Pr	OCM obscures all					52			48			
SA-2B		M		P	Cly						purple color					64			17	19		
SA-3A (Kd)	W	M	G	G	Cly						limonite stain	X	X			100						
SA-4	B	F	G	Fr	Cly			T	T?	T			X			87			1	12		
SA-5A	W	F	G	Fr	Cly		0			Cm			X			100						
SA-5B	Gy	F		P						Cm	dark					71	17				12	
SA-6	Gy	F	G	Fr	Cly		0				green + red	X	X			82	11				7	
SA-7	Gy	F	G	G	Cly	Al	0		Tr	Pr	dark	X	X			100						
SA-8	Gn	F	G	G		Pa	0				dark		X			62			20	18		
SA-9 green	Gn	M	G	G	Cly		0		Pr	Pr		X	X	X		99					1	
SA-9 red	R	M	G	G			0		Pr	Pr	hem. after pyrite		X			86	8				6	
SA-12	B	M	G	P	Cly					A		X				83	11				3	

Explanation: R = red C = coarse G = good Al = altered T = trace OCM = organic carbonaceous material
 B = brown M = medium Fr = fair Pa = partially altered Pr = present
 Gy = gray F = fine P = poor 0 = overgrowths Cm = common
 Gn = green A = abundant

-207-

Table 16

SEDIMENTARY PETROGRAPHY

SAMPLE	ALTERATION											CLAY HABIT									
	COLOR	GRAIN SIZE	SORTING	POROSITY	MATRIX	CALCITE	FELDSPAR	QUARTZ	HEAVY MIN.	PYRITE	REDISTRIBUTED OCM	PARTICULATE OCM	OTHER	PORE FILLING	GRAIN COATING	DETRITAL	KAOLINITE %	CHLORITE %	MONTMORILLONITE %	ILLITE %	I-M %
JJ 1A	W	M	P	Fr	cly								X			83					17
JJ 1B																20	T				80
JJ 2A	Gy	C	P	Fr	OCM	A			Cm	A	Cm		X			29				31	40
JJ 2B																6					94
JJ 3A	Gy	F	Fr	G	OCM		Pa		Cm	A	Pr										
JJ 3B	Gy	C	P	G	cly	Pr				Cm	Pr					50	25	4			21
JJ 3C wr	Gy	M	P	G	OCM				A	A	Cm					41	23		T		36
JJ 3C gry	Gy	F	Fr	G	cly				Cm		Cm		X			16					84
JJ 5A	W	F	Fr	G	cly		Pa						X			5	36	59			
JJ 5B	Gy	F	G	Fr	cly						Cm		X			27					73
JJ 6A	Gy	F	Fr	Fr	cly				Cm		Pr		X		X	52	14				34
JJ 6B	Gy	F	P	P	cly	A			T		A		X		X	46	T	T	T		54
JJ 7	R/W	F	G	G	cly				Pr		Cm		X								
JJ 8A	Gy	F	Fr	G	cly		Pa			A			X			100					
JJ 8B	Gy	M	G	G	cly		Al			A	Cm					92	8				
JJ 9A	Gy	F	Fr	G	OCM					A	Pr		X			55	45				
JJ 9B	Gy	F	Fr	G	cly		Pa		T		Pr		X	X		87	11	T	T		

Explanation: R = red C = coarse G = good Al = altered T = trace OCM = organic carbonaceous material
 B = brown M = medium Fr = fair Pa = partially altered Pr = present
 Gy = gray F = fine P = poor O = overgrowths Cm = common
 Gn = green
 W = white A = abundant

-208-

Table 17

SEDIMENTARY PETROGRAPHY

SEDIMENTARY PETROGRAPHY										ALTERATION				CLAY HABIT								
										COLOR	GRAIN SIZE	SORTING	POROSITY	MATRIX	CALCITE	FELDSPAR	QUARTZ	HEAVY MIN.	PYRITE	REDISTRIBUTED OCM	PARTICULATE OCM	OTHER
JJ 9C	W	F	P	G	cly								x	x	88					12		

Explanation:
R = red
C = coarse
G = good
Al = altered
T = trace
OCM = organic carbonaceous material

B = brown
M = medium
Fr = fair
Pa = partially altered
Pr = present

Gy = gray
F = fine
P = poor
O = overgrowths
Cm = common

Gn = green
A = abundant

W = white

Table 17 (continued)

SEDIMENTARY PETROGRAPHY

SAMPLE	ALTERATION												CLAY HABIT							
	COLOR	GRAIN SIZE	SORTING	POROSITY	MATRIX	CALCITE	FELDSPAR	QUARTZ	HEAVY MIN.	PYRITE	REDISTRIBUTED OCM	PARTICULATE OCM	OTHER	PORE FILLING	GRAIN COATING	DETRITAL	KAOLINITE %	CHLORITE %	MONTMORILLONITE %	ILLITE %
MLAKE-1	Blk	F	G	G					T	A						64	17		3	16
MLAKE-2	Blk	F	Fr	G					Pr	A						58	15		17	25
MLAKE-3	Blk	M	Fr	G					T	A						78	9		T	13
MLAKE-4	Blk	M	G	G					Pr	A						48	15		2	35
MLAKE-5	Blk	M	G	G					Pr	A						64	25			11
MLAKE-6	Blk	F	G	G					T	A						97	T			T
MLAKE-7	Blk	F	Fr	G					T	A						52	28			20
MLAKE-8	Blk	M	G	G					T	A										
MLAKE-9	Blk	F	Fr						Pr	A										
MLAKE-10	Blk	M	G	G	cly				T	A						81	11			8
MLAKE-11	Blk	M	Fr	G					T	A						68	15			17

Explanation: R = red C = coarse G = good Al = altered T = trace OCM = organic carbonaceous material
 B = brown M = medium Fr = fair Pa = partially altered Pr = present
 Gy = gray F = fine P = poor O = overgrowths Cm = common
 Gn = green
 W = white
 Blk = black

-210-

Table 18

SEDIMENTARY PETROGRAPHY

SAMPLE	ALTERATION											CLAY HABIT										
	COLOR	GRAIN SIZE	SORTING	POROSITY	MATRIX	CALCITE	FELDSPAR	QUARTZ	HEAVY MIN.	PYRITE	REDISTRIBUTED OCM	PARTICULATE OCM	OTHER	PORE FILLING	GRAIN COATING	DETRITAL	KAOLINITE %	CHLORITE %	MONTMORILLONITE %	ILLITE %	I-M %	
D-2	Gy	M	Fr	Fr	CaCO ₃	A			A	A		OCM as grain coats	X			Cm						
D-3	W/B	M	Fr	G	CaCO ₃	Pr				Cm			X								35	
D-4	B/W	M	P	G	cly				Pr	T			X	X	X	56					44	
D-4A			G	P	cly							clay gall			X	64					36	
D-5A	Gy	C	P	G	cly		Pa		Cm	A			X			28					72	
D-5B			G	P	cly		Pa	T				clay gall	X		X	70					30	
D-6	Gy	M	P	Fr	CaCO ₃	Cm	Pa		T	A	Cm		X			Pr						
D-8A	Gn	F	G	Fr	cly					A					X	62					38	
D-9A	Gy	M	P	P	CaCO ₃	A		Pr	Cm	A		pyrite as galls	X			32					68	
D-9B			G	P	cly							clay gall			X	4					96	
D-10	Gy	M	P	P	CaCO ₃	A	Pa				Pr		X			25					75	
D-11	Gn	F	G	P	cly	T									X	2					98	
D-12	W	M	P	Fr	CaCO ₃	A							X		X	73					27	

Table 19

Explanation: R = red C = coarse G = good Al = altered T = trace OCM = organic carbonaceous material
 B = brown M = medium Fr = fair Pa = partially altered Pr = present
 Gy = gray F = fine P = poor O = overgrowths Cm = common
 Gn = green
 W = white
 Blk = black A = abundant

SEDIMENTARY PETROGRAPHY

SAMPLE	ALTERATION										CLAY HABIT									
	COLOR	GRAIN SIZE	SORTING	POROSITY	MATRIX	CALCITE	FELDSPAR	QUARTZ	HEAVY MIN.	PYRITE	REDISTRIBUTED OCM	PARTICULATE OCM	OTHER	PORE FILLING	GRAIN COATING	KAOLINITE %	CHLORITE %	MONTMORILLONITE %	ILLITE %	I-M %
JOM-1	B	M	P	G	cly					Pr		native Se (Pr)		X	70	21				9
JOM-2	B	M	P	G	cly	Pr	Pa				X	secondary U min.	X	X	55	23				22
JOM-3	B/W	C	P	G	cly		Pa			Cm	Cm	native Se (Pr)	X	X	76	13				11
JOM-4 ox	R/Gn	F	G	P	cly					Cm	Cm	no Kspar	X	X	11	27				62
JOM-4 gry	Gy	C	P	G	cly		Pa			Pr	Pr	Apatite present	X		71	22				7
JOM-5 ore	Blk	M	P	G	OCM		Pa		Pr	A		fetid odor	X		45	30				25
JOM-5 cly	Gn/R	F	G	P	cly						Cm			X		54				46
JOM-6	B	M	P	G	cly		Pa	T	Pr	Pr			X		25					75
JOM-7	B/W	M	P	Fr			Pa				T	well indurated	X	X	68	14				18
JOM-8	W	F	G	Fr	cly	Cm		T			X	well indurated	X	X	38	33				29
JOM-9	R	M	Fr	Fr	cly	Cm				T		well indurated	X		67					33

Explanation: R = red C = coarse G = good Al = altered T = trace OCM = organic carbonaceous material
 B = brown M = medium Fr = fair Pa = partially altered Pr = present
 Gy = gray F = fine P = poor O = overgrowths Cm = common
 Gn = green
 W = white
 Blk = black A = abundant

SEDIMENTARY PETROGRAPHY

SAMPLE	ALTERATION										CLAY HABIT										
	COLOR	GRAIN SIZE	SORTING	POROSITY	MATRIX	CALCITE	FELDSPAR	QUARTZ	HEAVY MIN.	PYRITE	REDISTRIBUTED OCM	PARTICULATE OCM	OTHER	PORE FILLING	GRAIN COATING	DETRITAL	KAOLINITE %	CHLORITE %	MONTMORILLONITE %	ILLITE %	I-M %
23-2 ore	Blk	M	G	P	OCM		Al			Cm	X		X	X			27	47			26
23-3A (ore)	Blk	M	P	G	OCM		Pa			Pr	X			X	X		49	36			15
23-3A Bleached	Gy	F	P	G						A	T						17	39			44
23-3A Redtop	B	F	G	Fr	cly	T	Pa					T	feldspar > 10%	X			77				23
23-3B	B	F	Fr	Fr	CaCO ₃	A	Pa					T		X	X		54	30			16
23-4	Gy	-	P	Fr	cly	T	Pa			Cm		Pr	native Se	X	X		72	28			
23-76-4	B	M	G	G	cly		Pa			Pr		T		X	X		89	T			11
23-76-A	Gy	F	G	G	OCM		Pa			Pr	X	X		X	X		35	25			40
23-76-B	Gy	F	G	Fr	Silt		Pa			Cm		X		X		X	45	35	20		

Explanation: R = red C = coarse G = good Al = altered T = trace OCM = organic carbonaceous material
 B = brown M = medium Fr = fair Pa = partially altered Pr = present
 Gy = gray F = fine P = poor O = overgrowths Cm = common
 Gn = green A = abundant
 W = white
 Blk = black

SEDIMENTARY PETROGRAPHY

SAMPLE	ALTERATION											CLAY HABIT										
	COLOR	GRAIN SIZE	SORTING	POROSITY	MATRIX	CALCITE	FELDSPAR	QUARTZ	HEAVY MIN.	PYRITE	REDISTRIBUTED OCM	PARTICULATE OCM	OTHER	PORE FILLING	GRAIN COATING	DETRITAL	KAOLINITE %	CHLORITE %	MONTMORILLONITE %	ILLITE %	I-M %	
36-1A	R	F	P	Fr	cly			T		Cm		hematite stain	X	X		29	35				36	
36-1B	Gy	M	P	G	OCM	T	Pa	T		Cm		hematite stain	X	X								
36-2A	Gn/R	F	P	P	cly	Cm	Pa	T		Pr		hematite stain				24	33				43	
36-2B	-	M	P	-	cly	-	Pa			Cm		hematite stain		X		23	15				62	
36-2C	Gy	M	P	G	OCM	Cm		Pr		A		kspar=10-15%	X			29	18				58	
36-3	Gy	M	P	G						A						17					83	
36-4	Gy	M	Fr	-	OCM					A			X			65	22				13	
36-5	Gy	M	P	P	cly	Pr	Pa			A		U mineral (Pr)	X			83	17				10	

Explanation: R = red C = coarse G = good Al = altered T = trace OCM = organic carbonaceous material
 B = brown M = medium Fr = fair Pa = partially altered Pr = present
 Gy = gray F = fine P = poor O = overgrowths Cm = common
 Gn = green
 W = white A = abundant

Table 23

Figure 168 -2u

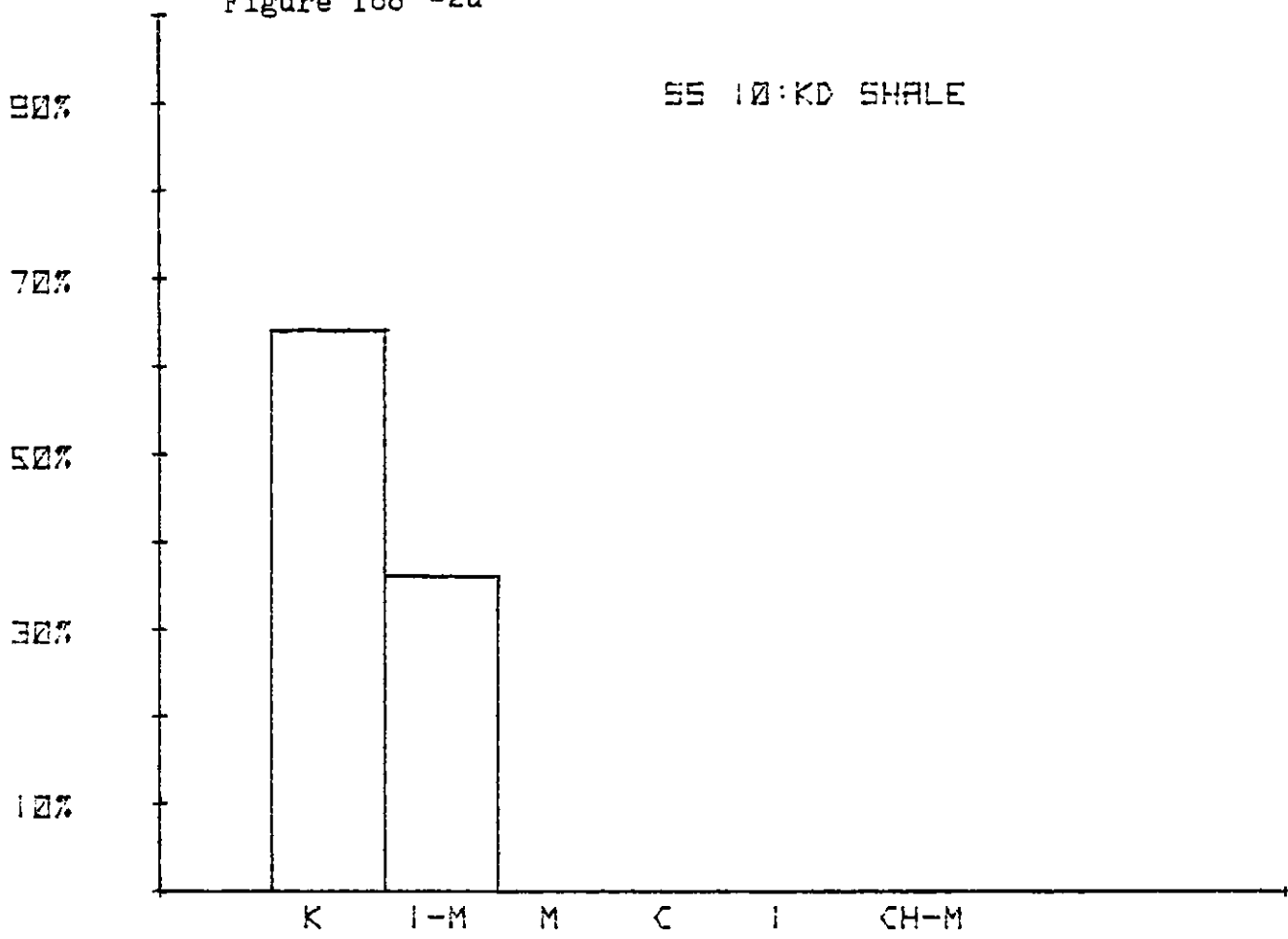


Figure 169 -2u

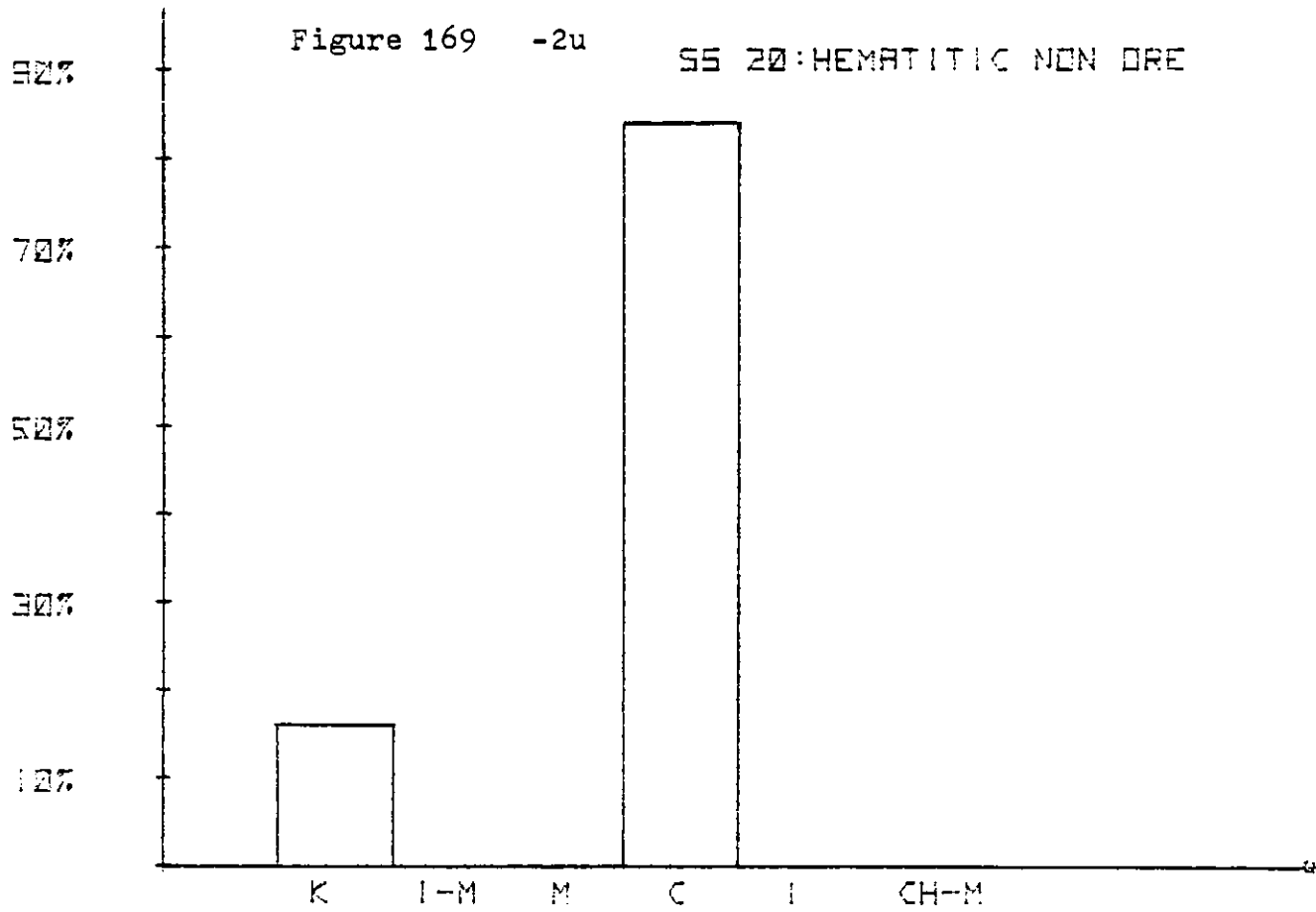


Figure 170

-2u

SS 30: DRE BERRING

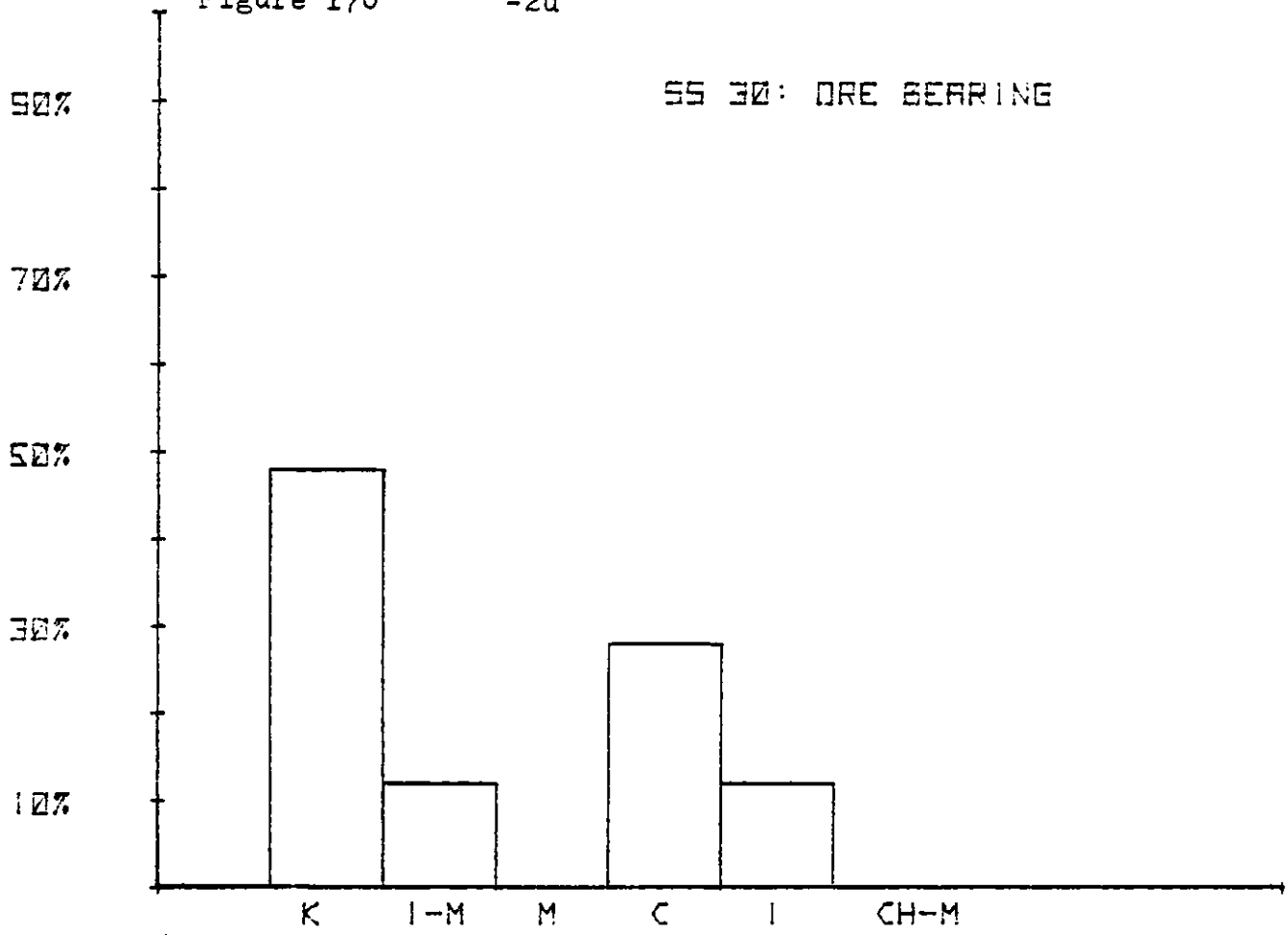


Figure 171

SS 40

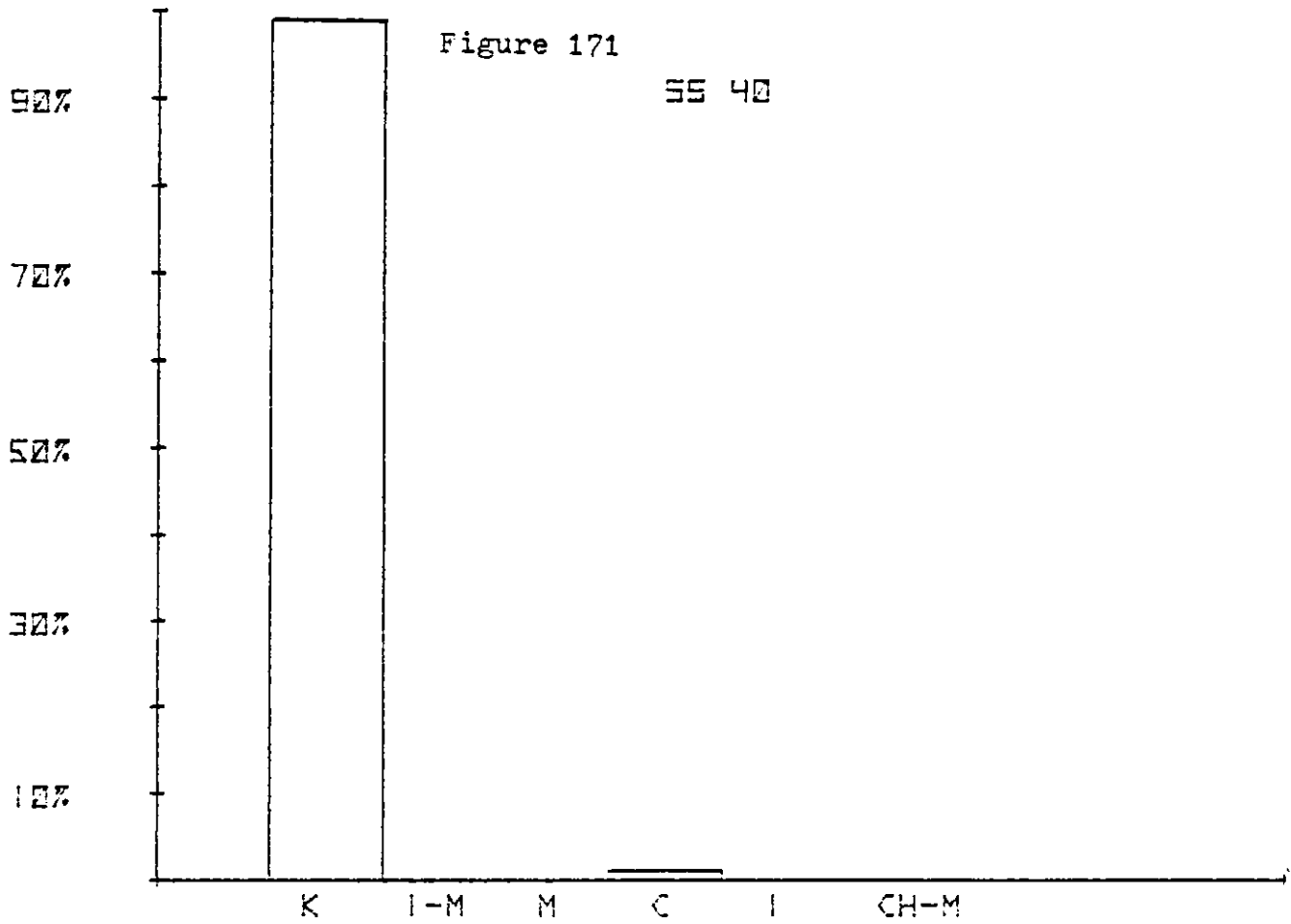


Figure 172

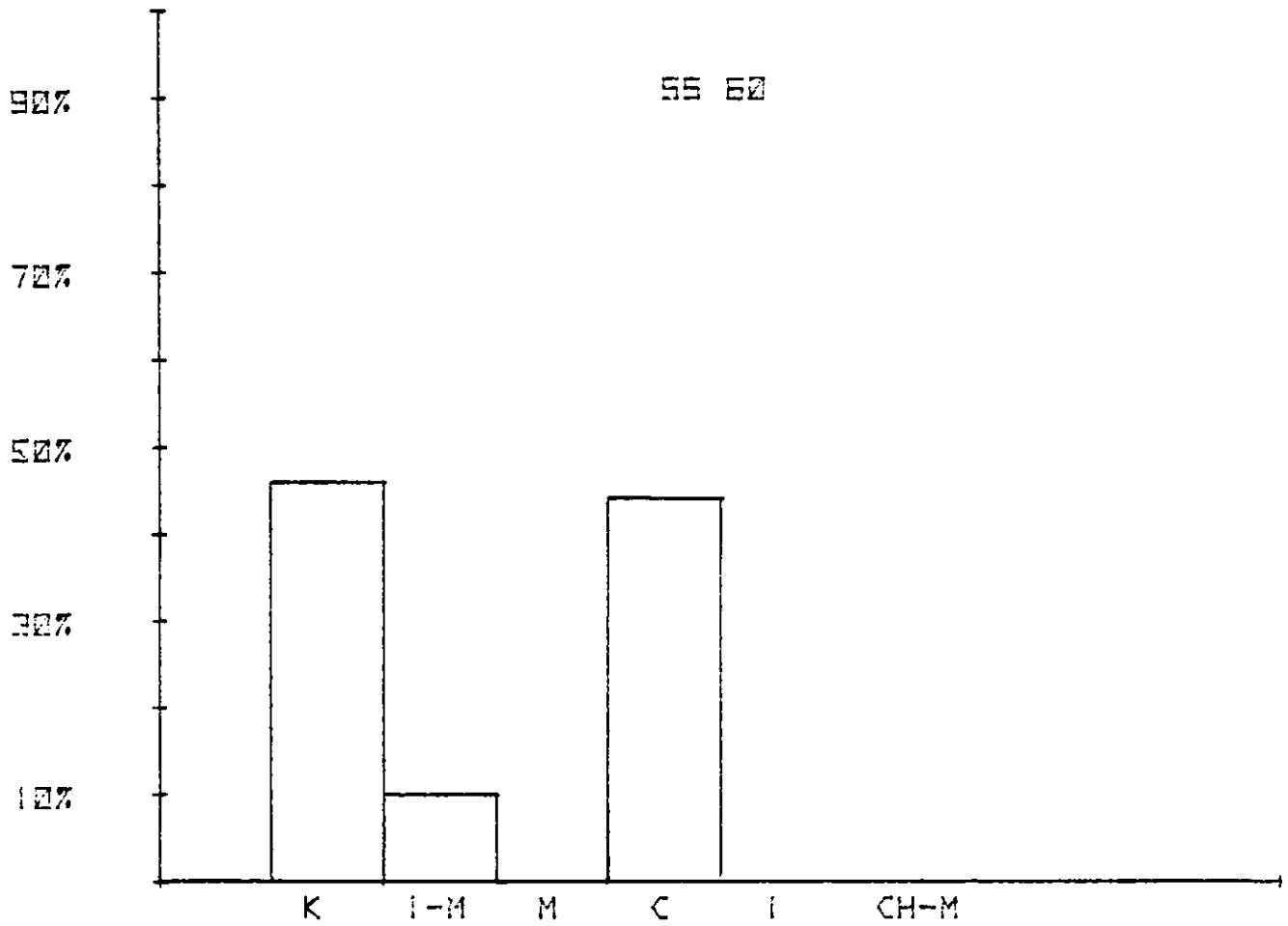


Figure 173

SR I

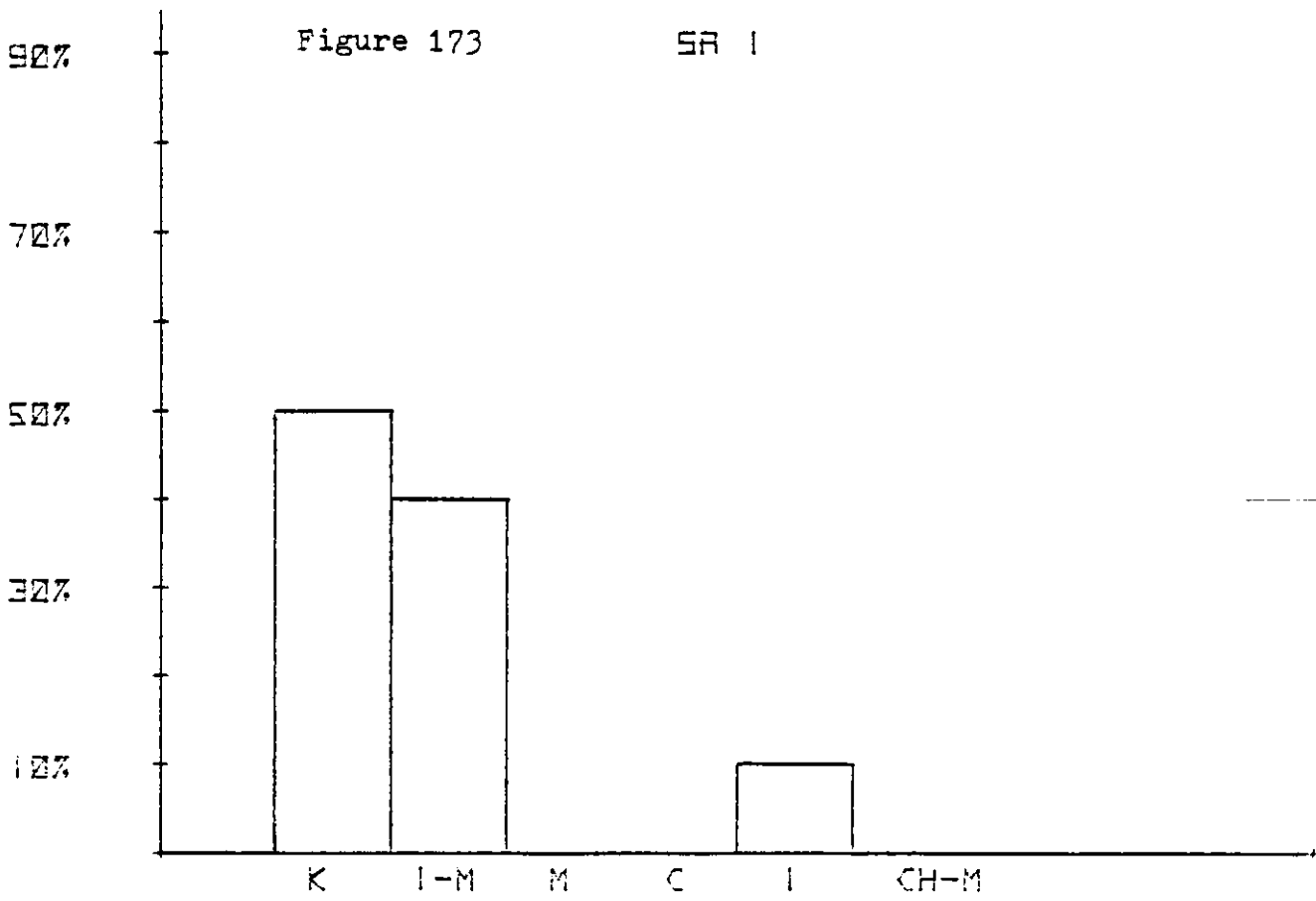


Figure 174

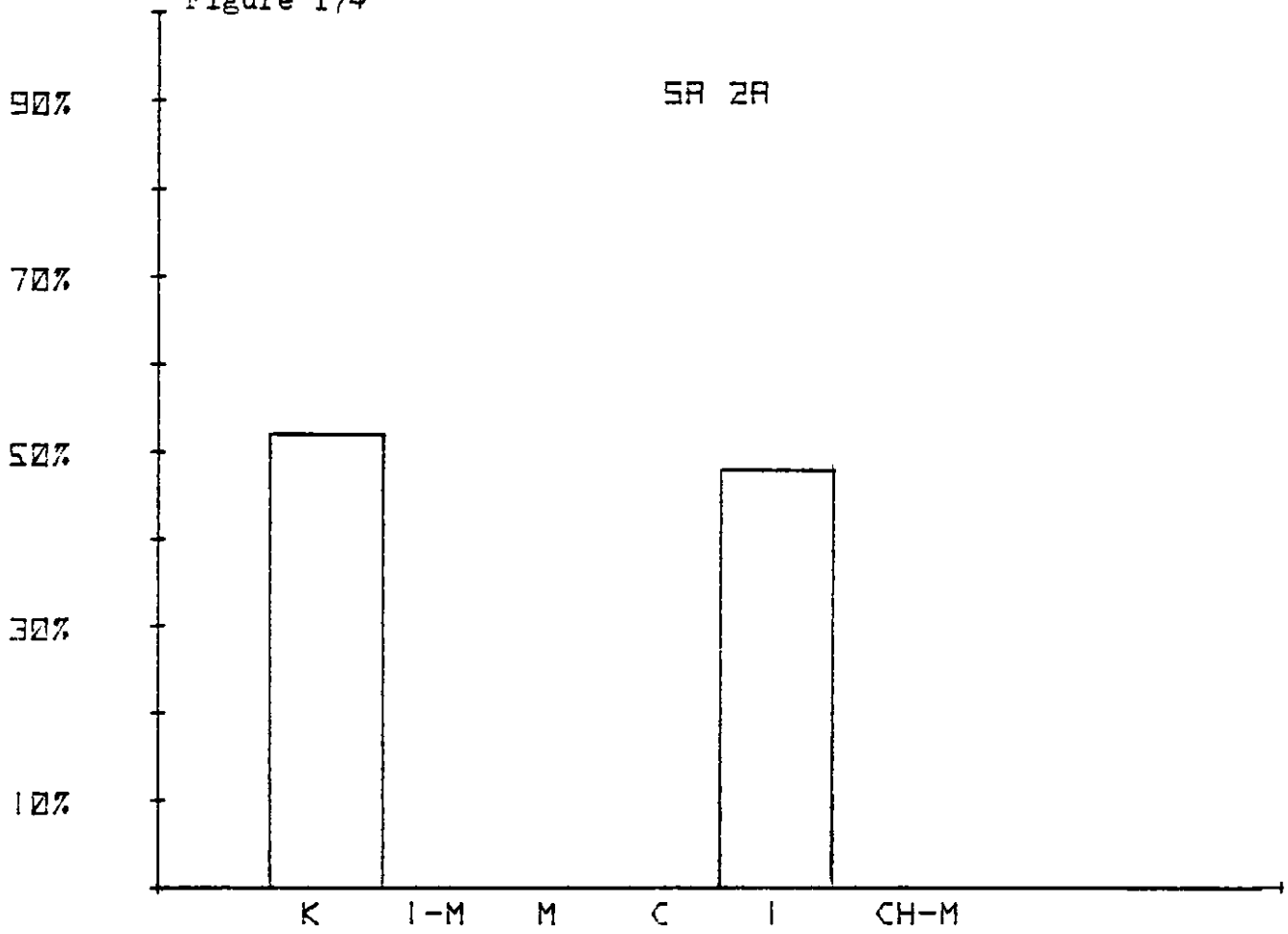


Figure 175

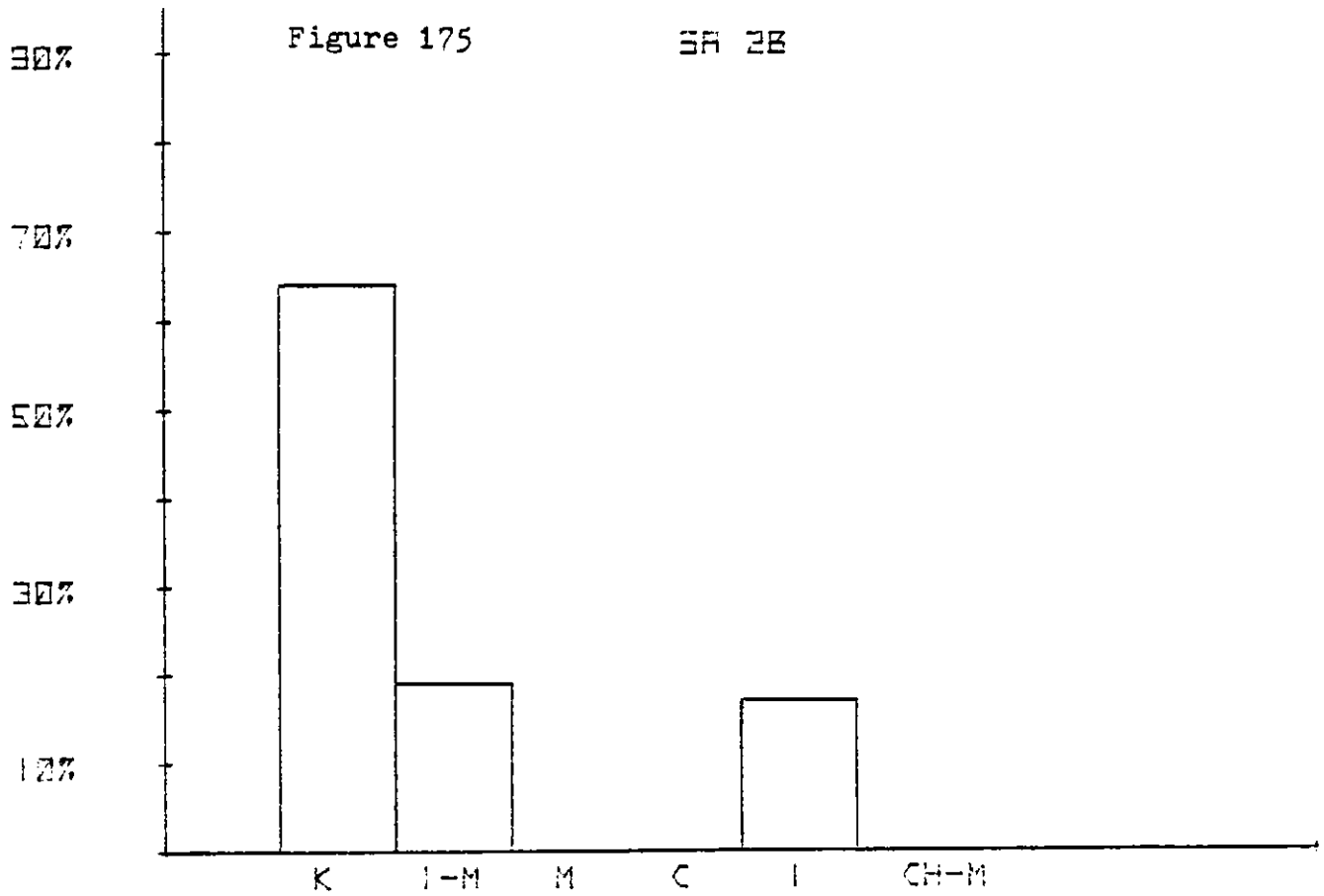


Figure 176

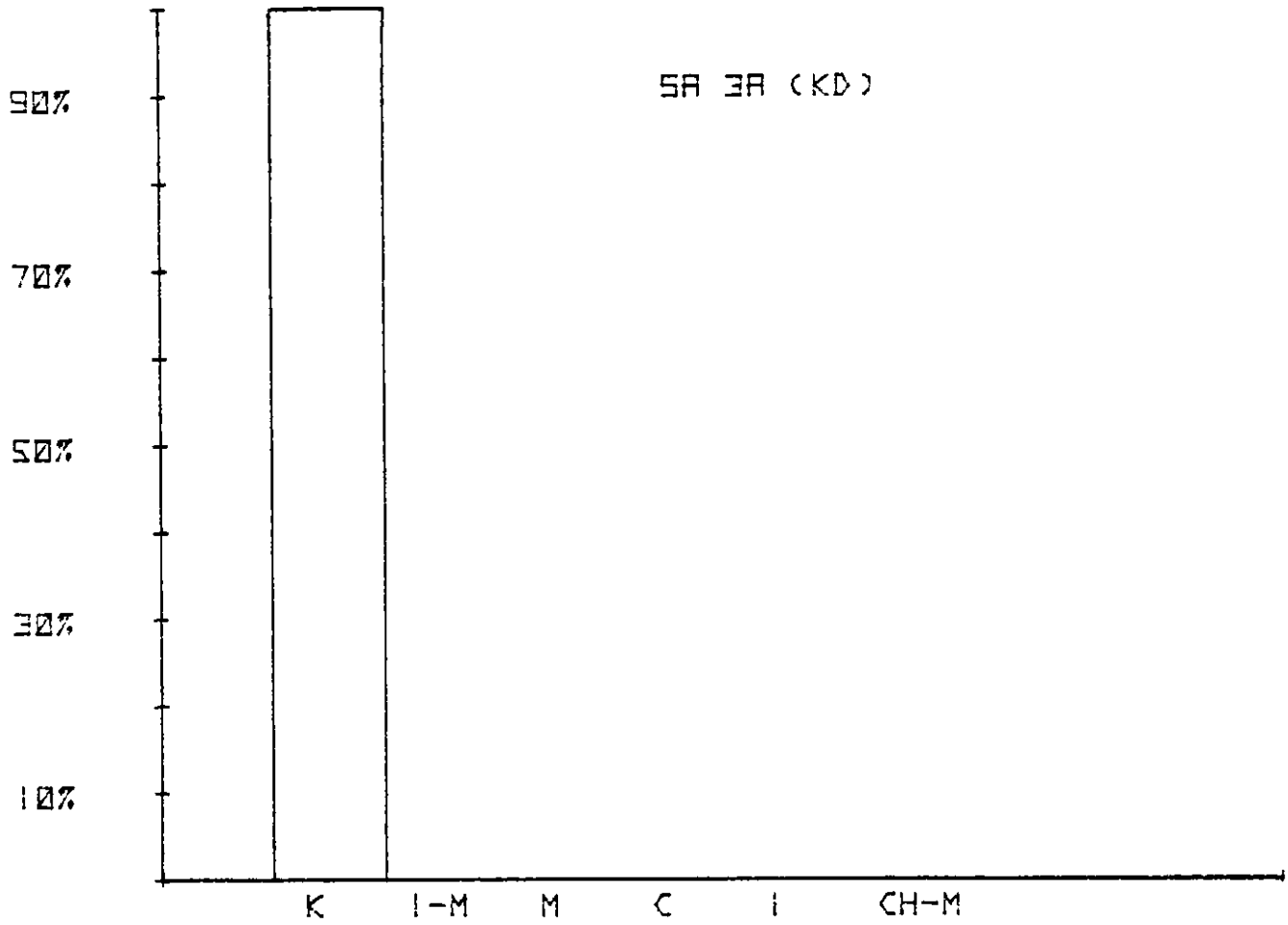


Figure 177 SA 4

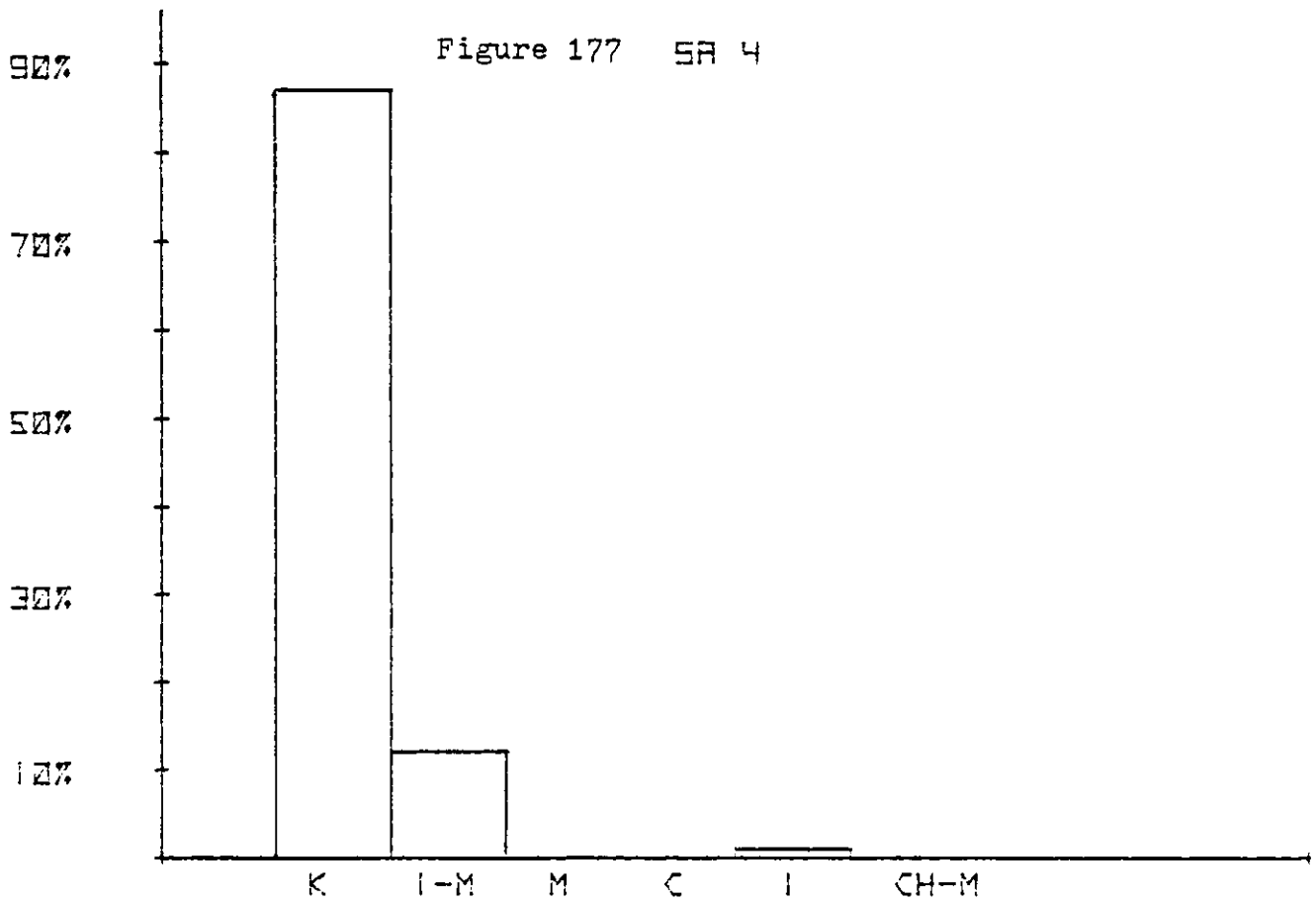


Figure 178

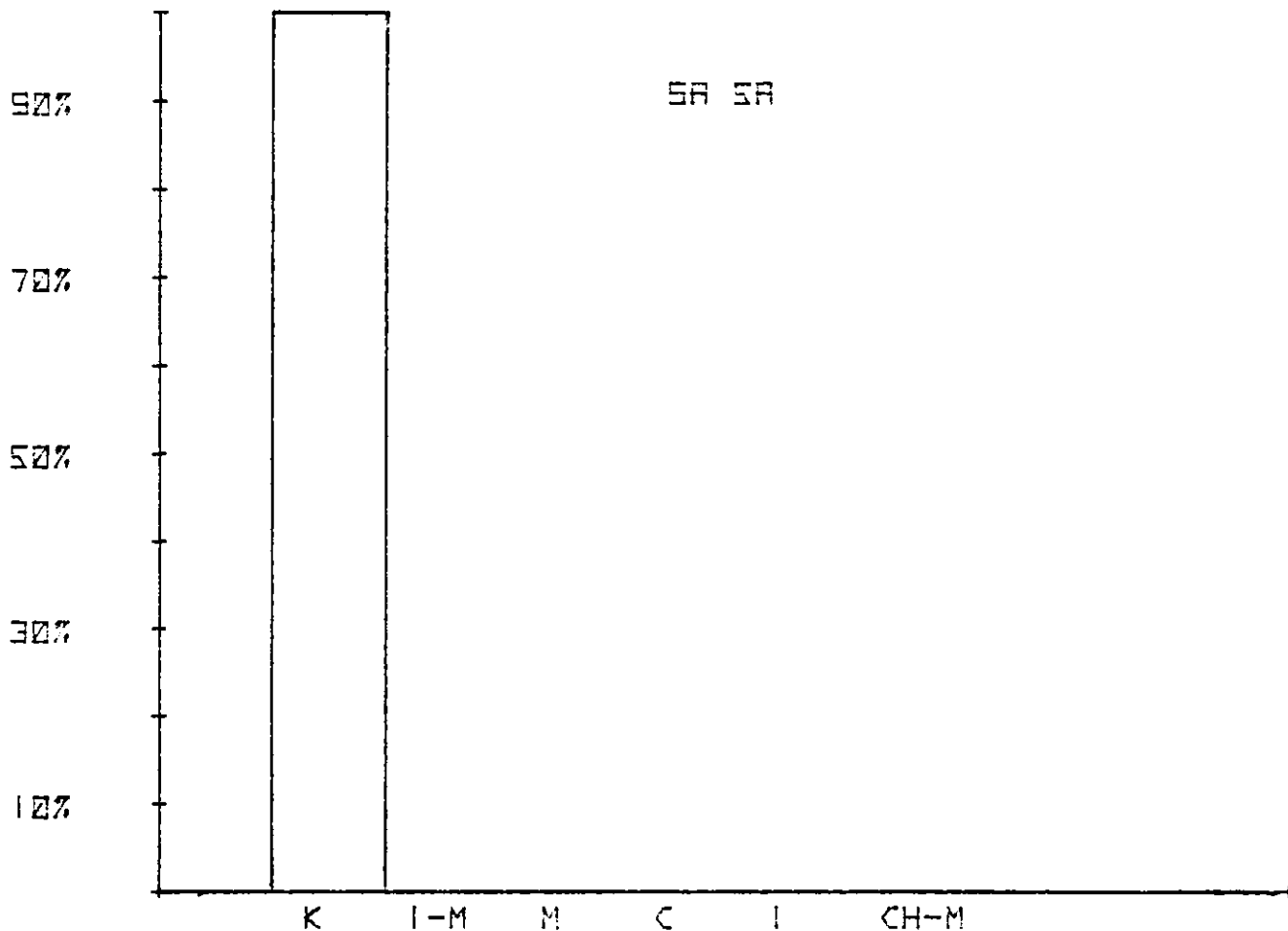


Figure 179

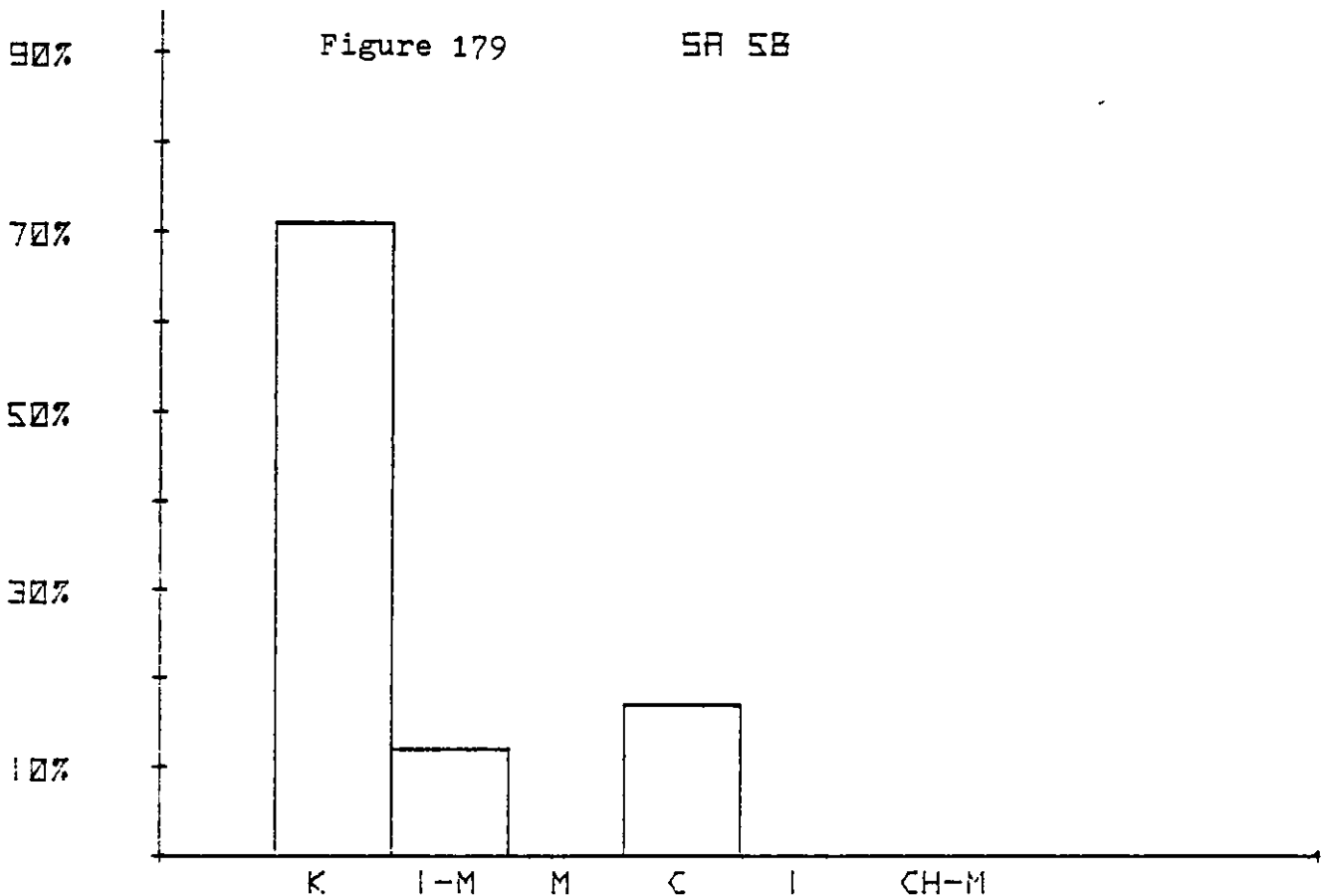


Figure 180

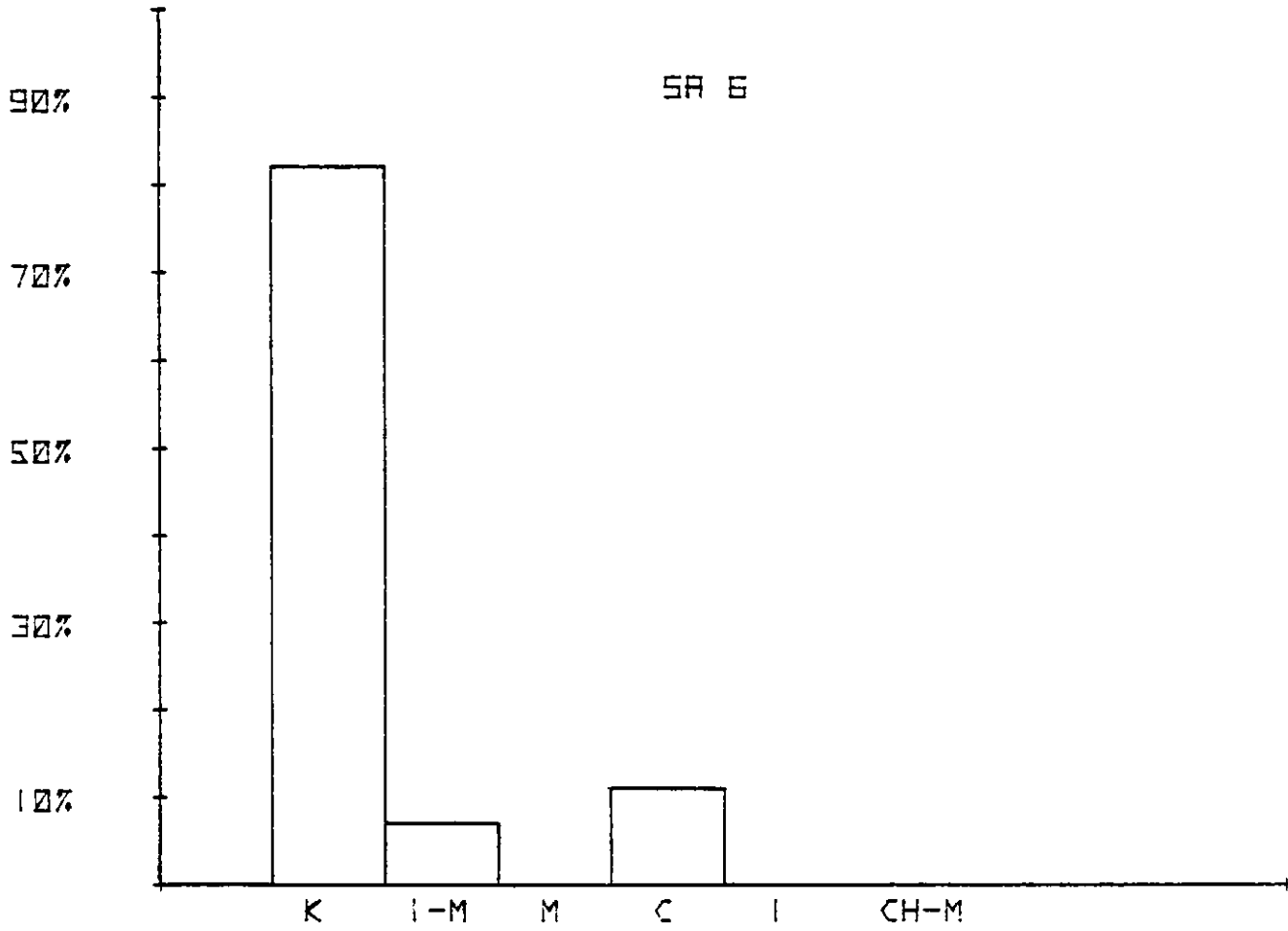


Figure 181

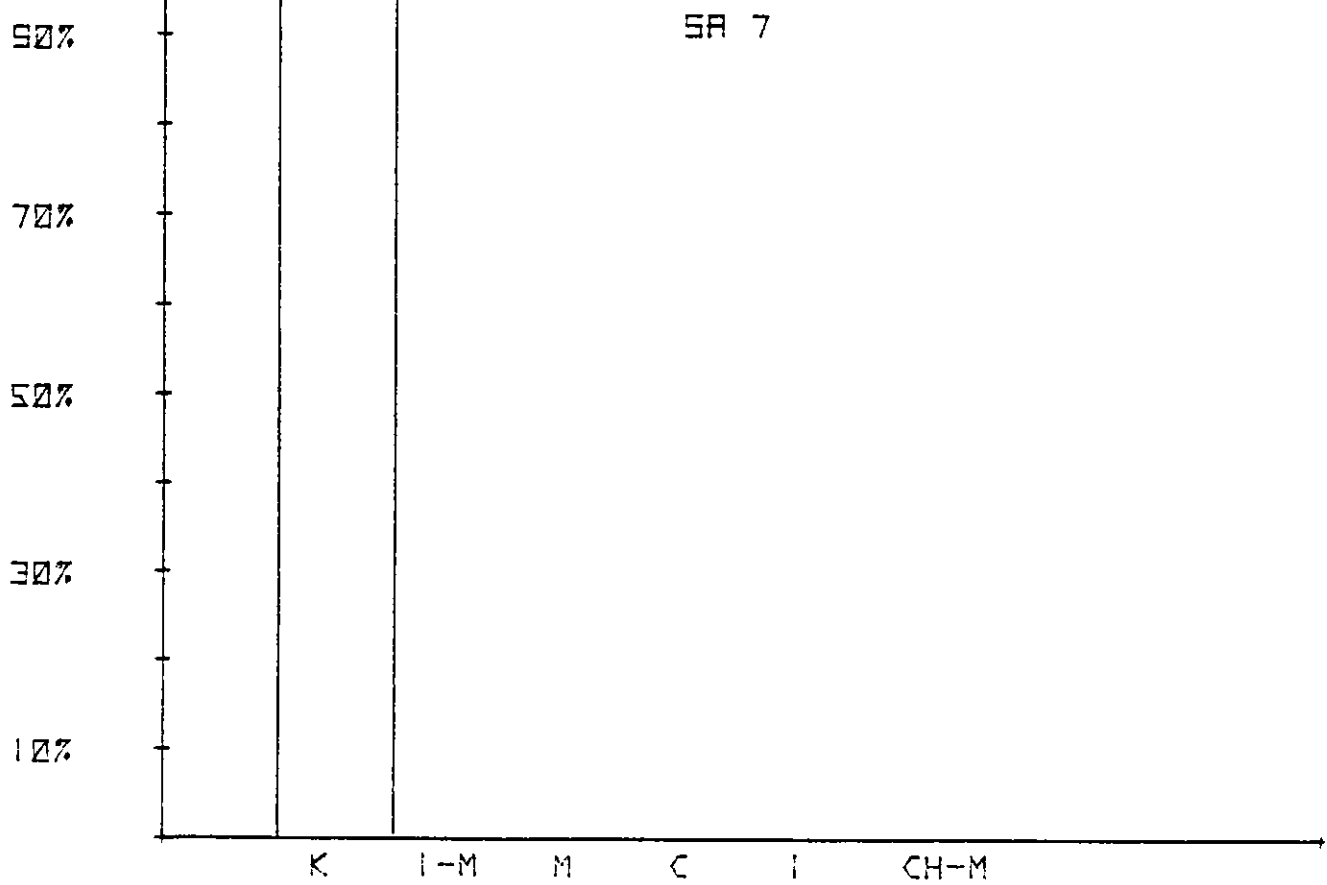


Figure 182

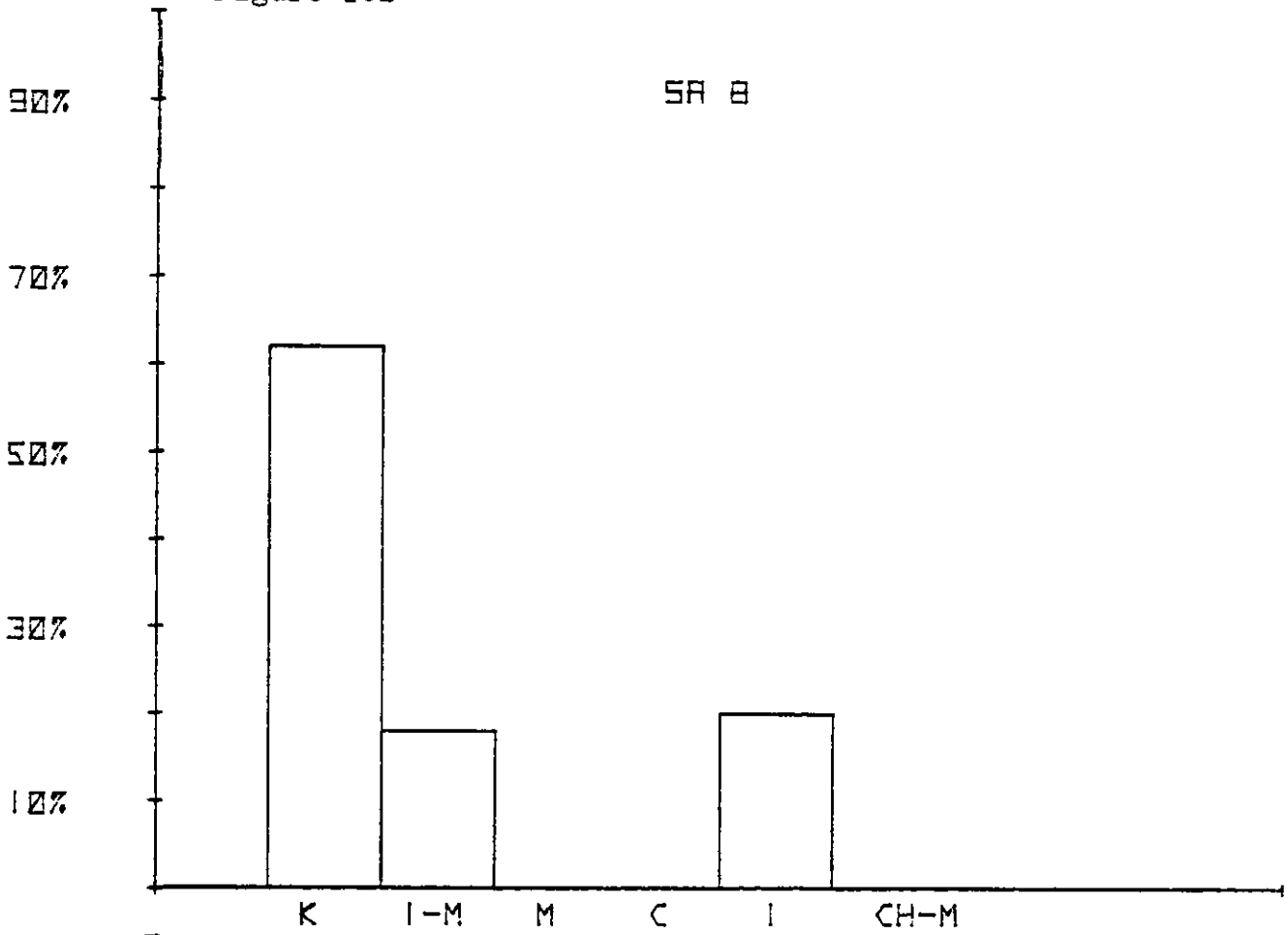


Figure 183

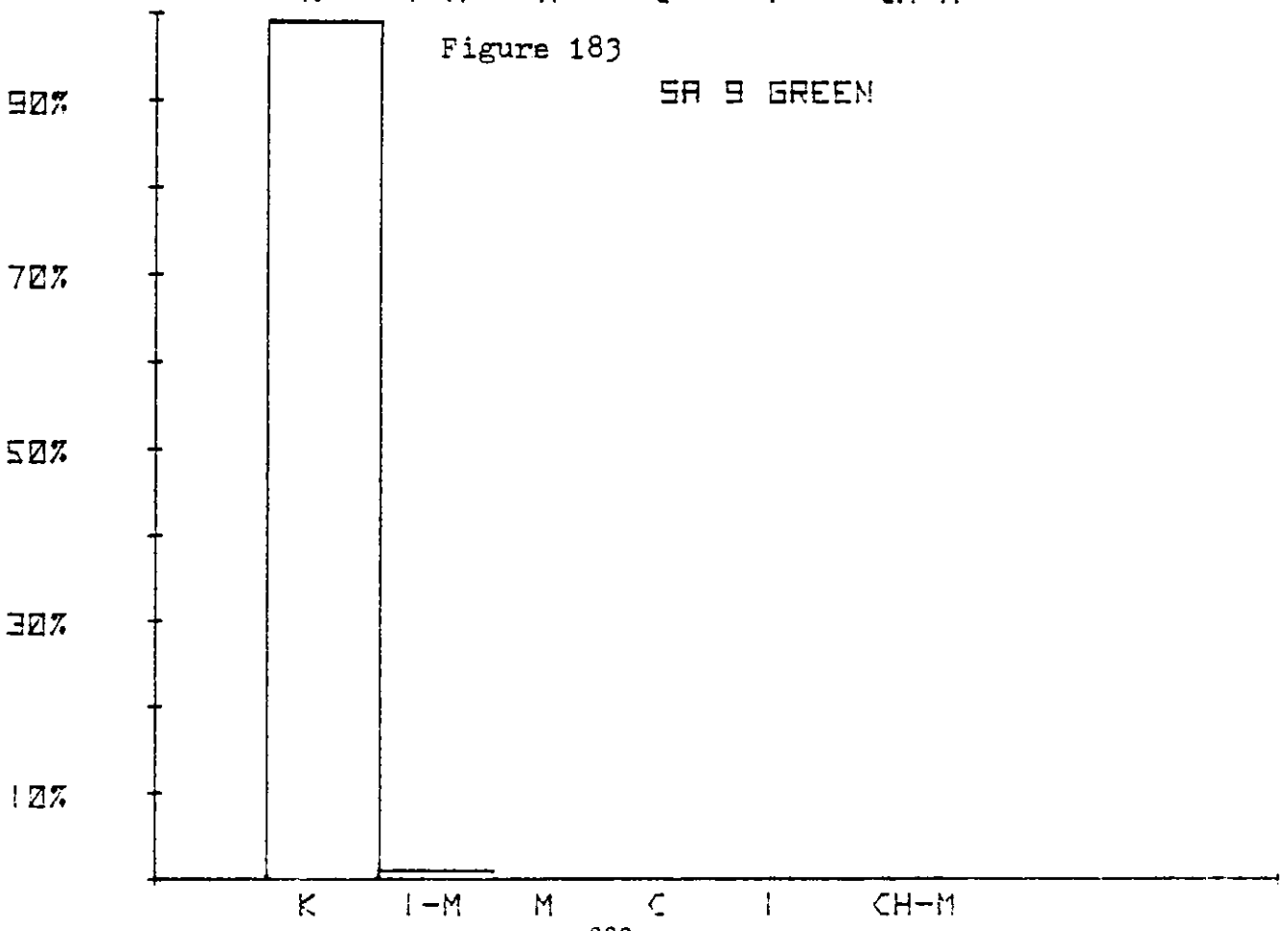


Figure 184

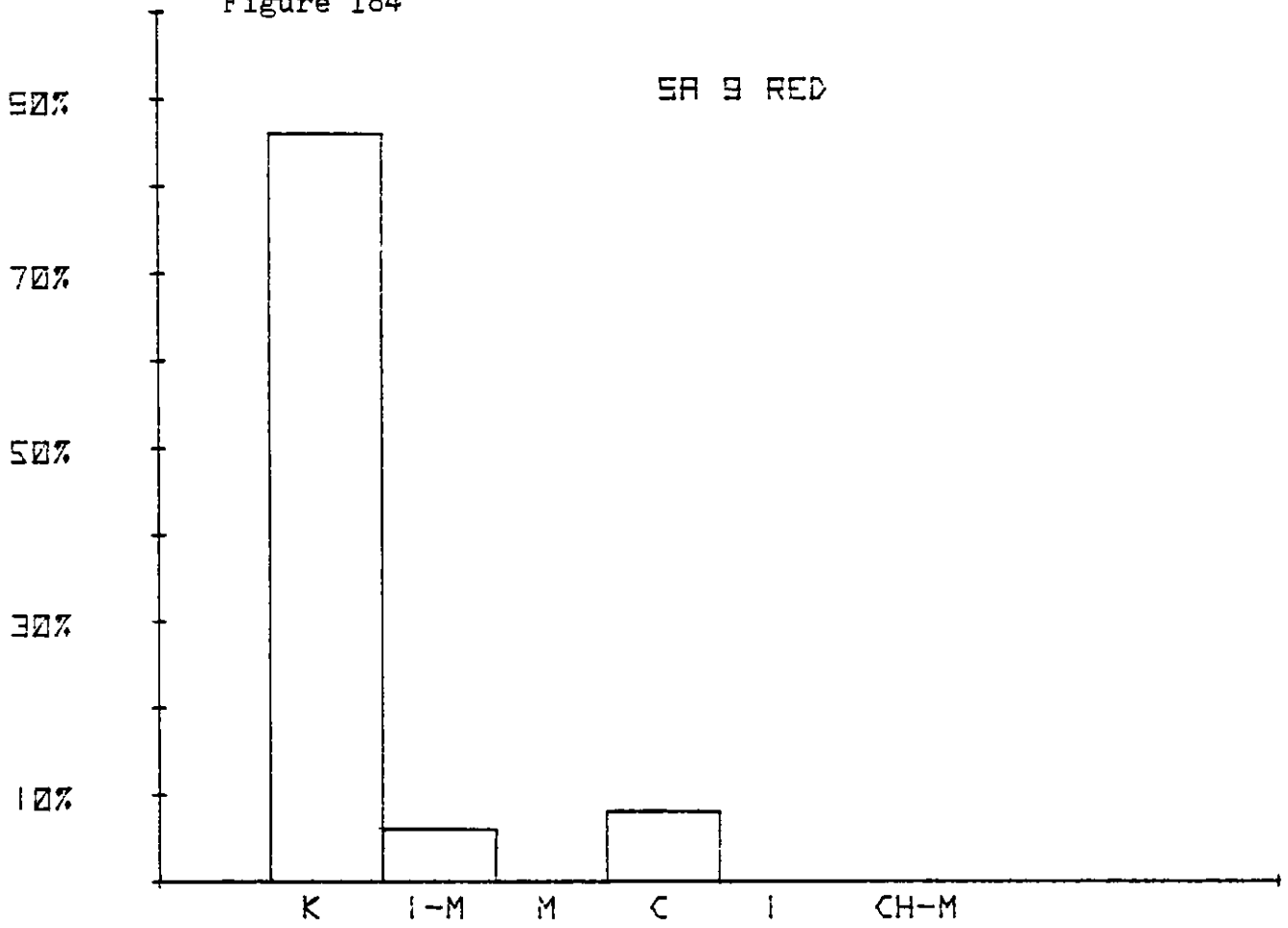


Figure 185 SA 12

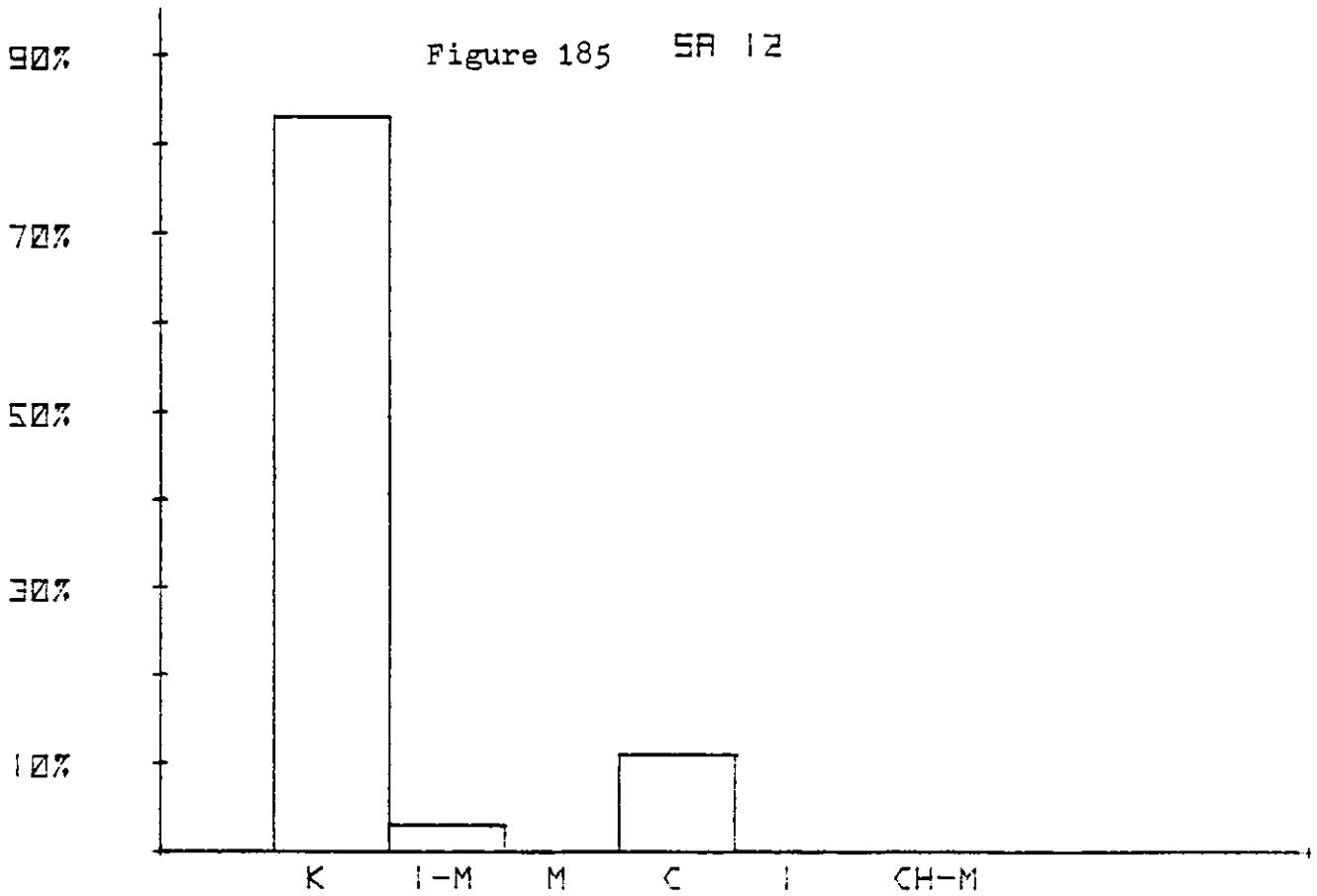


Figure 186 (near ore zone)

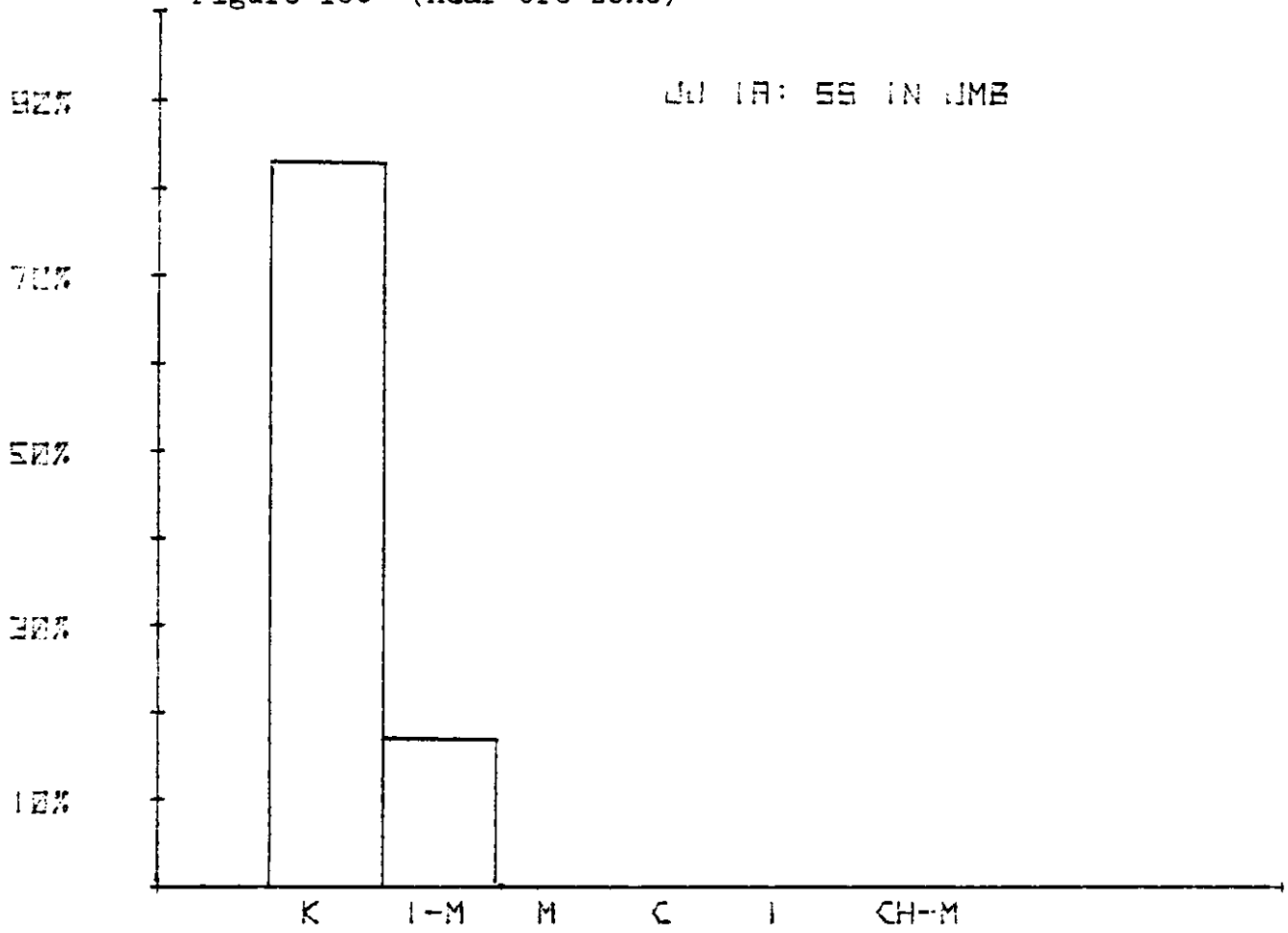


Figure 187

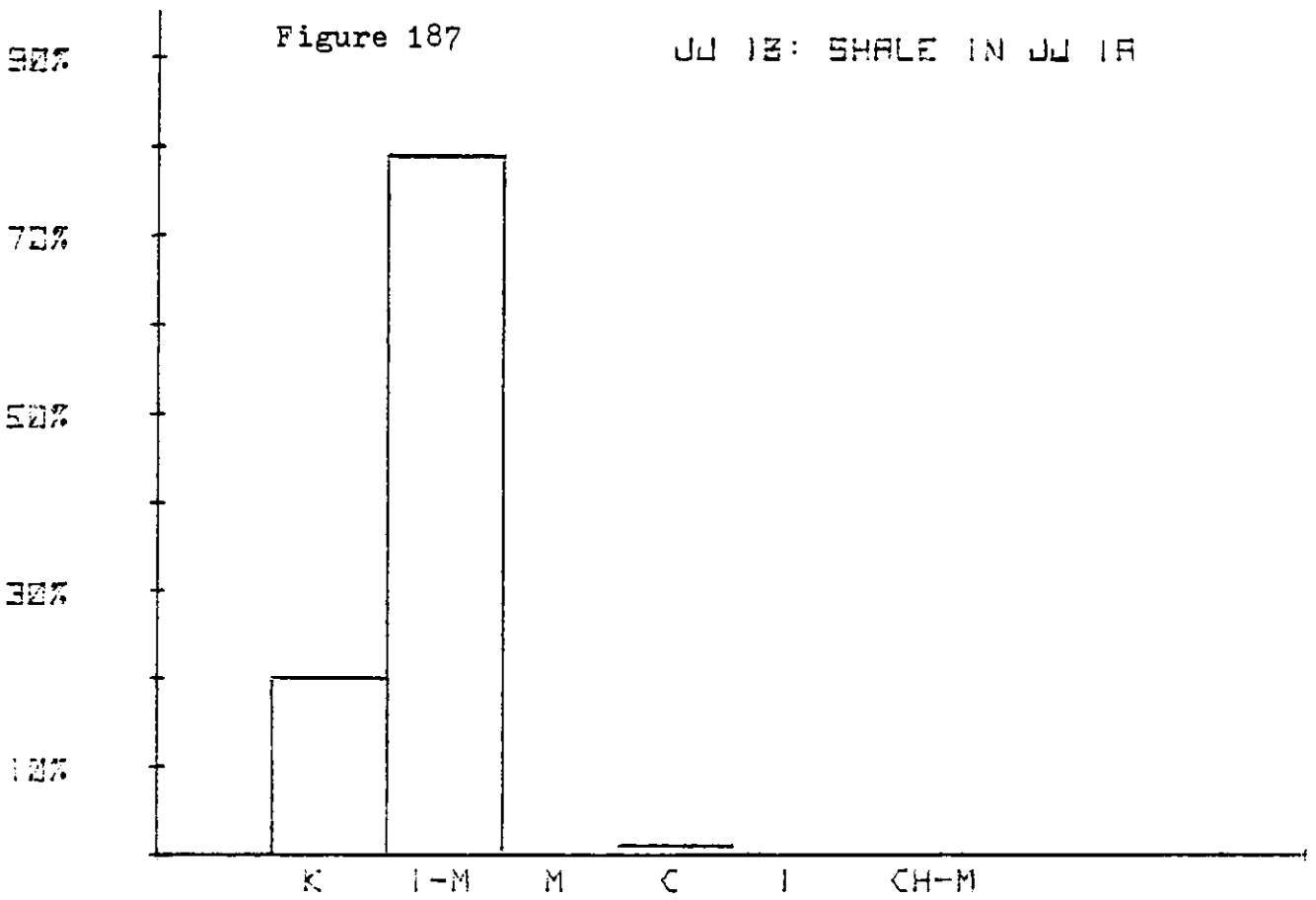


Figure 188

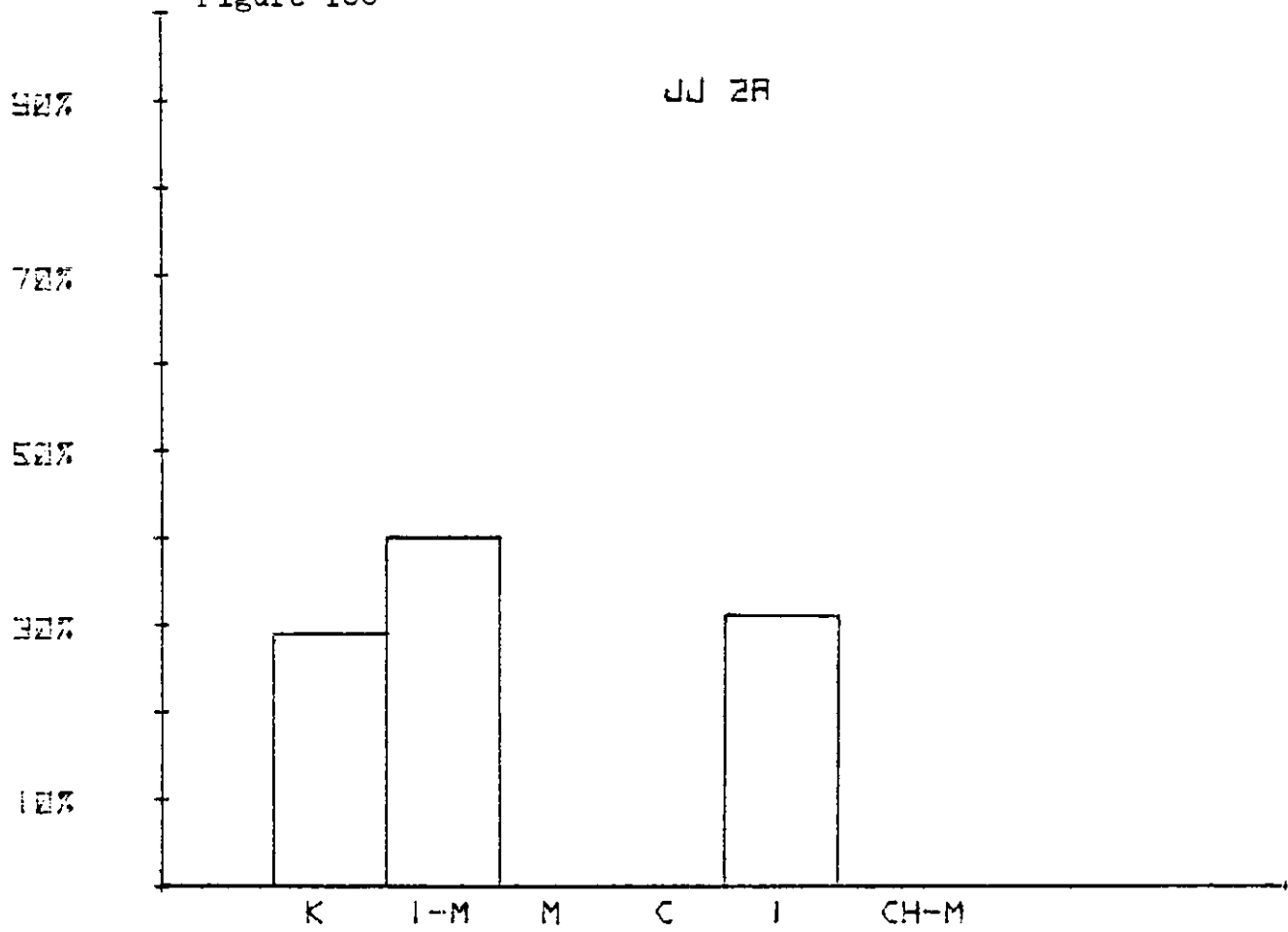


Figure 189

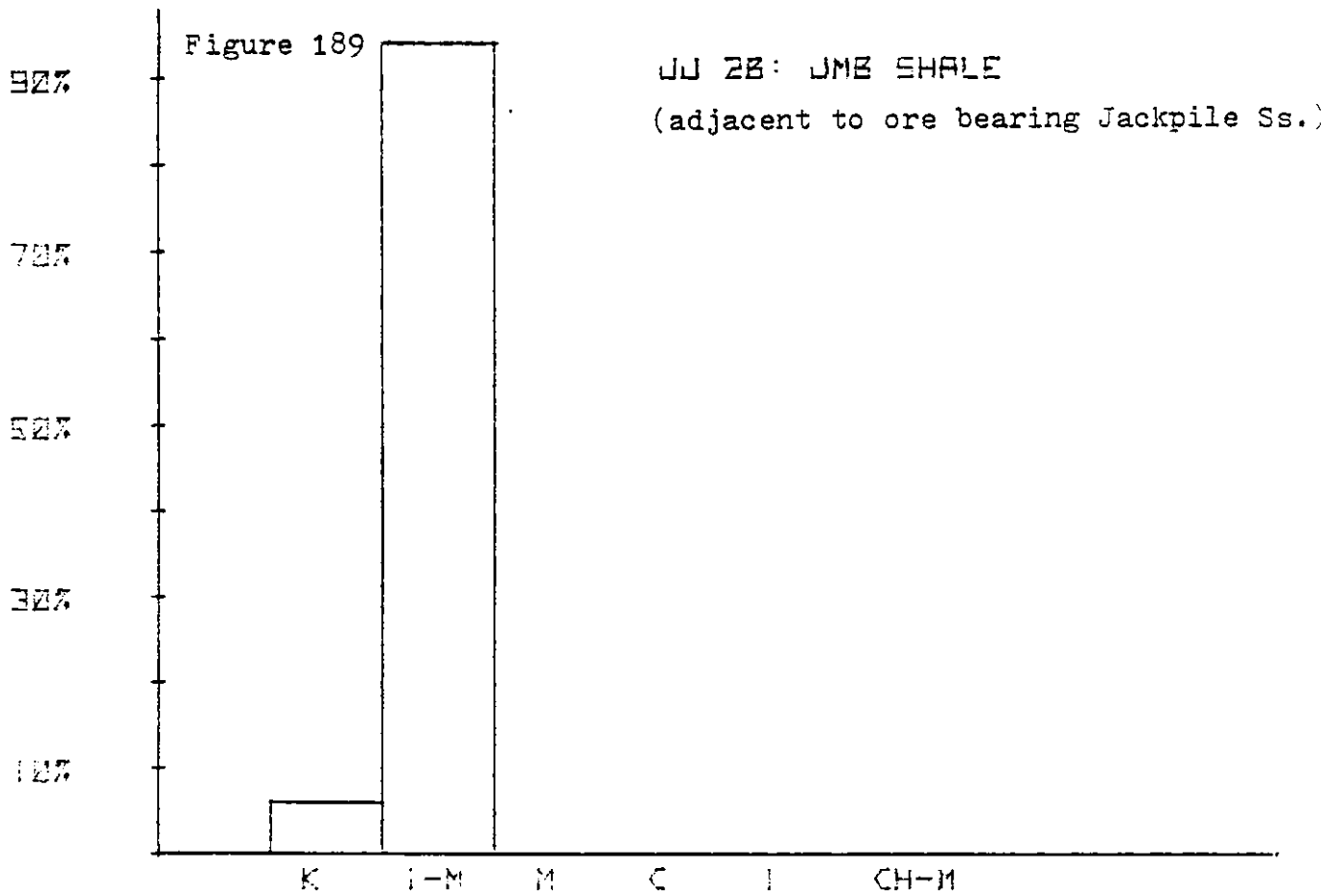


Figure 190

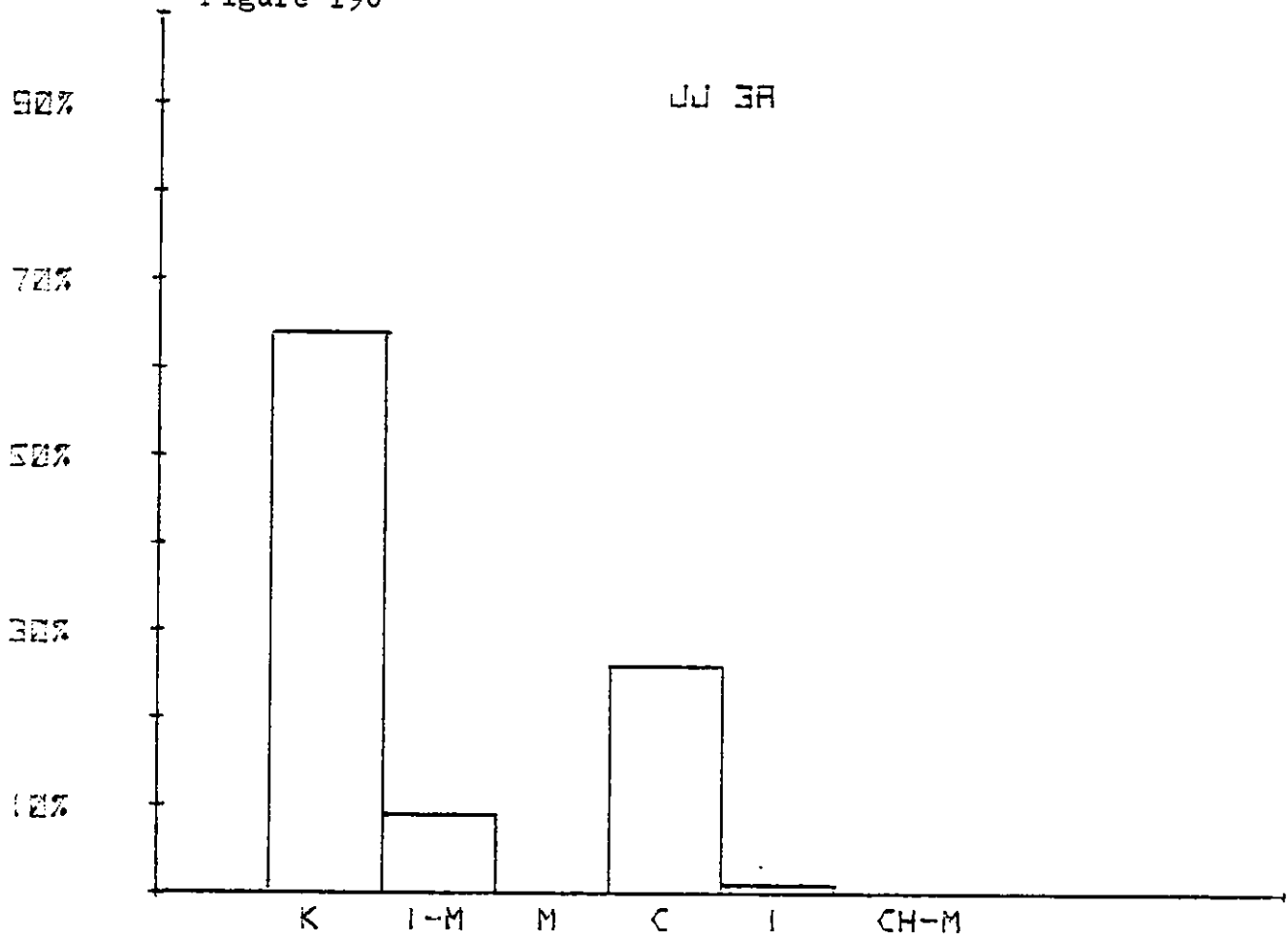


Figure 191

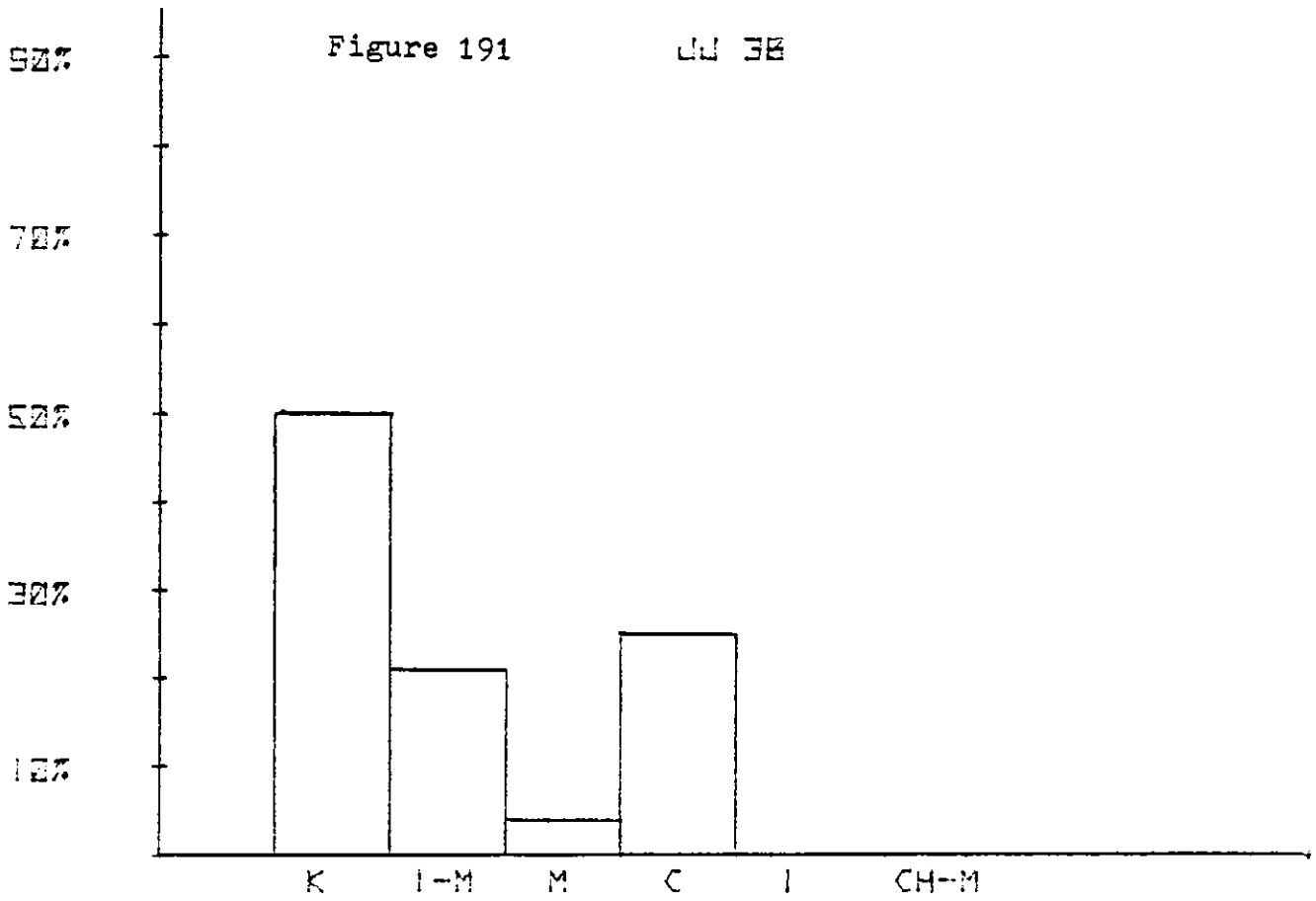


Figure 192

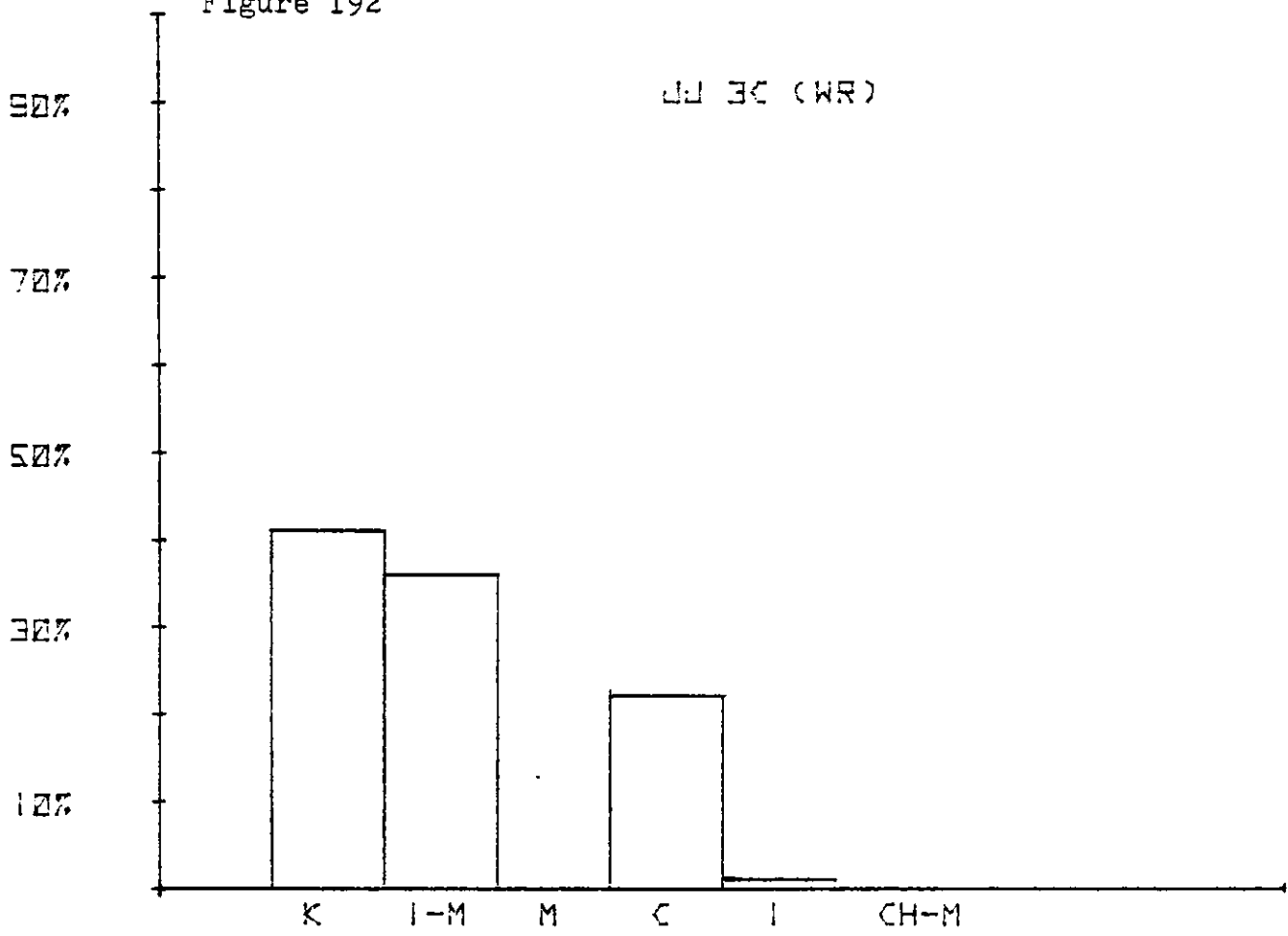


Figure 193

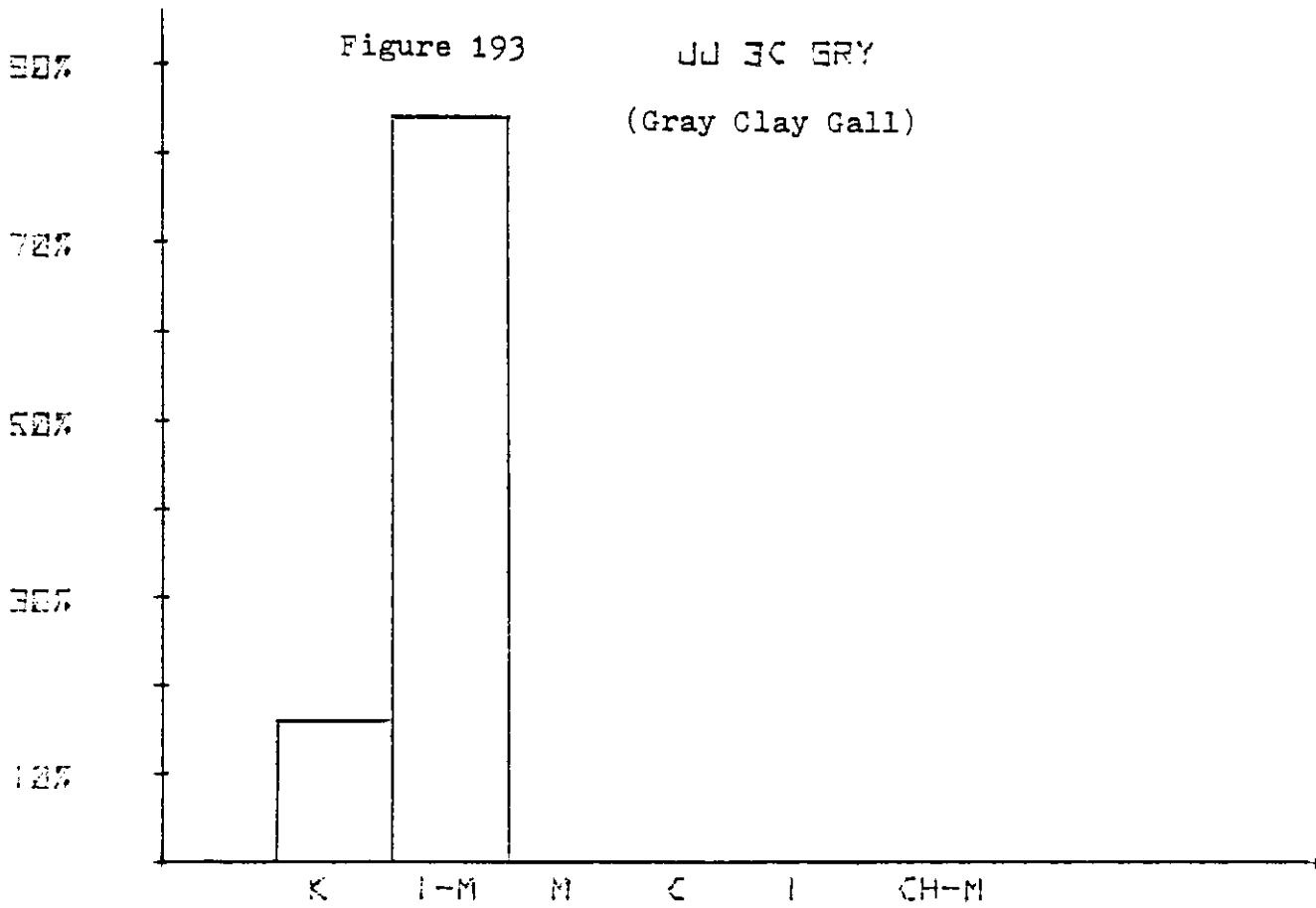


Figure 194

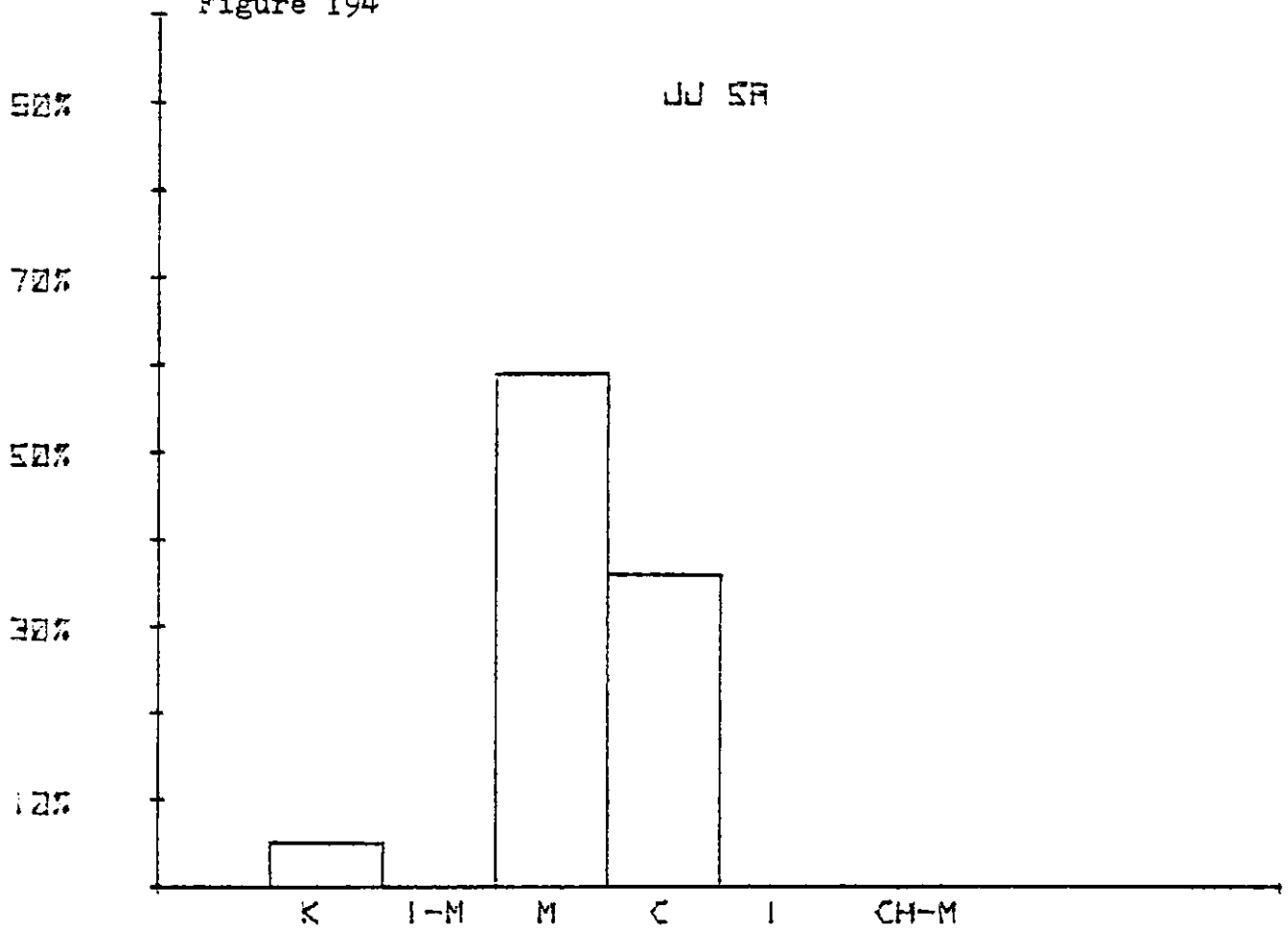


Figure 195

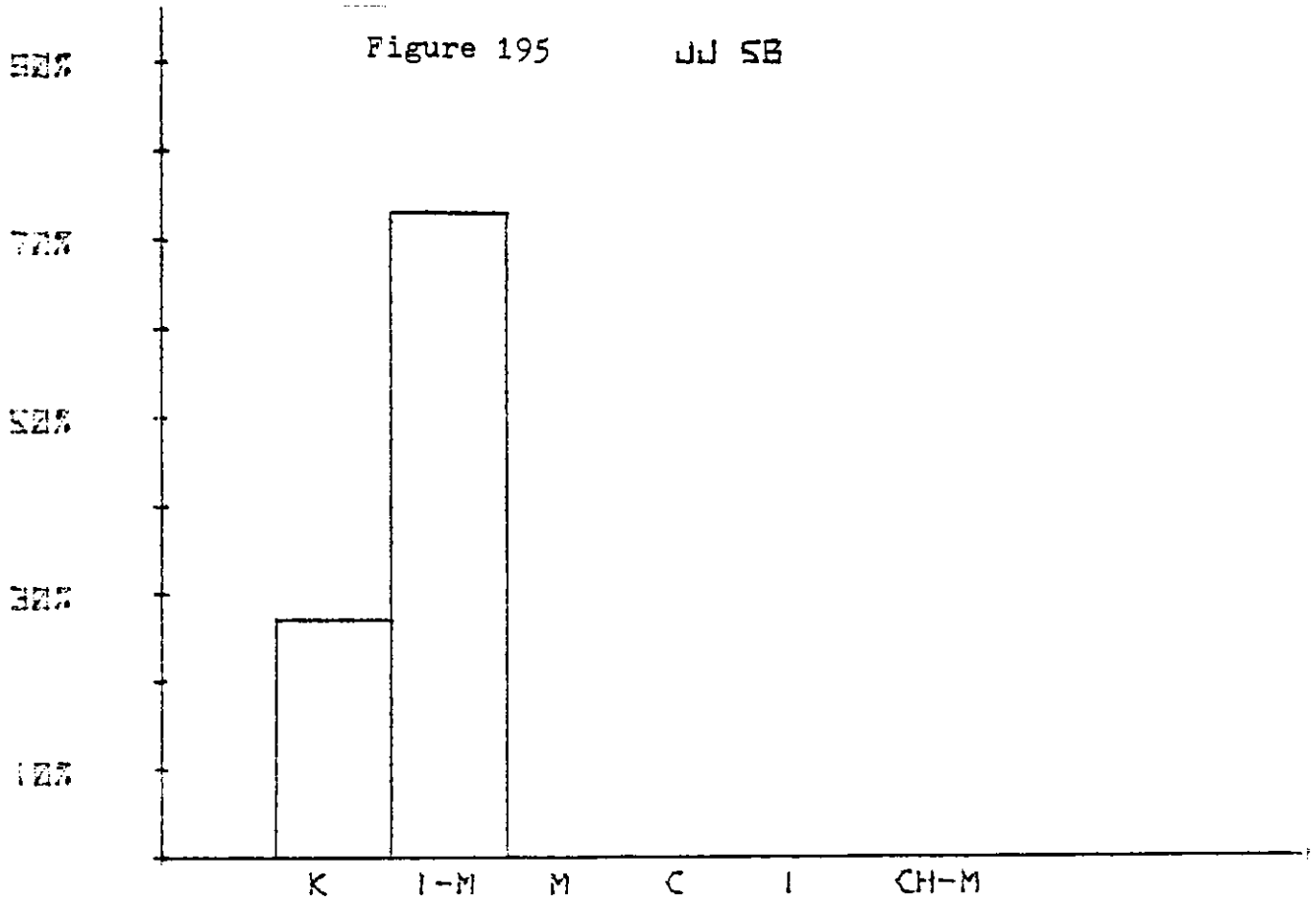


Figure 196

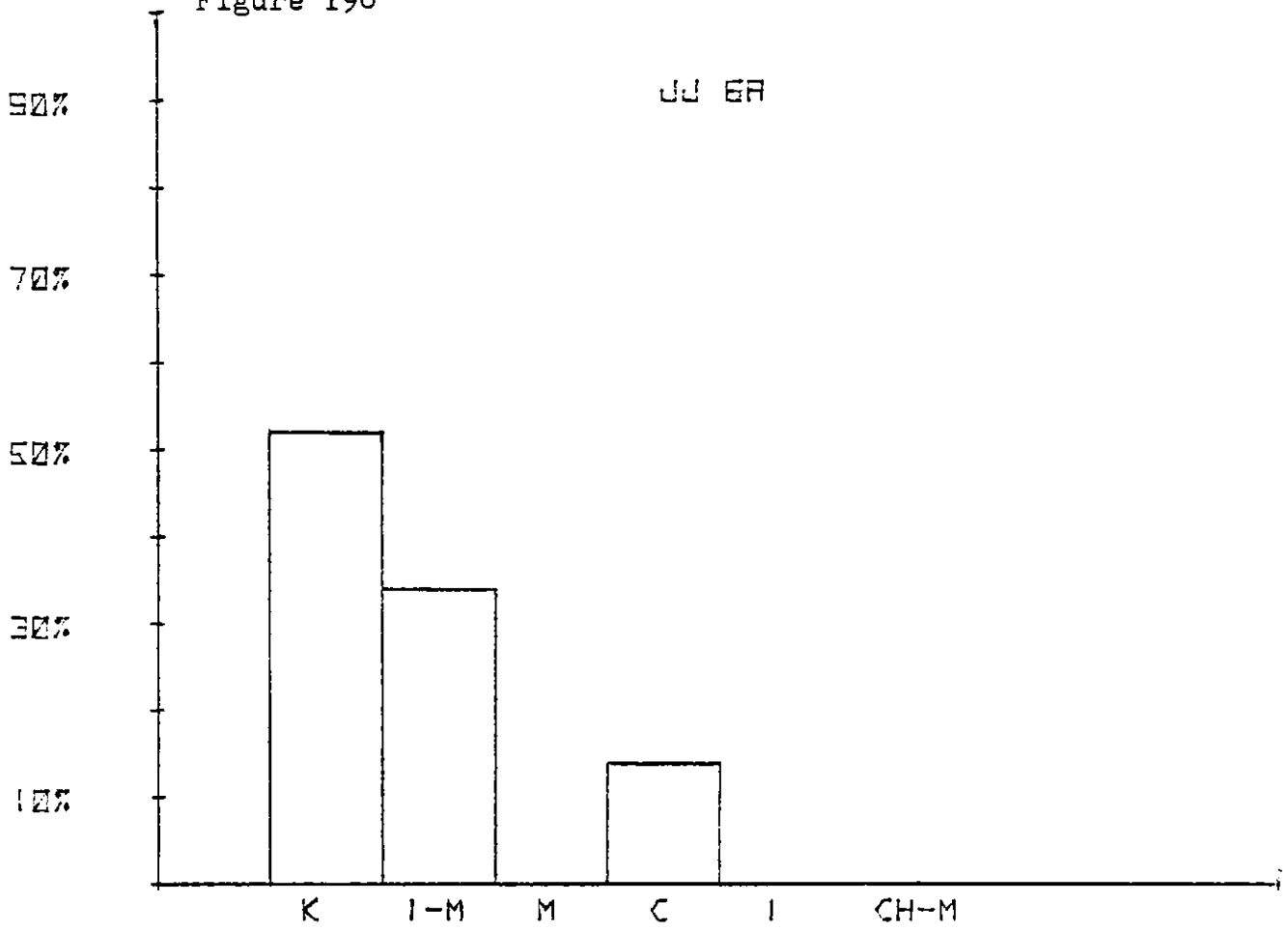


Figure 197

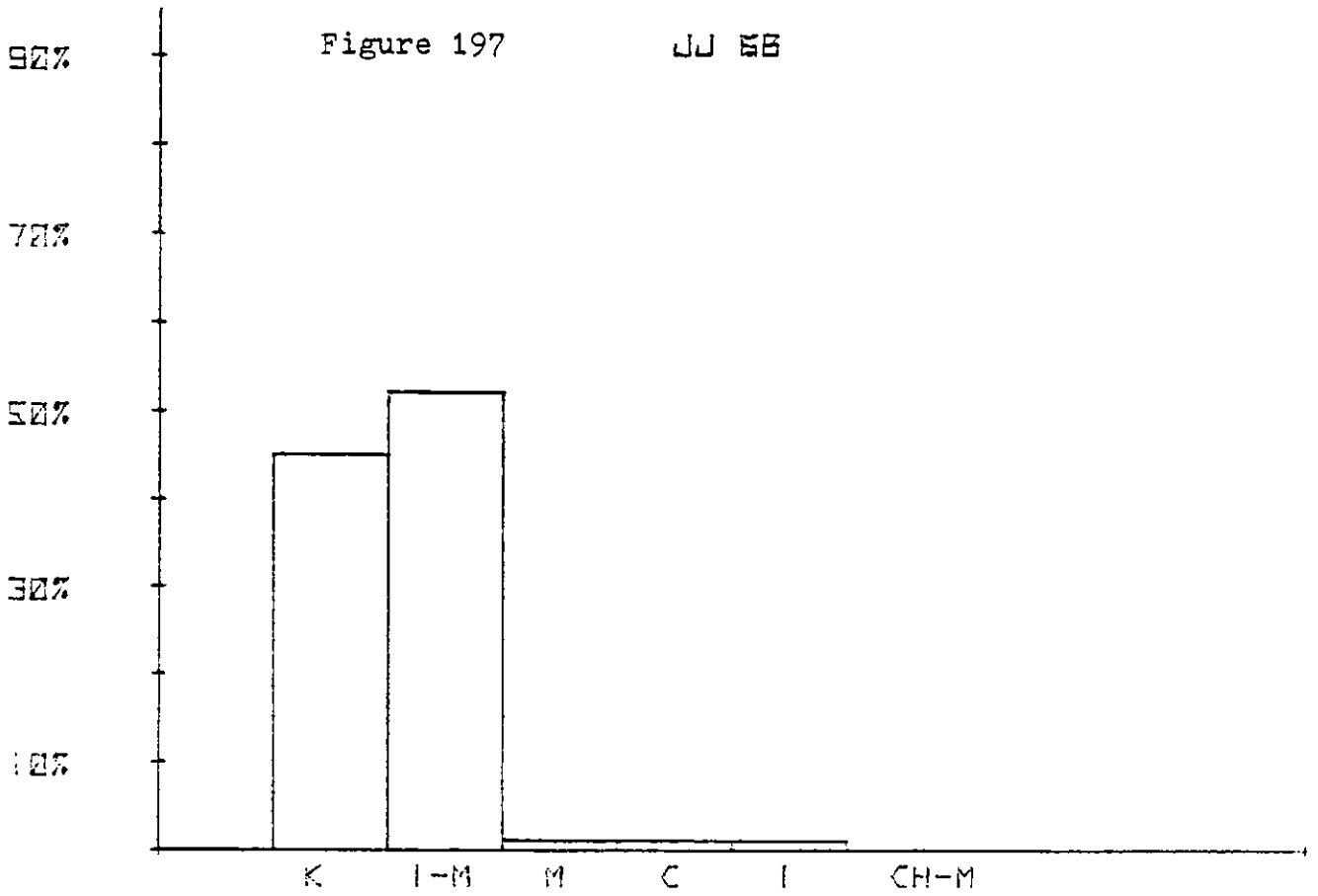


Figure 198

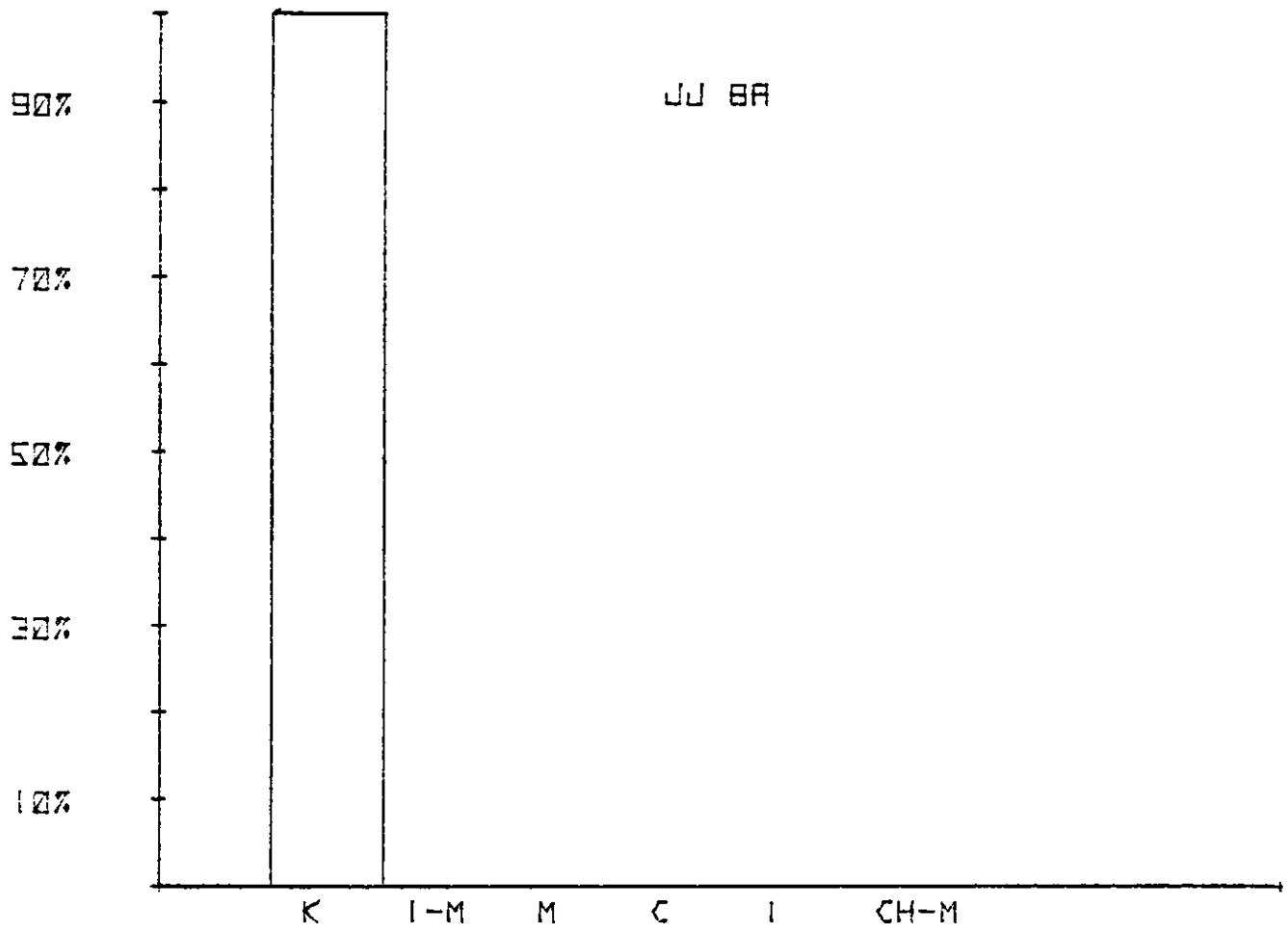


Figure 199

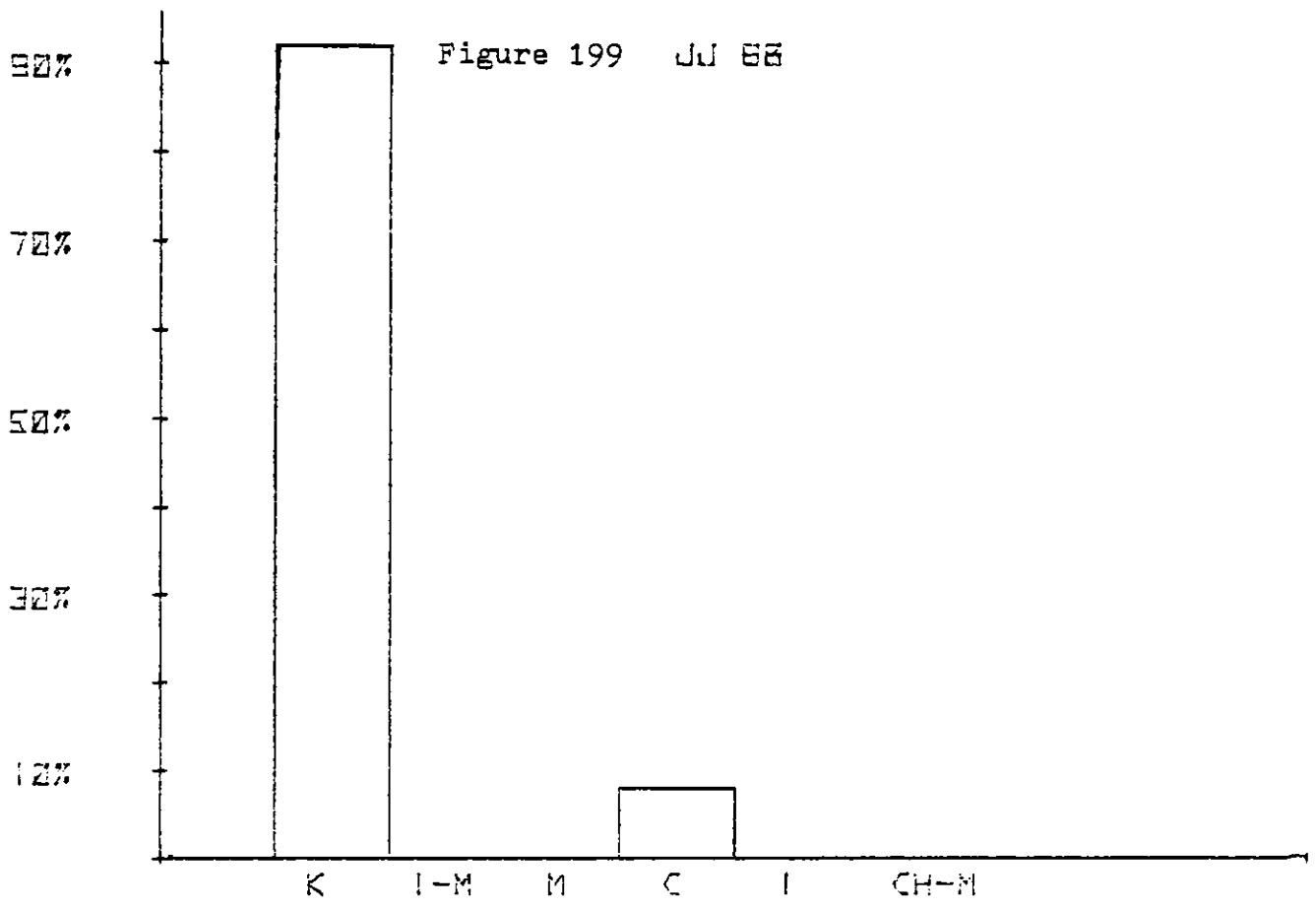


Figure 200

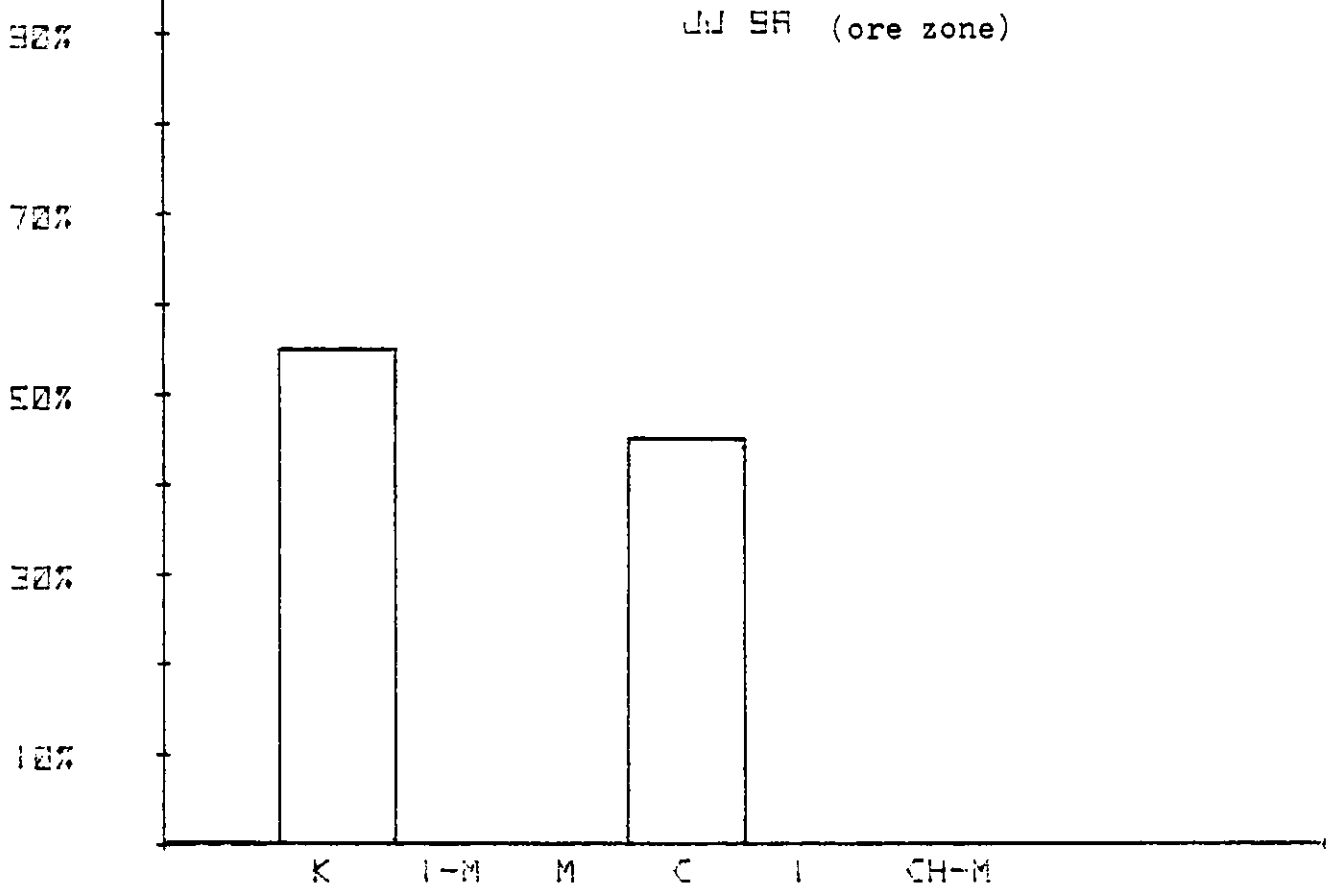


Figure 201

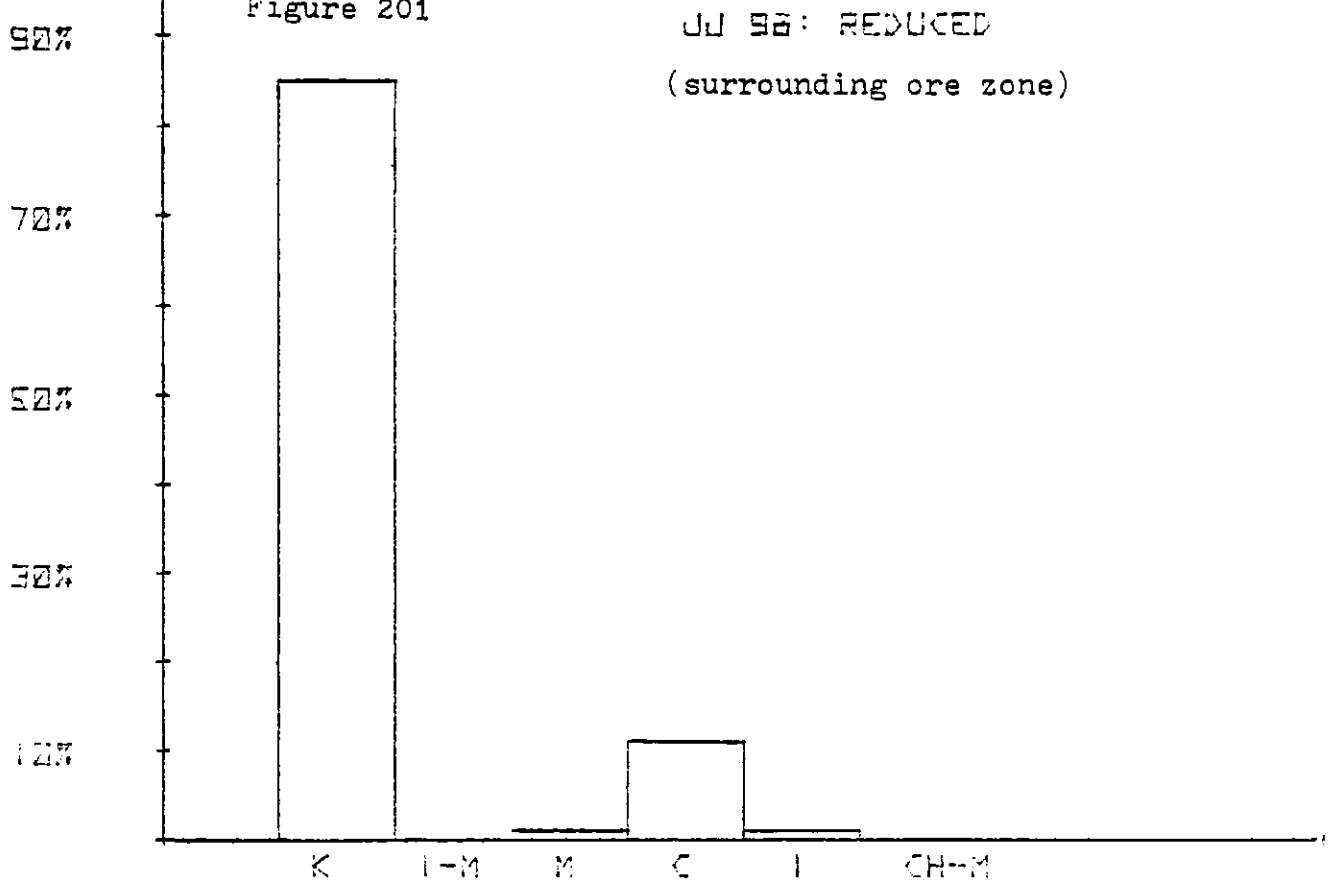


Figure 202

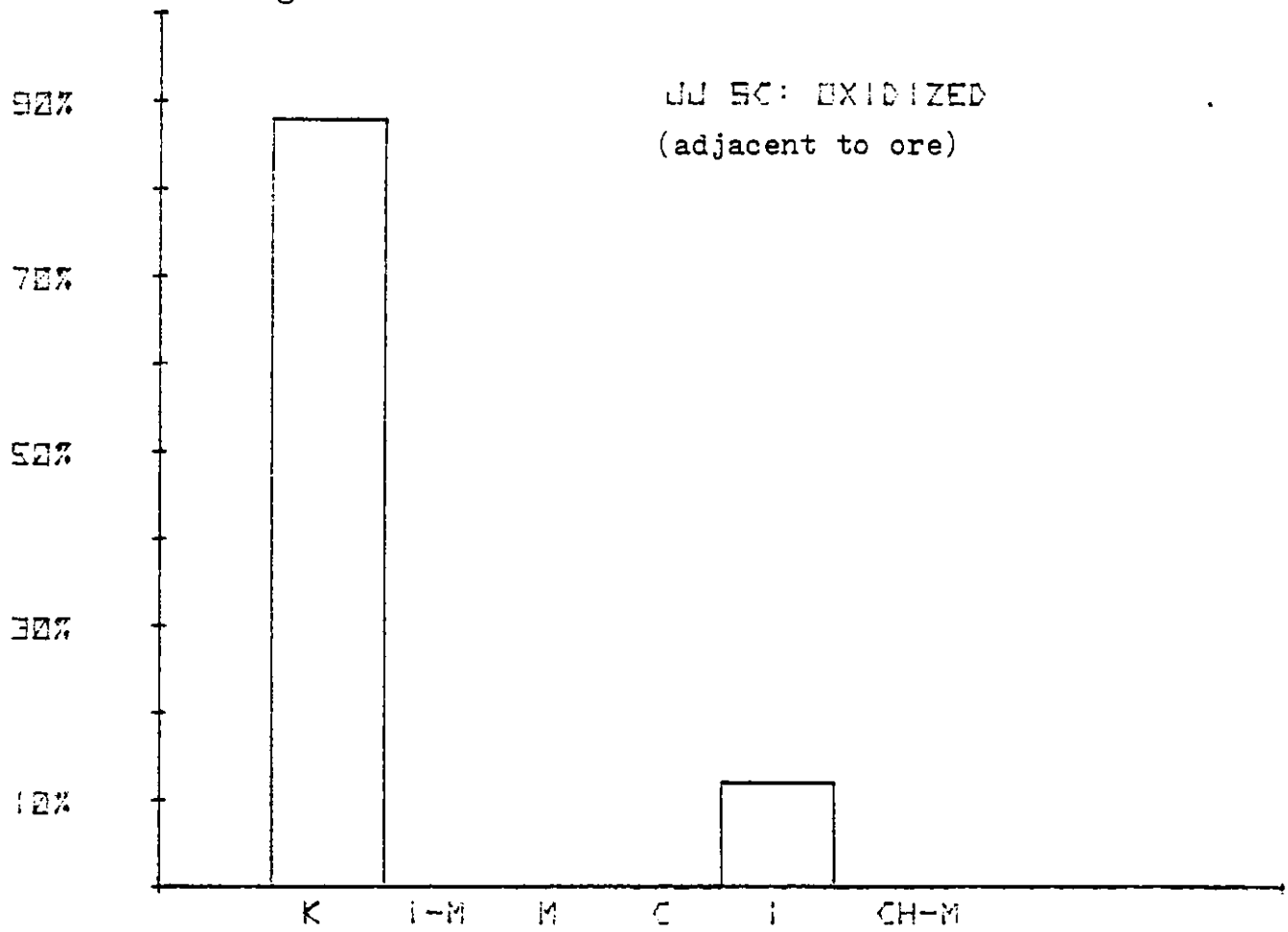


Figure 203

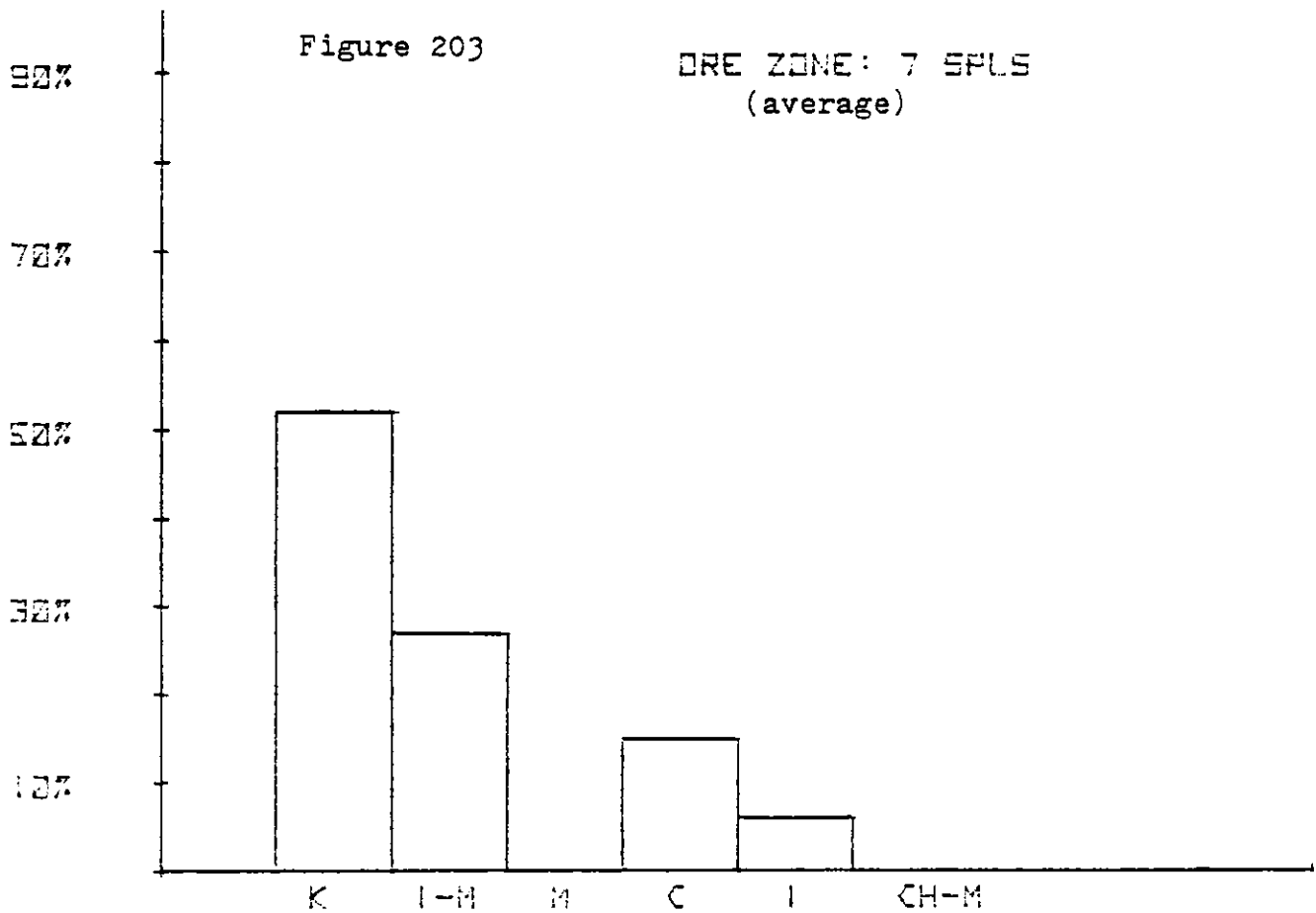


Figure 204

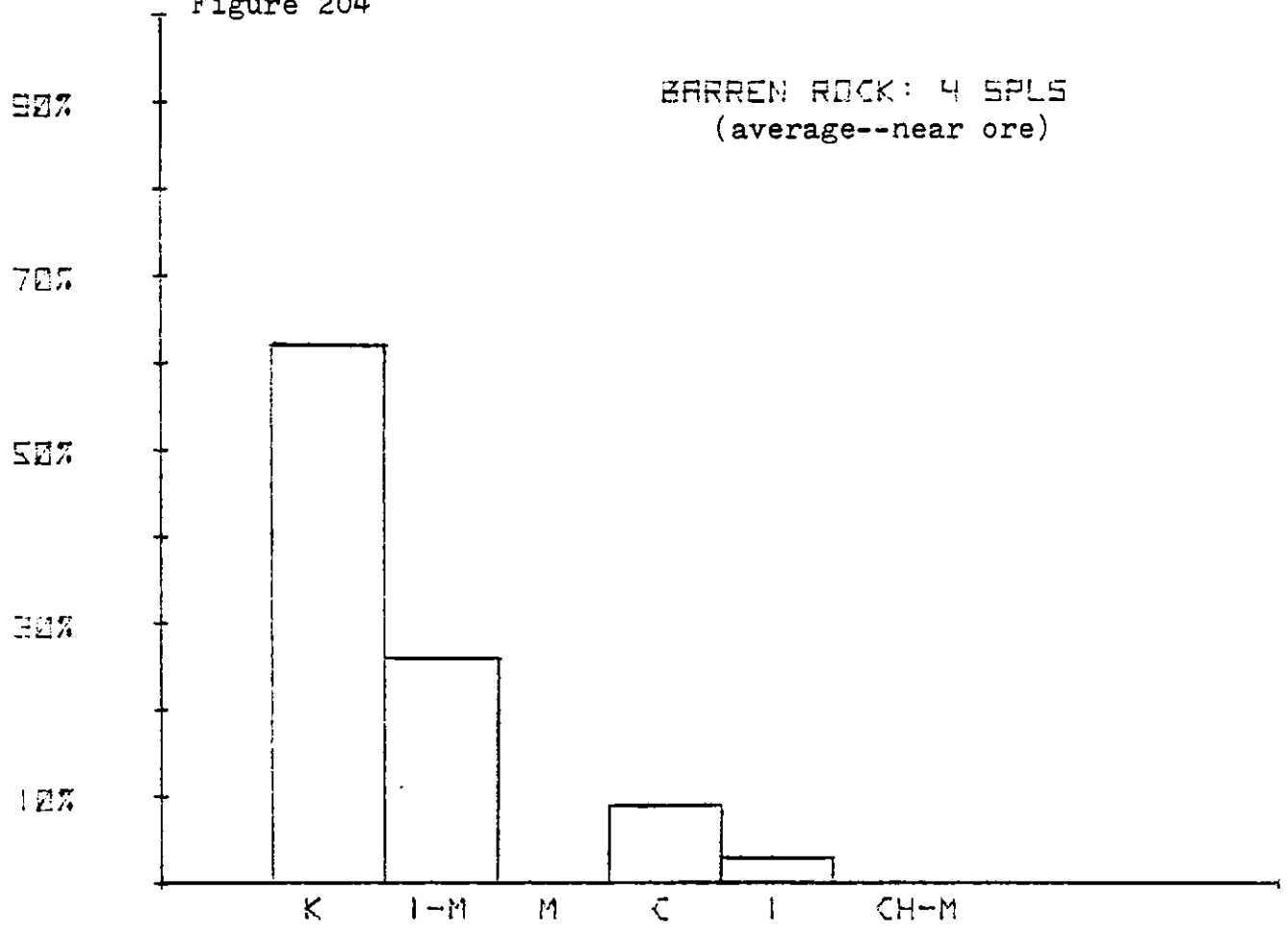


Figure 205

M. LAKE #1

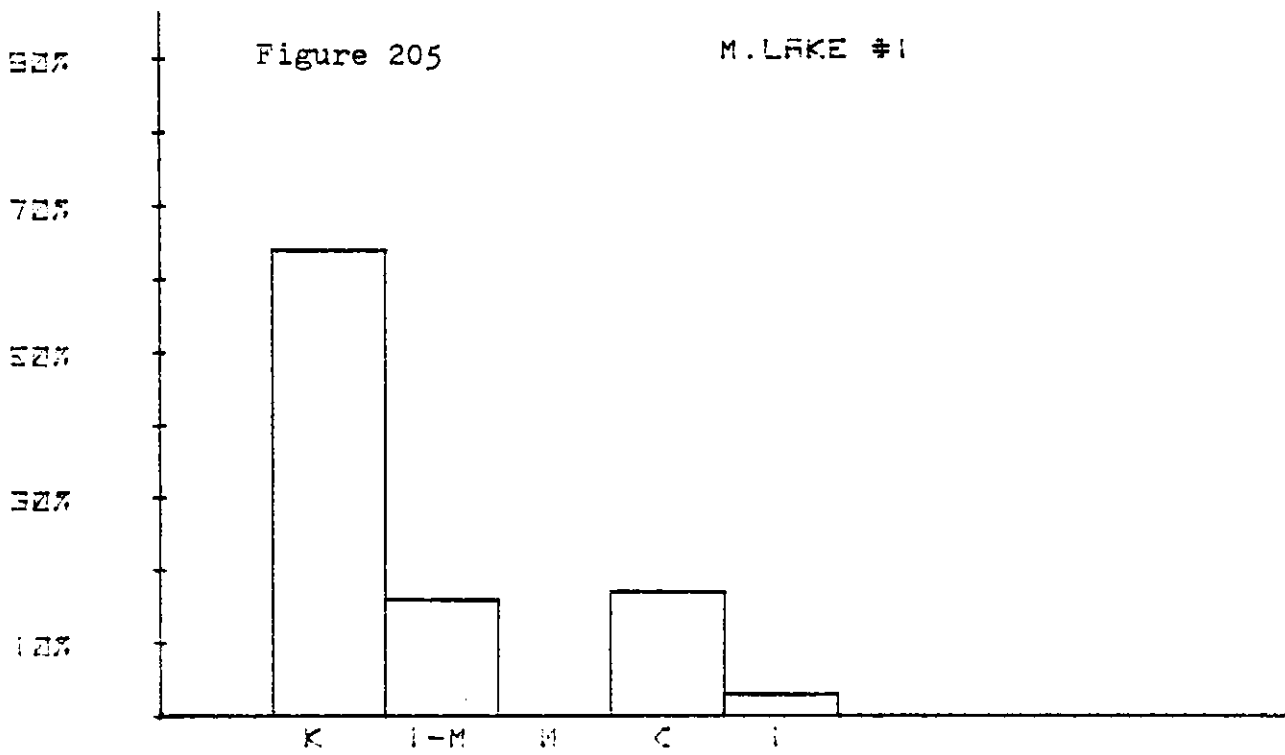


Figure 206

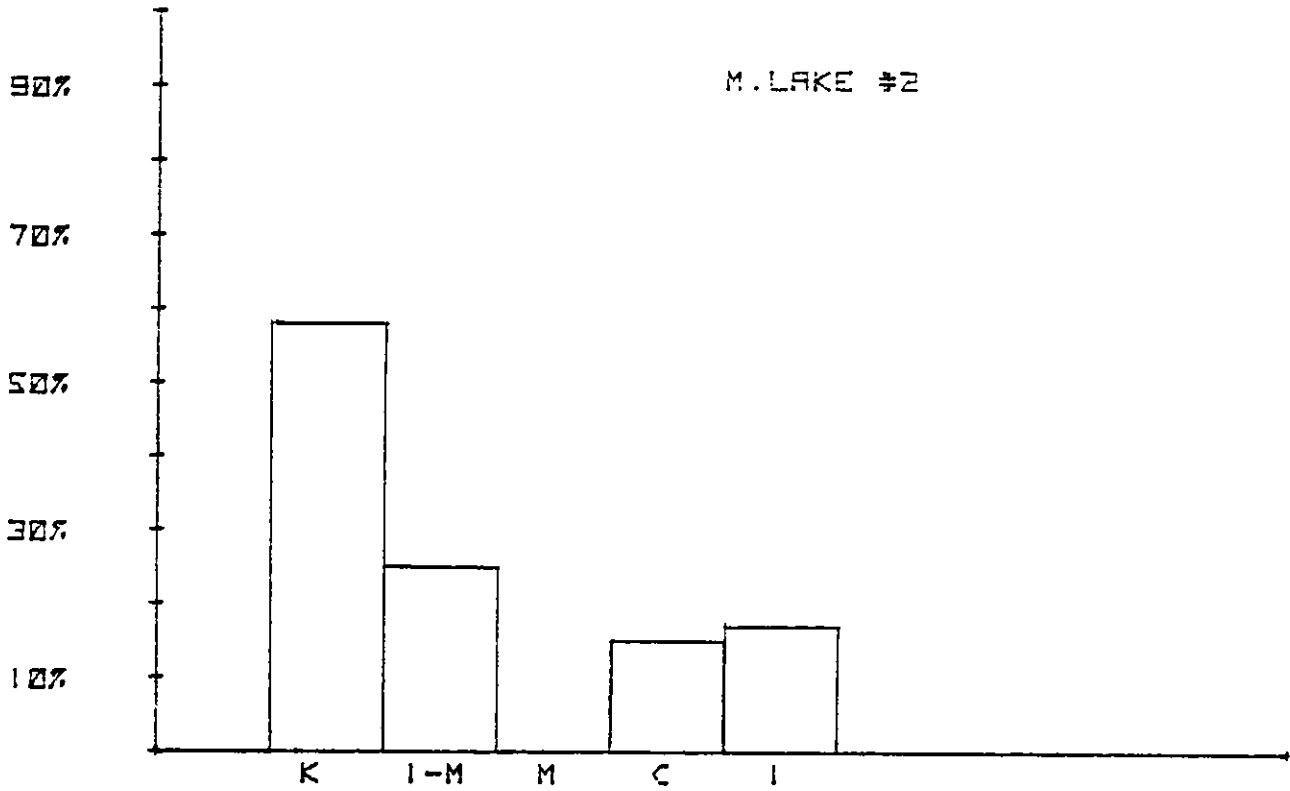


Figure 207

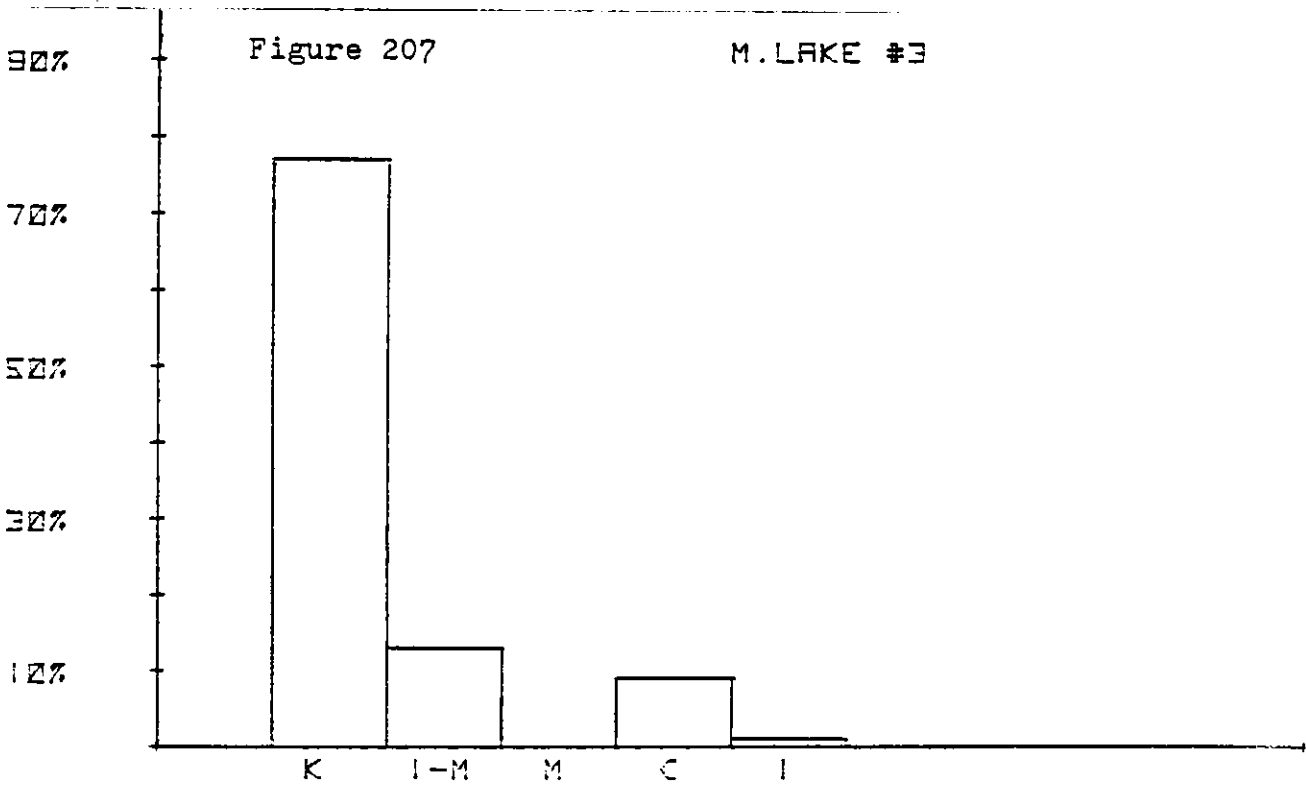


Figure 208

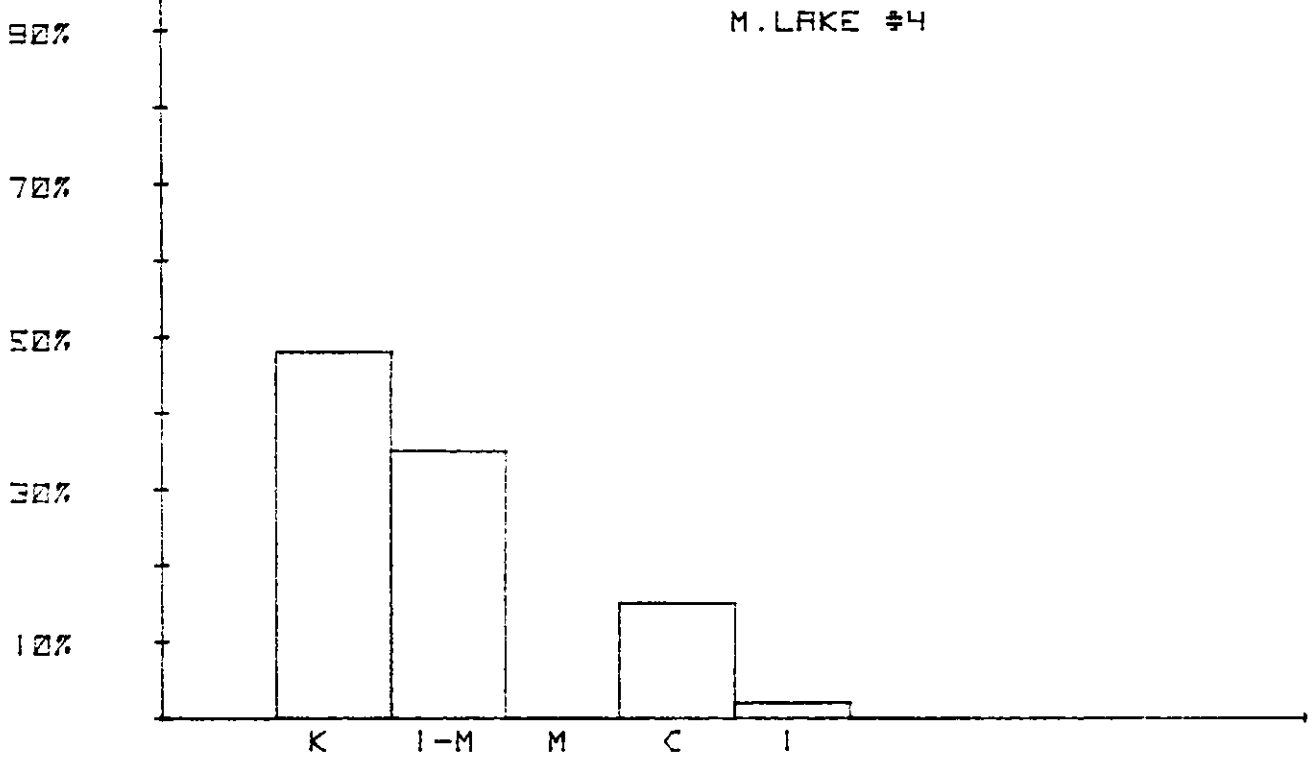


Figure 209

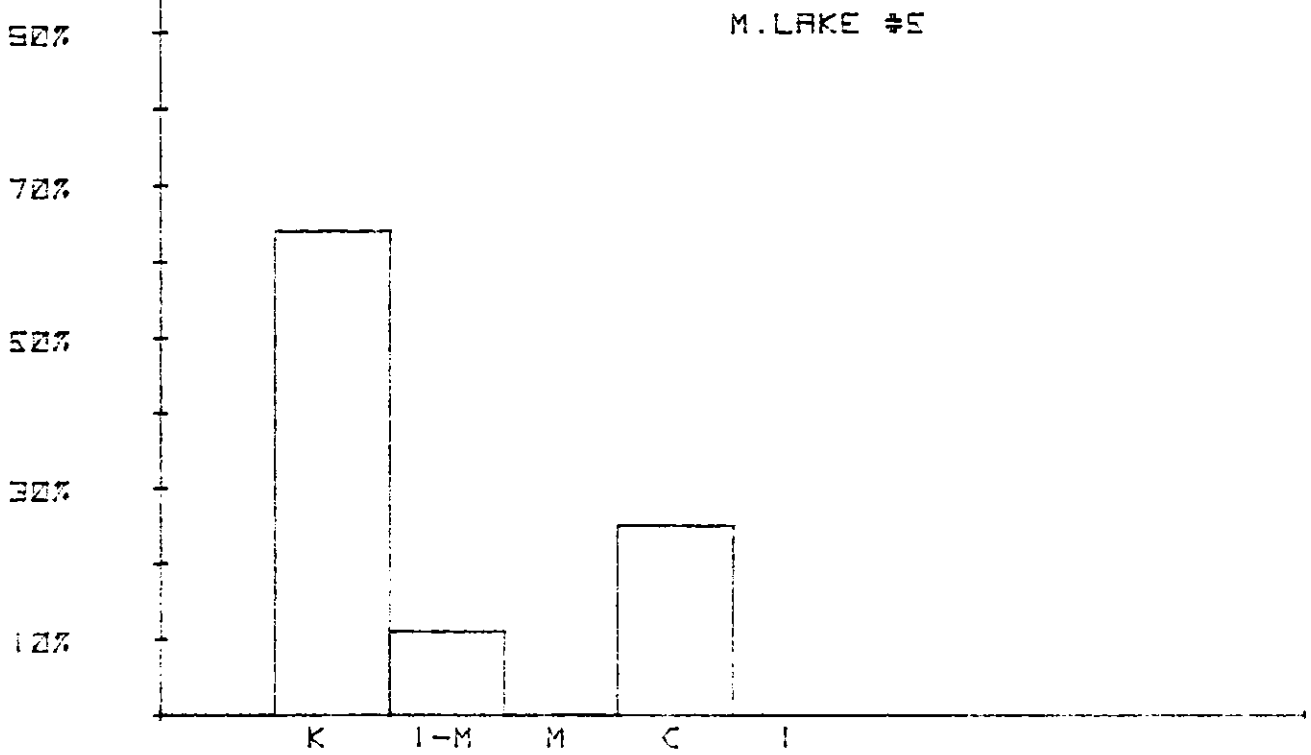


Figure 210

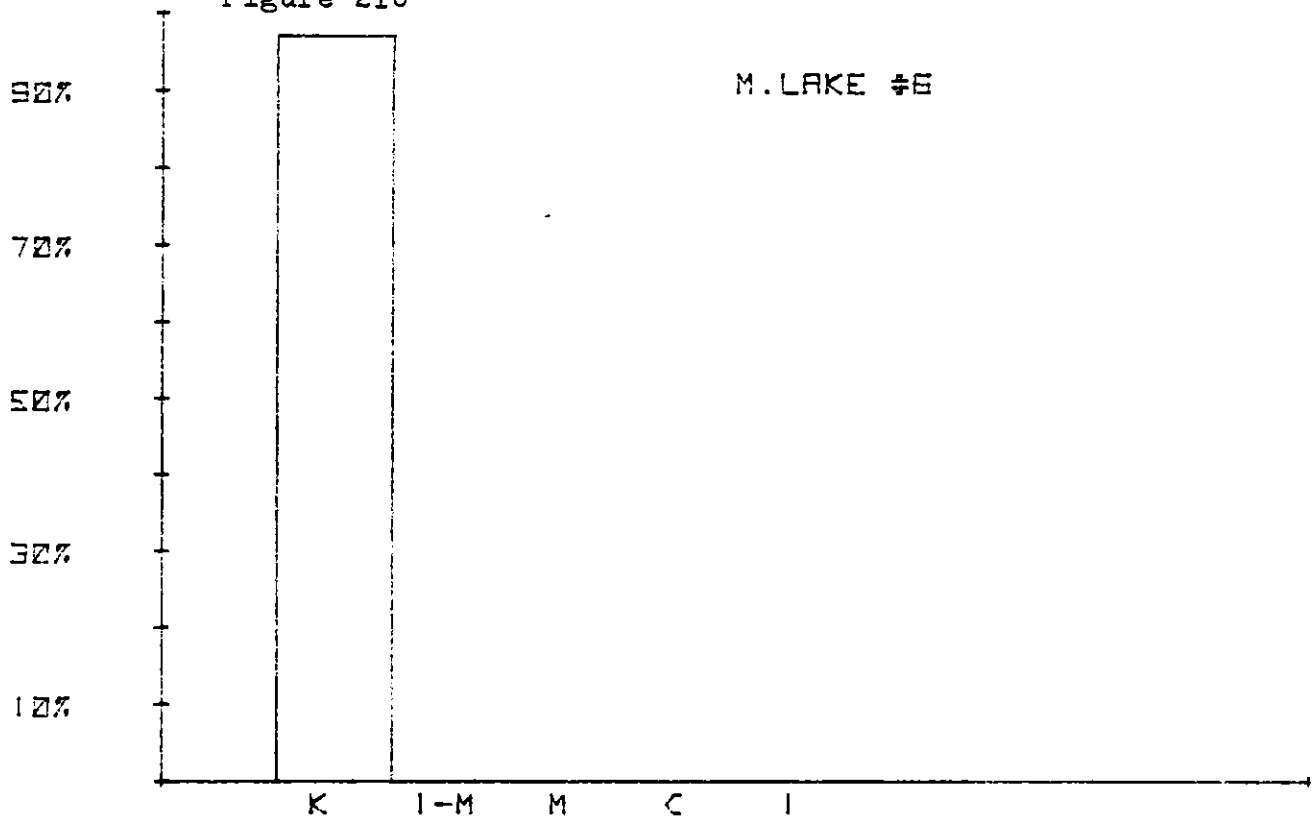


Figure 211

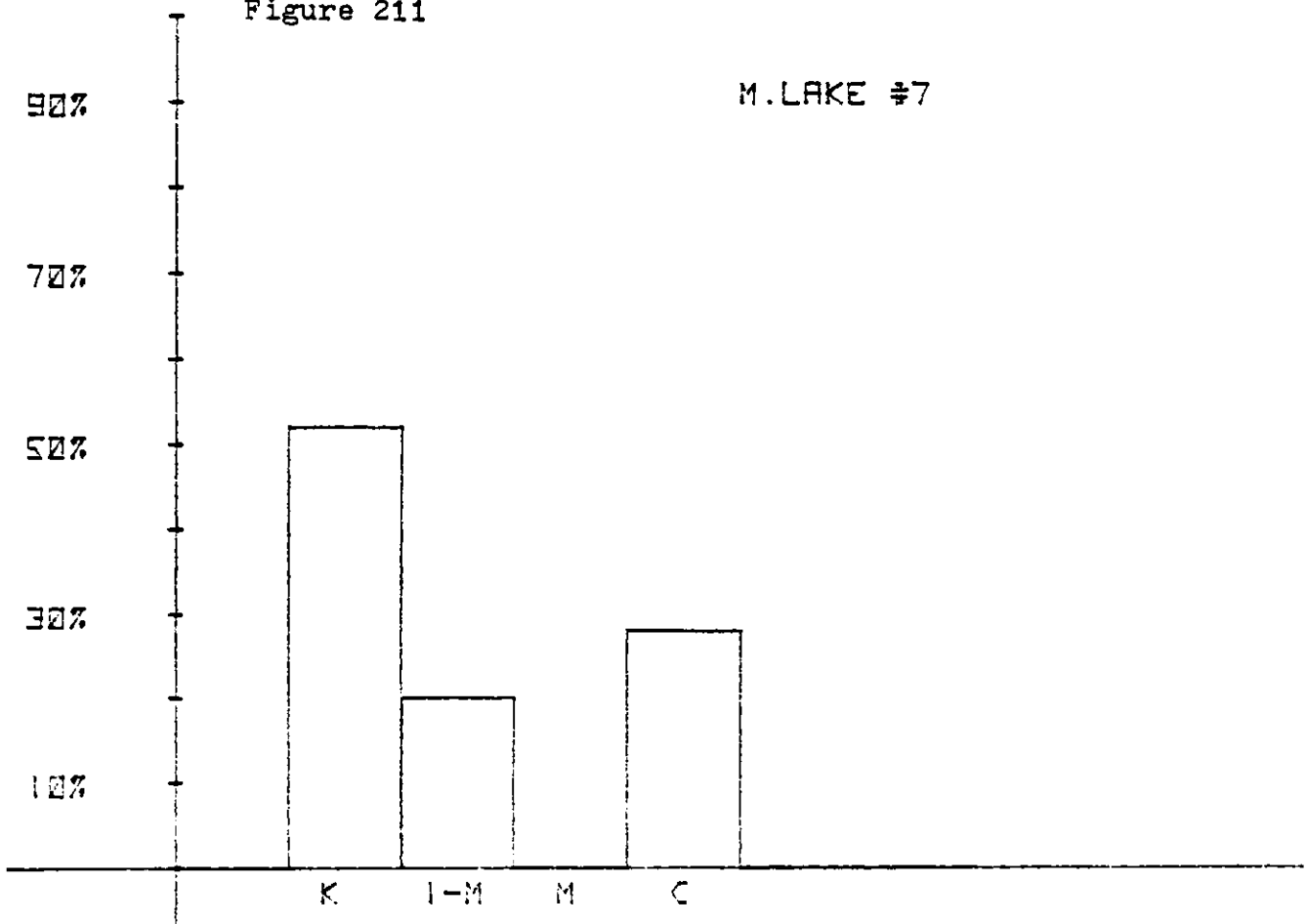


Figure 212

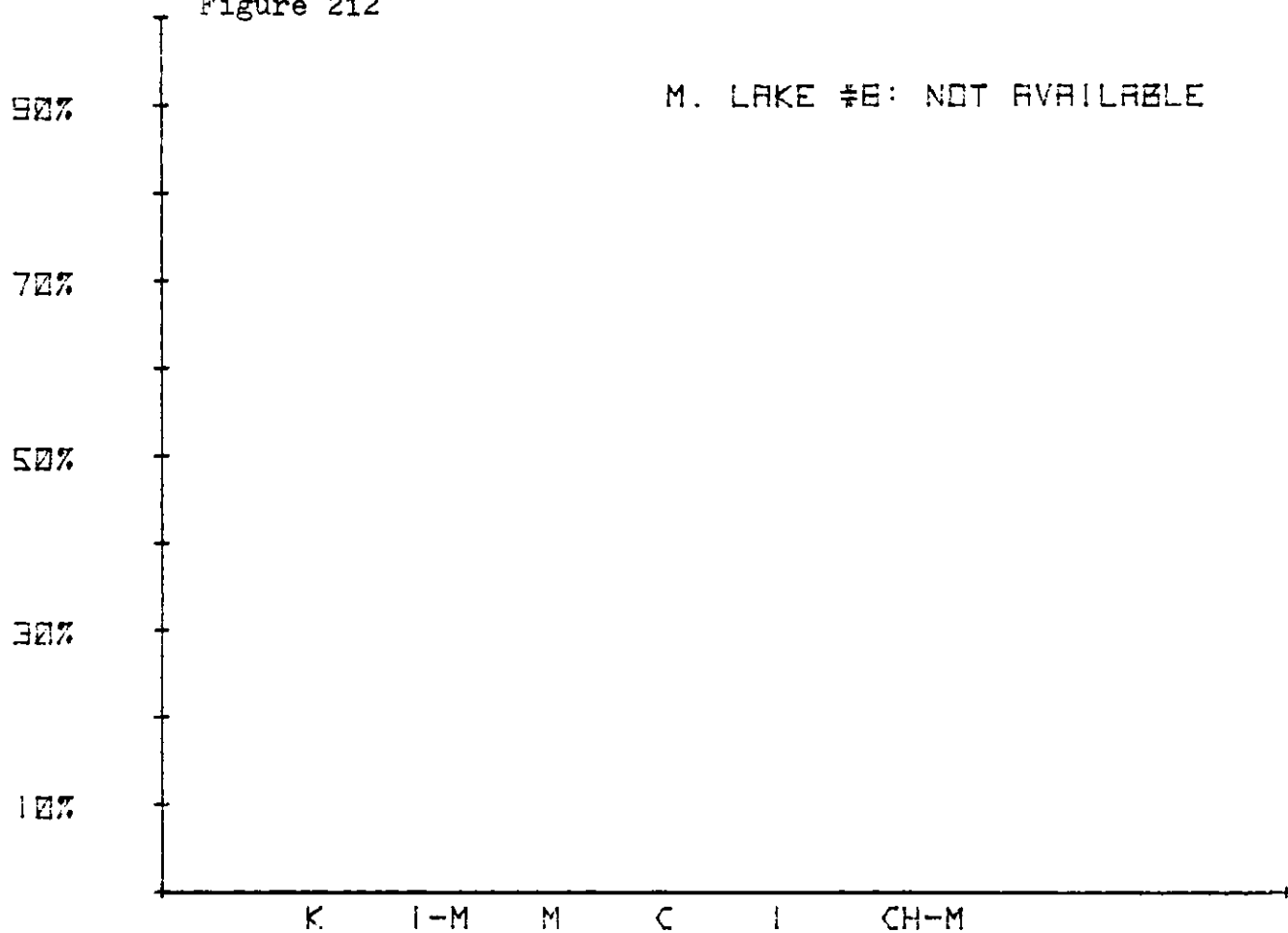


Figure 213

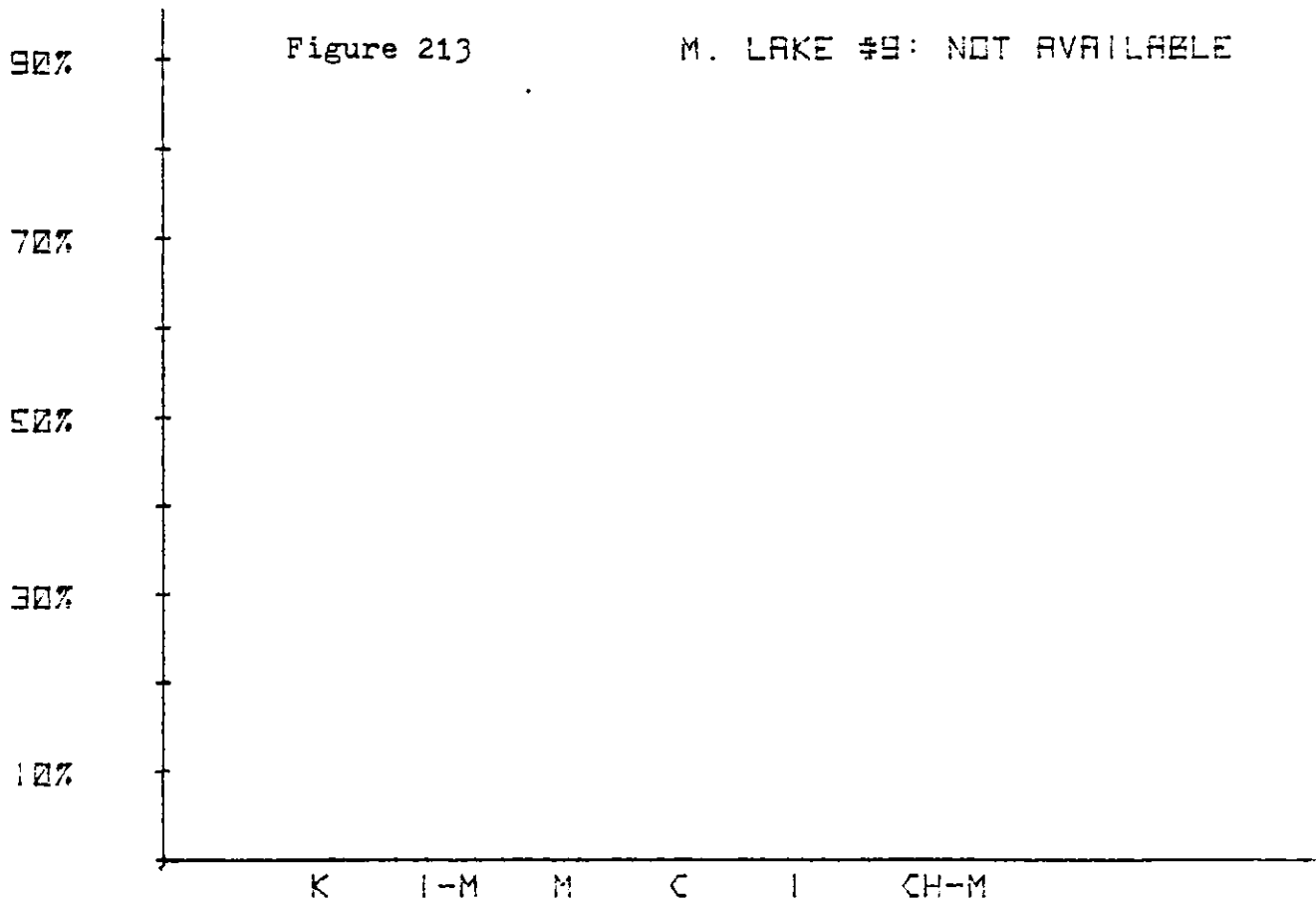


Figure 214

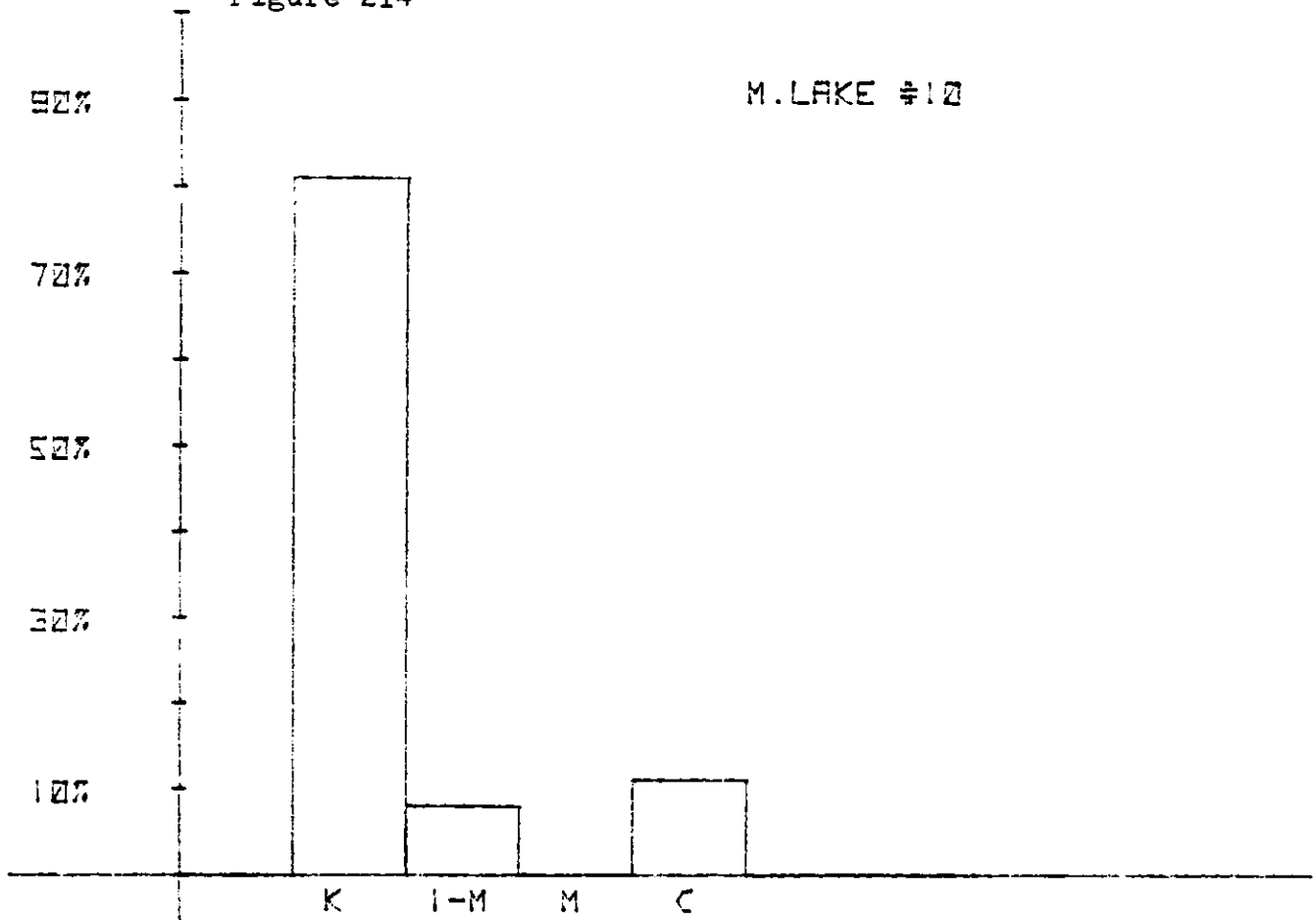


Figure 215

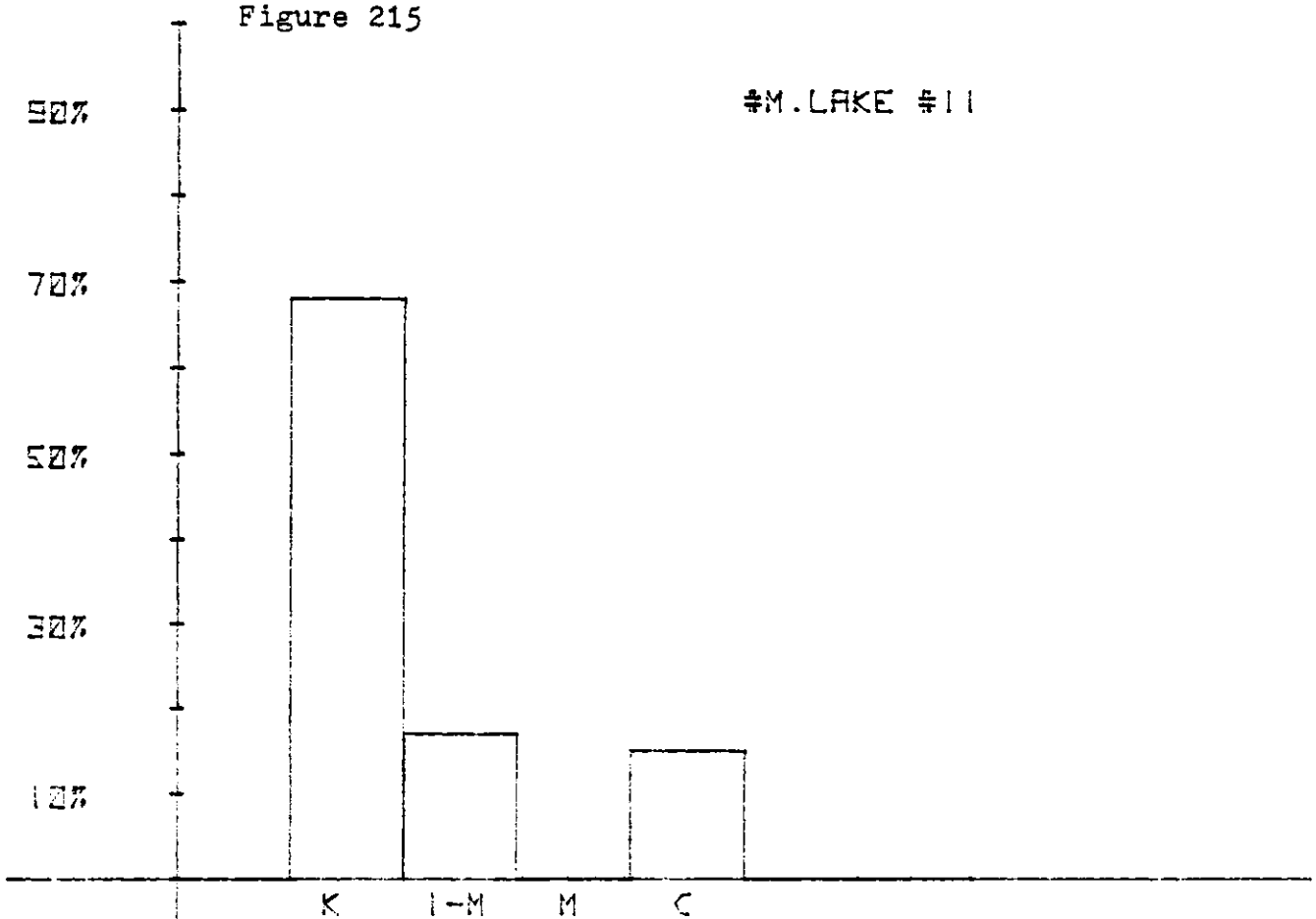


Figure 216

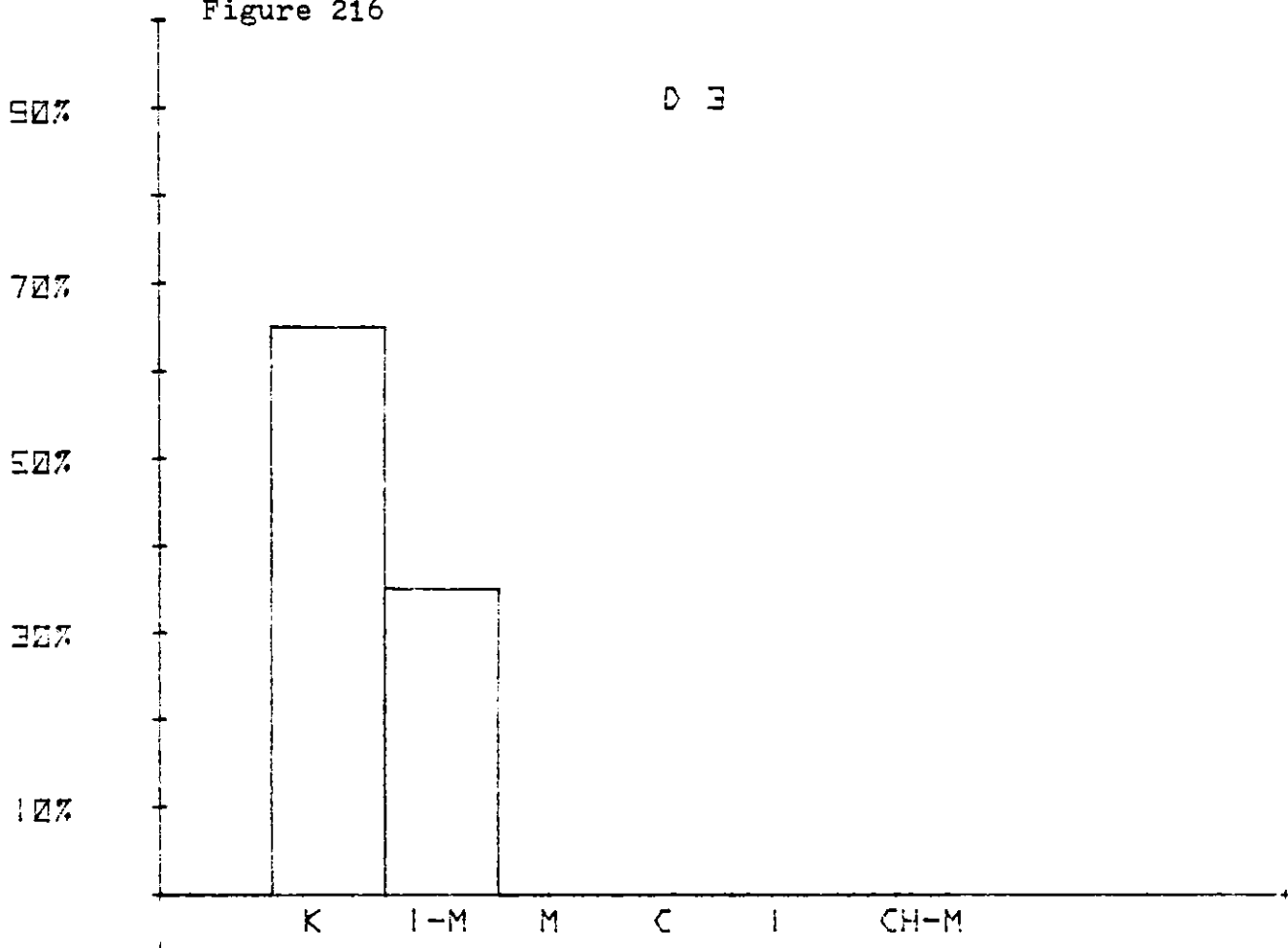


Figure 217

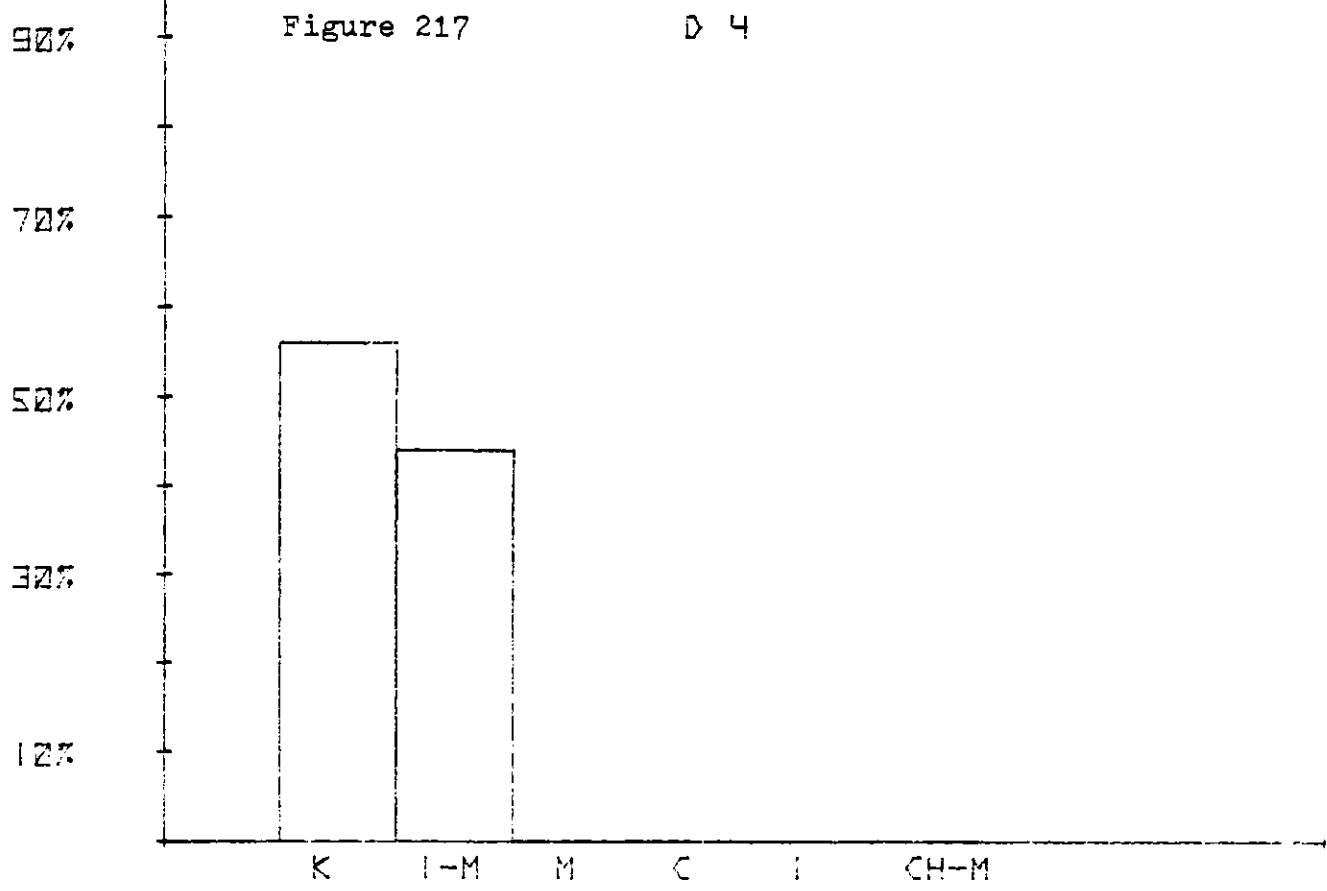


Figure 218

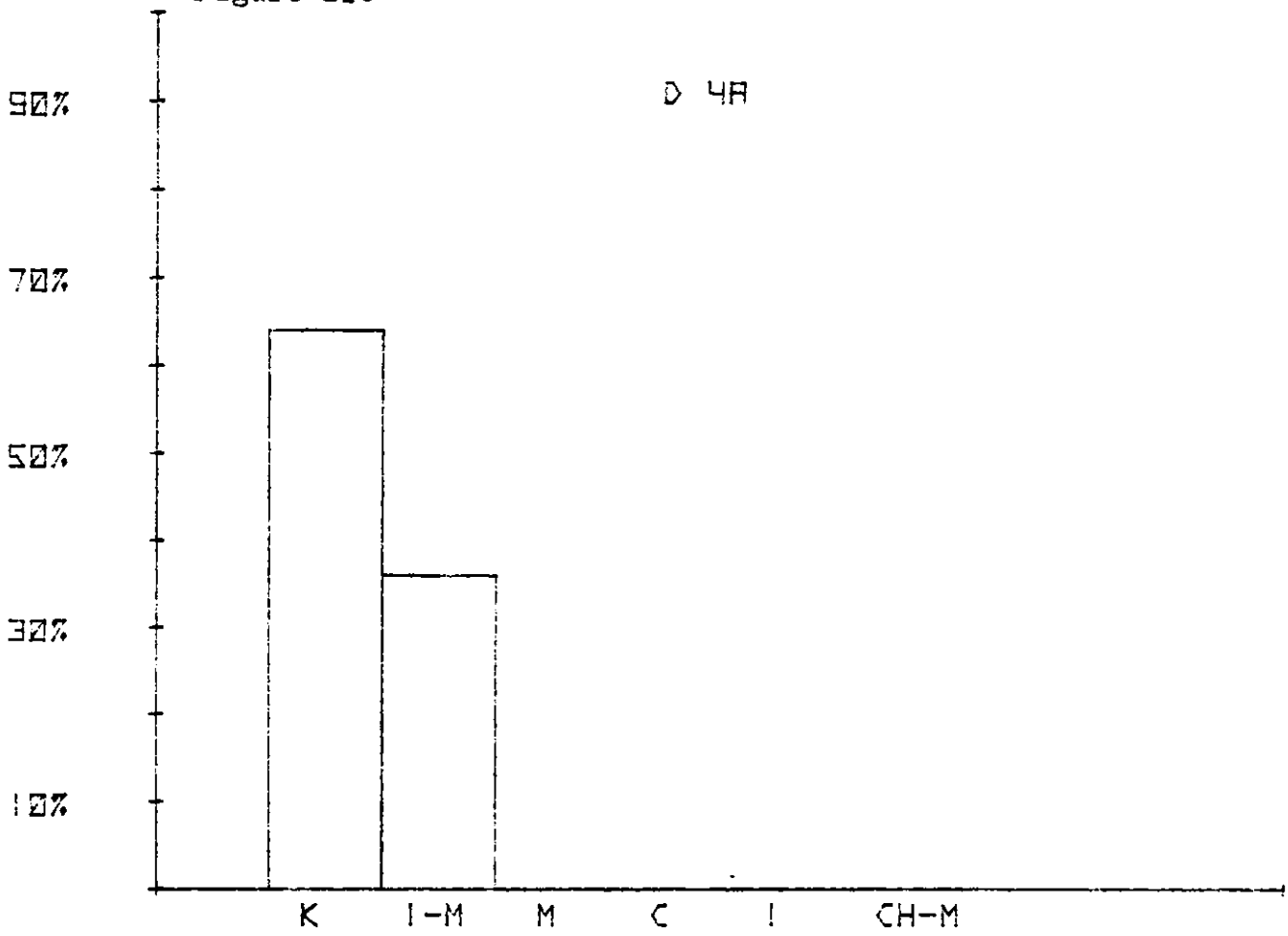


Figure 219

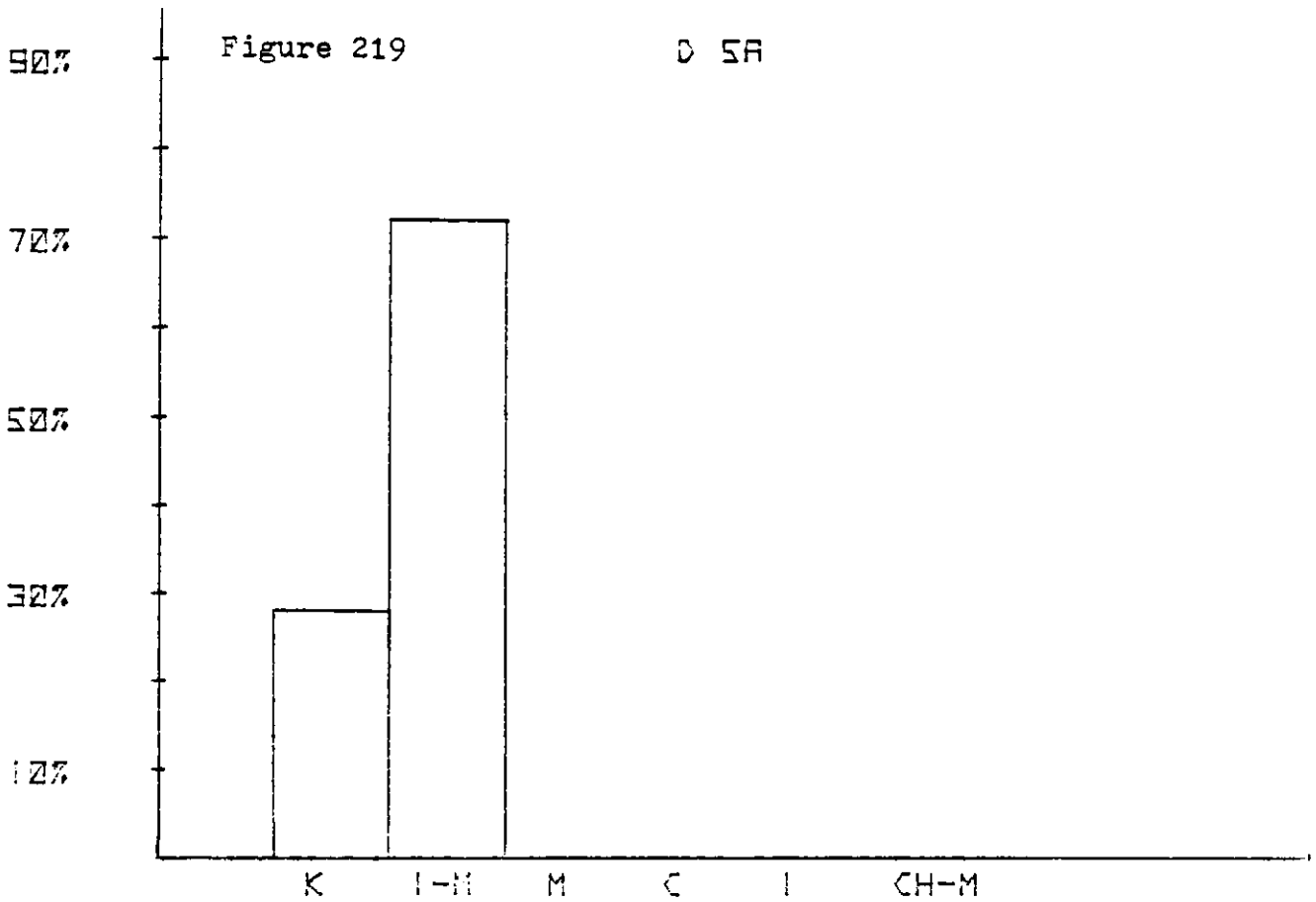
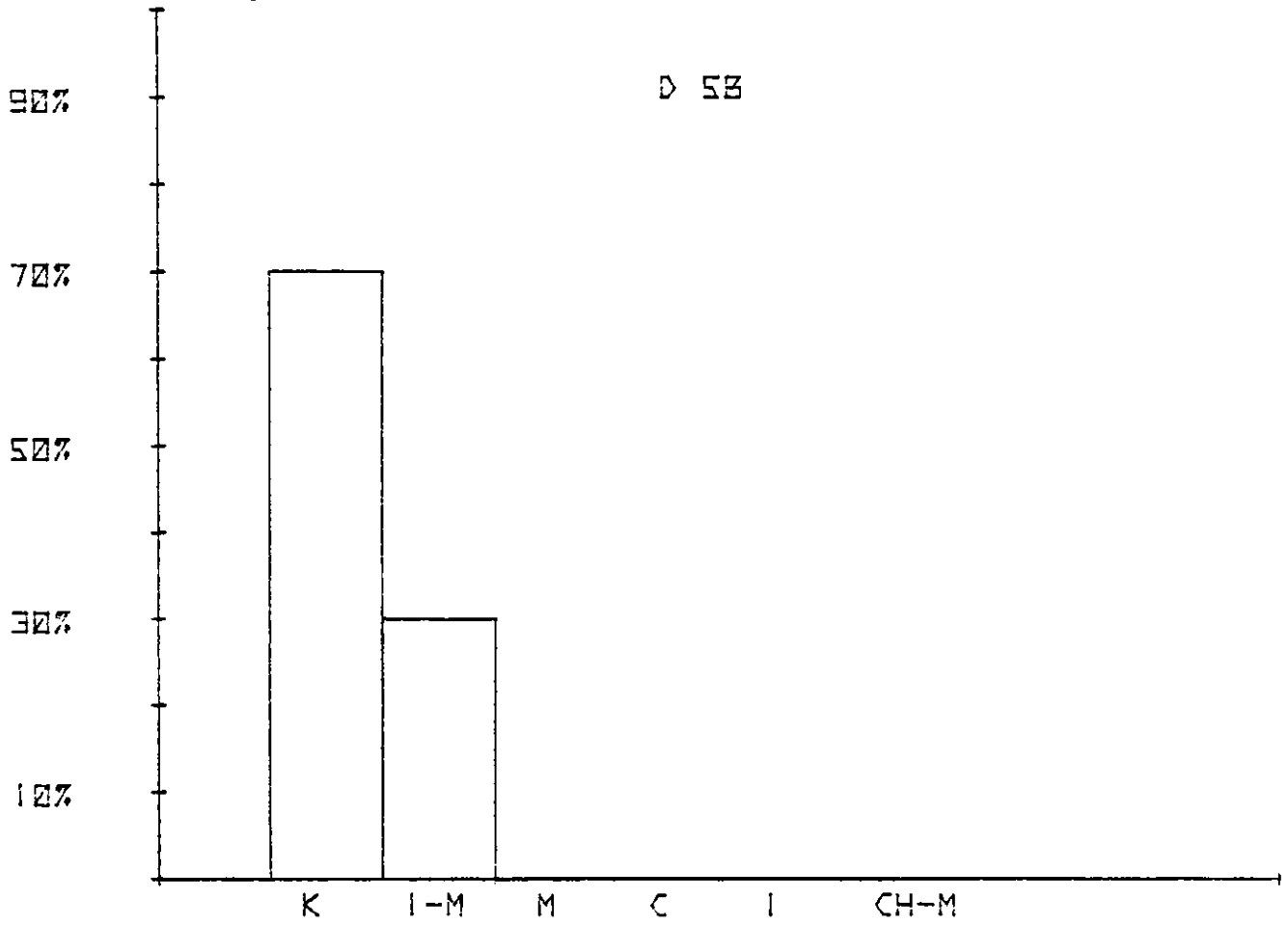
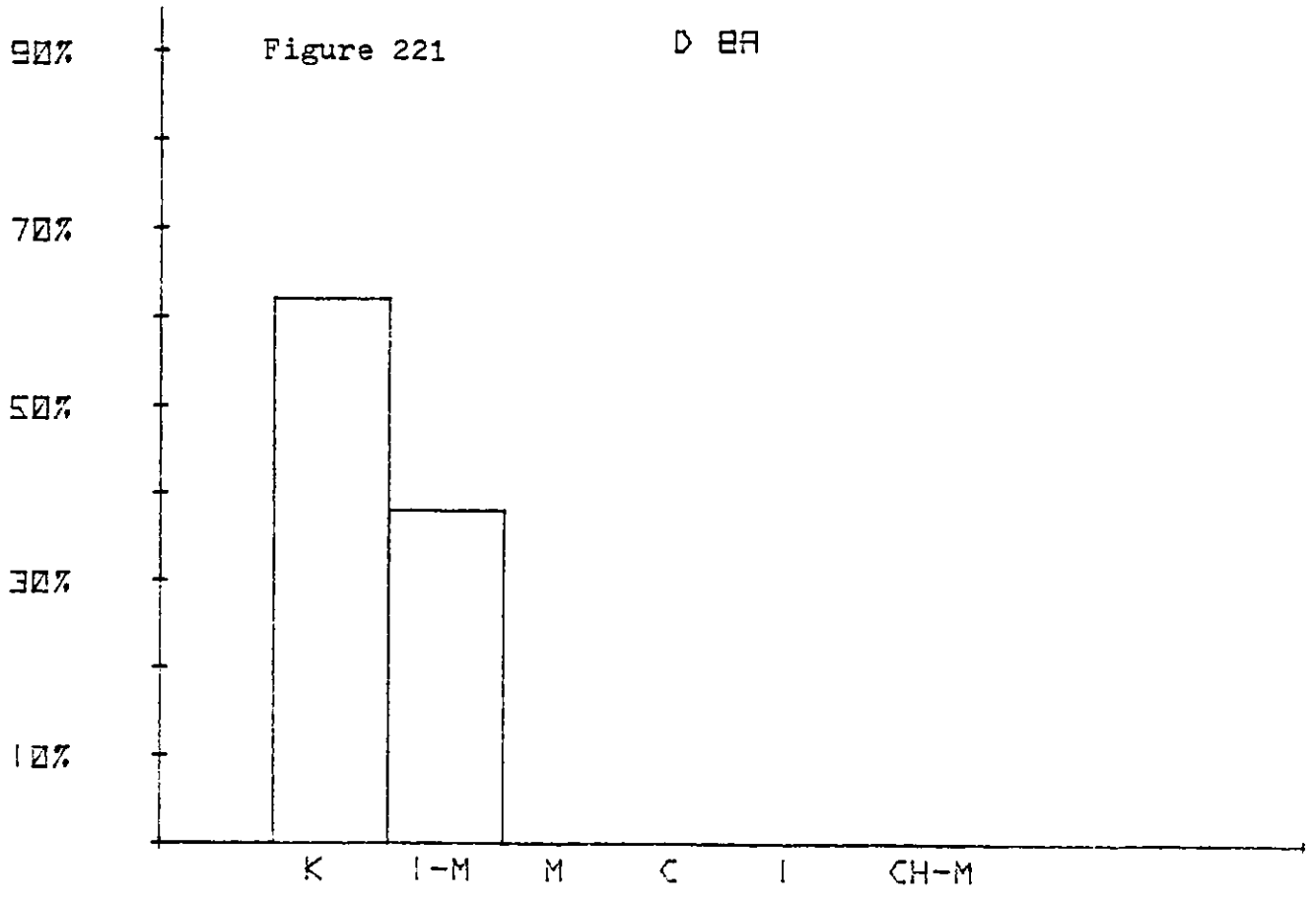


Figure 220



D 53

Figure 221



D 88

Figure 222

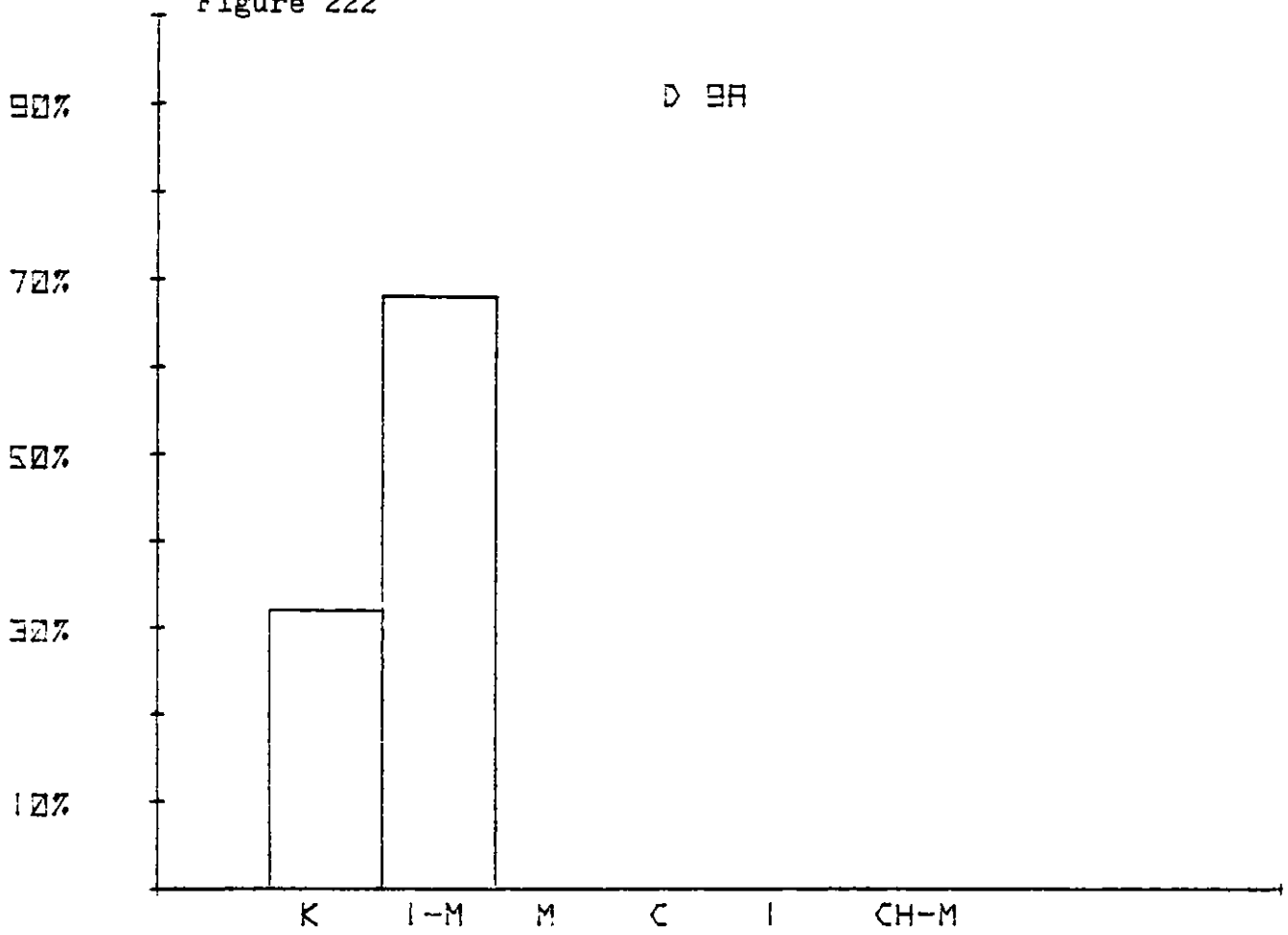


Figure 223

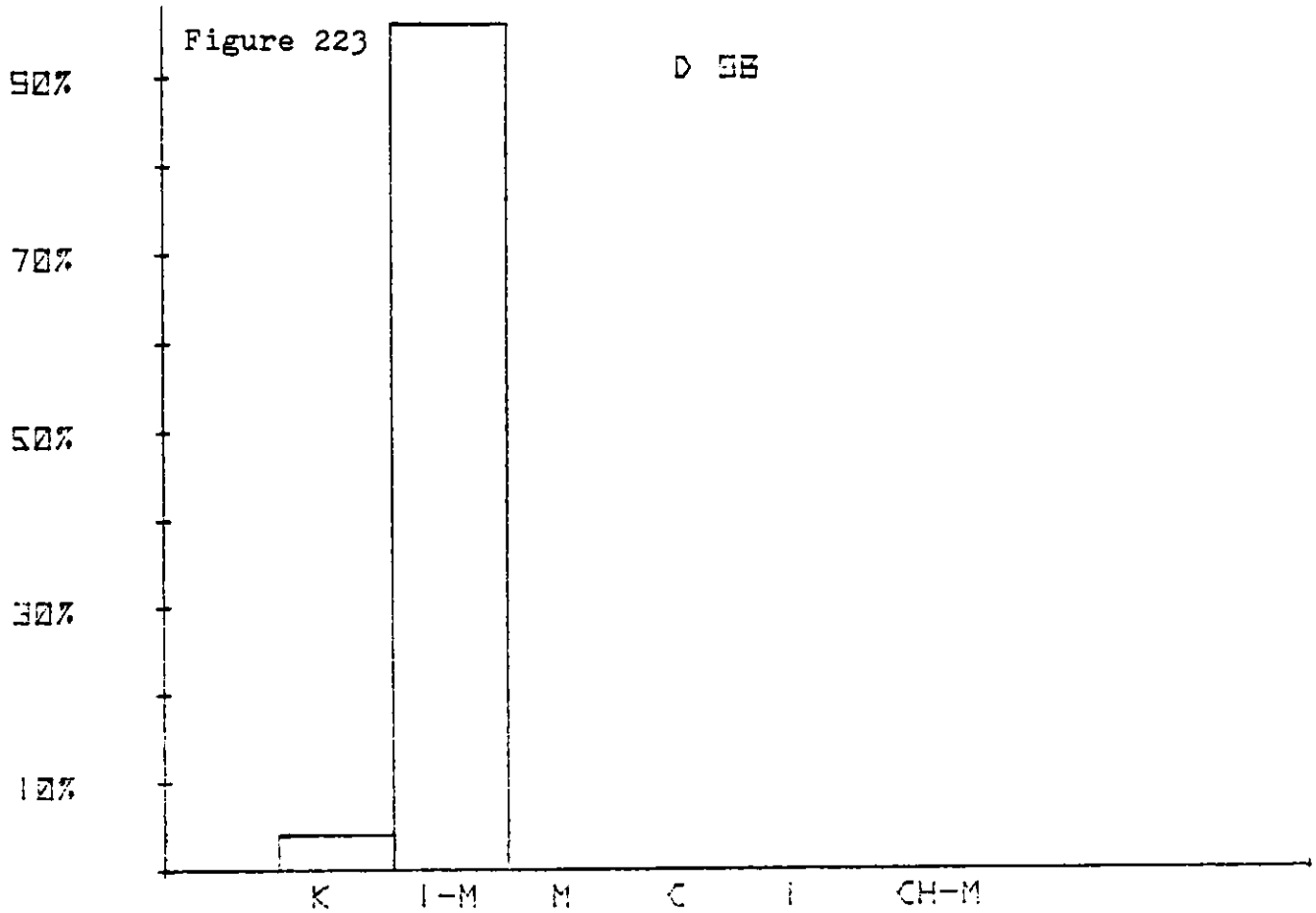


Figure 224

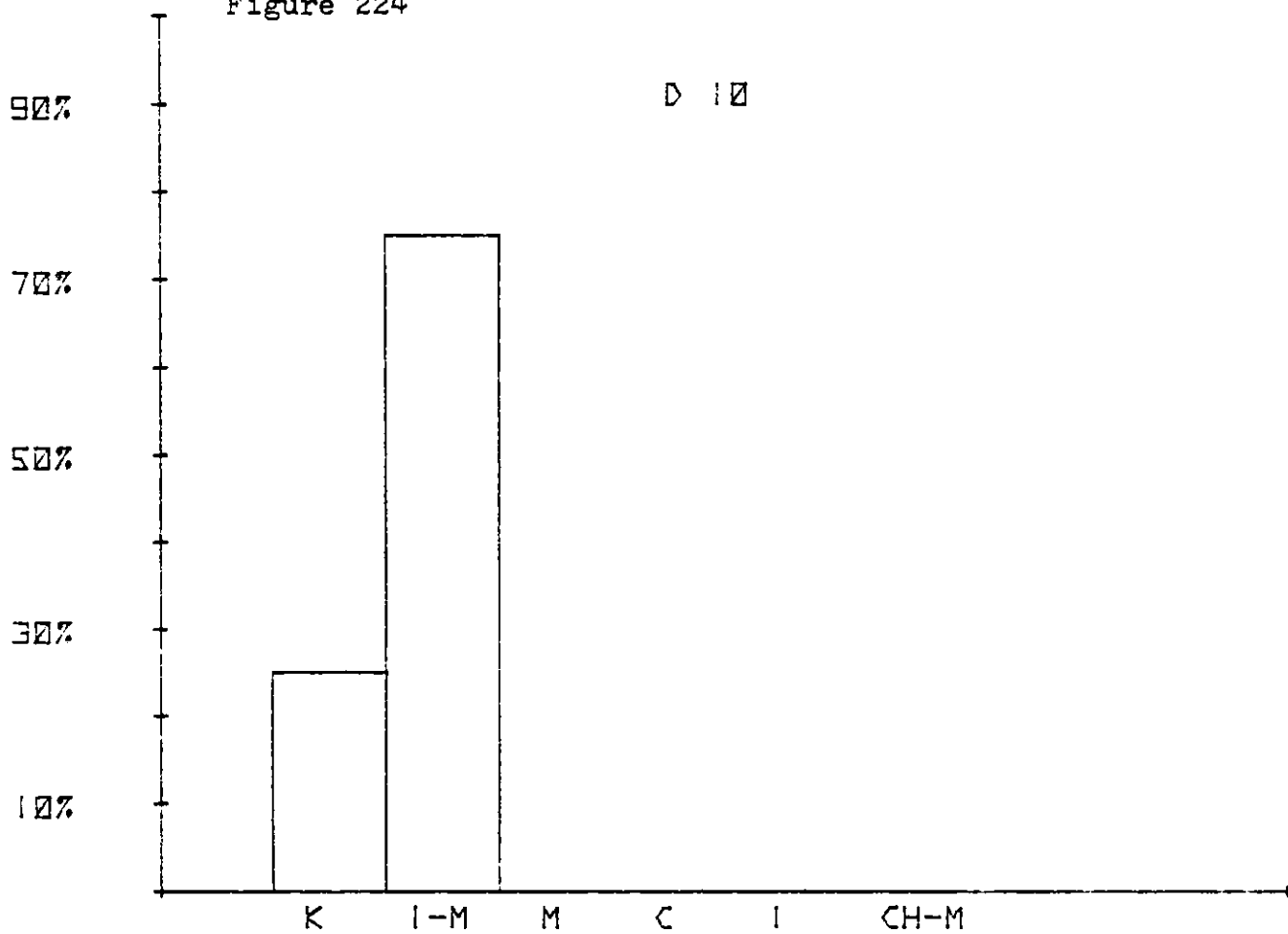


Figure 225

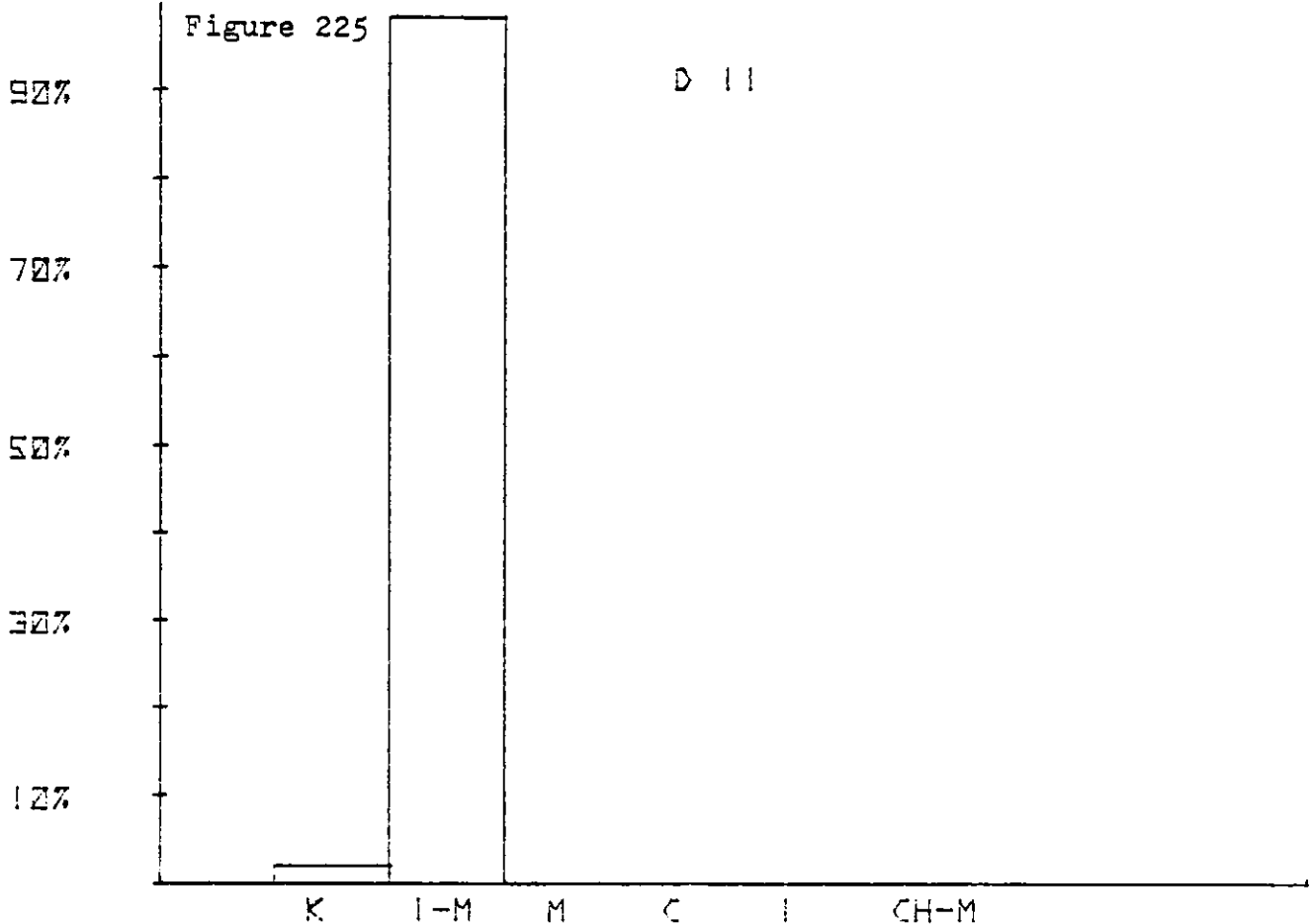
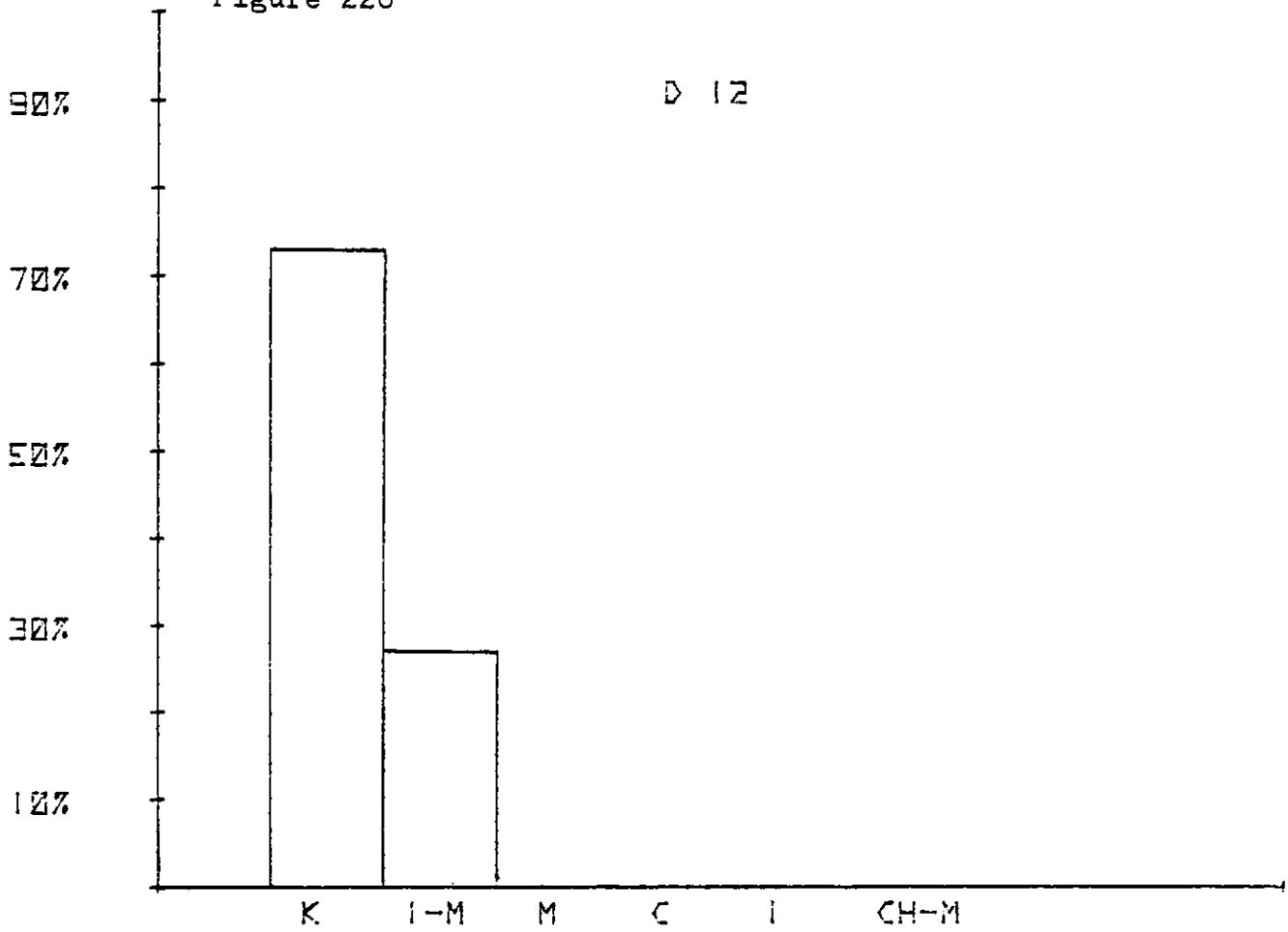
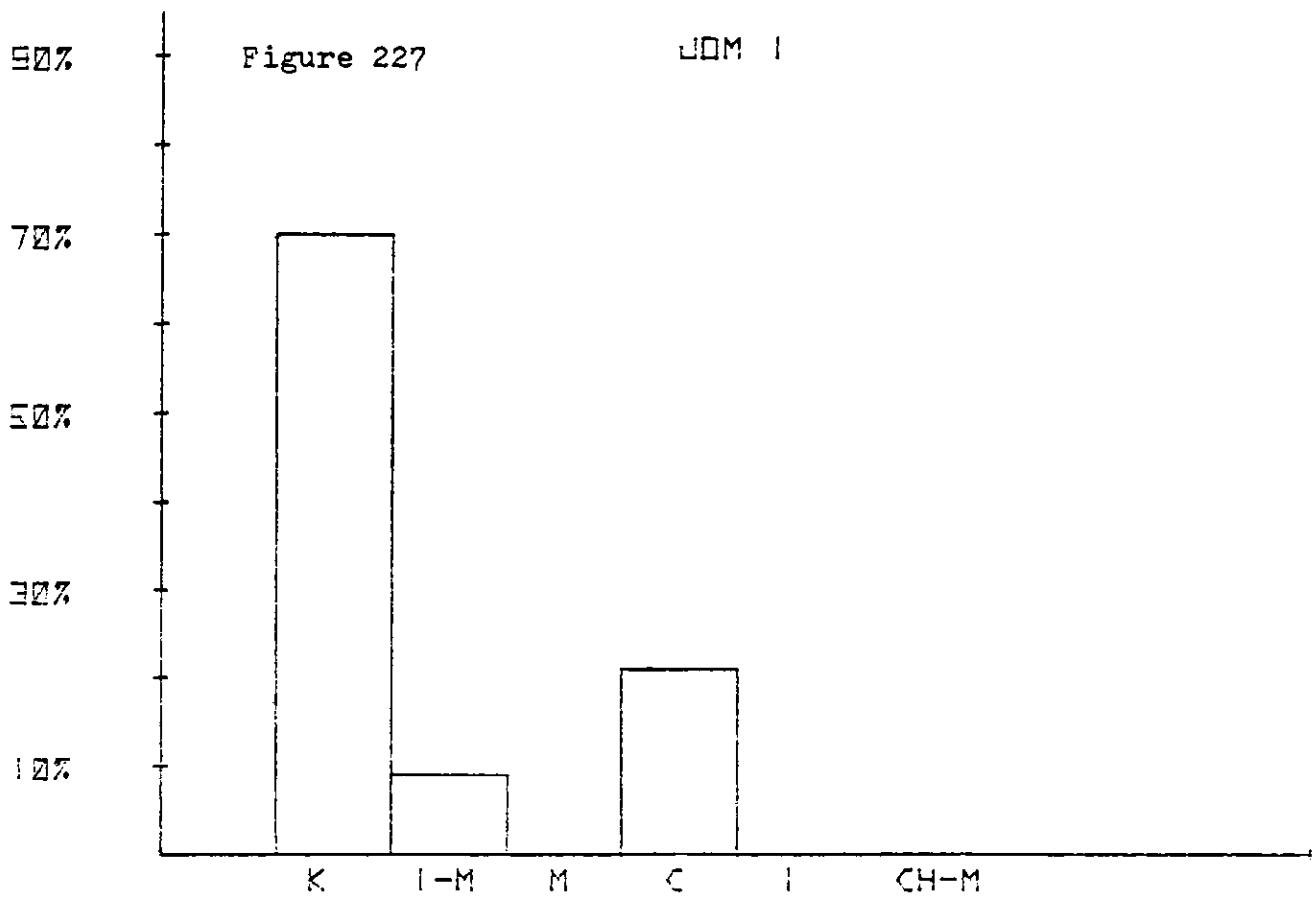


Figure 226



D 12

Figure 227



DOM 1

Figure 228

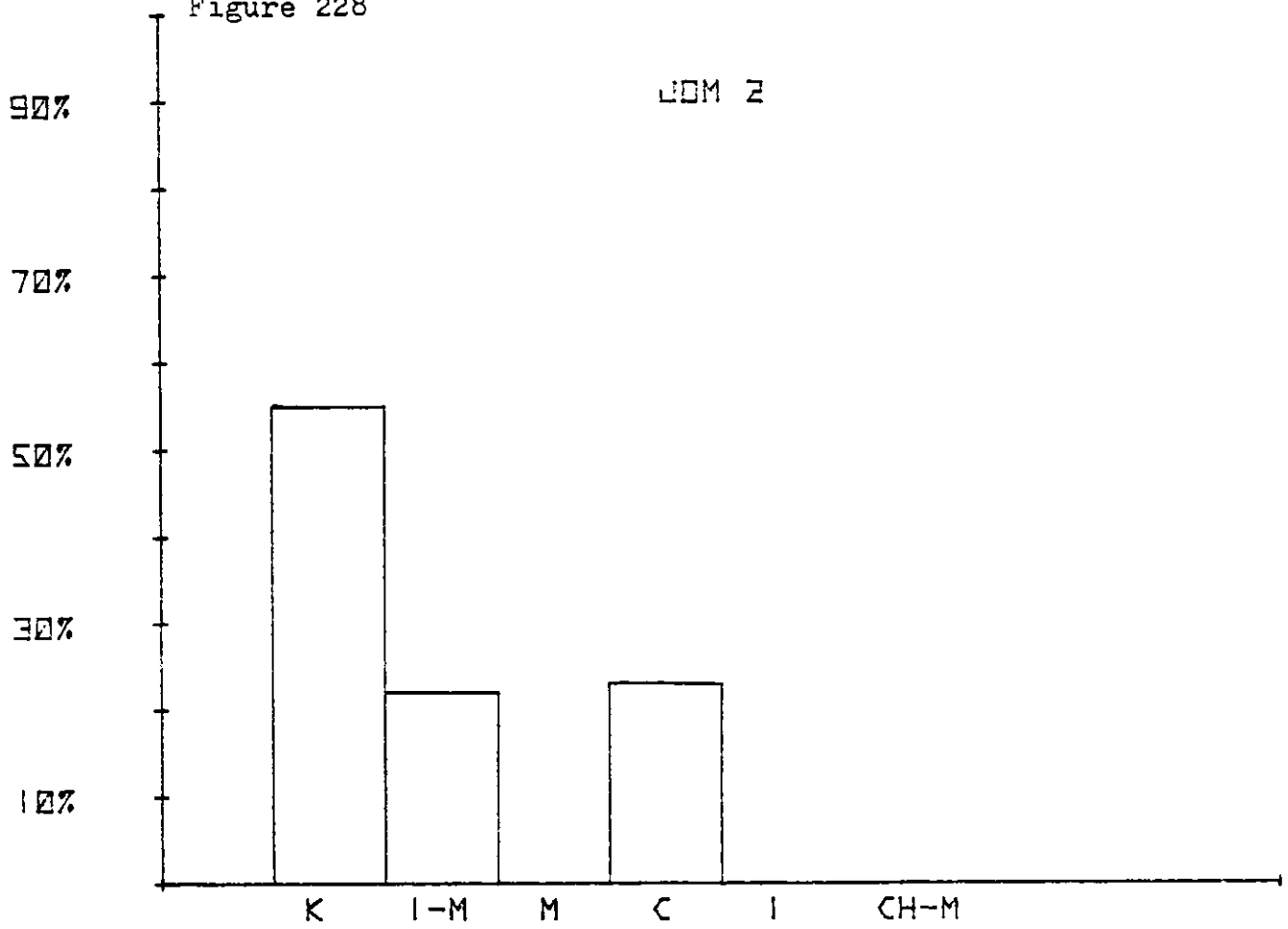


Figure 229

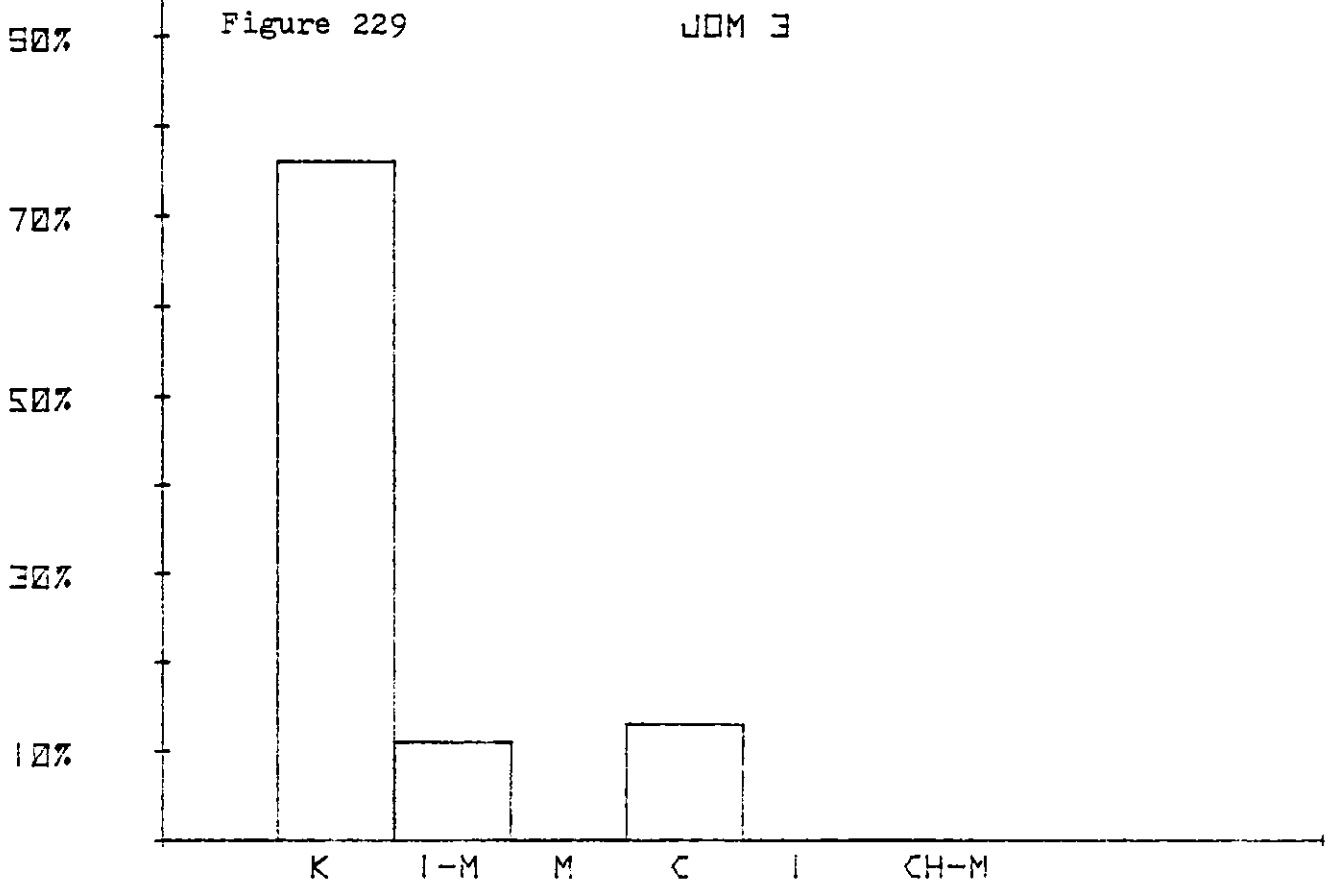


Figure 230

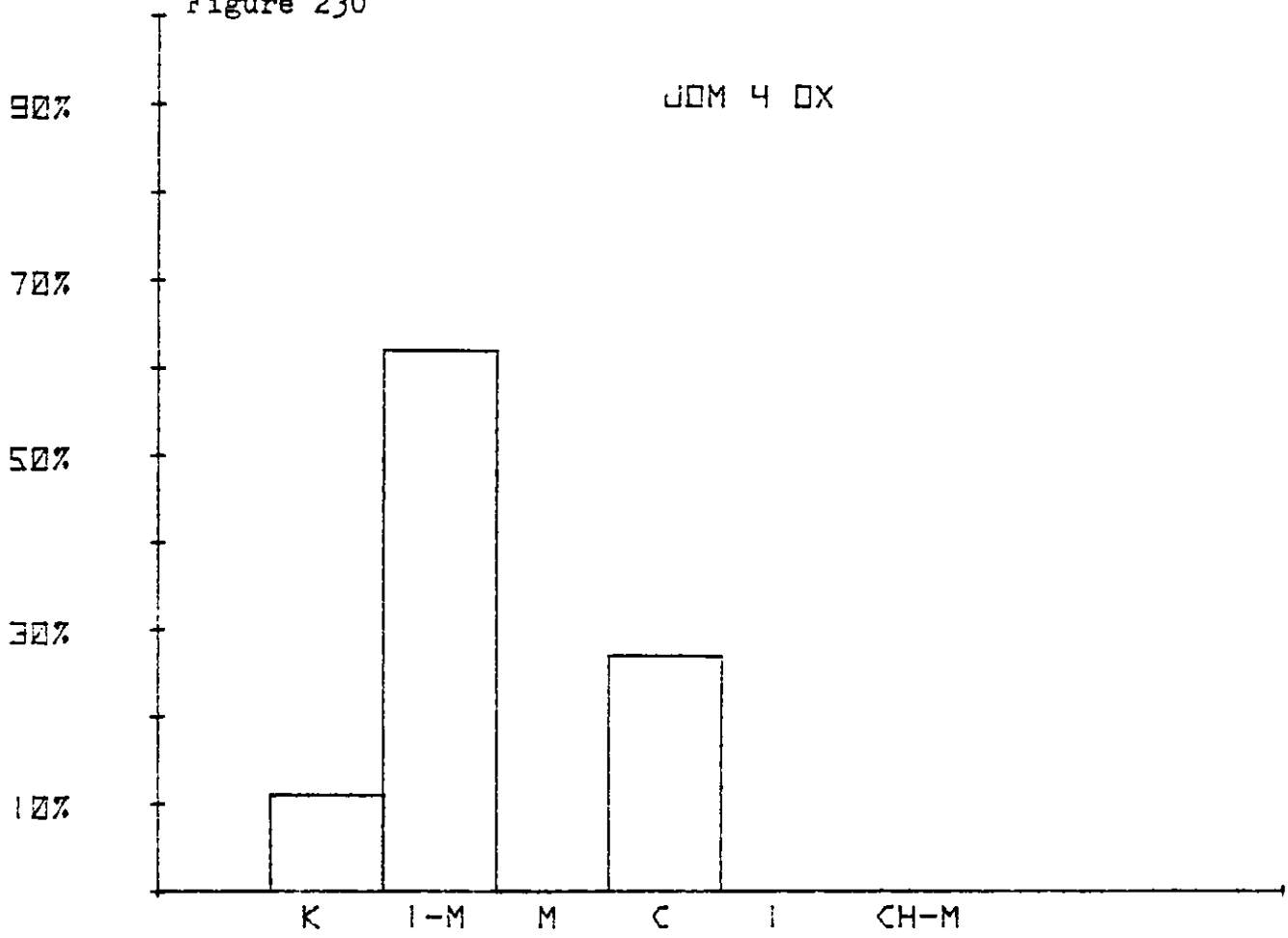


Figure 231

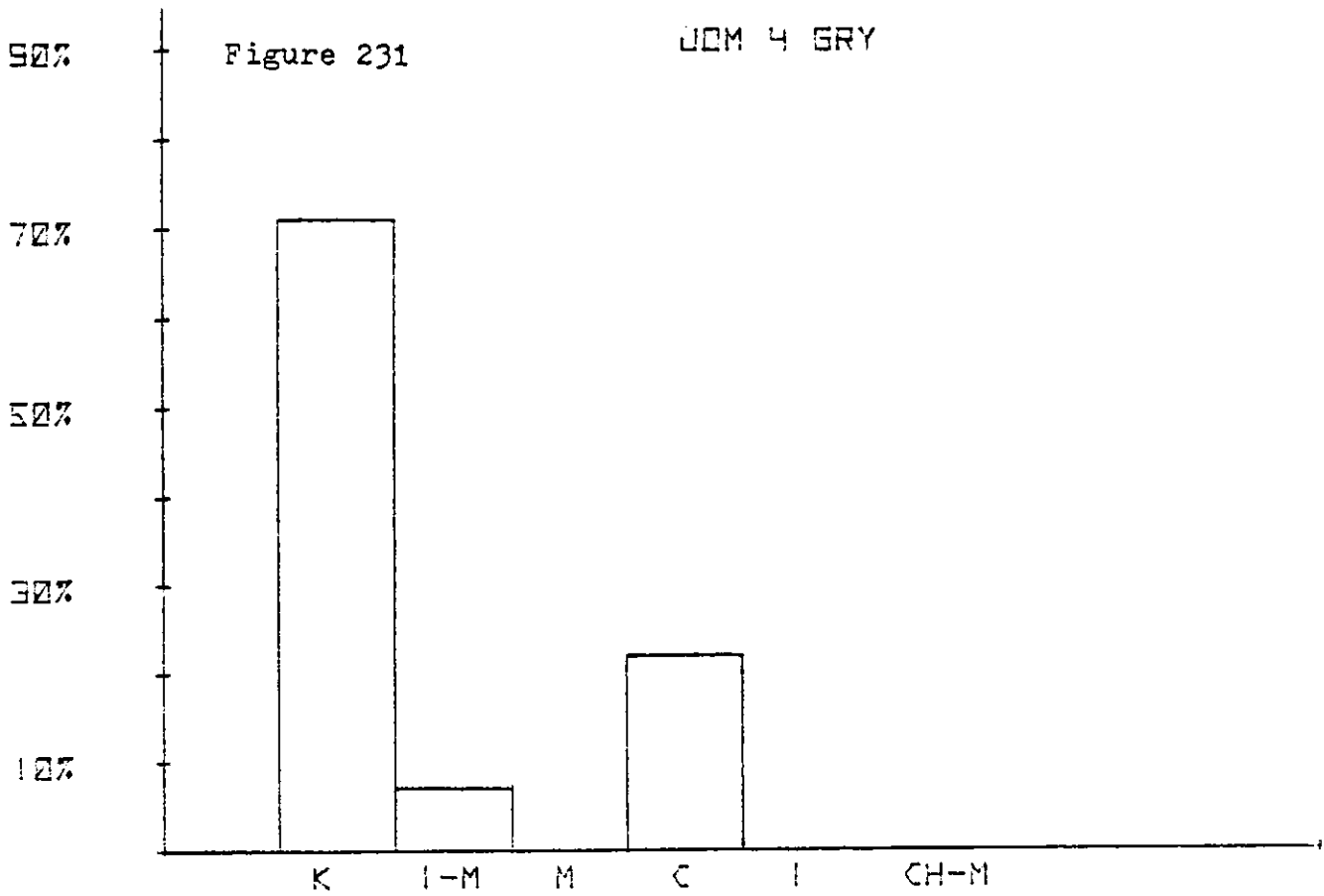


Figure 232

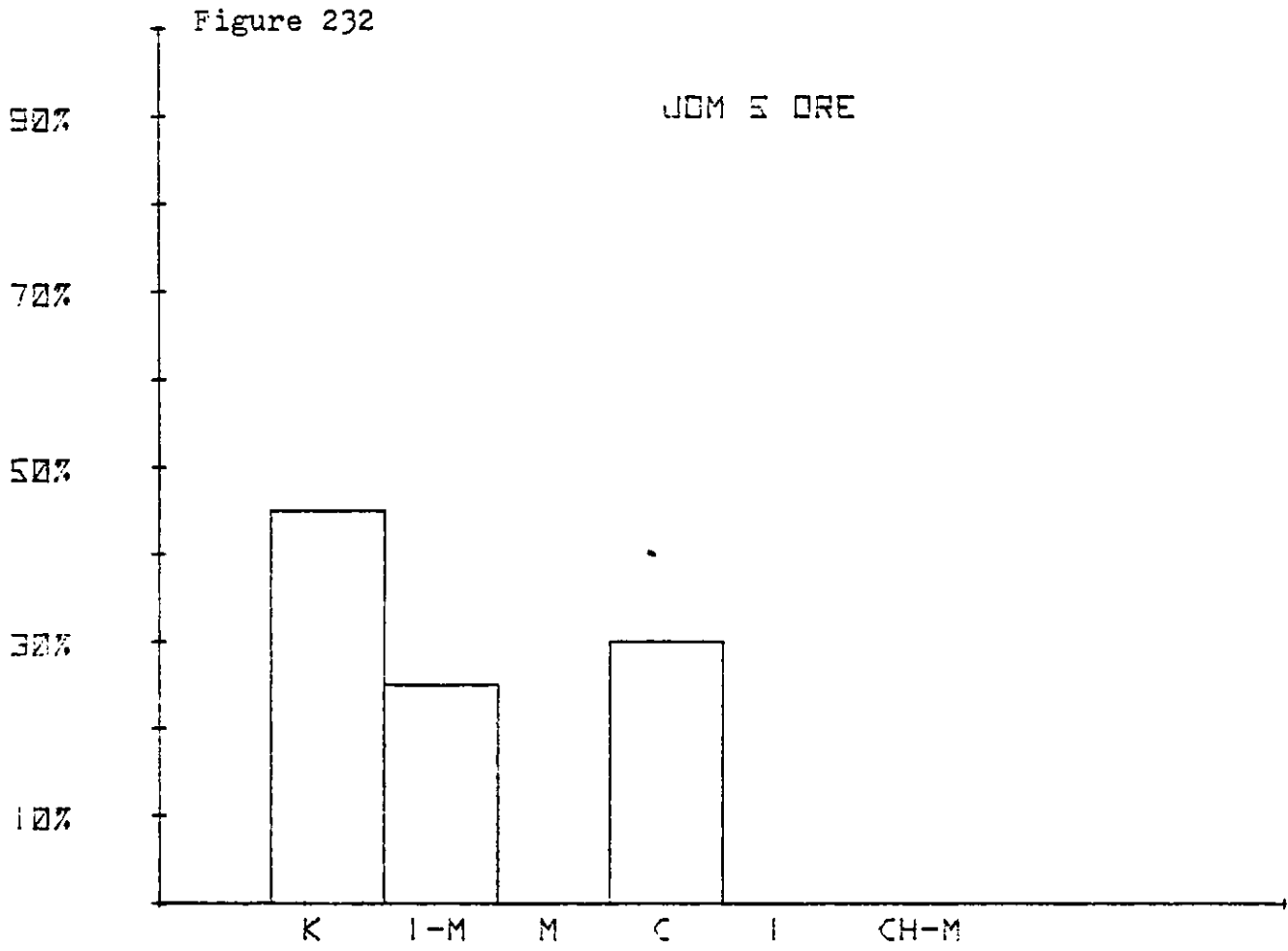


Figure 233

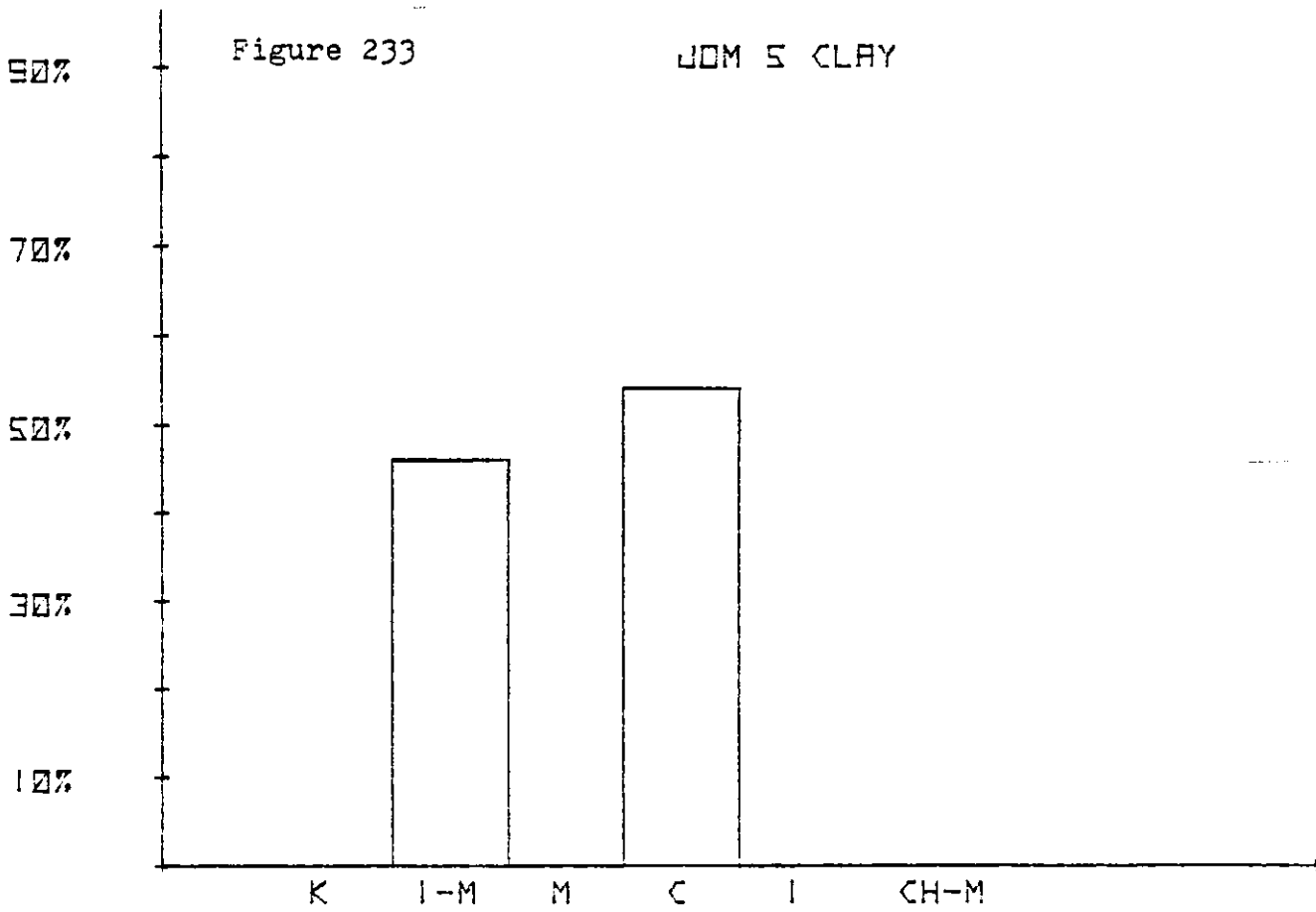


Figure 234

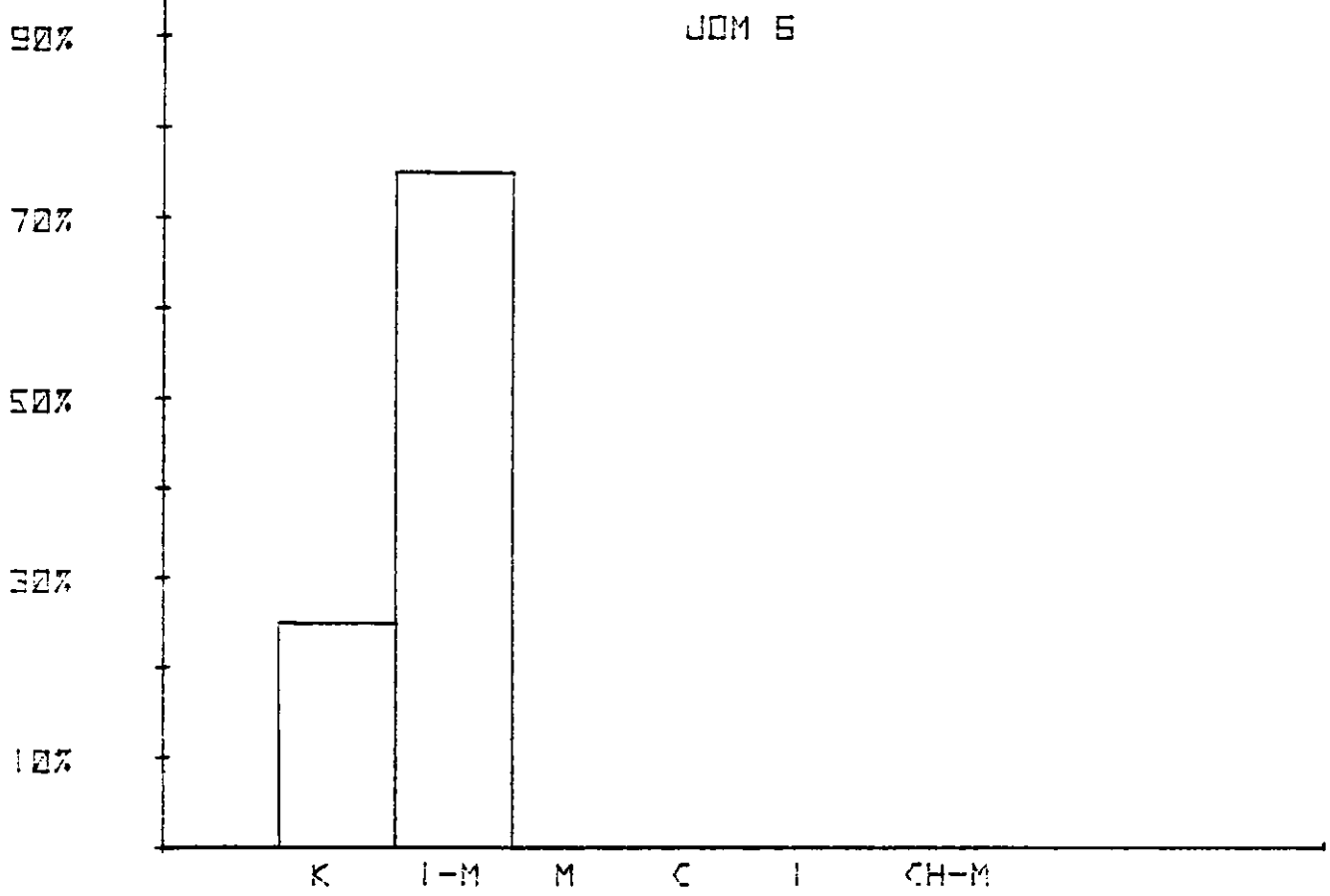


Figure 235

JOM 7

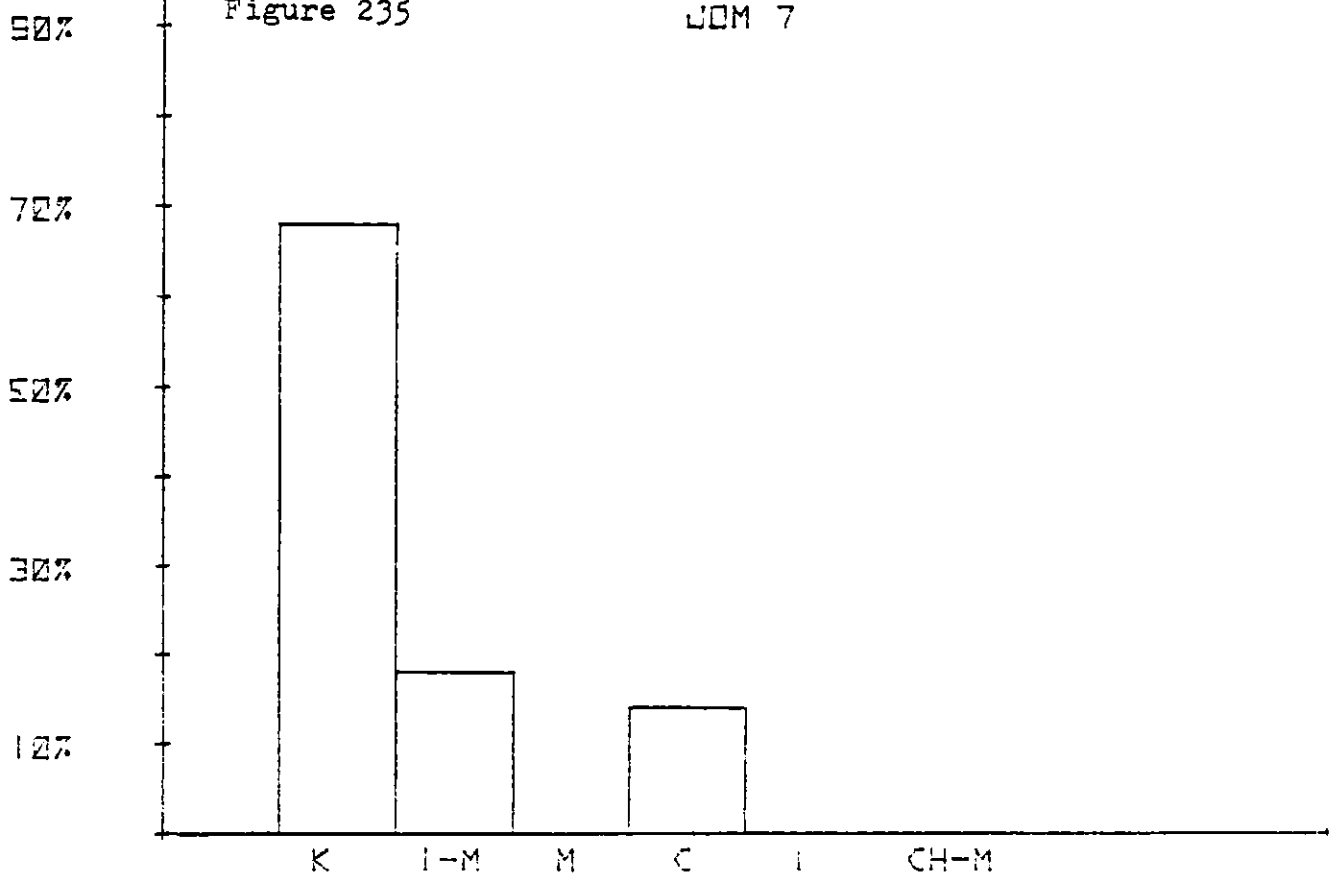


Figure 236

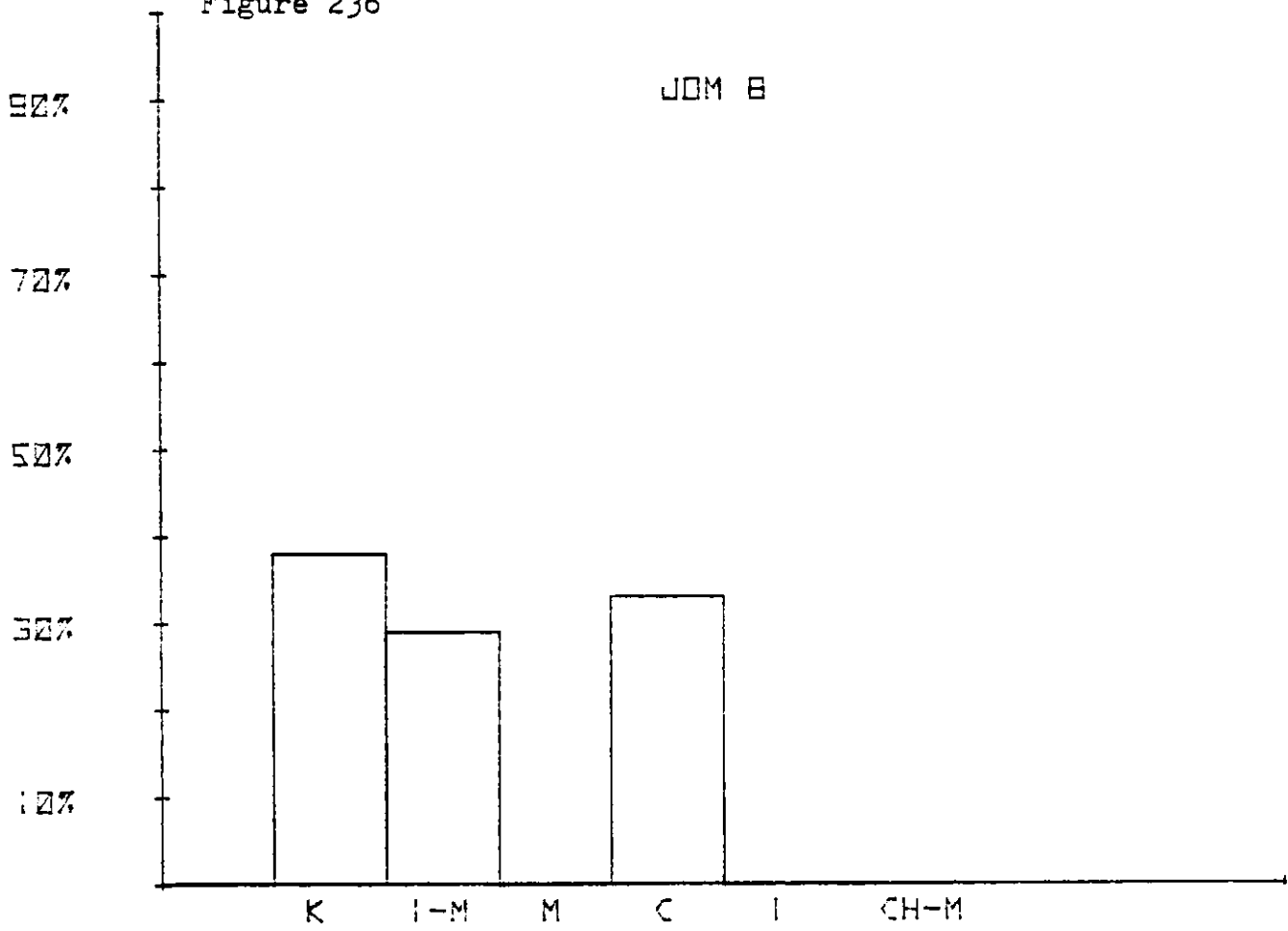


Figure 237

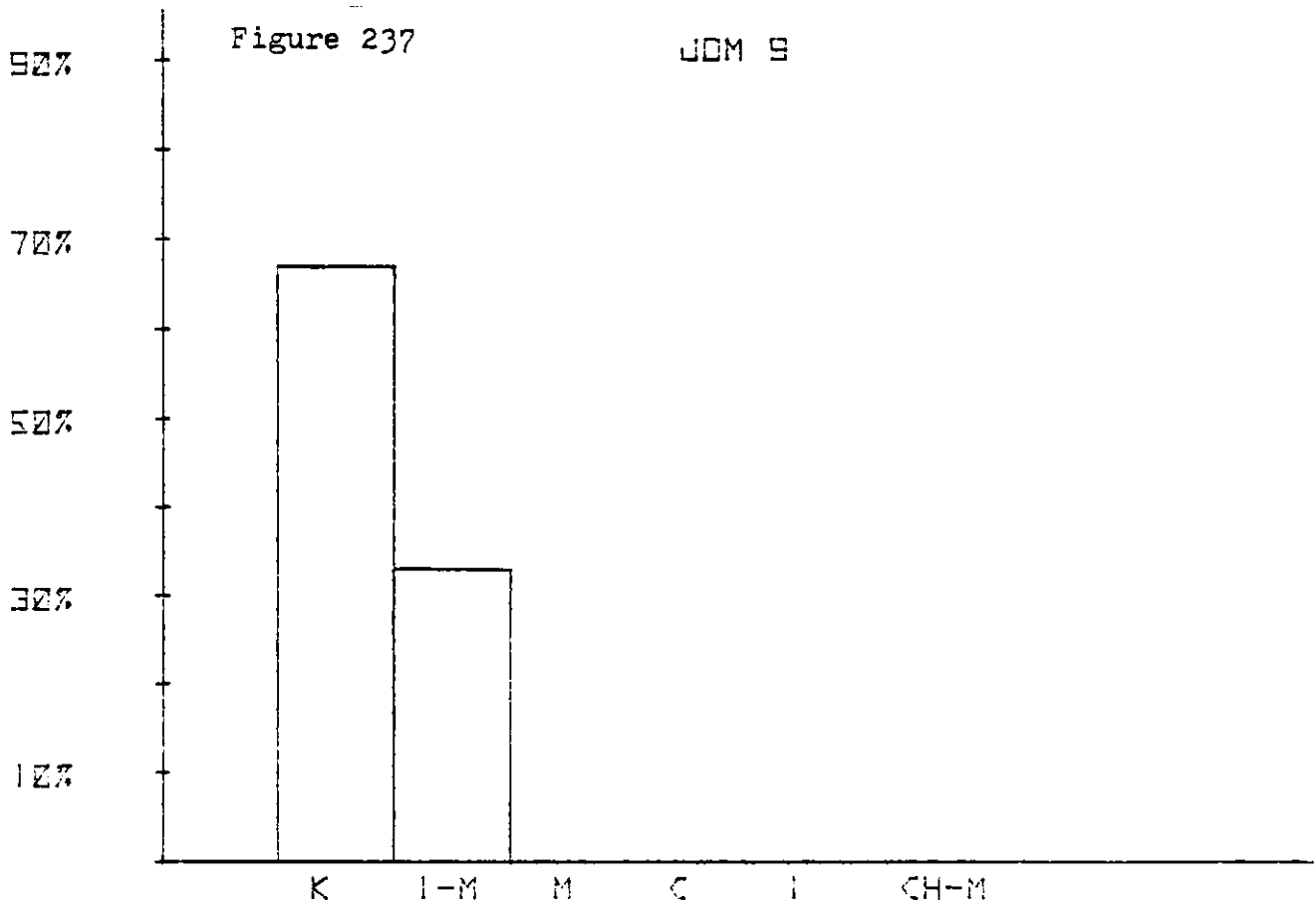


Figure 238

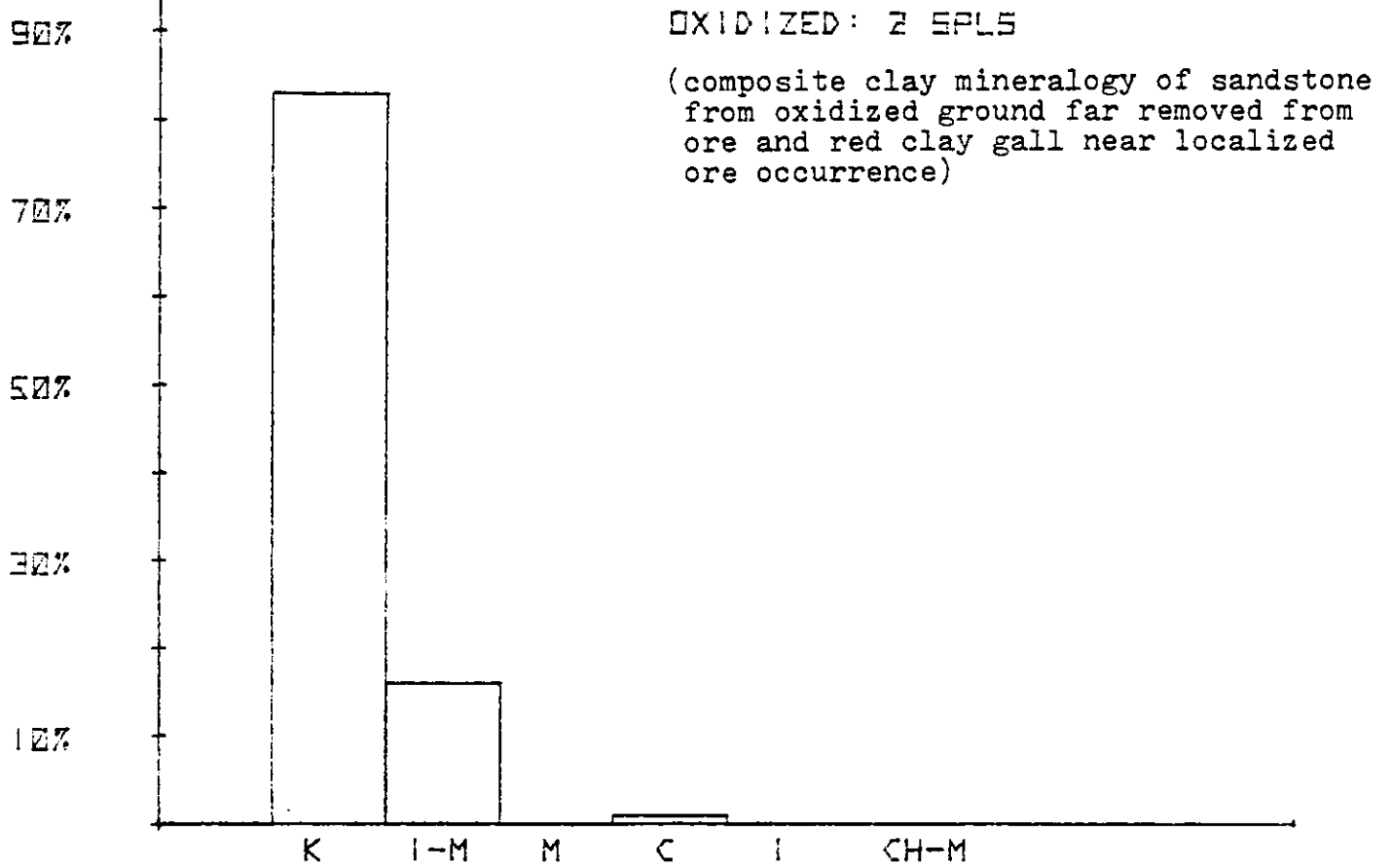
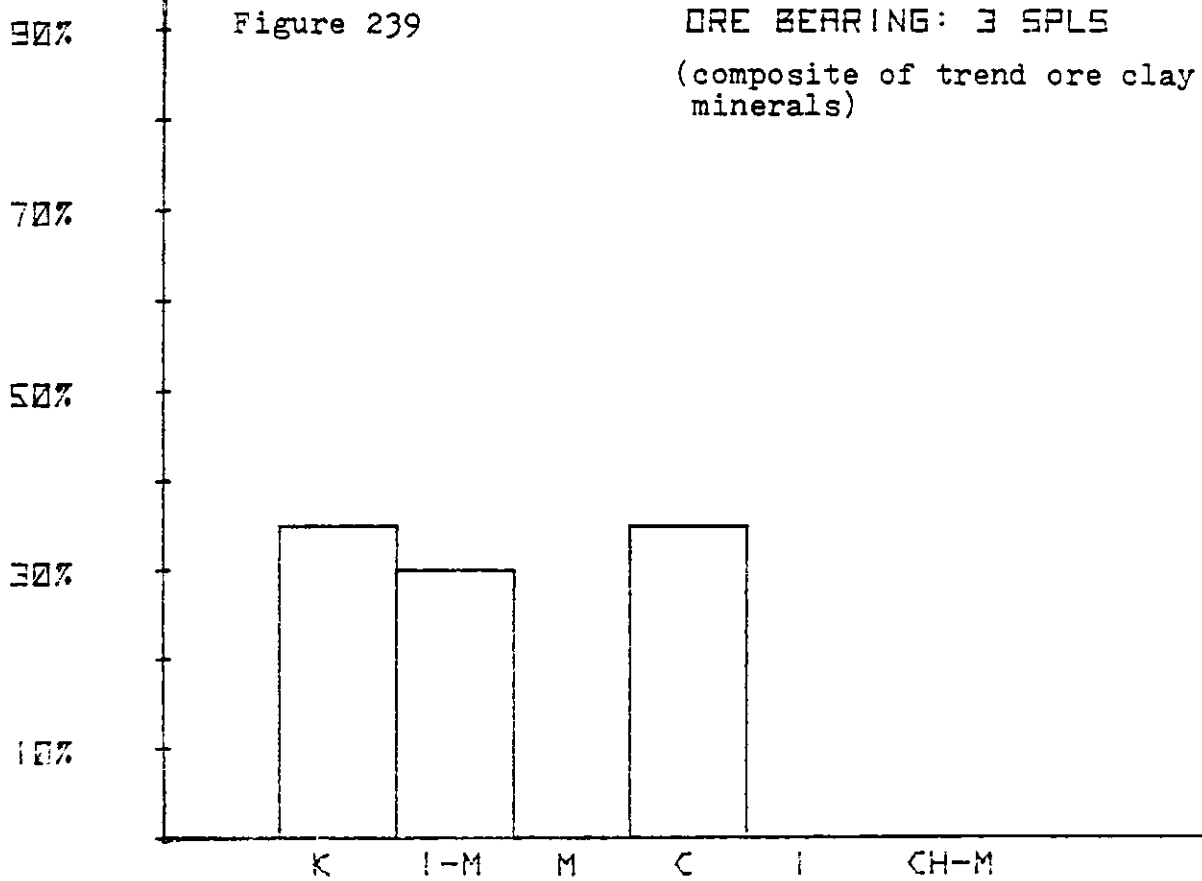


Figure 239



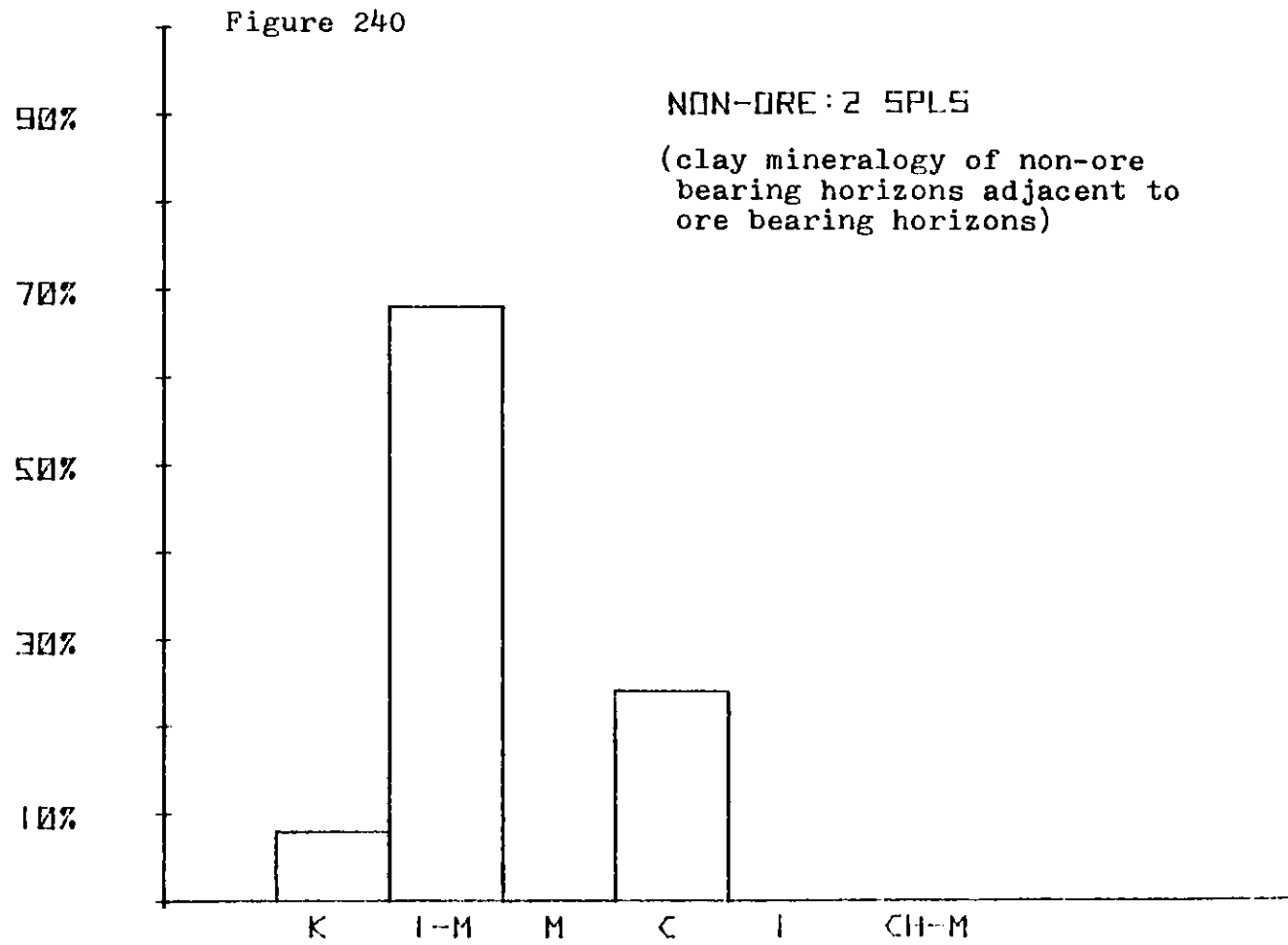
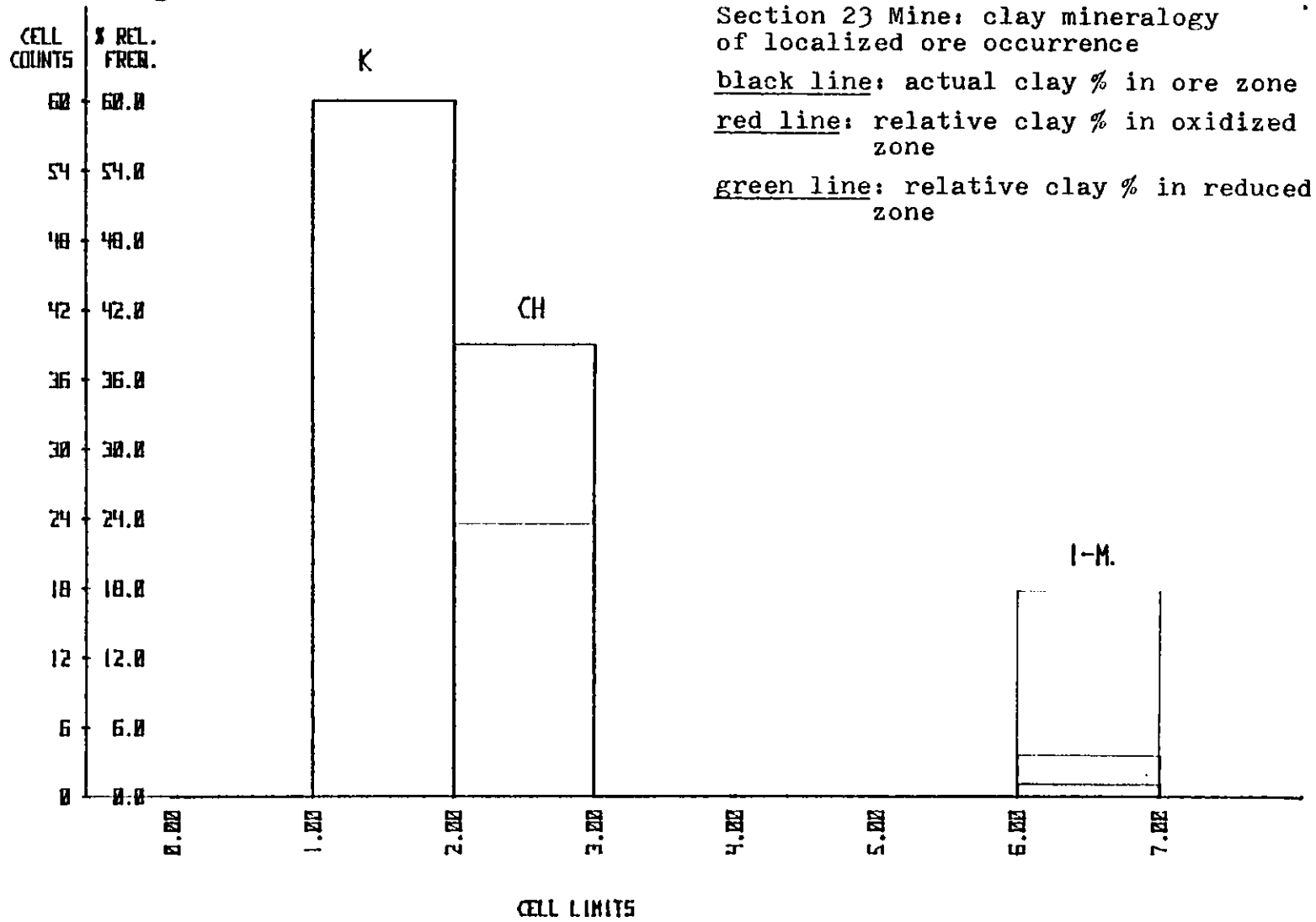


Figure 241



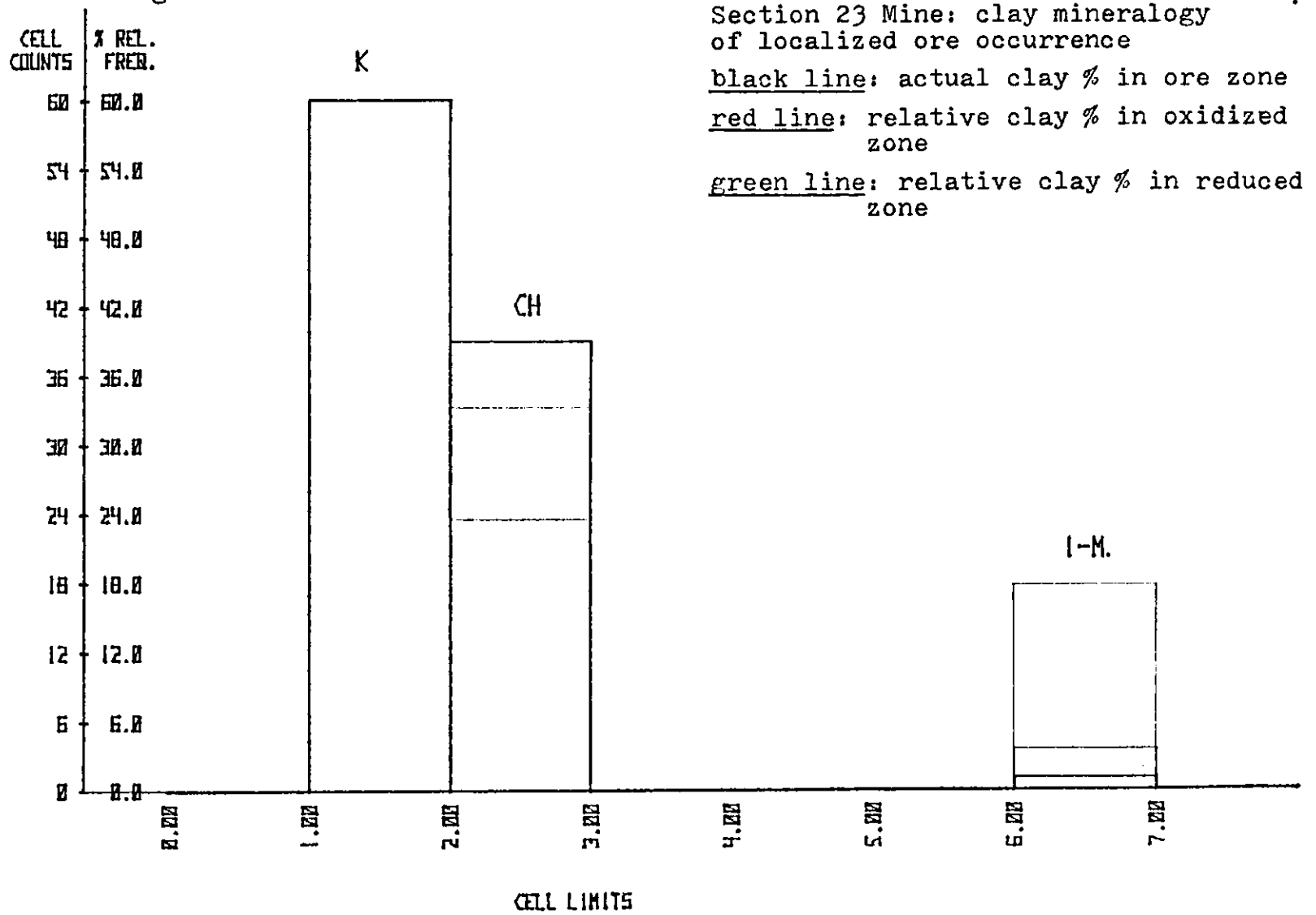
Section 23 Mine: clay mineralogy
of localized ore occurrence

black line: actual clay % in ore zone

red line: relative clay % in oxidized
zone

green line: relative clay % in reduced
zone

Figure 241



Section 23 Mine: clay mineralogy of localized ore occurrence

black line: actual clay % in ore zone
red line: relative clay % in oxidized zone

green line: relative clay % in reduced zone

Figure 242

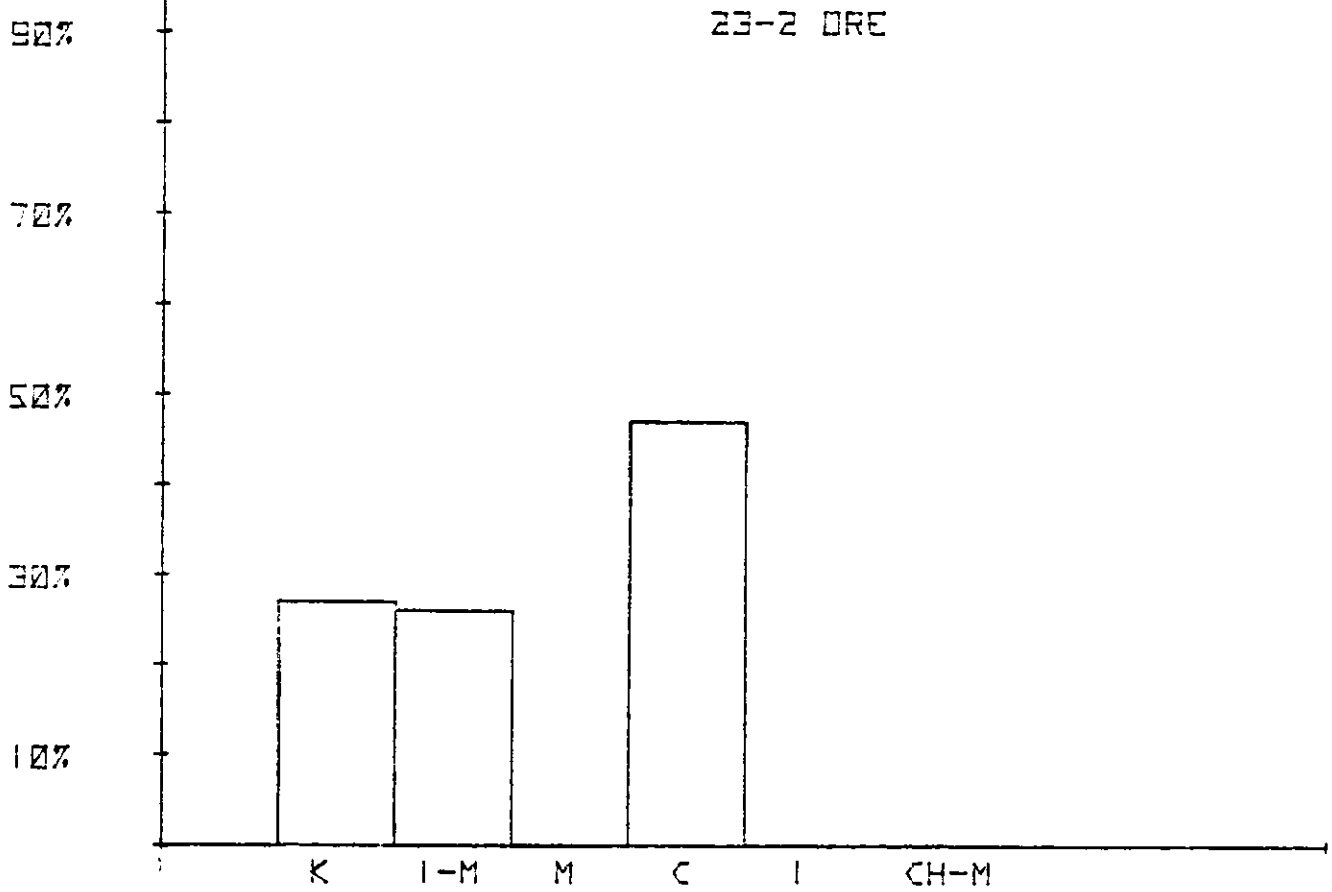


Figure 243

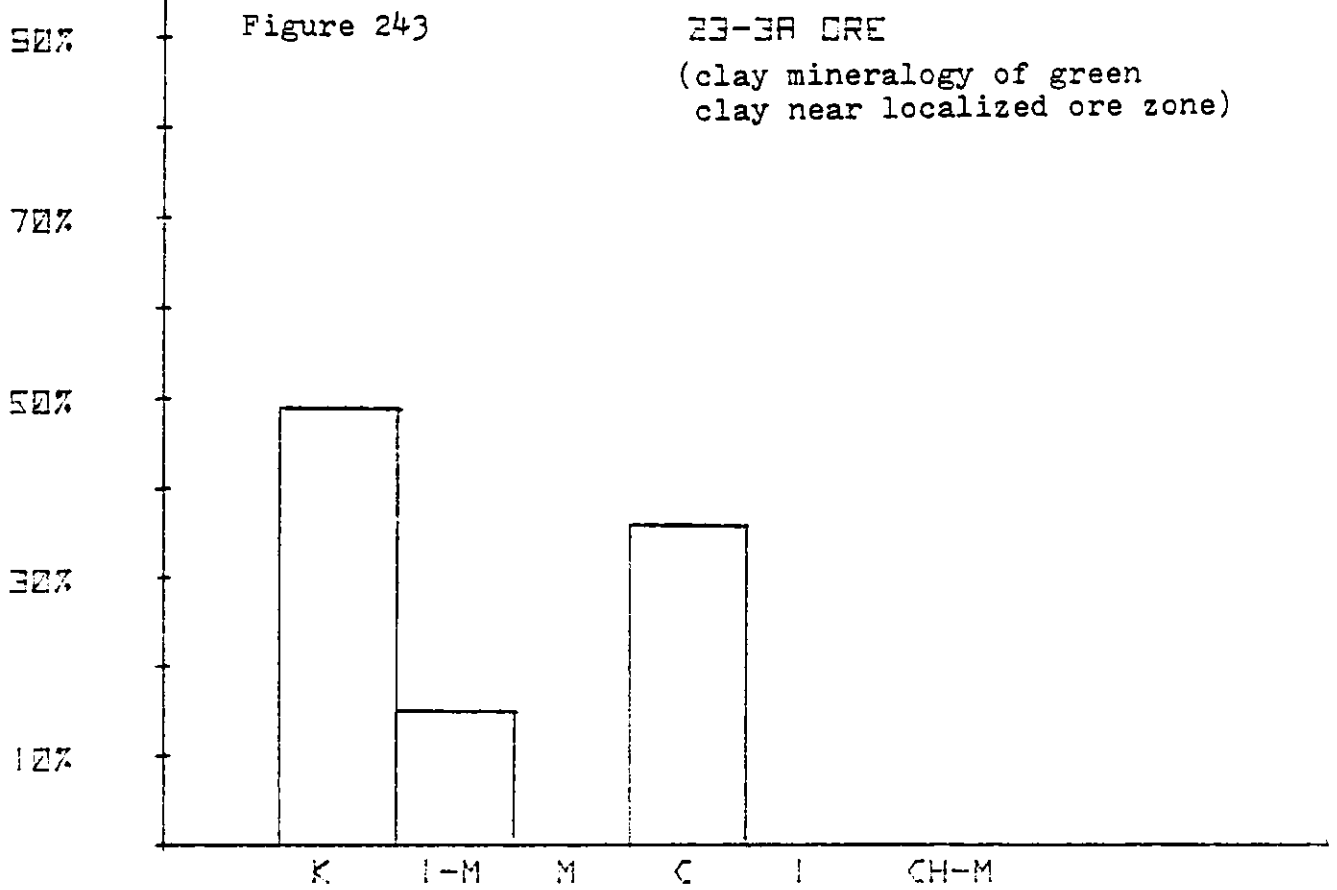


Figure 244

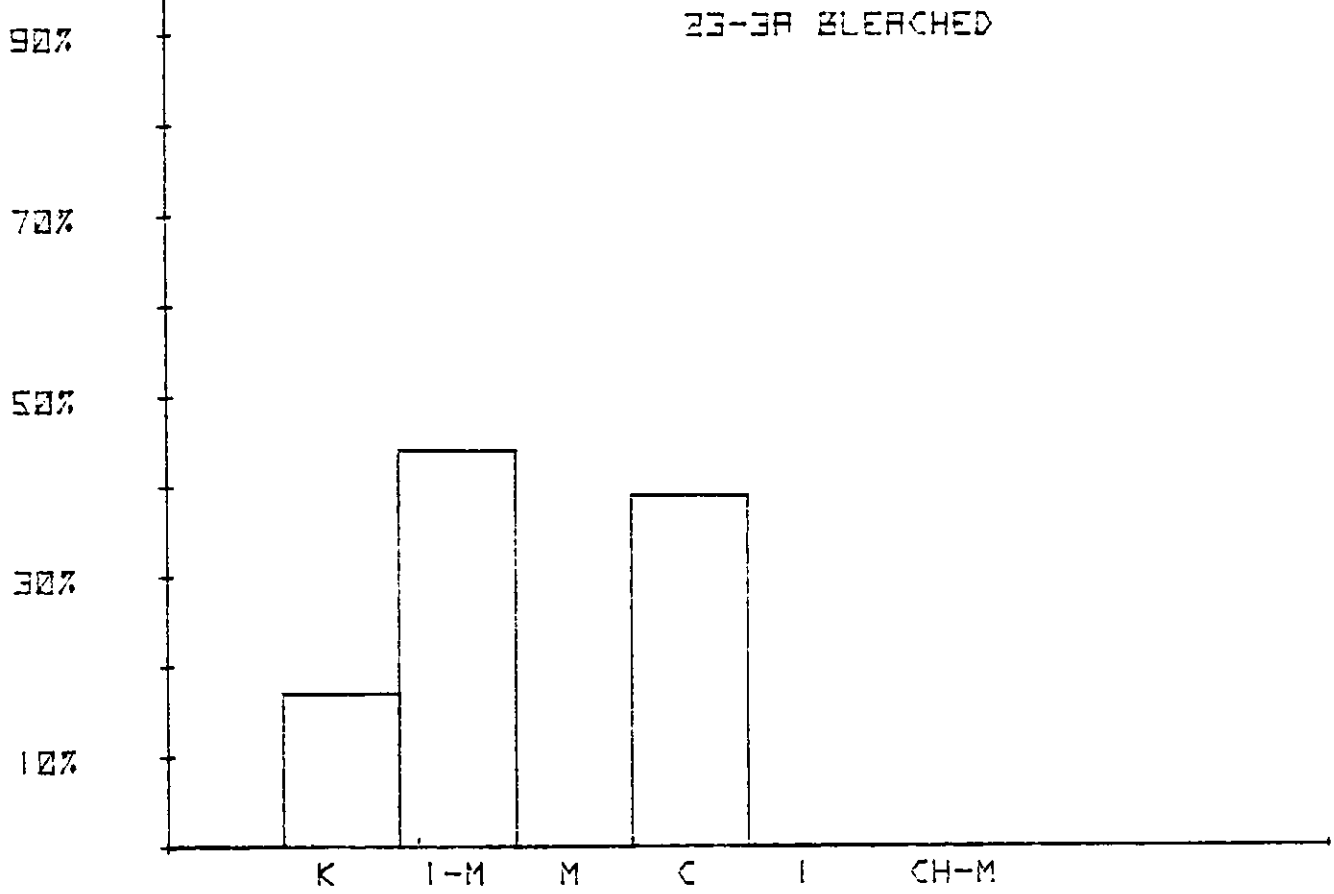


Figure 245

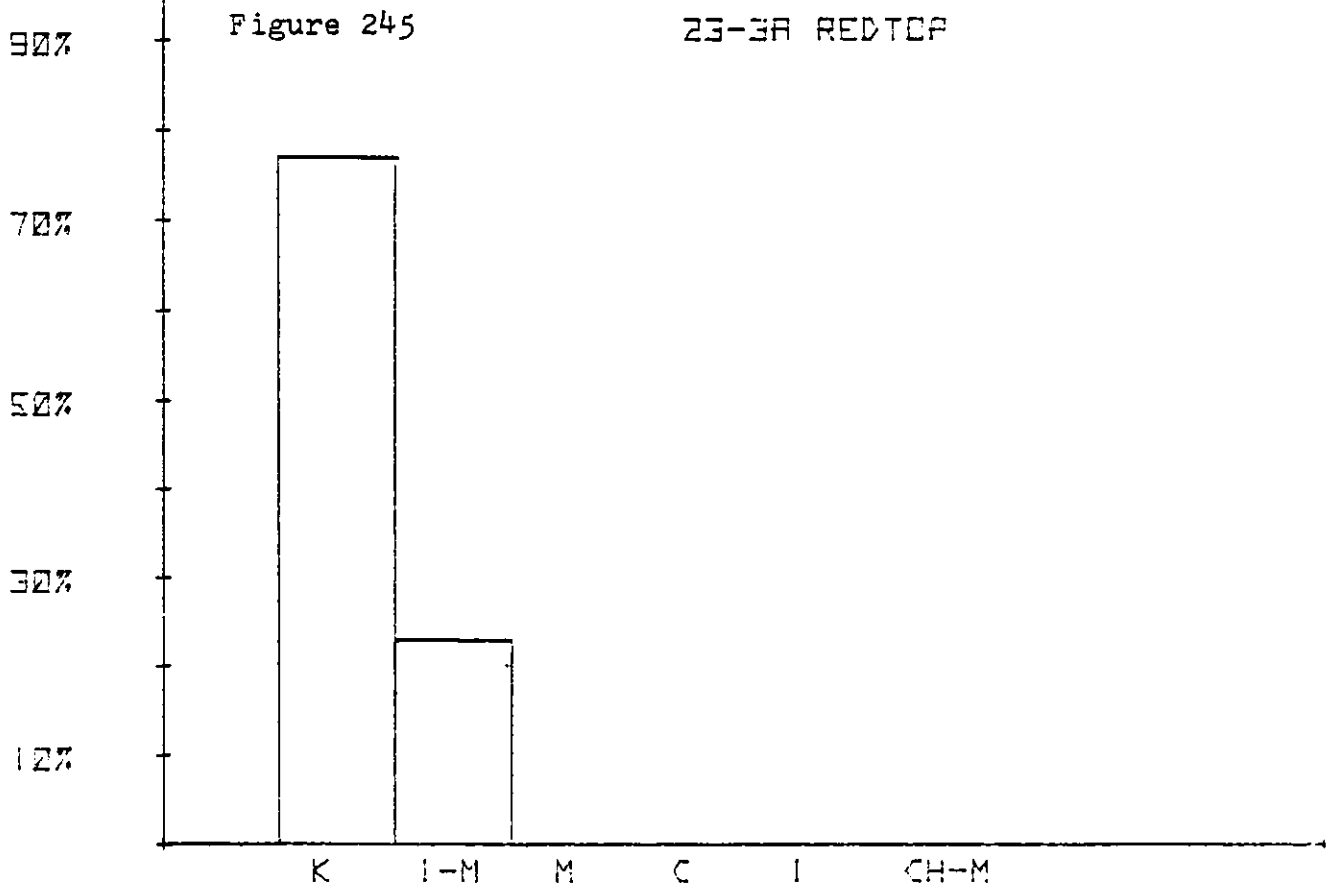


Figure 246

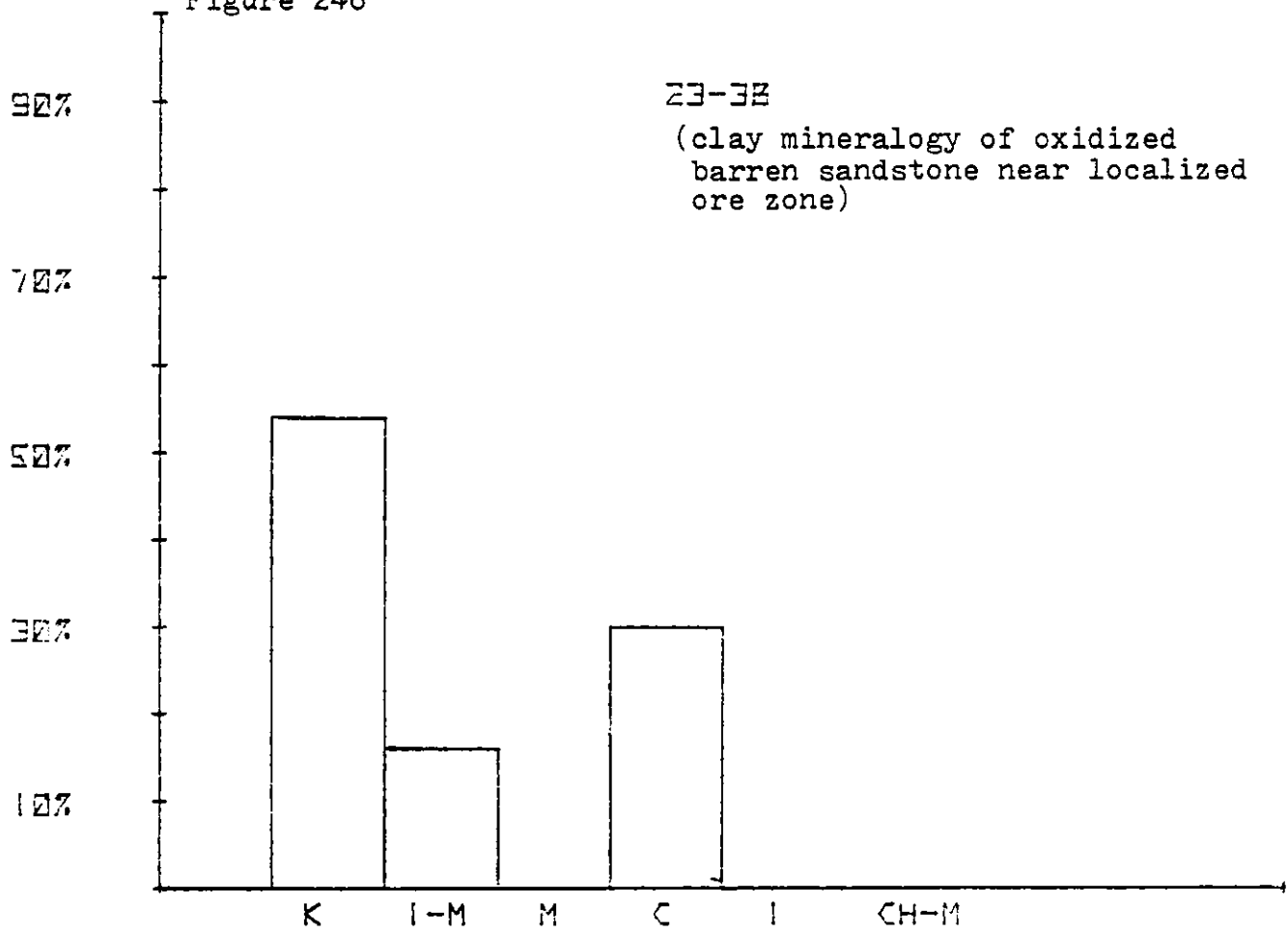


Figure 247

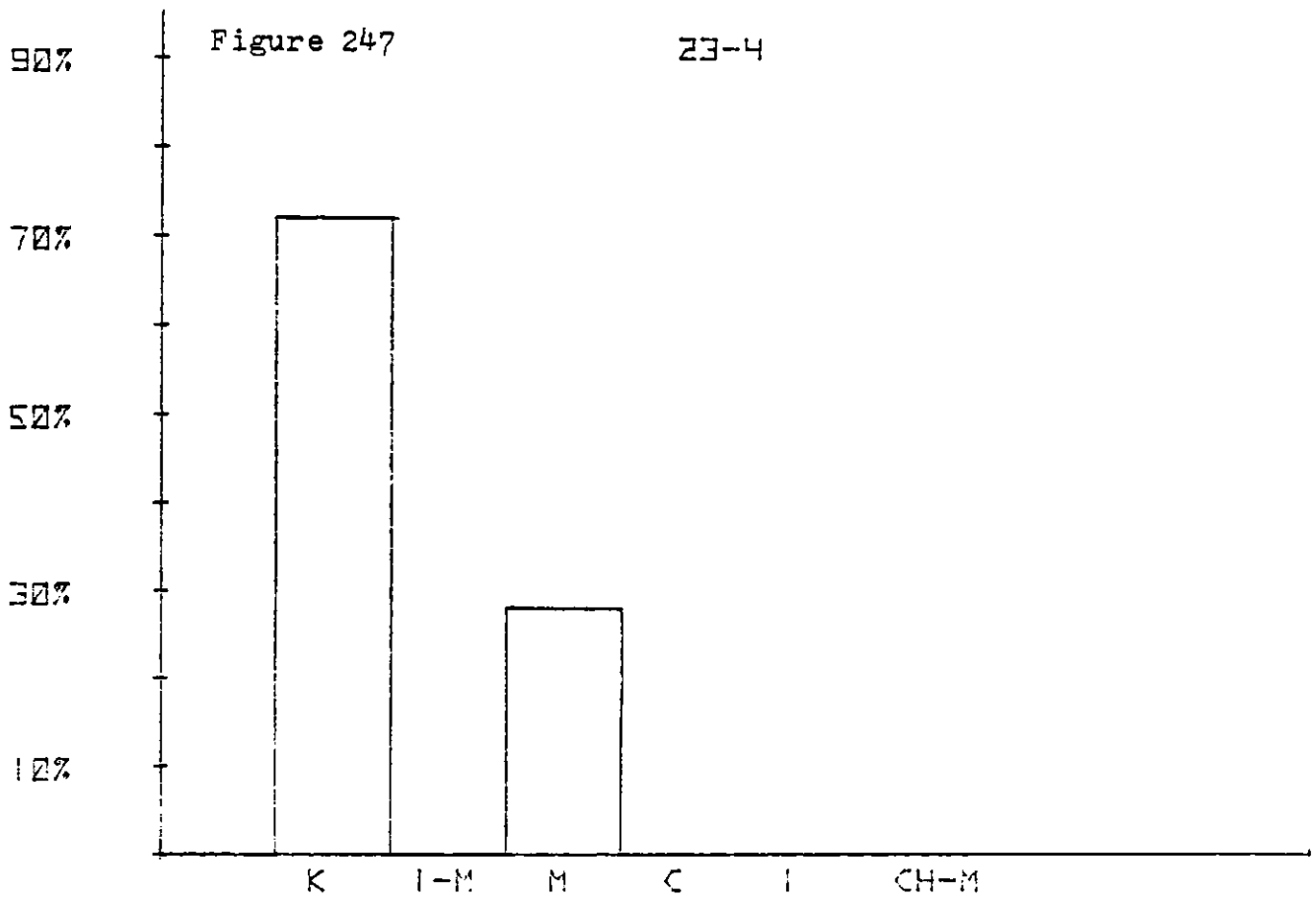


Figure 248

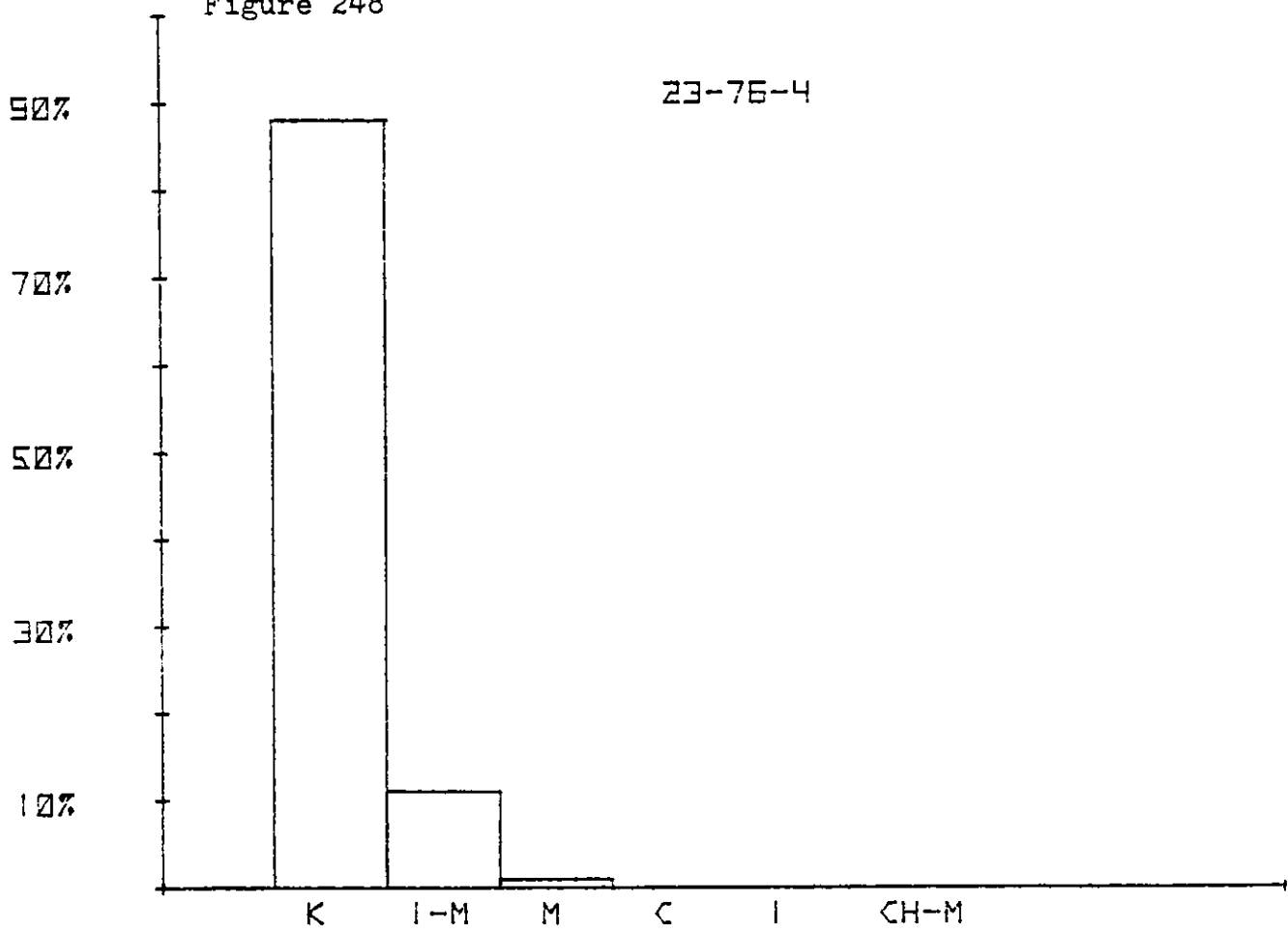


Figure 249

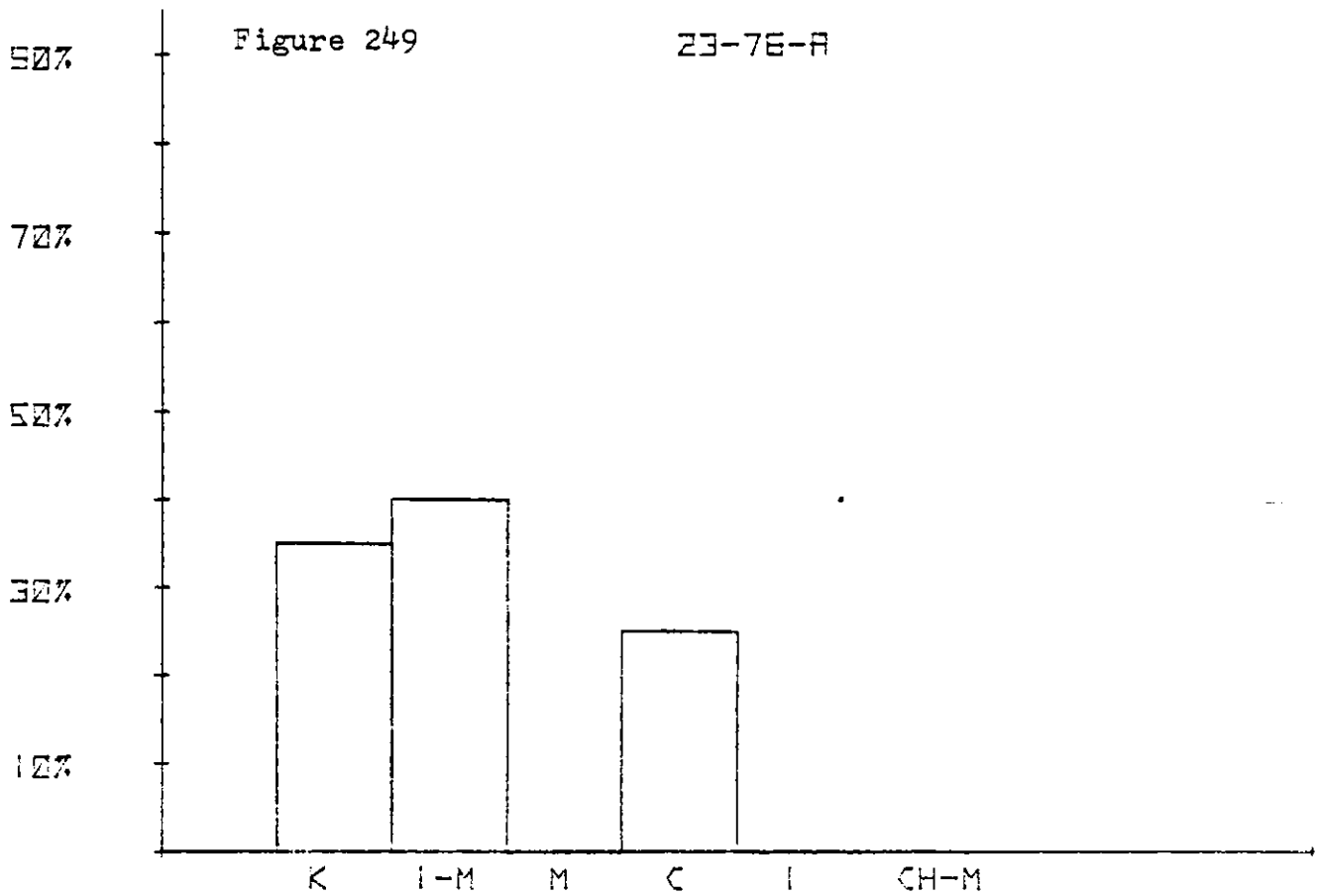


Figure 250

23-76-B

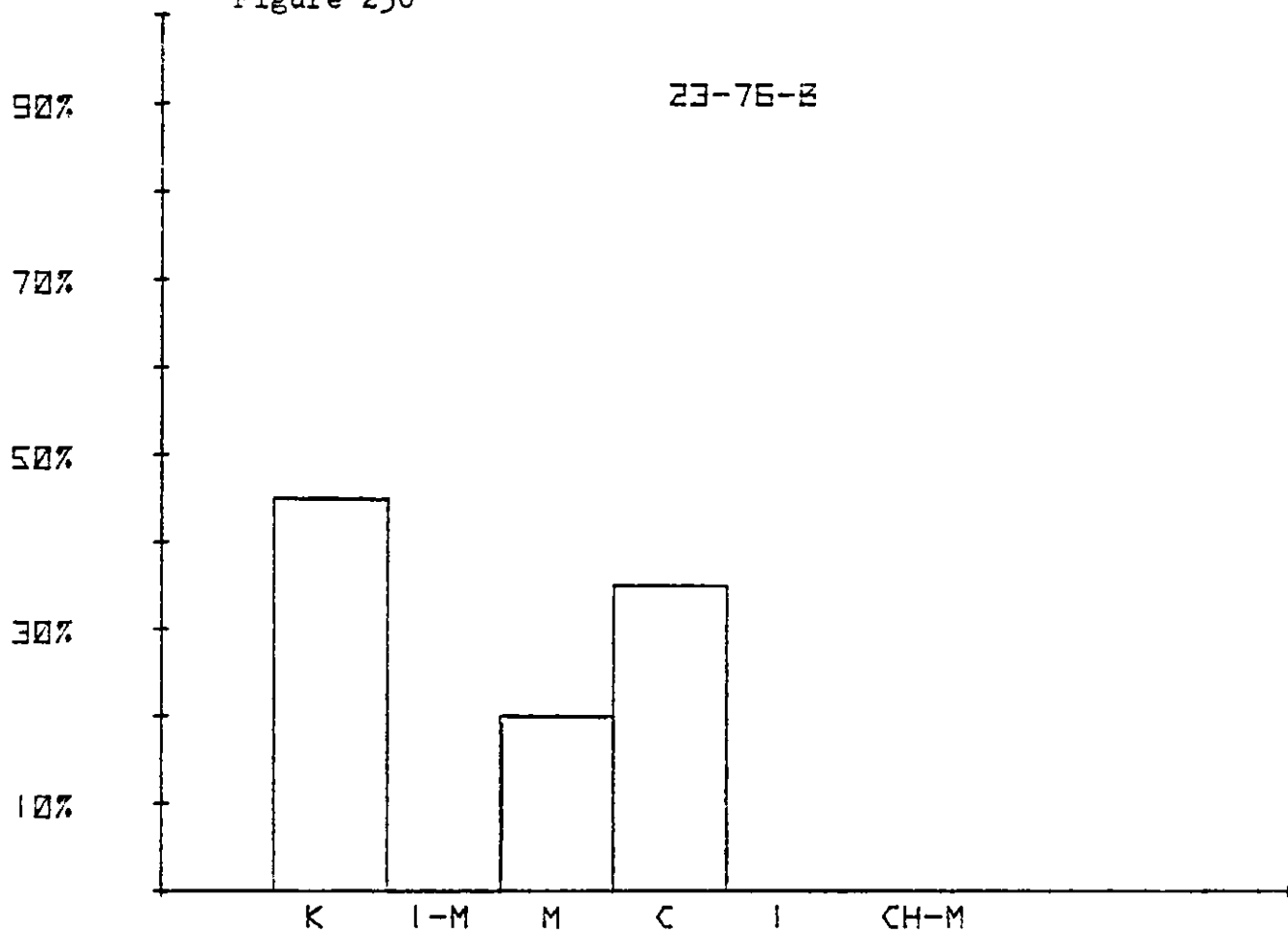


Figure 251

30 I

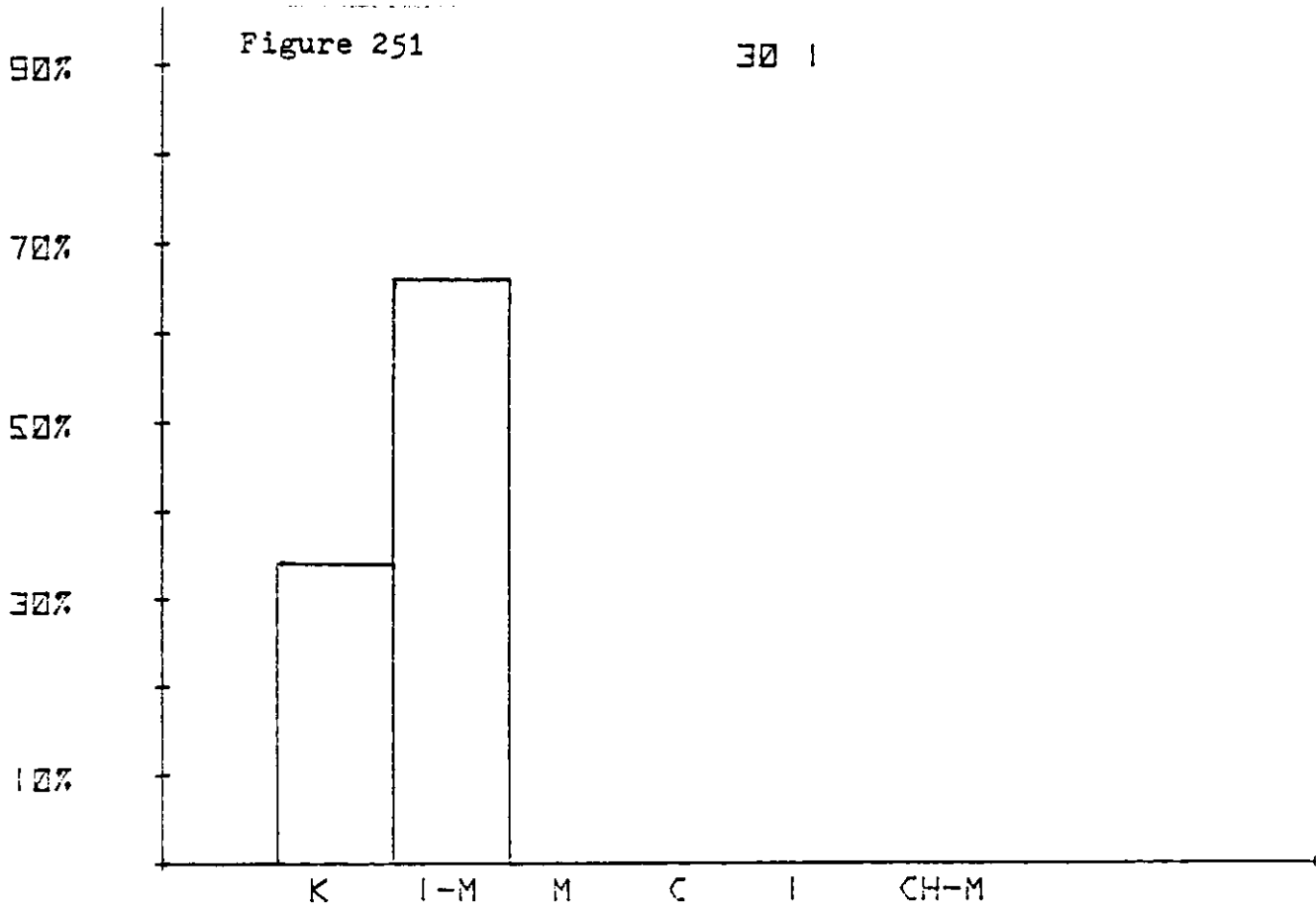


Figure 252

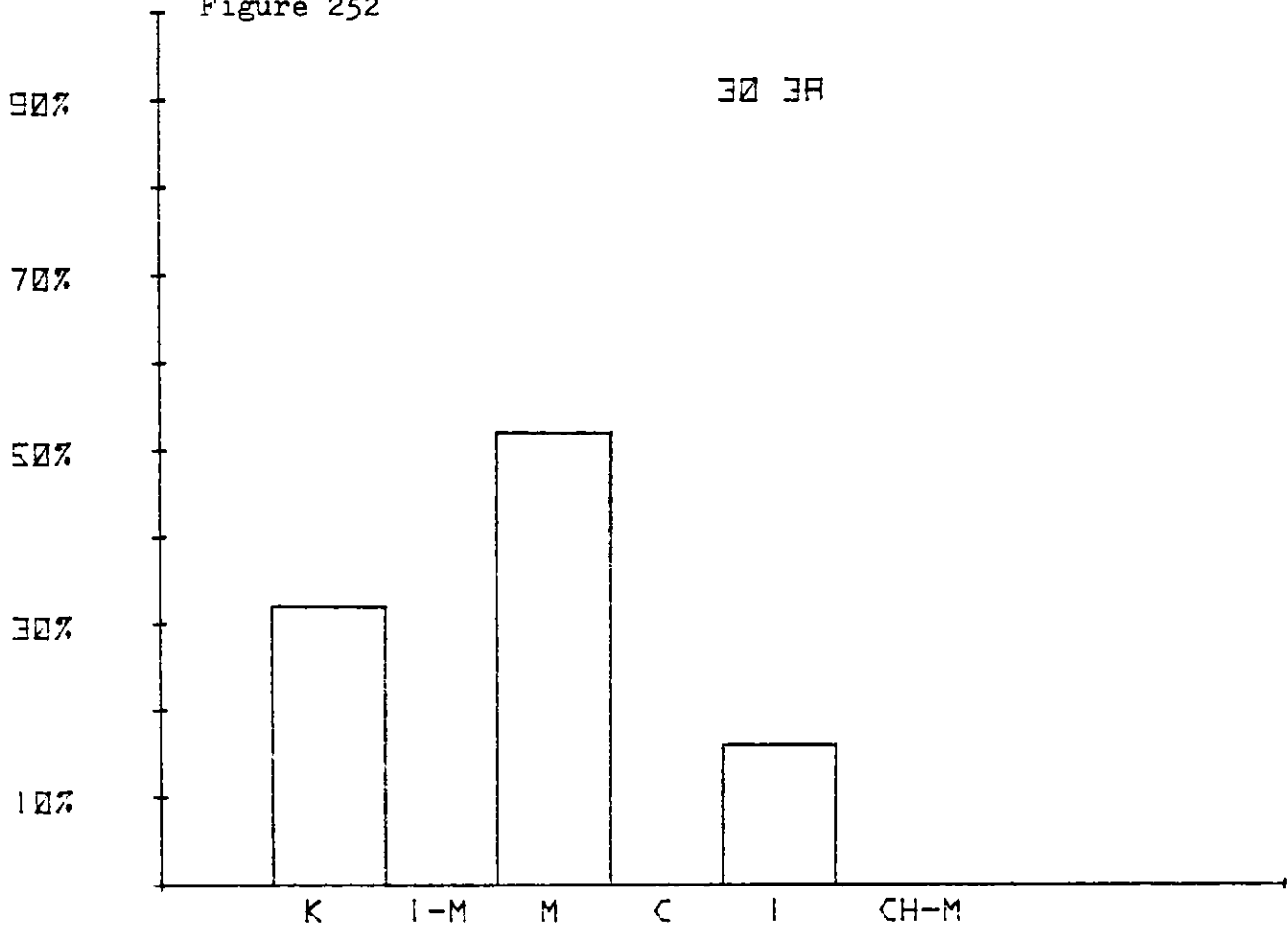


Figure 253

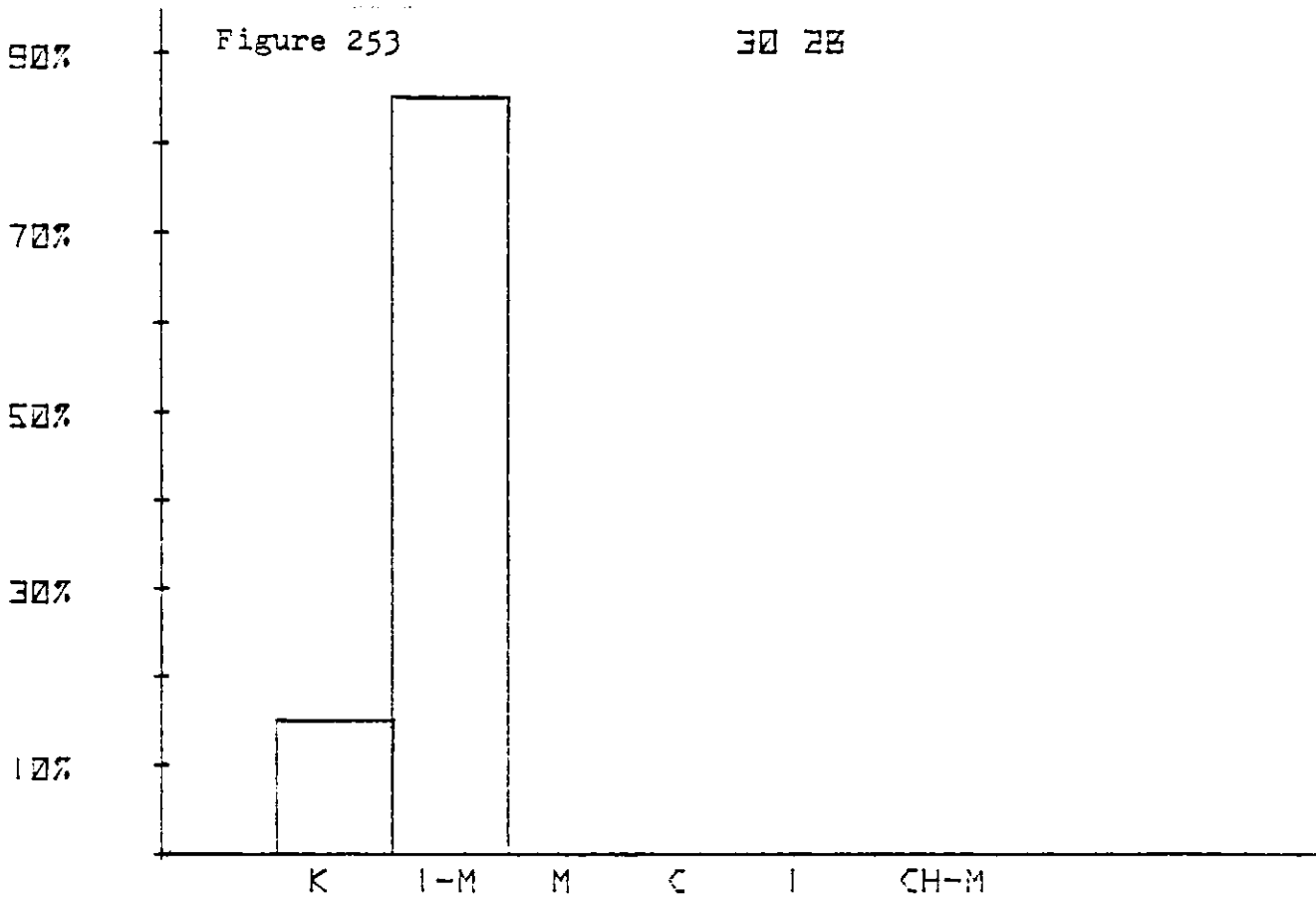


Figure 254

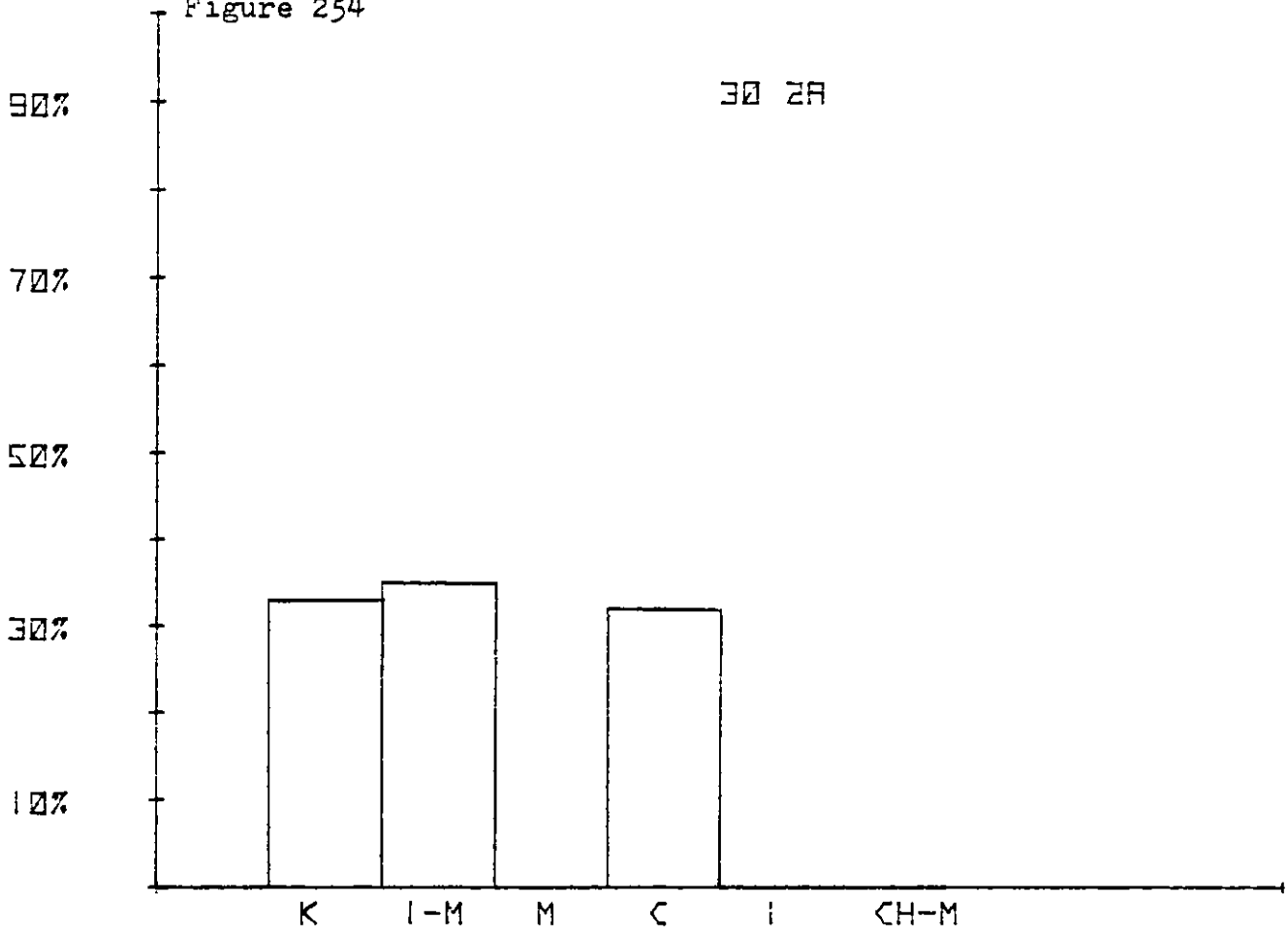


Figure 255

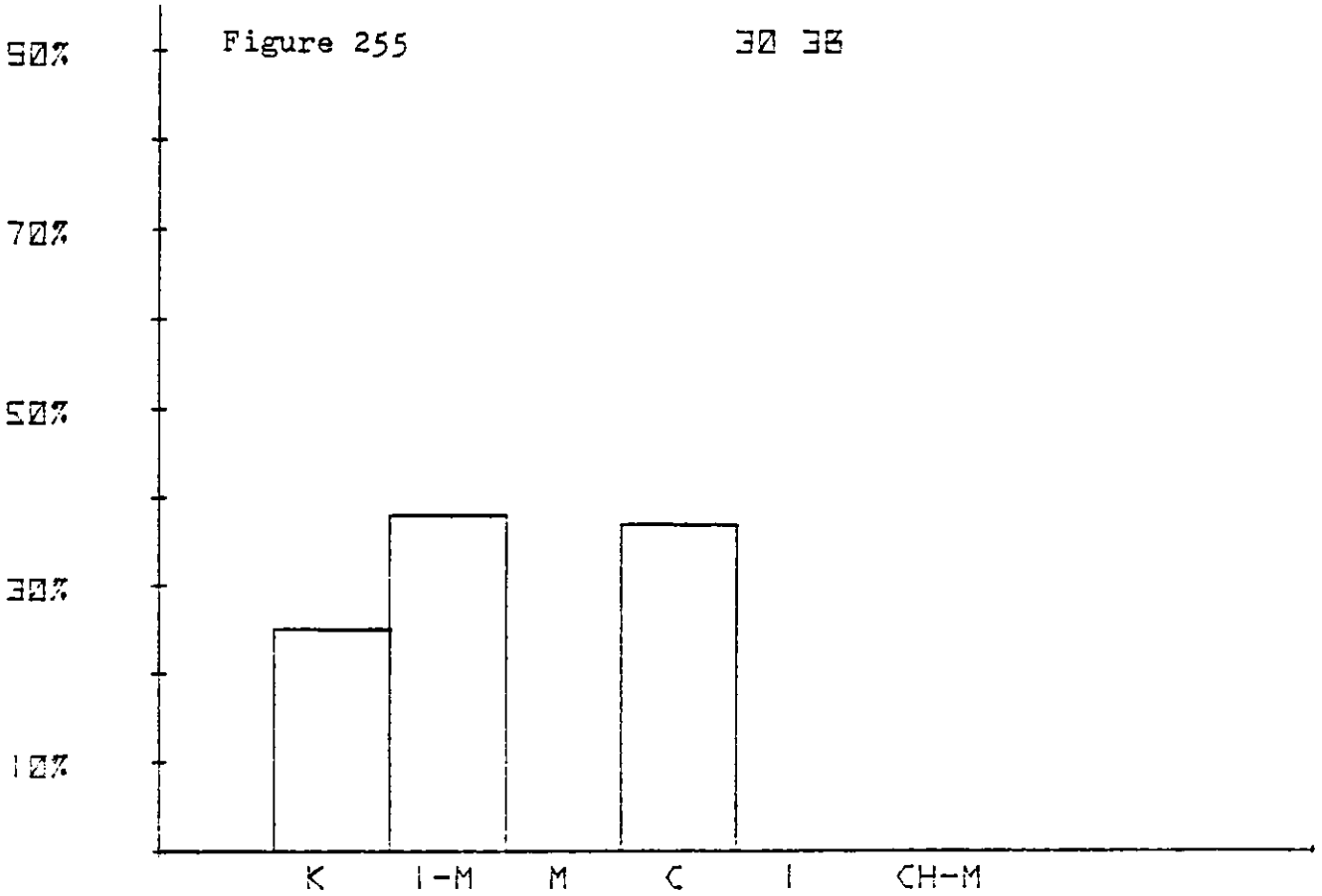


Figure 256

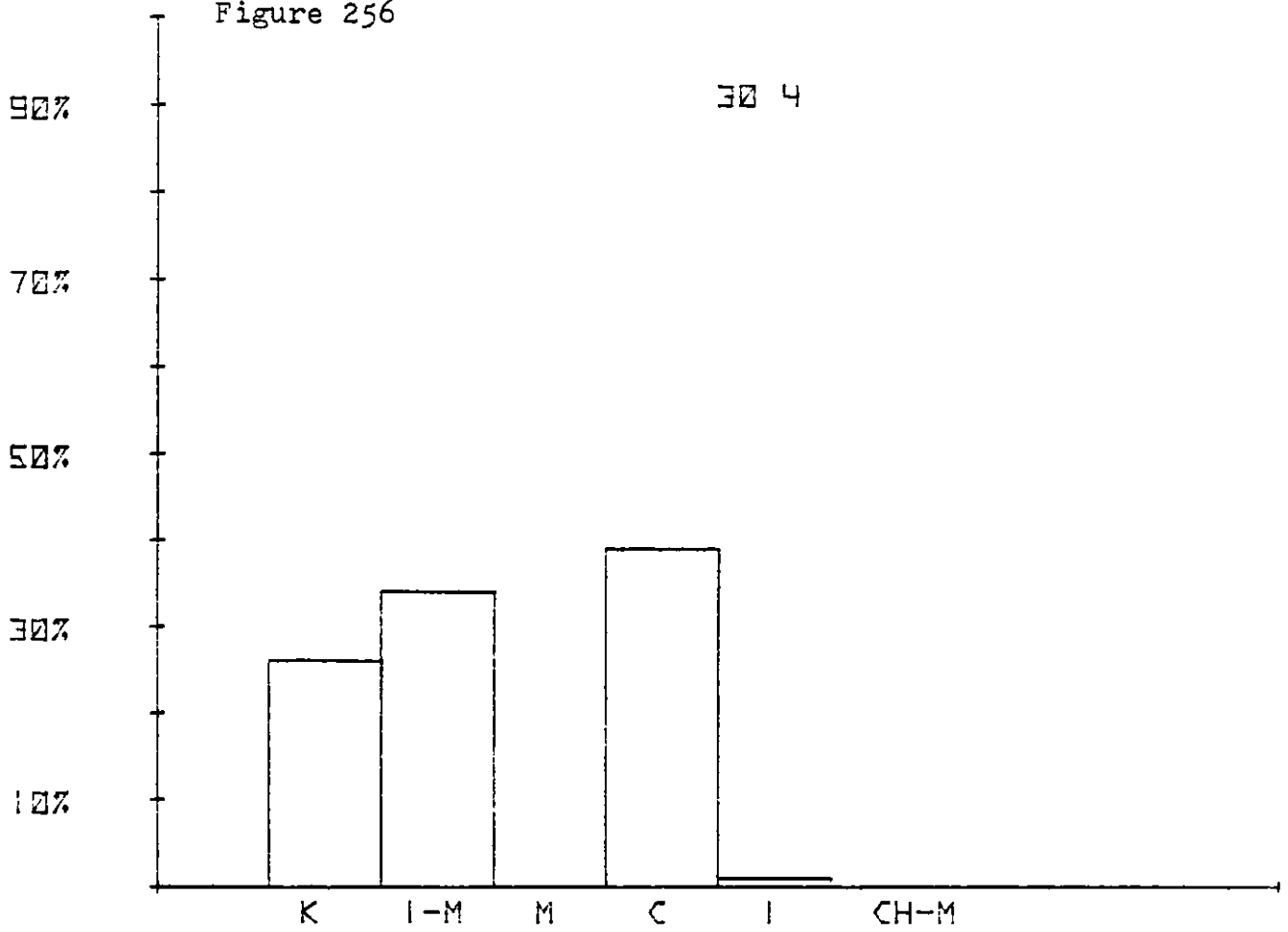


Figure 257

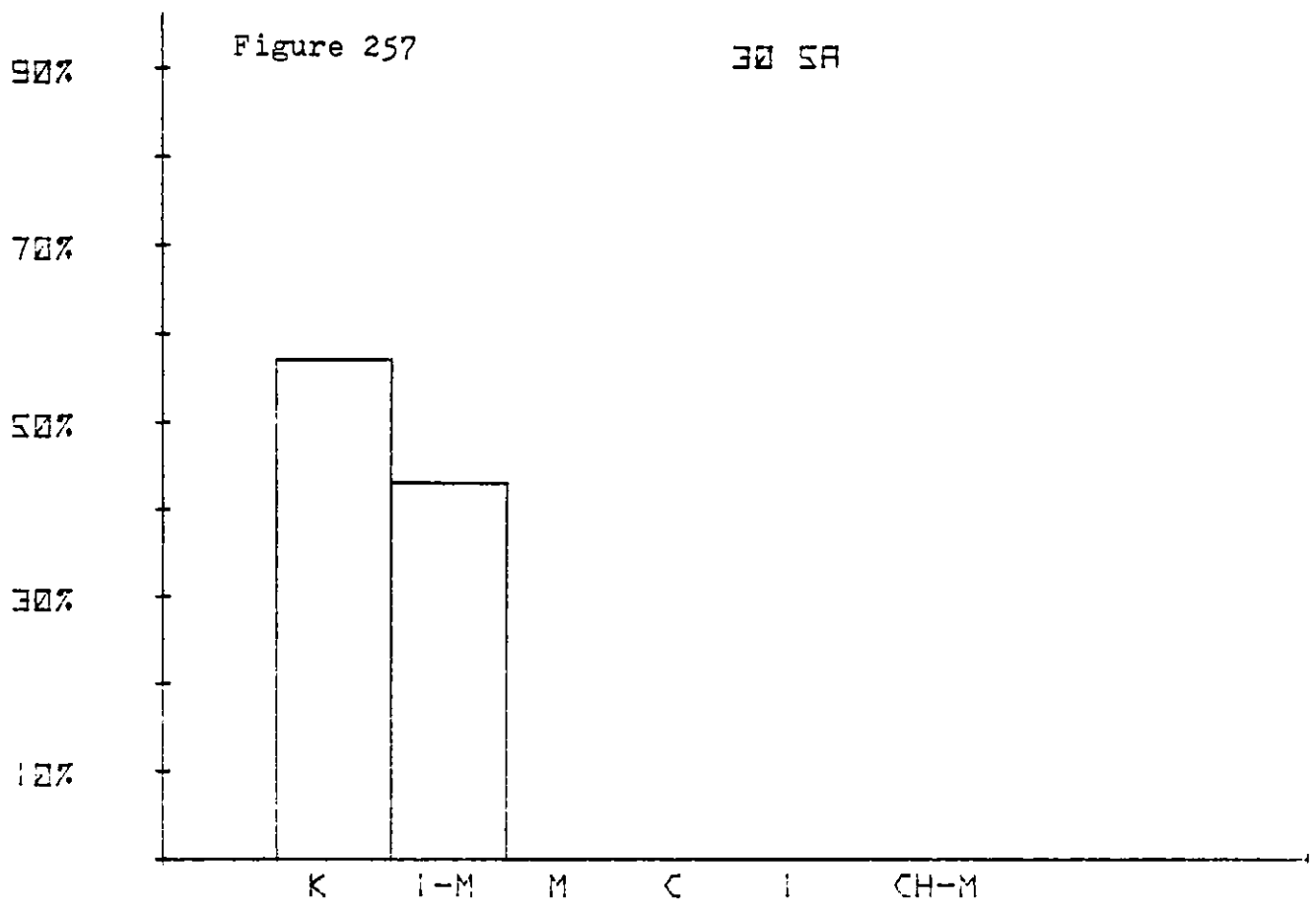
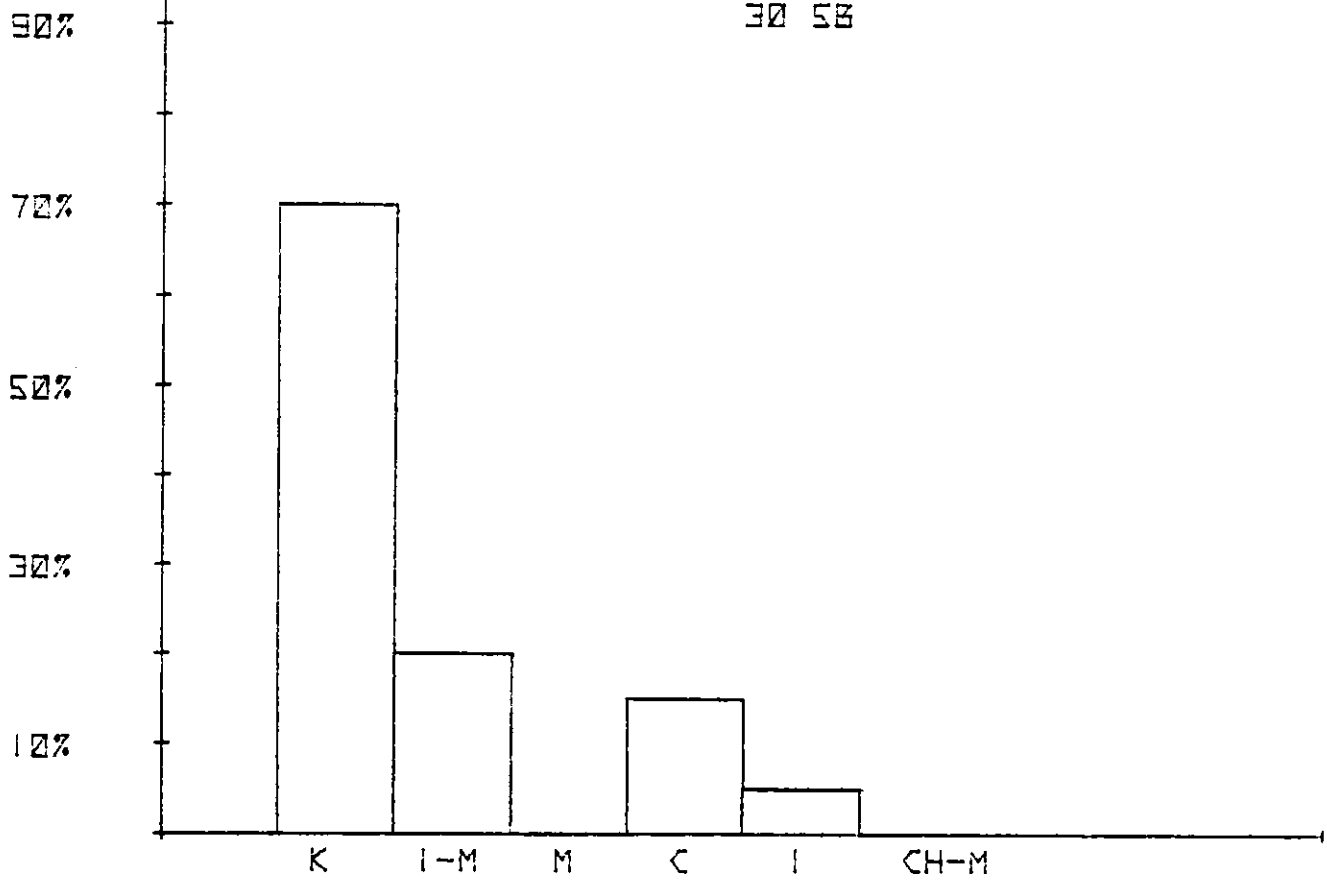
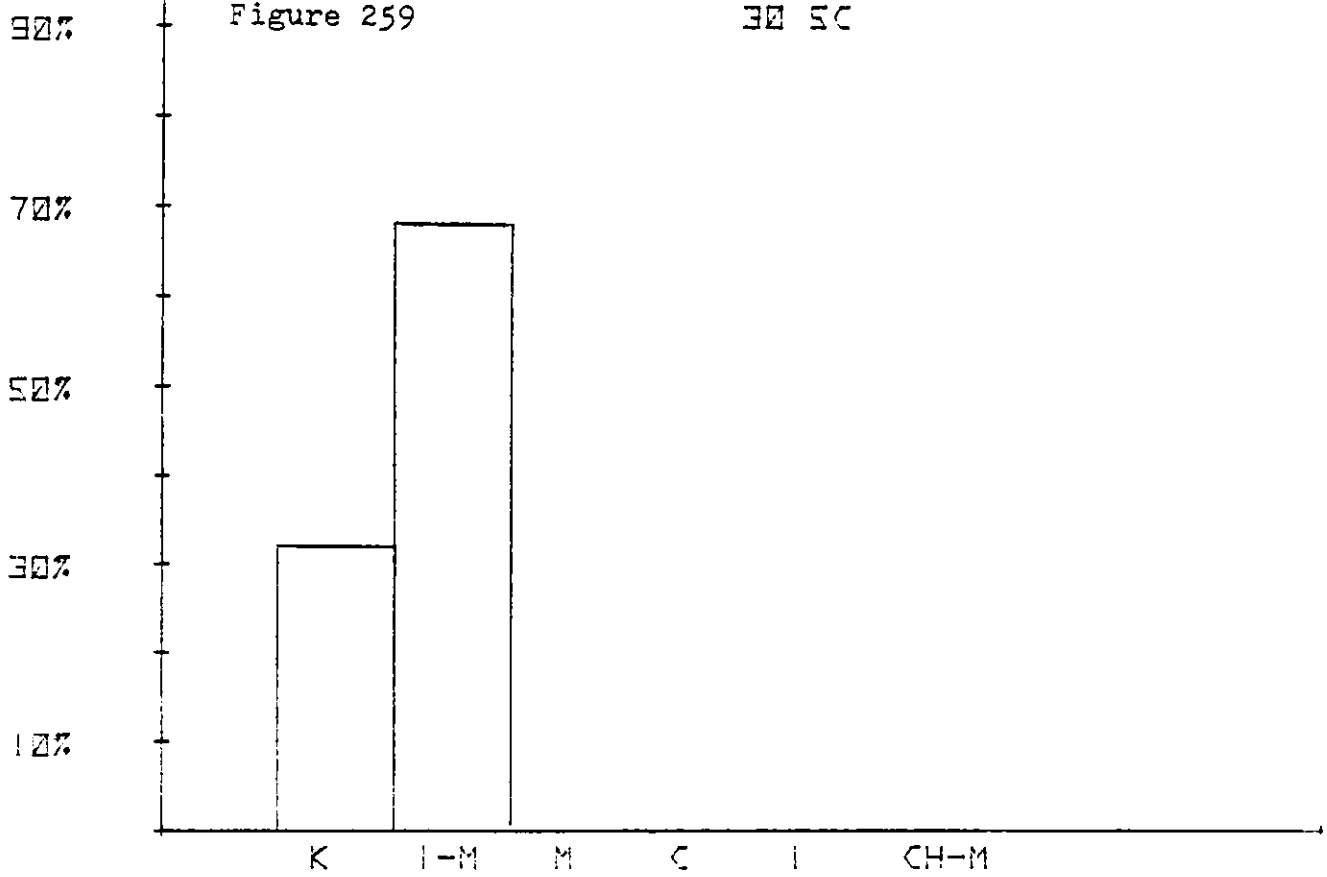


Figure 258



30 58

Figure 259



30 58

Figure 260

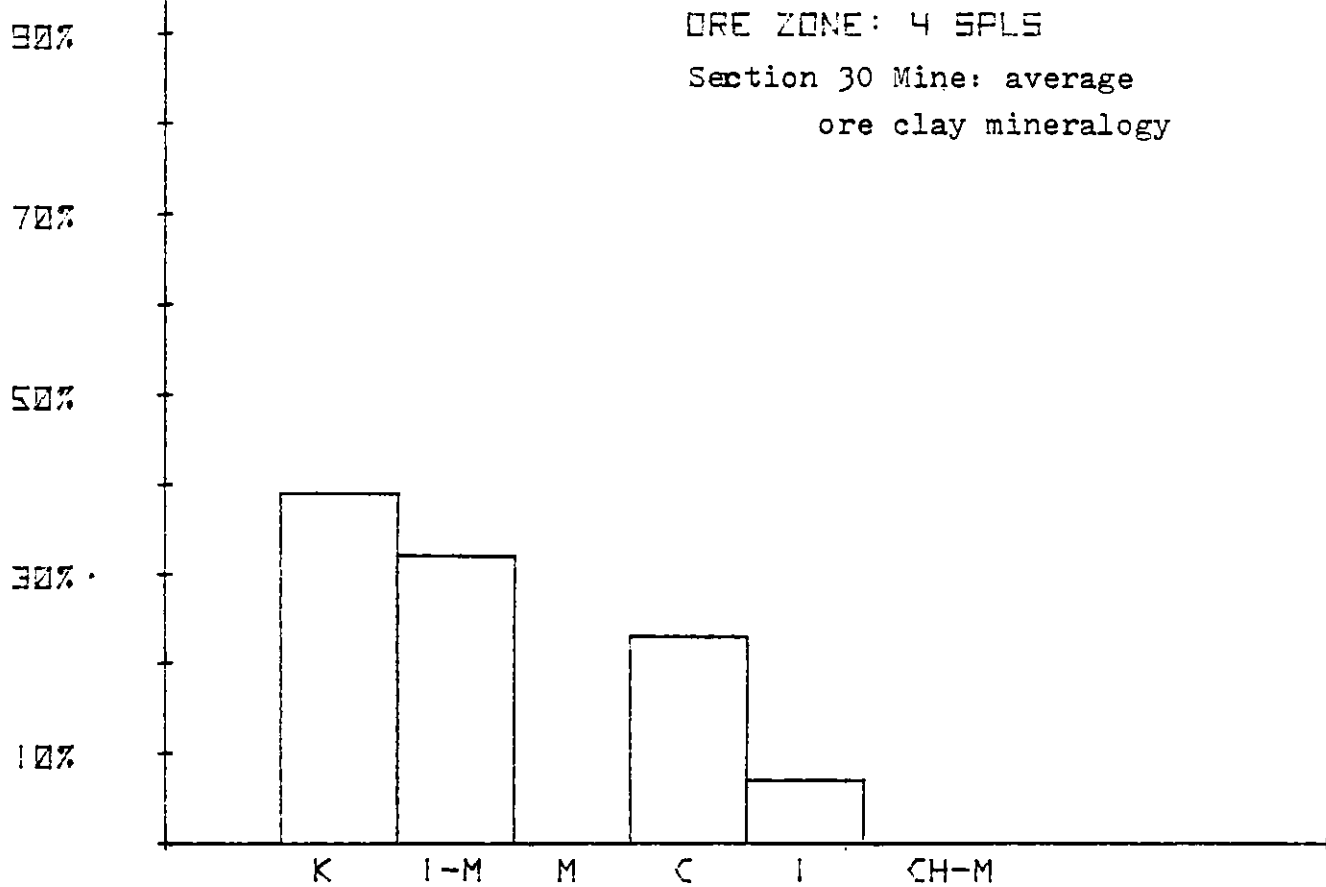


Figure 261

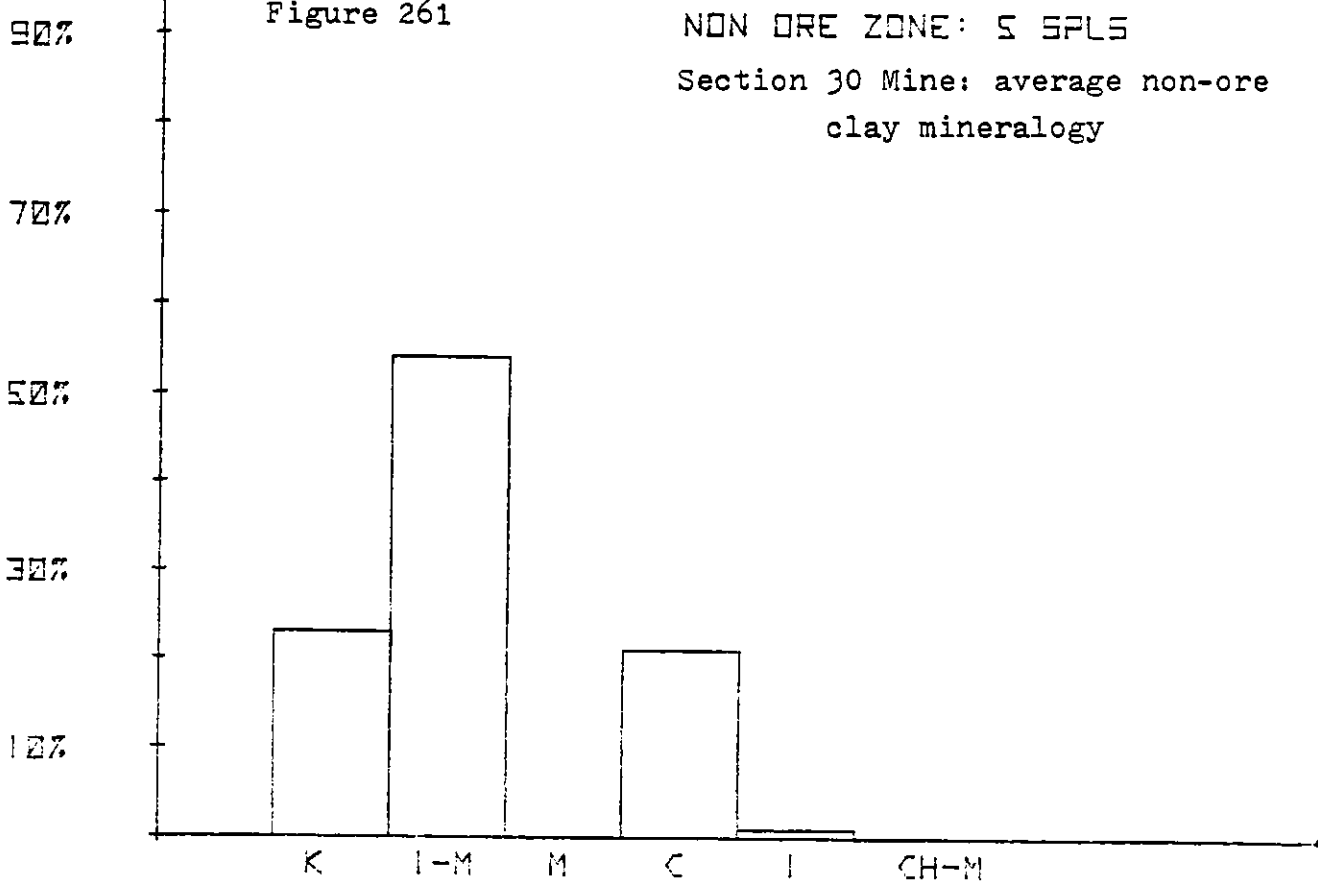


Figure 262

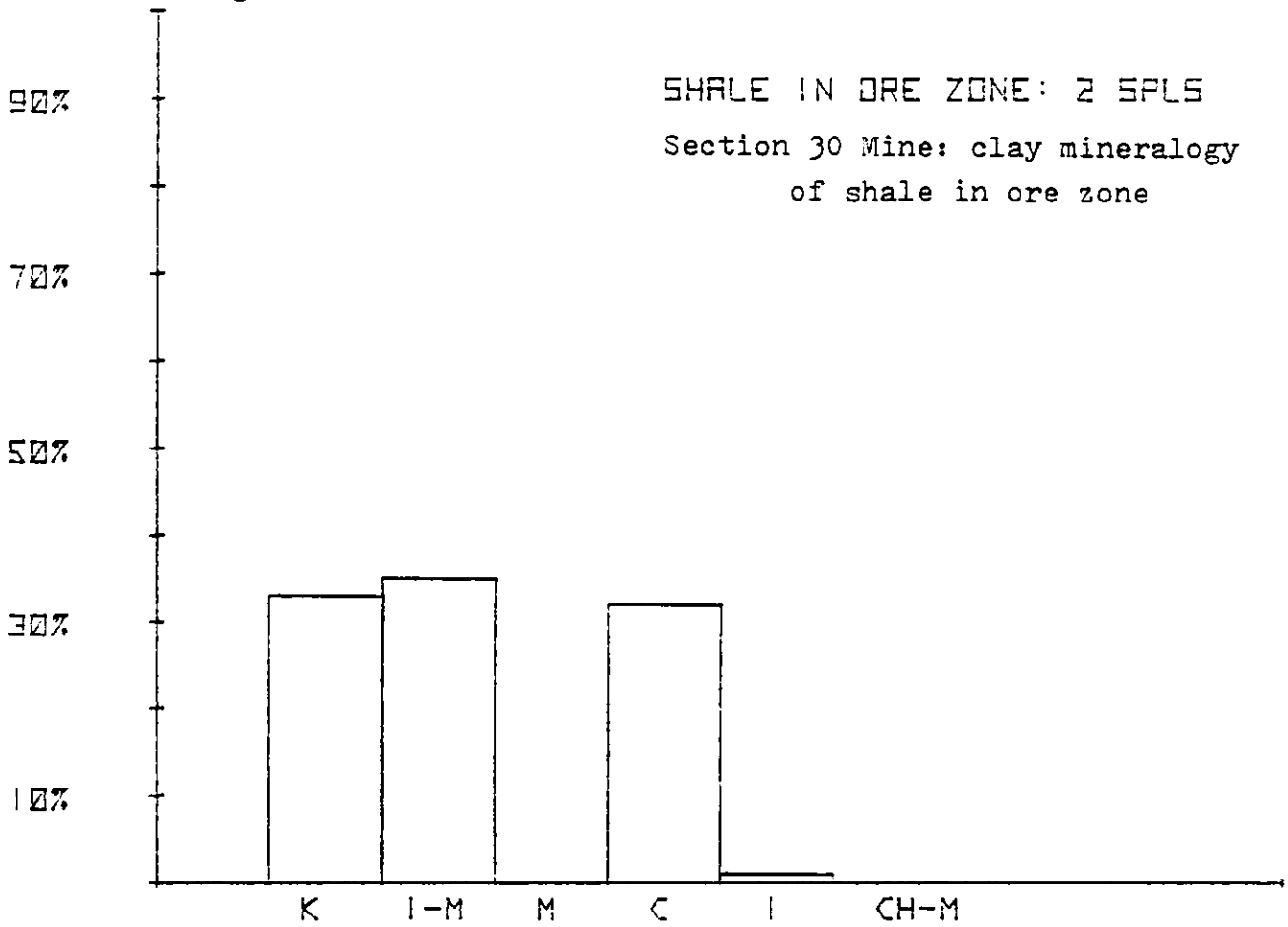
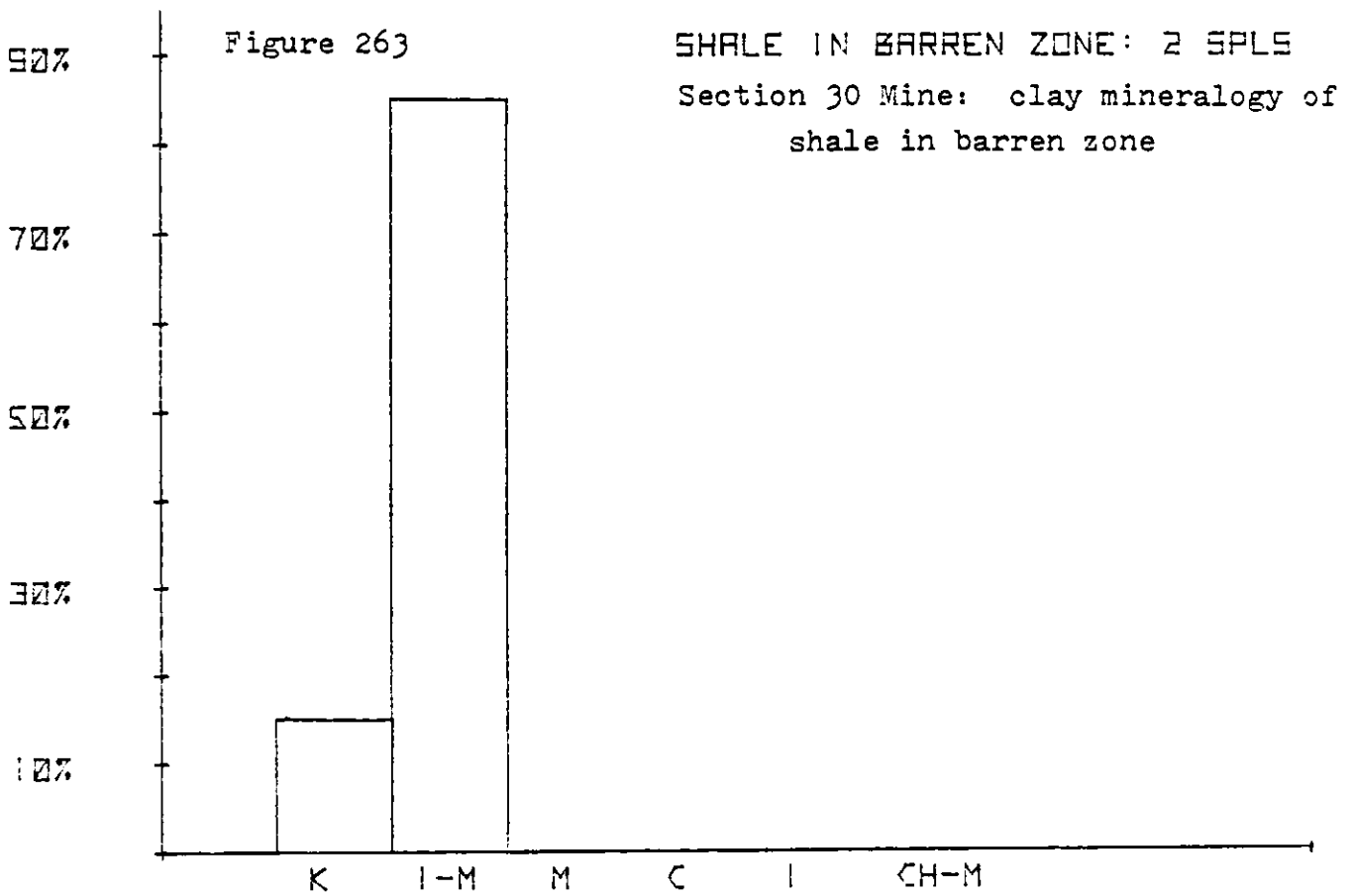


Figure 263



Chapter 7

INSTRUMENTAL NEUTRON ACTIVATION ANALYSIS

Introduction

Instrumental neutron activation analysis (I.N.A.A.) is one of the most sensitive techniques for the determination of the average abundance of elements in geological materials. Gordon and others (1968) showed the non-destructive analysis of standard rocks for 23 elements. Many other elements cannot be analyzed because of interfering reactions with Mn, La, Na, Sc and Co. One of the objectives of this investigation was to study and develop the technique of I.N.A.A. for the analysis of geological materials from the Grants mineral belt.

Sample Preparation

Samples were crushed in agate mortar and pestle by hand and passed through nylon sieves to less than 200 mesh. La, Co and Ni contamination was apparent in samples treated in a steel ball mill. Agate mortar and pestle and sieve sets were washed with dilute acids and distilled water between samples to minimize contamination.

Experimental

The most commonly used source of neutrons for activation analysis is the nuclear reactor. The samples in this study were irradiated at the Omega West Reactor (OWR). The OWR is a thermal, heterogeneous, tank type research reactor operated by the Los Alamos Scientific Laboratory. The reactor is light water moderated and cooled. At the 8 megawatt level the reactor provides fluxes of up to 8×10^{13} neutrons / cm^2 -sec in the experimental facilities.

The samples are loaded into polyvials and introduced to a high thermal neutron flux using a He charged pneumatic transfer (rabbit system). A small piece of Cr wire (nichrome resistance wire: 15% Cr, 25% Fe, 60% Ni) is run with each sample to monitor variations in the reactor flux. Large changes in the wire count will alert one to problems which may have occurred during the irradiation. For example, samples in the rabbit system may bounce back in an unexpected flux position. It is critical to be in the same position to take advantage of the optimum thermal/epithermal ratios.

Since several polyvials are run simultaneously, flux monitors are necessary to record the neutron flux decreases. The flux decreases as the distance of the sample from the core increases. After several experiments this drop down was recorded as 10.7% in 8 cm. The advantages of using the Cr wire flux monitor can be seen as follows (Sellschop et al., 1973):

- (1) Samples can be individually monitored.
- (2) An average dosage is measured as the flux contours do not change significantly within the size of the rabbits (0.8cm).
- (3) The $^{50}\text{Cr} (n,\gamma) ^{51}\text{Cr}$ can be used to measure the thermal flux and the $^{54}\text{Fe} (n,p) ^{54}\text{Mn}$ can monitor the fast neutron flux. Using this method epithermal and thermal neutrons can be monitored at the same time.
- (4) A large mass of Cr wire can be irradiated because of the relatively low cross section. A mass of 20-30 mg allows the weight of the monitor to be accurately determined.

In practice, the following technique is used. Sample polyvials (0.8cm) are filled with 80 to 100 mg of less than 200 mesh powdered sample. The vial is placed in a large polyvial (4 cm), which can accommodate 4 small polyvials and their Cr wires. Each sample and its flux monitor is separated

by quartz wool. Eight small polyvials (two large polyvials) can be accommodated for each irradiation period. Each irradiation lasts from 6 to 8 hours. After irradiation the Cr wires are removed and the ^{54}Mn and ^{51}Cr activities are determined. The values obtained are compared to a standard ^{60}Co source and a flux number for each sample is calculated. The absolute neutron flux can also be calculated if needed. The flux monitor can be compared to sample position to check for spurious values. Epithermal flux corrections are almost never needed since the rabbit used had an extremely high thermal/epithermal ratio.

The gamma spectroscopy system used consisted of a Ge(Li) detector connected to a 4000 channel analyzer. The detector used in this study is a Princeton Gamma Tech Ge(Li) detector with a 110cm^3 crystal. The detector shows a peak to Compton ratio of 36:3 at 1.33 Mev. After proper amplification the pulses were analyzed by aid of a Canberra 8100 (4096 channel) analyzer. This system gave a resolution of 2.41 Kev full width half mass and 5.47 Kev (Full width full mass) at 1.33 Mev using a ^{57}Co source.

A small displacement of the sample can introduce a large error in the measured activity. For this reason the sample was:

- (1) Mounted on Al counting plates. The sample was carefully centered each time.
- (2) Placed on shelf 10 (approx. 10 cm from the crystal). This large distance from the detector serves to minimize sample geometry effects.

Count rate effects are especially noticed in high Na, La and Mn samples. As the count rate handled by a gamma spectroscopy system is increased, the spectrum quality radically diminishes. The parameters affected are as follows:

- (1) The resolution (Full width half mass) is decreased. This means that closely spaced peaks can no longer be resolved (Sellschop et al., 1973).
- (2) The peak to Compton ratio decreases, resulting in a higher detection limit for low energy peaks which are lost in the Compton continuum (Sellschop et al., 1973).
- (3) Symmetrical peaks may result. Symmetrical peaks can make the determination of the peak boundaries difficult. This will result in erroneous peak area determinations (Sellschop et al., 1973).

Count rate effects are the major source of error in I.N.A.A. work. Samples analyzed have to be screened carefully or have interfering elements separated.

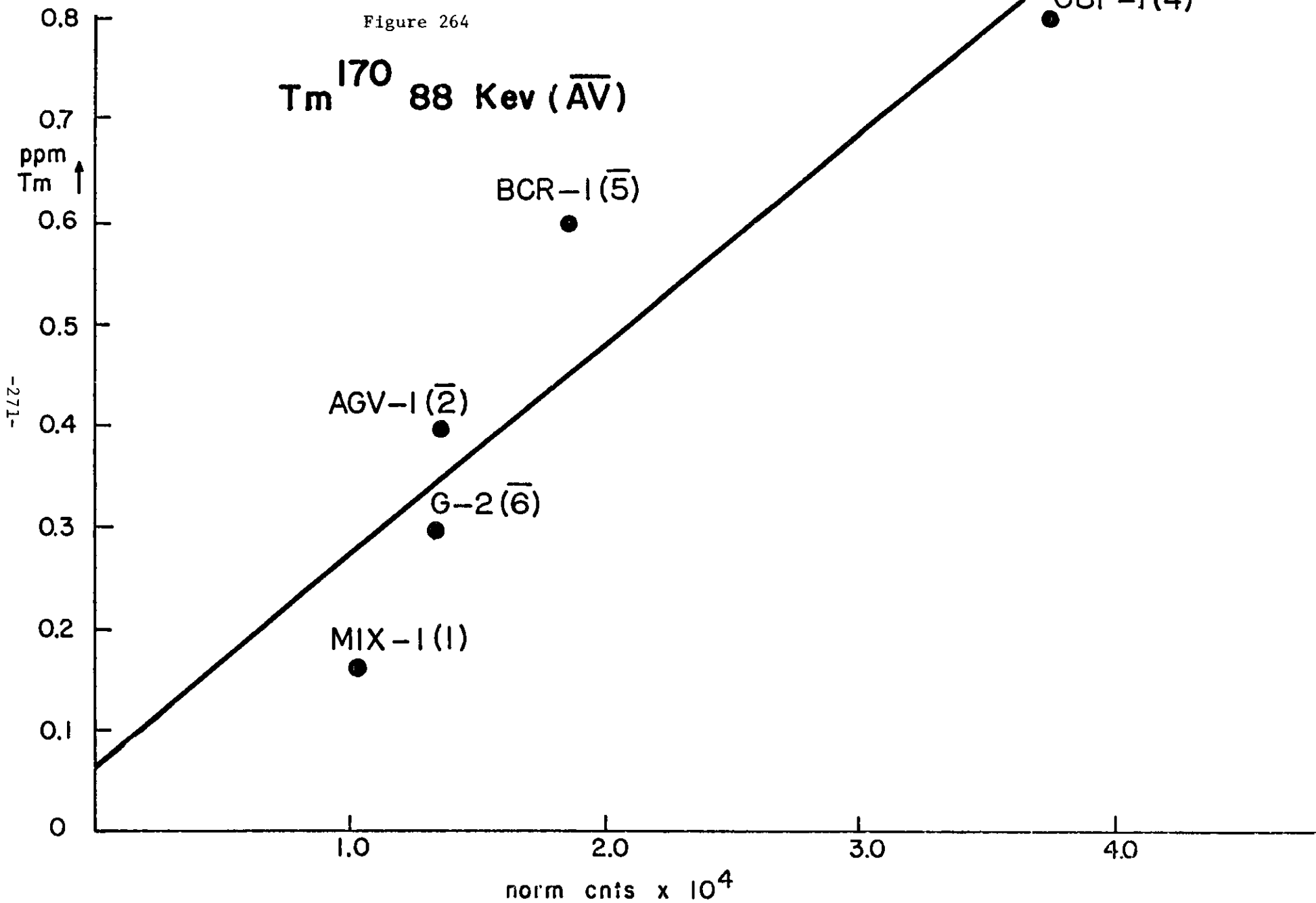
Results

By means of high resolution Fe(Li) detectors and instrumental activation analysis, 24 elements have been determined in six standard rocks. These standard rocks are U.S.G.S. series G-2, BCR-1, GSP-1, DTS-1, PCC-1 and AGV-1. In addition to the six U.S.G.S. standard rocks a mix (mix-1) was established from 46.47 wt.% PCC-1 and 53.53 wt.% G-2. Table 24 shows the currently accepted values for the trace elements analyzed. These values were used to calibrate the instrumental neutron activation analysis technique used at the Los Alamos Scientific Laboratory facilities. Table 25 shows the element analyzed with its product nuclide measured, peak used, best time after irradiation for counting, estimated errors and lower limit of detection. Figures 264-288 are calibration curves for various elements analyzed in this study. Please note that $\text{Ag}^{110\text{m}}$ is a working line and is still having data added for it. Many of these calibrations are an average of 5 or 6 determinations for each U.S.G.S. standard.

Figures 289-300 show the energy spectra for the various elements analyzed. These figures exhibit the high Compton scattering at the 100 to 600 channel range.

Figure 264

Tm^{170} 88 Kev (\bar{AV})



-271-

Figure 265

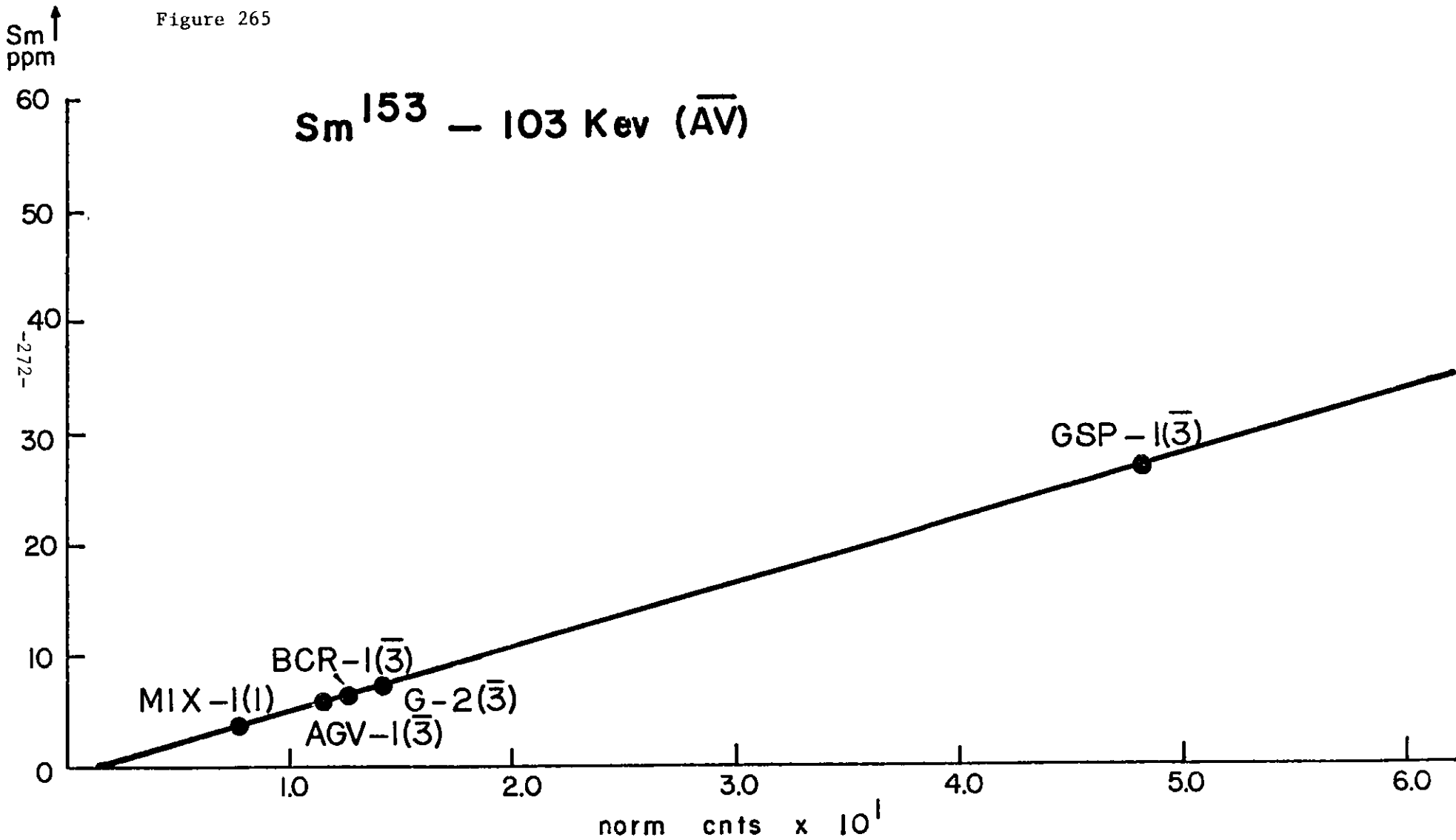


Figure 266

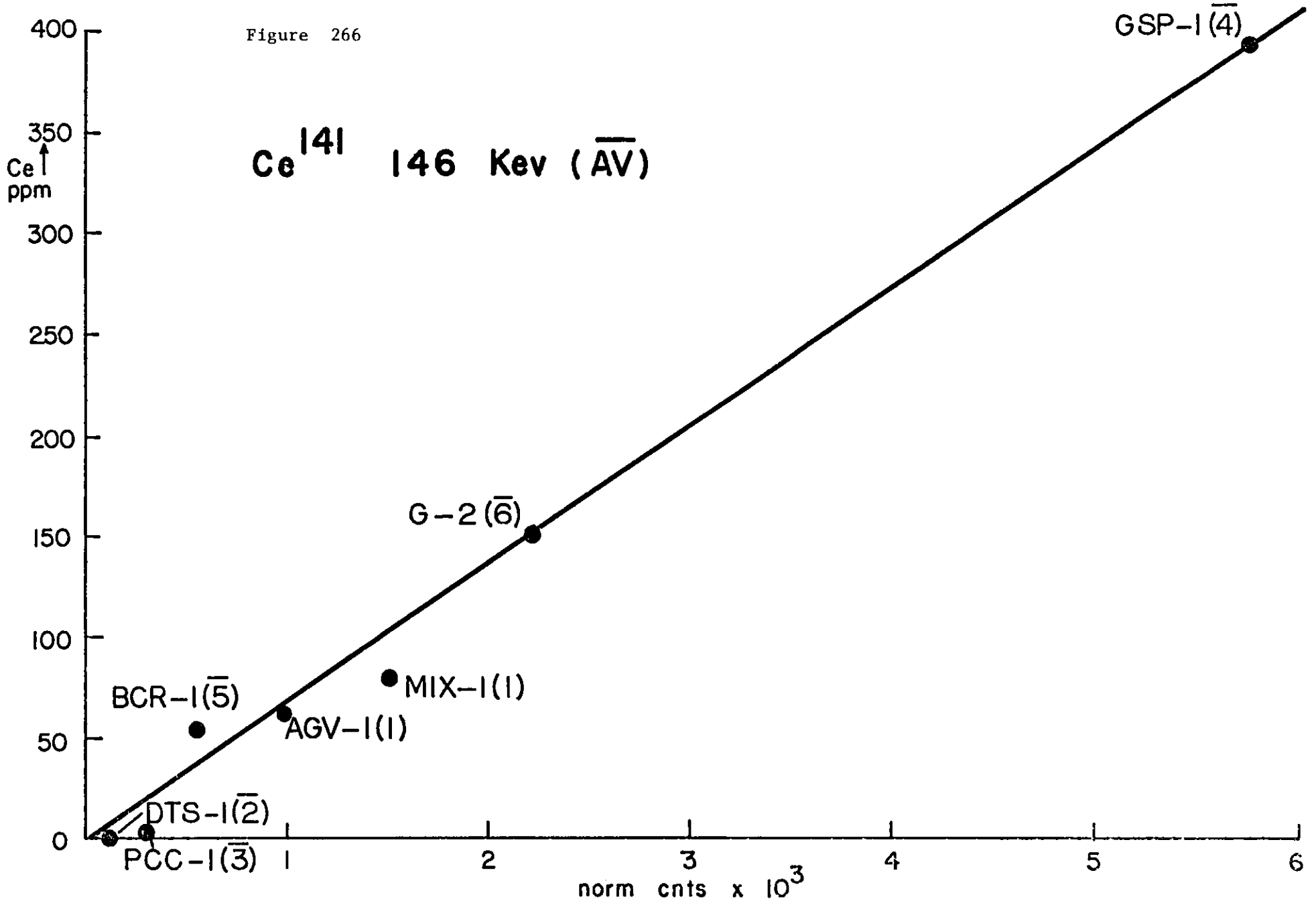


Figure 267

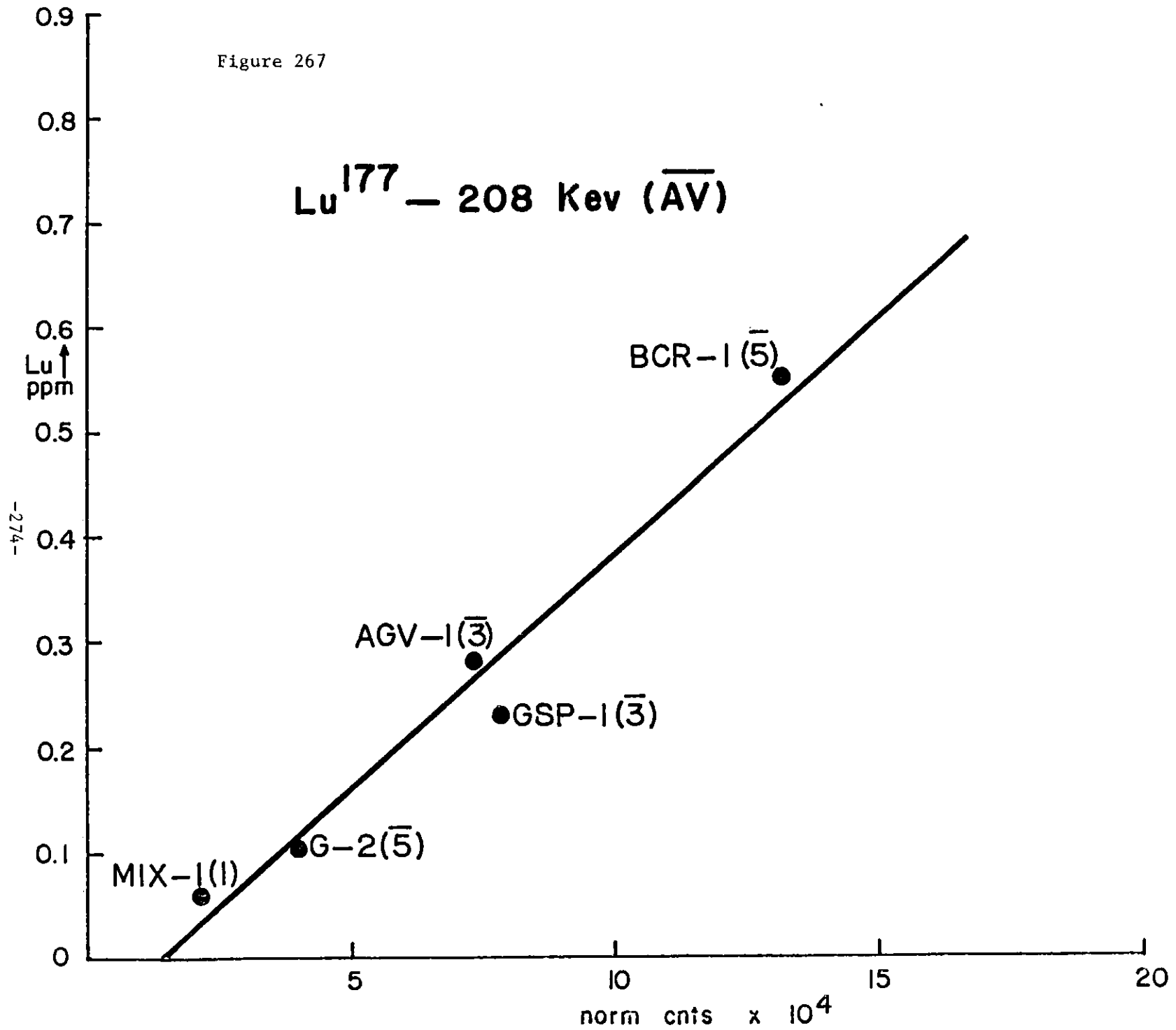


Figure 268

$\text{Yb}^{175} - 283 \text{ Kev } (\bar{AV})$

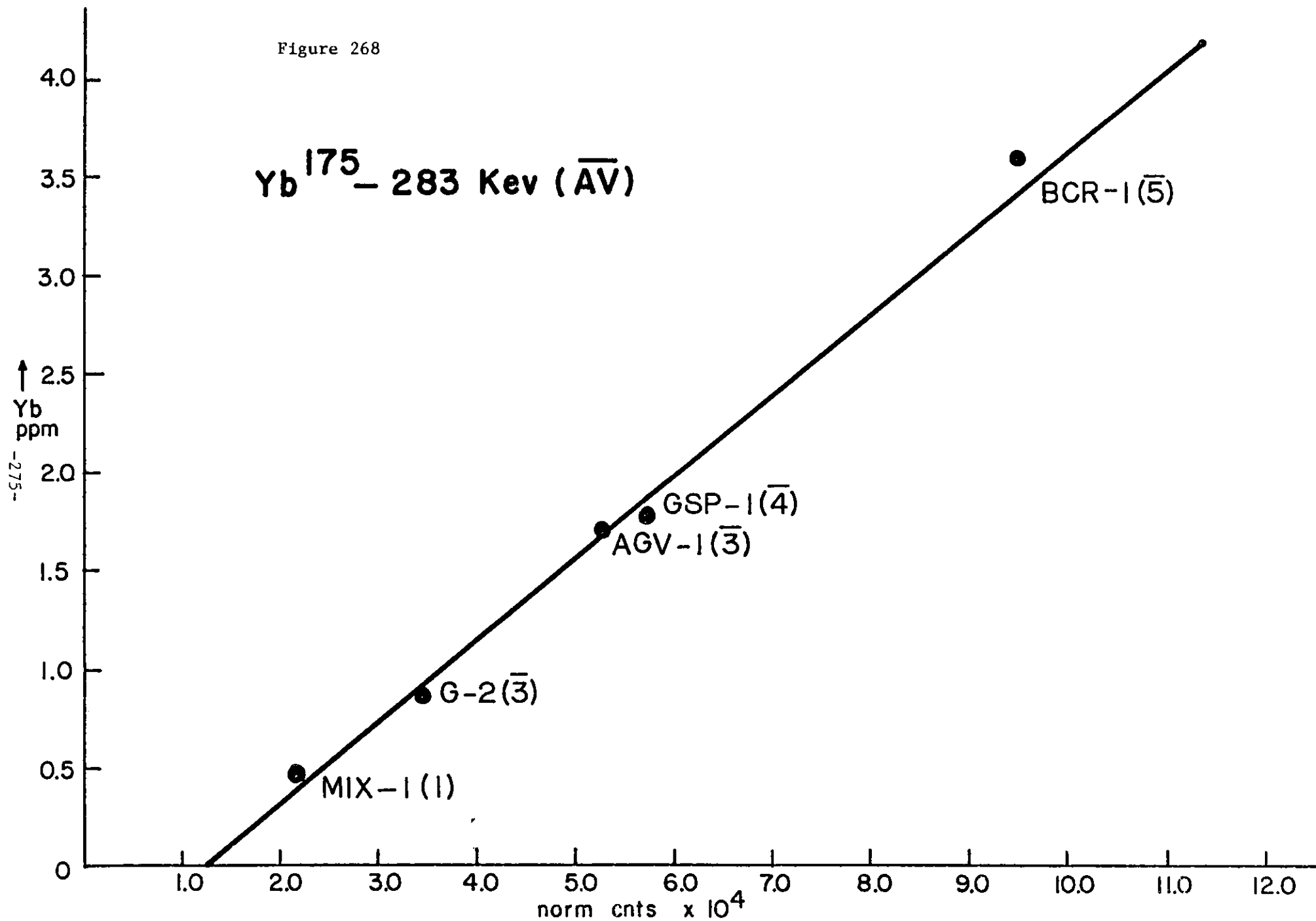


Figure 269

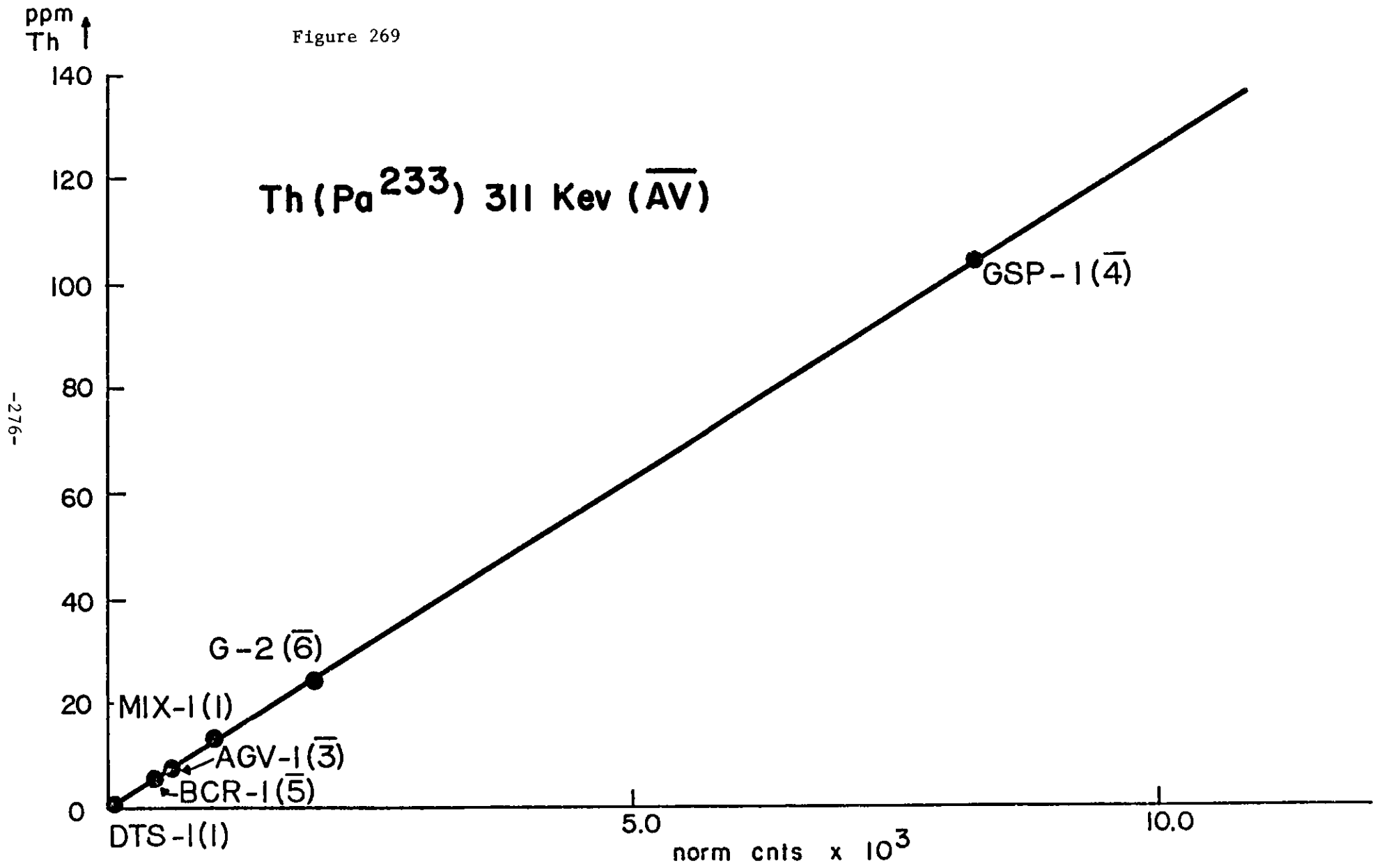


Figure 270

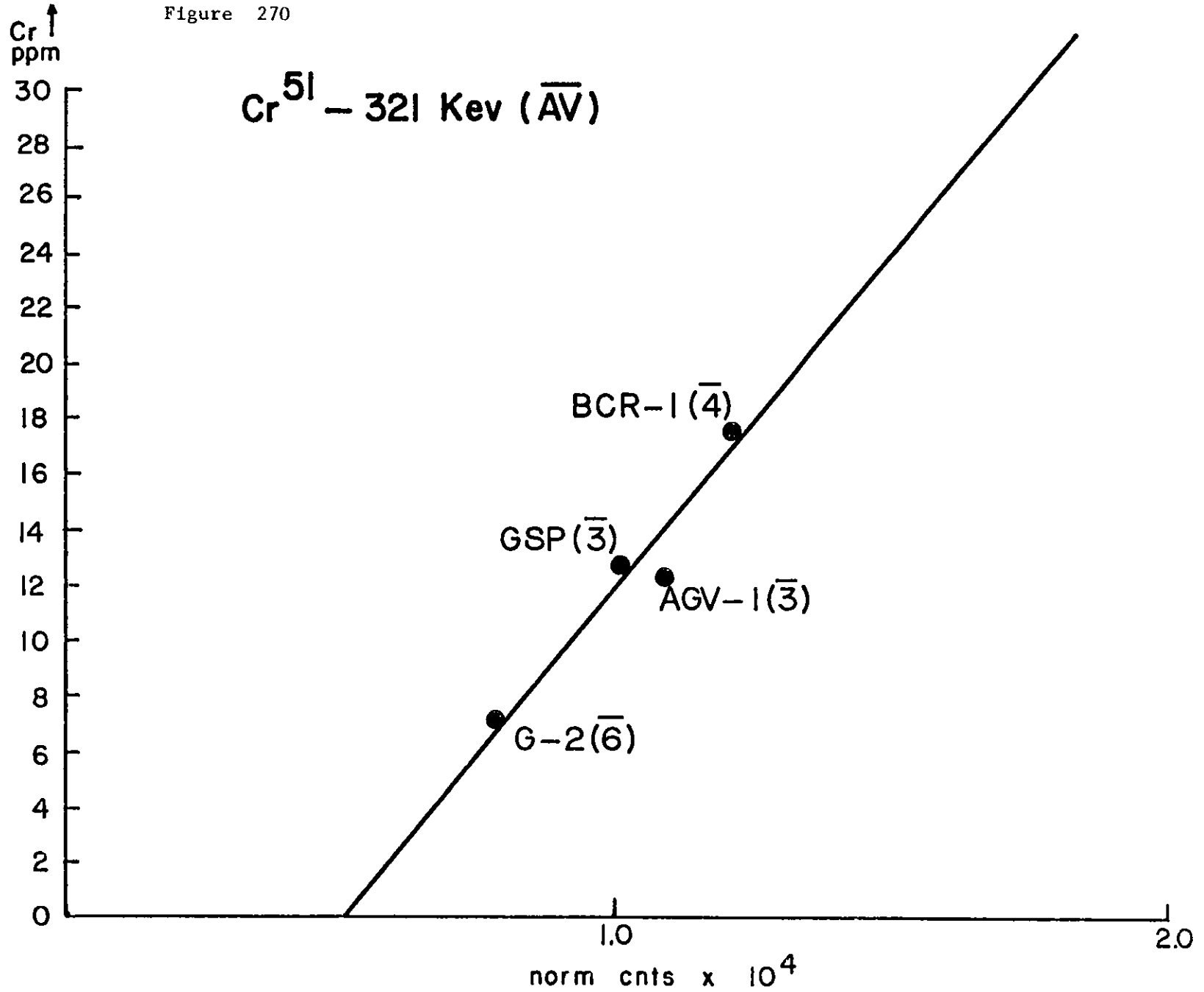


Figure 271

$\text{Hf}^{181} - 483 \text{ Kev } (\bar{AV})$

-278-

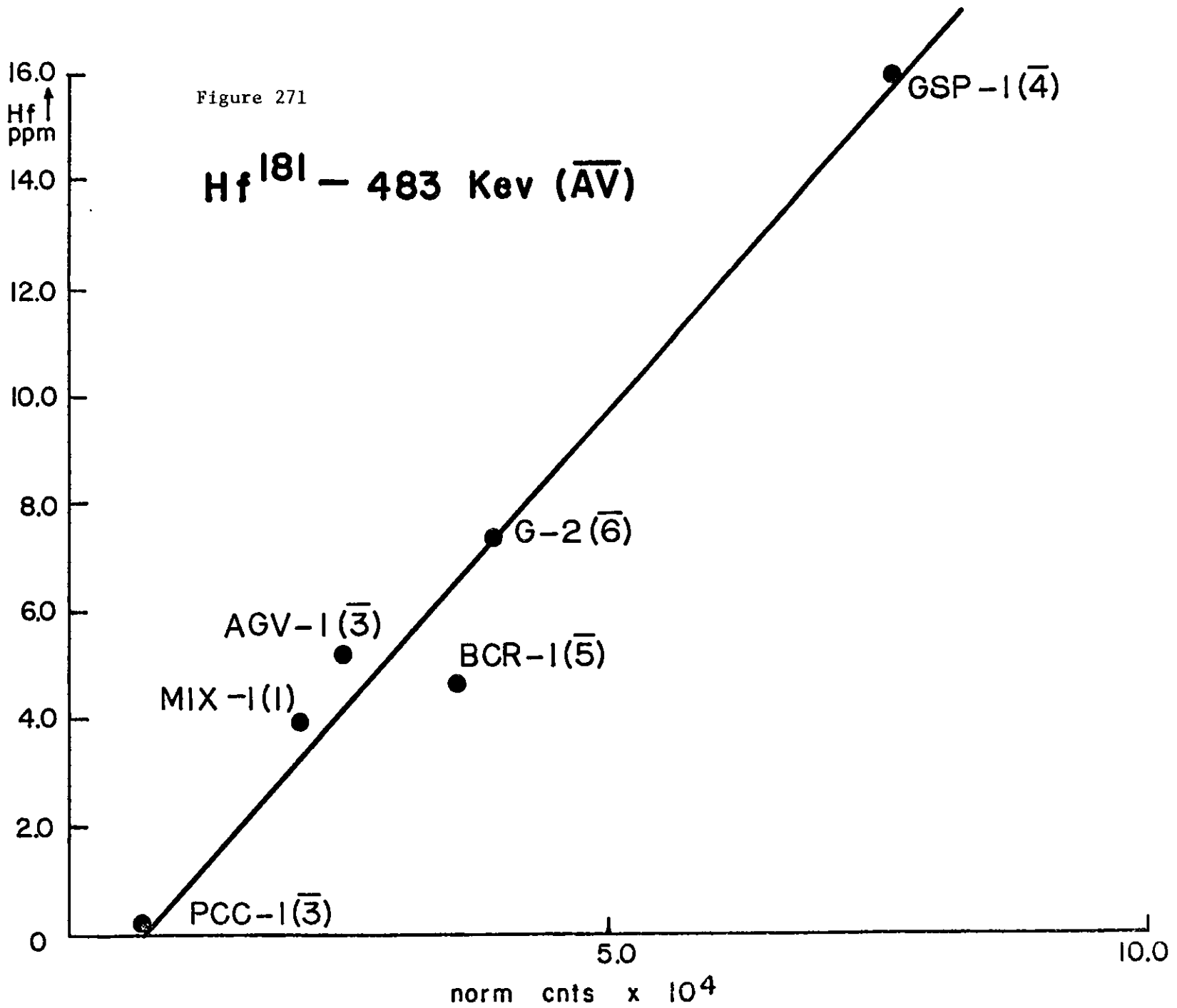
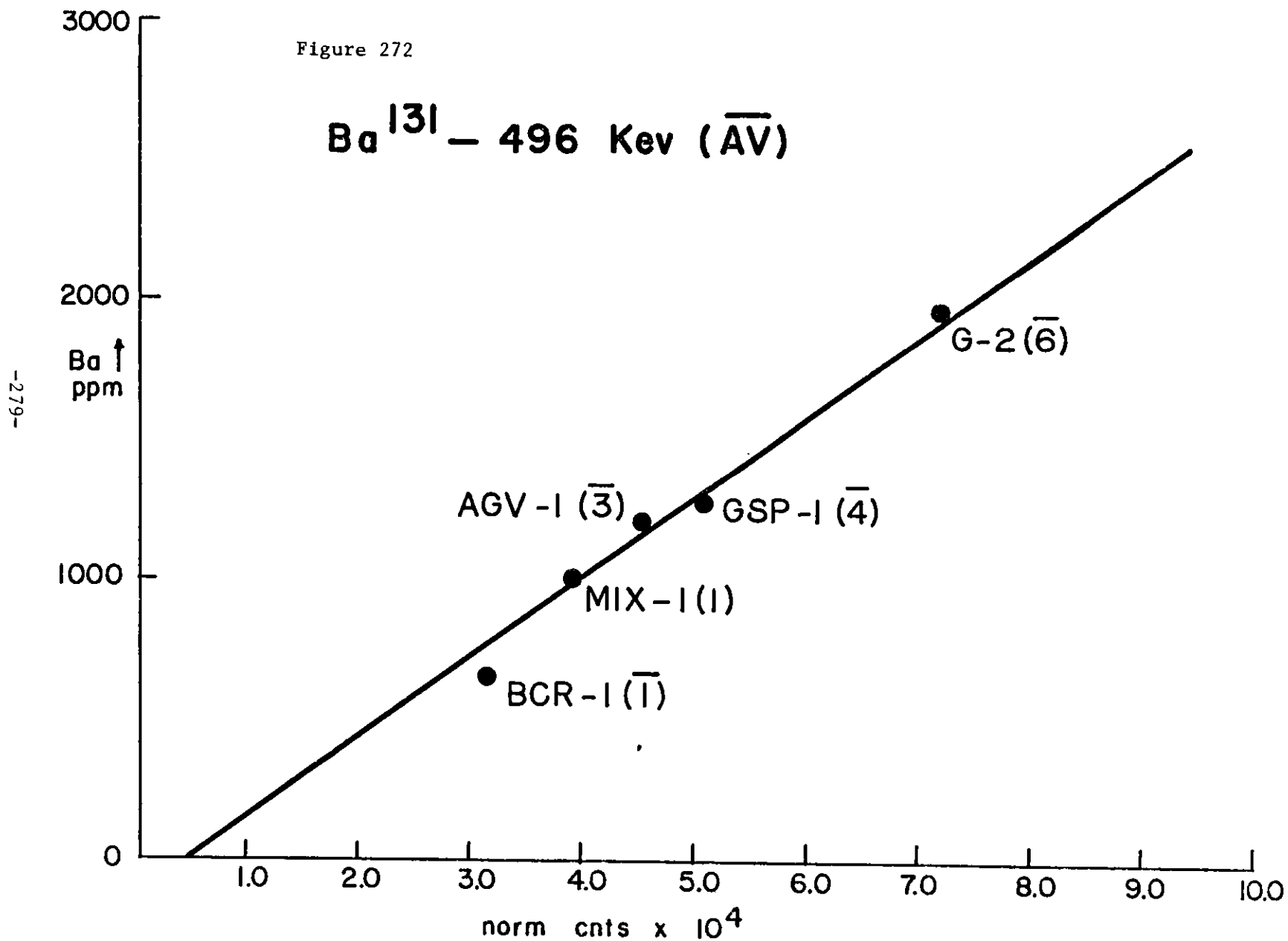


Figure 272

Ba¹³¹ - 496 Kev (\bar{AV})



-279-

Figure 273

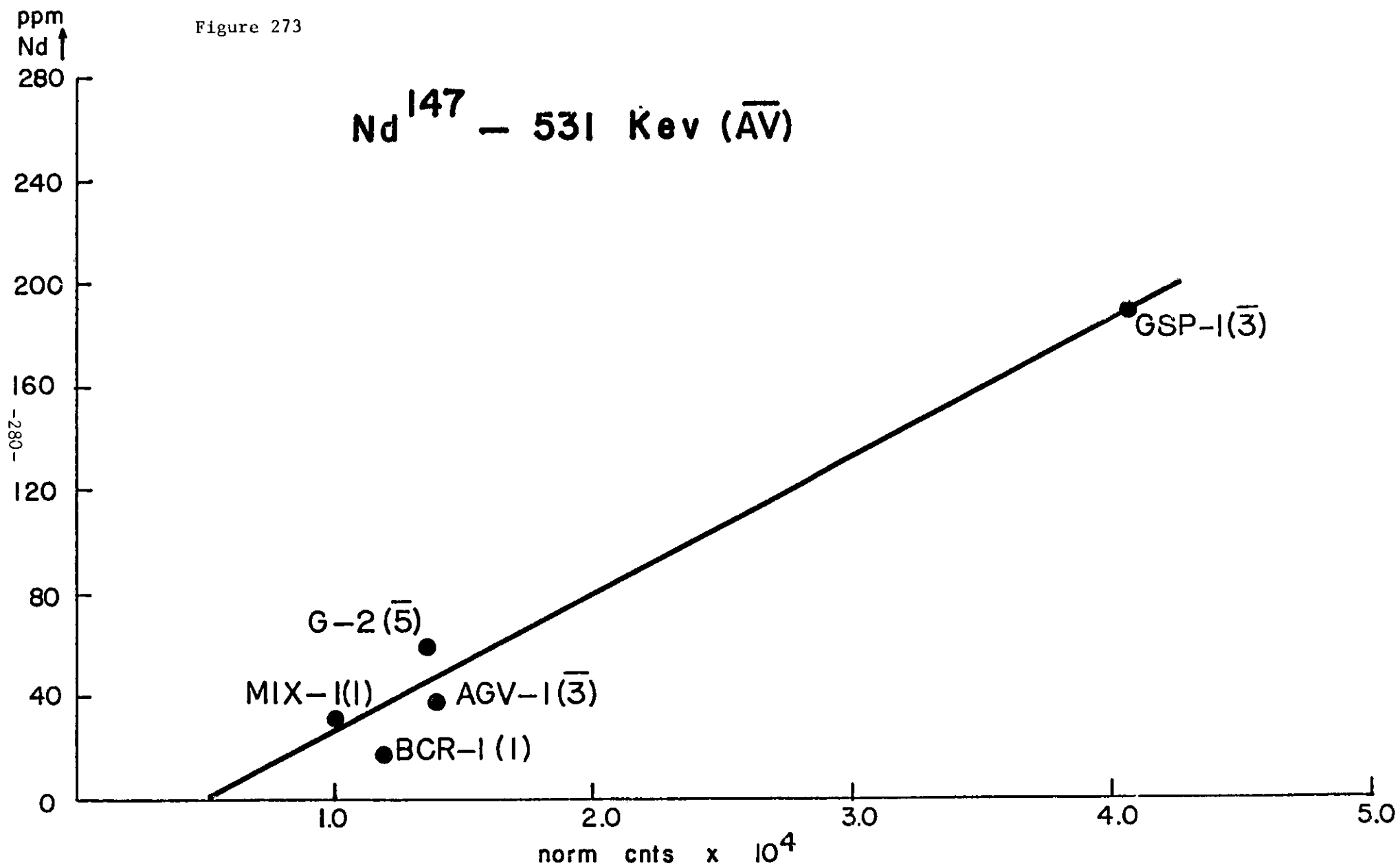


Figure 274

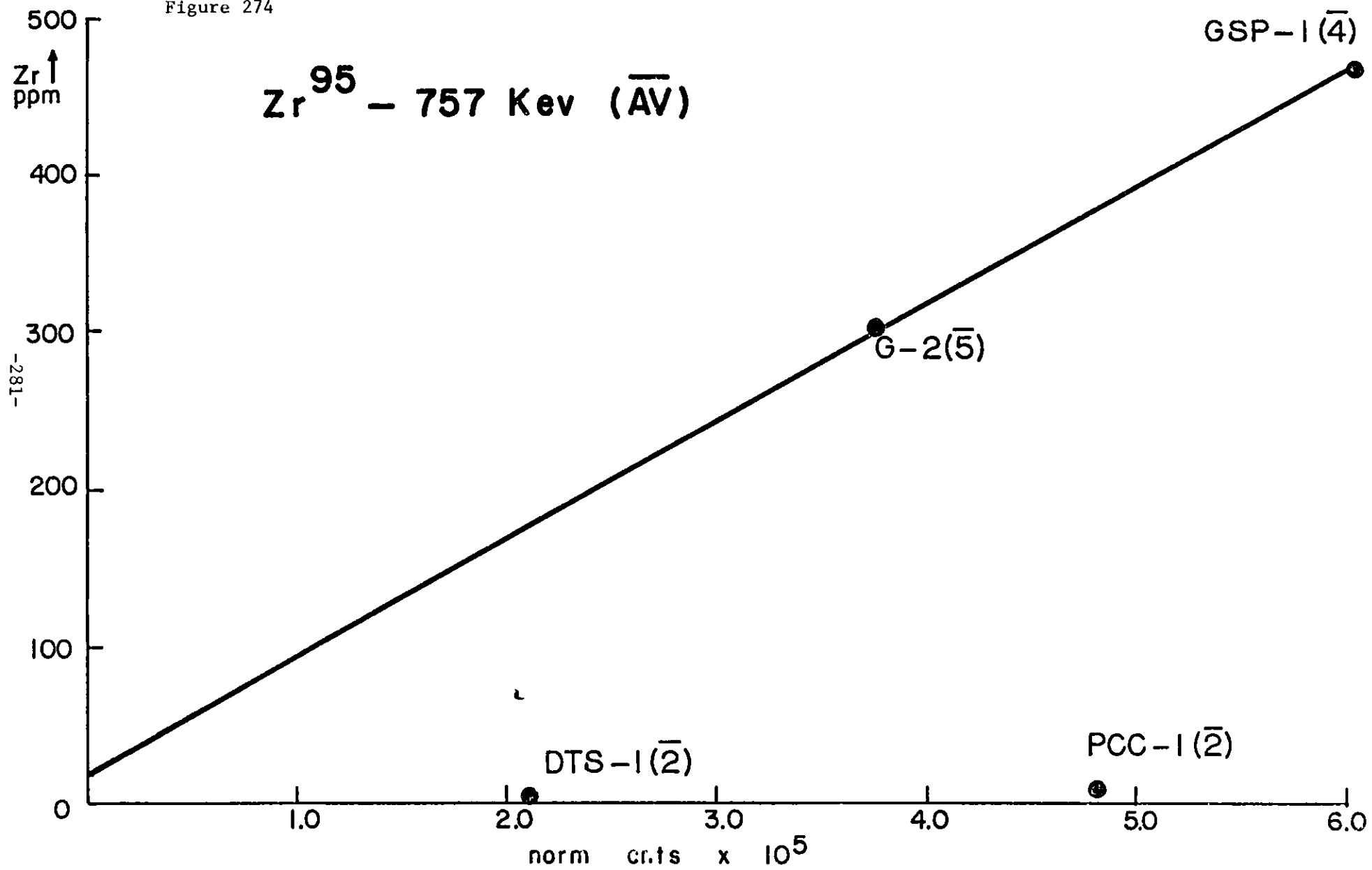


Figure 275

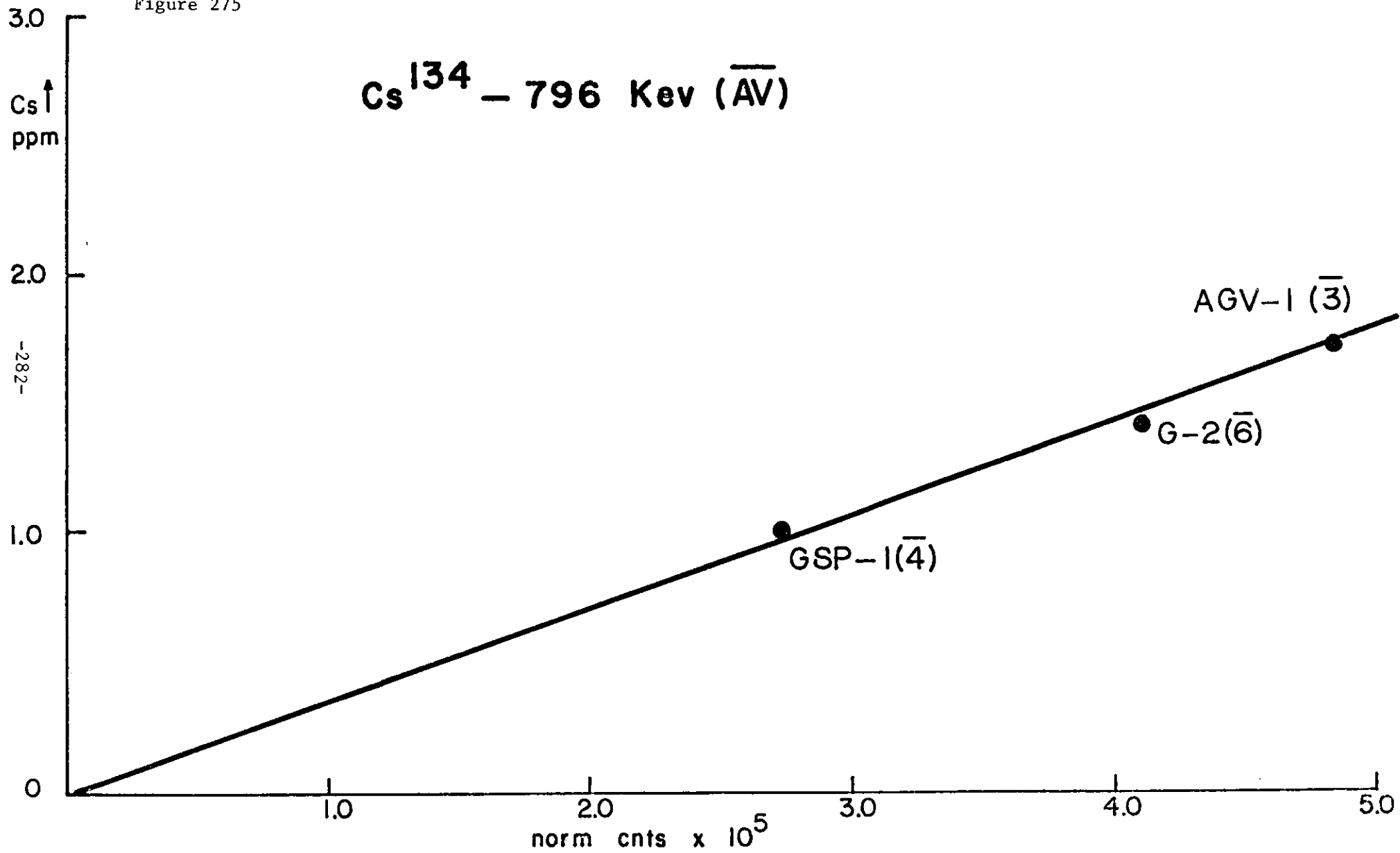


Figure 276

Ni (Co⁵⁸) - 809 Kev (\bar{AV})

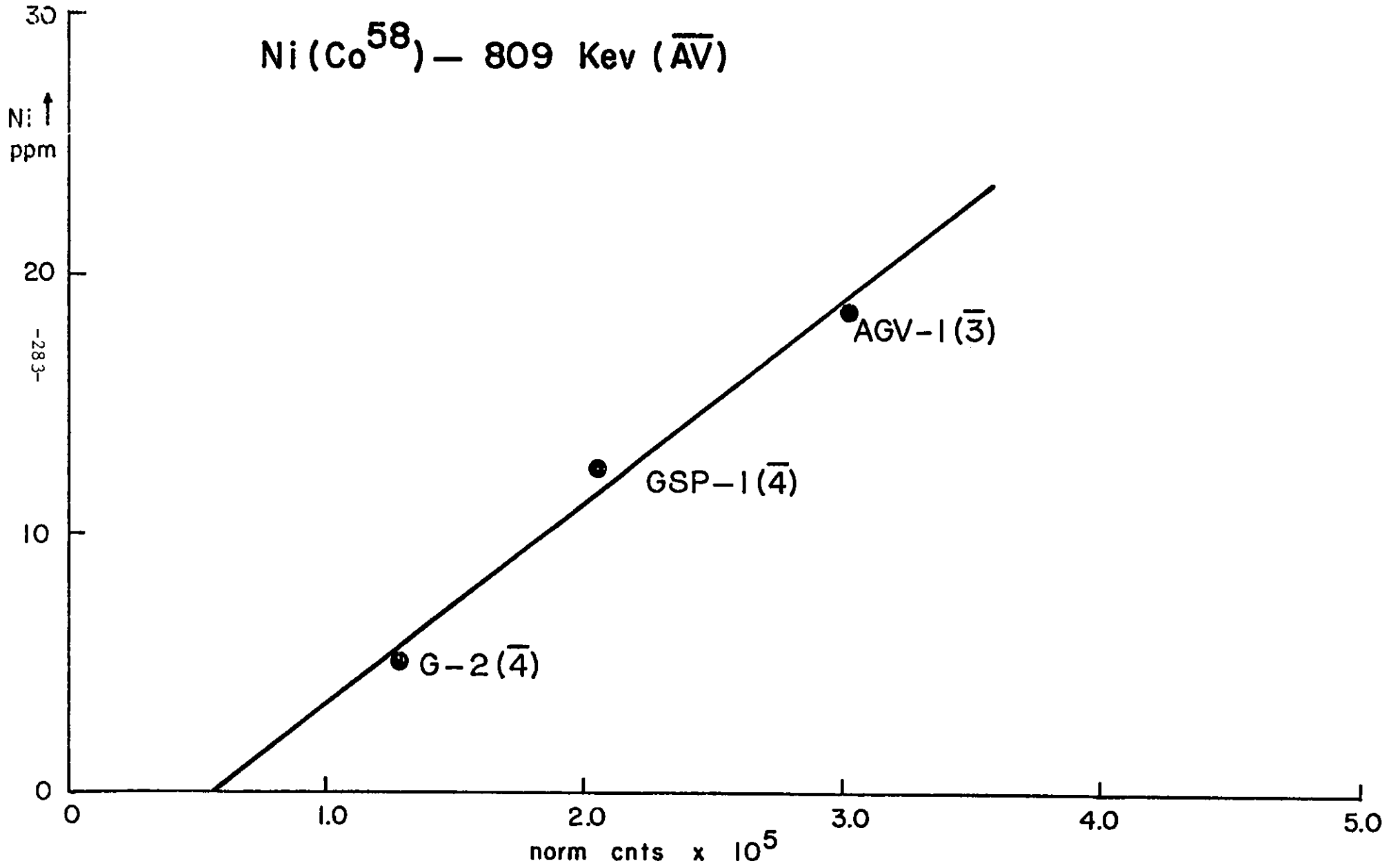


Figure 277

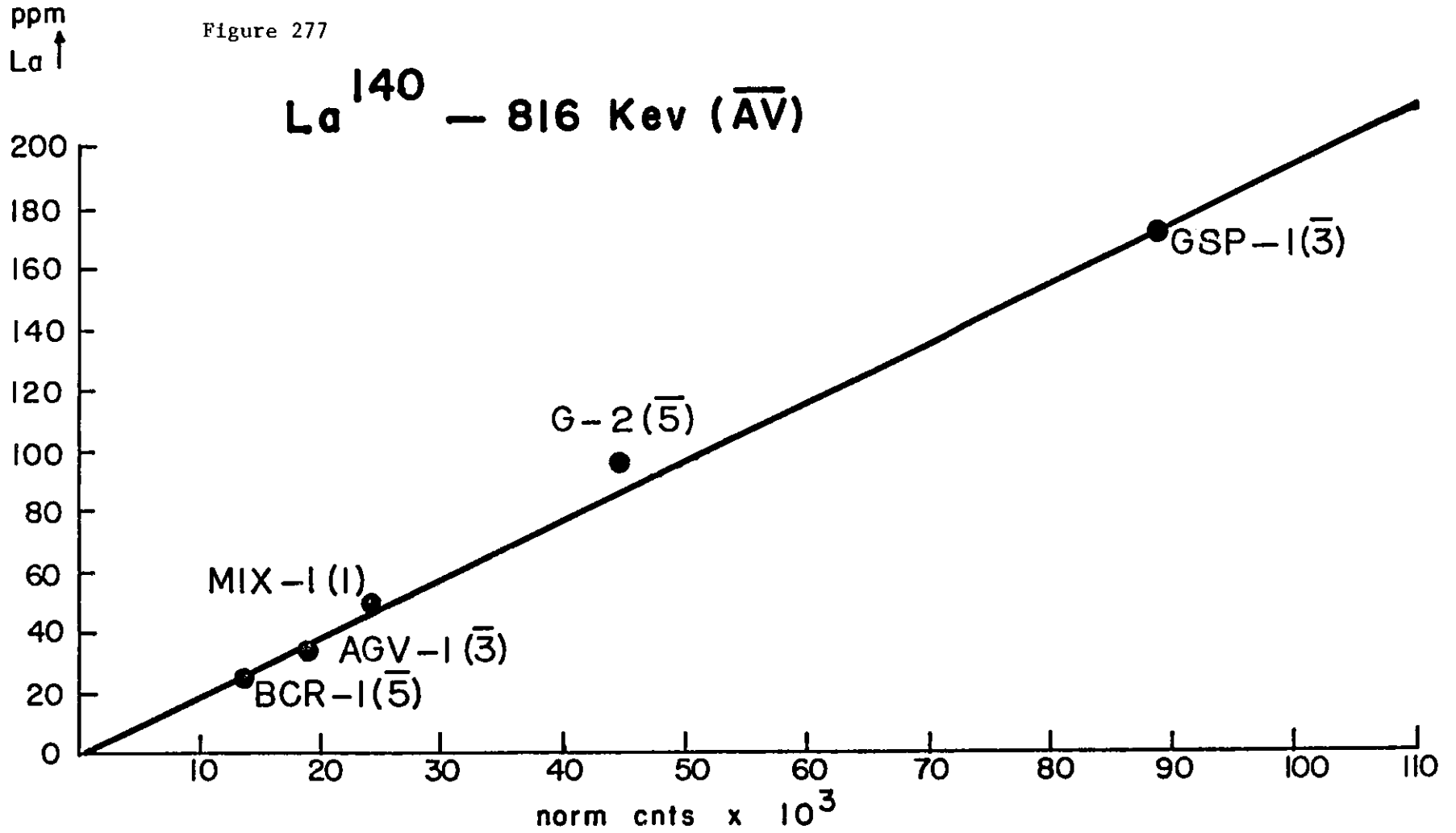


Figure 278

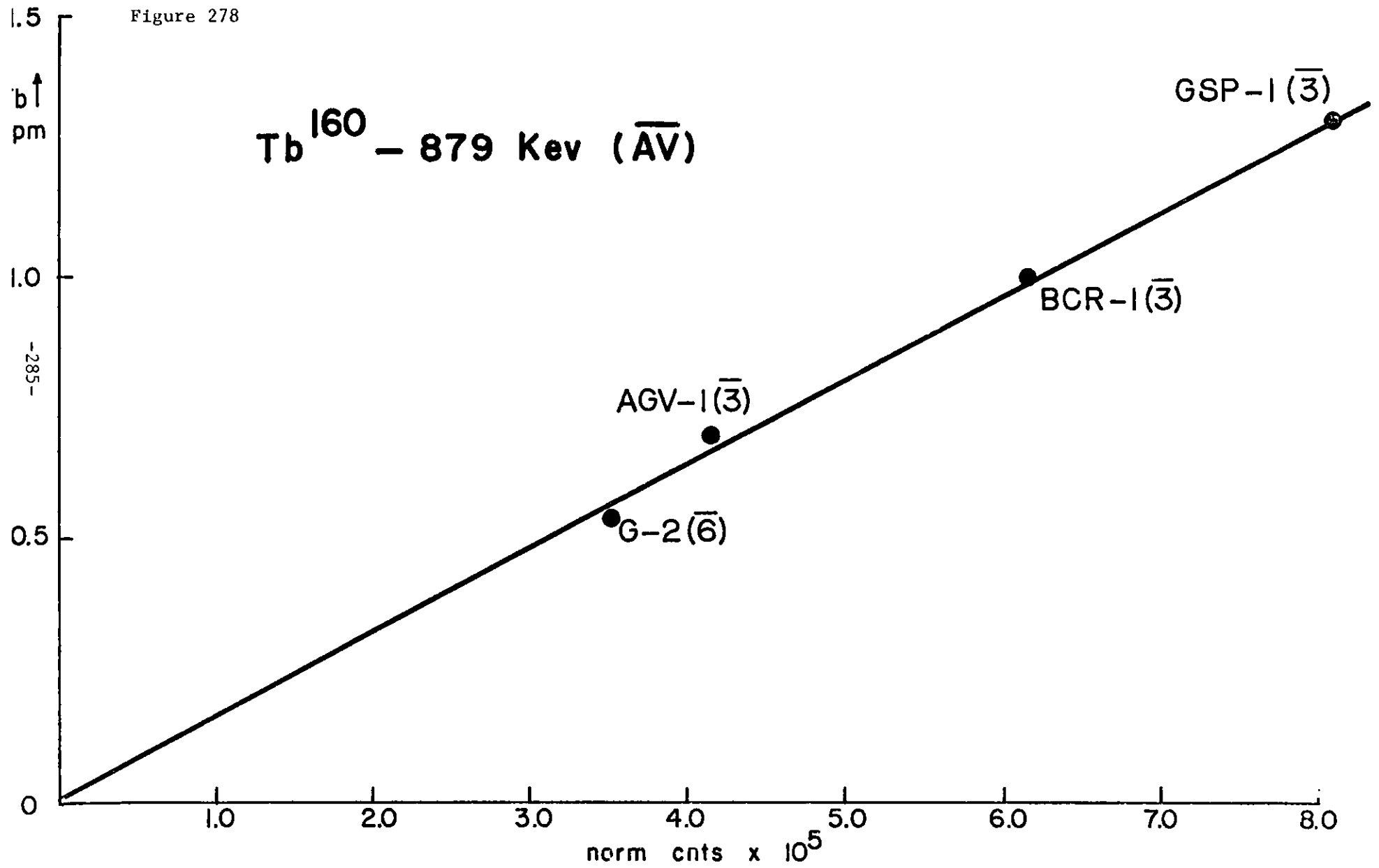


Figure 279

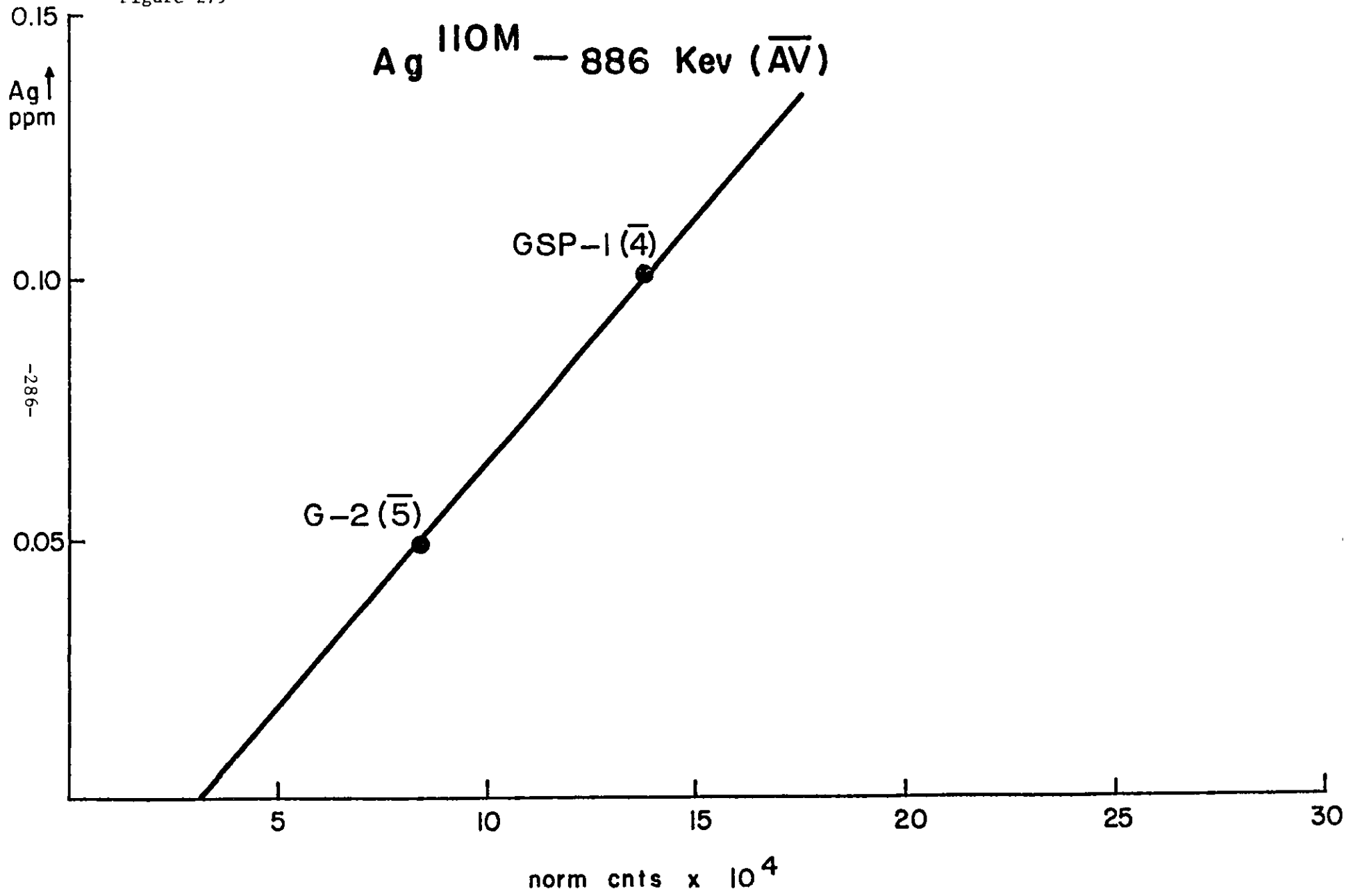


Figure 280

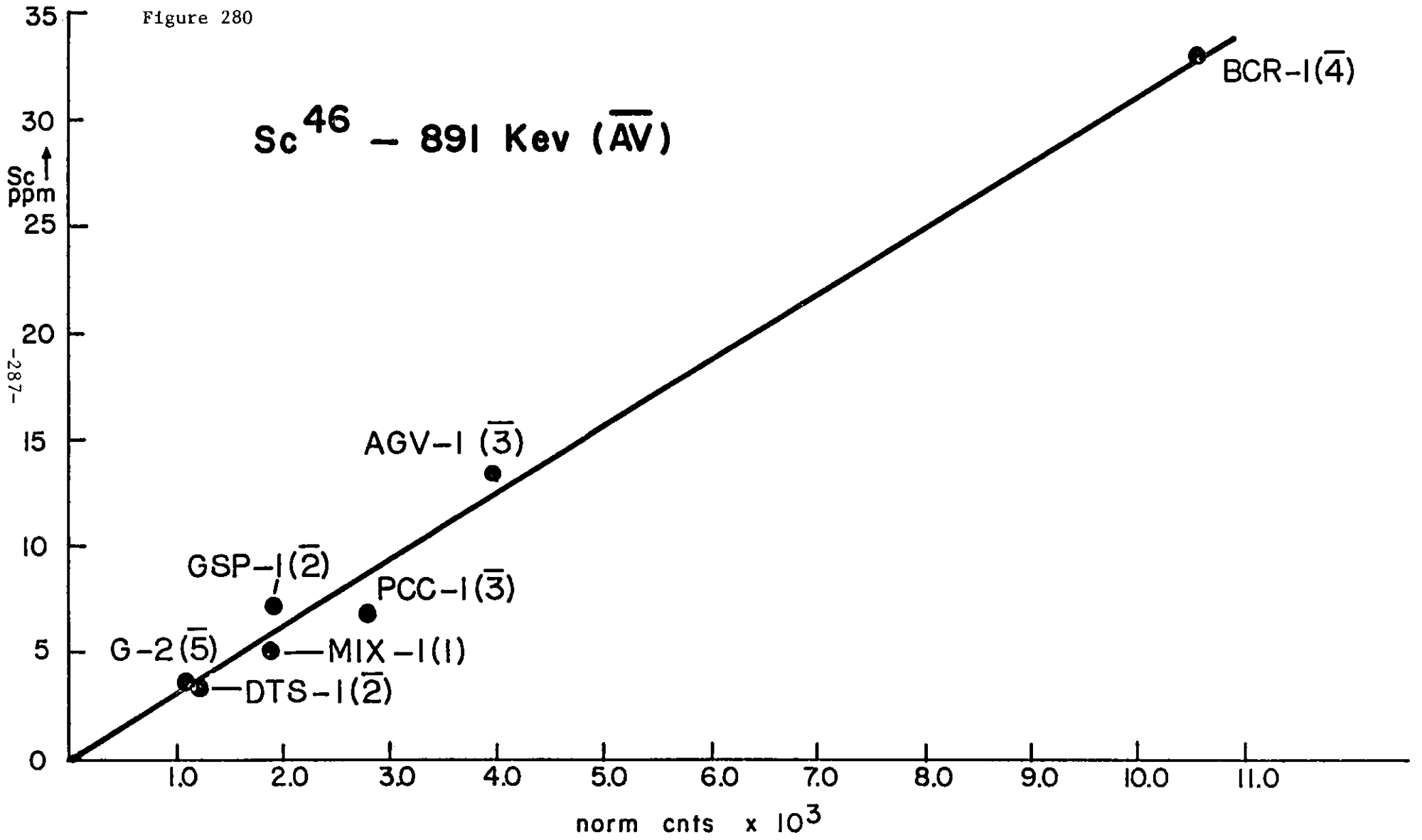


Figure 281

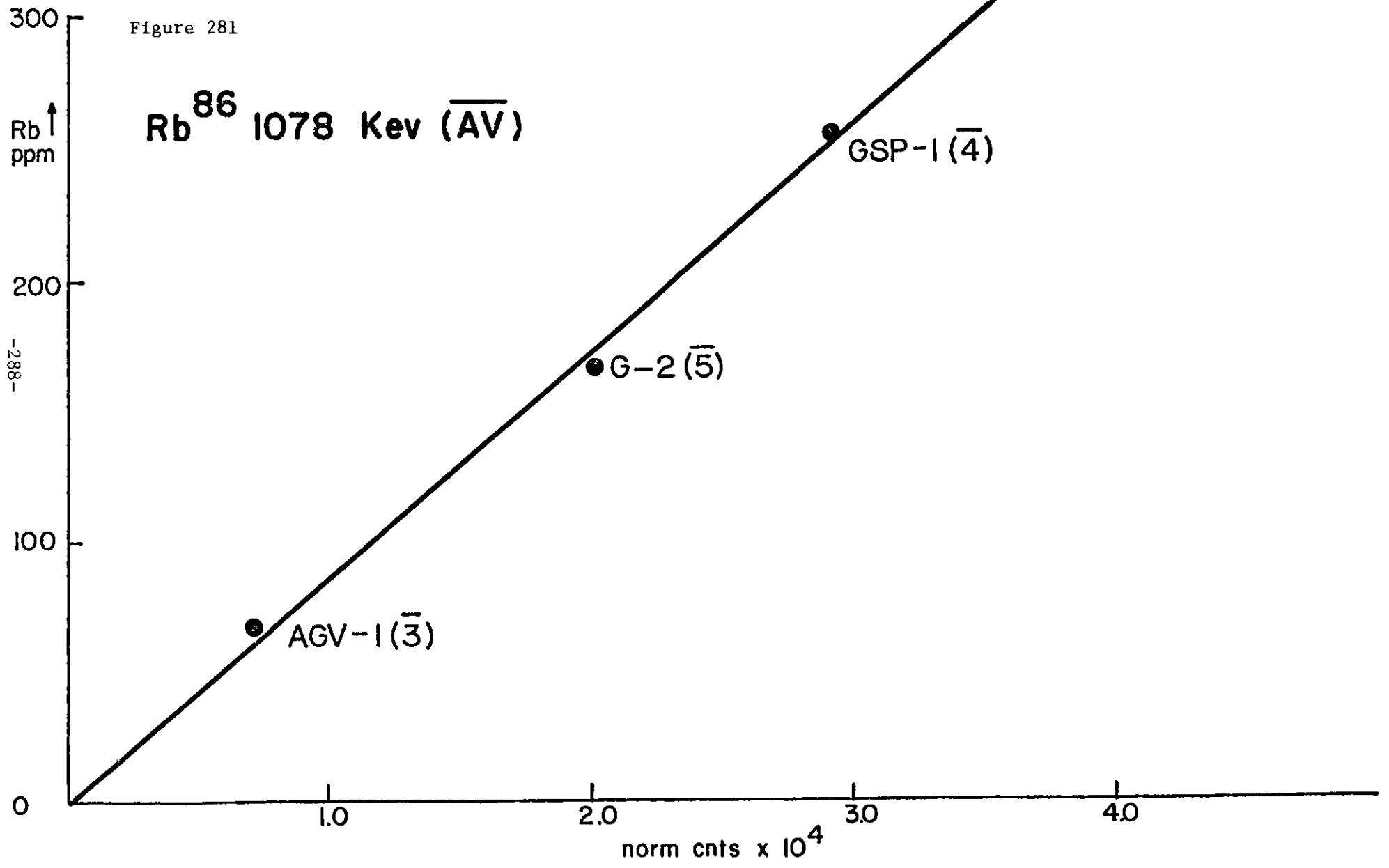
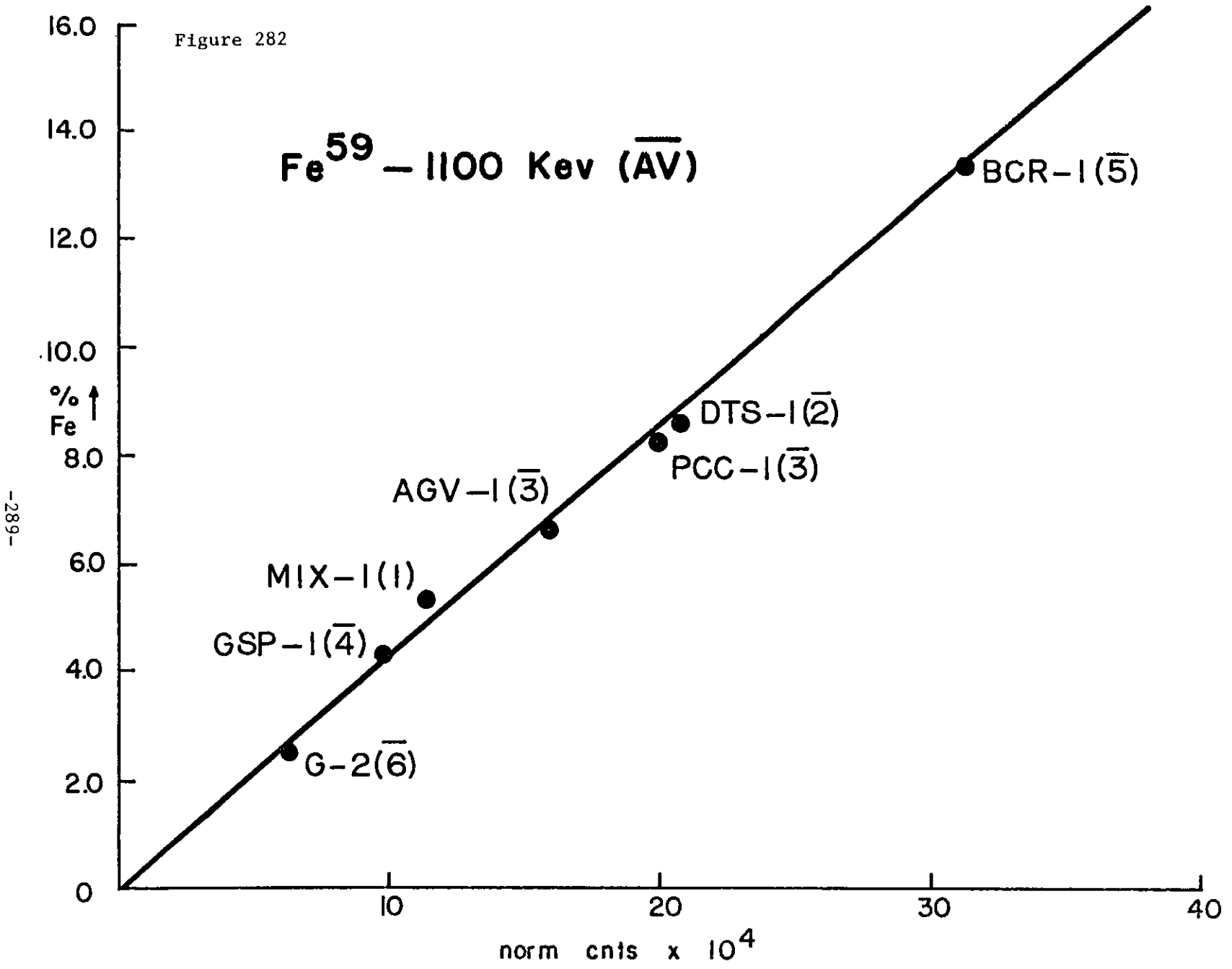


Figure 282

Fe^{59} - 1100 Kev ($\bar{A}\bar{V}$)



-289-

Ta ↑
ppm

Figure 283

Ta¹⁸² - 1229 Kev (\bar{AV})

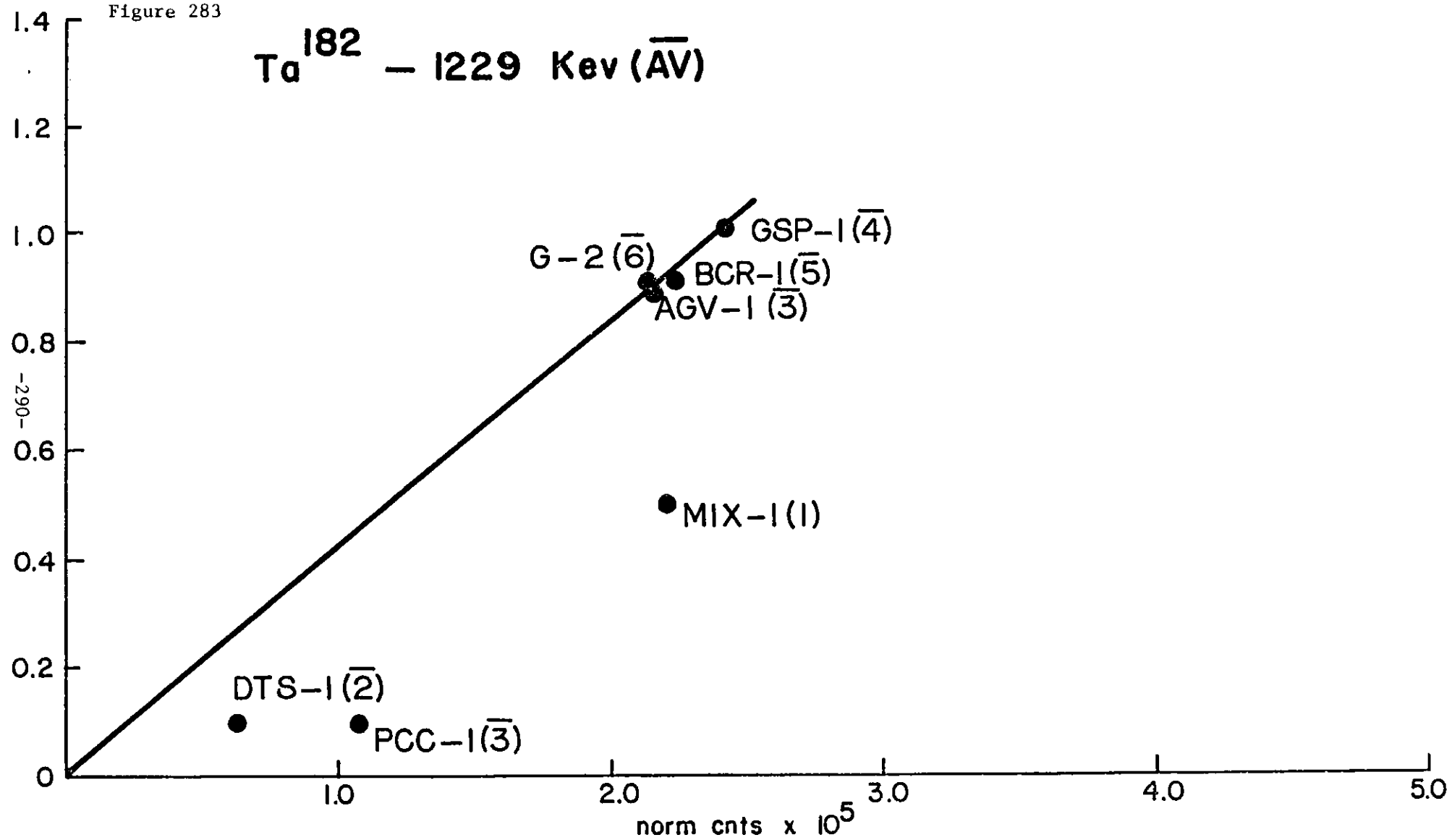
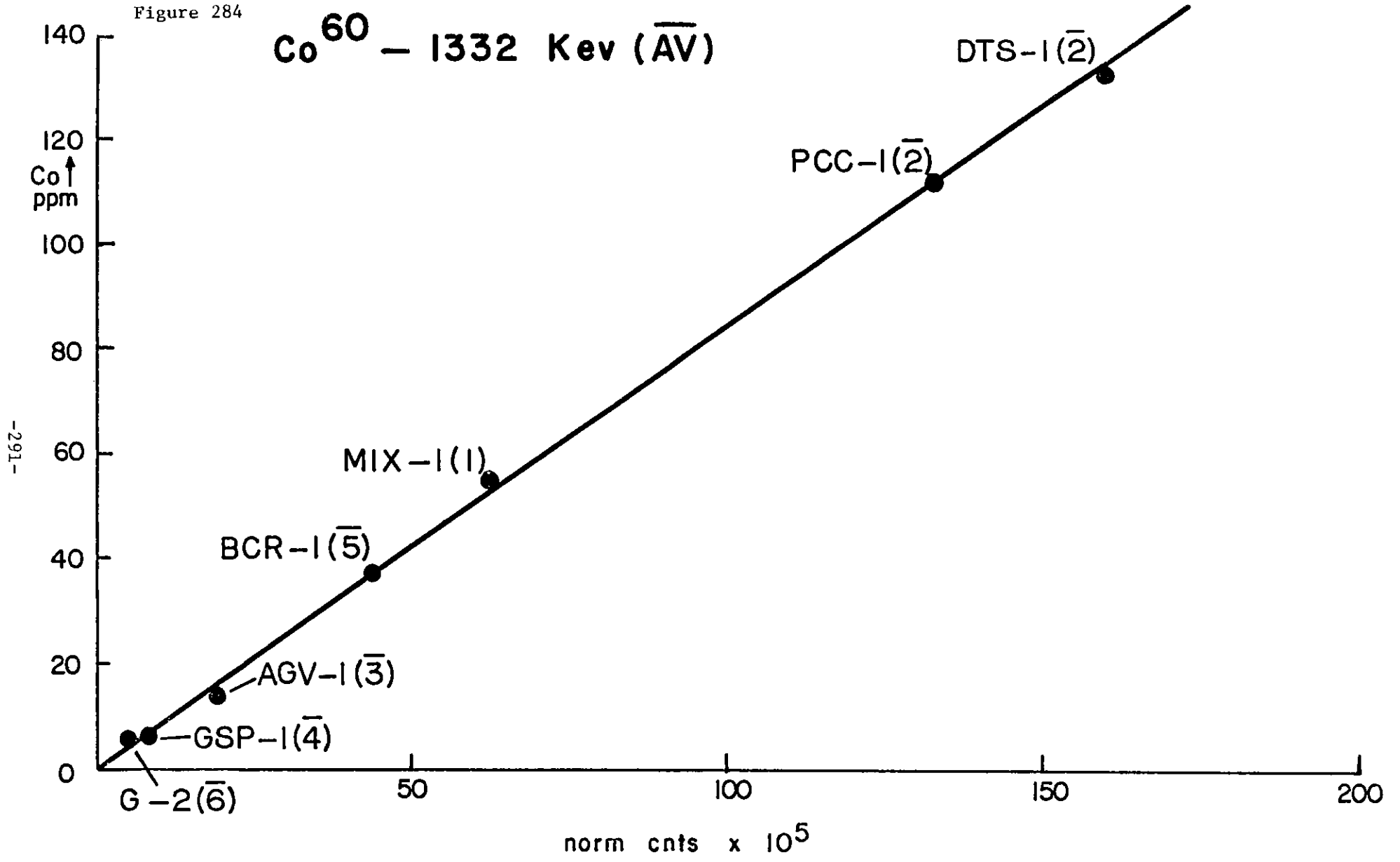


Figure 284

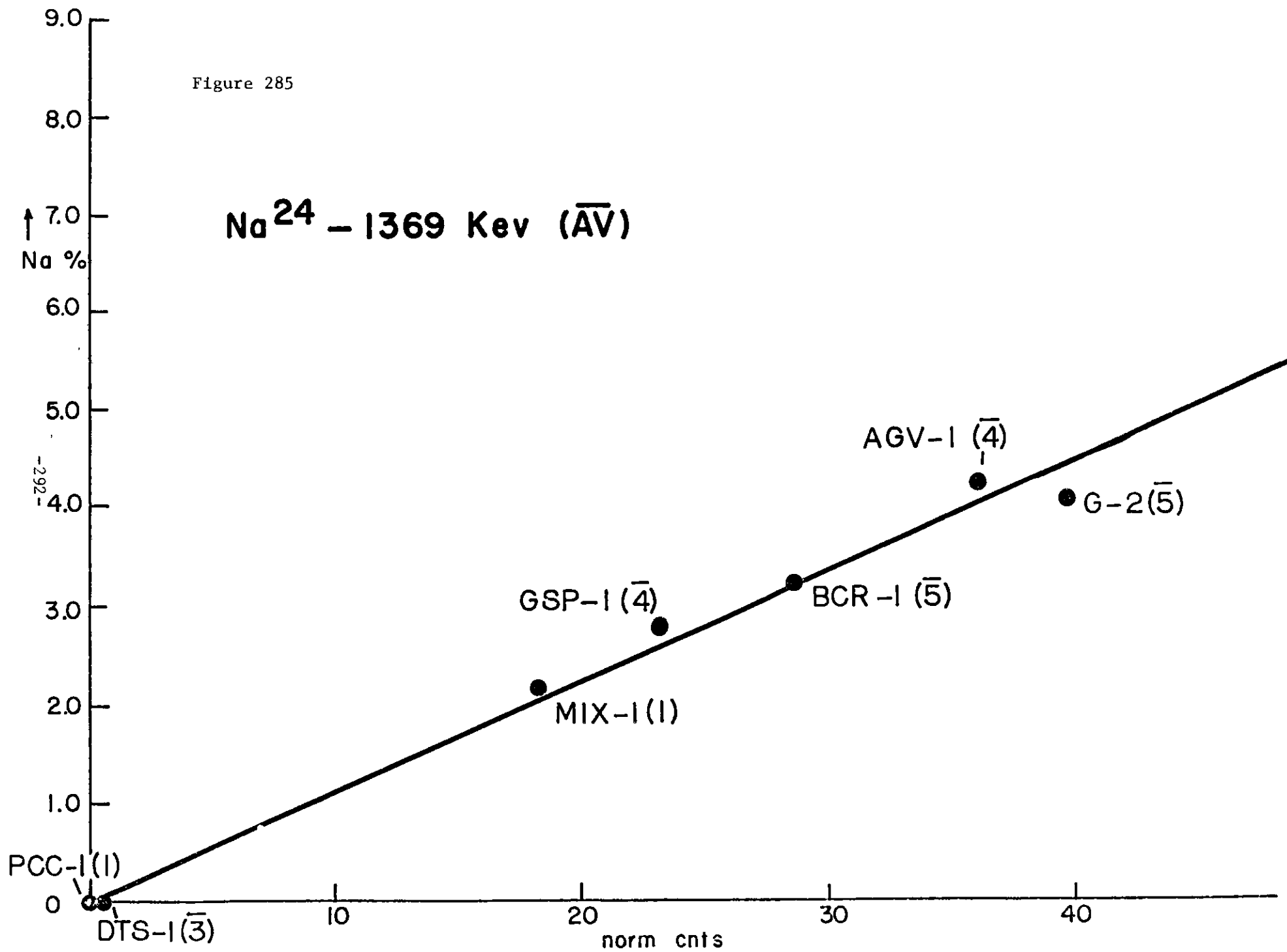
Co^{60} - 1332 Kev (\bar{AV})



-291-

Figure 285

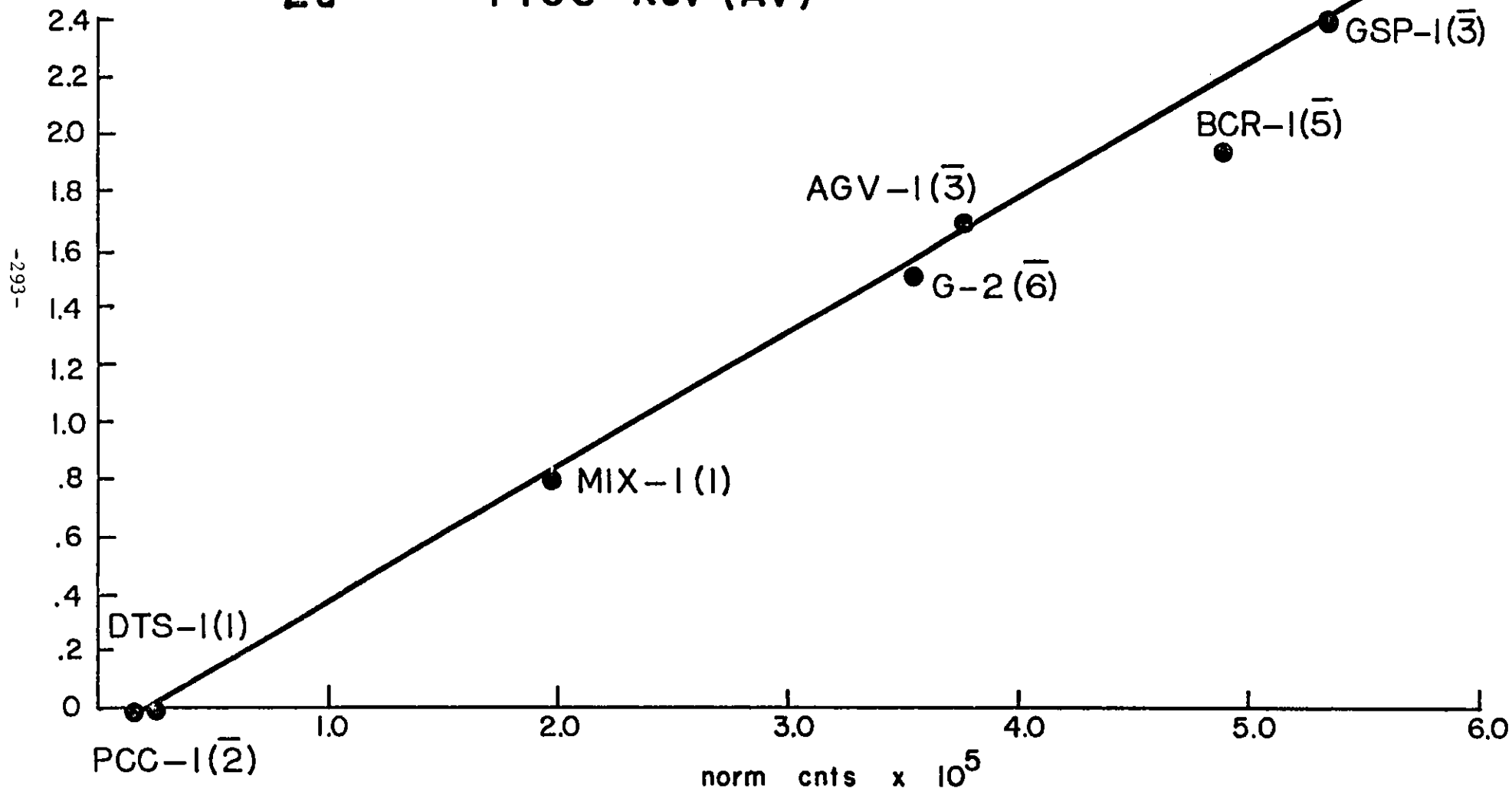
Na^{24} - 1369 Kev ($\bar{A}\bar{V}$)



Eu
ppm ↑

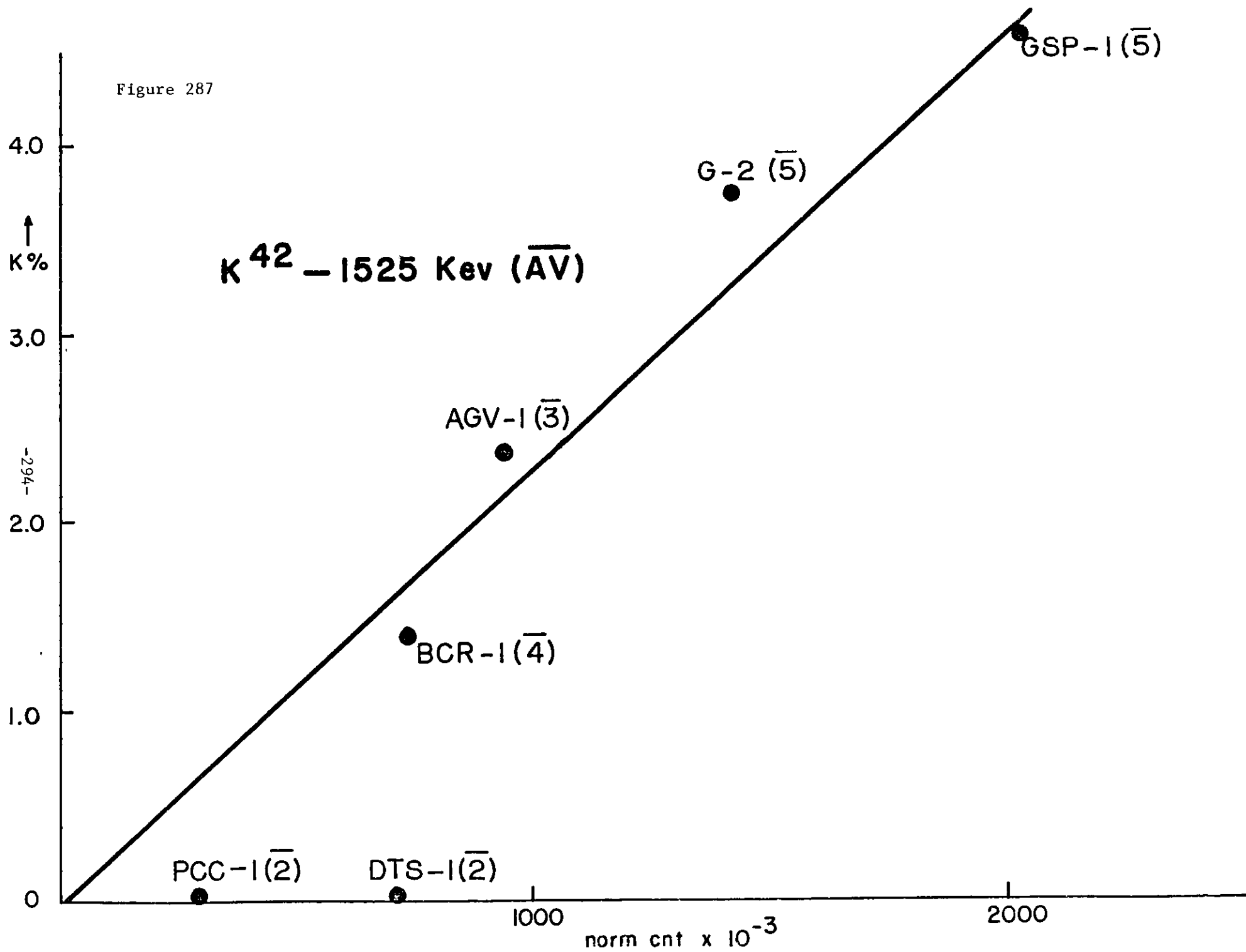
Figure 286

$\text{Eu}^{152} - 1408 \text{ Kev } (\bar{AV})$



-293-

Figure 287



Sb ↑
ppm

Figure 288

Sb¹²⁴ — 1691 Kev (\bar{AV})

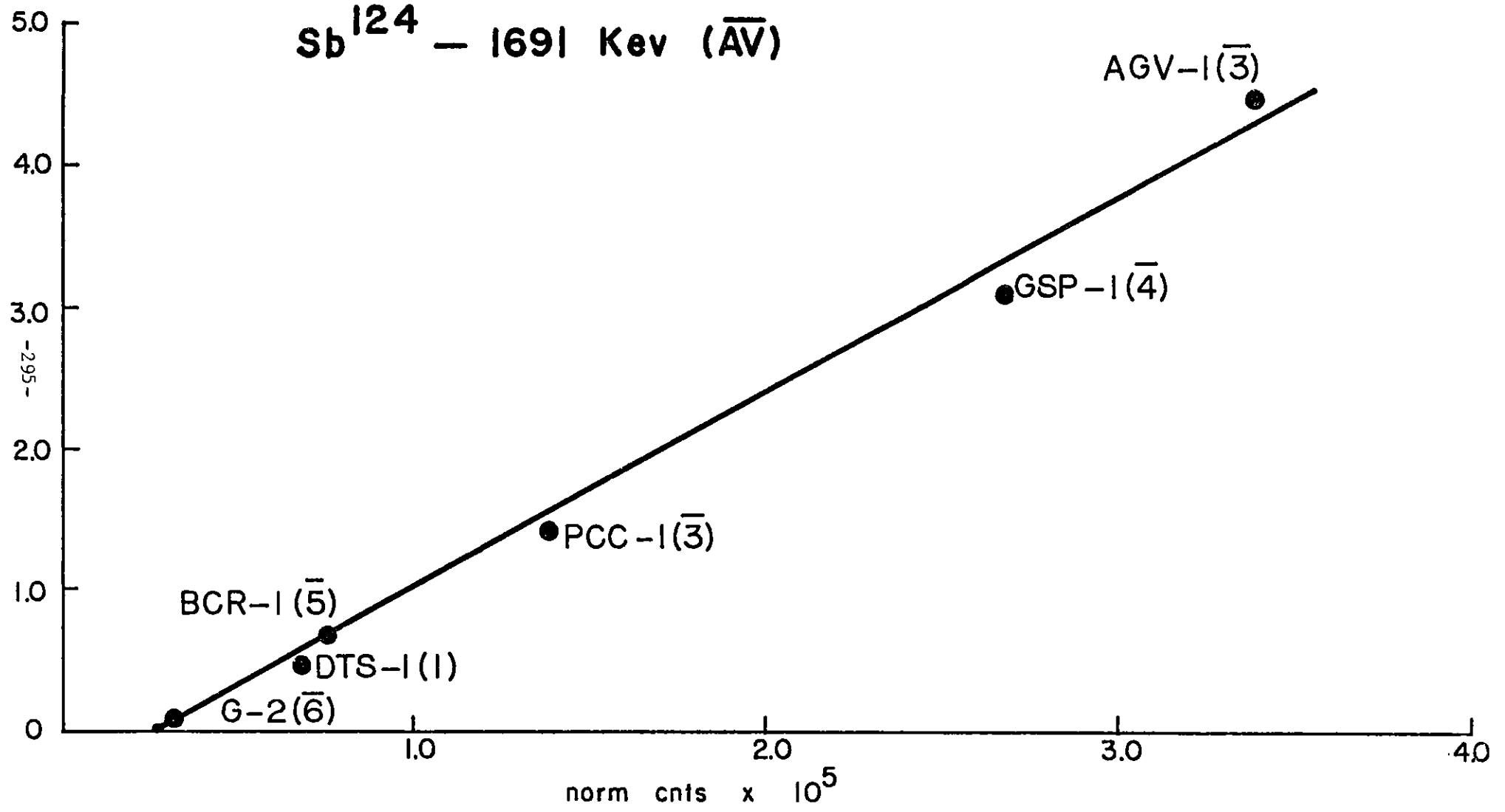


Table 24

Estimates for trace elements in
USGS Samples
(adapted from Flanagan, 1976)

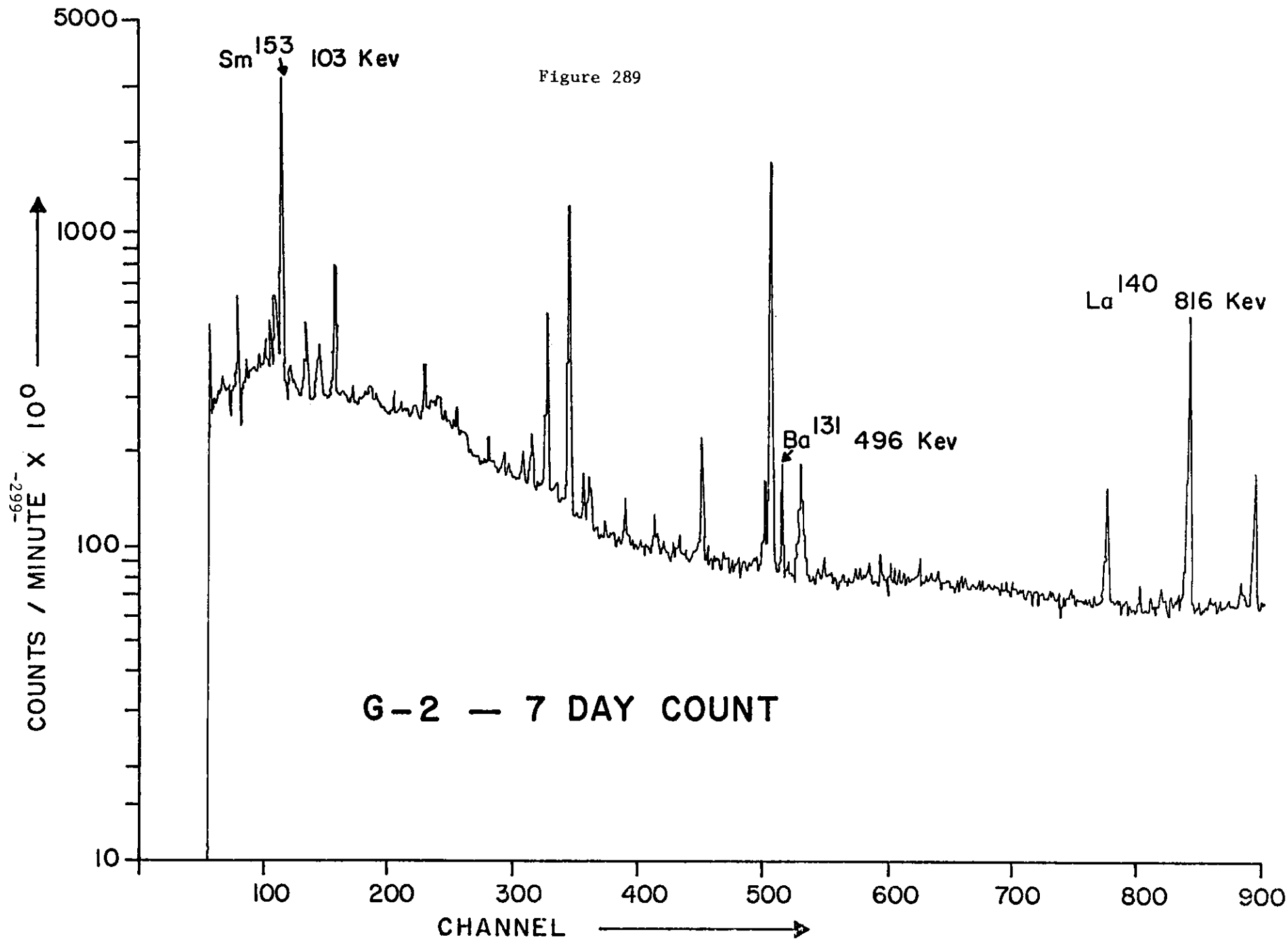
	G-2	BCR1	GSP-1	DTS-1	PCC-1	AGV-1	MIX-1
La	96.	26.	191.	.04	.15	35.	51.46
Ce	150.	53.9	394.	.06	.09	63	80.34
Nd	60.	29	188.	<0.02	-	39	32.12
Sm	7.3	6.6	27.1	.004	.008	5.9	3.91
Eu	1.5	1.94	2.4	.0009	.002	1.7	.80
Ho	0.4	1.2	<0.5	.003	-	0.6	.21
Tb	0.54	1.0	1.3	.0003	.001	0.7	.29
Yb	0.88	3.36	1.8	.01	.02	1.7	.48
Xu	0.11	.55	.23	.002	.006	.28	.06
Na(Na ₂ O)	4.07%	3.27%	2.80%	.007%	.006%	4.26%	2.18%
Rb	168	46.6	254	.053	.063	67.	89.96
Cs	1.4	.95	1.0	.006	.006	1.4	0.75
Ba	1870.	675.	1300	2.4	1.2	1208.	1001.57
Sc	3.7	33.	7.1	3.6	6.9	13.4	5.19
Cr	7	17.6	12.5	4000.	2730	12.2	1272.38
Fe(Fe ₂ O ₃)	2.65%	13.40%	4.33%	8.64%	8.35%	6.76%	5.30%
Co	5.5	38.	6.4	133.	112	14.1	54.99
Hf	7.35	4.7	15.9	.01	.06	5.2	3.96
Th	24.2	6.0	104	.01	.01	6.41	12.96
Zr	300	190	500	3	7	225	164
K(K ₂ O)	4.51%	1.70%	5.53%	.0012%	.004%	2.89%	2.42%

Table 24 (continued)

	USGS Samples						
	G-2	BCR1	GSP-1	DTS-1	PCC-1	AGV-1	MIX-1
Tm	0.3	0.6	-	0.001	-	0.4	0.16
As	0.25	0.70	0.09	.03	.05	0.8	0.16
Sb	0.1	0.69	3.1	0.46	1.4	4.5	0.70
Ta	0.91	0.91	1.0	<.1	<0.1	0.9	-
Ni	5.1	15.8	12.5	2269.	2339	1089.66	-

Table 25

<u>Measurement of Nuclides Observed</u>					Best Known
	<u>Isotope</u>	<u>Kev</u>	<u>Best Time</u>	<u>error</u>	<u>Lower limit of Detection</u>
Na	Na ²⁴	1369	7 days	+ 5%	0.06%
K	K ⁴²	1525	7 days	+ 15%	0.05%
Fe	Fe ⁵⁹	1100	49-56 days	+ 5%	0.15%
Cs	Cs ¹³⁴	796	49-56 days	+ 5%	1.07 ppm
Ba	Ba ¹³¹	496	7-14 days	+ 10%	80.0 ppm
Sc	Sc ⁴⁶	891	49-56 days	+ 10%	0.01 ppm
Zr	Zr ⁹⁵	757	49-56 days	+ 20%	50 ppm
Hf	Hf ¹⁸¹	483	49-56 days	+ 5%	0.4 ppm
Ta	Ta ¹⁸²	1229	49-56 days	+ 5%	0.05 ppm
Cr	Cr ⁵¹	321	28-35 days	+ 20%	0.54 ppm
Rb	Rb ⁸⁶	1078	28-35 days	+ 10%	5 ppm
Co	Co ⁶⁰	1332	49-56 days	+ 5%	0.35 ppm
Ni	Co ⁵⁸	809	49-56 days	+ 15%	5 ppm
Ag	NA	NA	NA	NA	NA
Sb	Sb ¹²⁴	1691	49-56 days	+ 10%	0.01 ppm
Th	Pa ²³³	311	28-35 days	+ 5%	0.41 ppm
La	La ¹⁴⁰	816	7-14 days	+ 5%	.5 ppm
Ce	Ce ¹⁴¹	146	28-35 days	+ 5%	1 ppm
Nd	Nd ¹⁴⁷	531	7-14 days	+ 5%	10 ppm
Sm	Sm ¹⁵³	103	7-14 days	+ 5%	0.3 ppm
Eu	Eu ¹⁵²	1408	49-56 days	+ 5%	0.01
Tb	Tb ¹⁶⁰	879	49-56 days	+ 5%	0.1 ppm
Tm	Tm ¹⁷⁰	88	49-56 days	+ 20%	0.1 ppm
Yb	Yb ¹⁷⁵	283	7-14 days	+ 10%	0.1 ppm
Lu	Lu ¹⁷⁷	208	7-14 days	+ 15%	0.1 ppm



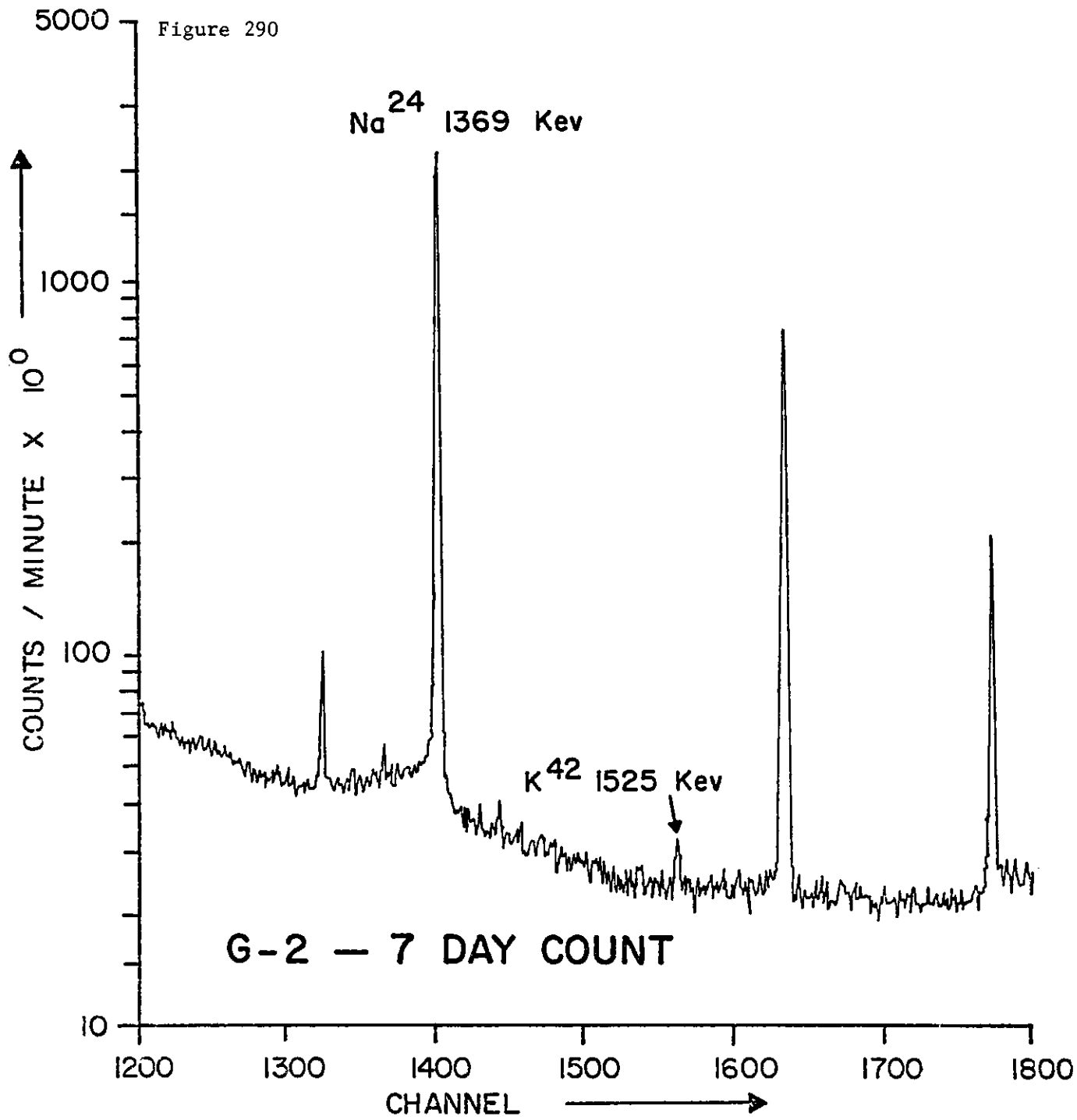
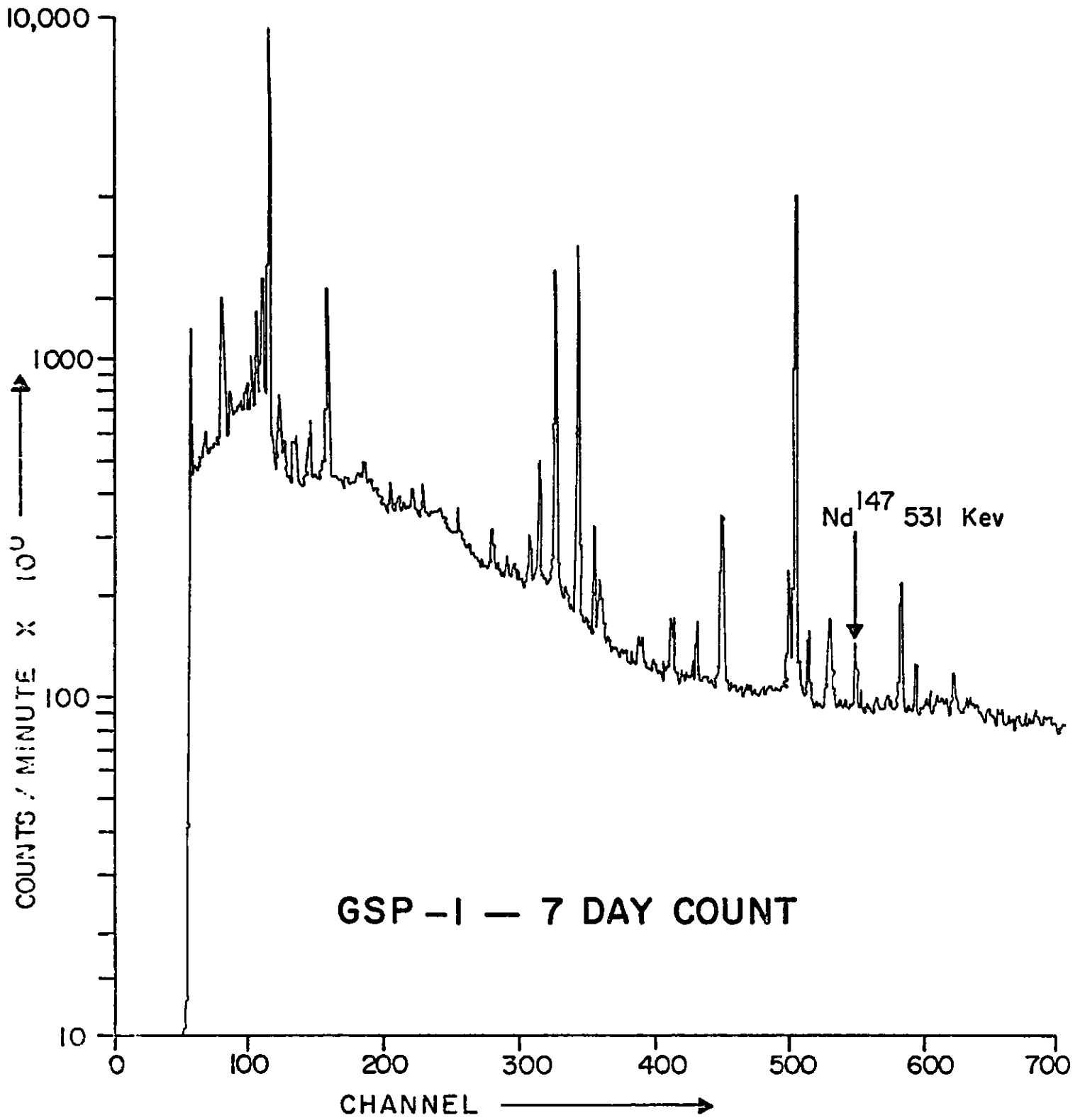
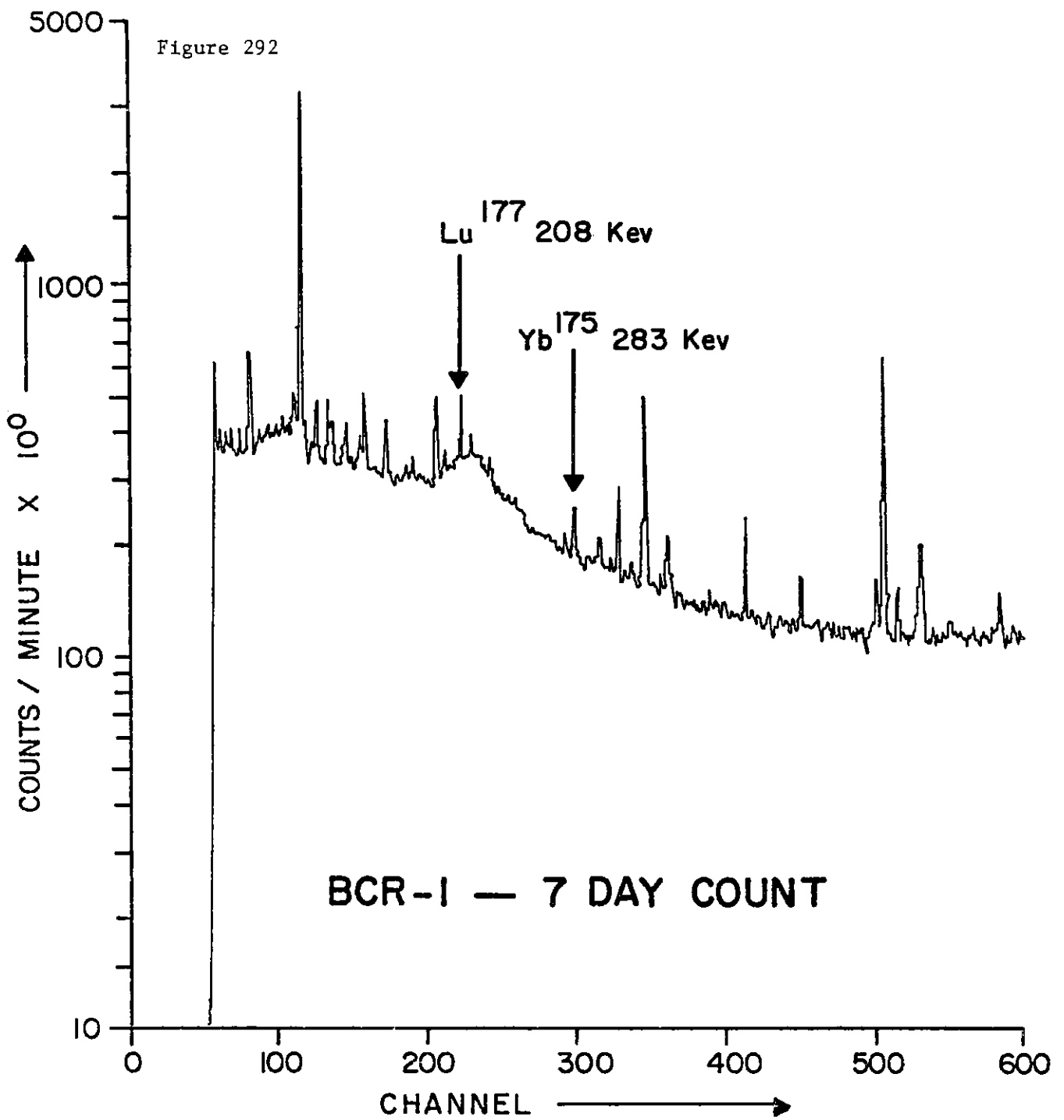


Figure 291





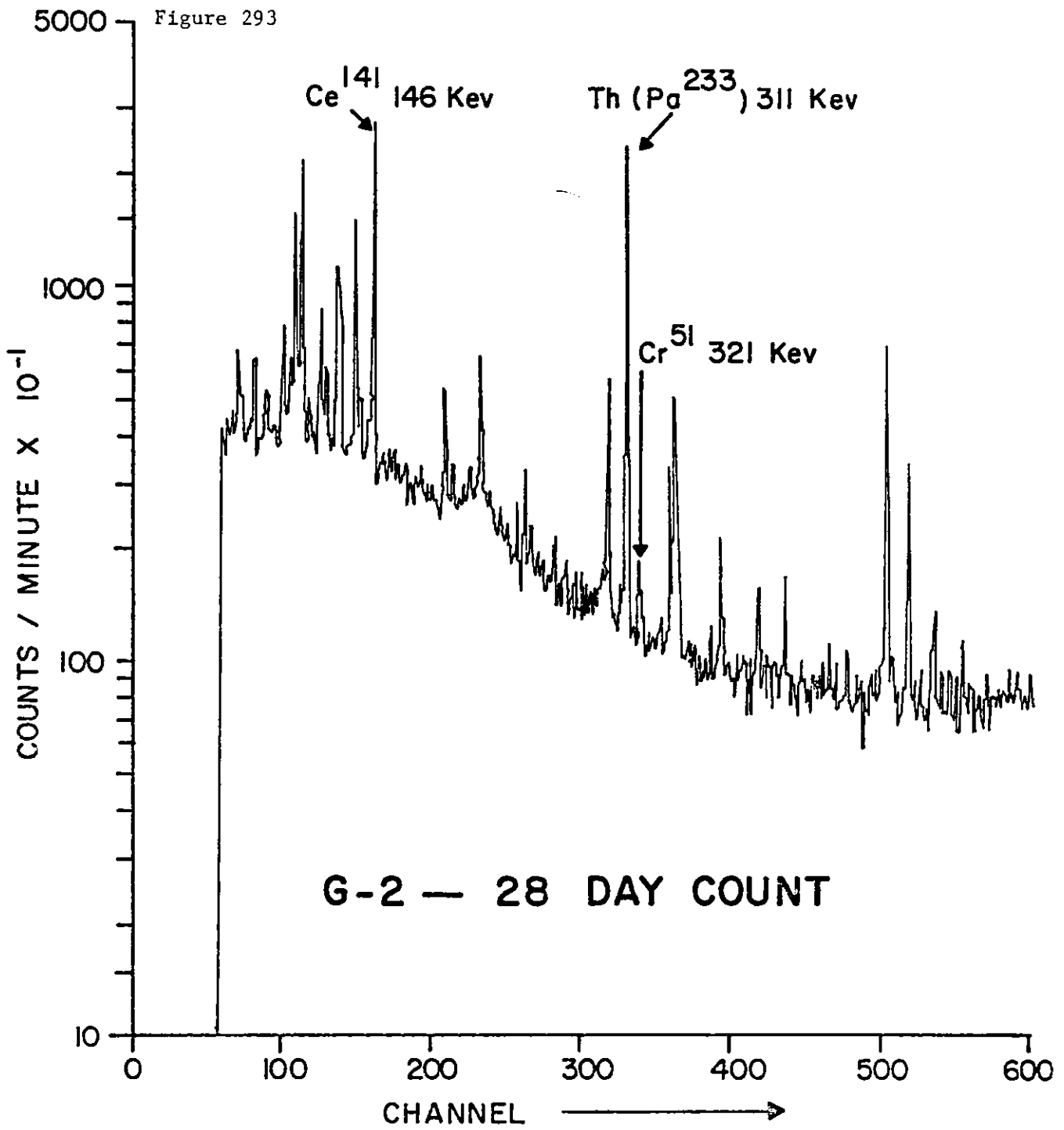


Figure 294

G-2 — 28 DAY COUNT

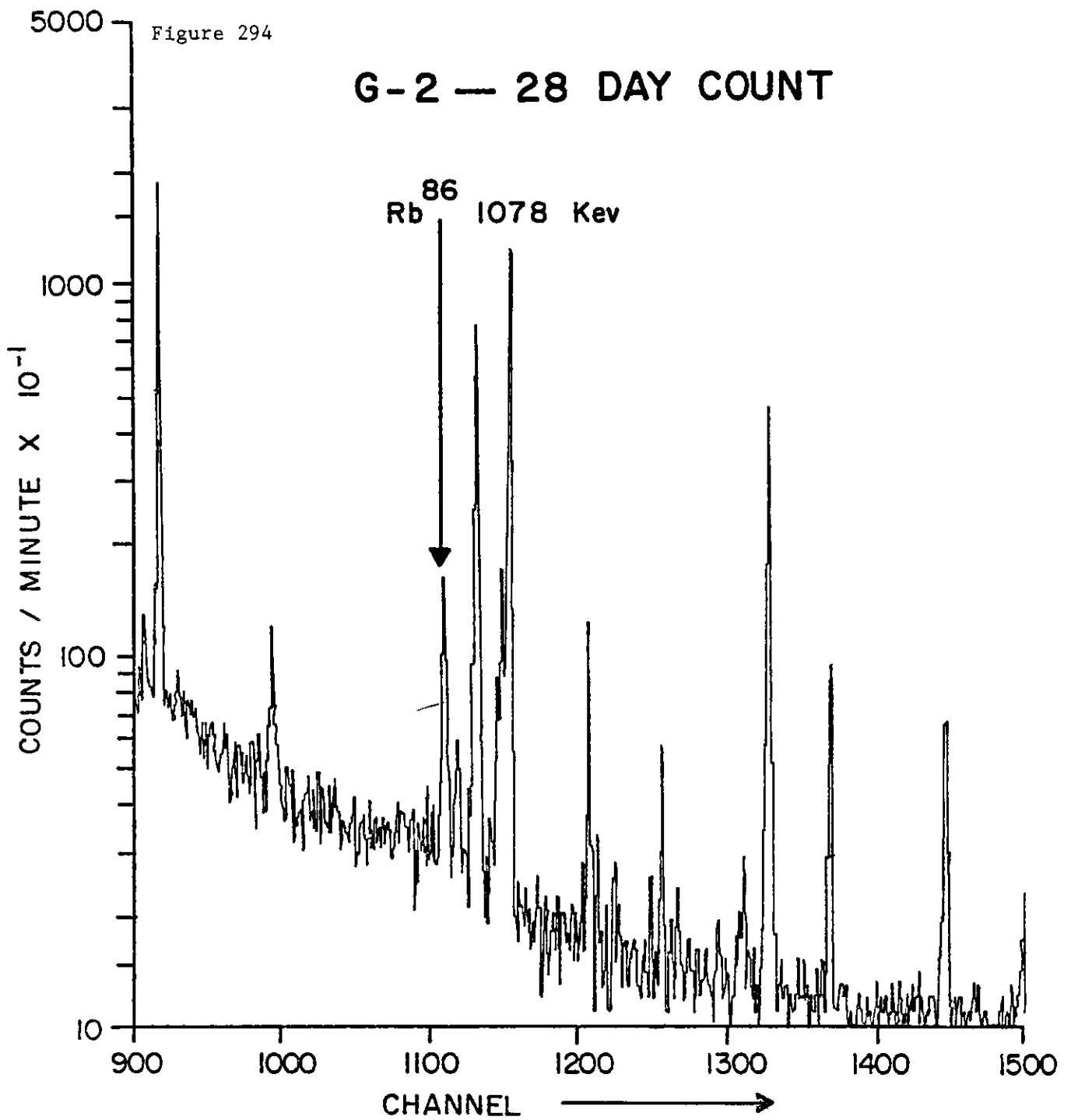


Figure 295

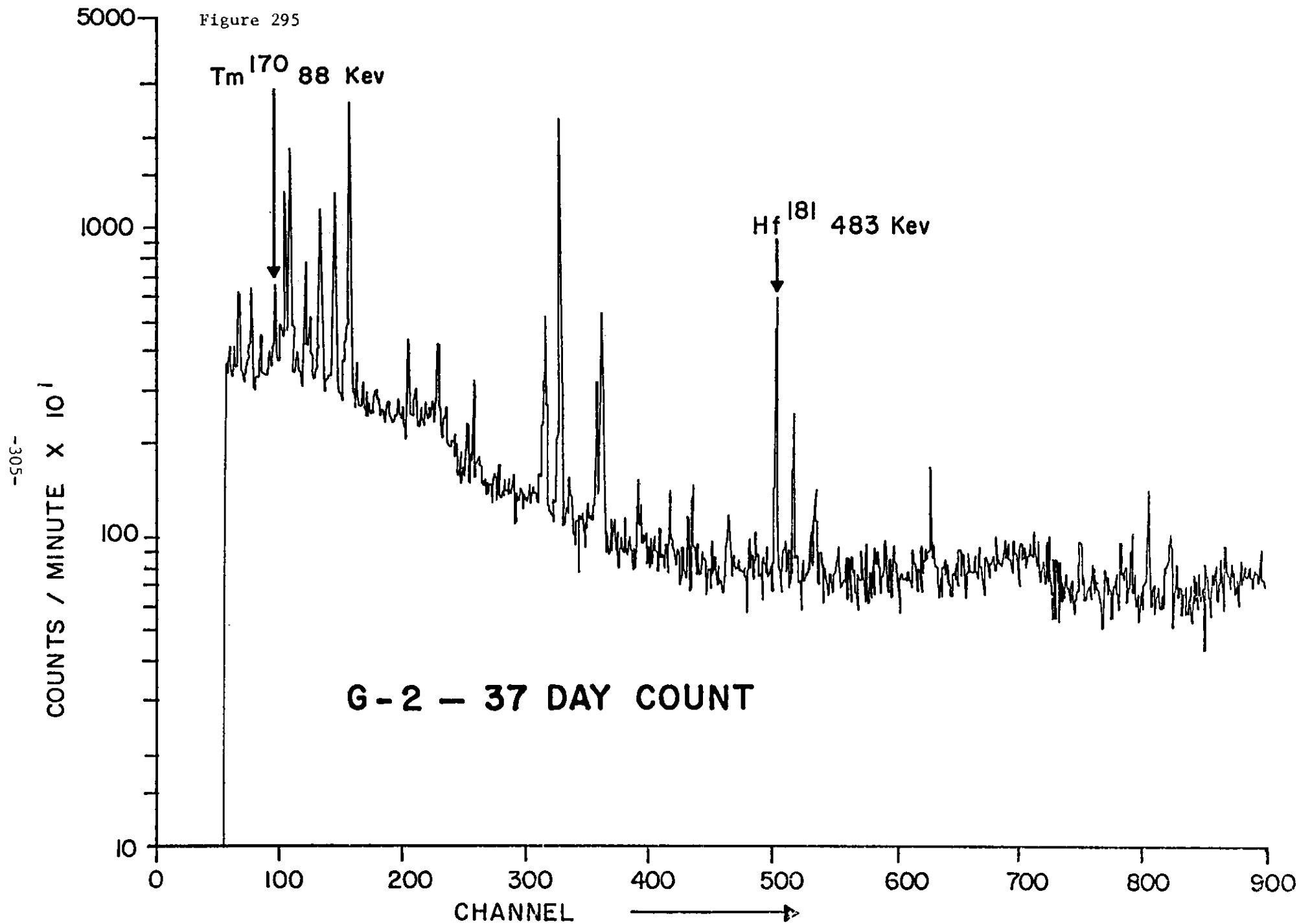


Figure 296

G-2 — 37 DAY COUNT

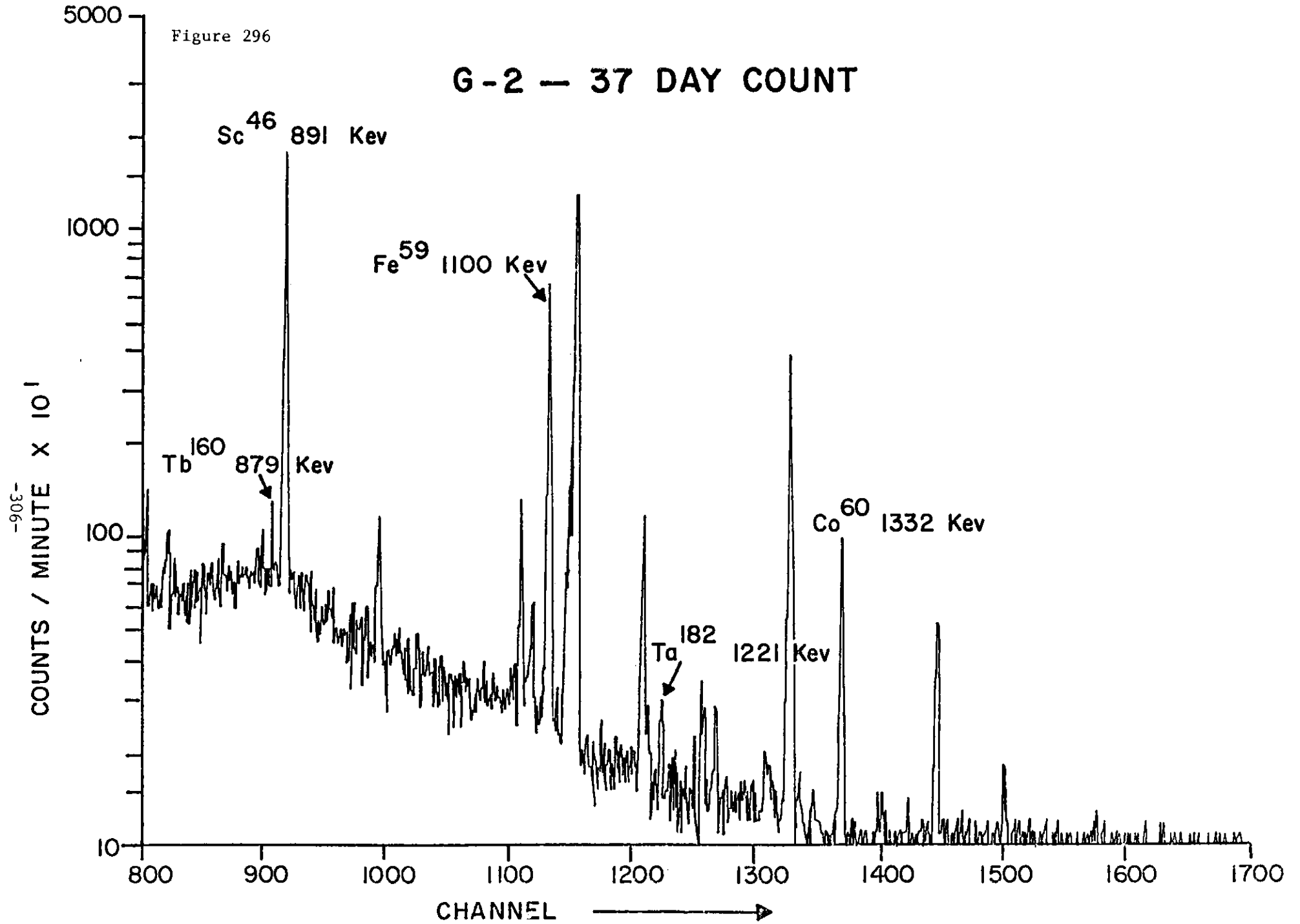
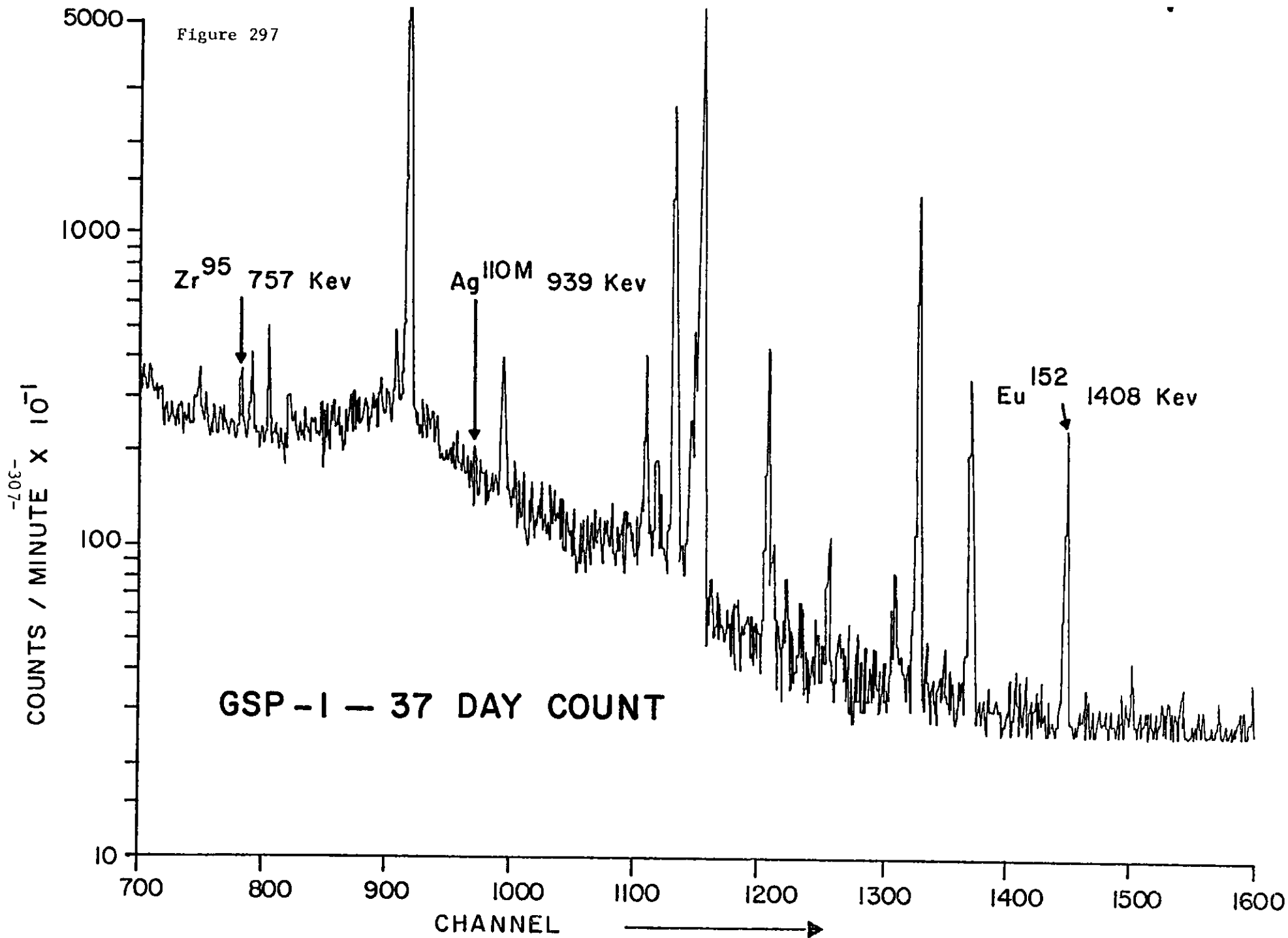


Figure 297



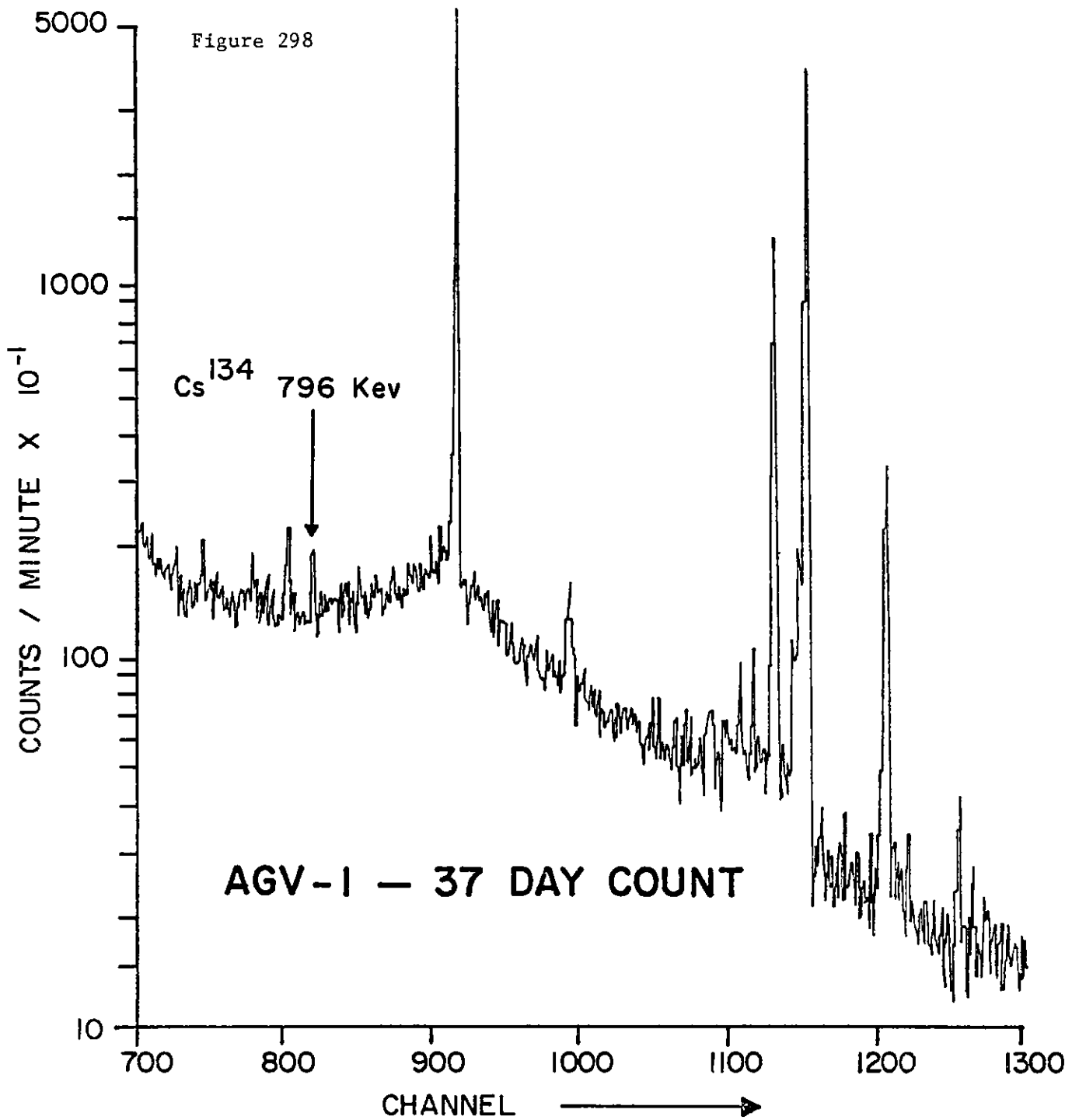


Figure 299

AGV - 1-37 DAY COUNT

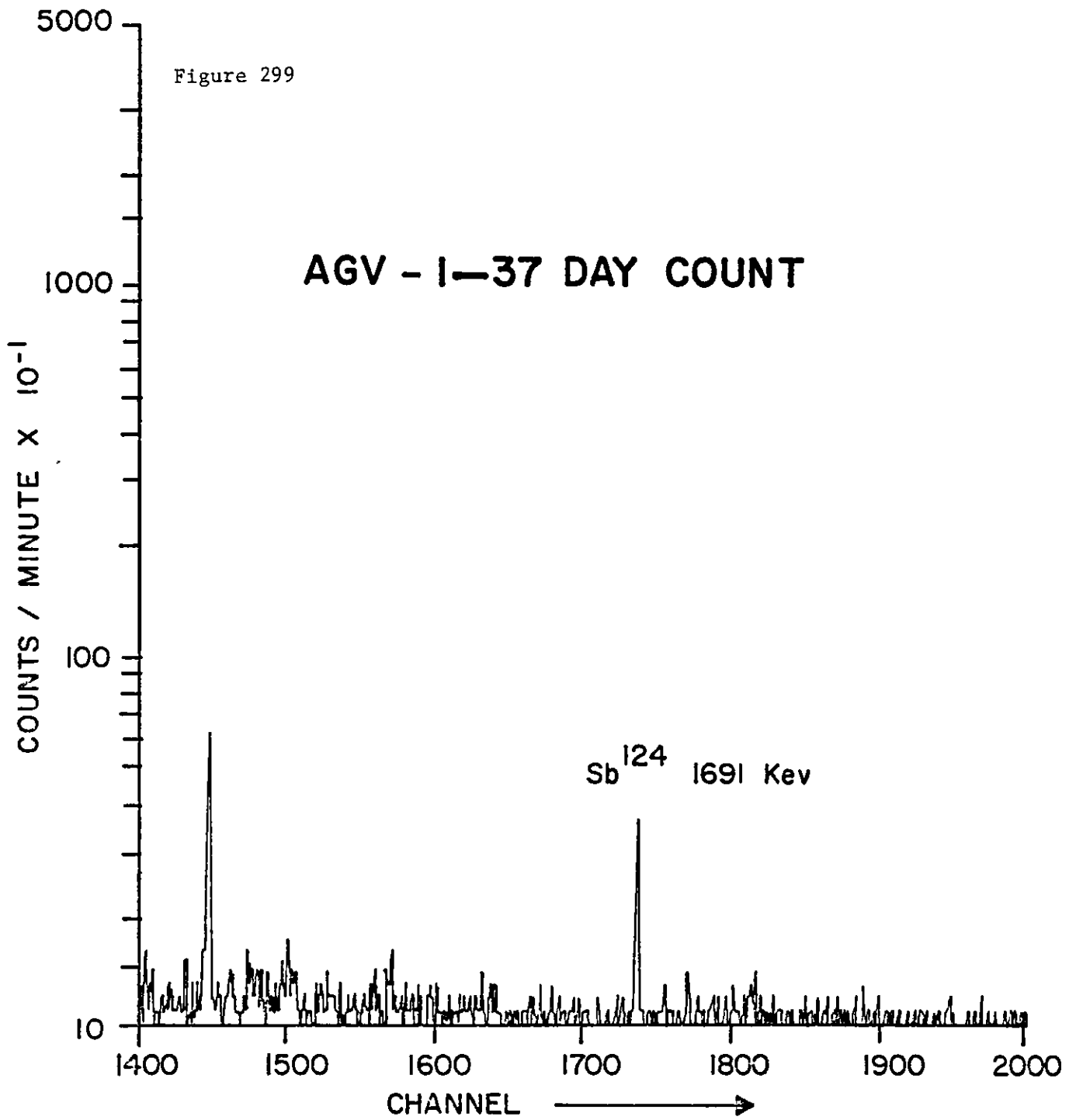


Figure 300

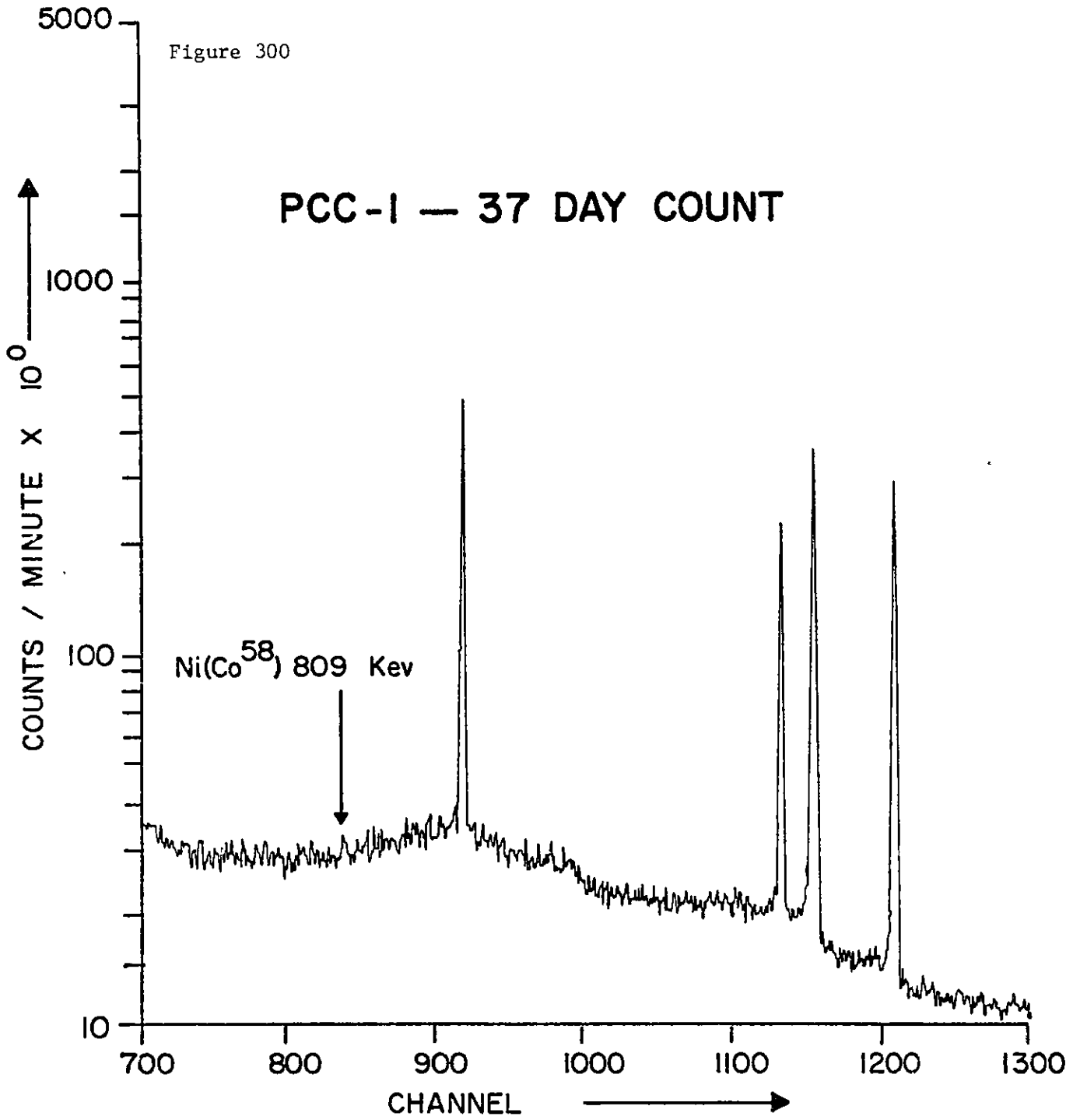


Table 26

Mancos Shale

(data in ppm except where noted)

	<u>Whole Rocks</u>		<u>-2μ Fraction</u>	
		<u>n</u>		<u>n</u>
Na (%)	0.83	29	0.22	18
K (%)	2.67	29	1.43	18
Fe (%)	4.03	29	6.43	18
Cs	5.16	29	15.38	18
Ba	288.64	29	225.71	18
Sc	8.91	29	17.01	18
Zr	283.99	29	378.46	18
Hf	6.63	29	6.03	18
Ta	1.25	29	1.41	18
Cr	53.28	29	99.30	18
Rb	127.27	29	184.02	18
Co	6.98	29	12.33	18
Ni	11.75	29	31.76	18
Sb	0.40	29	0.78	18
Th	15.35	29	22.32	18
La	37.84	29	45.66	18
Ce	75.49	29	93.97	18
Nd	49.79	29	57.90	18
Sm	6.58	29	6.76	18
Eu	1.19	29	1.40	18
Tb	0.77	29	6.12	18
Tm	0.38	29	0.56	18
Yb	2.52	29	2.64	18
Lu	0.43	29	0.53	18
Σ REE	174.81	29	205.55	18

Table 27

Dakota Formation
(data in ppm except where noted)

	Whole Rocks		-2 μ Fraction	
		<u>n</u>		<u>n</u>
Na (%)	.23	23	.19	20
K (%)	.63	20	.77	19
Fe (%)	1.74	23	4.12	20
Cs	.99	8	2.56	10
Ba	331.13	13	585.86	20
Sc	5.04	22	10.18	20
Zr	317.91	19	347.36	18
Hf	8.00	22	8.21	20
Ta	1.33	17	.55	10
Cr	58.54	15	28.55	17
Rb	41.97	21	59.31	19
Co	3.47	23	6.48	20
Ni	7.92	15	26.60	17
Sb	.72	17	1.33	17
Th	21.21	23	43.30	20
La	63.44	19	107.95	20
Ce	89.50	23	192.90	20
Nd	45.93	23	87.50	20
Sm	7.58	23	14.92	20
Eu	1.24	23	2.63	20
Tb	0.76	22	1.48	20
Tm	0.38	22	0.73	20
Yb	2.42	18	3.14	20
Lu	1.05	22	0.69	20
Σ REE	198.41	23	416.38	20

Table 28

Jackpile Sandstone
(data in ppm except where noted)

	<u>Whole Rocks</u>		<u>-2μ Fraction</u>	
		<u>n</u>		<u>n</u>
Na (%)	.62	7	.15	8
K (%)	1.90	7	3.35	7
Fe (%)	1.39	7	3.46	8
Cs	nd	0	nd	0
Ba	1578.17	3	649.4	7
Sc	2.77	7	11.36	8
Zr	987.74	7	725.15	8
Hf	5.08	7	6.14	8
Ta	.58	7	2.14	8
Cr	42.72	7	43.52	8
Rb	56.52	7	106.91	6
Co	2.20	7	7.12	8
Ni	25.61	5	21.08	1
Sb	.36	5	1.19	8
Th	9.14	7	24.48	8
La	178.88	7	238.61	8
Ce	250.80	7	336.77	8
Nd	120.24	7	157.18	8
Sm	25.98	7	36.6	8
Eu	4.79	7	7.87	8
Tb	3.51	6	5.20	8
Tm	1.14	7	1.83	8
Yb	15.54	6	12.6	8
Lu	3.01	7	5.04	8
Σ REE	607.09	7	805.27	8

Table 29

Brushy Basin Member
(data in ppm except where noted)

	Whole Rocks		-2 μ Fraction	
		<u>n</u>		<u>n</u>
Na (%)	1.10	16	.24	15
K (%)	2.19	15	1.81	15
Fe (%)	2.89	15	3.79	15
Cs	3.31	4	1.33	1
Ba	651.93	14	230.66	13
Sc	10.18	15	12.08	13
Zr	329.8	14	442.5	13
Hf	9.14	15	5.70	15
Ta	1.39	13	1.24	11
Cr	47.5	13	49.1	14
Rb	136.5	14	157.9	13
Co	4.92	15	58.3	15
Ni	13.89	7	17.44	11
Sb	.57	14	.71	15
Th	19.82	15	16.78	15
La	26.90	16	37.0	15
Ce	51.7	15	81.6	15
Nd	36.3	12	52.3	14
Sm	6.08	15	7.52	15
Eu	.99	15	1.03	15
Tb	.65	12	.93	15
Tm	.41	15	.40	13
Yb	2.34	16	3.26	15
Lu	.56	16	.84	15
Σ REE	101.89	15	138.9	15

Table 30

Poison Canyon Sandstone
(data in ppm except where noted)

	Whole Rocks		-2 μ Fraction	
		n		n
Na (%)	1.51	39	.60	24
K (%)	1.93	37	1.10	22
Fe (%)	1.28	39	6.01	25
Cs	2.48	13	2.57	5
Ba	518.96	39	433.18	25
Sc	2.03	39	9.50	25
Zr	172.84	36	346.36	23
Hf	2.18	39	3.58	25
Ta	.35	28	1.55	16
Cr	24.80	25	57.48	24
Rb	104.89	39	118.54	25
Co	1.87	39	13.79	25
Ni	10.43	21	24.25	16
Sb	.36	27	2.70	24
Th	4.41	39	19.35	25
La	20.08	39	95.10	25
Ce	36.42	39	154.07	25
Nd	21.19	38	92.51	25
Sm	4.13	39	14.17	25
Eu	.97	39	2.63	25
Tb	.44	38	1.10	24
Tm	2.50	37	.51	25
Yb	1.21	35	5.52	22
Lu	.27	39	1.71	25
Σ REE	87.21	38	367.32	24

Table 31

Westwater Canyon Member
(data in ppm except where noted)

	<u>Whole Rocks</u>		<u>-2μ Fraction</u>	
		<u>n</u>		<u>n</u>
Na (%)	.74	36	.35	21
K (%)	1.90	30	1.94	19
Fe (%)	1.81	34	7.50	23
Cs	2.02	9	3.4	3
Ba	381.50	35	511.59	23
Sc	3.84	32	12.90	19
Zr	256.78	34	484.68	15
Hf	4.18	34	3.83	23
Ta	.47	28	1.31	16
Cr	33.10	26	92.12	22
Rb	92.90	35	84.54	22
Co	3.2	34	12.37	23
Ni	6.49	21	16.05	14
Sb	.32	15	.61	16
Th	4.98	34	13.99	20
La	17.60	35	47.49	23
Ce	43.73	36	87.30	23
Nd	26.48	36	59.83	23
Sm	5.36	36	10.66	23
Eu	.82	34	2.08	23
Tb	.48	33	1.23	22
Tm	.44	32	.43	22
Yb	1.53	34	4.29	21
Lu	.39	36	1.00	23
Σ REE	94.88	35	223.73	23

Table 32

Recapture Member
(data in ppm except where noted)

	Whole Rocks		-2 μ Fraction	
		<u>n</u>		<u>n</u>
Na (%)	.65	8	.12	7
K (%)	1.43	7	2.11	7
Fe (%)	3.62	8	5.36	7
Cs	3.36	4	nd	0
Ba	269.5	8	170.8	7
Sc	6.60	8	9.84	7
Zr	300.1	7	335.4	6
Hf	6.52	8	4.12	7
Ta	1.00	5	.90	3
Cr	25.90	7	30.00	7
Rb	106.9	8	168.5	7
Co	7.26	8	11.48	7
Ni	8.09	4	15.24	5
Sb	.87	6	.44	6
Th	8.93	8	8.29	7
La	22.60	8	15.19	7
Ce	42.08	8	32.33	7
Nd	29.91	8	39.40	7
Sm	4.81	8	6.99	5
Eu	.94	8	.72	7
Tb	.75	8	.77	4
Tm	.33	8	.29	7
Yb	2.13	8	1.67	6
Lu	.46	8	.51	7
Σ REE	103.97	8	95.50	7

Table 33 Smith Lake

Neutron Activation Analysis & Delayed Neutron Activation Analysis

Sample Number	NAA																							DNAA						
	Na	K	Fe	Cs	Ba	Sc	Zr	Hf	Ta	Cr	Rb	Co	Ni	Ag	Sb	Th	La	Ce	Nd	Sm	Eu	Tb	Tm	Yb	Lu	ΣREE	Th	U	Th/U	
SL 271 AB WR-1	0.93%	2.01%	1.25%	NA	412.9	1.12	170.3	3.42	0.43	19.20	74.54	3.59	0.75	NA	LLD	3.87	11.54	26.35	9.40	2.33	0.50	0.20	0.20	0.51	0.16	51.19				

Concentrations in ppm except where noted

-318-

Table 34 San Mateo area

(Jmb & Jmw)

Neutron Activation Analysis & Delayed Neutron Activation Analysis

Sample Number	NAA																						DNAA						
	Na	K	Fe	Cs	Bo	Sc	Zr	Hf	Ta	Cr	Rb	Co	Ni	Ag	Sb	Th	La	Ce	Nd	Sm	Eu	Tb	Tm	Yb	Lu	ΣREE	Th	U	Th/U
SM 13-53 3311.0-3312.0 WR	1.14%	2.74%	4.20%	NA	274.6	10.49	332.5	LLD	NA	LLD	178.3	6.30	LLD	NA	0.01	12.28	30.45	67.84	32.04	5.72	1.29	0.81	0.33	2.78	0.48	141.7		NA	
SM 13-53 3311.0-3312.0 <2u	0.50%	1.86%	5.17%	NA	317.2	15.55	650.2	6.42	NA	18.68	190.1	7.36	41.78	NA	0.15	14.19	24.58	58.08	48.11	5.60	1.31	0.85	0.44	2.85	0.48	142.3		2.25	
SM 13-53 3346.0-3347.0 WR	2.38%	2.87%	1.18%	NA	0.14%	1.39	223.8	2.27	NA	21.70	134.9	2.35	16.60	NA	0.69	4.37	26.70	43.42	41.67	3.67	1.25	0.65	0.21	0.71	0.15	118.4		4.15	
SM 13-53 3346.0-3347.0 <2u	0.87%	1.32%	10.27%	NA	0.14%	11.81	481.1	4.53	NA	59.31	83.20	2.58	2.94	NA	0.53	12.20	39.95	95.38	85.16	8.70	1.20	1.54	0.44	3.27	0.68	236.3		21.35	
SM 13-53 3351.0-3352.0 WR	2.13%	1.57%	1.93%	NA	474.6	3.19	151.0	3.99	NA	16.26	109.2	2.47	9.96	NA	1.07	5.51	21.50	38.28	39.53	4.53	0.98	0.31	0.22	1.61	0.27	107.2		9.98	
SM 13-53 3351.0-3352.0 <2u	0.58%	1.35%	14.15%	NA	314.2	16.29	299.7	3.31	NA	56.80	127.8	17.48	0.27	NA	1.52	15.61	26.69	74.39	52.45	9.36	1.25	1.01	0.43	LLD	0.84	866.4		30.95	
SM 13-53 3356.0-3357.0 WR	3.11%	2.78%	2.27%	NA	0.15%	2.63	411.3	7.41	NA	48.64	152.0	4.05	14.50	NA	0.72	8.03	44.84	71.27	45.05	8.00	1.75	0.94	0.30	2.15	0.54	174.8		8.76	
SM 13-53 3356.0-3357.0 <2u	1.42%	3.99%	28.90%	NA	0.29%	21.83	0.17%	5.26	NA	157.6	271.8	45.29	41.70	NA	2.38	45.50	131.7	156.4	218.1	99.19	4.96	3.17	1.05	9.36	4.09	567.9		-	
SM 13-53 3456.0-3457.0 WR	1.51%	1.30%	1.12%	NA	646.2	1.75	160.6	3.03	NA	16.78	75.88	1.91	1.61	NA	0.64	3.86	16.35	30.55	19.50	5.14	0.81	0.35	0.17	LLD	0.29	73.2		14.64	
SM 13-53 3456.0-3457.0 <2u	0.05%	0.05%	0.22%	NA	LLD	0.08	6.7	LLD	NA	LLD	4.98	0.52	LLD	NA	LLD	0.01	LLD	LLD	10.0	4.31	LLD	0.03	0.07	LLD	LLD	4.48		175.30	
SM 13-53 3459.0-3460.0 WR	1.48%	1.17%	0.96%	NA	796.3	1.16	88.5	1.47	NA	2.12	55.35	1.59	0.49	NA	0.36	2.53	9.14	20.57	16.30	4.00	0.36	0.23	0.16	0.20	0.31	51.3		17.41	
SM 13-53 3459.0-3460.0 <2u	0.68%	1.74%	12.20%	NA	0.15%	12.90	0.10%	3.96	NA	59.00	163.6	17.73	30.10	NA	0.87	19.27	47.27	130.3	91.09	0.47	1.77	1.05	0.22	4.27	2.99	279.4		18.26	
SM 14-38 2833.0-2834.0 WR	4.48%	4.32%	1.88%	NA	0.16%	2.80	259.5	2.79	NA	43.52	234.8	3.47	5.15	NA	0.83	5.95	39.93	80.25	56.93	3.02	2.23	0.75	0.29	1.70	0.73	192.8		15.04	

Concentrations in ppm except where noted

-316-

Table 34 (cont'd)

Neutron Activation Analysis & Delayed Neutron Activation Analysis

Sample Number	NAA																								DNAA				
	Na	K	Fe	Cs	Ba	Sc	Zr	Hf	Ta	Cr	Rb	Co	Ni	Ag	Sb	Th	La	Ce	Nd	Sm	Eu	Tb	Tm	Yb	Lu	ΣREE	Th	U	Th/U
SM 14-38																													
2833.0-2834.0 <2u	1.03%	2.33%	10.90%	NA	0.18%	13.57	0.11%	2.61	NA	74.2	LTD	26.94	20.98	NA	1.90	17.30	63.06	160.1	239.8	41.13	2.65	1.76	0.61	9.95	3.22	522.2		157.40	
SM 14-38																													
2838.0-2839.0 WR	4.37%	2.96%	3.43%	NA	0.12%	3.78	314.7	5.56	NA	20.0	165.2	4.00	18.77	NA	0.49	6.74	34.35	76.2	55.7	16.98	1.95	0.75	0.35	0.62	0.94	188.8		22.10	
SM 14-38																													
2838.0-2839.0 <2u	0.87%	1.43%	17.30	NA	0.20%	27.82	0.18%	6.15	NA	107.0	137.3	31.04	57.70	NA	0.86	18.45	57.51	99.1	163.8	0.84	3.65	0.92	0.68	7.00	4.20	337.7		NA	
SM 14-38																													
2841.0-2842.0 WR	4.17%	4.83%	2.78%	NA	0.17%	3.86	513.2	9.01	NA	36.6	223.5	4.24	24.49	NA	0.76	8.62	51.95	97.2	78.0	20.48	2.18	0.56	0.29	2.84	1.18	254.6		159.80	
SM 14-38																													
2841.0-2842.0 <2u	0.88%	0.95%	16.80%	NA	0.14%	15.36	0.15%	4.11	NA	120.5	119.0	36.56	46.61	NA	1.22	21.41	63.69	168.8	129.0	0.53	5.02	1.21	0.59	11.70	3.16	383.7		16.9%	
SM 14-38																													
2845.0-2846.0 WR	3.94%	3.50%	1.60%	NA	0.16%	2.48	368.8	2.62	NA	29.2	205.2	3.38	7.83	NA	0.55	6.27	45.33	76.1	51.6	14.23	2.04	0.83	0.29	3.02	0.71	194.1		192.30	
SM 14-38																													
2845.0-2846.0 <2u	0.80%	1.86%	9.05%	NA	0.14%	13.49	923.3	2.76	NA	42.1	175.3	23.38	LTD	NA	0.54	15.04	65.68	161.2	108.7	43.40	2.52	1.67	0.57	2.35	3.65	389.7		101.10	
SM 14-38																													
2949.0-2950.0 WR	0.58%	2.40%	3.90%	NA	556.4	11.11	842.0	5.75	NA	23.4	194.4	6.85	LTD	NA	0.12	12.37	36.05	92.6	70.8	24.49	1.87	1.23	0.41	1.20	2.05	230.6	NA	NA	
SM 14-38																													
2949.0-2950.0 <2u	0.24%	2.96%	6.14%	NA	386.8	15.63	417.2	6.81	NA	13.5	340.0	9.06	53.25	NA	0.82	14.98	47.53	106.2	91.3	17.41	2.20	1.00	0.58	5.07	1.46	272.7		3.58	
SM 14-38																													
2954.0-2955.0 WR	0.93%	1.36%	3.37%	NA	254.0	2.09	0.14%	3.91	NA	26.5	69.24	4.06	13.82	NA	1.05	3.22	5.77	23.2	15.2	1.40	0.76	0.54	0.14	0.02	0.14	47.5		19.04	
SM 14-38																													
2954.0-2955.0 <2u	0.23%	1.01%	19.30%	NA	210.8	9.09	466.2	1.50	NA	35.6	74.02	19.71	24.85	NA	0.57	6.50	7.41	64.2	22.4	4.51	0.66	0.65	0.35	0.31	0.46	100.7		2.2%	
SM 14-38																													
2957.0-2958.0 WR	1.32%	3.54%	2.16%	NA	398.8	3.08	372.8	5.10	NA	20.2	88.43	3.81	10.64	NA	0.27	5.48	15.55	28.8	26.0	2.75	1.09	0.66	0.21	6.12	0.21	75.5		9.46	
SM 14-38																													
2957.0-2958.0 <2u	1.04%	3.74%	21.60%	NA	811.9	30.40	73.8	7.47	NA	104.6	349.1	35.34	52.39	NA	1.94	20.97	56.72	69.8	55.2	12.52	2.60	2.22	0.85		1.29	207.3			

Concentrations in ppm except where noted

-320-

Table 35 DOE Drill Core (Morrison Fm.)

Neutron Activation Analysis & Delayed Neutron Activation Analysis

Sample Number	NAA																							DNAA					
	Na	K	Fe	Cs	Ba	Sc	Zr	Hf	Ta	Cr	Rb	Co	Ni	Ag	Sb	Th	La	Ce	Nd	Sm	Eu	Tb	Tm	Yb	Lu	ΣREE	Th	U	Th/U
R-2; 3906 M-WR	0.72%	0.82%	1.25%	NA	152.1	1.30	150.6	5.82	0.41	2096.0	70.21	2.24	1.16	NA	LLD	2.92	12.72	30.85	17.75	2.40	0.62	0.33	0.18	0.47	0.13	65.45			
R-3; 2661 A1-WR	1.86%	2.06%	1.16%	13	844.0	1.09	99.4	1.32	0.30	102.2	92.98	2.62	8.34	NA	LLD	1.97	12.10	22.81	16.92	2.22	0.88	0.32	0.13	0.78	0.14	56.30	2.80	3.30	0.85
R-3; 2661 A2-WR	0.53%	0.35%	0.93%	NA	708.9	0.96	113.5	0.81	0.38	48.7	73.64	2.51	LLD	NA	LLD	1.63	10.22	20.68	9.99	1.47	0.74	0.32	0.17	0.30	0.09	43.98			
R-3; 2661 AT-WR	0.32%	0.21%	1.74%	NA	219.9	1.31	92.8	1.68	0.57	29.7	60.75	2.52	1.33	NA	LLD	7.74	11.54	41.77	9.43	2.30	0.95	0.48	0.25	0.46	0.13	67.31			
R-5; 3826 AN1-WR	1.25%	1.41%	1.61%	NA	322.5	2.37	173.9	7.06	LLD	31.4	77.32	2.47	LLD	NA	0.02	4.08	14.35	28.28	33.78	3.51	0.72	0.38	0.19	0.87	0.25	82.30			
R-5; 3826 AN2-WR	1.24%	1.46%	1.66%	NA	389.36	2.24	283.6	5.96	0.64	21.6	81.01	2.64	LLD	NA	LLD	7.95	13.96	34.29	15.01	3.55	0.56	0.35	0.20	0.94	0.27	69.13			
R-5; 3826 AN <2u	0.22%	0.33%	8.27%	NA	464.6	10.93	635.1	1.96	1.74	34.6	105.5	13.13	36.46	NA	LLD	8.29	7.03	23.02	29.91	LLD	1.47	0.86	0.29	0.83	0.91	64.32	44.29	0.19	
R-7; 2661-1 WR	1.61%	1.83%	1.74%	NA	592.6	2.40	83.4	4.51	0.29	22.8	109.9	2.58	4.00	NA	LLD	5.08	16.90	39.76	19.76	2LLD	0.99	0.28	LLD	0.87	0.48	79.04			
R-7; 2660-2 WR	0.56%	0.34%	1.67%	NA	627.3	2.48	375.9	3.92	0.54	25.5	116.0	2.59	7.70	NA	0.24	4.12	8.93	35.76	32.03	3.65	0.87	0.36	0.17	1.47	0.47	83.71			
R-7; 2660 <2u	0.05%	1.27%	6.95%	NA	571.1	488.7	394.4	3.13	1.26	44.5	100.5	9.94	LLD	NA	0.67	7.64	24.80	7.64	43.19	5.61	0.64	LLD	0.35	2.17	0.43	84.83	13.73	0.56	
R-8; 2666 B-1 WR	1.24%	1.30%	1.35%	NA	374.0	1.38	66.4	1.16	0.28	7.7	91.46	2.32	3.56	NA	LLD	3.02	11.28	22.66	18.82	1.82	0.38	0.15	0.12	0.19	0.10	55.52			
R-8; 2666 B-2 WR	1.37%	1.73%	1.52%	NA	422.1	LLD	53.1	1.40	0.18	15.8	81.52	2.90	LLD	NA	LLD	2.47	11.67	22.38	15.71	2.41	0.60	LLD	0.13	0.11	0.10	53.11			
R-8; 2666 B <2u	0.12%	1.04%	9.59%	NA	LLD	8.96	171.2	3.48	0.89	10.3	45.73	13.09	5.44	NA	LLD	3.09	8.08	41.55	LLD	1.36	0.47	0.19	0.33	0.56	0.14	52.58	6.77	0.46	
R-8; 2666 C-1 WR	1.75%	1.51%	1.17%	NA	634.2	1.09	2.4	0.92	0.26	25.0	100.9	2.53	LLD	NA	LLD	2.04	11.70	25.32	16.38	2.18	0.83	0.12	0.16	0.58	0.10	57.37	5.23	3.35	1.56
R-8; 2666 C-NAg	0.11%	0.19%	73.08%	NA	398.1	9.04	LLD	13.17	LLD	246.5	LLD	41.83	LLD	NA	0.60	39.22	42.88	93.04	53.51	LLD	2.04	LLD	LLD	1.09	1.39	199.00	63.11	0.62	
R-8; 26667 - WR	0.89%	1.07%	1.75%	NA	253.4	1.43	25.8	1.98	0.64	16.8	55.87	2.40	LLD	NA	LLD	5.21	17.94	41.22	22.96	3.45	0.99	0.50	0.22	0.72	0.16	88.16			
R-8; 3823 L-1 WR	0.27%	0.48%	3.19%	NA	208.1	7.99	193.3	4.26	0.64	31.2	122.3	4.28	LLD	NA	NA	9.46	15.81	56.32	25.51	3.77	1.21	0.79	0.35	2.37	0.43	106.60			
R-8; 3823 L-2 WR	0.73%	2.28%	3.31%	NA	191.3	8.22	170.7	3.43	0.51	24.7	142.1	3.85	4.36	NA	NA	8.40	24.49	50.74	55.59	6.33	1.32	LLD	LLD	2.54	0.45	141.50			
R-8; 3823 L <2u	0.20%	2.18%	5.20%	NA	978.7	13.20	704.1	4.10	1.60	38.5	173.0	5.79	LLD	NA	LLD	11.32	29.61	65.40	30.87	6.78	1.23	1.76	LLD	1.95	0.59	138.20	--	16.51	0.69

Concentrations in ppm except where noted

-321-

Table 37 (cont'd)

Neutron Activation Analysis & Delayed Neutron Activation Analysis

Sample Number	NAA																								DNAA				
	Na	K	Fe	Cs	Ba	Sc	Zr	Hf	Ta	Cr	Rb	Co	Ni	Ag	Sb	Th	La	Ce	Nd	Sm	Eu	Tb	Tm	Yb	Lu	ΣREE	Th	U	Th/U
ZS - 1 Pica	2.98%	3.18%	2.71%	NA	863.0	8.75	356.6	10.52	NA	29.21	211.1	2.48	22.64	NA	0.13	0.32	109.6	161.1	88.51	13.20	3.10	1.88	0.72	7.79	1.07	387.00			
ZS - 2 Pica	0.35%	2.86%	1.38%	NA	287.3	2.70	158.9	4.18	NA	16.51	344.6	1.14	1.86	NA	LLD	27.32	24.1	81.0	20.51	4.73	0.21	0.82	0.49	5.12	0.86	137.80			
ZS - 3 Pica	4.02%	1.59%	2.44%	NA	712.0	4.19	246.8	2.62	NA	19.34	83.26	5.45	5.34	NA	LLD	5.67	16.4	32.6	14.00	2.49	0.72	0.36	0.17	1.12	0.14	68.02			
ZS - 4 Pica	3.81%	2.45%	3.70%	NA	0.10%	7.29	287.3	5.56	NA	53.83	175.1	9.31	6.51	NA	LLD	7.76	37.2	63.7	36.47	4.70	1.43	0.72	0.24	1.20	0.18	45.90			
ZS - 5 Pica	2.13%	2.41%	3.04%	NA	0.13%	8.87	253.1	7.63	NA	19.85	235.0	5.01	19.05	NA	2.71	12.88	37.2	79.3	53.00	7.31	1.89	0.75	0.45	4.22	0.65	84.70			
ZS - 6 Pica	2.89%	4.07%	1.60%	NA	302.9	3.73	316.7	6.19	NA	19.30	287.6	1.63	19.55	NA	0.16	28.06	54.5	103.1	81.74	10.13	0.56	1.57	0.64	5.70	0.98	258.90			
ZS - 7 Pica	1.27%	0.32%	1.73%	NA	725.9	5.12	310.0	7.80	NA	16.45	174.4	1.92	33.31	NA	0.52	8.75	56.2	102.2	45.65	10.34	1.96	1.33	0.56	5.47	0.94	224.70			
ZS - 8 Pica	1.32%	2.59%	1.02%	NA	LLD	LLD	LLD	5.40	NA	18.93	252.7	0.73	LLD	NA	0.19	0.61	13.3	47.6	15.76	5.24	0.34	1.11	0.54	6.42	1.00	91.36			

Concentrations in ppm except where noted

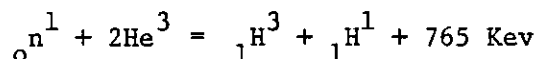
DELAYED NEUTRON ACTIVATION ANALYSIS

DNAA Method for U

It has been recognized that the determination of uranium and thorium at trace levels in a complex matrix is a problem. XRF techniques can offer no better than 30 ppm detection limits for U or Th. Lower limits of detection can be reached by XRF but not without considerable difficulty. U and Th analysis can be run routinely if a sample is irradiated in the neutron flux of a nuclear reactor. The sample is then transported by a pneumatic tube to a neutron sensitive counter. The delayed neutrons emitted by the sample can then be counted.

Experimental

Helium (^3He) filled proportional counter use the following reactions with thermal, epithermal and fast neutrons:



The free proton can then be accelerated to the negative pole. During its path it creates an electron pair in a filler gas (usually argon). It is these electrons which create a voltage drop, and through proper amplification are counted.

The design of the counter used is seen in figure 301. Although the He^3 counters can use epithermal neutrons in the reaction, the efficiency greatly increases toward the thermal end. Thus the counter was designed with a polypropylene moderator. Calibration of the counter was accomplished using USGS standards and LASL standards.

DNAA Method for Th

In geological materials, the transuranic elements may be considered non-existent; so that the only fissionable nuclides present will be ^{232}Th , ^{235}U

and ^{238}U (Gale, 1967). In a mixed thermal and fast neutron flux the thermal neutrons will fission ^{235}U and the fast neutrons will fission ^{238}U and ^{232}Th . However, fission of ^{235}U predominates (99.7%) (Gale, 1967). When the sample is irradiated inside a cadmium or boron sheath, to screen out the thermal neutrons, only ^{232}Th and ^{238}U will fission. Since cross-sections for ^{232}Th and ^{238}U are similar, Th analysis will have a serious error. Two measurements of the sample, one with slow and the other with fast neutrons, enables the uranium to be subtracted. This is the method used to determine Th in the present study.

Experimental

Approximately 1.5 grams of sample is loaded into a polyvial. The sample is then sent to the detector which sits below 6 meters of water in a pool. This is to insure minimum cosmic ray and stray gamma influence. A delay time of 20 seconds is used to insure little interference from short lived isotopes produced in the irradiation. The sample is counted for 80 seconds, then stored in a pig. The samples are then reloaded into the thermal rabbit for uranium analysis using the same timing sequence.

The advantage to doing U and Th by the above method is:

- (1) U and Th determinations on the same aliquot (this is useful in determining accurate Th/U ratios).
- (2) Large numbers of samples can be analyzed routinely.

Interferences

There are four possible types of interference in the DNAA (Delayed Neutron Activation Analysis) technique (Gale, 1967):

- (1) Interference from other fissionable nuclides (not likely in geological samples).

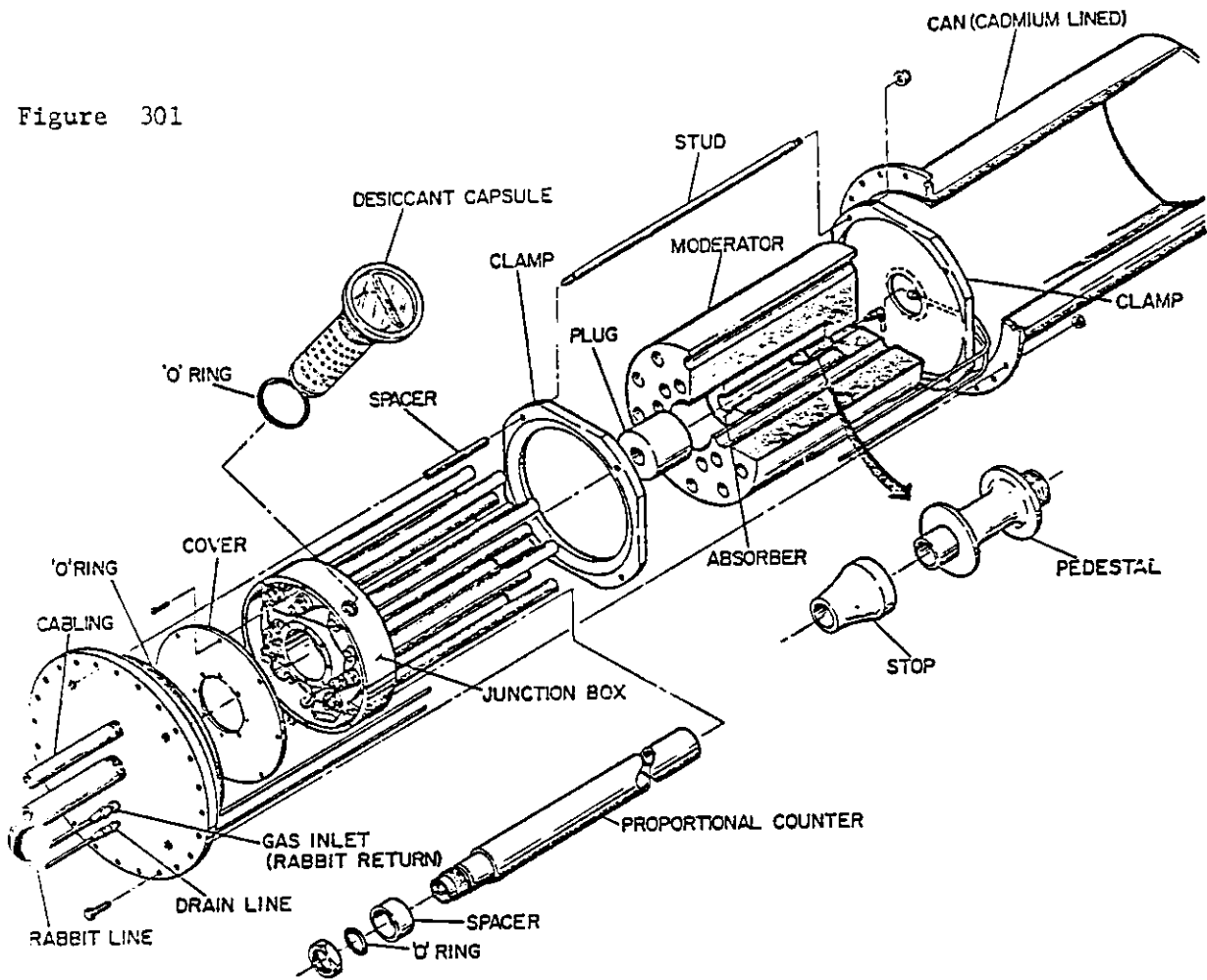
- (2) Delayed neutron emitters formed by primary or secondary (n,p) or (n, γ) reactions (low probability).
- (3) Intense gamma production (possible in high Na samples).
- (4) Self shielding effects and dead time effects (usually occurs in 3% or more U more).

Normal geological samples will not be affected by the above interferences.

Results

Table 38 shows the standards used, their U and Th values, lower limits of detection for U and Th and errors for U and Th analysis. Figures 302 and 303 show the calibration lines obtained for U and Th.

Figure 301



Schematic of the DNAA Counter at LASL (After Balestrini et al., 1976)

Table 38

Uranium and Thorium Standards

<u>#</u>	<u>Standard</u>	<u>U ppm</u>	<u>Th ppm</u>	<u>Description</u>
S-1	G-2	2.15	24.0	USGS standard
S-2	BCR-1	1.81	5.26	" "
S-3	GSP-1	2.54	106.9	" "
S-4	PCC-1	.007		" "
S-5	0 + S-1	.004	-	" "
S-6	AGV-1	2.20	5.37	" "
S-7	SL 201	13.1		LASL STD determined by Mass Spectrometer Isotope Dilution
S-8	SL 207	25.30		" "
S-9	SL 138	39.3		" "
S-10	SL 213	55.0		" "
S-11	SL 204	853.		" "
S-12	SL 130	2778.		" "
S-13	W-1	0.58	2.67	" "

	Lower Limit of Detection	Error
U	1.0 ppm	+ 5%
	.05 ppm	+ - 75%
Th	1.0 ppm	+ 15%

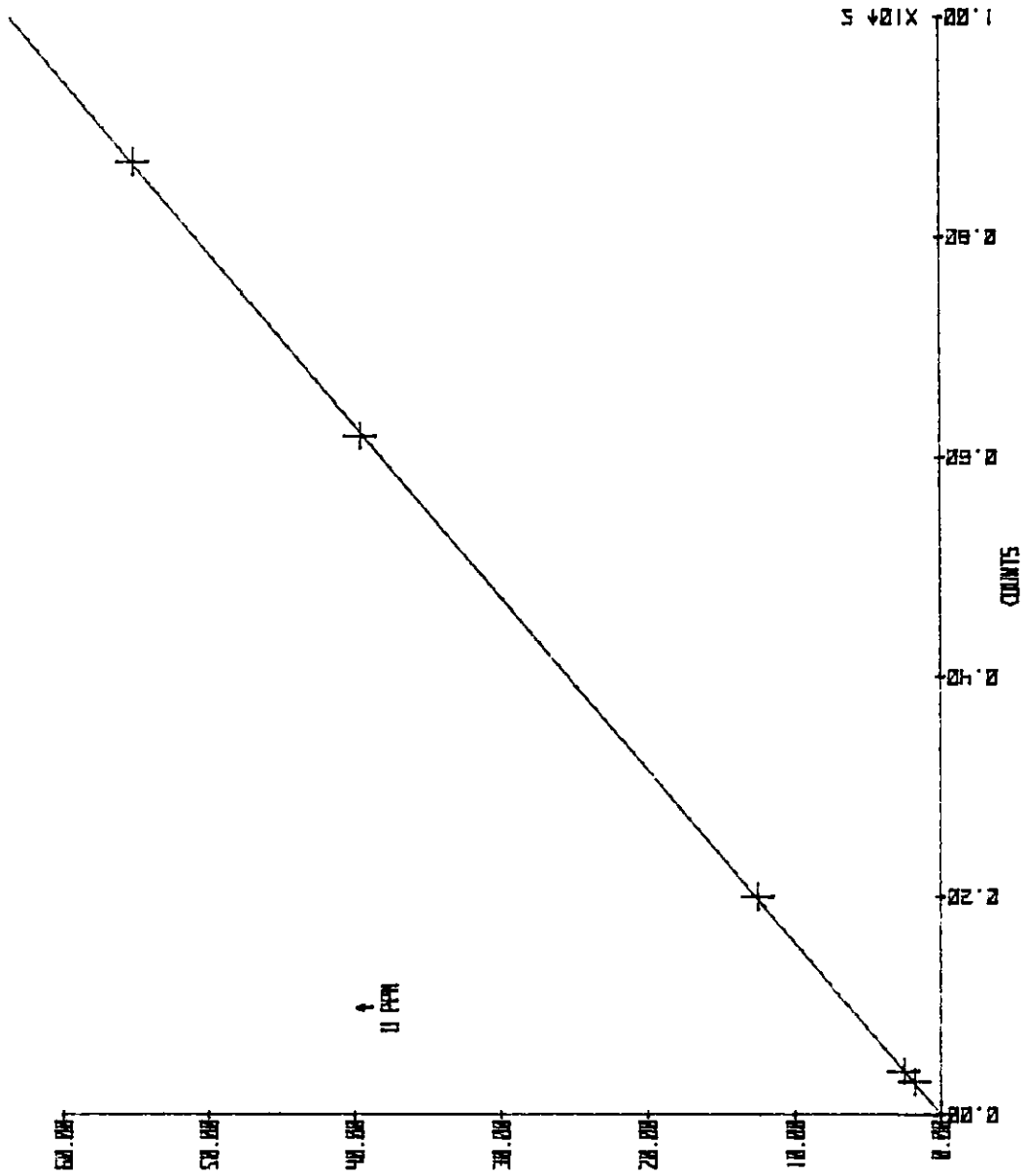


Figure 302

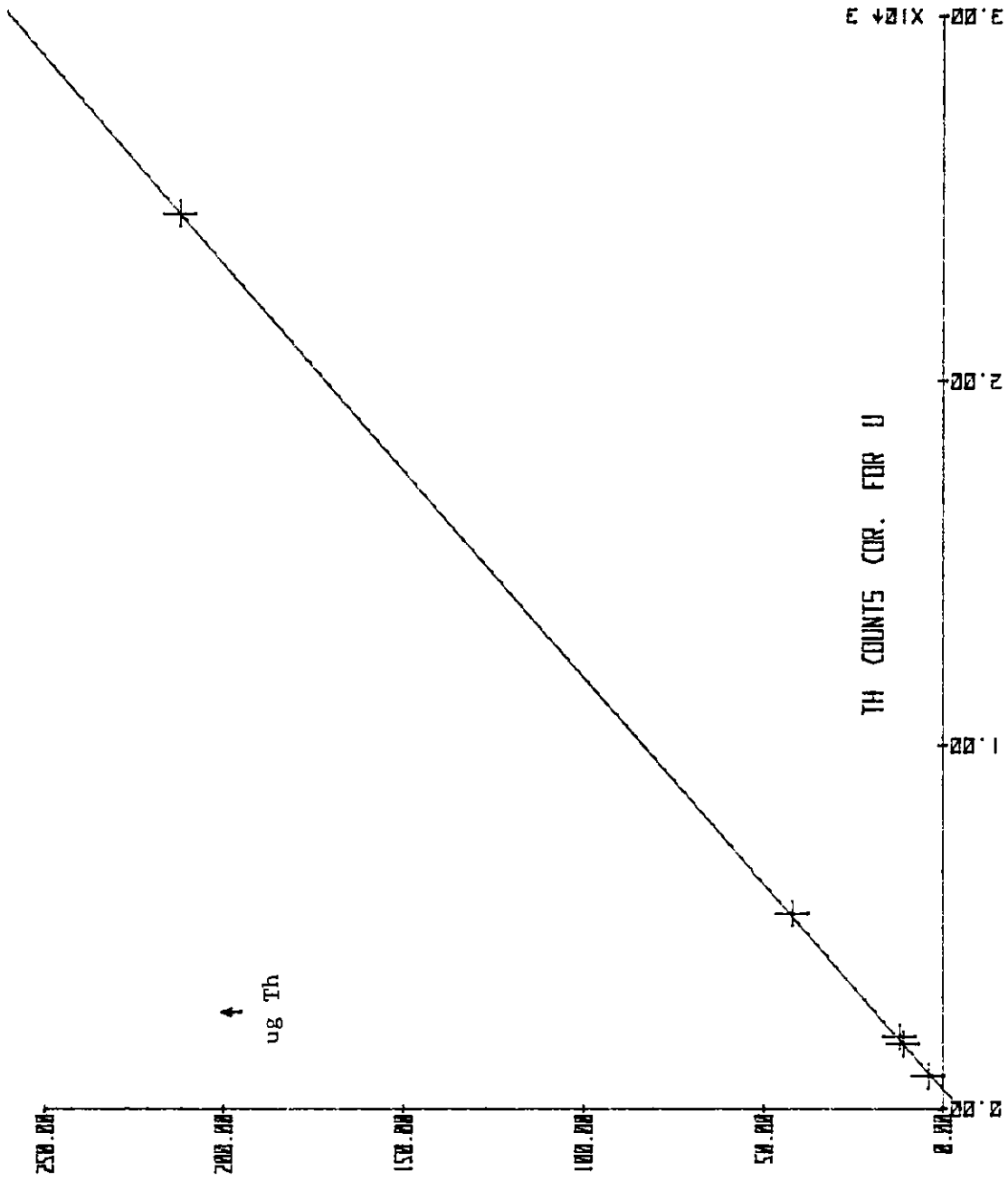


Figure 303

Table 39 Mancos Shale

MANCOS SHALE

<u>SAMPLE</u>	<u>U</u>	<u>Th</u>	<u>Th/U</u>
KMS 1 (WR)	4.61		
KMS 2 (WR)	4.99		
KMS 3 (WR)	4.82		
KMS 4 (WR)	4.24		
KMS 5 (WR)	2.85		
KMS 6 (WR)	3.89		
KMS 7 (WR)	3.58		
KMS 8 (WR)	3.41		
KMS 9 (WR)	3.59		
KMS 12 (WR)	3.77		

Table 40

DAKOTA

<u>SAMPLE</u>	<u>U</u>	<u>Th</u>	<u>Th/U</u>
Kds - 1J (WR)	5.32		
Kds - 4J (WR BENT)	11.99		
Kds - 8J WR BENT	6.23		
Kds - 9J WR BENT	14.64		
Kds - 12J WR	6.12		
Kds - 1 PC WR	6.15		
Kds - 4PC WR	0.72		
Kds - 6 PC WR	0.37		
Kdss - 3 PC WR	0.52		
Kdss - 4 2u	5.97		
Kdsh - 7 PC	5.27		
TQ Kd 1	0.63		
TQ Kd 6	0.51		
MQ Kd	0.71	LLD	-
MQ Kd	0.36		

Table 41

JACKPILE SANDSTONE

<u>SAMPLE</u>	<u>U</u>	<u>Th</u>	<u>Th/U</u>
MQ Kd-Jmj (WR)	7.70	41.76	5.42
MQ Kd-Jmj (WR)	12.30		
LQ Jmj 5 (WR)	5.22	9.53	1.83
LQ Jmj 5 (WR)	4.87		
MQ Jmj 1 (WR)	4.12	15.67	3.80
MQ Jmj 1 (WR)	3.50		
MQ Jmj 1 (WR)	26.7		
MQ Jmj 2 (WR)	32.46	16.38	.50
MQ Jmj 2 (WR)	29.60		
MQ Jmj 4 (WR)	24.76	LLD	-
MQ Jmj 4 (WR)	16.70		
MQ Jmj 5 (2u)	10.24		

Table 42

BRUSHY BASIN

<u>SAMPLE</u>	<u>U</u>	<u>Th</u>	<u>Th/U</u>
LQ Jmb 1 (WR)	8.58	13.24	1.54
LQ Jmb 1 (WR)	8.07		
LQ Jmb 3 (2u)	8.01		
LQ Jmb 5 (WR)	2.65		
TQ Jmb 1 (2u)	17.92		
TQ Jmb 1 (WR)	14.51		
TQ Jmb 2 (WR)	7.66	8.46	1.10
TQ Jmb 2 (WR)	7.00		
TQ Jmb 5 (WR)	3.11	8.84	2.84
DLQ Jmb 1 (2u)	11.83		
DLQ Jmb 1 (WR)	10.2		
DLQ Jmb 2 (WR)	22.19	16.63	.75
DLQ Jmb 2 (WR)	20.10		
DLQ Jmb 4 (WR)	4.23	12.00	2.84
DLQ Jmb 4 (WR)	3.77		

POISON CANYON

Table 43

<u>SAMPLE</u>	<u>U</u>	<u>Th</u>	<u>Th/U</u>
PCL 2 (WR)	2.63		
PCL 3 (WR)	3.72		
PCL 3 (WR)	3.95		
PCL 4 (WR)	4.49		
PCL 5 (WR)	31.07		
PCL 6 (WR)	12.99		
PCL 7 (WR)	4.55		
PCL 8 (WR)	1.97		
PCL 9 (WR)	2.89		
PCL 10 (WR)	10.48		
PCL 11 (WR)	3.83		
PCL 12 (WR)	4.32		
PCL 12 (WR)	4.15		
PCU 1 (WR)	4.03		
PCU 3 (WR)	4.91		
PCU 4 (WR)	5.07		
DLQ Jmpc 1 (WR)	7.59	6.79	.89
DLQ Jmpc 1 (WR)	7.07		
DLQ Jmpc 3 (WR)	10.56	7.82	.74
DLQ Jmpc 3 (WR)	15.10		
DLQ Jmpc 4 (WR)	31.3		

Table 44

WESTWATER CANYON

<u>SAMPLE</u>	<u>U</u>	<u>Th</u>	<u>Th/U</u>
Jmw 1-2d (WR)	4.06		
DLQ Jmw 1 (WR)	2.21	3.55	1.61
DLQ Jmw 4 (WR)	11.85	5.01	.42
DLQ Jmw 4 (WR)	2.01		
DLQ Jmw 4 (WR)	10.20		
DLQ Jmw 4 (2u)	215.72		
DLQ Jmw 5 (WR)	7.45	12.62	1.69
DLQ Jmw 5 (WR)	6.93		
DLQ Jmw 6 (WR)	11.15	5.04	.46
DLQ Jmw 6 (WR)	10.30		
DLQ Jmw 6 (2u)	29.43		
LQ Jmw 1 (WR)	1.13		
LQ Jmw 5 (WR)	1.30	3.19	2.45
LQ Jmw 5 (WR)	.91		
LQ Jmw 7 (WR)	3.62		
LQ Jmw 7 (2u)	12.21		
LQ Jmw 7 (WR)	1.47		
TQ Jmw 1 (WR)	1.80	3.89	2.16
TQ Jmw 1 (WR)	1.35		
TQ Jmw 3 (WR)	2.53	4.16	1.64
TQ Jmw 3 (WR)	2.25		
TQ Jmw 7 (WR)	1.54	.81	.53
TQ Jmw 7 (WR)	1.22		
TQ Jmw 7 (2u)	12.21		
TQ Jmw 9 (WR)	2.87	6.48	2.26

Table 44 (cont'd) WESTWATER (cont'd)

TQ Jmw 9 (WR)	2.46		
TQ Jmw 9 (2u)	5.15		
TQ Jmw 11 (WR)	1.87		
TQ Jmw 12 (WR)	3.44	10.28	2.99
TQ Jmw 12 (WR)	2.82		

Table 45

San Mateo

<u>SAMPLE</u>	<u>U</u>	<u>Th</u>	<u>Th/U</u>
13-53-3304	3.99		
13-53-3305	2.66		
13-53-3306	2.52		
13-53-3307	1.73		
13-53-3307	1.94		
13-53-3308	1.52		
13-53-3311	2.09		
13-53-3311	2.25		
13-53-3344	2.69		
13-53-3345	3.56		
13-53-3346	4.15		
13-53-3346	3.94		
13-53-3346	21.35		
13-53-3347	4.56		
13-53-3350	6.83		
13-53-3351	9.88		
13-53-3351	30.95		
13-53-3351	9.98		
13-53-3352	10.95		
13-53-3353	14.48		
13-53-3354	11.19		
13-53-3355	8.35		
13-53-3356	8.76		
13-53-3356	9.43		

Table 45 (cont'd)

San Mateo (cont'd)

<u>SAMPLE</u>	<u>U</u>	<u>Th</u>	<u>Th/U</u>
13-53-3356	16.32		
13-53-3361	55.32		
13-53-3454	1.65		
13-53-3455	2.96		
13-53-3456	14.64		
13-53-3456 (2u)	175.27		
13-53-3458	12.94		
13-53-3459	17.13		
13-53-3459	18.26		
13-53-3459	17.41		
14-38-2805	2.33		
14-38-2807	4.41		
14-38-2808	4.50		
14-38-2809	4.46		
14-38-2810	-		
14-38-2830	15.48		
14-38-2831	-		
14-38-2832	11.73		
14-38-2832	8.80		
14-38-2833	-		
14-38-2833	-		
14-38-2834 2M	157.37		
14-38-2834	15.04		
14-38-2834	13.13		

Table 45 (cont'd)

San Mateo (cont'd)

<u>SAMPLE</u>	<u>U</u>	<u>Th</u>	<u>Th/U</u>
14-38-2835	27.57		
14-38-2836	20.78		
14-38-2837	22.78		
14-38-2838	22.26		
14-38-2839	22.10		
14-38-2839	21.73		
14-38-2840	22.41		
14-38-2841	18.90		
14-38-2842 2u	159.75		
14-38-2842	21.07		
14-38-2842			
14-38-2843	-		
14-38-2844	-		
14-38-2845	-		
14-38-2846	12.32		
14-38-2846 2u	192.31		
14-38-2846	16.91		
14-38-2846			
14-38-2847	28.65		
14-38-2848	24.20		
14-38-2849	17.18		
14-38-2858			
14-38-2946	3.53		
14-38-2947	3.84		

Table 45 (cont'd)

San Mateo (cont'd)

<u>SAMPLE</u>	<u>U</u>	<u>Th</u>	<u>Th/U</u>
14-38-2948	132.27		
14-38-2949	8.78		
14-38-2950 2u	5		
14-38-2950	101.08		
14-38-2950	-		
14-38-2952	9.62		
14-38-2953	14.91		
14-38-2954	8.24		
14-38-2955	3.58		
14-38-2955 2u	19.04		
14-38-2955	3.81		
14-38-2956	3.27		
14-38-2957	1.65		
14-38-2958	2.21		
14-38-2958 2u	9.46		
14-38-2958	3.10		
14-38-2959	2.21		
14-38-2960	2.23		
14-38-2961	2.22		
SM 15-24-2594	77.8		
15-24-2608	65.2		
15-24-2611	17.26		
SM 15-25-2596	2.36		
15-25-2604	294.66		
15-25-2609	311.88		
15-25-2610	4.39		

Table 45 (cont'd)

San Mateo (cont'd)

<u>SAMPLE</u>	<u>U</u>	<u>Th</u>	<u>Th/U</u>
15-25-2627	8.36		
15-25-2632	12.12		
SM 15-28-2650	17.73		
15-28-2674	22.25		
15-28-2680			
15-28-2684	-		
15-31-2763	1.65		
SM 15-31-2810	2.51		
15-31-2840	1.69		
15-31-2868	6.68		
15-31-2869	4.72		
SM 15-36-2576	4.01		
15-36-2585	9.59		
15-36-2588	343.33		
15-36-2590	22.44		
15-36-2597	-		
SM 15-43-2564	2.19		
15-43-2582	8.42		
15-43-2592	2705.54		
15-43-2593	-		
15-43-2605	65.19		
15-43-2611	43.53		
15-43-2635	6.81		
15-43-2641	2.33		
SM 15-48-2582	61.11		

Table 45 (cont'd)

San Mateo (cont'd)

<u>SAMPLE</u>	<u>U</u>	<u>Th</u>	<u>Th/U</u>
15-48-2591	31.94		
15-48-2618	31.55		
15-48-2618			
15-48-2626	80.35		
15-48-2637	58.36		
15-48-2666	17.29		
15-48-2670	14.59		
22-14-2627	7.11		
22-14-2645	3.56		
22-14-2651	35.61		
22-14-2655	333.41		
22-14-2660	2.04		
22-14-2672	5.99		
22-14-2673	70.61		
22-15-2635	5.44		
22-15-2658	4076.0		
22-15-2690	3738.92		
23-15-2804	30.07		
23-15-2809	9.82		
23-15-2815	16.93		

Table 46 DOE Drill Core

<u>SAMPLE</u>	<u>U</u>	<u>Th</u>	<u>Th/U</u>
LP 2661 A (WR)	3.30	2.80	.85
LP 2661 D (WR)	1.39	1.95	1.40
LP 2665 B (WR)	1.86	2.61	1.46
LP 2665 E (WR)	3.39	7.10	2.09
LP 2666 C (WR)	2.86		
LP 2666 C (WR)	3.35	5.23	1.56
3823 L (2u)	16.51		
LP 3824 A (WR)	4.11	6.84	1.66
LP 3824 E (WR)	2.73	4.67	1.71
LP 3825 b (WR)	2.60	2.73	1.05
LP 3825 E (WR)	2.37	7.00	2.95
LP 3825 K (WR)	1.58	2.66	1.68
3826 AN 2663C (2u)	44.29		
2660-3824 A (2u)	13.73		
266C MG (WR)	6.77		
266 B (2u)	63.11		

Table 47

RECAPTURE

<u>SAMPLE</u>	<u>U</u>	<u>Th</u>	<u>Th/U</u>
TQ Jmr 1	4.03		
TQ Jmr 1	4.56	0.47	.10
TQ Jmr 2	5.42		
TQ Jmr 4	3.17		
TQ Jmr 4	3.73		
DLQ Jmr 1 (2u)	25.58		
DLQ Jmr 1	11.51	17.74	1.54
DLQ Jmr 1	10.5		
DLQ Jmr 2	21.1		
DLQ Jmr 4	0.81	1.55	1.91
DLQ Jmr 4	0.63		
DLQ Jmr 5	1.93	5.34	2.77
DLQ Jmr 5	1.63		
DLQ Jmr 6	2.61	8.75	3.35

Table 48

Uranium Analyses of Some Sedimentary Rocks (from Brookins and Della Valle, 1977)

FORMATION (or Map Unit)	RANGE (ppm U)	N	(ppm U)	REMARK(S)
1. Todilto (Jurassic)	0.57 - 3.45	12	1.39	Limestone and gypsum
2. Morrison (Jurassic)				
a) Brushy Basin Member	2.65 - 20.10	5	9.08	Non-ore; outcrop
b) Jackpile Sandstone	3.50 - 29.6	5	13.39	Non-ore; near Jackpile Mine
c) Poison Canyon	1.97 - 31.30	19	9.05	Non-ore; near Poison Canyon Mine
d) Westwater Canyon Member				
i)	0.91 - 10.30	13	3.63	non-ore; outcrop
ii)	1.65 - 65.20	20	14.50	core; oxidized zone*
iii)	2.04 - 70.61	11	20.64	core; reduced zone*
e) Recapture Member	0.63 - 21.10	7	6.64	non-ore; outcrop
3. Dakota (Cretaceous)				
a) Bentonite-rich	5.32 - 14.64	5	8.86	near San Ysidro*
b) sandstone	0.36 - 6.15	8	1.82	near Ambrosia Lake*
4. Mancos Shale (Cretaceous)	2.85 - 4.99	10	3.98	---
5. Madera (Pennsylvanian-Permian)	1.68 - 16.90	19	5.65	limestone, shale

*Comments:

- 1) The Dakota sandstone samples from Ambrosia Lake fall in two distinct groups based on U analyses: 1. low U; 0.3 - 0.7 ppm; high U; 5.2 - 6.2 ppm. Bentonite-rich samples from San Ysidro are rich in U (\bar{X} = 8.86 ppm).
- 2) Madera Formation samples are included for comparison. The high (\bar{X} = 5.65 ppm) U average is significant in that these samples were all collected from areas well removed from the Grants Mineral Belt.
- 3) Samples of both oxidized and reduced ground in an exploratory drill hole core from the (general) Ambrosia Lake District yield high U contents. Interpretation of these data must await other trace element work.

Table 49

JEMEZ ROCKS

<u>SAMPLE</u>	<u>U</u>	<u>Th</u>	<u>Th/U</u>
Qbo (pumice)	17.16		
Qbt (tuff)	8.13		

Table 50

ZUNI ROCKS

<u>SAMPLE</u>	<u>U</u>	<u>Th</u>	<u>Th/U</u>
Z 10 (WR)	3.7		
Z 13 (WR)	5.88		
Z 16 (WR)	3.95		
Z 17 (WR)	5.97		
Z 25A (WR)	3.20		
Z 25B (WR)	3.31		
Z 25C (WR)	2.99		
Z 28 (WR)	3.06		
Z 30 (WR)	2.58		
Z 35 (WR)	3.04		
Z 39 (WR)	2.68		
Z 40 (WR)	3.05		
Z 41 (WR)	8.22		
Z 101 (WR)	3.35		
Z 102 (WR)	4.39		
Z 103 (WR)	3.35		
Z 104 (WR)	7.23		
Z 105 (WR)	3.24		
Z 106 (WR)	5.28		
Z 108 (WR)	1.82		
Z 109 (WR)	2.61		
Z 109 (WR)	3.02		
Z 110 (WR)	4.74		
Z 111 (WR)	3.19		
Z 112 (WR)	3.77		
Z 114 (WR)	3.22		

Table 50 (cont'd)

<u>SAMPLE</u>	<u>U</u>	<u>Th</u>	<u>Th/U</u>
Z 115A	2.28		
Z 115B	2.40		
Z 115C	2.46		
Z 115D	3.42		
Z 115E	2.95		
Z 116	3.94		
Z 117	3.62		
Z 118	2.54		

Table 51

URANIUM ANALYSES: HOPI BUTTES

<u>RK TYPE</u>	<u>SPL #</u>	<u>PPM U</u>
tuff	MM-1	33.30
tuff-breccia	MM-2	31.66
tuff	MM-6	39.08
tuff	MM-7	35.60
ls/tuff	MM-8	22.84
tuff	MM-9	5.51
tuff-breccia	MM-10	16.49
tuff	MM-11	3.53
tuff-breccia	MM-12	5.35
clay	MM-12a	7.46
tuff	MM-3	27.77
ls.	MM-5	42.35
tuff-breccia	CB-1	6.72
tuff	CB-2	1.76
tuff-breccia	CB-3	10.06
tuff/clay	CB-4	6.99
tuff	14-2	31.79
tuff	14-3	11.21
welded tuff	14-5	4.65
tuff-breccia	14-6	10.61
breccia	MM-19	102.35
scoria	MM-19a	78.28
ls.	MM-20	76.86
"basalt"	CB-5a	8.76
"basalt"	14-8	4.61
agglomerate	H-2	10.08
tuff-breccia	H-3	9.14
agglomerate	HC-4	2.95
agglomerate	HC-5	5.85
tuff-breccia	HC-6	6.50
clay	HC-7	7.32
tuff	HC-3	2.90

Chapter 8

RARE EARTH ELEMENT (REE) STUDIES

In a previous report (Brookins, 1976a) it was noted that the REE were enriched in many of the ore zone samples studied. Further examination of these samples showed also that this enrichment was due to enrichment in the clay size (-2μ) fraction (Brookins, 1976a; Lee, 1976; Brookins et al., 1978). Of further interest from these studies was the observation in ore zone samples from the Grants mineral belt that not only were the REE enriched in the clay size fraction but that a positive Eu anomaly was commonly noted. Europium is commonly (along with Ce) used as a valuable petrogenetic indicator among the REE because it can occur in nature as both Eu^{2+} and Eu^{3+} ions in the water stability field at 25°C and 1 atmosphere pressure. The Eh-pH diagram for Eu is shown as figure 64 in Chapter 4. The presence of the small field of Eu^{2+} in figure 64 close to the lower stability limit for water indicates extremely reducing conditions and over a narrow range in pH. Not shown (due to lack of data) is the stability field of EuCO_3 nor the field of $\text{Eu}_2(\text{CO}_3)_3$ is probably close to the position for the Eu tricarbonat.

Although sedimentary rocks have not been studied as intensively as igneous rocks for their REE distribution and abundance, workers in recent years (Haskin et al., 1966; Cullers et al., 1975; Wildman and Haskin, 1975) have compiled enough data to make some interesting observations. First, Precambrian sedimentary and metasedimentary rocks exhibit a positive Eu anomaly and slight enrichment in the light REE. The positive Eu anomaly is possibly due to a more reducing atmosphere prior to about 1.6 billion years ago.

For Phanerozoic rocks an opposite pattern is commonly noted; a negative Eu anomaly (relative to chondrites) and only slight and usually random light or heavy REE enrichment or depletion to NAS (North American Shale Composite). The common explanation for the negative anomaly in Phanerozoic rocks is a more oxidizing atmosphere such that any first formed Eu^{2+} would be easily oxidized to Eu^{3+} and lost to weathering solutions whereas the other trivalent REE would not be so easily removed.

The second factor is the possibility of removing disproportionately high amounts of Eu during the early- to mid-Precambrian as mentioned above so that on a World wide basis Eu has become depleted in younger rocks. These factors are not fully understood nor to be accepted without further information.

In the following figures are shown the REE plots for the -2μ total REE and the total REE for aliquots of the whole rocks from which the -2μ fractions were removed. All plots are normalized to NAS and reported in conventional fashion.

In addition to the entire data (Tables 26-37) and the information in table 52 the following information is of interest. The ranges for total REE in the -2μ fractions, and in the whole rocks and the ranges and arithmetic means for -2μ REE/WR REE (Column A: Range in Total REE for -2μ fraction(2μ REE); Column B: Range in Total REE for Whole Rocks (WR REE); Column C: Ranges in -2μ REE/WR REE for each rock unit; Column D: Arithmetic mean ($R_{\bar{x}}$) for the ranges shown in Column C.).

	A.	B.	C.	D.
	<u>-2μ REE</u>	<u>WR REE</u>	<u>R</u>	<u>$\frac{R}{X}$</u>
Mancos Shale	68-147	75-110	0.9-1.5	1.22
Dakota Fm.	307-502	13-413	1.2-34.4	14.3
Jackpile Ss.	266-3100	91-1500	2.1-3.3	2.78
Poison Canyon	23-498	48-186	0.3-8.8	2.89
Brushy Basin	50-238	41-536	0.3-3.0	1.74
Westwater Canyon	82-409	44-388	1.1-3.8	2.06
Jm-Mt. Taylor	101-568	47-255	1.0-5.5	2.28
Jm-DOE	55-138	55-106	0.9-1.3	1.06
Recapture Shale	68-147	75-110	0.9-1.5	1.22

These data are of extreme interest because the $\frac{R}{X}$ values are all greater than 1.0. While the mudstones (Mancos, Brushy Basin, Recapture, mudstones within sands) all show values between 1.06 and 1.74 the values for the sandstones (including argillaceous sandstones) vary from 2.06 to 14.3. Most sandstones fall between 2.06 and 2.89, however, the Dakota Sandstone being anomalously high (14.3).

Older, conventional ideas concerning the REE suggested that they should be enriched in resistate fractions of sediments and thus values of $\frac{R}{X}$ should under most circumstances be less than 1.0. That all units studied to date show values in excess of 1, and sandstones in excess of 2, clearly show that the hydrolyzate fraction plays a major role in abundance and distribution of the REE.

The following REE plots and data are provided on an individual sample basis so that the reader may examine the variation from barren to uraniferous samples. The REE are associated with clay minerals in ore zones, but it has not been unequivocally demonstrated that the REE are located in the clay

mineral structures or whether they may be absorbed as surface oxides-hydroxides (Brookins et al., 1978). Incorporation of the REE into calcite (or other carbonates or in sulfates) is deemed unlikely in the ore zones although these minerals warrant study for carbonate- and sulfate-rich parts of units such as the Todilto Formation (proposed for Phase III).

High REE enrichment may be useful as an indicator of provenance as well, and either positive or negative Eu and Ce anomalies useful for a variety of interpretive reasons (see Chapter 10).

Rare Earth Comparisons: Selected Samples*

Table 52

A. Mancos Shale

Sample	2M REE	WR REE	2 /WR
KMS 1A	224.3	155.2	1.44
KMS 1B	212.9	174.9	1.22
KMS 3A	196.5	259.2	0.76
KMS 3B	193.5	270.5	0.72
KMS 4A	298.5	178.9	1.67
KMS 4B	189.7	183.4	1.03
KMS 5	387.7	133.8**	2.90
KMS 8	160.0**	179.3	0.89
KMS 9	212.4	209.7**	1.01
KMS 11	174.9	209.1**	0.84
KMS 12	206.9	144.5**	1.43

B. Dakota Formation

KDSS 3PC	343.8	23.3	14.8
KDSS 4PC	307.3	23.2	13.2
KDSS 4PC	453.8	13.2	34.4
KDSS 6PC	311.8	16.2	19.2
KDSH 7PC	452.8	145.3	3.12
KDSS 9J	501.7	413.2	1.21

C. Morrison Fm - Jackpile Sandstone

MQ JMJ 1	391.0	144.9	2.70
MQ JMJ 3	3100	1500	2.07
MQ JMJ 5	265.7	91.15	2.91
LQ JMJ 5A	314.9	94.26	3.34

D. Morrison Formation - Brushy Basin Member

Sample	REE	WR REE ratio	M/WR
LQ JMB 1A	143.2	129.7	1.10
LQ JMB 1B	234.79	78.47	2.99
DLQ JMB 2	238.0	117.5	2.03
LQ JMB 3A	131.4	112.6	1.17
LQ JMB 3B	169.6	41.21	4.12
LQ JMB 3C	175.9	79.7	2.21
DLQ JMB 4A	88.4	108.3	0.82
DLQ JMB 4B	157.5	536.2	0.29
LQ JMB 5	50.21	51.29	0.98

E. Morrison Formation - Poison Canyon Member

JMPC 3	245.2	80.27	3.05
PCL 4	52.61	186.6	0.28
PCL 6	237.6	141.5	1.68
PCL 7	234.6	67.87	3.46
PCL 8	202.6	78.53	2.58
PCL 10	497.6	56.20	8.85
PCL 11	179.2	45.22	3.72
PCU 1	239.4	96.6	2.48
PCU 3	348.9	89.9	3.88
PCU 4	208.8	77.13	2.71
PCU 9	23.36	79.93	0.29
PCU 10	104.6	63.29	1.65

F. Morrison Fm. - San Mateo Area

SM 13-53 3311-2	142.3	141.7	1.00
SM 13-53 3346-7	236.3	118.4	2.00
SM 13-53 3351-2	166.4	107.2	1.55
SM 13-53 3356-7	567.9	174.8	3.25
SM 13-53 3459-60	279.4	51.3	5.47
SM 14-38 2833-4	522.2	192.8	2.71
SM 14-38 2838-9	337.7	188.8	1.79
SM 14-38 2841-2	383.7	254.6	1.51
SM 14-38 2845-6	389.7	194.1	2.01
SM 14-38 2949-50	272.7	230.6	1.18
SM 14-38 2954-5	100.7	47.5	2.12
SM 14-38 2957-8	207.3	75.6	2.74

G. Morrison Formation - Westwater Canyon Member

CLY GL	409.5	387.6	1.06
DLQ JMW6	177.9	72.48	2.45
TQ JMW4	183.4	71.45	2.57
TQ JMW7	93.63	64.05	1.46
TQ JMW9	290.0	114.0	2.54
JMWI-2D	168.0	44.22	3.80
JMWI-3A	176.8	98.38	1.80
LQJMW7A	82.29	55.6	1.48
LQJMW9	104.6	75.6	1.38

H. Morrison Fm - Recapture Member

TQ JMR - 2	68.82	75.61	0.91
DLQ JMR -2	147.84	96.91	1.53
DLQ JMR - 6	126.56	110.14	1.14
HG JMR - 2	100.22	77.67	1.29

I. DOE Drill Core

R8 2666 B-1	52.58	55.52	0.95
R7 2660 -1	84.83	79.04	1.07
R5 3826 AN2	64.32	69.13	0.93
R8 3823 L	138.2	106.6	1.30

Figures 304 to 353: Typical rare earth plots for Jurassic and Cretaceous Formations from the Grants mineral belt and for some volcanic and granitic rocks. All rare earth values are normalized to the North American Shale (NAS) Composite.

Figures 304-306 and 307-309: Mancos Shale whole rocks and clay size fractions (-2μ) exhibit very typical patterns for Phanerozoic shales with total rare earth contents ranging from 148 to 260 ppm for whole rocks and the clay size fractions from 175 to 217 ppm. Slight oxidation effects for the clay minerals are possibly indicated by the negative slopes near Ce and Eu. The apparent low for Yb may be due to analytical uncertainty.

Figures 310-317: Dakota Sandstone samples chosen show a tremendous range for whole rocks (9.0 to 430 ppm) while the -2μ fractions are highly enriched in the REE (343 to 527 ppm). The two lowest whole rocks show negative Eu anomalies and depletion in the light REE whereas the -2μ fractions are somewhat enriched in the light REE. This is interpreted to indicate control by the -2μ fraction and, more important, a granitic provenance for the Dakota sediments different from that for the Mancos Shale.

Figures 318-323: Jackpile Sandstone: The whole rocks chosen show very high total REE (0.11 to 0.31%) whereas the four -2μ fractions show a range from 315 to 560 ppm. The data of table 52 (D) show, however, enrichment of the REE in the -2μ fraction relative to the whole rocks. Mixed provenance is indicated with some enrichment of both light and heavy REE indicated. A different provenance for the Jackpile sediments from the Dakota source is indicated.

Figures 324-329: Brushy Basin Shale: Total REE in whole rocks vary from 60 to 80 ppm while a range in REE from 131 to 176 ppm for the -2μ fraction is noted. Both the whole rock and -2μ fractions are typical for Phanerozoic shales; the changes in slope toward the heavy REE is due to analytical uncertainties for Tm and/or Yb. Some Lu enrichment is noted, however.

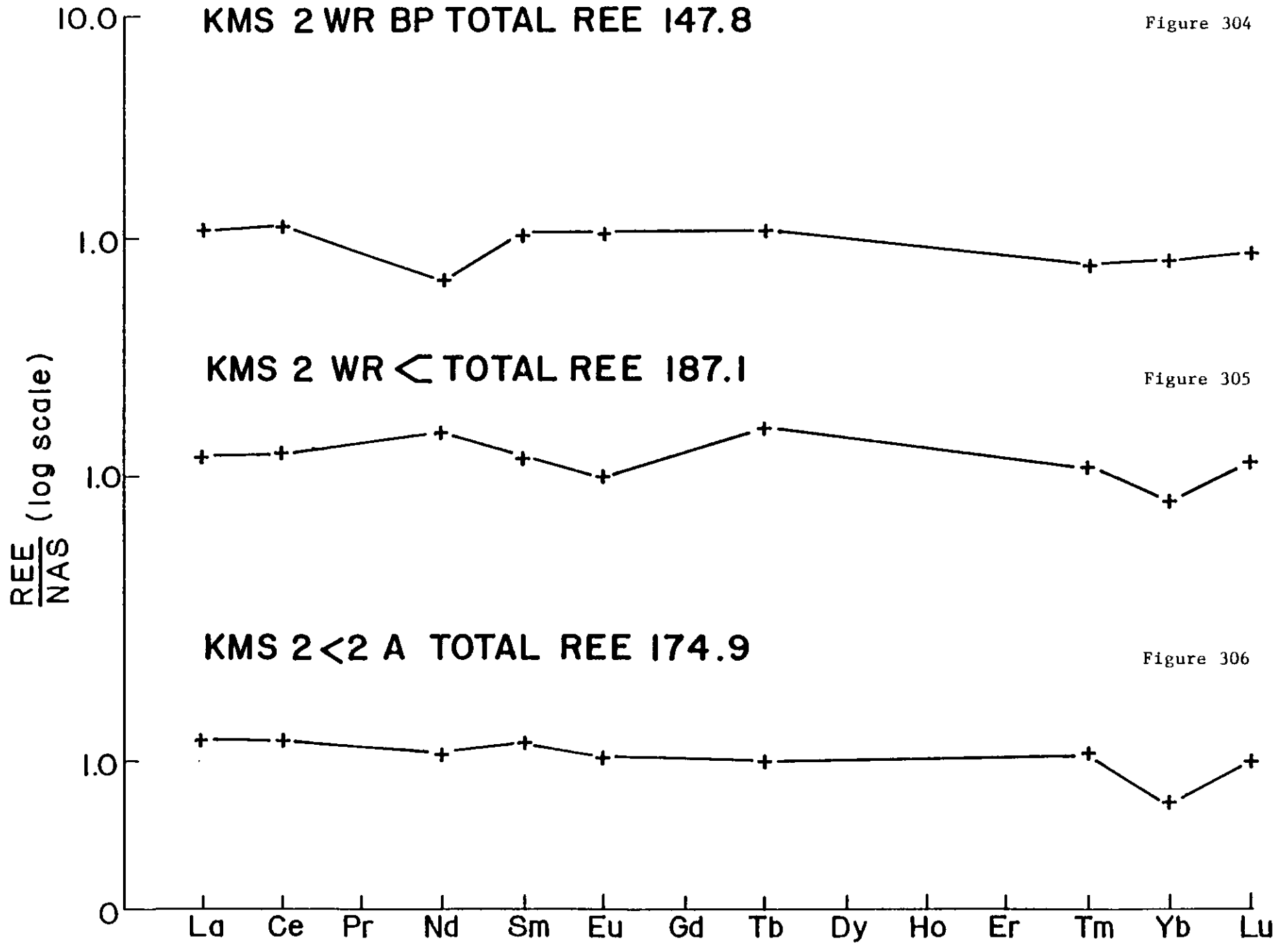
Figures 330-335: Poison Canyon Sandstone whole rocks yield total REE from 63 to 79 ppm while the -2μ fraction ranges from 202 to 235 ppm for the two samples chosen. Positive Eu anomalies are noted for five of the six samples shown; this is taken to indicate lack of oxidizing solutions.

Figures 336-341: Westwater Canyon Sandstone whole rocks range from 64 to 104 ppm while the -2μ fractions range from 76 to 293 ppm. In general, the Westwater Canyon -2μ fraction/whole rock ratio is less than that for the Poison Canyon Sandstone; this suggests different provenance or different diagenetic or later (and possibly local) conditions of infiltration of the Poison Canyon sandstone by slightly oxygenated waters.

Figures 342-347: Recapture Shale whole rocks (5) range from 70 to 150 ppm while the one -2μ fraction shown yields 108 ppm. The data from table 52H show enrichment of the REE in the -2μ fraction. In all, the general patterns are typical for Phanerozoic shales and the distributions only slightly different from those for the Brushy Basin shale.

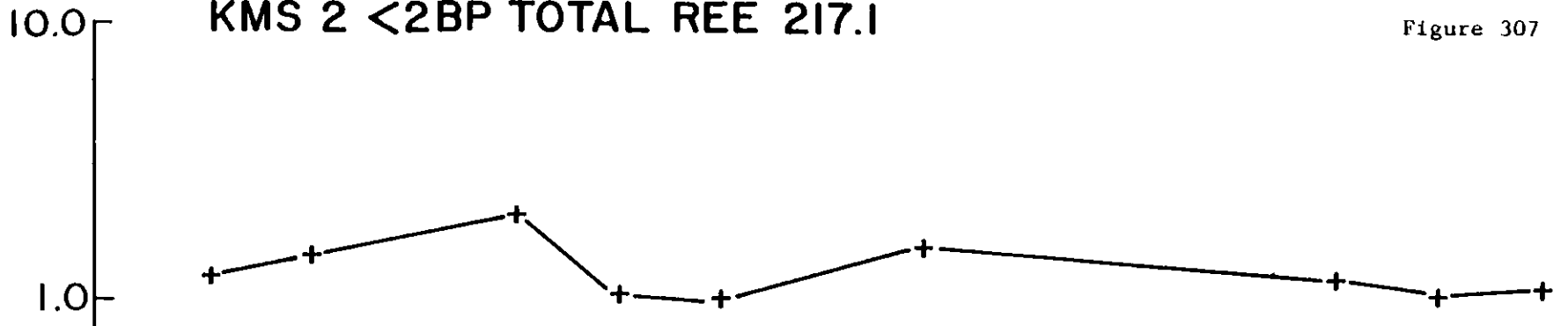
Figures 348-350: Quaternary volcanics show pronounced Eu negative anomalies for 2 of 3 samples; this is the usual trend for such rocks. Interestingly, the light REE are not as enriched as one might predict.

Figures 351-353: Granitic rocks from the Zuni Mountains show normal total REE from 130 to 210 ppm and, more important, pronounced negative Eu, lesser negative Ce and overall negative light REE anomalies. If this material provided detritus to the Grants mineral belt these trends would be expected in the low total REE sandstones but such trends are not observed.



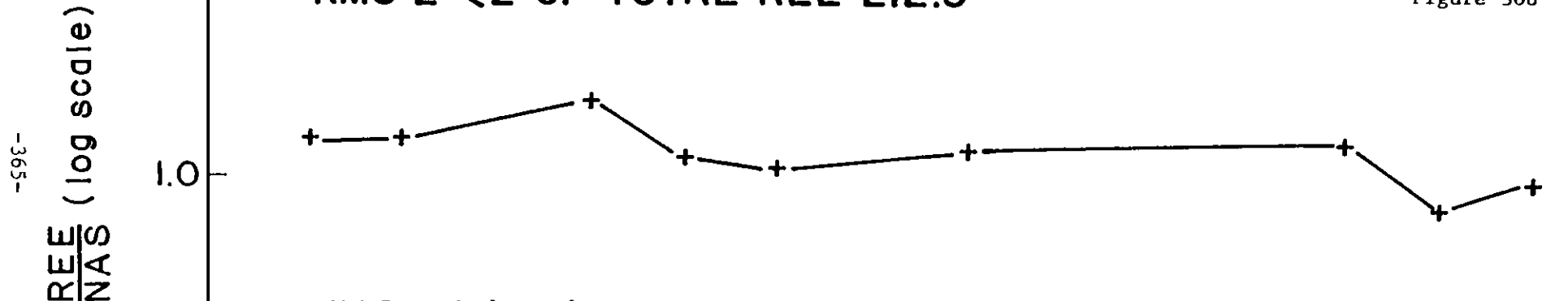
KMS 2 <2BP TOTAL REE 217.1

Figure 307



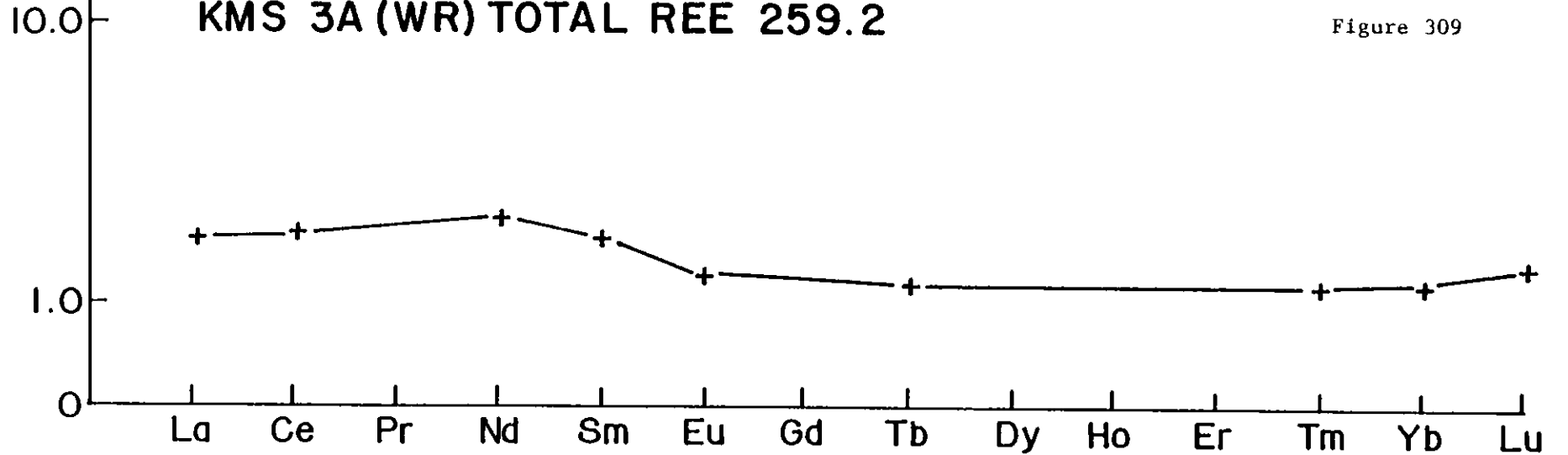
KMS 2 <2 CP TOTAL REE 212.3

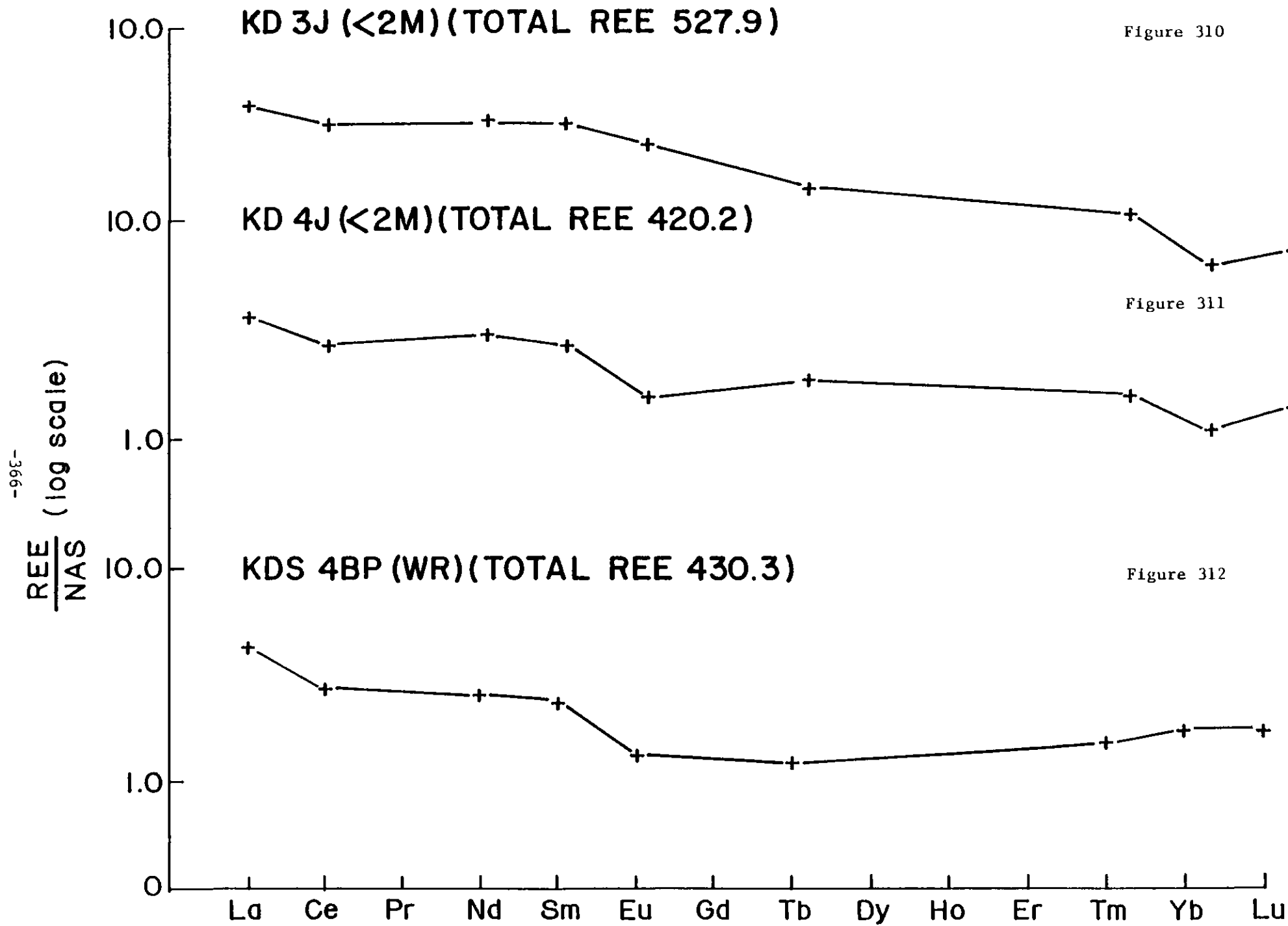
Figure 308



KMS 3A (WR) TOTAL REE 259.2

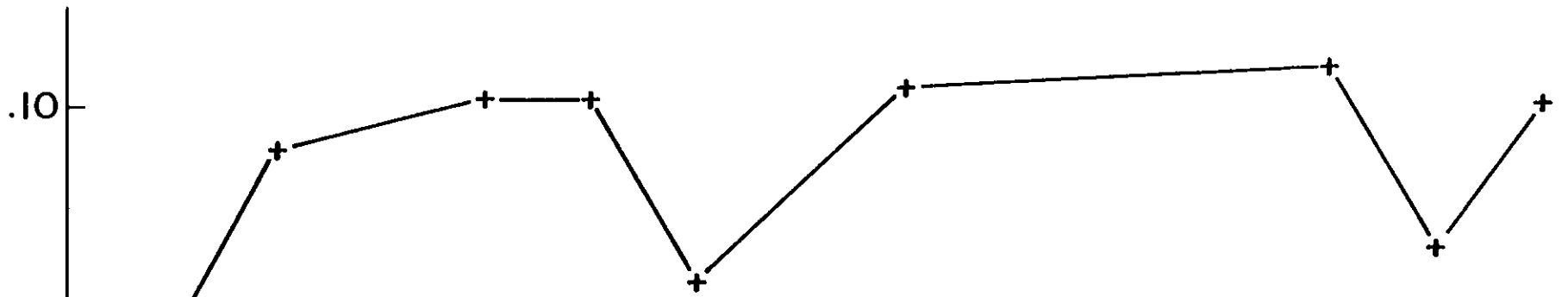
Figure 309





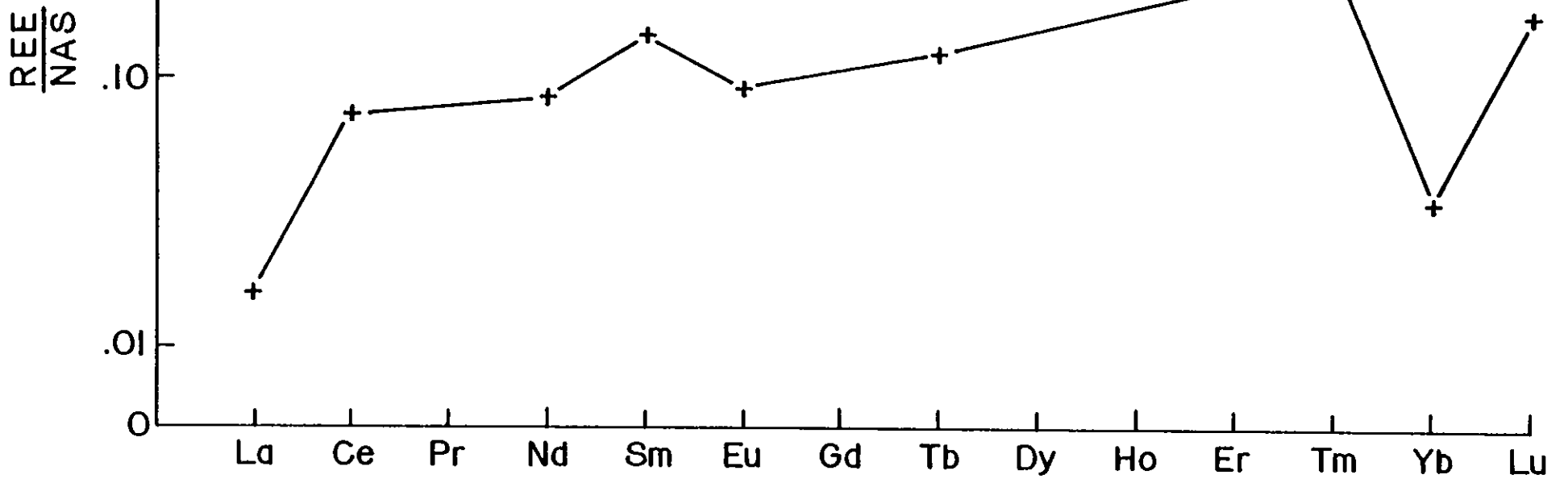
TQ KD IA (WR) TOTAL REE 9.12

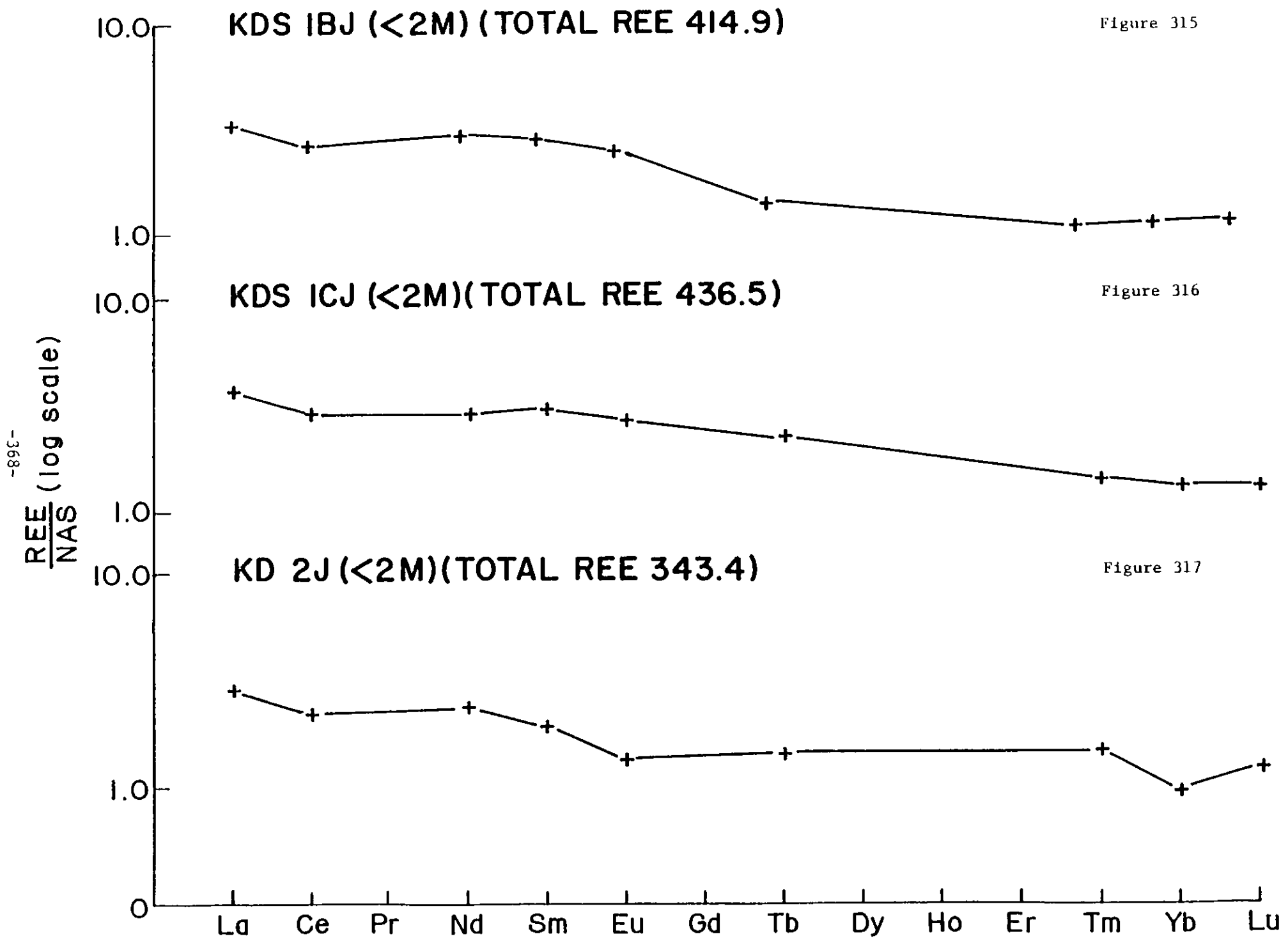
Figure 313

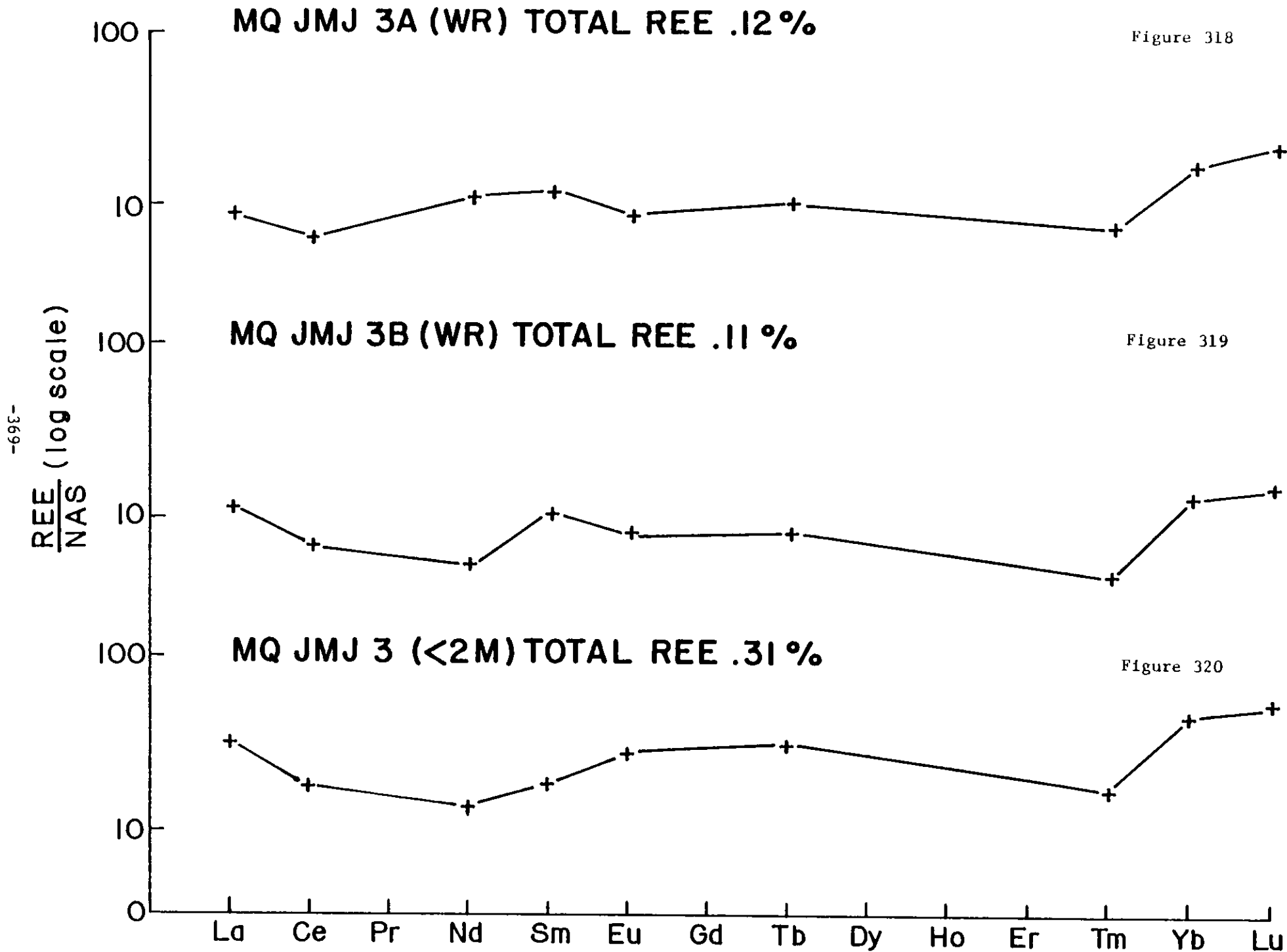


TQ KD IB (WR) TOTAL REE 8.76

Figure 314

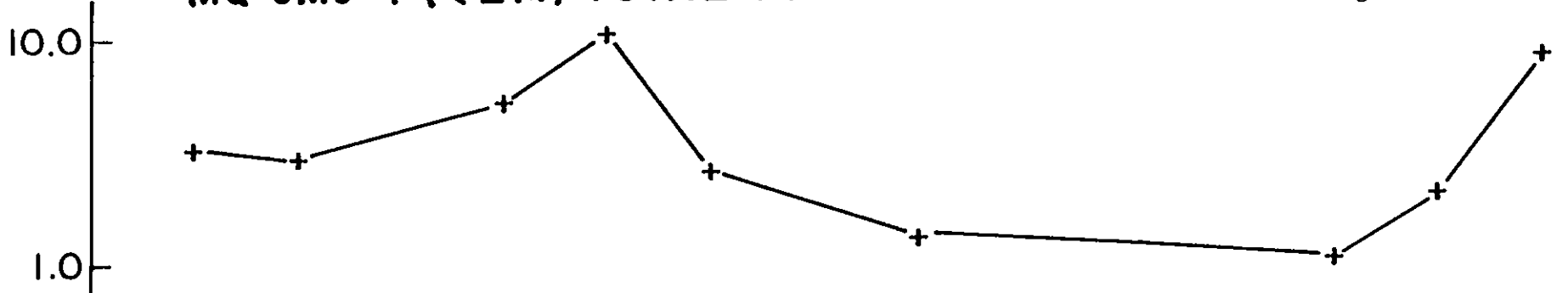






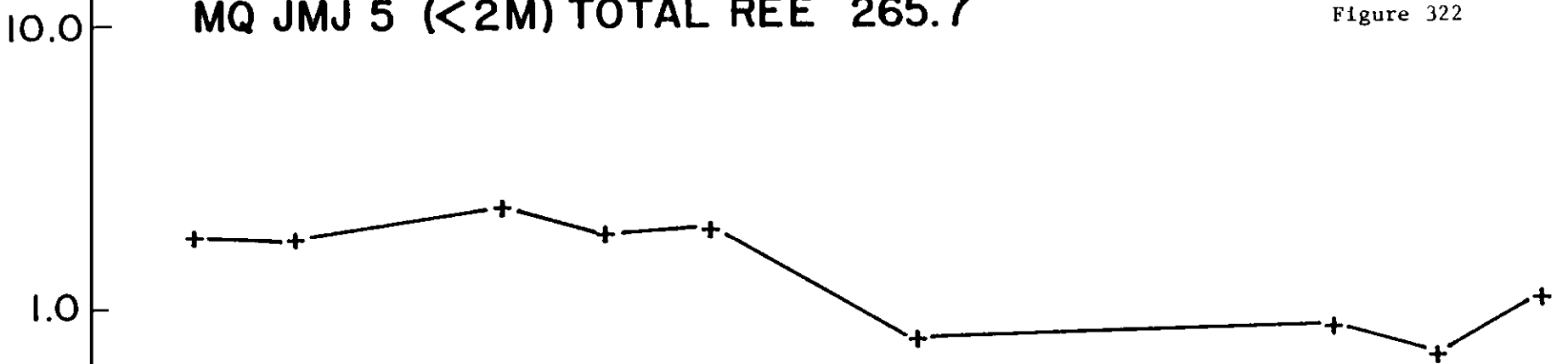
MQ JMJ 4 (<2M) TOTAL REE 560.5

Figure 321



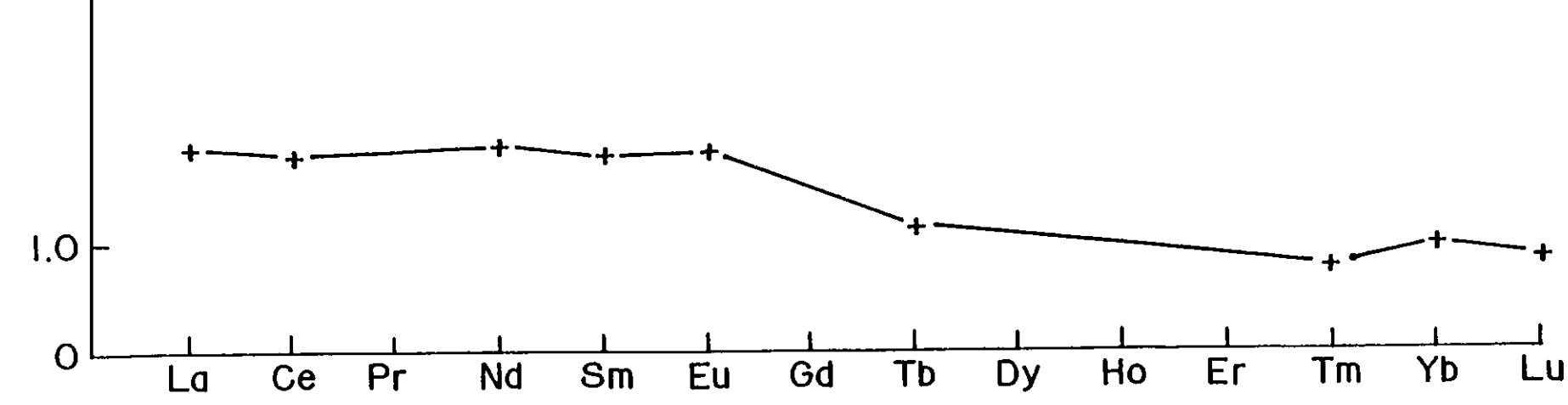
MQ JMJ 5 (<2M) TOTAL REE 265.7

Figure 322



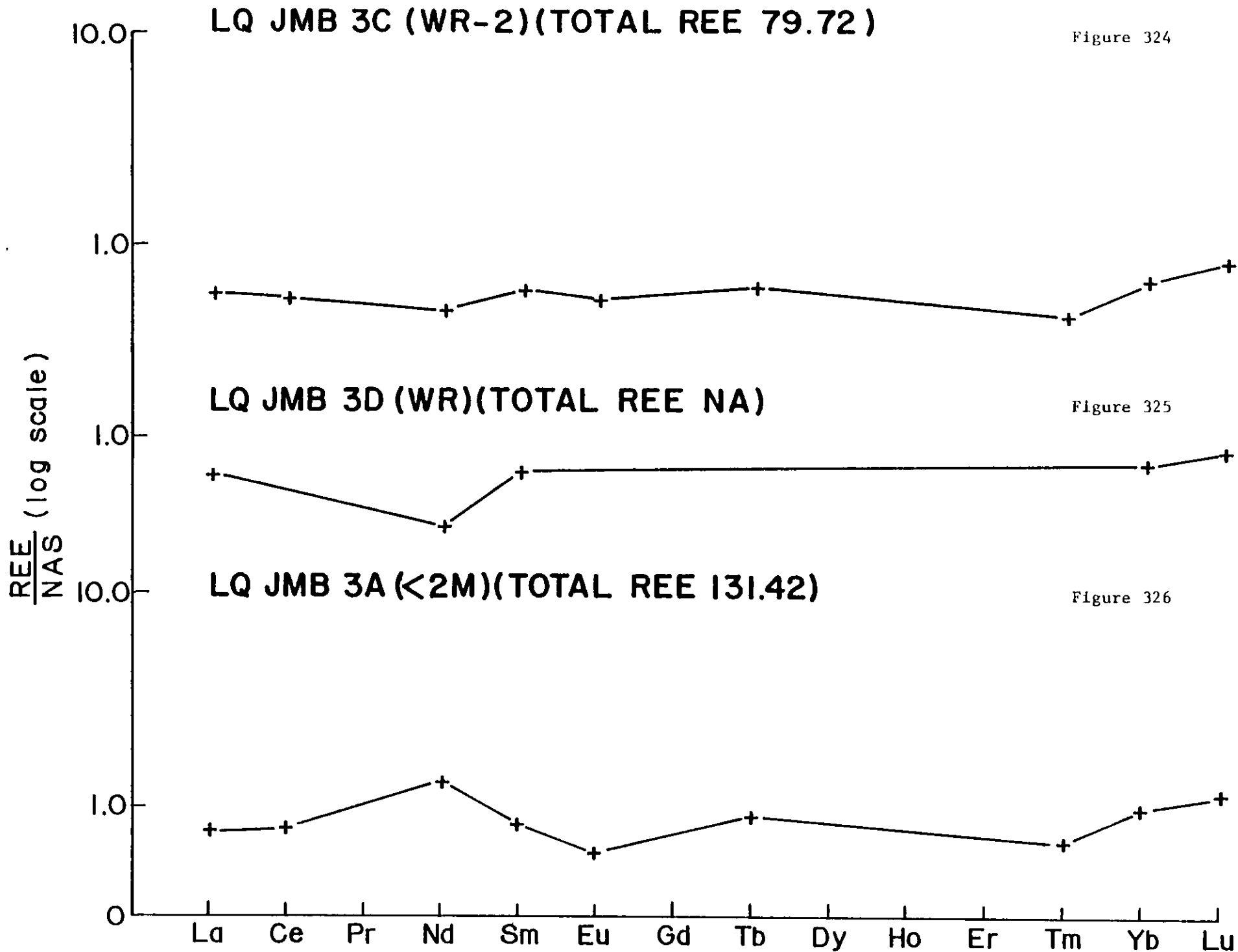
MQ JMJ 5A (<2M) TOTAL REE 314.9

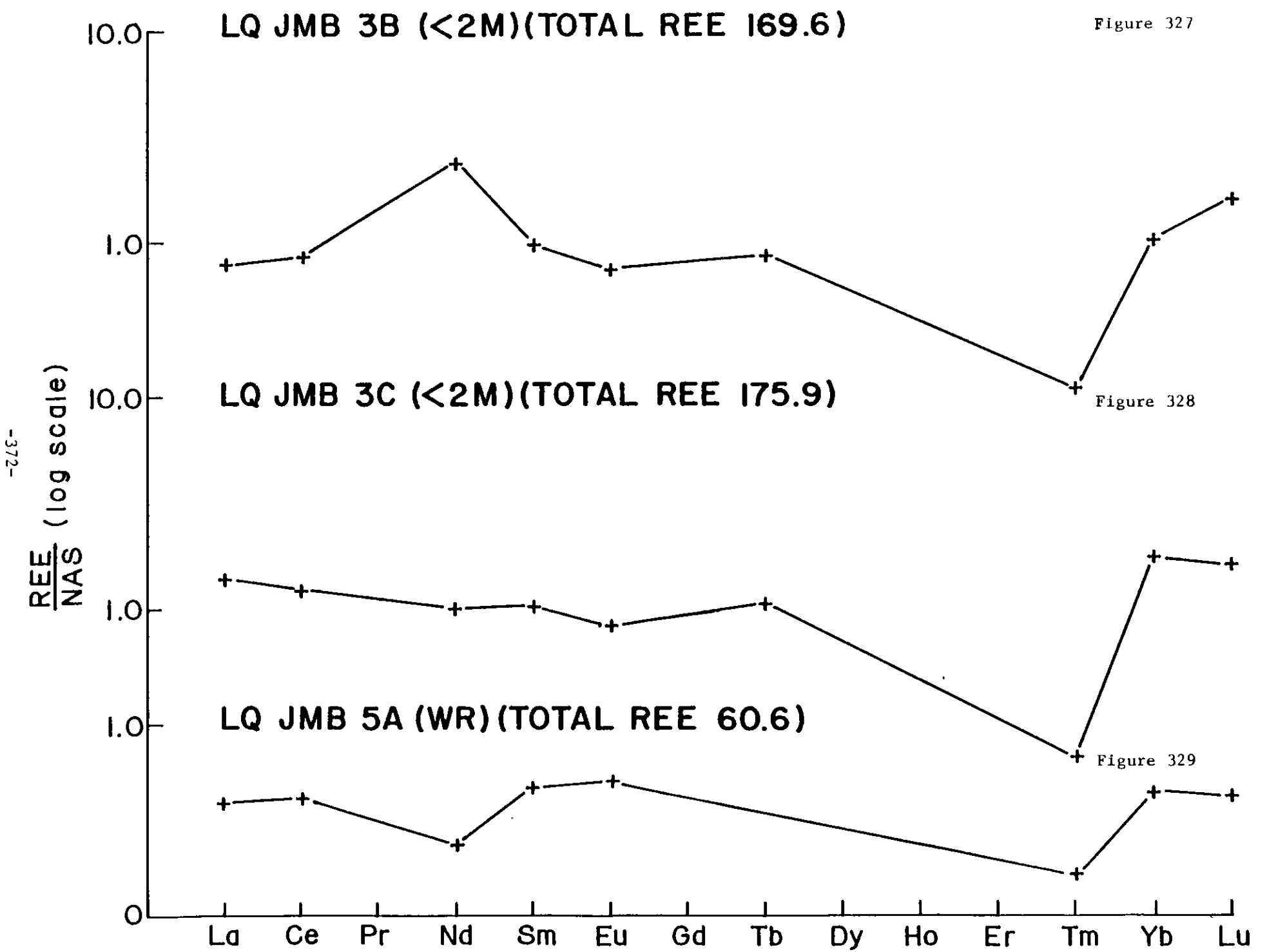
Figure 323

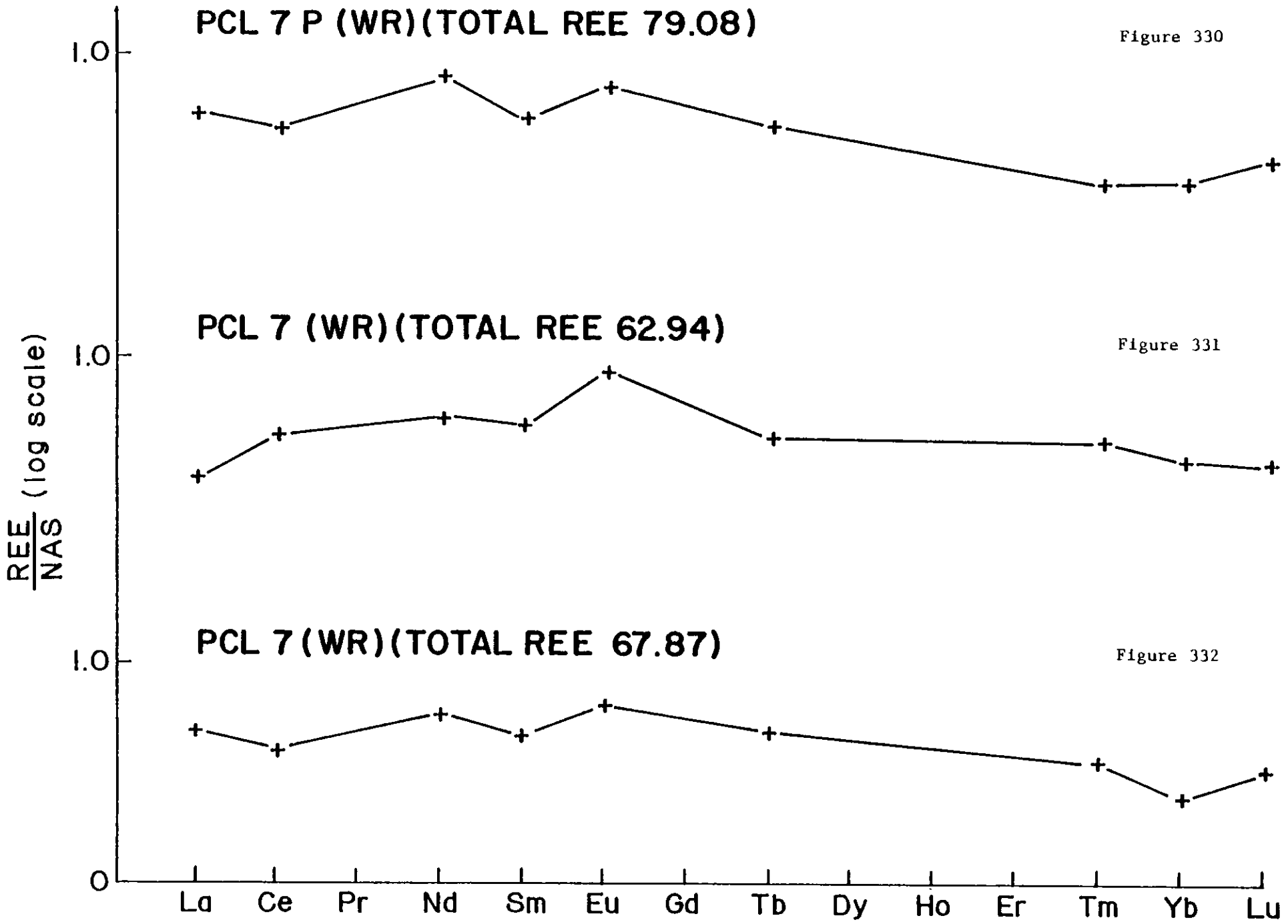


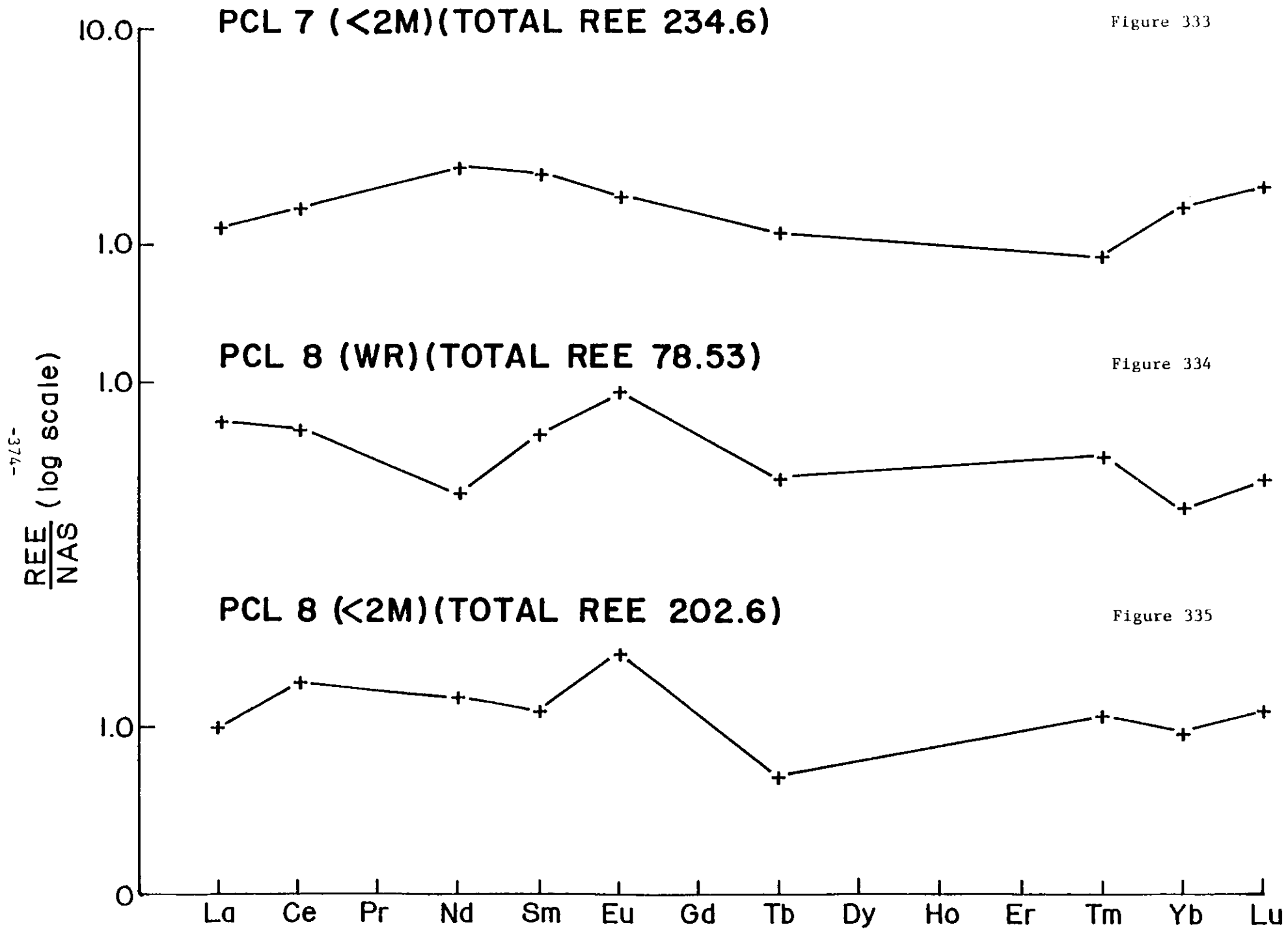
-370-

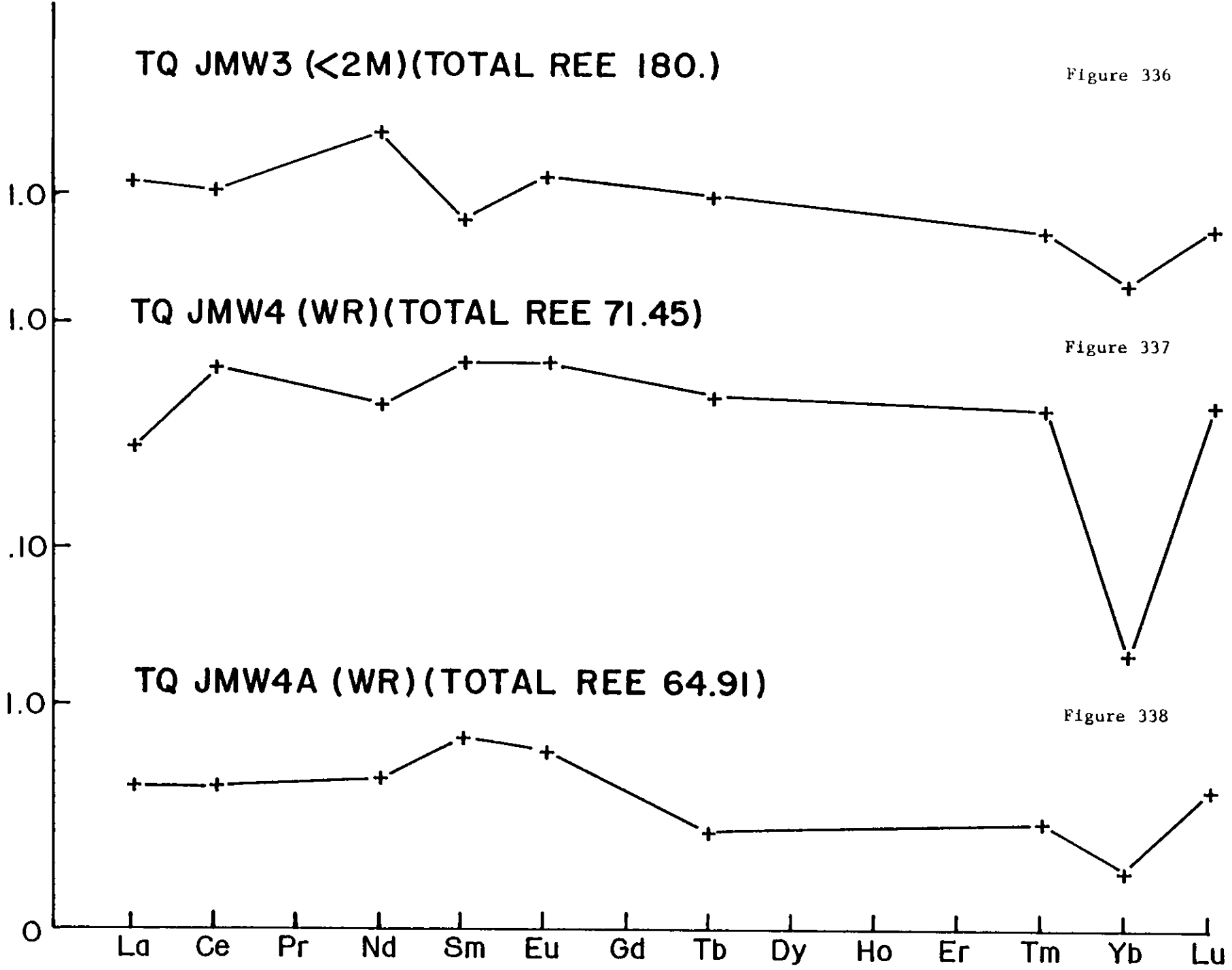
REE/NAS (log scale)

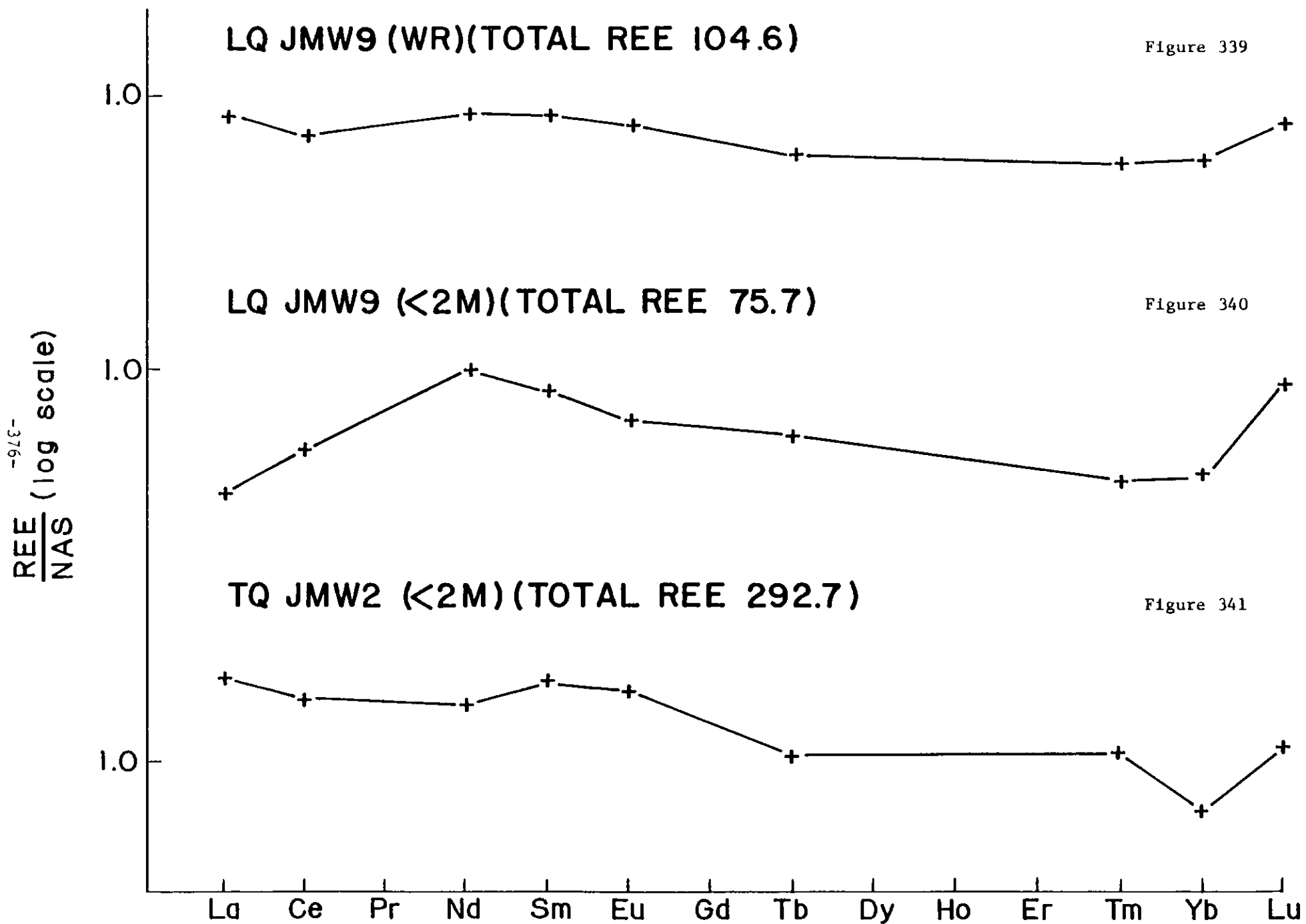


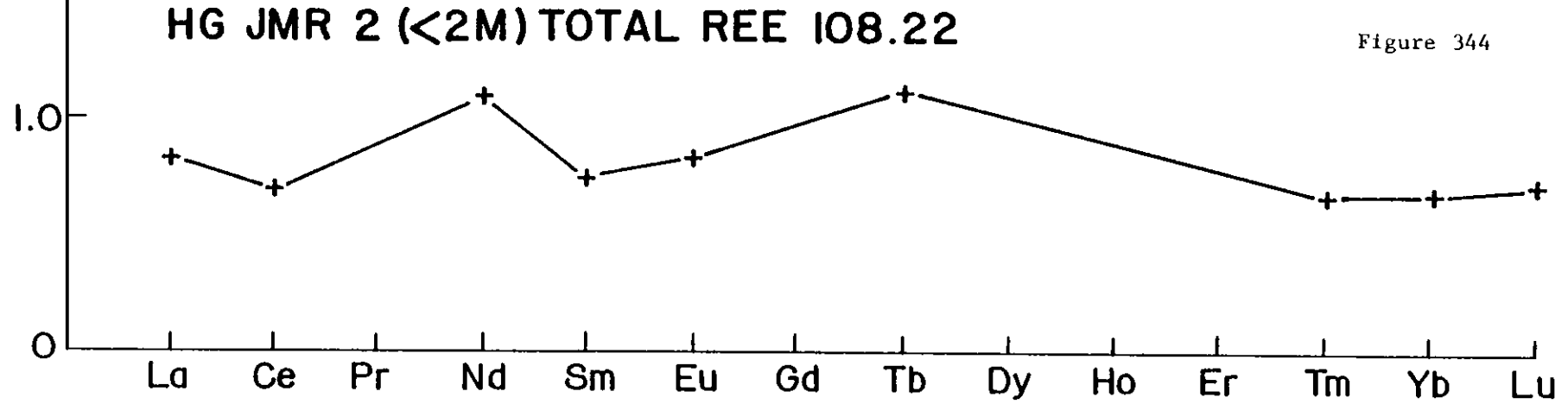
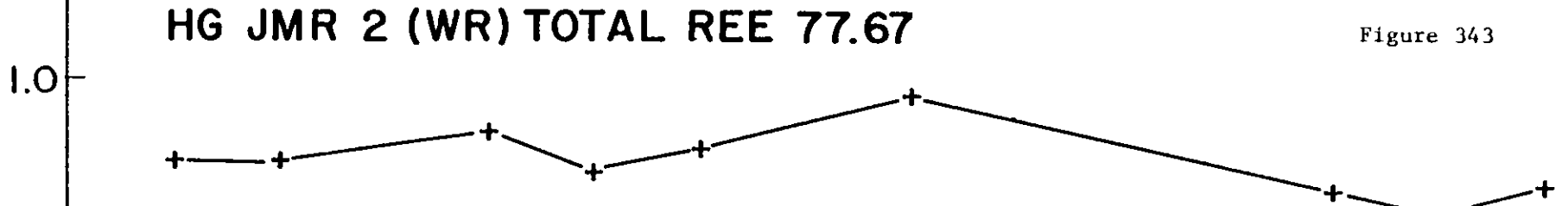
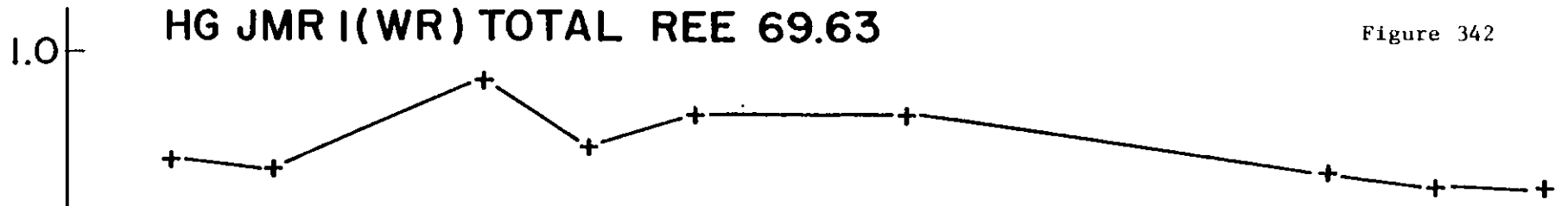


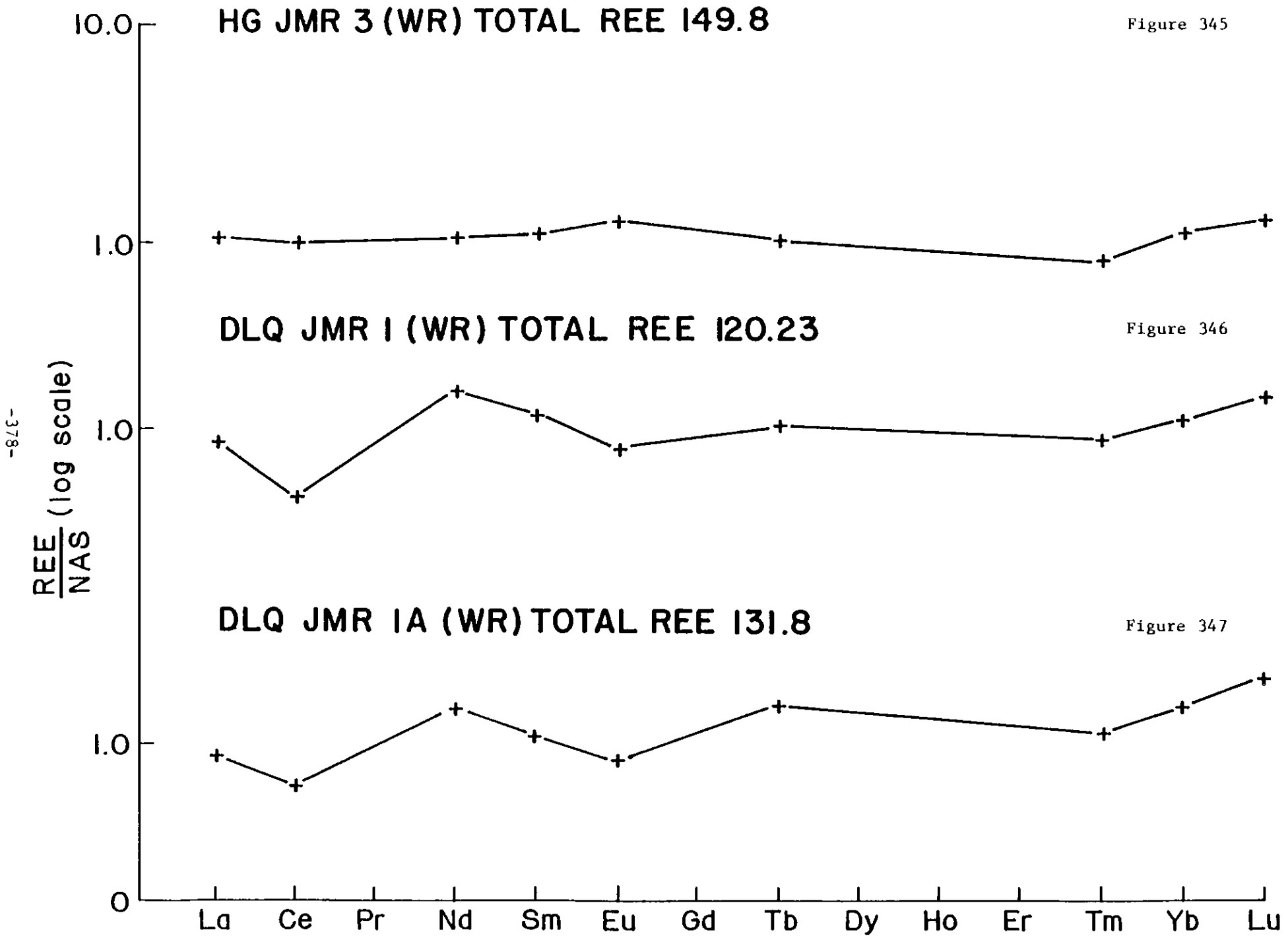






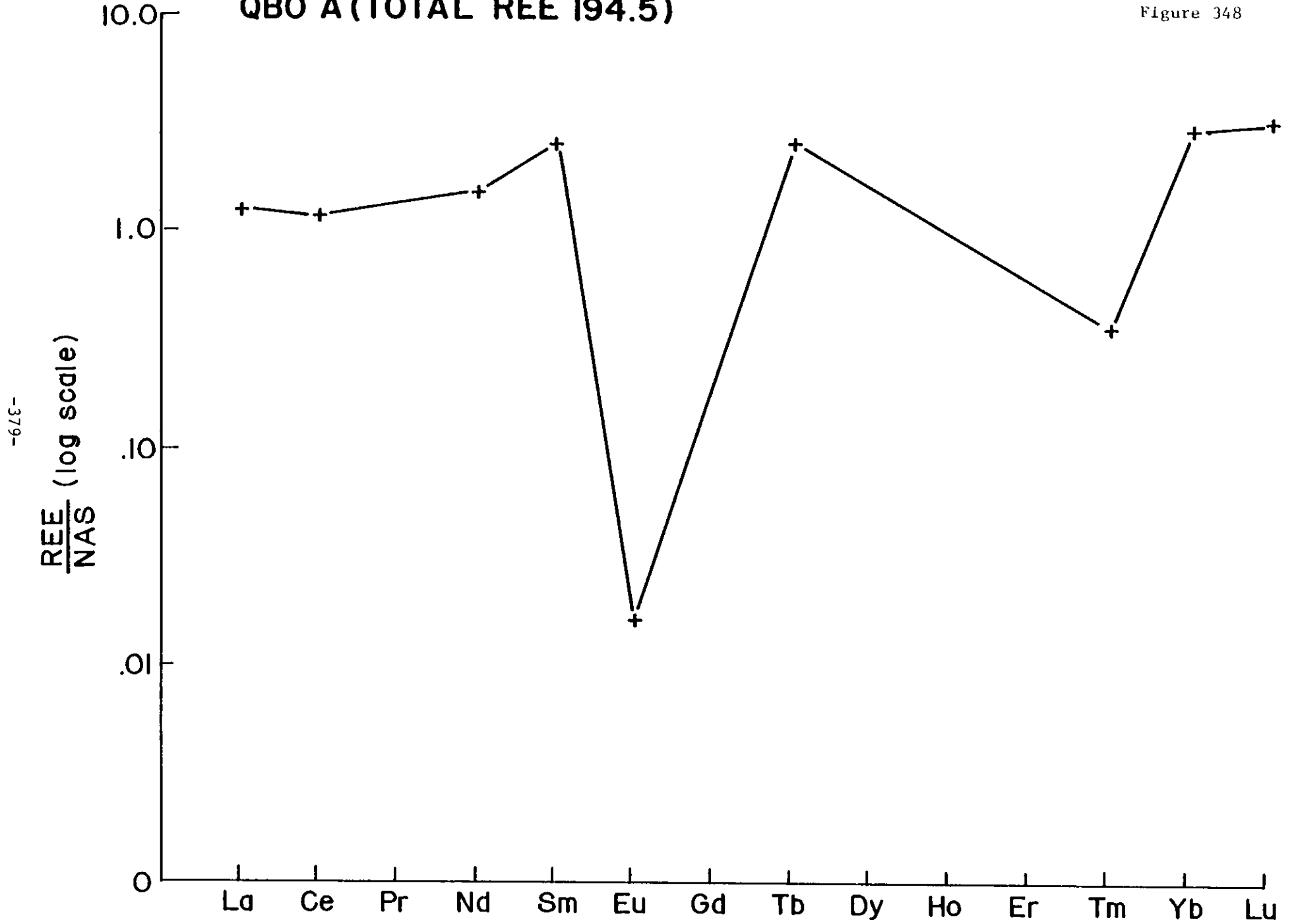




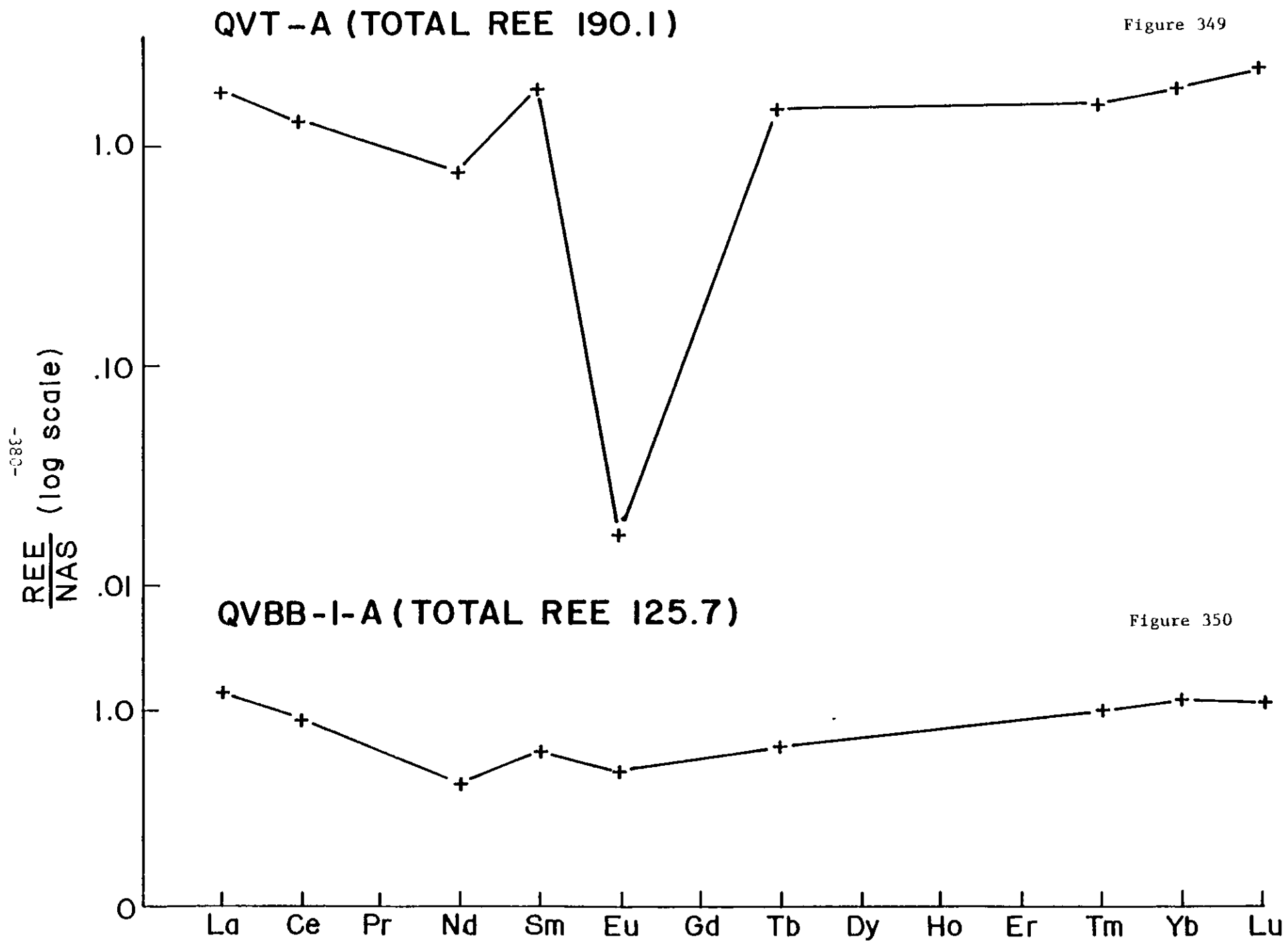


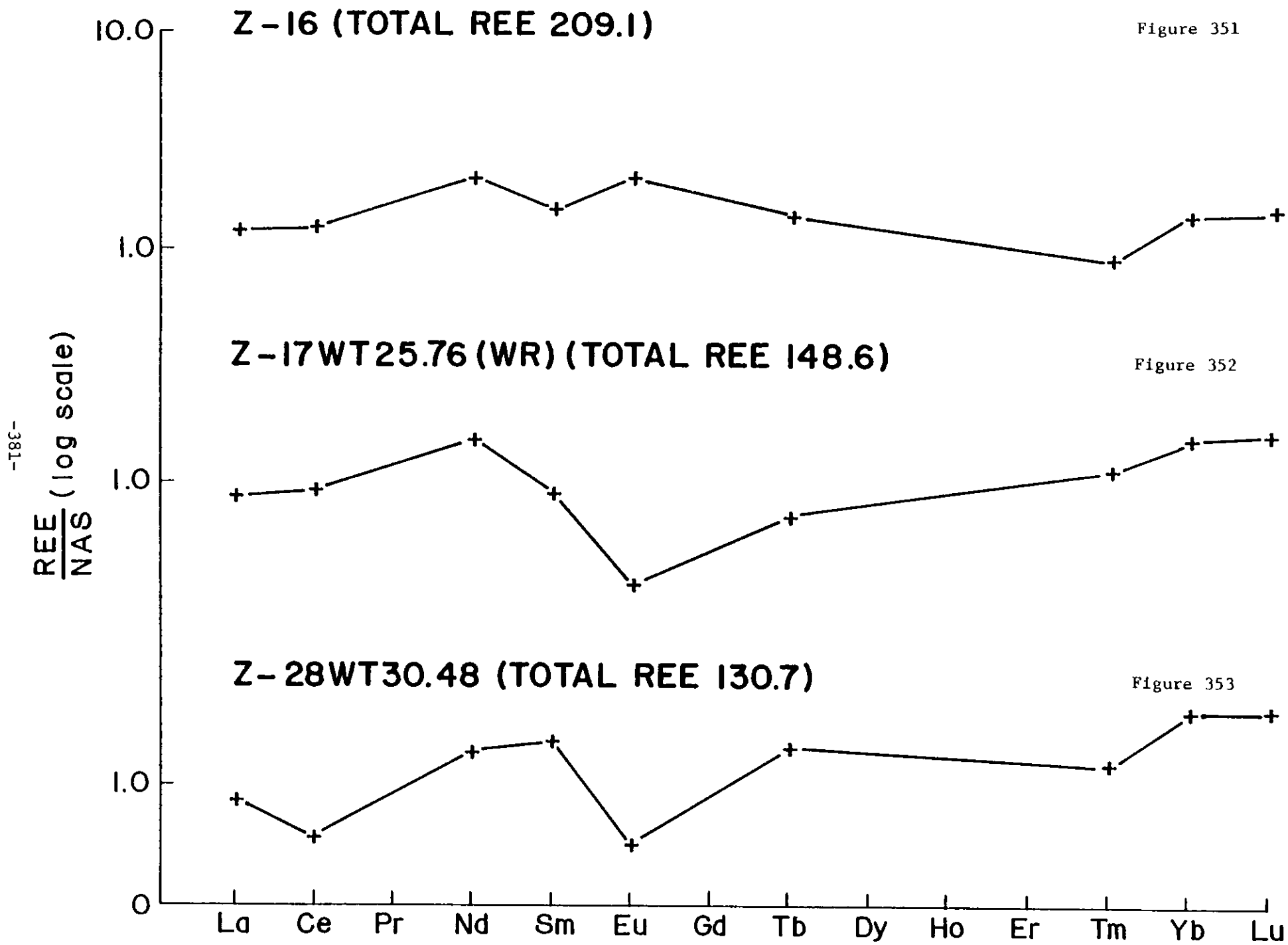
QBO A (TOTAL REE 194.5)

Figure 348



-379-





Chapter 9

THORIUM AND URANIUM ABUNDANCES IN THE ZUNI MOUNTAINS:

IMPLICATIONS TO THE GRANTS MINERAL BELT

As part of a State of New Mexico funded project the uranium and thorium abundance in a wide variety of all major Precambrian rocks exposed in the Zuni Mountains have been determined by DNAA. The data include surface samples from fresh outcrop (ZS), from quarry or road cut (Z) and from shallow drilling (ZM). The data are of interest in that the Zuni Mountains lie to the southwest of and parallel to the Grants mineral belt. If the ancestral Zuni Mountains directly or indirectly served as a source for uranium for the Grants mineral belt then this should be reflected in the Th and U abundances and in the Th/U ratio remaining in presently exposed rocks. While it is generally accepted that the presently exposed rocks were covered by Paleozoic rocks during the deposition of the Jurassic Morrison Formation, at least part of the area may have been uplifted in the Cretaceous and certainly in post-Laramide time. Consequently, if the uranium for the Grants mineral belt was deposited in Cretaceous or younger time then the Zuni Mountains are a convenient source due to their location at the southwestern edge of the San Juan Basin with the regional drainage presumably to the northeast.

While data for uranium are available for 57 samples only 25 samples have yet been analyzed for Th. The data are shown in table 53. The Th samples vary from 4 to 29 ppm with a mean of 17.5 ppm while U varies from 1.8 to 7.4 ppm with a mean of 3.9 ppm. For the Th/U ratios, variation is noted between 2.27 and 7.82 with a mean of 4.55.

The Th, U contents and the Th/U ratios are typical of rocks which have not lost appreciable amounts of U or else very low U contents and proportionately higher Th/U ratios (i.e., 20-50) would be common. Since the REE plots also indicate normal behavior for granitic rocks (Fig. 628) then, in support of other evidence, we propose that the presently exposed rocks of the Zuni Mountains were not important contributors for the uranium of Grants mineral belt.

Table 53

Zuni Mts.

<u>SAMPLE</u>	<u>Th</u>	<u>U</u>	<u>Th/U</u>
ZMIA-2P	18.79	5.98	3.14
ZSIP	15.98	3.53	4.53
ZS4P	7.92	2.14	3.70
ZMIA 6P	18.02	3.37	5.35
ZS 3P	4.07	1.79	2.27
ZMEA 5P	20.51	3.65	5.62
ZS7P	18.30	5.33	3.43
ZS2P	30.36	5.60	5.42
ZS5P	11.29	3.49	3.23
ZM6 5P	16.86	2.94	5.73
ZMIA-1	22.76	2.91	7.82
ZMIA-4	21.91	4.02	5.45
ZMIA-7P	20.24	3.64	5.56
ZS8P	28.60	5.02	5.70
ZM62P	14.02	2.97	4.72
ZM64P	16.54	4.44	3.73
ZM77P	17.48	3.28	5.33
ZM76P	13.63	3.46	3.94
Z10P	24.35	4.32	5.64
Z16P	14.04	4.07	3.45
ZM78P	13.44	2.64	5.09
ZM6 1P	11.98	3.46	3.46
ZM63P	12.22	3.67	3.33
Z25P	15.79	3.74	4.22
Z41P	29.15	7.37	3.96

Table 53 (cont'd.)

- 1) Samples for uranium analyses
A) Zuni Mountains
i) granites

<u>no.</u>	<u>U(ppm)</u>	<u>no.</u>	<u>U(ppm)</u>
Z-10	3.70	ZU-101	3.35
Z-13	5.88	ZU-103	3.35
Z-16	3.95	ZU-105	3.24
Z-17	5.97	ZU-108	1.82
Z-25a	3.20		
Z-25b	3.31	ZU-112	3.77
Z25c	2.99	ZU-114	3.22
Z-28	3.06	ZU-104	7.23
Z-30	2.58	ZU-115A	2.28
Z-35	3.04	ZU-115B	2.40
Z-39	2.68	ZU-115C	2.46
Z-40	3.05	ZU-115D	3.42
Z-41	8.22	ZU-115E	2.95

- ii) Metarhyolites

ZU-106	5.28
ZU-109	2.61
ZU-110	4.74
ZU-111	3.19
ZU-116	3.94
ZU-117	3.62
ZU-118	2.54

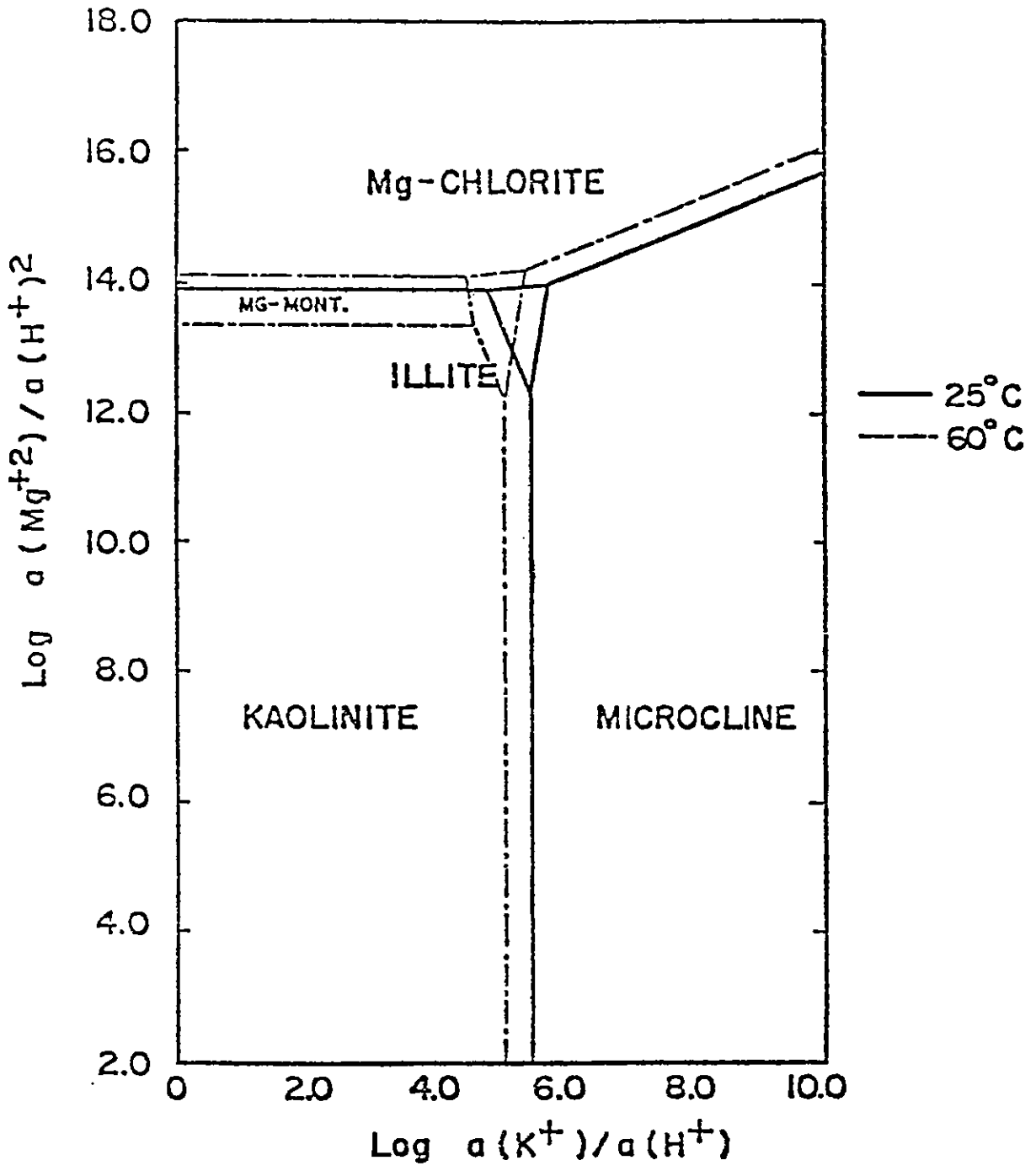
Chapter 10

DISCUSSION AND CONCLUSIONS

Clay Mineral Relationships and their Bearing on Uranium Mineralization

The importance of clay minerals to the uranium mineralization noted in the Grants mineral belt has been discussed in earlier reports (Lee, 1976; Brookins, 1976a, 1976b, 1977a, 1977b); discussion of earlier work by Granger (1962), Keller (1962), Kendall (1972) and others are discussed by Lee (1976) and Brookins (1976a,b). In brief, enrichment of Mg in ore zones is frequently observed, especially in ore reduced ground, removed from the redox interface. Chlorite is commonly the product of some of these reactions. Under other conditions, illite, mixed layer illite-montmorillonite and montmorillonite are penecontemporaneous with the primary uranium minerals. Kaolinite is present in several generations: (a) In bleached, oxidized ore, presumably secondary in formation to the oxidation. (b) As nests in both reduced and oxidized rocks, again presumably as secondary as it fills post-ore (or other primary mineral) voids and fissures as opposed to coating grains. (c) As grain coatings commonly associated with stack (redistributed) ore; commonly at ore enriched at the main redox interface are probably penecontemporaneous with some uranium ore (see discussion elsewhere in this section).

Any discussion of the Grants mineral belt clay mineral reactions is made easier by consideration of the activity - activity diagrams constructed by Helgeson et al. (1969) and with reference to the studies of Huang and Keller (1970, 1971, 1972) on the role of organic acids affecting detrital rock forming minerals, authigenic clay minerals and release of dissolved species by organic acid attack. Reference is made to figure 354 which is



System Mg-K-Al-Si-O-H (1 atm.) for quartz saturation. Mont. = Montmorillonite.

Figure 354

a plot of $\log (a_{\text{Mg}}^{2+}/a_{\text{H}^+})^2$ vs. $\log a_{\text{K}^+}/a_{\text{H}^+}$ in the temperature range of 25°C to 60°C at one atmosphere pressure and under conditions of quartz saturation are demonstrated by the occurrence of quartz overgrowths. Clay minerals can commonly be described by use of figure 354 for sediment rich in organic matter which in some manner facilitates chlorite formation. The use of Mg-Si-K-Al-O-H as variables exclusive of other major elements is justified because much of the Fe is incorporated in either hematite or pyrite (depending on Eh) or possibly in Fe-bearing chlorites (discussed below) which react to form Mg-chlorites in ore zones. Calcium is probably released from plagioclase during organic acid attack but either removed from the system or else incorporated into newly formed calcite with the source of dissolved CO_2 (as HCO_3^-) likely to have formed by oxidation of organic carbon (G. P. Landis; unpub. data). Na from destroyed feldspars may either be removed from the system or, less commonly, be removed from solution as zeolites. The aluminum is commonly retained in the species being destroyed and newly formed (i.e., K-feldspar and clay minerals in figure 34). Any Al released to solution should either be precipitated as $\text{Al}(\text{OH})_3$ (amorphous) or in $(\text{Fe}, \text{Al}(\text{OH})_3)$ under more oxidizing conditions. The data of Phoenix (1959) tend to support the use of figure 354 as waters from the Morrison Formation are typically classified as Ca-Mg- CO_3 - SO_4 varieties (note: the overall role of SO_4 is discussed below; SO_4 as true SO_4^{2-} ion is important under only oxidizing conditions). Adams and others (1977) have presented results from the Jackpile Mine to support the lack of Na in or near ore zones (except as zeolite) and that Ca is present in only calcite not including secondary U(VI)-Ca minerals such as andersonite, bagleyite, rutherfordine, etc.

The SEM photomicrographs shown earlier indicate several key reactions to take place for primary or trend ore removed from the redox front down dip, well into reduced ground.

(1) Ubiquitous chlorite with variable Fe content, commonly forming edge-to-face habits and presumed to be authigenic; this habit of Mg, Fe-chlorite is usually not associated by direct contact with ore.

(2) Rosettes of Mg-chlorite intimately mixed with coffinite (more rarely pitchblende), organic carbonaceous matter, pyrite. This variety of chlorite apparently forms from pre-existing Fe, Mg-chlorite but more commonly from pre-existing montmorillonite or illite or mixed layer montmorillonite-illite.

(3) Typical honeycomb-habit montmorillonite is authigenic and usually partially or completely reacted to form rosette chlorite or illite; the same is true for the common mixed layer montmorillonite-illite. Because mixed layer montmorillonite-illite may be considered as a mechanical stacking of varying proportions of montmorillonite and illite (Tardy and Garrels, 1974), then mixed layer montmorillonite-illite formed authigenically can only be distinguished from montmorillonite-illite by habit. The former still defines typical honeycomb structure but with more disoriented edges and the latter forms feathery stackings (See Fig. 27).

(4) Illite as feathery and filamentous growths may be primary but is more commonly interpreted as secondary. Secondary varieties in addition to montmorillonite-illite and unmixed illite (usually as the 1Md polytype) include illite-chlorite mixed layered assemblages and even more complex illite-chlorite-montmorillonite. All these assemblages are to be expected by inspection of figure 354. Some illite has been, along with chlorite

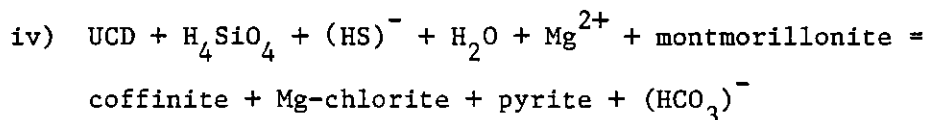
(See Fig. 43), has formed from K-feldspar which is interpreted to indicate a high Mg/H ratio.

A summary of commonly observed reactions and the ΔG_R° for each are:

- | | | | |
|------|-----------------|----------------|--|
| i) | Montmorillonite | to Mg-chlorite | $\Delta G_R^{\circ} = - 105 \text{ kcal.}$ |
| ii) | Illite | to Mg-chlorite | $\Delta G_R^{\circ} = - 95 \text{ kcal.}$ |
| iii) | Montmorillonite | to Illite | $\Delta G_R^{\circ} = - 25 \text{ kcal.}$ |

These changes have been discussed by Brookins (1976b) who points out that due to the large errors in ΔG_f° data reactions (i) and (ii) are more likely than (iii); further, since illite occupies only a small area in figure 354 mixed layer structures are to be expected. The reactions also indicate not only a high Mg/H ratio but slightly alkaline conditions (i.e., for fixed dissolved $\text{H}_4\text{SiO}_4 = 10^{-3.5}$ molal, pH must be greater than 7 for chlorite to form from K-feldspar). Most kaolinite in primary ore deposits is younger than the Mg-chlorite-montmorillonite-illite as indicated by SEM and petrography.

Of further interest is that Fe is considered in the starting clay mineral reactants (i-iii above) will, under reducing conditions, be released as Fe^{2+} which will then combine with $(\text{HS})^-$ or H_2S from the organic matter present to form pyrite. Further, released H_4SiO_4 will react with UDC to facilitate coffinite formation. Thus the addition of reduced sulfur actually accounts for a strong partitioning of Mg into clay mineral products and Fe into pyrite. A general reaction for (i) is then more properly written:



for which the ΔG_R° is close to -100 kcal.

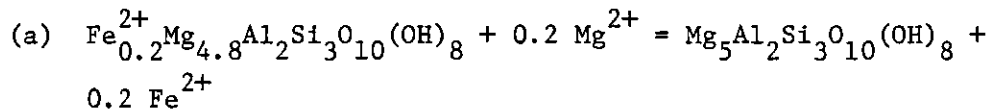
Of interest in this (iv) reaction is that, in view of the different host phases for U, V, Mo, Se under reducing conditions, the most likely host for V^{3+} is in octahedral sites in chlorites or similar Mg, Fe-bearing minerals. This has been demonstrated by Lee (1976). If the V content is very high it will be incorporated into roscoelite (See LaPointe and Markos, 1977) although this mineral is rare in the Grants Mineral Belt (i.e., low V/U) while common in the Uravan Belt (high V/U). When oxidizing waters affect the V-bearing clay minerals, the result is oxidation of V(iii) to V(iv) and V(v). Both V^{4+} and V^{5+} are, however, still retained in the original clay mineral as the difference of ionic radius between V^{3+} and V^{5+} is only 5 percent and thus all species (V^{3+} , V^{4+} , V^{5+}) can easily substitute for Mg^{2+} and/or Fe^{2+} . Only by actual severe alteration or actual destruction of the original clay minerals can the V^{5+} be released into solution as an oxyanion or VO_2^+ .

Both Mo and Se (and presumably Sb and As as well) will be more strongly affected by redox reactions affecting sulfur species. Native selenium may form secondary enrichments from pre-existing ferroselite or seleniferous pyrite.

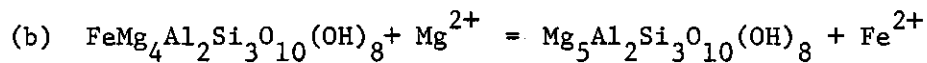
Arsenic should follow pyrite fairly closely, yet data are not adequate to unequivocally demonstrate this point. Similarly, Mo should be close to or intermixed with pyrite. Antimony, on the other hand, will upon oxidation be more likely left behind in the near-ore oxidized zone than Mo or As due to the ease of formation of Sb_2O_5 . This may result in slight enrichment of Sb in limonitic or hematitic stained rocks and thus may be useful for pathfinder element purposes.

Chlorite-Pyrite Reactions

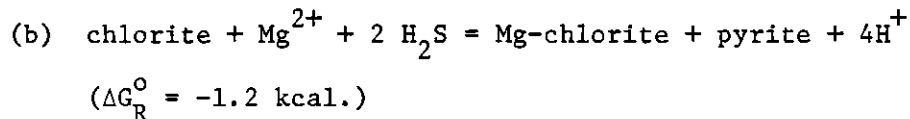
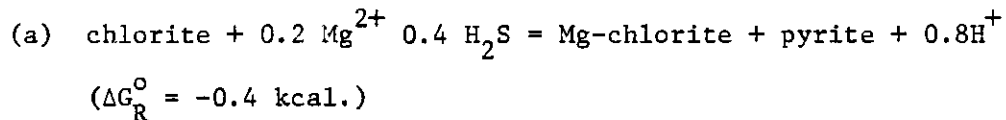
Granger (1962), Brookins (1976a), Lee (1976) have pointed out that chlorites associated with pyrite in uranium ore zones are more magnesium-rich than chlorite removed from ore. Consider the following reactions for which thermodynamic data are available (Nriagu, 1975; Robie and Waldbaum, 1968):



and

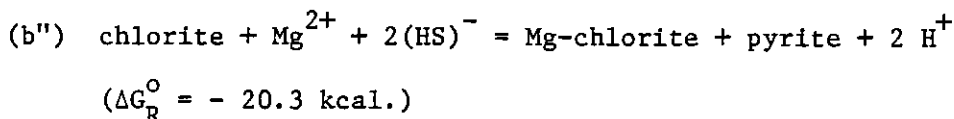
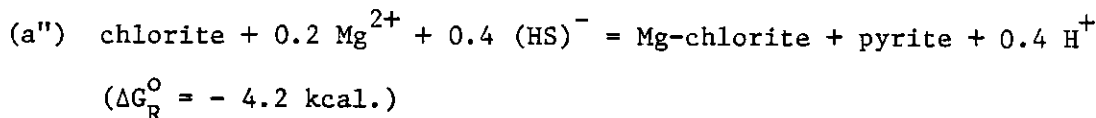


The free energies of reactions (a) and (b), ignoring errors in the data, are: + 0.5 kcal. and + 3.5 kcal. respectively. Thus mere displacement of Fe^{2+} by stoichiometric amounts of Mg^{2+} is not, at first glance, consistent with observation. However, if reactions (a) and (b) are now considered first in the presence of H_2S and then $(\text{HS})^-$ as reactants with pyrite as a product (i.e., $2 \text{H}_2\text{S}$ or $2(\text{HS})^- = \text{FeS}_2 + 4\text{H}^+$ or 2H^+), then the free energies for reactions (a) and (b) are (re-written as (a') and (b')):



(note: electrons produced in (a') and (b') are not included).

Alternately, if $(HS)^-$ is used instead of H_2S , then the free energies for (a) and (b) are written as (a'') and (b''):

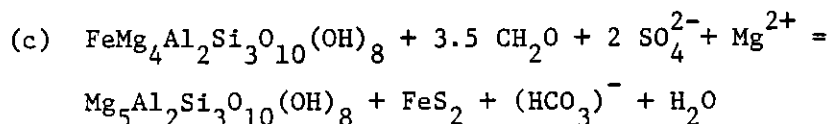


Very simply, at pH conditions where $(HS)^- > H_2S$ (i.e., $pH > 7$), then pyrite formation facilitates Mg-chlorite formation. Even under $pH < 7$, pyrite formation results in more Mg-rich chlorite being formed but the ΔG_R^0 is much smaller. Since Mg-chlorites in the Grants mineral belt are presumed penecontemporaneous with pyrite (and coffinite) formation then slightly alkaline as opposed to slightly acidic conditions are indicated by the reactions above.

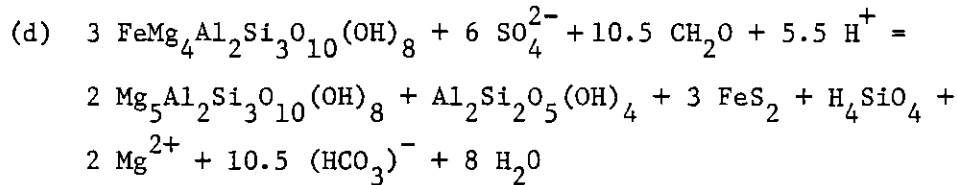
Reactions Involving Organic Carbon, Chlorite, Sulfur Species,

(⁺) Kaolinite in Redox Zones

The presence of kaolinite in ore zones can be explained as due to younger material formed in post-ore time or possibly due to kaolinite formed penecontemporaneously with the ore. For reactions involving just sulfide-sulfate redox reactions in the presence of organic carbon (written as CH_2O by convention) and chlorite one may write:



for which $\Delta G_R^0 = - 114 \text{ kcal.}$ If, as proposed by Siever and Kastner (1972), kaolinite may also form by a similar reaction such as:



for which $\Delta G_R^0 = -432$ kcal. This reaction (d) is modified from that of Siever and Kastner (1972) to allow use of chlorites for which ΔG_f^0 are known (Nriagu, 1975). The Mg^{2+} released during this reaction will facilitate formation of additional Mg-chlorite by reaction (c) in the redox zone, or, if transported a short distance into the reduced ground, facilitate reactions (a) and (b) discussed above. The released silica (as H_4SiO_4) will aid in coffinite formation or, in the absence of uranium, for quartz overgrowths.

The point made for reactions (a) through (d) that pyrite formation is predictable when Mg-chlorites are forming due to various reactions involving organic carbon. If (a) and (b) are modified to include organic carbon as a reactant and $(\text{HCO}_3)^-$ as a product, the reactions are even more efficient.

Clay Minerals from Barren Rocks

The clay minerals associated with different uranium deposits have been tabulated in Chapter 6 (Tables 15-23; Figs. 169-266). It is interesting to compare uranium-clay mineral assemblages with the clay minerals from barren rock.

The Cretaceous Mancos Shale and Dakota Formation can be summarized as follows. The Mancos Shale is characterized by both variable amounts of kaolinite and illite plus illite-montmorillonite. The kaolinite content commonly varies from 33-61 percent while combined illite and illite-montmorillonite vary between 25-62 percent. Illite plus illite-montmorillonite are always enriched relative to montmorillonite and only two samples show

chlorite enrichment. Since the Mancos Shale is commonly enriched in organic carbonaceous matter then the absence of chlorite is important as reactions involving organic carbon plus chlorite are important to uranium mineralization in the Grants mineral belt (See below).

The Dakota Formation can be divided into those samples rich in bentonites and/or shales relative to those rich in sandstone. The former are conspicuously montmorillonite-rich with variable (2-40 percent) kaolinite. Illite and illite-montmorillonite are very rare. The sandstones, on the other hand are always rich in kaolinite (72-95 percent) with lesser amounts of illite and illite-montmorillonite and virtually no montmorillonite.

The Morrison Formation units studied for this report include, in descending order, of the Jackpile Sandstone which cuts and is commonly included as the uppermost sand of the underlying Brushy Basin Shale. At the approximate bottom of the Brushy Basin Shale is found the Poison Canyon Sandstone. The Poison Canyon Sandstone is interpreted as either a separate Member or as the lowermost sand of the Brushy Basin (See discussion in Lee, 1976). The Westwater Canyon Member underlies the Poison Canyon Sandstone and is the dominant host for uranium in the Ambrosia Lake District as well as the western portion of the Grants mineral belt. The Westwater Canyon Member overlies the Recapture Shale Member which contains little uranium relative to the overlying Westwater Canyon.

Of the six barren Jackpile Sandstone samples studied only two are very kaolinite-rich (91-93 percent) while three others show enrichment in the -2μ fraction in combined montmorillonite: montmorillonite-chlorite: illite: illite.

The Brushy Basin Member is typically rich in montmorillonite or illite-montmorillonite although illite and/or chlorite are enriched in some samples.

When chlorite is present it is always present as the face on edge habit characteristic of chlorites removed from ore but not necessarily removed from organic matter.

The Poison Canyon Sandstone samples are from barren ground but not spatially removed far from areas of known mineralization (i.e., either in the Poison Canyon Sandstone or uppermost recognized sands of the Westwater Canyon Member). Of the twenty-two samples studied, twenty are sandstones containing variable but abundant amounts of kaolinite (25-85 percent) and illite-montmorillonite plus illite (24-60 percent); the two mudstones are enriched in illite plus illite-montmorillonite and montmorillonite plus illite-montmorillonite.

The clay minerals from the Westwater Canyon Member barren rocks contain less kaolinite than other sandstones of the Morrison Formation considered in this report. Only 8 of 24 samples contain ten or more percent kaolinite (17-67 percent) while enrichment in ferromagnesian clay minerals is common chlorite in excess of 5 percent noted in ten samples, chlorite-montmorillonite in excess of 5 percent in nine samples, and eleven samples contain 40 percent or more illite-montmorillonite.

The Recapture Rock Member rocks are typically less sand rich than the Brushy Basin Member. Kaolinite varies from 0 to 24 percent for the nine samples inspected, montmorillonite is abundant in three samples, and illite plus illite-montmorillonite very abundant (85-100 percent) in four samples. Only one sample (TQ Jmr-2) is rich in chlorite (19 percent); this sample is interesting in that it is also enriched in both kaolinite (24 percent) and montmorillonite (43 percent) whereas combined illite and illite-montmorillonite total only 14 percent.

For descriptions of the barren rocks from the DOE Drill Hole Locations and from the Mount Taylor Area (San Mateo) the reader is referred to description in Chapter 2 and 3 of this report and to Brookins (1976a) and Lee (1976).

Clay Minerals from Ore-Bearing and Near-Ore Rocks from Mines

Only the Silver Spur Mine was sampled to obtain samples from a mine in the Dakota Formation. Kaolinite is common in only one sample (SS-40) which contains the most redistributed ore and organic carbonaceous matter. Chlorite is enriched in three of the six samples for which XRD studies were conducted, illite in one, and illite-montmorillonite in three. The presence of chlorite is considered important as is the lesser abundances of either chlorite with illite-montmorillonite or abundant illite-montmorillonite alone in view of the abundance of unmixed montmorillonites in bentonites and shales from barren rocks and kaolinite in sandstones. Either the presence of chlorite or illite-montmorillonite may be used with caution to indicate areas of mineralization. The age of mineralization at the Silver Spur uranium deposit is unknown. Three possibilities are: (1) Cretaceous mineralization. (2) Post-Laramide mineralization by far-removed fluids. (3) Post-Laramide mineralization by remobilization of Jurassic ore. At present these alternatives cannot be separated but structural control may favor (3).

Deposits from the Jackpile Sandstone for this report include 14 samples from the Saint Anthony Mine and 16 samples from the JJ Mine. Both mines are close to the Jackpile-Paguete Mines discussed in detail by Nash (1968) and also reported on by Brookins (1976a) and Lee (1976).

Whereas the barren Jackpile rocks are too few to allow one to distinguish definite trends in clay minerals, the clay minerals from the Jackpile Sandstone deposits tend to be about evenly divided in terms of enrichment in chlorite and illite-montmorillonite or just in illite-montmorillonite. The JJ mine samples tend to be less kaolinite-rich than those from the Saint Anthony Mine. As Nash (1968) has pointed out, mixed layer illite-montmorillonite and chlorite are both commonly associated with ore at the Jackpile Mine. Our previous findings (Brookins, 1976a) and the present study support this view.

Clay minerals from the ore at the Mariano Lake Mine from the Poison Canyon Sandstone are of interest in that kaolinite is abundant in all ore samples and always greater in abundance than chlorite or illite-montmorillonite (including illite) which are present in about equal abundance. The presence of abundant kaolinite may be explained here by reactions such as those involving kaolinite and chlorite forming from pre-existing material when sulfide-sulfate reactions take place in the presence of organic carbon. Chlorite is considered very important as a possible ore guide as it is usually absent, except in mudstone galls, in the barren Poison Canyon rocks.

The uranium of the Doris M. Mine occurs in an upper sand of the Westwater Canyon Member. The Doris M. Mine samples are characterized by a calcite-rich matrix and kaolinite and illite-montmorillonite are both common (with about 50:50 division of one more common than the other). The absence of chlorite in the ore zones may be due to the high calcite matrix or to other factors (i.e., temperature) not yet studied. Certainly the calcite-illite-montmorillonite is more typical of ore-bearing samples than barren samples.

At the Johnny M. Mine from deeper in the Westwater Canyon Member the clay minerals associated with ore are still kaolinite-rich but chlorite plus illite-montmorillonite are more abundant than kaolinite in 6 of 11 samples. The matrix is clay-rich and carbonate-poor and this may account for the greater abundance of chlorite.

Samples from Section 23, Section 30 and Section 36 Mines at Ambrosia Lake have been studied further since the reports by Brookins (1976a) and Lee (1976). Each mine apparently has a somewhat unique suite of clay minerals. Chlorite is most important at the Section 23 Mine, illite-montmorillonite (8 of 9 samples) and chlorite (4 of 9 samples) are abundant at the Section 30 Mines, and all samples from the Section 36 Mine contain both chlorite and illite-montmorillonite. The barren samples contain a clay mineral suite commonly rich in montmorillonite, less frequently in illite-montmorillonite, and chlorite is relatively rare. Kaolinite, too, is only enriched over 10 percent in about one-third the samples from barren rocks. The main difference between ore-bearing rocks and the barren rocks is thus the replacement of montmorillonite by chlorite and some illite-montmorillonite in the Ambrosia Lake district.

Concluding Statements

Conclusions we have reached from the research funded by U.S.D.O.E./ B.F.E.C. Contract #76-029-E are as follows:

- (1) SEM Photomicrographs allow one to carefully work out the clay mineralogic history of the paragenesis of those minerals which are authigenic and not associated with ore, those minerals which are intimately mixed with the ore and presumed congenetic with it, those minerals which represent younger periods of alteration. The SEM material represented here is only a small part of the total SEM collection. The bulk of the 1300 SEM views will be published as an appendix to this report.
- (2) Evaluation of the Mount Taylor uranium deposit and associated area reveal that (a) clay minerals zone across the ore body, (b) certain trace elements and ratios of trace elements as determined by XRF are valuable as pathfinder for this deposit but may not, without further work, be safely applied to other deposits, (c) tartaric acid, one of the constituent derivative acids of humic or fulvic acid, is the most effective of the acids used for leaching of Mt. Taylor samples. Ways to rapidly identify tartic acid component of humic materials will be useful in assessing the role of organics in uranium deposits, (d) total organic carbon in the -2μ fraction correlates well with uranium; total organic carbon is more common throughout certain rock sequences where contents are low and variable.
- (3) Eh-pH are useful in depicting the sequence of uranium and associated mineralization in the Grants mineral belt. Further, trace element data, used in conjunction with the Eh-pH diagrams and clay mineral

assemblages, may allow one to predict favorability of rocks either re-reduced or re-oxidized from pre-existing redox fronts.

- (4) Several periods of mineralization are noted in the Grants mineral belt as outlined in Chapter 5. Syngenetic or early epigenetic mineralization at about 135-140 m.y. ago during deposition of the Morrison Formation. Mineralization during the mid-Cretaceous in part of the Laguna district. Possible mineralization during the Late Cretaceous (note: further dating will allow an evaluation of primary Cretaceous vs. remobilized Late Jurassic or other ore into Cretaceous rocks), Laramide mineralization, post-Laramide mineralization. The testing of remobilized versus newly introduced uranium by the Rb-Sr method can be accomplished in a relatively straightforward manner.

Finally, the Rb-Sr ages on the Late Jurassic rocks and on the Cretaceous Dakota and Mancos Formations attests to the reliability of the Rb-Sr method for dating of many sedimentary rocks previously thought undatable by radiometric means.

Provenance for detritus should also be determinable with combined geochronologic and geochemical work.

- (5) Clay mineralogic studies have proven to be most valuable. One can convincingly argue for chlorite and/or chlorite plus illite-montmorillonite and/or illite-montmorillonite to be commonly associated with ore whereas more montmorillonitic sequences are typical of barren rocks. Kaolinitic rocks pose problems, but in some cases (i.e., Laramide or post-Laramide (?)) deposits kaolinite and chlorite appear to both be associated with ore. This is consistent with uranium mineralization under reducing conditions for the kaolinite-absent assemblages and to sulfide-sulfate reactions when kaolinite and

chlorite are both present. Barren rocks can usually be distinguished from mineralized rocks based on combined clay mineralization and a characteristic suite of trace elements.

- (6) The trace element data for barren rocks of the Grants mineral belt have been refined by both instrumental and delayed neutron activation analysis (INAA and DNAA). The former data can probably be used for large and subtle halo effects based on first inspection; these data are being carefully scrutinized to verify or refute this idea at present. The uranium and thorium data allow one to distinguish more obvious haloes near ore bodies. Further, the lack of high Th/U in the Brushy Basin can be interpreted to mean a far removed provenance for the uranium of the Westwater Canyon Member as opposed to some local provenance (i.e., Dakota or Brushy Basin Source). The trace element data by INAA allow for the first time an adequate data bank for background values for many trace elements for both total rocks and their constituent clay minerals to be established. The accuracy and the precision of the INAA and DNAA techniques have been demonstrated using the Omega West Reactor Facilities of the Los Alamos Scientific Laboratory.
- (7) The Rare Earth Element (REE) studies conducted show that barren rocks are quite different from each other and, more important, different from ore zone rocks. This is clearly reflected in examination of the -2μ fractions of ore where the REE, and especially Eu, are enriched (Brookins, 1976a) whereas such enrichment is less and sporadic in other rocks. The whole rocks and clay minerals of the arenaceous rocks provides one with a powerful tool for distinguishing between them.

Differences between argillaceous rocks are more subtle and reliance on other trace elements must be made.

- (8) A combination of data from Phase I (Brookins, 1976a) and Phase II (this report) plus anticipated data from Phase III (pending) will allow inspection of various genetic models for the Grants mineral belt to be tested. We anticipate use of the collective data already reported (including this report) plus unpublished stable isotope and other data to allow us to address problems of (a) genetic model for the Grants mineral belt, (b) evaluation of preliminary drilling before planning major, closed spaced programs, (c) assessment of provenance and therefore other areas of possible potential, (d) a more exact chronology of primary and subsequent periods of mineralization in the Grants mineral belt (i.e., therefore allowing one to either follow up on or eliminate areas for detailed drilling if the geochronologic and geochemical data both suggest the route to take).
- (9) The presently exposed Precambrian core rocks of the Zuni Mountains possess normal U and Th abundances and the Th/U ratio is typical of many granitic rocks. No evidence for removal of large amounts of uranium are indicated; this, coupled with the geologic evidence, argue against the Zuni Mountains core rocks as a source of uranium for the Grants mineral belt.
- (10) Unpublished data (UNM) and some published geochronologic and uranium data for rocks from southwestern New Mexico and southeastern Arizona suggest that these rocks should be inspected for possible provenance.

REFERENCES CITED

- Adams, S. S., Hafen, P. L. and Salek-Nejad, H., 1975, Aspects of detrital and authigenic mineralogy of the Jackpile Sandstone, northwestern New Mexico; (abs.) Am. Assoc. Petrol. Geol., Rocky Mtn. Section, 24th Annual Meeting.
- Balestrini, S. J., Balagna, J. P. and Menlove, H. O., 1976, Two specialized delayed-neutron detector designs for assays of fissionable elements in water and sediment samples: Nuc. Instrum. Methods, v. 136, p. 521-524.
- Brookins, D. G., 1976a, Uranium deposits of the Grants, New Mexico Mineral Belt: U.S.E.R.D.A. Final Rpt. GJO-1636-1, 120 p.
- _____, 1976b, The Grants Mineral Belt, New Mexico: comments on the coffinite-uraninite relationship, clay mineral reactions, and pyrite formation: N.M. Bur. Mines Min. Res. Spec., Vol. 6, p. 158-166.
- _____, 1976c, Position of uraninite and/or coffinite accumulations to the hematite-pyrite interface in sandstone-type deposits: Economic Geol., v. 71, p. 944-948.
- _____, 1977a, Geochemical Genesis of Uranium in the Southern San Juan Basin: Uranium Geology Symposium, Vol. GJO:BFEC-78, p. 10-28.
- _____, 1977b, Uranium deposits of the Grants Mineral Belt: geochemical constraints: Rocky Mtn. Assoc. Geol. Gdbk, p. 337-352.
- Brookins, D. G. and Della Valle, R. S., 1977a, Uranium abundance in some Precambrian and Phanerozoic rocks from New Mexico: Rocky Mtn. Assoc. Geol. Gdbk, p. 353-362.
- _____, Lee, M. J. and Reise, W. C., 1977b, Trace Elements as Possible Prospecting Tools for Uranium in the Southern San Juan Basin: N.M. Geol. Soc. 28th Gdbk., p. 263-270.
- Brookins, D. G., Della Valle, R. S. and Lee, M. J., 1978a, Rare earth element study of whole rocks and clay minerals from the southern San Juan Basin, New Mexico: EOS Trans. Am. Geophys. Un., v. 59, p. 388.
- _____, 1978b, Rb-Sr geochronologic investigation of Precambrian silicic rocks from the Zuni Mountains, New Mexico: The Mountain Geologist, v. 15, p. 67-71.
- Cullers, R. L., Chadhuri, S., Arnold, B., Lee, M. and Carlton, W. W., 1975, Rare earth distributions in clay minerals and in the clay-sized fraction of the Lower Permian Havensville and Eskridge shales of Kansas and Oklahoma: Geochimica et Cosmochimica Acta, 1975, Vol. 39, pp. 1691 to 1703.

- Finch, W. I., 1967, Geology of epigenetic uranium deposits in sandstone the United States: U.S. Geol. Survey Prof. Paper 538, 12 p.
- Flanagan, F. J. 1976, Descriptions and Analyses of eight new USGS rock standards: U.S.G.S. Prof. Paper 840, 19 p.
- Gale, N. H., 1967, Development of delayed-neutron technique as rapid and precise method for determination of uranium and thorium at trace levels in rocks and minerals- with applications to isotope geochronology. In: Radioactive Dating and Methods of Low-Level Counting. International Atomic Energy Agency, Vienna, p. 431-452.
- Garrels, M. R. and Christ, C. L., 1965, Solutions, Minerals and Equilibria: Harper and Row, New York, 450 p.
- Gordon, G. E., Randle, K., Goles, G. G., Corlis, J. B., Beeson, M. H. and Oxley, S. S., 1968, Instrumental activation analysis of standard rocks with high-resolution γ -ray detectors, Geochim Cosmochim. Acta, v. 32, p. 369-396.
- Granger, H. C., 1962, Clays in the Morrison Formation and their spatial relationship to the uranium deposits at Ambrosia Lake, New Mexico: U.S. Geol. Survey Prof. Paper 450-D, p. 15-20.
- _____, 1968, Localization and control of uranium deposits in the southern San Juan Basin Belt, New Mexico - An Hypothesis; U.S. Geol. Survey Prof. Paper 600B, p. B60-70.
- Harshman, E. N., 1970, Uranium ore rolls in the United States: in Uranium Exploration Geology: Int. At. Ener. Agy., Vienna, Austria, p. 219-232.
- Haskin, L. A., Wildeman, T. R., Frey, F. A., Collins, K. A., Keedy, C. R. and Haskin, M. A., 1966, Rare earths in sediments, J. Geophys. Res. 71, p. 6091-6105.
- Helgeson, H. E., Brown, T. H. and Leeper, R. H., 1969, Handbook of theoretical activity diagrams depicting chemical equilibria in geologic systems involving an aqueous phase at one atm. and 0 to 300°C; Freeman, Cooper and Co., San Francisco, 253 p.
- Hem, J. D., 1977, Reactions of metal ions at surfaces of hydrous iron oxide: Geochim. Cosmochim. Act, v. 41, p. 527-538.
- Hostetler, P. B., 1960, Uranium deposits of the San Juan Basin, New Mexico; Econ. Geol., v. 55, p. 429-464.
- _____ and Garrels, R. M., 1962, Transportation and precipitation of uranium and vanadium at low temperatures with special reference to sandstone-type uranium deposits; Econ. Geology, v. 57, p. 137-167.

- Howard, J. H., 1977, Geochemistry of selenium: formation of ferroselite and selenium behavior in the vicinity of oxidizing sulfide and uranium deposits, *Geochim. Cosmochim. Acta*, v. 41, p. 1665-1678.
- Huang, W. H. and Keller, W. D., 1970, Dissolution of rock-forming silicate minerals in organic acids: Simulated first-stage weathering of fresh minerals surfaces; *Am. Mineralogist*, v. 55, p. 2076-2094.
- _____, 1971, Dissolution of clay minerals in dilute organic acids at room temperature; *Am. Mineralogist*, v. 56, p. 1082-1095.
- _____, 1972, Organic acids as agents of chemical weathering of silicate minerals; *Nature*, v. 239, p. 149-151.
- Keller, W. D., 1962, Clay minerals in the Morrison Formation of the Colorado Plateau: U.S. Geol. Survey, Bull. 1150, 90 p.
- Kelley, V. C., 1955, Regional tectonics of the Colorado Plateau and relationships to the origin and distribution of uranium; Univ. New Mexico Publications in Geology, No. 5, Albuquerque, New Mexico, 120 p.
- _____, Ed., 1963, Geology and technology of the Grants uranium region; New Mexico Bur. Mines and Min. Res., Memoir 15, 277 p.
- _____, and Clinton, N. J., 1958, Fracture systems and tectonic elements of the Colorado Plateau; U.S. Atomic Ener. Comm., RME-108, 107 p.
- Kendall, E. W., 1971, Trend ore bodies of the Section 27 Mine, Ambrosia Lake uranium district, New Mexico: unpub. Ph.D. thesis, Univ. of Calif., Berkeley, 167 p.
- Langmuir, D., 1978, Uranium solution-mineral equilibria at low temperatures with applications to sedimentary ore deposits: *Geochim. et Cosmochim. Acta*, Vol. 42, pp. 547-569.
- LaPoint, D. J. and Markos, G., 1977, Geochemical interpretation of ore zonation at the Rifle vanadium mine, Colorado: U.S. Geol. Survey Circ. 753, p. 53-55.
- Lee, M. J., 1976, Geochemistry of the sedimentary uranium deposits of the Grants Mineral Belt, southern San Juan Basin, New Mexico: unpub. Ph.D. thesis, Univ. of New Mexico, 241 p.
- _____ and Brookins, D. G. (in press), Rb-Sr investigation of the Morrison Formation (Late Jurassic), Grants Mineral Belt, New Mexico: minimum ages of sedimentation-uranium mineralization, and provenance: *Amer. Assoc. Petrol. Geo. Bull.*

- Lisitsin, A. K. and Kuznetsova, E. C., 1967, Role of micro-organisms in development of geochemical reduction barriers where limonitization bedded zones wedge-out, Intl. Geol. Rev. 9, p. 1180-1191.
- Ludwig, K. R., 1977, Effect of initial radioactive-daughter disequilibrium on U-Pb isotope apparent ages of young minerals: Jour. of Res. U.S.G.S., Vol. 5, p. 663-667.
- Melvin, J. W., 1976, Systematic Distribution of large uranium deposits in the Grants uranium region, New Mexico: in Tectonics and Mineral Resources of Southwestern North America, Woodward, L. A. and Northrop, S. A., eds., N.M. Geol. Soc. Spec. Pub. No. 6, p. 144-150.
- Naumov, G. B., Ryzhenko, B. N. and Khodakovsky, I. L., 1974, Handbook of thermodynamic data, Natl. Tech. Info. Service., U.S. Dept. of Commerce, Springfield, Va.
- Nash, J. T., 1968, Uranium deposits in the Jackpile Sandstone, New Mexico: Econ. Geology, v. 63, p. 737-750.
- Nord, G. L., 1977, Characteristics of fine-grained black uranium ores by transmission electron microscopy. Short Papers of the U.S. Geol. Survey, Uranium-Thorium Symposium (Ed. J. A. Campbell), U.S. Geol. Survey Circ. 753, p. 29-31.
- Nriagu, J. O., 1975, Thermochemical approximations for clay minerals: Amer. Mineralogist, v. 60, p. 834-839.
- Ong, H. L., Swanson, V. E. and Busque, R. E., 1970, Natural organic acids as agents of chemical weathering: U.S. Geol. Survey Res. 1970, p. C130-137.
- Phoenix, D. A., 1959, Occurrence and chemical character of groundwater in the Morrison Formation; U.S. Geol. Survey Prof. Paper 320, p. 55-64.
- Ragland, P. C., 1977, Uranium potential of the crystalline rock areas of the southeastern U.S.: 1977 NURE Uranium Geology Symposium, U.S.D.O.E., pp. 173-182.
- Riese, W. C., 1977, Geology and geochemistry of the Mount Taylor uranium deposit, Valencia County, New Mexico: Univ. of New Mexico masters thesis, 146 p.
- _____, Brookins, D. G. and Della Valle, R., 1978, The effectiveness of organic acids in providing uranium mineralization in the Grants Mineral Belt, New Mexico: an experimental study (abs't.): Bull. N.M. Acad. Sci., v. 18, n. 1, p. 18.

- Roach, C. M. and Thompson, M. E., 1959, Sedimentary structures and localization and oxidation of ore at the Peanut Mine, Montrose County, Colorado: U.S. Geol. Survey, Prof. Paper 320, p. 197-202.
- Robie, R. A. and Waldbaum, D. R., 1968, Thermodynamic properties of minerals and related substances at 298.15°K (25.0°C) and one atmosphere (1.013 bars) pressure and at higher temperatures; U.S. Geol. Survey Bull. 1259, 256 p.
- Roeber, M. M., Jr., 1972, Possible Mechanics of lateral enrichment and physical positioning of uranium deposits, Ambrosia Lake area, New Mexico: N.M. Bur. Mines and Min. Res., Circ. 118, 16 p.
- Rubin, B., 1970, Uranium roll front zonation in the southern Powder River Basin, Wyoming: Wyoming Geol. Assoc., Earth Sci. Bull., Dec. 1970.
- Sellschop, J. P. F., Steele, T. W., Rasmussen, S. E. and Fesq, H. W., 1973, Neutron activation analysis of samples from the Kimberly Reef conglomerate: Natl. Institute for Metallurgy, Univ. of the Witwatersrand, Johannesburg, 241 p.
- Siever, R. and Kastner, M., 1972, Shale petrology by electron microprobe: pyrite-chlorite relations: Jour. of Sedimentary Petrology, v. 42, No. 2, p. 350-355.
- Tardy, y. and Garrels, R. M., 1974, A method of estimating the Gibbs energies of formation of layer silicates; Geochim. et Cosmochim Acta, v. 38, p. 1101-1116.

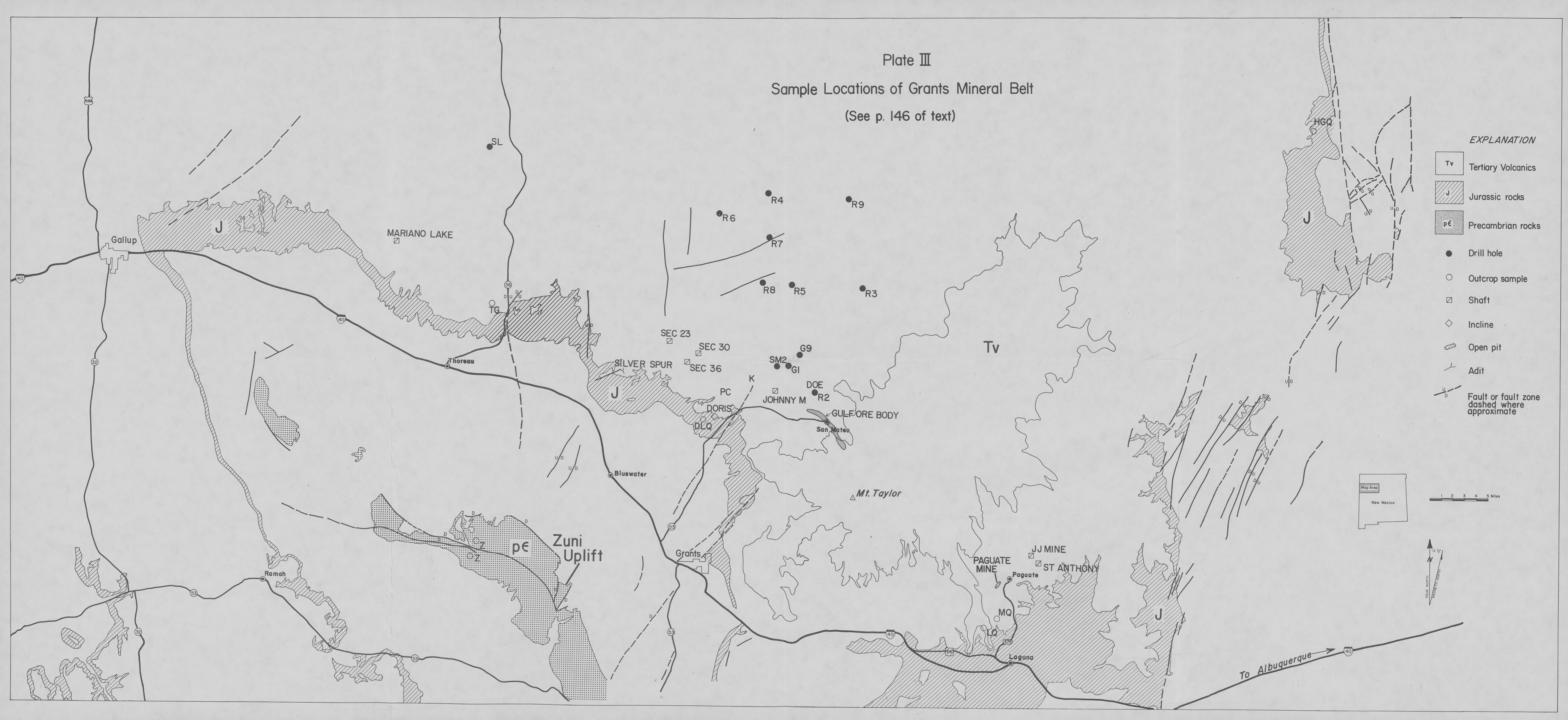
Publications Resulting from
AEC-ERDA-DOE/BFEC Funding

1. Brookins, D.G., and Lee, M.J., (1974), "Uranium Mineralization: Carbonaceous Matter: Clay Mineral Relationships in the South San Juan Mineral Belt, New Mexico": Geol. Soc. Amer. Abs. with Progs, w. 6, p. 669.
2. Lee, M.J., Brookins, D.G., Mudhopadhyay, B. (1975), "Clay mineralogy of the uranium-organic matter enriched and barren zones in the Morrison Formation, Ambrosia Lake District": Amer Assoc. Petroleum Geologists, Rocky Mtn. Sec., 1975, Bull. AAPG, v. 59, p. 914.
3. Brookins, D.G., (1975), "Coffinite-uraninite stability relations in the Grants Mineral Belt": Amer. Assoc. Petroleum Geol., Rocky Mtn. Sec., Bull. AAPG, v. 59, p. 905.
4. Brookins, D.G., (1975), "Uranium resources 1975-2000: reserves and exploration potential in the United States": Amer. Soc. Mech. Engineers Symposium, 1975, p. 11-20.
5. Hafenfeld, S.R., and Brookins, D.G., (1975), "Mineralogy of Uranium Deposits Northeast of the Laguna District, Sandoval County, New Mexico": Amer. Assoc. Petroleum Geol., Rocky Mtn. Sec., 1975, Bull. AAPG, v. 59, p. 910-911.
6. Brookins, D.G., (1976a), The Grants Mineral Belt, New Mexico: comments on the coffinite-uraninite relationship, clay mineral reactions, and pyrite formation: N.M. Bur. Mines Min. Res. Spec. Vol. No. 6, p. 158-166.
7. Brookins, D.G., (1976b), Uranium deposits of the Grants, New Mexico Mineral Belt: U.S.E.R.D.A. Final Rpt. GJO-1636-1, 120 p.
8. Brookins, D.G., (1976c), Position of uraninite and/or coffinite accumulations to the hematite-pyrite interface in sandstone-type deposits: Economic Geol. v. 71, p. 944-948.
9. Riese, W.C., and Brookins, D.G., (1976), Geochemistry of Uranium deposits east and northeast of the San Mateo Springs Grant, McKinley and Valencia Counties, New Mexico: Geol. Soc. Amer. Abs. w. Prog., v. 8, p. 622.
10. Lee, M.J., and Brookins, D.G. (1976), "Role of Argillaceous Units in the Formation of Uranium Deposits, Grants Mineral Belt, New Mexico": Geol. Soc. Amer. Prog. w. Abs., v. 8, p. 974-975.
11. Brookins, D.G., Riese, W.C., and Lee, M.J., (1977), "Rare earth and other trace elements as prospecting guides in the Grants Mineral Belt, New Mexico": Amer. Assoc. Petrol. Geol. Bull., v. 61, p. 612.
12. Brookins, D.G., Lee, M.J., and Shafiqullah, M., (1977), "K-Ar ages for clay and silt-size fractions of uranium ore from the Grants Mineral Belt, New Mexico": Isochron/West, n. 18, p. 17-19.

13. Brookins, D.G., Lee, M.J., and Riese, W.C., 1977 Trace Elements as Possible Prospecting Tools for Uranium in the Southern San Juan Basin: N.M. Geol. Soc. 28th Gdbk., p. 263-270.
14. Brookins, D.G., (1977a), Uranium deposits of the Grants Mineral Belt: geochemical constraints: Rocky Mtn. Assoc. Geol. Gdbk, p. 337-352.
15. Brookins, D.G., and Della Valle, R.S., (1977), Uranium abundance in some Precambrian and Phanerozoic rocks from New Mexico: Rocky Mtn. Assoc. Geol. Gdbk, p. 353-362.
16. Lee, M.J., and Brookins, D.G., (in press), Rb-Sr investigation of the Morrison Formation (Late Jurassic), Grants Mineral Belt, New Mexico minimum ages of sedimentation-uranium mineralization, and provenance: Amer. Assoc. Petroleum Geo. Bull.
17. Riese, W.C., and Brookins, D.G., (1977), Subsurface stratigraphy of the Morrison Formation in the Mount Taylor area and its relation to uranium ore genesis: N.M. Geol. Soc. Gdbk., p. 271-277.
18. Riese, W.C., Lee, M.J., and Brookins, D.G., (1977), Scanning electron microscopy of uranium ores, Grants Mineral Belt, New Mexico: application to U:C:pyrite distribution: Geol. Soc. Amer. Prog. w. Abs., v. 9, n. 7, p. 1142.
19. Brookins, D.G., 1977b; Geochemical Genesis of Uranium in the Southern San Juan Basin: Uranium Geology Symposium Vol. GJO:BFEC-78, p. 10-28.
20. Brookins, D.G., Della Valle, R.S., and Lee, M.J., (in press, 1978), Rb-Sr geochronologic investigation of Precambrian silicic rocks from the Zuni Mountains, New Mexico: The Mountain Geologist.
21. Brookins, D.G., (1978) Geochemical study of the uranium deposits of the southern San Juan Basin, New Mexico: U.S.D.O.E. Open File Rpt.GJBX-12(78),p. 67-86.
22. Brookins, D.G., (in press, 1978) The geochemistry of sandstone type uranium deposits: C. 7 in The Occurrence and Geologic Setting of Uranium Deposits, Energy and Power Research Inst. Spec. Pub.
23. Riese, W.C., Brookins, D.G., Lee, M.J., and Della Valle, R.S., (in press) Application of trace element geochemistry to prospecting for sandstone-type uranium deposits: Jour. Geochem. Expl.
24. Riese, W.C., Brookins, D.G., and Della Valle, R.S., (1978 in press), A scanning electron microscopic study of the Mount Taylor uranium deposit, Valencia County, N.M.: N.M. Acad. Sci.
25. Riese, W.C., and Brookins, D.G., (in press, 1978) The effectiveness of organic acids in providing uranium mineralization in the Grants Mineral Belt, N.M.: N.M. Acad. Sci.

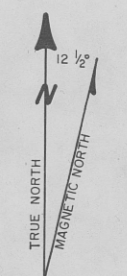
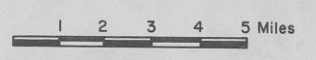
26. Brookins, D.G., Della Valle, R.S., and Lee, M.J. (1978), Rare earth element study of whole rocks and clay minerals from the southern San Juan Basin, New Mexico: EOS Trans. Am. Geophys. Un., v. 59, p. 388.
27. Sullivan, C.E., Della Valle, R.S., and Brookins, D.G. (1978 in press), Uranium, rare earth and other trace element distribution in the Hopi Buttes, northern Arizona: N.M. Acad. Sci.
28. Place, J.T., Della Valle, R.S., and Brookins, D.G. (1979 in press), "The mineralogy and geochemistry of the Mariano Lake uranium deposit, Grants mineral belt": Grants Uranium Sym., AAPG, May 1979.
29. Riese, W.C., and Brookins, D.G. (1979 in press), "The Mount Taylor uranium deposit, San Mateo, New Mexico": Grants Uranium Sym., AAPG, May 1979.
30. Riese, W.C., Brookins, D.G., Lee, M.J., and Della Valle, R.S. (1979 in press), "Scanning electron microscopy investigation of the Paragenesis of uranium deposits, Grants mineral belt, New Mexico": Grants Uranium Sym., AAPG, May 1979.
31. Brookins, D.G. (1979 in press), "Periods of mineralization in the Grants mineral belt, New Mexico": Grants Uranium Sym., AAPG, May 1979.
32. Della Valle, R.S., and Brookins, D.G. (1979 in press), "Geochemical studies of the Grants mineral belt, New Mexico": Grants Uranium Sym., AAPG, May 1979.
33. Brookins, D.G. (1979 in press), "Mechanisms for uranium deposition in the Grants mineral belt": Grants Uranium Sym., AAPG, May 1979.
34. Hicks, R.T., Lowy, R.M., Della Valle, R.S., and Brookins, D.G. (1979 in press), "Comparative clay mineralogy of the Jackpile Sandstone (Late Jurassic) and the Dakota Sandstone (Cretaceous), Grants mineral belt": Grants Uranium Sym., AAPG, May 1979.
35. Della Valle, R.S., Hicks, R.T., Lowy, R.M., and Brookins, D.G. (1979 in press), "Petrology and geochemistry of the Westwater Canyon Member, Morrison Formation, northern San Juan Basin: Similarities and differences with the Grants mineral belt": Grants Uranium Sym., AAPG, May 1979.

Plate III
 Sample Locations of Grants Mineral Belt
 (See p. 146 of text)



EXPLANATION

Tv	Tertiary Volcanics
J	Jurassic rocks
pC	Precambrian rocks
●	Drill hole
○	Outcrop sample
□	Shaft
◇	Incline
○	Open pit
—	Adit
—	Fault or fault zone dashed where approximate



To Albuquerque →

